DEPARTMENT OF CIVIL ENGINEERING
UNIVERSITY OF STRATHCLYDE
GLASGOW

THE NUMERICAL MODELLING OF TIDE AND FLOOD MOVEMENT IN TWO-DIMENSIONAL SPACE USING IMPLICIT FINITE DIFFERENCE METHODS

THESIS SUBMITTED IN FULFILMENT OF
THE REQUIREMENTS FOR THE
DEGREE OF DOCTOR OF PHILOSOPHY

GARETH PENDER
1985

ABSTRACT

The non-linear hyperbolic partial-differential equations governing long wave propagation in one and two plan dimensions are derived. By application of the Preissmann or 'box' finite difference scheme two numerical models of long wave behaviour are developed.

The first, based on the one plan dimensional form of the partial differential equations, is intended for the solution of flood routing problems in natural river systems. The model has two constituent parts. A main channel algorithm reproducing flood wave behaviour in the main channel of the drainage system and a washland algorithm modelling the behaviour of lateral storage ponds on the river banks. The main channel algorithm possesses the ability to handle: natural channel cross-sections, variable distance increments, tributary inflows, calibration with both distance and stage, rating curve boundary conditions, the formation and drowning of controls and the analysis of controls. On completion of development trials the model was used to assess the effect a new road embankment would have on flood levels in the River Aire in Yorkshire.

The second, based on the two plan dimensional partial differential equations, employs an alternating direction application of the Preissmann finite difference scheme to model tide and storm surge behaviour in estuaries and coastal seas. Special consideration was given to boundary conditions in the model and these include a

moving shore line boundary condition permitting the flooding and drying of sand flat areas to be modelled and a "weir" flow boundary condition, enabling the overtopping of obstructions with a width considerably less than the grid size of the model to be represented. A practical assessment of the model's capabilities was accomplished by simulating tide and storm surge propagation in the Firth of Clyde and Humber Estuary.

ACKNOWLEDGEMENTS

The author would like to express his gratitude to Dr. J. Ellis, Department of Civil Engineering, University of Strathclyde, for his guidance and constructive criticism during the period of this research. Thanks are also due to Mrs. M. Barrie for typing the manuscript, and also to Mr. M. Garey of Clydeforth Office Equipment Ltd for use of his firm's typing and photocopying facilities.

The assistance of Associated British Ports and Hydraulics Research in supplying and permitting the reproduction of the field data from the Humber Estuary is gratefully acknowledged, as is the help of Messrs Babtie, Shaw and Morton, Consulting Civil and Structural Engineers, in providing the information regarding the River Aire flood study.

CONTENTS

NOMENCLATURE

SYMBOL	DEFINITION
A	Cross-sectional flow area perpendicular to the flow direction.
As	Surface area of washland.
a	Body forces acting on a fluid element.
B	Width of cross-section at free surface elevation.
Bl	Bank level
C	Chezy coefficient in empirical roughness law.
Co	Discharge coefficient for a free barrier.
C_s	Discharge coefficient for a submerged barrier.
Cr	Courant number
c	Wave celerity.
Dso	Median bed material diameter.
E	Total fluid energy.
Fr	Froude number.
Gj	Right hand side of finite difference continuity equation.
g	Acceleration due to gravity.
H	Head above flood banks
Hj	Right hand side of finite difference dynamic equation.
h	Water depth
h'	Instantaneous variation from mean water depth.
J_+, J_-	Riemann invariants
j	Computational Point index.

SYMBOL	DEFINITION
jj	Total number of computational points in x-direction.
K	Channel conveyance factor; wind stress coefficient.
k	Computational Point Index.
kk	Total number of computational points in y-direction.
M	Any point in x-t space.
n	Manning coefficient in empirical roughness laws; time step index.
P	Wetted perimeter; pressure in a liquid.
Pa	Atmospheric pressure.
Q	Volumetric water discharge.
Q_{CR}	Critical flow.
Ql	Tributary inflow.
qb	Sediment flow rate per unit breadth.
ql	Lateral flow.
qx	Flow per unit breadth x-direction.
qy	Flow per unit breadth y-direction.
R	Hydraulic radius.
Sf	Slope of energy line.
So	Slope of water surface.
t	Time.
Δt	Time between two computational intervals.
U	Depth averaged velocity in the direction of x-axis.
u	Velocity in direction of x-axis.
V	Depth averaged velocity in the direction of y-axis.
v	Velocity in the direction of y-axis.
W	Wind speed above water surface.

SYMBOL	DEFINITION
Wl	Waterlevel.
w	Velocity in direction of z-axis.
x	Space co-ordinate in horizontal plane.
Δx	Distance between two computational points in the x-direction.
y	Space co-ordinate in horizontal plane.
Δy	Distance between two computational points in the y-direction.
z	Vertical space co-ordinate above datum.
zb	Elevation of barrier.
zo	Elevation of bed.
α	Energy gradient weighting coefficient.
β	Angle of wind measured from north.
β'	Non-uniform velocity distribution coefficient.
θ	Weighting coefficient in finite difference approximations of functions and their space derivatives.
λ	Wavelength; damping parameter.
π	Constant 3.14159.
ρ	Fluid density.
ρ_a	Air density.
τ	Shear stress.
τ_o	Bed shear stress.
γ	Mass per unit weight of water.
γ_s	Mass per unit weight of sand
φ	Latitude
ω	Angular Velocity

CHAPTER ONE

INTRODUCTION

1.1.

Recent technological advances have provided the means to design and construct civil engineering works of greater technical complexity and scale than were previously possible. Such projects have the potential to affect the environment over distances ranging from their immediate vicinity to hundreds of miles. Parallel to this increasing technical ability there has been a steady growth in society's environmental conscience; awareness of man's increasing potential to irreversibly damage his surroundings. Together these have placed greater emphasis on the engineering profession's responsibility to assess the environmental impact of proposed engineering works long before the construction phase.

Civil engineering hydraulics is one branch of engineering to which the above statements are particularly applicable. As, when proposed works influence flows in rivers and seas there is considerable potential for economic and environmental damage. Economic damage may result from inundation of valuable land or adverse effects on shipping lanes or the inshore fishing industry. Environmental damage can occur through damage to wild life habitats or the loss of a recreational amenity.

To solve the complex problems of cause and effect

posed by alterations to hydraulic flow systems recourse is made to physical or numerical modelling. Both of these techniques have their own particular advantages and disadvantages. In the case of numerical modelling the advantages include: flexibility in the sense that the structure of the model does not depend on data from the prototype, and hence the same basic model can be used for entirely different cases, also numerical models can be stored easily with minimum costs. Although possessing these advantages numerical models are not yet sufficiently advanced to totally replace physical models; as only by physical modelling can full three dimensional flow behaviour and fine geometrical detail be included in a study.

In the early days numerical modelling found application only in projects with a large capital expenditure, as in these projects the cost of numerical modelling research and development are small compared with the overall project cost. Today, however, numerical modelling is used for projects with capital expenditure ranging from tens of thousands to hundreds of millions of pounds. This popularising of numerical modelling results from two sources. Firstly, the availability of published information allowing numerical schemes to be developed with a small budget by capitalising on research investments made for the earlier projects and secondly the increased availability and reduced costs of computing facilities.

One of the aims of this research project is to build on current numerical modelling expertise to provide low cost numerical models for the solution of tide and flood propagation problems in two plan dimensions. It is hoped that the resulting models will be of use to hydraulic engineers with access to standard office computing facilities.

1.2. ECONOMIC ASPECTS OF NUMERICAL HYDRAULIC MODELS

The commercial considerations governing the internal operation of a numerical modelling organisation are presented in detail both by Abbott (1979a) and Cunge, Holly and Verway (1980). From the point of view of a practising engineer the economics can be viewed in a relatively simple light. To him a numerical model is an engineering tool which should provide reliable engineering information at as low a cost as is possible. This applies if he purchases a software system to operate on his own inhouse computer facilities or if he employs a numerical modelling organisation to carry out a study for him.

The costs incurred when using inhouse facilities to solve a particular problem may be subdivided as follows:

i. The cost of basic surveying and field measurement campaign. This cost exists for all studies and its value depends to a large extent on local conditions.

ii. The cost of purchasing or developing

the necessary software to solve the problem. This can be significantly reduced if the model is applicable to a number of problems permitting initial development or purchasing costs to be discounted over a number of applications. Such is the economic reasoning behind the design system approach Abbott (1976).

A design system consists of a main computational algorithm for the solution of the mathematical equations governing the physical problem linked to subsidiary programmes for data and result processing. The main computational algorithm is developed with a high degree of flexibility enabling it to be applied to as wide a range of problem types and geometrical configurations as possible. The subsidiary programmes lower costs by reducing the manhours required for data and result processing. A flow chart for a general design system is shown in Figure 1.1

iii. The cost of computer time. This cost exists for all studies. It can be minimised firstly, by the use of efficient programming techniques, secondly by careful assessment,

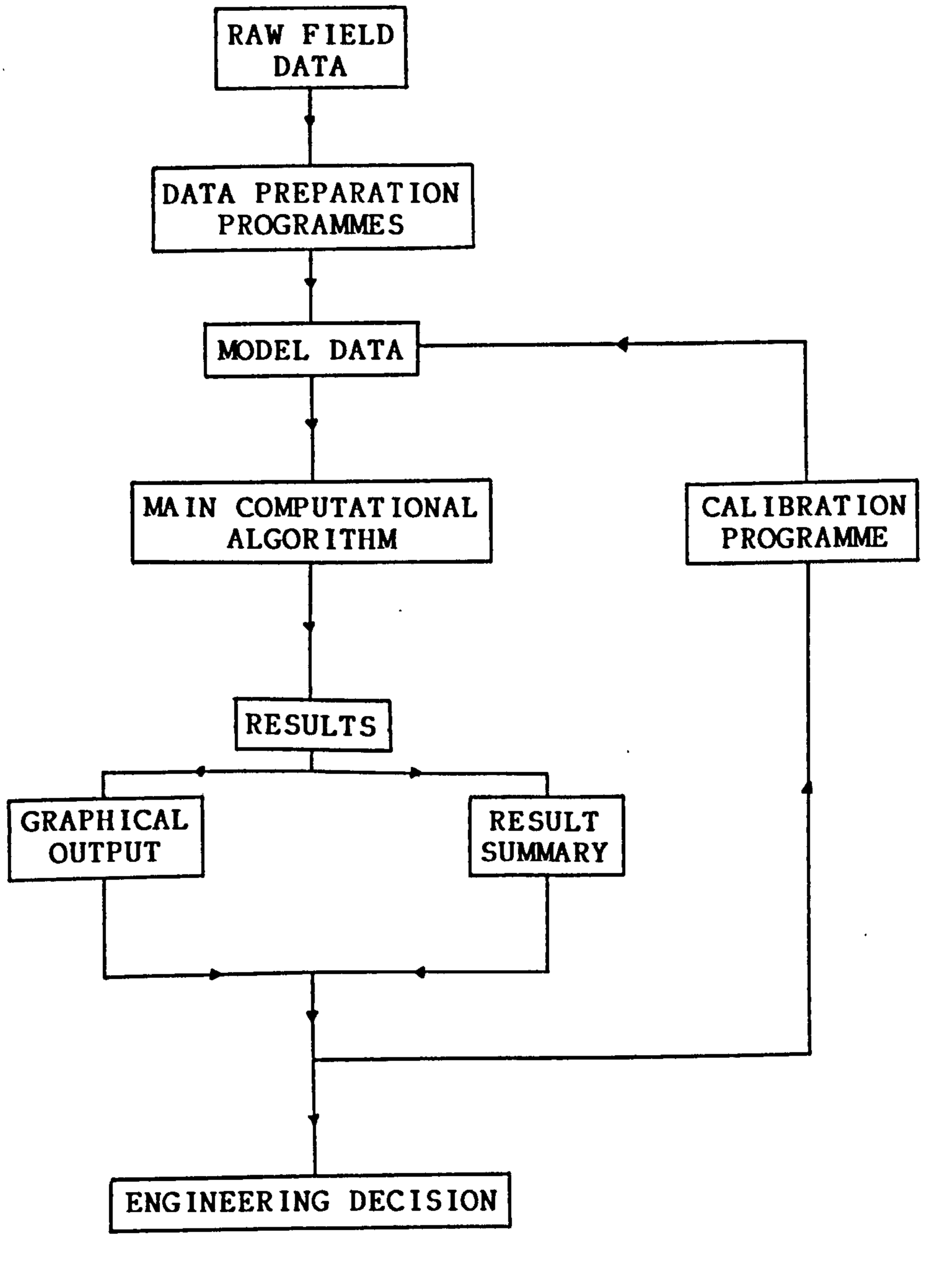

FIGURE 1.1
FLOW CHART FOR A DESIGN SYSTEM.

at the planning stage, of exactly what information is required from the study.

The advantage for a practicing engineer in adopting a policy of using inhouse numerical modelling is that after the initial development or purchasing outlay for the numerical model has been met his organisation then has direct control over charges for any modelling contract. Autonomy of this kind permits the strategic use of numerical models where the engineering firm may choose to subsidise numerical model studies for a client in the hope that such a study will eventually lead to a much more valuable contract.

If the practicing engineer employs a modelling organisation to carry out a study on his behalf the cost of the operation is outwith his control and will depend to a large extent on economic forces operating within the numerical modelling market at that time.

In most engineering firms numerical modelling studies will consist of a mixture of inhouse studies and external numerical modelling contracts.

1.3. SCOPE OF THE CURRENT RESEARCH

In the following chapters the development and application of two numerical models is described. One for the modelling of flood wave propagation in a natural river channel and its associated washland areas and the other for the modelling of tide and storm surge propagation

in coastal waters.

1.3.1. FLOOD ROUTING MODEL

The aim of the flood routing model, listed in Appendix B, is to provide an estimate of variations in flows and water levels during the passage of a flood through a natural river system by solving the governing hydraulic equations. This requires that the model take account of flows both in the main river channel and into and out of washland areas. To achieve this two algorithms are employed within the model; one for the solution of the continuity and dynamic equation in the main channel and the other for volume conservation in washland areas.

The main channel algorithm employs an implicit finite difference method to solve the governing equations as this permits use of the most economic combinations of time and distance increments. In addition to solving for flows and water levels along the main channel length it was desirable that the model contain the facility for handling the following features:

i. The ability to operate using the geometry of the natural river channel.

ii. The ability to use variable distance increments between solution nodes. This enables easy inclusion of sections of hydraulic interest such as bridges and weirs in the numerical schematisation.

iii. A facility for handling tributary inflows as in many rivers a large percentage of downstream main channel flow comes from upstream tributary flows.

iv. Be capable of detecting and analysing control sections. This includes both man made weirs and natural control sections which may be present at low flows and drowned out at high flows. An initial survey of the technical literature indicated that such a requirement may pose computational difficulties especially in reaches with relatively steep bed slopes, Price and Samuels (1980).

v. Calibration with both distance and stage allowing local energy losses at meanders and bridge sections to be included along with variations in channel roughness with water level.

vi. The use of a rating curve for the downstream boundary condition. Through this the influence of conditions downstream of the model area are included in the solution.

Washland areas are represented by a number of

storage pockets on both banks of the main channel. The pockets are separated from each other and the main channel by a system of flood banks. Flows between the main channel and the washlands are calculated from a weir flow equation of the form $q \propto H^{3/2}$. The degree of submergence is taken into account by the use of a submergence factor. Within each washland compartment waterlevel is calculated by an explicit solution of the continuity equation. The use of an explicit calculation allows the washland model to be contained in a separate routine. This adds to programme flexibility as the main channel model can be applied in rivers where no washland system exists. Since individual washland compartments may border an appreciable stretch of river channel it was thought desirable to accommodate the possibility of simultaneous inflow to and outflow from a washland. Such a circumstance may develop, for example, at a meander loop. Upstream of the meander the river level is relatively high and a proportion of the river flow enters the flood plain within the loop of the river. Downstream of the meander the river level is significantly lower due to head losses within the meander and flow may take place from the flood plain to the river at this point.

Programming of the numerical model was done in such a way as to be compatible with an existing programme library at the University of Strathclyde. The library provides supplementary programmes for the generation of main channel section properties from raw survey data, the calculation

of starting conditions in the form of steady flow profiles and calibration.

On completion the flood routing model was used for a flood study of the River Aire in Yorkshire. The purpose was to assess the effect of flood levels when a proportion of the existing washland was lost due to the construction of a new road embankment.

1.3.2. TIDAL MODEL

Intended applications of the model are the simulation of tide and storm surge propagation in coastal areas. The model, listed in Appendix C, employs an alternating direction implicit finite difference scheme to solve the long wave equations in two plan dimensions for flows and water levels at every point in a numerical grid placed over the study area. Solution at every point in a numerical grid inevitably increases computational cost above those for methods solving flows and water levels at alternate grid points. However, it is hoped that the additional computer costs incurred will be offset by greater model flexibility particularly in the choice of boundary conditions.

Possible boundary conditions include:

i. Flow known as a function of time.

ii. Water level known as a function of time.

iii. An expanding boundary condition where the solution area may expand over

low-lying areas as water level increases. Such a condition will be particularly useful if it is required to assess the extent of flooding resulting from a storm surge.

iv. A weir flow boundary condition. This condition is of value in circumstances where an assessment of flow over an obstruction with a width considerably less than the grid size is required. Examples of such obstructions are sand-bars or causeways.

For development purposes the model was used to simulate tides and storm surges in the Firth of Clyde. The Firth of Clyde was chosen because of its highly variable bathymetry and the readily available data for both schematisation and verification. After completion of testing and calibration the opportunity was taken to obtain a direct comparison between the adopted alternating direction implicit method and a two-dimensional characteristic method. The results of Donald (1981) were used as the basis for this comparison.

Following the satisfactory conclusion of development tests in the Firth of Clyde, the model was applied to the Humber Estuary. Data for this estuary was available to provide direct comparisons between computed and observed water levels and velocities. The water level and velocity

observations were extracted from published works by the Humber Estuary Research Committee and the Hydraulics Research Station. In addition the sand flat areas in the Humber Estuary permitted testing of the expanding boundary condition while the weir flow boundary was tested by simulating the over topping of Spurn Head.

CHAPTER TWO

DERIVATION OF LONG WAVE EQUATIONS

2.1. WATER WAVES

Water waves are classified into three categories according to their "relative depth", which is the ratio of water depth to wave length. If the relative depth is greater than a half, the waves are called "deep-water waves" or "short waves", for which the wave celerity is dependent on the wave length only.

For the "shallow water waves", also called "long waves", the relative depth is less than one twentieth, and the wave celerity is dependent on the water depth only.

Waves having relative depths between these two limits are called "intermediate-depth waves", where the wave celerity is dependent on both the wave length and the water depth.

The present concern is with long waves as these are the dominant wave form during flood wave, tide and storm surge propagation.

2.2. GENERATION OF "LONG WAVES" IN SEAS

In sea areas long waves are generated by forces acting on the body of water. The resulting waves can be classified depending upon the generating forces. These are: tidal, meteorological surge and tsunami.

2.2.1. TIDES

Tidal waves are a result of:

a) The attractive force of the moon;

b) The attractive force of the sun;

c) The attractive force of the earth;

d) The centrifugal force caused by the earth about its axis.

Of these contributory forces, that of the moon is the greatest. If it were not for the effects of the shape and depth of the oceans, and the position of islands therein, and the shape of the coastlines, the rise and fall of the tides would closely follow the movement of the moon round the earth, varied to some extent in accordance with the momentary position of the moon, the earth and the sun in relation to each other. In fact, however, the manner in which the tides rise and fall in different seas and oceans varies considerably; the period of oscillation of the tide in one area differs from that in another, and varies from about six to twenty-four hours.

The combined attractive forces of the moon and the sun on the earth's large masses of water have their greatest effect when they are in line with the earth, i.e. at new moon and full moon, and their least effect when they are approximately at right angles to each other, i.e. at the first and last quarters of the moon.

These variations of this force affect the amplitude of the wave they produce and hence the range of the tide,

i.e. the difference in level between successive high and low waters, is also affected. Shortly after full and new moon a locality will experience its highest high waters and lowest low waters of that lunar month, and the tides in this period are called "spring tides". Conversely, around the times of first and last quarters of the moon, the lowest high waters and highest low waters of that lunar month will be experienced, at which period the tides are called "neap tides". Between these limits the height of successive tides increases or diminishes progressively. Spring tides around the British Isles occur from about one to one and a half days after full or new moon, and neaps occur at about the same interval after the first or last quarters of the moon. The time interval between successive spring and neap tides is variable, but for practical purposes it can be taken as being about seven and a half days, i.e. about one quarter of an average lunar month of twenty-nine and a half days.

2.2.2. METEOROLOGICAL SURGE

A meteorological surge wave is normally produced by conditions associated with a depression. An area of low pressure over an area of sea will set up a barometric slope, by causing a relative rising of the sea surface by about 10mm per mb. Appreciable surges are only likely to develop on this account when a progressive wave is built up by resonance which results from a depression travelling at a speed approaching $(gh)^{\frac{1}{2}}$. Associated strong winds can

also act to increase water level. Amplitudes of surges will only be small in deep water but will become magnified on account of shoaling effect on entering shallow water.

2.2.3. TSUNAMI

Tsunamis have a seismic origin and will thus be propagated from a faulted or orogenic area. Coastal engineers are usually concerned with tsunami that have degenerated into trains of long waves. On account of their relative infrequency and unpredictability much remains to be learned of their fundamental characteristics. As with storm surges the amplitudes of tsunami waves are also magnified on entering shallow water.

2.3. MODIFICATION OF LONG WAVES IN COASTAL AREAS

Long waves propagating in the open ocean generally have an amplitude of less than a metre. On entering coastal areas restrictions imposed by the surrounding land and the shallower water cause the wave crest to steepen and the wave amplitude to increase.

The steepening of the wave crest is a result of wave celerity depending on water depth. It can be shown, Doodson & Warburg (1941), that the celerity of any point in a wave is equal to:

$$C = [g(h + 3h')]^{\frac{1}{2}}$$

where h is the mean water depth and h' is the instantaneous variation above and below this mean. Clearly in shallow water high water will be accelerated and low water will

be retarded, significantly steepening the wave crest.

Amplification of wave amplitude in gulfs and estuaries results from two distinct causes:

i. By reason of tendency to resonance. It can be shown, Doodson and Warburg, (1941), that in estuaries of length less than half a wave-length tidal oscillations at the closed end are greater than at the mouth.

ii. By reason of the changes in the area of the cross-section of the channel. As the cross-sectional area diminishes the stream must increase to convey the same amount of volume and energy as before. This necessarily involves an increase in the elevation also.

2.4. INTERACTION OF LONG WAVES

Unpredictable surge waves, such as meteorological surges and tsunami, will be superimposed on any tide that may be present and the two will build up together in shallow water. If the crest of a surge coincides with high water a phenomenal high water will be produced, far above the predicted value. Disastrous effects may be experienced ashore, such as damage of man made structures or the inundation of valuable arable land.

2.5. DERIVATION OF THE TWO-DIMENSIONAL LONG WAVE EQUATIONS

Using Newton's laws and the principle of conservation of mass it is possible to derive the two-dimensional unsteady flow equations; which given continuous sets of boundary and geometrical data will describe the propagation of long

waves in two space dimensions. In the subsequent sections these equations are derived relative to a fixed co-ordinate system. The Cartesian axes 'x' and 'y' are taken counter-clockwise in an arbitrary horizontal plane, with the 'z' axis vertically upward.

2.5.1. THE CONTINUITY EQUATION

The law of conservation of mass states that the mass of fluid flowing across the boundaries into the fluid element shown in Figure 2.1 in time 'Δt' must be equal to the amount by which the mass of the element has increased in the same time interval. Let the dimensions of the element be Δx, Δy, and Δz and velocities in the 'x', 'y' and 'z' directions be given by 'u', 'v' and 'w' respectively.

The inflow of mass across face ACGE in time 'Δt' is:

$$\rho u \Delta z \Delta y \Delta t$$

where ρ is the mass per unit volume of the fluid. By Taylor's theorem, the inflow of mass across opposing face BDHF in time 'Δt' is approximately:

$$-\left[\rho u \Delta z \Delta y \Delta t + \frac{\partial(\rho u)}{\partial x} \Delta x \Delta z \Delta y \Delta t\right]$$

Adding the above pair of expressions yields the net inflow of mass in the x-direction during 'Δt':

$$-\frac{\partial(\rho u)}{\partial x} \Delta x \, \Delta z \, \Delta y \, \Delta t \quad .$$

The net inflow of mass into the volume element is the sum of the contributions of the three co-ordinate directions, i.e.:

$$\begin{matrix}\text{net flow across} \\ \text{all faces in } \Delta t\end{matrix} = -\left[\frac{\partial(\rho u)}{\partial x} + \frac{\partial(\rho v)}{\partial y} + \frac{\partial(\rho w)}{\partial z}\right]\Delta x \Delta y \Delta z \Delta t \qquad \text{Equation 2.1}$$

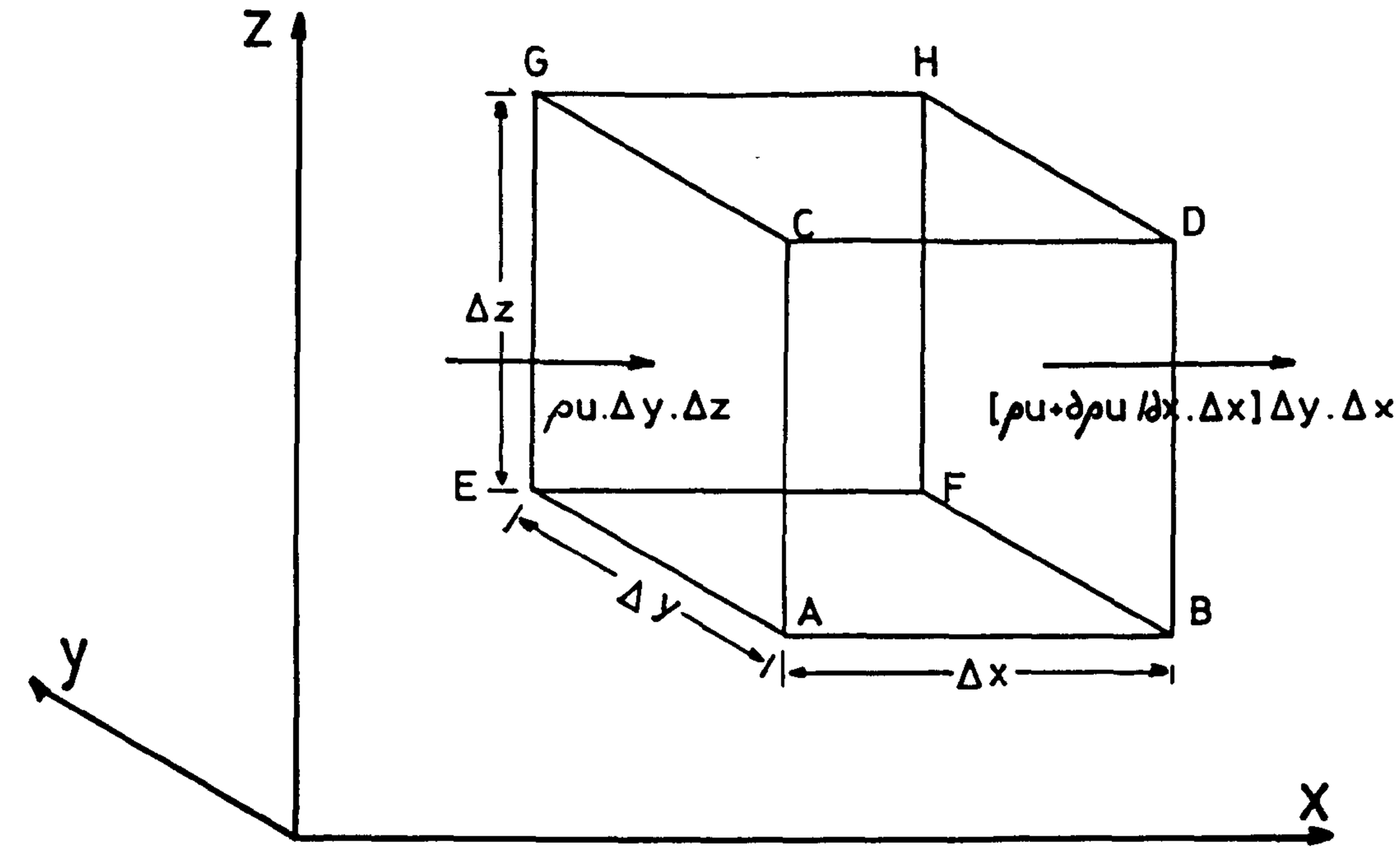

Figure 2.1
Flux through element in x-direction

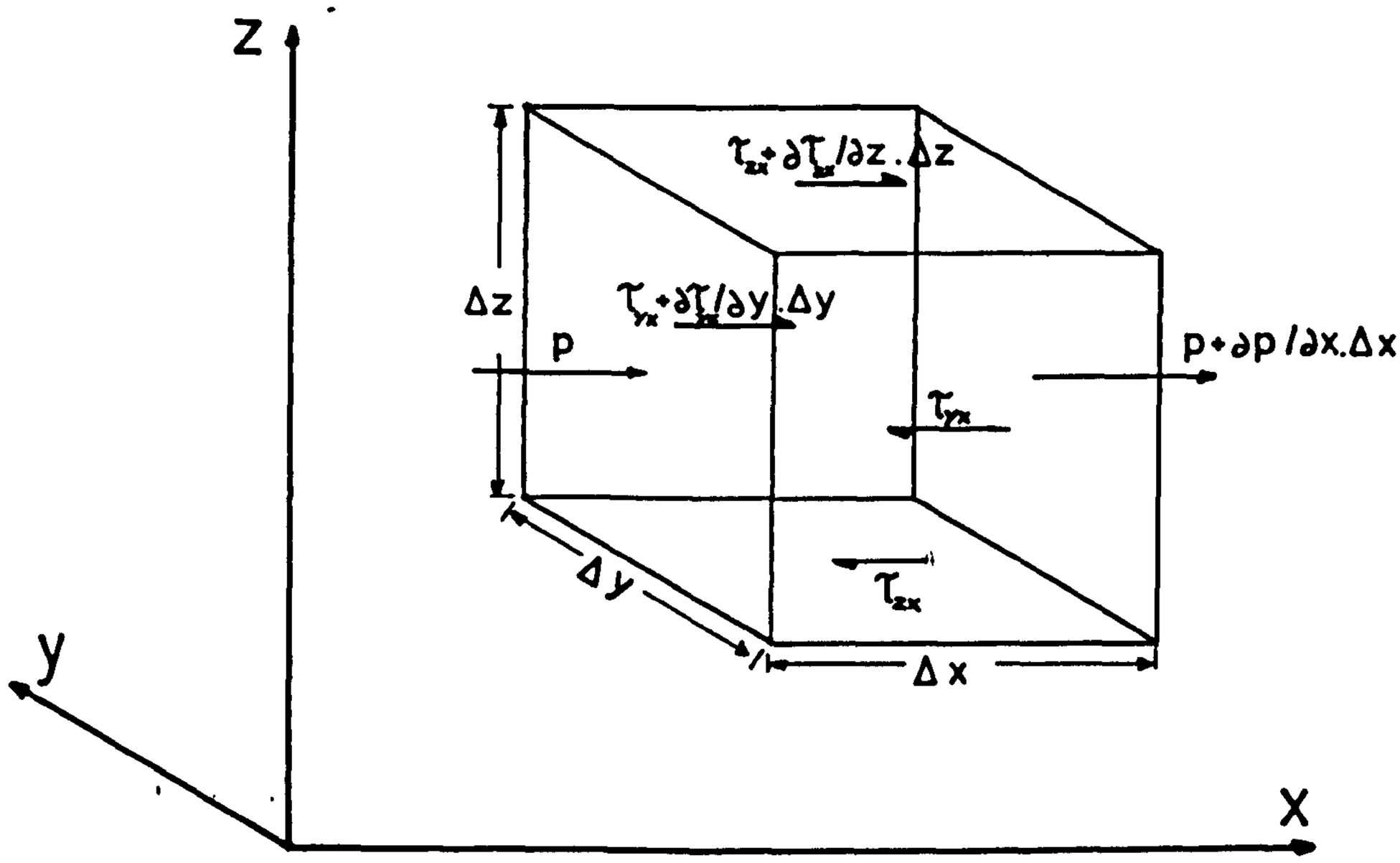

Figure 2.2
Pressure and shear stresses acting in the x-direction on fluid element.

If the mass present at time 't' is $\rho \Delta x \Delta y \Delta z$ then at time 't+Δt', from Taylor's formula, the mass present will be:

$$\rho \Delta x \Delta y \Delta z + \frac{\partial \rho}{\partial t} \Delta x \Delta y \Delta z \Delta t$$

Then,

net increase of mass within element in Δt = $\frac{\partial \rho}{\partial t} \Delta x \Delta y \Delta z \Delta t$ Equation 2.2.

In the absence of any creation of mass within the element this must be equal to the inflow of mass across the boundaries;

i.e. Equation 2.1. = Equation 2.2.

$$\frac{\partial \rho}{\partial t} = - \left[\frac{\partial (\rho u)}{\partial x} + \frac{\partial (\rho v)}{\partial y} + \frac{\partial (\rho w)}{\partial z} \right] \quad \text{Equation 2.3.}$$

Where a fluid may be considered incompressible equation 2.3. reduces to the volume conservation law of an incompressible fluid:

$$\frac{\partial u}{\partial x} + \frac{\partial v}{\partial y} + \frac{\partial w}{\partial z} = 0 \quad \text{Equation 2.4}$$

2.5.2. THE DYNAMIC EQUATION

Consider the forces shown acting, in the x-direction, on the fluid element in figure 2.2. A double subscript convention is used to identify shear stress components; the first subscript indicating the direction of the normal to the surface on which the shear stress acts, and the second, the direction of the component. Assuming all pressures to increase in the positive co-ordinate direction, the net pressure force on the element is: $- \frac{\partial P}{\partial x} \Delta x \Delta y \Delta z$. Similarly the net shear forces acting in the x-directions are: $\frac{\partial \tau_{yx}}{\partial y} \Delta y \Delta x \Delta z$ and $\frac{\partial \tau_{zx}}{\partial z} \Delta z \Delta x \Delta y$. Body forces, in the x-direction, acting on the fluid as a whole, e.g. tide generating forces and Coriolis force are represented by

the term a_x. Summating the above forces and applying Newton's second law in the x-direction gives:

$$\frac{du}{dt} = -\frac{1}{\rho}\frac{\partial P}{\partial x} + \frac{1}{\rho}\frac{\partial(\tau_{yx})}{\partial y} + \frac{1}{\rho}\frac{\partial(\tau_{zx})}{\partial z} + a_x \qquad \text{Equation 2.5.}$$

The acceleration term is provided by the differential equation for the total change in velocity u.

$$du = \frac{\partial u}{\partial x}dx + \frac{\partial u}{\partial y}dy + \frac{\partial u}{\partial z}dz + \frac{\partial u}{\partial t}dt$$

Similar equations can be derived for the y and z directions. Namely:

$$\frac{dv}{dt} = \frac{-1}{\rho}\frac{\partial P}{\partial y} + \frac{1}{\rho}\frac{\partial(\tau_{xy})}{\partial x} + \frac{1}{\rho}\frac{\partial(\tau_{zy})}{\partial z} + a_y \qquad \text{Equation 2.6.}$$

$$\frac{dw}{dt} = \frac{-1}{\rho}\frac{\partial P}{\partial z} + \frac{1}{\rho}\frac{\partial(\tau_{xz})}{\partial x} + \frac{1}{\rho}\frac{\partial(\tau_{yz})}{\partial y} + a_z \qquad \text{Equation 2.7.}$$

For the problems considered in the present work, (flow in rivers and estuaries), vertical components of local mean velocity are small. In consequence, vertical components of force due to changes of momentum and gradients of vertical shearing stresses are negligible compared with the force due to gravity.

Equations 2.5. to 2.7. can be simplified to:

$$\frac{\partial u}{\partial t} + u\frac{\partial u}{\partial x} + v\frac{\partial u}{\partial y} = \frac{-1}{\rho}\frac{\partial P}{\partial x} + \frac{1}{\rho}\frac{\partial \tau_{yx}}{\partial y} + \frac{1}{\rho}\frac{\partial \tau_{zx}}{\partial z} + a_x \qquad \text{Equation 2.8.}$$

$$\frac{\partial v}{\partial t} + u\frac{\partial v}{\partial x} + v\frac{\partial v}{\partial y} = \frac{-1}{\rho}\frac{\partial P}{\partial y} + \frac{1}{\rho}\frac{\partial \tau_{xy}}{\partial x} + \frac{1}{\rho}\frac{\partial \tau_{zy}}{\partial z} + a_y \qquad \text{Equation 2.9.}$$

$$\frac{1}{\rho}\frac{\partial P}{\partial z} = -g \qquad \text{Equation 2.10.}$$

It is assumed that the density is uniform and consequently the pressure is hydrostatic and a linear function of depth, i.e.

$$p(z) = \rho g h + Pa$$

where Pa is the atmospheric pressure. In tidal computations,

atmospheric pressure is usually assumed to remain constant over the problem area, however, pressure variations are important in the generation of storm surges. The derivatives of pressure in the horizontal directions now become a function of water level and atmospheric pressure:

$$\frac{\partial P}{\partial x} = \rho g \frac{\partial Wl}{\partial x} + \frac{\partial Pa}{\partial x}$$

where $\frac{\partial Wl}{\partial x}$ is the component of surface slope in the x-direction.

Equation 2.8 becomes:

$$\frac{\partial u}{\partial t} + u\frac{\partial u}{\partial x} + v\frac{\partial u}{\partial y} = -g\frac{\partial Wl}{\partial x} - \frac{1}{\rho}\frac{\partial Pa}{\partial x} + \frac{1}{\rho}\partial \tau_{yx}/\partial y + \frac{1}{\rho}\partial \tau_{zx}/\partial z + a_x \qquad \text{Equation 2.11}$$

Likewise, equation 2.9 can be written:

$$\frac{\partial v}{\partial t} + u\frac{\partial v}{\partial x} + v\frac{\partial v}{\partial y} = -g\frac{\partial Wl}{\partial y} - \frac{1}{\rho}\frac{\partial Pa}{\partial y} + \frac{1}{\rho}\partial \tau_{xy}/\partial x + \frac{1}{\rho}\partial \tau_{zy}/\partial z + a_y \qquad \text{Equation 2.12}$$

2.5.3 DEPTH AVERACED EQUATIONS

If the bed is at elevation z_o above the datum and $Wl - z_o$ = stream depth h equations 2.11 and 2.12 can be integrated throughout the depth:

$$\frac{1}{h}\int_{z_o}^{Wl}\left(\frac{\partial u}{\partial t} + u\frac{\partial u}{\partial x} + v\frac{\partial u}{\partial y}\right)dz =$$

$$-\frac{g}{h}\int_{z_o}^{Wl}\frac{\partial Wl}{\partial x}dz - \frac{1}{\rho h}\int_{z_o}^{Wl}\frac{\partial Pa}{\partial x}\,dz + \frac{1}{\rho h}\int_{z_o}^{Wl}\left(\partial \tau_{yx}/\partial y + \partial \tau_{zx}/\partial z\right)dz$$

$$+\frac{1}{h}\int_{z_o}^{Wl} a_x dz = -g\frac{\partial Wl}{\partial x} - \frac{1}{\rho}\frac{\partial Pa}{\partial x} + a_x + \frac{1}{\rho h}\int_{z_o}^{Wl}\partial \tau_{yx}/\partial x\,dz + \frac{1}{\rho}\tau_{sx} - \frac{1}{\rho}\tau_{bx}$$

$u\frac{\partial u}{\partial x}$ and $v\frac{\partial u}{\partial y}$ are non-linear terms and can only be integrated over the vertical if their distributions are known. Fortunately they are usually much smaller in magnitude than $\partial u/\partial t$

and it is sufficient to assume that:

$$\frac{1}{h}\int_{zo}^{wl}(u\frac{\partial u}{\partial x}+v\frac{\partial u}{\partial y})\,dz = \beta_1' U\frac{\partial U}{\partial x} + \beta_2' V\frac{\partial V}{\partial y}$$

where U and V are depth averaged velocities. Values of coefficient β' have been found for typical variations of velocity over the vertical β' seldom exceeds 1.05 in real flows, Henderson (1966). Because of the smallness of the terms, however, it is common practice to omit the term completely or take $\beta' = 1$.

Most estuaries are wider by an order of magnitude than they are deep, and shear stresses on the vertical planes are small except near steep banks and vertical walls. τ_{yx} and τ_{xy} are thus usually small and can be omitted from equations 2.11. and 2.12.

Dividing by g and rearranging equations 2.11. and 2.12. become:

$$\frac{1}{g}\frac{\partial U}{\partial t}+\frac{U}{g}\frac{\partial U}{\partial x}+\frac{V}{g}\frac{\partial U}{\partial y}+\frac{\partial Wl}{\partial x}+\frac{1}{\rho g}\frac{\partial Pa}{\partial x}-\frac{\tau_{sx}}{\rho gh}+\frac{\tau_{bx}}{\rho gh}=\bar{a}_x \qquad \text{Equation 2.13}$$

$$\frac{1}{g}\frac{\partial V}{\partial t}+\frac{U}{g}\frac{\partial V}{\partial x}+\frac{V}{g}\frac{\partial V}{\partial y}+\frac{\partial Wl}{\partial y}+\frac{1}{\rho g}\frac{\partial Pa}{\partial y}-\frac{\tau_{sy}}{\rho gh}+\frac{\tau_{by}}{\rho gh}=a_y \qquad \text{Equation 2.14}$$

The continuity equation can also be integrated over the depth of the stream:

$$\int_{z}^{wl}(\frac{\partial u}{\partial x}+\frac{\partial v}{\partial y}+\frac{\partial w}{\partial z})dz = 0$$

Putting $U = \frac{1}{h}\int_{zo}^{wl} u\,dz$ and $V = \frac{1}{h}\int_{zo}^{wl} v\,dz$

and noting that $W_{zs} = dWl/dt$ and $W_{zb} = 0$ we get:

$$\frac{\partial(hU)}{\partial x}+\frac{\partial(hV)}{\partial y}+\frac{dWl}{dt}=0 \qquad \text{Equation 2.15}$$

The foregoing is based on the discussion presented by McDowell and O'Connor (1977).

2.5.4. REPRESENTATION OF SURFACE AND BOTTOM SHEAR STRESSES

Common practice is that shear stress at the sea bed be expressed in terms of the well known Chezy friction coefficient 'C' as used in steady open channel flow. Equilibrium between gravitational and resistance forces can be expressed as

$$\tau_{br} = \rho g h S_o$$

where τ_{br} is the resultant shear stress proportional to the resultant depth averaged velocity $(U^2 + V^2)^{\frac{1}{2}}$ and S_o is the slope of the water surface. The resultant velocity may be deduced from De Chezy's empirical relationship namely:

$$(U^2 + V^2)^{\frac{1}{2}} = C(S_o h)^{\frac{1}{2}}$$

since h corresponds to the hydraulic radius in a very wide channel. From the previous pair of equations, it follows that the resultant frictional stress at the sea bed is given by:

$$\tau_{br} = \rho g (U^2 + V^2) / C^2$$

Also, the components of the resultant frictional stress which opposes fluid motion are expressed as follows:

$$\tau_{bx} = \rho g U(U^2 + V^2)^{\frac{1}{2}} / C^2 \qquad \text{Equation 2.16}$$

$$\tau_{by} = \rho g V(U^2 + V^2)^{\frac{1}{2}} / C^2 \qquad \text{Equation 2.17}$$

The frictional resistance factor 'C', which is used to establish these relationships between squared velocity and the bottom stress, can be found only by observation. This coefficient depends on the roughness of the bottom, the bottom material and depth.

The horizontal shear force at the free surface of the fluid as a result of wind stress, τ_{sr} may be determined from an empirical approach similar to that for investigation of bottom stress, Muir Wood and Fleming (1981). However, for wind stress the medium of flow is air not water. The components of wind stress, when the x-axis lies in a North-South direction, are expressed as:

$$\tau_{sx} = K \rho_a W W \cos \beta \qquad \text{Equation 2.18}$$

$$\tau_{sy} = K \rho_a W W \sin \beta \qquad \text{Equation 2.19}$$

where K is the wind stress coefficient, ρ_a is the density of air and W is the wind speed above the water surface.

2.5.5. EXTERNAL BODY FORCES

Body forces a_x and a_y include the effects of the earth's rotation and tide generating forces. Tide generating forces are negligibly small compared to other terms and are generally omitted from actual computations. Consequently, the only external force requiring consideration is that due to the earth's rotation. The Coriolis acceleration components, and the associated inertia forces are induced by the rotation of the earth with angular velocity ω and therefore depend on the latitude φ of the body of fluid. The inertia forces in the positive x and y directions are $\rho \Omega v$ and $-\rho \Omega u$ respectively, where $\Omega = 2\omega \sin\varphi$.

When these forces are integrated with respect to z and divided by the total depth h, the final form can be equated to the external forces as follows:

$$a_x = 2V \omega \sin\varphi \qquad \text{Equation 2.20}$$

$$a_y = -2U \omega \sin\varphi \qquad \text{Equation 2.21}$$

A comprehensive discussion of the coriolis force is given by Doodson and Warburg (1941), while a rigorous mathematical derivation of the term is presented by Raudkivi and Callander (1975).

2.5.6 THE COMPLETE EQUATIONS

The equations for long wave motion in two-plan dimensions can now be written as:

$$\frac{1}{g}\frac{\partial U}{\partial t} + \frac{U}{g}\frac{\partial U}{\partial x} + \frac{V}{g}\frac{\partial U}{\partial y} + \frac{\partial Wl}{\partial x} + \frac{1}{g\rho}\frac{\partial Pa}{\partial x} - \Omega V + \frac{\tau_{bx}}{g\rho h} - \frac{\tau_{sx}}{g\rho h} = 0 \qquad \text{Equation 2.22}$$

$$\frac{1}{g}\frac{\partial V}{\partial t} + \frac{U}{g}\frac{\partial V}{\partial x} + \frac{V}{g}\frac{\partial V}{\partial y} + \frac{\partial Wl}{\partial y} + \frac{1}{g\rho}\frac{\partial Pa}{\partial y} + \Omega U + \frac{\tau_{by}}{g\rho h} - \frac{\tau_{sy}}{g\rho h} = 0 \qquad \text{Equation 2.23}$$

$$\frac{\partial Wl}{\partial t} + \frac{\partial (hU)}{\partial x} + \frac{\partial (hV)}{\partial y} = 0 \qquad \text{Equation 2.24}$$

or setting $q_x = Uh$ and $q_y = Vh$

$$\frac{1}{g}\frac{\partial (q_x/h)}{\partial t} + \frac{(q_x/h)}{g}\frac{\partial (q_x/h)}{\partial x} + \frac{(q_y/h)}{g}\frac{\partial (q_x/h)}{\partial y} + \frac{\partial Wl}{\partial x} + \frac{1}{g}\frac{\partial Pa}{\partial x} - \Omega(q_y/h) + \frac{\tau_{bx}}{g\rho h} - \frac{\tau_{sx}}{g\rho h} = 0 \qquad \text{Equation 2.25}$$

$$\frac{1}{g}\frac{\partial (q_y/h)}{\partial t} + \frac{(q_x/h)}{g}\frac{\partial (q_y/h)}{\partial x} + \frac{(q_y/h)}{g}\frac{\partial (q_y/h)}{\partial y} + \frac{\partial Wl}{\partial y} + \frac{1}{g}\frac{\partial Pa}{\partial y} - \Omega(q_x/h) + \frac{\tau_{by}}{g\rho h} - \frac{\tau_{sy}}{g\rho h} = 0 \qquad \text{Equation 2.26}$$

$$\frac{\partial Wl}{\partial t} + \frac{\partial qx}{\partial x} + \frac{\partial qy}{\partial y} = 0 \qquad \text{Equation 2.27}$$

where:

$$\tau_{bx} = \rho g \frac{q_x}{h} \left[\left(\frac{q_x}{h}\right)^2 + \left(\frac{q_y}{h}\right)^2 \right]^{\frac{1}{2}} / C^2$$

$$\tau_{by} = \rho g \frac{q_y}{h} \left[\left(\frac{q_x}{h}\right)^2 + \left(\frac{q_y}{h}\right)^2 \right]^{\frac{1}{2}} / C^2$$

$$\tau_{sx} = K \rho_a W W \text{ Cos } \beta$$

$$\tau_{sy} = K \rho_a W W \text{ Sin } \beta$$

2.6 ONE DIMENSIONAL LONG WAVE EQUATIONS

In systems such as that shown in Figure 2.3 the lateral boundaries effectively restrict flow to one space dimension. Here the two-dimensional unsteady flow equations can be reduced to their one-dimensional form through certain simplifying assumptions. These one-dimensional long wave equations, also known as the de St Venant equations, are presented in the following.

2.6.1 ONE DIMENSIONAL CONTINUITY EQUATION

Under the conditions shown in Figure 2.3 the continuity equation becomes:

$$B \frac{\partial W1}{\partial t} + \frac{\partial Q}{\partial x} - q1 = 0 \qquad \text{Equation 2.28}$$

where 'B' is the section breadth, 'Q' is the average flow rate over the section area and 'q' is the average inflow or outflow per unit length.

2.6.2 ONE DIMENSIONAL DYNAMIC EQUATION

In one dimensional unsteady flow calculations the Coriolis acceleration, wind shear stress and variations

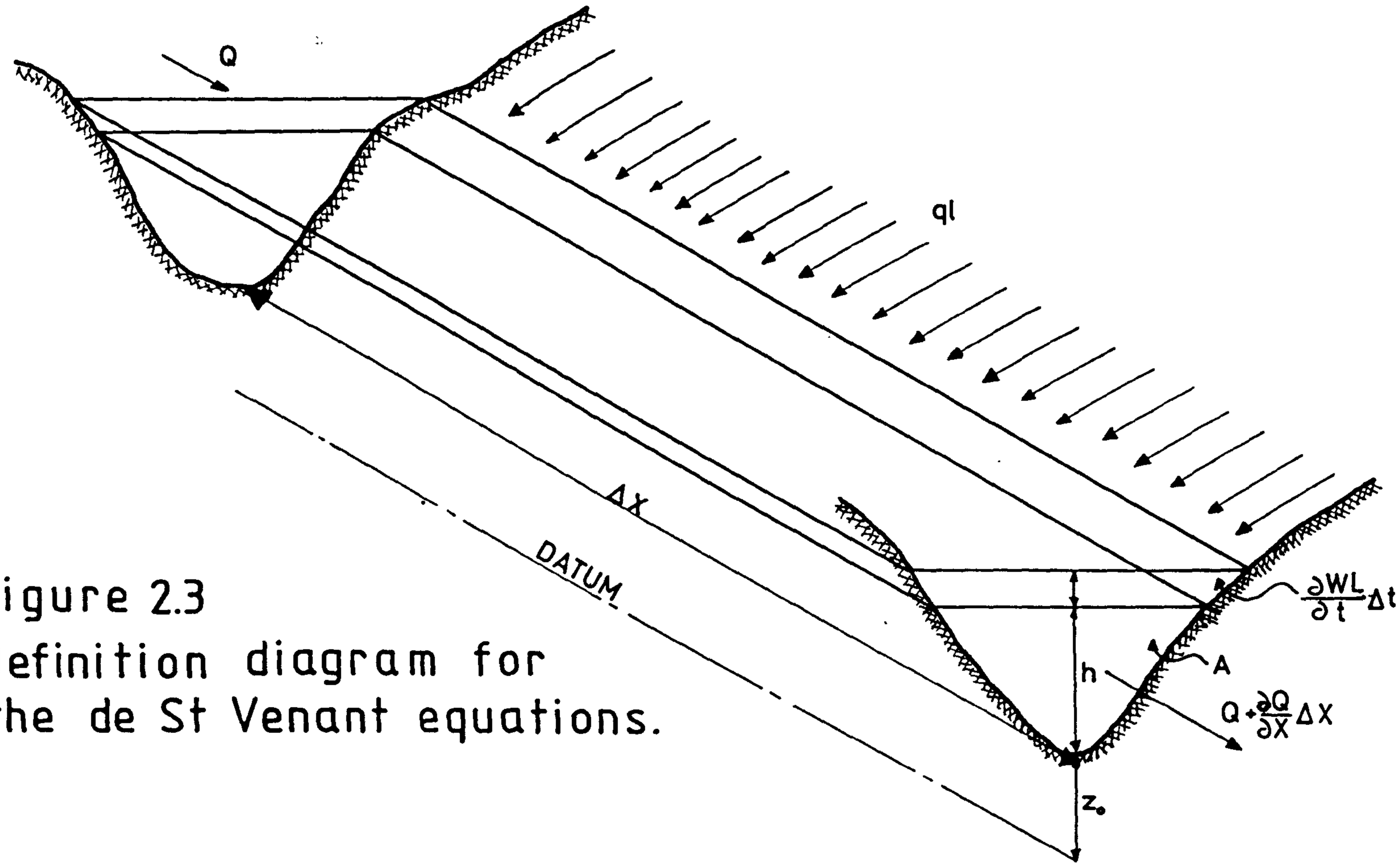

Figure 2.3
Definition diagram for
the de St Venant equations.

in barometric pressure are negligibly small, further the total change in velocity of time 'dt' is now provided by:

$$du = \frac{\partial u}{\partial x} \, dx + \frac{\partial u}{\partial t} \, dt$$

giving the one dimensional dynamic equation as:

$$\frac{\partial u}{\partial t} + g \frac{\partial Wl}{\partial x} + u \frac{\partial u}{\partial x} + \frac{\tau_{bx}}{\rho h} = 0$$

or,

$$\frac{1}{g} \frac{\partial u}{\partial t} + \frac{\partial Wl}{\partial x} + \frac{1}{2g} \frac{\partial u^2}{\partial x} + \frac{\tau_{bx}}{\rho g h} = 0$$

Substituting Q = uA provides:

$$\frac{1}{g} \frac{\partial (Q/A)}{\partial t} + \frac{\partial Wl}{\partial x} + \frac{1}{2g} \frac{\partial (Q/A)^2}{\partial x} + \frac{\tau_{bx}}{\rho g h} = 0 \qquad \text{Equation 2.29}$$

2.7 THE METHOD OF CHARACTERISTICS

Equations 2.25, 2.26 and 2.27 and equations 2.28 and 2.29 are sets of hyperbolic partial differential equations. Such equations can be combined linearly to produce characteristic equations. These equations have the property that they involve differentiation in one less direction than the original equations. For example, in one-dimensional unsteady flow, the characteristic equations become ordinary differential equations. Further, the characteristic equations define paths or surfaces in the solution domain along which disturbances propagate. It is this feature which provides the analogy between the physical system and its characteristic representation. The domain of dependence and region of influence for any point are rigorously defined

by the method of characteristics and correspond to those of the physical prototype. This feature is often quoted as being a major attraction when applying the method of characteristics to unsteady flow problems.

CHAPTER THREE

A NUMERICAL MODEL FOR LONG WAVE PROPAGATION IN A NATURAL RIVER CHANNEL

3.1 INTRODUCTION

Man's interest in river flow stems from his need to protect human life, property, and economic systems from the capriciousness of natural flow events and to exploit their potential benefits in terms of energy, agriculture, and navigation. In this overall context, mathematical modelling provides a tool by means of which man can study and gain an understanding of hydraulic flow phenomena, select and design sound engineering projects and predict extreme situations so as to be able to provide advanced warning of their occurrence and importance.

A numerical model to predict flow conditions in the main channel of a natural river system is developed in the following chapter. The main channel, shown in Figure 3.1, is considered to be the channel through which direct drainage from the system takes place. Particular attention is paid to the numerical representation of the lateral flow term in the continuity equation as this is of importance when linking the model to the washland algorithm presented in Chapter Four.

When applied to real problems the following numerical model will be the main constituent of a suite of programmes. The complementary programmes are designed to generate data, suitable for use by the main numerical model, from raw survey data. This facility will considerably reduce the total number of man hours required for the analysis

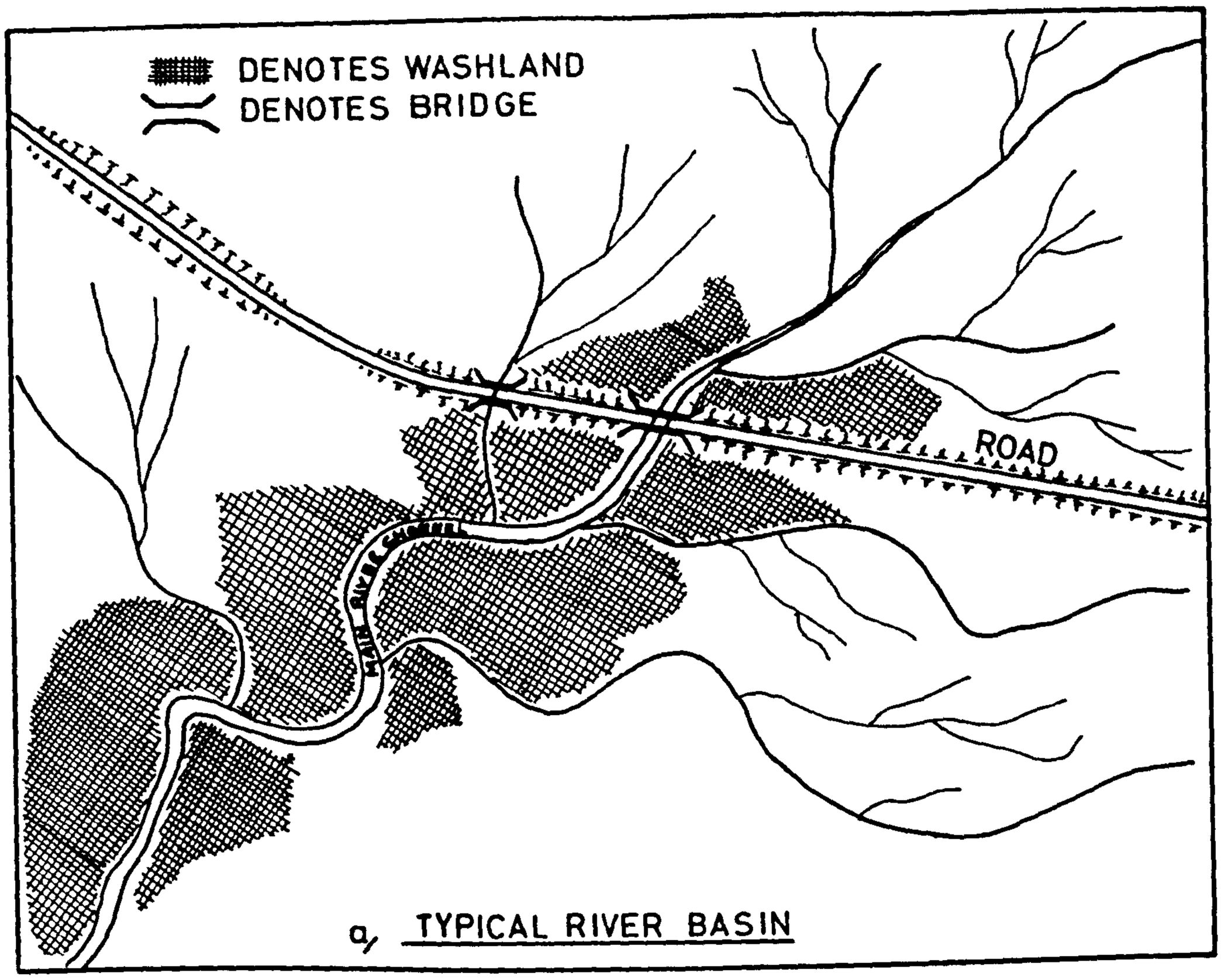

a/ TYPICAL RIVER BASIN

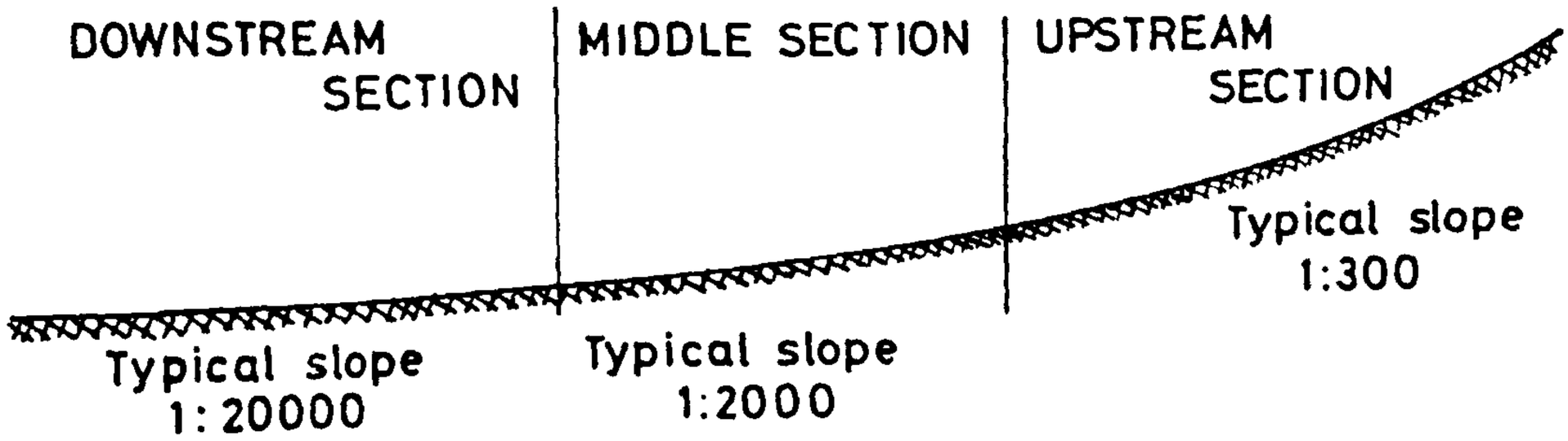

b/ LONGITUDINAL PROFILE

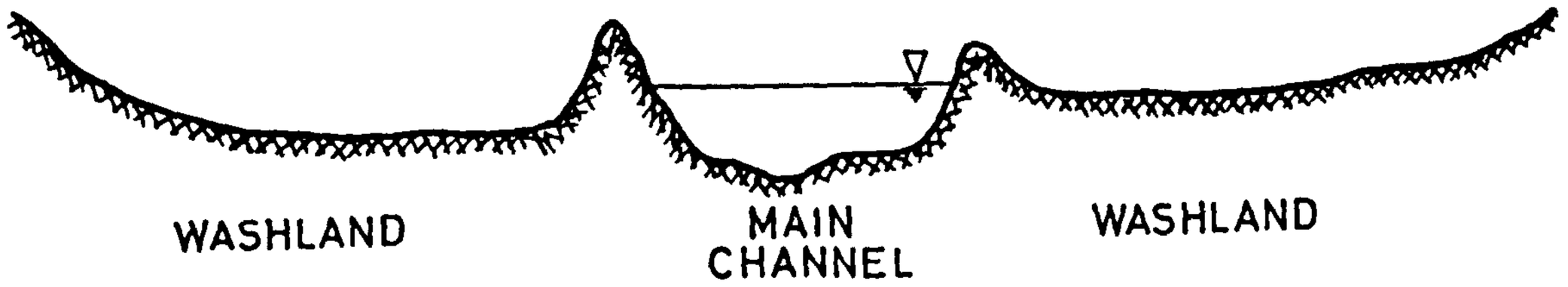

c/ TYPICAL CROSS SECTION

Figure 3·1

of flood routing problems. The complementary programmes and their interdependence are discussed in Section 5.6 and illustrated in Figure 5.5.

3.2 DISCRETIZATION OF THE ONE-DIMENSIONAL LONG WAVE EQUATIONS

The one-dimensional long wave equations define values of dependent variables, i.e. flow and water level, throughout a continuous flow field. For practical engineering purposes it is necessary to solve equations 2.28 and 2.29 for these variables at predetermined points in space and time. As these equations cannot be solved analytically approximate methods must be used. Approximate methods proceed through the process of discretization, where the continuous flow field is described in terms of discrete values at a finite number of points. These points at which variables are computed are called "grid points" or "nodal points". Discretized flow laws can then be solved to furnish approximate engineering solutions to the equations. Of the discrete methods available the finite difference approach is adopted in the present work, this being that most commonly used in engineering practice, see Cunge, Holly and Verwey (1980). The method requires the replacement of the partial differential operators in the continuum equations by finite difference operators, to give a finite difference analogue of the differential equations. The finite difference equations are then solved by numerical methods.

At the grid points geometrical information is given

to the calculation; rendering their position of considerable importance in natural river flood routing computations. As, if numerical computations are to include all aspects of energy loss by flow passing through a channel, irregularities and constrictions such as meanders, weirs and bridges must be defined in addition to typical channel cross-sections. Inclusion of such features generally requires that irregular distance increments be used to position grid points.

3.3 CHOICE OF FINITE DIFFERENCE SCHEME

Of the host of available finite difference schemes a variation of the Preissman scheme, described by Abbott (1979b) was considered the most appropriate in the present circumstances. The reasons are two fold.

Firstly, the rate of rise of a flood may be said to be relatively slow in the majority of circumstances. Thus, from the point of view of representing the time dependent behaviour of a flood wave, a relatively large time increment may be selected in any step-by-step numerical computation. Large time steps are desirable from an economic standpoint in that a reduced computer time is employed. However, modelling of the spatial variations of flow parameters requires that relatively close distance intervals be chosen between adjacent solution points within the computational scheme. Such considerations militated against the use of an explicit method of solution of the equations of motion and accordingly, for the calculations of time dependent variables in the river channel, an implicit technique is desirable.

Secondly, the scheme solves for both dependent variables at every grid point throughout the solution domain. This means that no weighting of differences is required for local centering to second-order accuracy with non-equidistant grid points, Price (1974) and Abbott and Isonescu (1967). Special conditions that relate dependent variables at discrete points, such as weir flow and stage discharge curves can be conveniently introduced.

3.4 IMPLICIT FINITE DIFFERENCE SCHEME

The following variation of the Preissmann finite difference scheme is applied, see Figure 3.2 Let it be assumed that all variables are known at all points of the network on the row 't^n' which is at time step 'n' and that it is desired to find the values of the variables on the row 't^{n+1}', that is the computations are advanced to the time step $t^{n+1} = t^n + \Delta t$. Choosing a four point grid identified by the intersections of the vertical lines x_j and x_{j+1} with the horizontal lines t^n and t^{n+1}, the equations of unsteady flow are applied in the finite difference form within the four point grid. At the point m, the average values and the partial derivatives of a function f are represented by:

$$f(m) = \frac{(1-\theta)}{2} (f_j^n + f_{j+1}^n) + \frac{\theta}{2} (f_j^{n+1} + f_{j+1}^{n+1}) \qquad \text{Equation 3.1}$$

$$\frac{\partial f(m)}{\partial x} = \frac{1}{\Delta x} \left[(1-\theta) (f_{j+1}^n - f_j^n) + \theta (f_{j+1}^{n+1} - f_j^{n+1}) \right] \qquad \text{Equation 3.2}$$

$$\frac{\partial f(m)}{\partial t} = \frac{1}{2\Delta t} \left[(f_j^{n+1} + f_{j+1}^{n+1}) - (f_j^n + f_{j+1}^n) \right] \qquad \text{Equation 3.3}$$

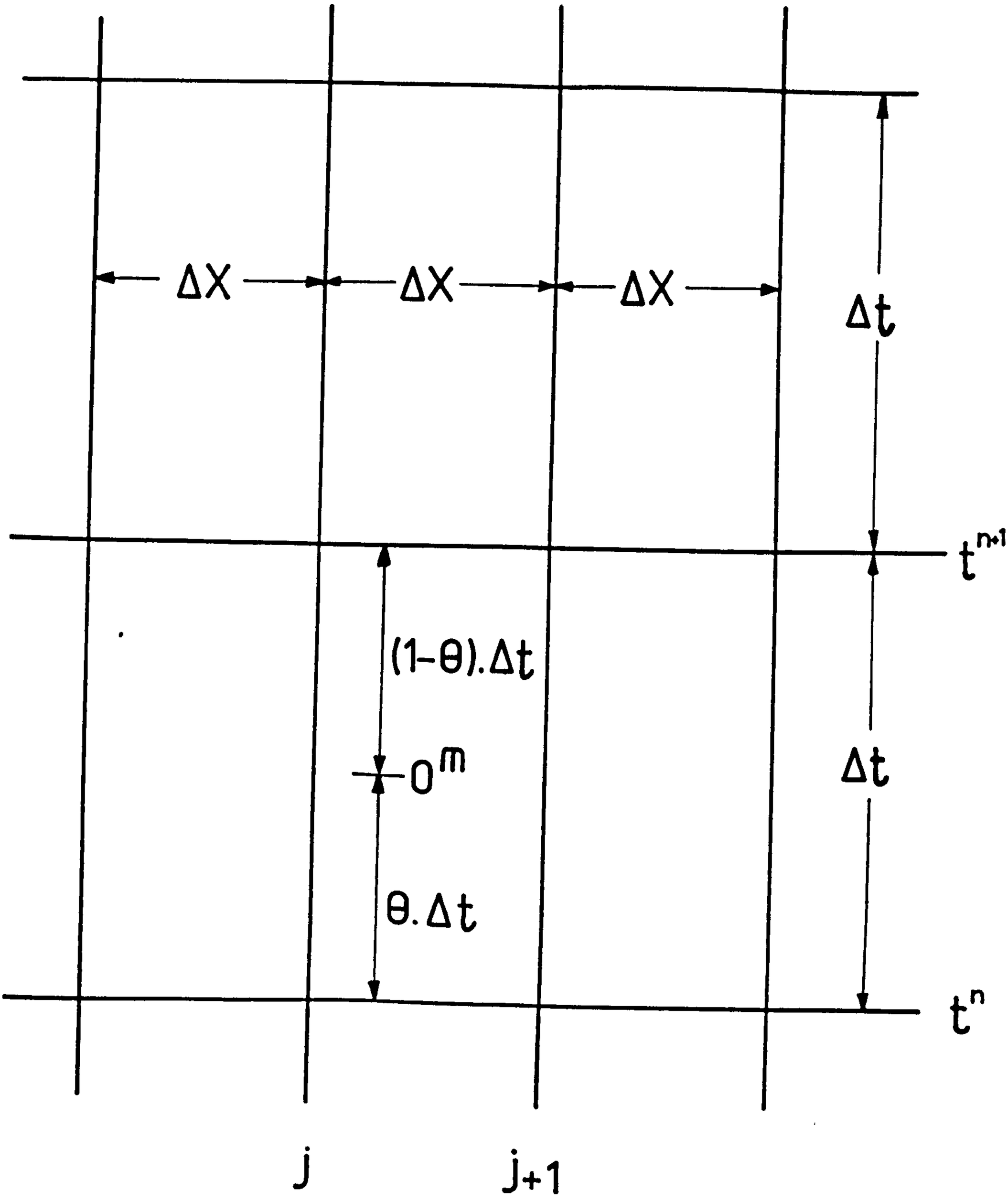

Figure 3.2

In equations 3.1 through 3.3 f may represent Q, Wl, S_f so that Q, Wl, $\frac{\partial Q}{\partial x}$, $\frac{\partial Q/A}{\partial t}$, $\frac{\partial Wl}{\partial x}$, $\frac{\partial Wl}{\partial t}$, at the point m are presented in terms of the values of the variables at the four corner grid points.

With $\Theta = 0.5$ this scheme is similar to that used successfully by Amein and Fang (1970). More recently Price and Samuels (1980) developed a numerical model based on the scheme and applied it to the River Lagan in Northern Ireland.

3.5 CONSISTENCY, CONVERGENCE AND STABILITY

Before a finite difference analogue of the continuum equations can be considered of value its properties of consistency, convergence and stability must be examined.

3.5.1 CONSISTENCY

Consistency can be defined in terms of the local truncation error, as defined by Smith (1978). That is, if the value of the finite difference terms tends to the true value of the partial differential terms as the grid lengths tend to zero then the finite difference scheme is consistent with the partial differential equations.

The consistency of the Preissmann scheme described in the previous section can be investigated by taking Taylor series expansions about the point m to give:

$$f_{j+1}^{n} = f_{j+\frac{1}{2}}^{n+\theta} + \frac{\partial f}{\partial x}\left(\frac{\Delta x}{2}\right) + \frac{\partial^2 f}{\partial x^2}\frac{(\Delta x/2)^2}{2} + O\left((\Delta x/2)^3\right)$$

$$-\frac{\partial f}{\partial t}(\theta \Delta t) + \frac{\partial^2 f}{\partial t^2}\frac{(\theta \Delta t)^2}{2} - O\left((\theta \Delta t)^3\right)$$

$$f_j^n = f_{j+\frac{1}{2}}^{n+\theta} - \frac{\partial f}{\partial x}\left(\frac{\Delta x}{2}\right) + \frac{\partial^2 f}{\partial x^2}\frac{(\Delta x/2)^2}{2} - O\left((\Delta x/2)^3\right)$$

$$- \frac{\partial f}{\partial t}(\theta\Delta t) + \frac{\partial^2 f}{\partial t^2}\frac{(\theta\Delta t)^2}{2} - O((\theta\,\Delta t)^3)$$

$$f_{j+1}^{n+1} = f_{j+\frac{1}{2}}^{n+\theta} + \frac{\partial f}{\partial x}\left(\frac{\Delta x}{2}\right)^2 + \frac{\partial^2 f}{\partial x^2}\frac{(\Delta x/2)^2}{2} + O\left(\left(\frac{\Delta x}{2}\right)^3\right)$$

$$+ \frac{\partial f}{\partial t}\left((1-\theta)\Delta t\right) + \frac{\partial^2 f}{\partial t^2}\frac{((1-\theta)\Delta t)^2}{2}$$

$$+ O(((1-\theta)\Delta t)^3)$$

$$f_j^{n+1} = f_{j+\frac{1}{2}}^{n+\theta} \frac{\partial f}{\partial x}\left(\frac{\Delta x}{2}\right) + \frac{\partial^2 f}{\partial x^2}\frac{(\Delta x/2)^2}{2} - O\left(\left(\frac{\Delta x}{2}\right)^3\right)$$

$$+ \frac{\partial f}{\partial t}\left((1-\theta)\Delta t\right) + \frac{\partial^2 f}{\partial t^2}\frac{((1-\theta)\Delta t)^2}{2}$$

$$+ O\left((1-\theta)\Delta t)^3\right)$$

Substitution of the above terms into equation 3.2 gives:

$$\frac{\partial f(m)}{\partial x} = \frac{\partial f}{\partial x} + O(\Delta x^2) \qquad \text{Equation 3.4}$$

or equation 3.3 gives:

$$\frac{\partial f\ (m)}{\partial t} = \frac{\partial f}{\partial t} + O(\Delta t) \qquad \text{Equation 3.5}$$

Clearly, the finite difference operators tend to the partial differential operators as Δx and Δt tend to zero. Further, equations 3.4 and 3.5 show the scheme to be of second order accuracy in space and first order accuracy in time.

3.5.2 CONVERGENCE AND STABILITY

The mathematical foundations for the questions of convergence and stability of numerical schemes are well-

developed only for linear systems. The results from linear theory are used as guidelines to non-linear problems, the justification depending on numerical experiments.

A convergent finite difference scheme is defined mathematically as one in which all values of the finite difference solution approach the continuum differential equation solution as the finite difference mesh size approach zero. This condition is linked to stability of a linear scheme through the equivalence theorem of Lax:

Given a properly posed initial-value problem and a finite difference approximation to it that satisfies the consistency condition, stability is the necessary and sufficient condition for convergence.

Lax and Richtmyer (1956) define stability by requiring a bounded extent to which any component of the initial data can be amplified in the numerical procedure.

A local stability analysis for the scheme applied to the linearized long-wave equations was undertaken by Evans (1977), who concluded that for $\theta = 0.5$ the scheme has no amplitude error, but does have phase error and is thus dispersive. For $0.5 < \theta \leq 1.0$ the scheme is stable and damping of short-period waves occurs, the degree of damping depending on the number of grid points per wave length and moves up the wave spectrum as the Courant number is increased. In practical terms none of this is relevant to river modelling where the number of grid points per wave length is very large, and even with high Courant numbers there is little phase error. Indeed,

Abbott (1974) suggests that "accuracy may actually be increased by operating at high Courant numbers, due to the solution being continually "refreshed" by the "boundary conditions"."

3.6 FINITE DIFFERENCE CONTINUITY EQUATION

Leaving aside the lateral flow term for the present, replacing the differential operators by the following difference operators:

$$B \frac{\partial Wl}{\partial t} = B_j^n/2\Delta t \ (Wl_j^{n+1} - Wl_j^n) + B_{j+1}^n/2\Delta t \ (Wl_{j+1}^{n+1} - Wl_{j+1}^n)$$

$$\frac{\partial Q}{\partial x} = \frac{1}{2\Delta x} \ (Q_{j+1}^{n+1} - Q_j^{n+1}) + \frac{1}{2\Delta x} \ (Q_{j+1}^n - Q_j^n)$$

gives the finite difference continuity equation:

$$B_j^n/2\Delta t \ (Wl_j^{n+1} - Wl_j^n) + B_{j+1}^n/2\Delta t \ (Wl_{j+1}^{n+1} - Wl_{j+1}^n) + \frac{1}{2\Delta x} (Q_{j+1}^{n+1} - Q_j^{n+1}) + \frac{1}{2\Delta x} (Q_{j+1}^n - Q_j^n) = 0$$

Rearranging:

$$(B_j^n/2\Delta t) \ Wl_j^{n+1} - \frac{1}{2\Delta x} Q_j^{n+1} + (B_{j+1}^n/2\Delta t) Wl_{j+1}^{n+1} + \frac{1}{2\Delta x} Q_{j+1}^{n+1} = G_j$$

Equation 3.6

where

$$G_j = B_j^n/2\Delta t \ Wl_j^n + B_{j+1}^n/2\Delta t \ Wl_{j+1}^n + \frac{1}{2\Delta x}(Q_j^n - Q_{j+1}^n)$$

Equation 3.7

3.6.1 LATERAL FLOW TERM

In the present study the lateral flow term at any

section may consist of two components:

a) a tributary inflow (Ql)

In finite difference form this is the average of the known tributary flows at times n and n^{n+1} within a reach between two nodal points,

$$Ql_{mean} = 0.5\ (Ql_j^{n+1} + Ql_j^n)$$

b) an overbank lateral flow (ql)

This is a complicated term to formulate in finite difference form, as the lateral overbank flow is a function of both channel water level and washland water level. During a time increment variations in both of these water levels may be large enough to significantly influence the lateral flow. Therefore, the finite difference term has two components. An initial lateral flow ql_j^n and a gradient term compensating for variation of lateral flow with river water level, $\Delta ql/\Delta Wl\ (Wl_j^{n+1} - Wl_j^n)$. The total lateral flow term then becomes:

$$Qlt_j^n = \frac{1}{2\Delta x}\ (Ql_j^{n+1} + Ql_j^n) + (ql_j^n + 0.5\ \frac{\Delta ql}{\Delta Wl}(Wl_j^{n+1} - Wl_j^n))\frac{1}{\Delta x}$$

Equation 3.8

The influence of the washland water level is modelled using a submergence factor. Details of this are described in the following chapter.

3.6.2 FINITE DIFFERENCE CONTINUITY EQUATION INCLUDING LATERAL FLOW

Inserting equation 3.8 in equation 3.6 provides the complete finite difference continuity equation,

$$(B_j^n/2\Delta t - \frac{1}{2\Delta x}\ \Delta q1/\Delta W1)\ W1_j^{n+1} - \frac{1}{2\Delta x}\ Q_j^{n+1} +$$

$$(B_{j+1}^n/2\Delta t)\ W1_{j+1}^{n+1} + \frac{1}{2\Delta x}\ Q_{j+1}^{n+1} = G_j \qquad \text{Equation 3.9}$$

with G_j^* modified to:

$$G_j^* = G_j + \frac{1}{2\Delta x}\ (Q1_j^{n+1} + Q1_j^n - (\Delta q/\Delta W1)W1_j^n - 2q1_j^n)$$

Equation 3.10

3.7 FINITE DIFFERENCE DYNAMIC EQUATION

Ignoring energy losses due to friction for the present and replacing the differential operators by the following difference operators:

$$\frac{1}{g}\ \frac{\partial(Q/A)}{\partial t} = \frac{1}{2g\Delta t}\ (Q_j^{n+1}/A_j^n - Q_j^n/A_j^n + Q_{j+1}^{n+1}/A_{j+1}^n - Q_{j+1}^n/A_{j+1}^n)$$

$$\frac{\partial W1}{\partial x} = \frac{\Theta}{x}\ (W1_{j+1}^{n+1} - W1_j^{n+1}) + \frac{(1-\Theta)}{x}\ (W1_{j+1}^n - W1_j^n)$$

$$\frac{1}{g}\ \frac{\partial(Q^2/A^2)}{\partial x} = \frac{\Theta}{\Delta x}\ (Q_{j+1}^{n+1}\ Q_{j+1}^n/2g(A_{j+1}^n)^2 - Q_j^{n+1}\ Q_j^n/2g\ (A_j^n)) +$$

$$((Q_{j+1}^n)^2/2g\ (A_{j+1}^n)^2 - (Q_j^n)^2\ /2g(A_j^n)^2\ )\ \frac{(1-\Theta)}{\Delta x}$$

gives the finite difference dynamic equation:

$$\frac{1}{2g\ \Delta t}\ (Q_j^{n+1}/A_j^n - Q_j^n/A_j^n + Q_{j+1}^{n+1}/A_{j+1}^n - Q_{j+1}^n/A_{j+1}^n) +$$

$$\frac{\Theta}{\Delta x}(W1_{j+1}^{n+1} - W1_j^{n+1}) + \frac{(1+\theta)}{\Delta x}\ (W1_{j+1}^n - W1_j^n) +$$

$$\frac{\Theta}{2g\Delta x}(Q_{j+1}^{n+1}\ Q_{j+1}^n/(A_{j+1}^n)^2 - Q_j^{n+1}Q_j^n/(A_j^n)^2\ ) + \frac{(1-\theta)}{2g\Delta x}((Q_{j+1}^n)^2/(A_{j+1}^n)^2 - (Q_j^n)^2/(A_j^n)^2) = 0$$

Rearranging:

$$(\frac{-\theta}{\Delta x})\ Wl_j^{n+1} + (Q_j^{n+1}/2gA_j^n)(\frac{1}{\Delta t} - \theta Q_j^n/A_j^n\Delta x) + \frac{\theta}{\Delta x}\ Wl_{j+1}^{n+1} +$$

$$(Q_{j+1}^{n+1}/2gA_{j+1}^n)(\frac{1}{\Delta t} + \theta Q_{j+1}^n/A_{j+1}^n\Delta x) = H_j \qquad \text{Equation 3.11a}$$

where

$$H_j = \frac{-(1-\theta)}{\Delta x}\ (Wl_{j+1}^n - Wl_j^n) + \frac{1}{2g\Delta t}\ (Q_j^n/A_j^n + Q_{j+1}^n/A_{j+1}^n) -$$

$$\frac{(1-\theta)}{2g\Delta x}((Q_{j+1}^n)^2/(A_{j+1}^n)^2 - (Q_j^n)^2/(A_j^n)^2) \qquad \text{Equation 3.11b}$$

3.7.1 ENERGY GRADIENT

In this study an estimate of the energy gradient is obtained from Mannings equation for the flow, Q, in an open channel under uniform conditions, i.e. the total energy line has a constant gradient and is parallel to the invert level,

$$Q = \frac{A}{n}\ R^{\frac{2}{3}}\ So^{\frac{1}{2}}$$

where A is the channel cross-sectional area, R is the hydraulic radius, n is Mannings constant and So is the invert or energy gradient. In the non-uniform flow case the energy gradient, Sf, is estimated by rearranging the above equation:

$$Sf = n^2\ Q^2/(A^2\ R^{4/3})$$

or,

$$Sf = Q^2/k^2 \qquad \text{Equation 3.12}$$

where k, the conveyance is given by

$$k = A\ R^{\frac{2}{3}}/n \qquad \text{Equation 3.13}$$

With reference to Figure 3.2, it is desirable that the finite difference term be representative of conditions within the region bounded by the lines j , j+1, n and n+1. That is, some average of Sf_j^n , Sf_{j+1}^n , Sf_j^{n+1} and Sf_{j+1}^{n+1} . This creates two problems. Firstly, the question of calculating an average energy gradient through the reach. Secondly how to obtain a realistic representation of the unknown friction gradients at time n+1.

3.7.2 VARIATION OF ENERGY GRADIENT WITH TIME

The problem created here is that the friction gradients Sf_j^{n+1} and Sf_{j+1}^{n+1} are quadratic functions of the unknown flow Q^{n+1} and conveyance k^{n+1} , which in turn is a function of the unknown water level Wl^{n+1} . A variety of alternative formulations is possible to overcome this impasse. Three possibilities are discussed below.

a) The simplest formulation is based on the assumption that conveyance will not vary significantly during a time increment, so that k_j^{n+1} may be replaced by k_j^n then linearising the problem in Q_j^{n+1} by considering Q_j^{n+1}. Q_j^n to be representative of $(Q_j^{n+1})^2$.

Resulting in:

$$Sf_j^{n+1} = Q_j^{n+1}Q_j^n/(k_j^n)^2 \qquad \text{Equation 3.14}$$

Application of this approximation is limited to channels where the above assumptions are justifiable. Namely, where cross-sectional properties vary gradually with water

level and where flow and water level vary little within the implicit time increment.

b) As above, assume conveyance to vary slowly with time and replace k_j^{n+1} by k_j^n. To linearise the problem in Q_j^{n+1} assume $Q_j^{n+1} = Q_j^n + \Delta Q$. Then,

$$(Q_j^{n+1})^2 = (Q_j^n + \Delta Q)^2$$

$$= Q_j^{n2} + 2Q_j^n \Delta Q + \Delta Q^2$$

Considering ΔQ^2 to be negligibly small and putting

$$\Delta Q = Q_j^{n+1} - Q_j^n$$

gives

$$Q_j^{n+1^2} \simeq 2Q_j^n Q_j^{n+1} - (Q_j^n)^2$$

Sf_j^{n+1} may then be represented by

$$Sf_j^{n+1} \simeq (2Q_j^n Q_j^{n+1} - (Q_j^{n2})) / (k_j^{n2}) \qquad \text{Equation 3.15}$$

This approximation is applicable where flow varies significantly during a time increment, but is limited as variations in section properties with water level must be gradual.

c) The following representation of energy gradient at time n+1 is linearised in unknowns by the use of the differential expression for total change in Sf from changes in both flow and conveyance.

$$Sf = Q^2/k^2$$

$$dSf = (2Q_j^n/(k_j^{n2}))\, dQ - (2Q_j^{n2})/(k_j^{n3}))\, dk$$

$$= 2Sf_j^n ((Q_j^{n+1} - Q_j^n)/Q_j^n - (k_j^{n+1} - k_j^n)/k_j^n)$$

$$= 2Sf_j^n \left(Q_j^{n+1}/Q_j^n - k_j^{n+1}/k_j^n\right) \qquad \text{Equation 3.16}$$

Utilizing

$$k_j^{n+1} = k_j^n + \frac{\Delta k}{\Delta Wl}\left(Wl_j^{n+1} - Wl_j^n\right) \qquad \text{Equation 3.17}$$

equation 3.16 expands to

$$dSf = 2Sf_j^n \left(Q_j^{n+1}/Q_j^n - 1 - \frac{\Delta k/\Delta Wl}{k_j^n}\left(Wl_j^{n+1} - Wl_j^n\right)\right)$$

Sf_j^{n+1} may be written as

$$Sf_j^{n+1} = Sf_j^n + dSf = Sf_j^n + 2Sf_j^n \left(Q_j^{n+1}/Q_j^n - \frac{\Delta k/\Delta Wl}{k_j^n}\left(Wl_j^{n+1} - Wl_j^n\right) - 1\right)$$

Equation 3.18

This representation is applicable in channels where both flow and conveyance vary significantly during a time increment.

3.7.3 VARIATION OF ENERGY GRADIENT WITH DISTANCE

Since Sf is expressed in the form

$$Sf = Q^2/k^2$$

and flows Q and conveyance k are known only at the solution nodes, the problem arises as to how to interpolate between them in expressing Sf. Cunge, Holly and Verwey (1980) outline a number of methods developed by different modellers. These include the following interpolation formulae:

$Sf_1 = Q^2 / (\alpha k_1^2 + (1-\alpha)k_2^2)$ (weighted average of k^2)

$Sf_2 = Q^2 (\alpha/k_1^2 + (1-\alpha)/k_2^2)$ (weighted average of Sf)

$Sf_3 = Q^2/k_1^{2\alpha} \; k_2^{2-2\alpha}$ (weighted geometric mean of k^2)

$Sf_4 = Q^2/(\alpha k_1 + (1-\alpha)k_2)^2$ (weighted average of k)

in which a steady flow situation has been assumed, where

α = a weighting coefficient. Cunge, Holly and Verwey show how with a factor of two difference in conveyance between two adjacent points and $\alpha = 0.5$, the friction slope for each reach could vary by some 50% depending on the conveyance interpolation scheme chosen.

During the development of the current scheme it was noted that if equal weighting is given to energy gradients at both ends of a reach, i.e. $\alpha = 0.5$, steep local energy gradients at sections where cross sectional area is restricted, see Figure 3.3, have an excessive influence on the calculations. In order to reduce this influence to proportions similar to those found in the physical system a flexible weighting coefficient is used in the numerical model.

$$Sf_m = \alpha_j Sf_j + \alpha_{j+1} Sf_{j+1} \qquad \text{Equation 3.19a}$$

where

$$\alpha_j = Sf_{j+1}/(Sf_j + Sf_{j+1}) \qquad \text{Equation 3.19b}$$

$$\alpha_{j+1} = Sf_j/(Sf_j + Sf_{j+1}) \qquad \text{Equation 3.19c}$$

Here the weighting coefficient varies from reach to reach depending on the relative magnitude of the energy gradients. Adoption of such a scheme is justified by the following example:

The equation for total energy E:

$$E = z + h + u^2/2g$$

can be differentiated with respect to x to give

Figure 3.3

$$\alpha_j = S_{j+1}/(S_j + S_{j+1})$$

$$\alpha_{j+1} = S_j/(S_j + S_{j+1})$$

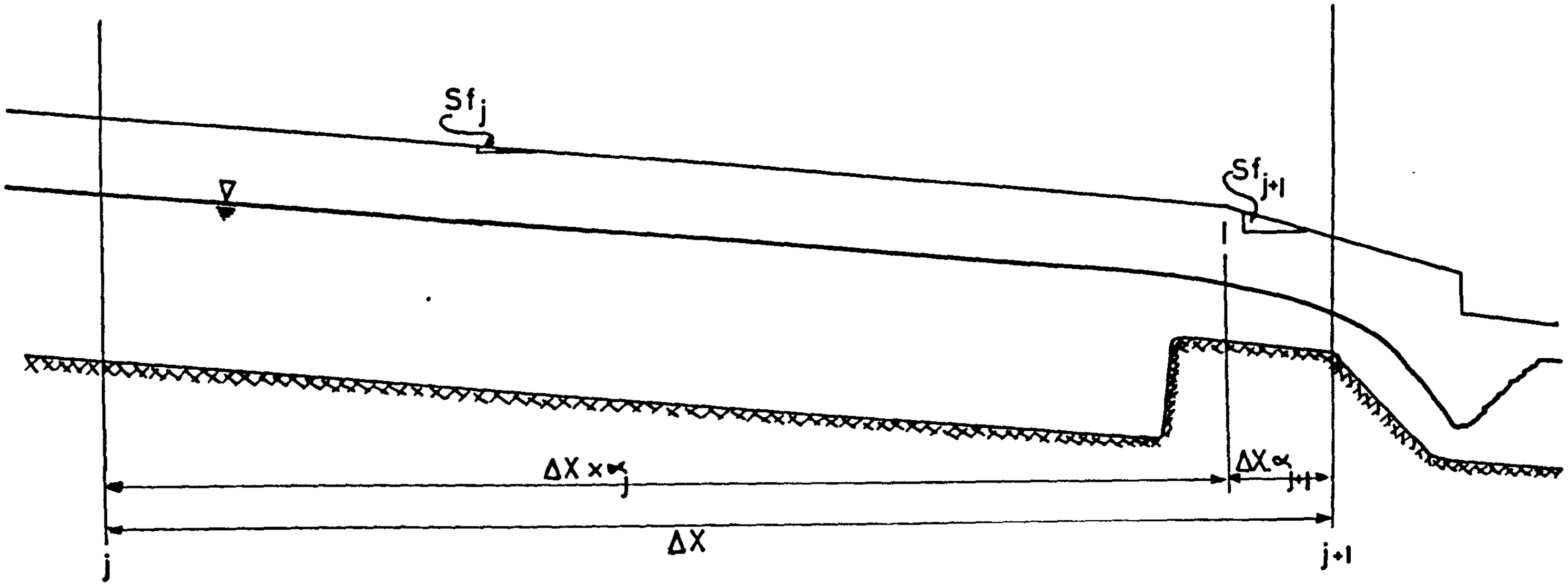

$$\frac{dE}{dx} = \frac{d}{dx}(z + h + v^2/2g) = -Sf = {}^{v^2}/_{CR}$$

or,

$$\frac{d}{dx}(h + v^2/2g) = So - Sf$$

The above equation can be written in finite difference form as:

$$\frac{\Delta H}{\Delta x} = \frac{\Delta(h + v^2/2g)}{\Delta x} = So - Sf \qquad \text{Equation 3.20}$$

When flow conditions are known at a point equation 3.20 can be integrated back up the channel in a stepwrise manner. Although not providing an exact solution this technique will furnish a reasonable approximation to the profile of the energy line in the physical system.

Consider the case of a trapezoidal channel with a base width of 6m and side slopes of $1\frac{1}{2}H$: 1V laid on a bed slope of 1/1000 and carrying a discharge of $30m^3/s$. The channel terminates in a free overfall and has a Mannings' roughness coefficient of n = 0.025. Section properties can be calculated from:

$$A = h(6 + 1.5h)$$

$$P = 6 + 2\sqrt{3.25}\, h$$

$$B = 6 + 3h$$

The critical depth h_c existing at the free overfall can be calculated from:

$$\frac{Q^2 B}{gA^3} = 1$$

or on substituting the above section properties

$$30^2 (6+3h_c) = gh_c^3 (6+1.5h_c)^3$$

whence by trial

$$h_c = 1.226m$$

The numerical integration to a distance of 410m upstream of the control is carried out in Table 3.1. The energy line profile from this table is plotted in Figure 3.4.

Consider a reach bounded by j 200m before the free overfall to j+1 at the free overfall. The friction gradients at j and j+1 are 0.0016 and 0.0068 respectively. Calculating the factors from equations 3.19b and 3.19c gives

$$\alpha_j = \frac{(0.0016)}{(0.0016 + 0.0068)} = 0.19$$

$$\alpha_{j+1} = \frac{(0.0068)}{(0.0016 + 0.0068)} = 0.81$$

The total gain in specific energy in passing from j to j+1 calculated from equation 3.19a is:

$$H = - (0.0068 \times 0.19 + 0.0016 \times 0.81) \times 200 + 0.001 \times 200 = -0.32m$$

This can be compared with the loss measured from Figure 3.4 H = -0.3m. If an arithmetic mean were used the calculated specific energy loss through the reach would be:

$$H = - (0.0068 + 0.0016) \times 0.5 \times 200 + 0.001 \times 200 = -0.64m$$

It is obvious that in areas where locally steep energy gradients occur use of an arithmetic mean will cause considerable errors in computed energy gradients. Adoption of the flexible weighting coefficients brings the computed energy gradients closer to those of the physical

Y m	A m^2	P m	R m	C^2 m/s^2	V m/s	$V^2/2g$ m	E m	V^2/C^2R	$(V^2/CR)m$	$(So-V^2/CR)m$	ΔE m	Δx m	$x = \sum \Delta x$ m
1.226	9.61	10.42	0.922	1557	3.121	0.497	1.723	0.0068					
1.35	10.83	10.87	0.996	1598	2.770	0.391	1.741	0.0048	0.0058	-0.0048	0.018	-3.75	-3.75
1.50	12.38	11.41	1.085	1644	2.433	0.299	1.799	0.00329	0.0040	-0.0030	0.058	-19.33	-23.08
1.65	13.98	11.95	1.170	1686	2.146	0.235	1.885	0.00233	0.0028	-0.0018	0.086	-47.77	-70.85
1.80	15.66	12.49	1.254	1725	1.916	0.187	1.987	0.00170	0.0020	-0.001	0.102	-102.00	-172.85
1.95	17.40	13.03	1.335	1762	1.724	0.151	2.101	0.00126	0.00148	-0.00048	0.114	-237.50	-410.35

Table 3.1

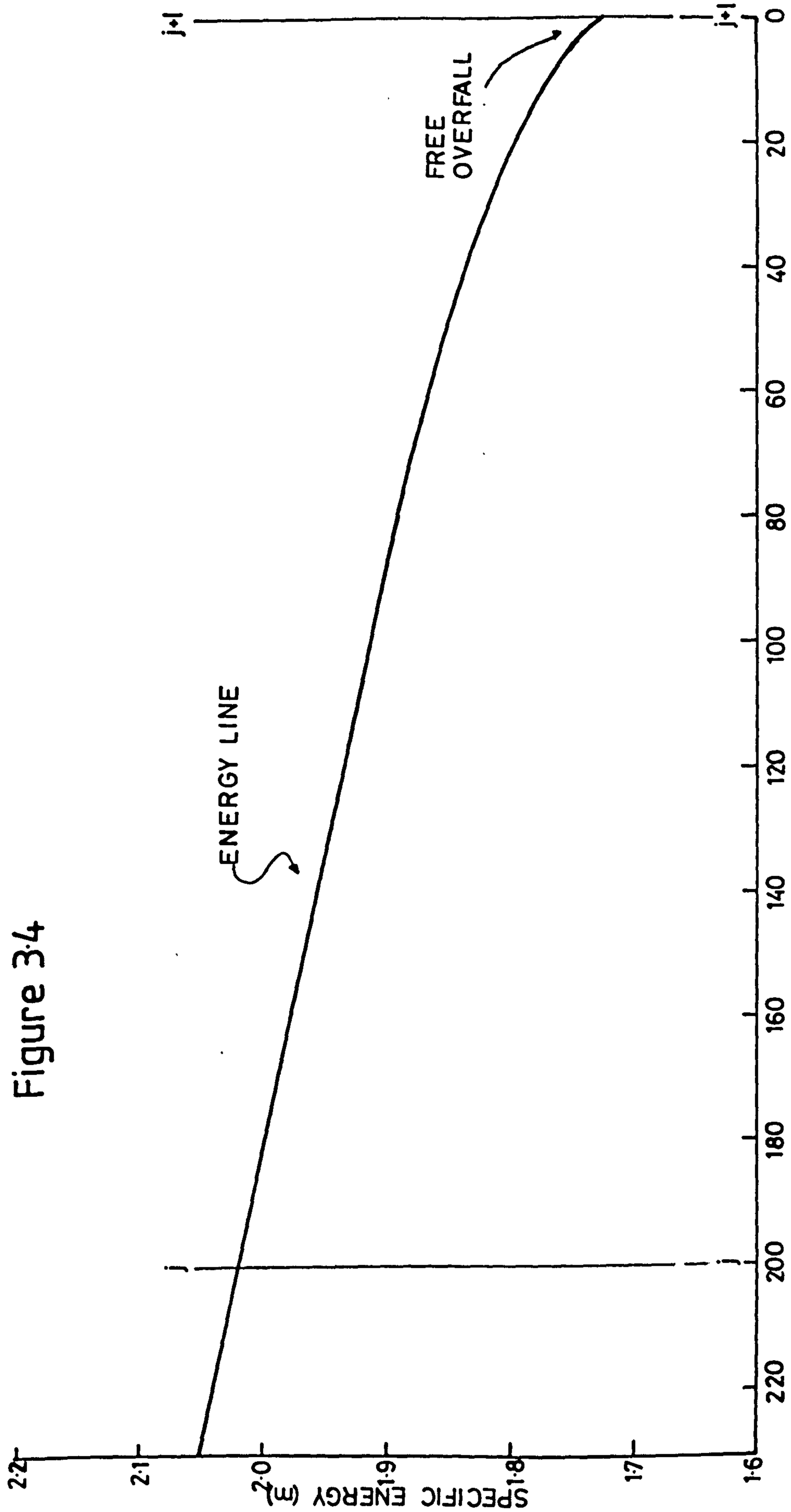
j+1
FREE OVERFALL
ENERGY LINE
j
SPECIFIC ENERGY (m)
2·2
2·1
2·0
1·9
1·8
1·7
1·6
0
20
40
60
80
100
120
140
160
180
200
220
DISTANCE FROM FREE OVERFALL (m)

Figure 3.4

system in this circumstance.

3.7.4. ENERGY GRADIENT REPRESENTATION

From an economic view point, within the bounds of required accuracy, it is desirable to have representation of all terms as simple as possible. Greater complexity means greater computational effort. Each of the representations given in section 3.7.2 a, b and c and section 3.7.3. is of use; the choice depends upon the rate of change of boundary conditions and the variation of the channel geometry.

Trial runs showed that for the case of flood propagation through a natural channel with steep bed slopes (1:500 and greater) the energy gradient representation is particularly important during the formation and operation of control sections as constrictions of area both natural and manmade create large local values of energy gradient.

A similar problem prevented Price and Samuels (1980) applying their unsteady flow model to the River Rhymney in Wales. The average bed slope of this river is 1:250. Later they successfully modelled unsteady flow conditions in the middle portion of the River Lagan in Northern Ireland with a bed slope of 1:1700. Although not mentioning problems with control sections they relied on a back water curve analysis of the upstream and downstream sections with bed slopes of 1:400 and 1:500 respectively.

The finite difference form of the energy gradient used in the present model is that derived in section 3.7.2.c, modified by the factors of section 3.7.3. The complete

term is therefore:

$$Sf = (1-\theta)\ (\alpha_j\ Sf_j^n + \alpha_{j+1} Sf_{j+1}^n) + \theta(\alpha_j Sf_j^{n+1} + \alpha_{j+1} Sf_{j+1}^{n+1})$$

with Sf_j^{n+1} and Sf_{j+1}^{n+1} defined by equation 3.18 giving:

$$Sf = (1-\theta)\ (\alpha_j Sf_j^n + \alpha_{j+1} Sf_{j+1}^n) +$$

$$\theta[\alpha_j (Sf_j^n + 2Sf_j^n\ (Q_j^{n+1}/Q_j^n - \frac{(\Delta k_j/\Delta Wl_j)}{k_j^n}\ (Wl_j^{n+1} - Wl_j^n) - 1)) +$$

$$\alpha_{j+1} (Sf_{j+1}^n + 2Sf_{j+1}^n (Q_{j+1}^{n+1}/Q_{j+1}^n - \frac{(\Delta k_{j+1}/\Delta Wl_j)}{k_{j+1}^n} (Wl_{j+1}^{n+1} - Wl_{j+1}^n) - 1))]$$

Equation 3.21

3.7.5 FINITE DIFFERENCE DYNAMIC EQUATION INCLUDING ENERGY GRADIENT

Introducing the energy gradient term from section 3.7.4 into equation 3.11 gives the complete one-dimensional finite difference dynamic equation:

$$\left(-\frac{\theta}{\Delta x} - (2\theta\alpha_j Sf_j^n\ \Delta k/\Delta Wl_j)/k_j^n \right)\ Wl_j^{n+1} + (1/2gA_j^n\ \left(\frac{1}{\Delta t} - \theta Q_j^n/A_j^n \Delta x\right) + 2\theta\alpha_j Sf_j^n) Q_j^{n+1} + \left(\frac{\theta}{\Delta x} - (2\theta\alpha_{j+1} Sf_{j+1}^n\ \Delta k/\Delta Wl_{j+1})/k_{j+1}^n\right) Wl_{j+1}^{n+1}$$

$$+ 1/2gA_{j+1}^n\ \left(\frac{1}{\Delta t} - \theta Q_{j+1}^n/A_{j+1}^n \Delta x\right) + 2\theta\alpha_{j+1} Sf_{j+1}^n/Q_{j+1}^n)\ Q_{j+1}^{n+1}$$

$$= H_j^* \qquad \text{Equation 3.22a}$$

where

$$H_j^* = H_j - \alpha_j Sf_j^n\ (1 + 2\theta\ (\ (\Delta k/\Delta Wl_j\ /k_j^n) Wl_j^n - 1\ ) - \alpha_{j+1} Sf_{j+1}^n$$

$$(1 + 2\theta\ (\ \frac{\Delta k/\Delta Wl_{j+1}}{k_{j+1}^n}\ Wl_{j+1}^n) - 1\ ) \qquad \text{Equation 3.22b}$$

3.8 BOUNDARY CONDITIONS

3.8.1 EXTERNAL BOUNDARY CONDITIONS

When the finite difference scheme described previously is applied between each of the jj solution nodes defining the solution domain, a total of 2(jj-1) simultaneous equations are obtained. To solve for the 2jj dependent variables necessitates that additional boundary equations are available at the external boundaries.

As the type of appropriate boundary conditions may vary from application to application the ability of the model to operate with a variety of boundary conditions is an important consideration from the point of view of flexibility. Hence during the development of the present model care was taken to provide facilities for handling all foreseeable upstream and downstream conditions.

For the upstream boundary these are:

i Water level as a function of time $WL = \emptyset(t)$

ii Flow as a function of time $Q = \emptyset(t)$

Possible downstream boundary conditions are:

i Water level as a function of time $Wl = \emptyset(t)$

ii Flow as a function of time $Q = \emptyset(t)$

iii Flow as a function of water level $Q = \emptyset(Wl)$

Any combination of these upstream and downstream boundary conditions can be used to provide an additional pair of equations giving a total of 2jj simultaneous equations. These are solved for the 2jj dependent variables using the modified Gaussian elimination routine described in Appendix A.

3.8.2 OCCURRENCE OF CRITICAL FLOW

Before proceeding with the implicit calculations to advance the river solution forward to time $(n+1)\Delta t$ a check is made to determine if critical flow conditions exist at any solution node within the model. Existence of critical flow is determined by comparing conditions of flow, at each node, with the corresponding relationship between water level and discharge for a control section. The occurrence of critical flow indicates that the flow contains the minimum specific energy necessary for it to pass through the section. The condition provides an unique relationship between flow and water level and it is essential that subsequent solutions adhere to this relationship as failure to do so implies a violation of Newton's second law.

3.8.3 OPERATION OF CONTROLS

Once the existence of a control section has been determined adherence of subsequent solutions to the minimum energy condition is ensured by inserting an internal boundary at this section. For example, if a control is found at section 'i' in Figure 3.5b then the channel is divided into two reaches 1 to i and i + 1 to jj, the new boundary condition at i being the relationship between water level and critical flow, i.e. boundary type (iii). For the new upstream boundary condition at section i+1 the computed flow through the control section is used i.e. a boundary of type (ii).

It is noteworthy that in subsequent solutions controls

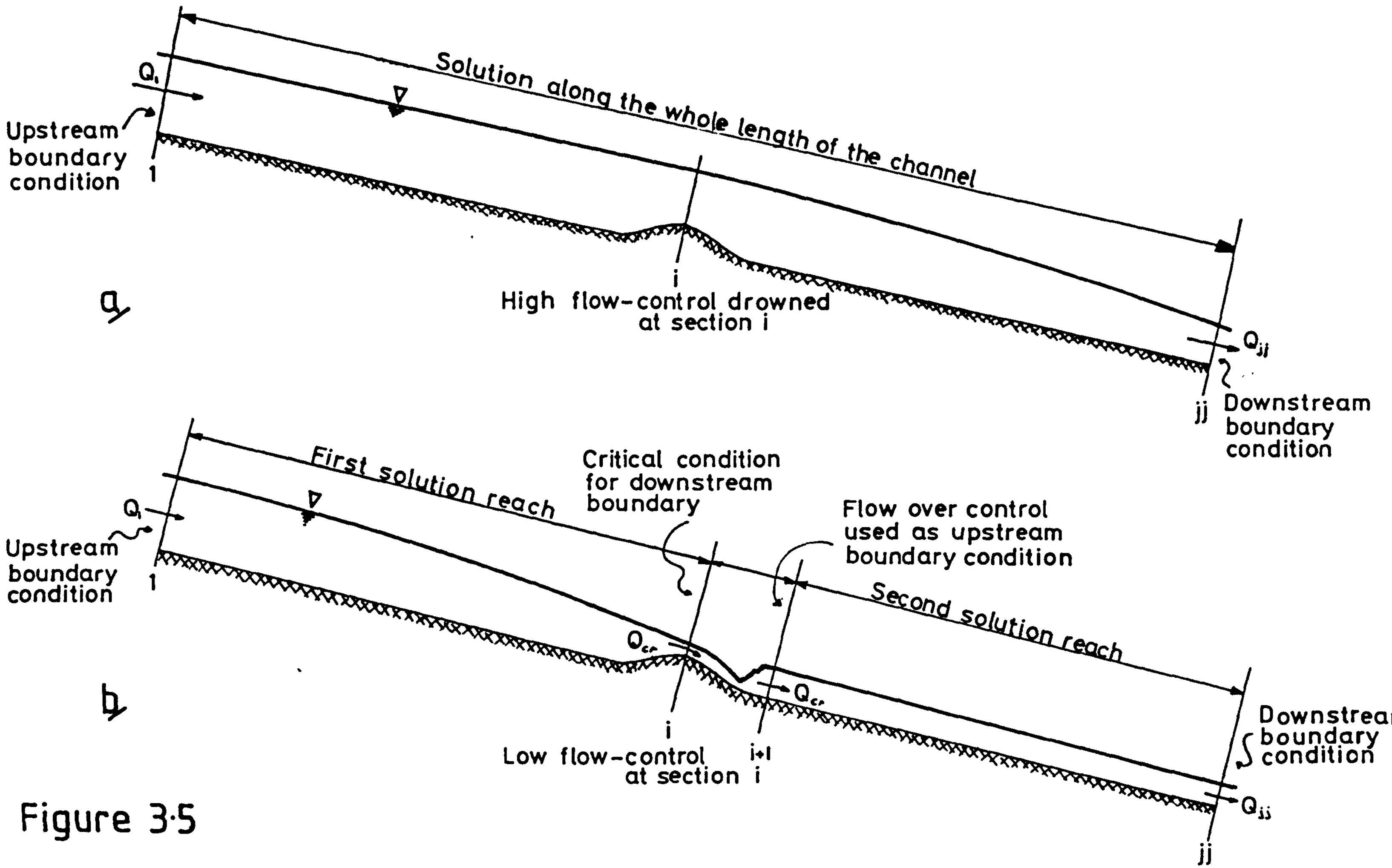
Solution along the whole length of the channel
Q_1
Upstream boundary condition
1
i
High flow-control drowned at section i
Q_{jj}
jj
Downstream boundary condition
a
First solution reach
Critical condition for downstream boundary
Flow over control used as upstream boundary condition
Second solution reach
Q_{cr}
Low flow-control at section i
i+1
Downstream boundary condition
b

Figure 3·5

may form in reaches 1 to i or i to jj. In this case the reaches are subdivided further and more internal boundaries introduced.

3.8.4 DROWNING OF CONTROLS

During the propagation of a flood wave through the main channel it is possible that conditions at a control section will cease to be critical. This circumstance arises when the influence of a downstream control extends up the channel and raises the energy at the upstream control above the critical value. The mathematical model tests for this occurrence by comparing the total energy at the control with the total energy downstream plus the friction losses occurring in the reach between the two. If the downstream energy plus the friction loss is found to be greater than the critical energy at the control then the control is drowned and the two reaches are joined as shown in Figure 3.5a. The implicit solution now takes place along the reach from 1 to jj.

CHAPTER FOUR

A NUMERICAL MODEL OF WASHLAND AREAS

4.1 INTRODUCTION

In general, engineering flood routing problems require that conditions in both the river and its associated washland areas be modelled. Many rivers and adjoining washlands can be considered to respond to flood discharges in a fashion similar to a complex run-of-river regulating reservoir. The river channel is segregated from the washlands by a system of flood-banks. Interaction between the river and its washland areas results from lateral over bank flows, which depend on both the main channel and the washland water levels.

Within each washland, individual compartments are separated from their neighbours by a complex system of cross-banks.

4.2 DESCRIPTION OF WASHLAND ALGORITHM

The primary requirements of the washland algorithm is that it accurately represents lateral over-bank flows and washland water levels.

4.2.1 CALCULATION OF WASHLAND WATER LEVELS

Computation of changes in the water level of a washland are based upon an explicit solution of the equation of conservation of volume. An explicit solution was chosen as it was considered that rates of change in the washland would be modest compared to those in the main channel. Further, an explicit solution can be contained in a separate

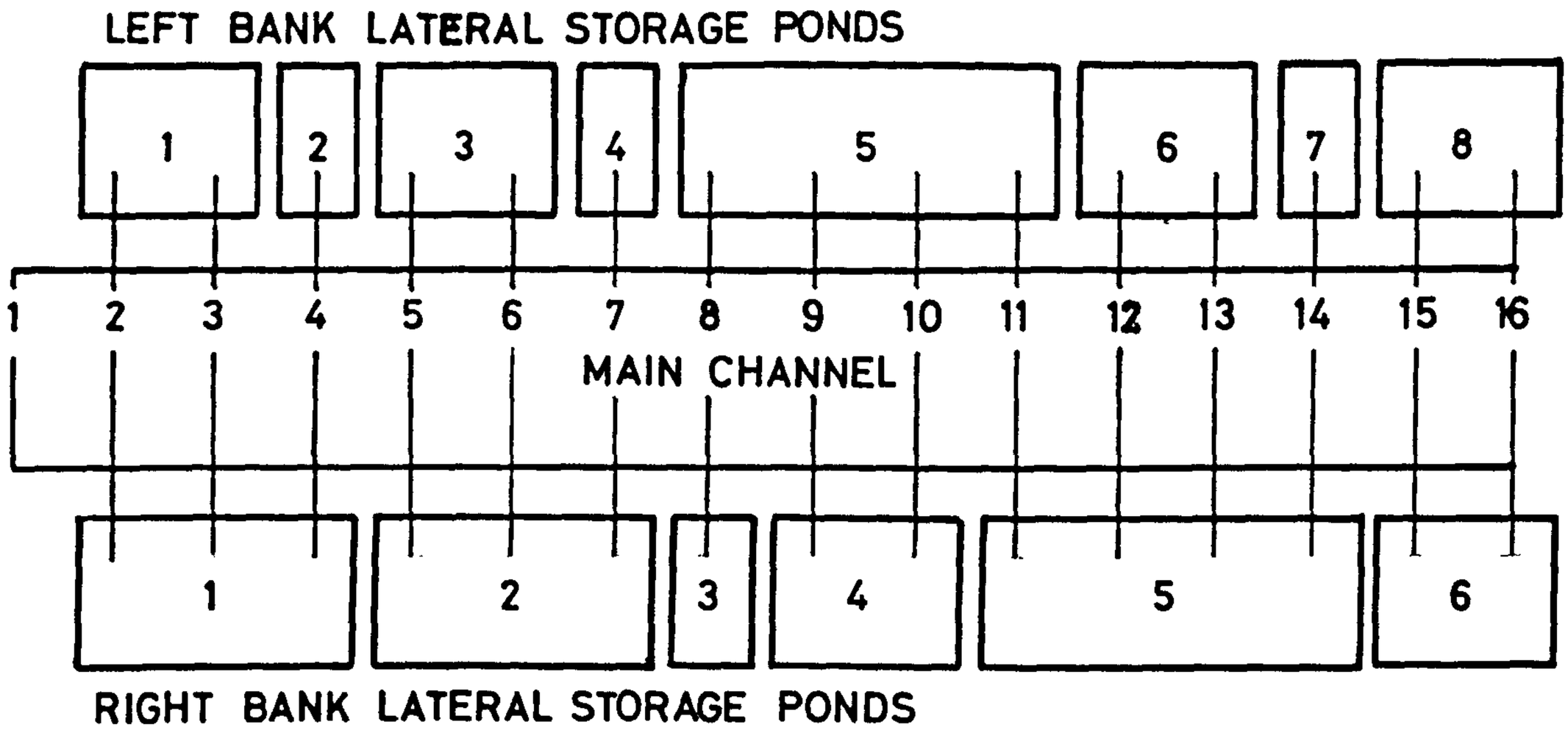

FIGURE 4.1a

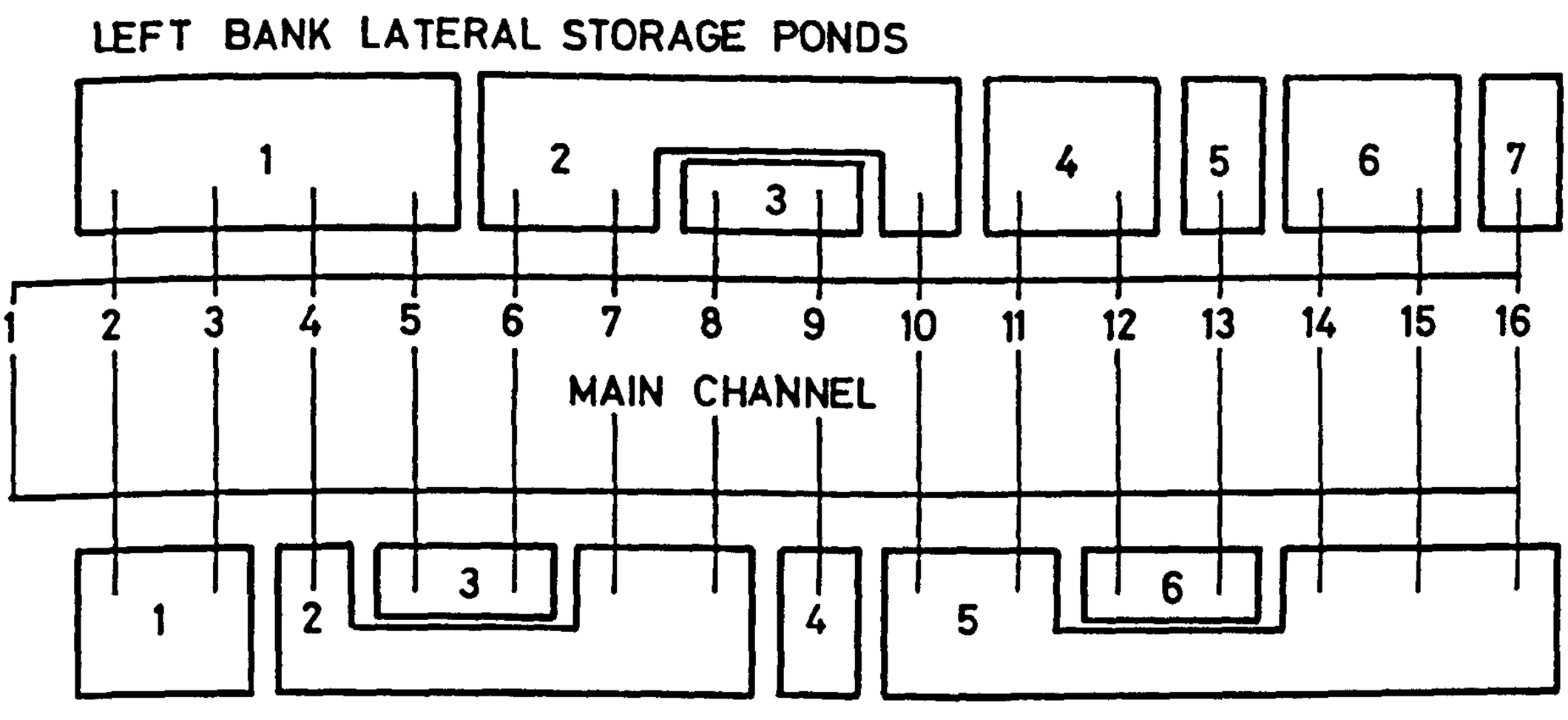

FIGURE 4.1 b
SCHEMATIC DIAGRAM OF LATERAL STORAGE PONDS.

routine and need only be included in the model when topographical features warrant it. An implicit solution on the other hand would require modification of the main channel finite difference equations.

The volume conservation equation for a washland area can be written as:

$$ql = As \frac{dWl}{dt}p \qquad \text{Equation 4.1}$$

where ql is the total lateral flow to or from the washland and As is the surface area of the washland. Equation 4.1 can be written in finite difference form as:

$$\sum_{j=JStart}^{JFinish} \overline{qlj} \quad \Delta t/As = \Delta Wl_p \qquad \text{Equation 4.2}$$

where $\overline{qlj}$ is the average lateral flow from reach j during a time increment. The sumation is required as the washland can be fed from more than one main channel reach, see Figure 4.1a. Indeed, the reaches feeding a washland need not be consecutive, Figure 4.1b; in this case the sumation reads:

$$\sum_{j=JStart1}^{JFinish1} \overline{qlj} \quad + \quad \sum_{j=JStart2}^{JFinish2} \overline{qlj}$$

4.2.2 CALCULATION OF LATERAL FLOWS

Flows entering or leaving the main channel to or from the washland are dependent upon the level of water in the river and in the washlands. Figure 4.2 illustrates the types of behaviour which may develop during a flood event which exceeds the bank full stage.

i. Flood level rising in the river with no flow into the washland:

Overbank flow = O.O

The washland may contain water from a previous flood.

ii. River level exceeds bank full level, "weir" flow occurs to the washlands and the water level in the washland starts to rise:

Overbank flow = Ø (river level).

iii. River level rising; washland level exceeds bank level and "submerged weir" flow occurs:

Overbank flow = Ø (river level, washland level).

iv. River level starts to fall but is still above bank full stage. Then "submerged weir" flow to the river occurs:

Overbank flow = Ø (washland level, river level).

v. River level below bank level; washland level exceeds bank level and "weir" flow from the washland occurs:

Overbank flow = Ø (washland level).

Calculation of the magnitude of overbank flows is based upon a weir flow equation of the form:

$$ql \propto H^{3/2} \quad \text{x submergence factor}$$

Bank data is processed to yield tables of lateral flow versus water level above bank level. These are stored

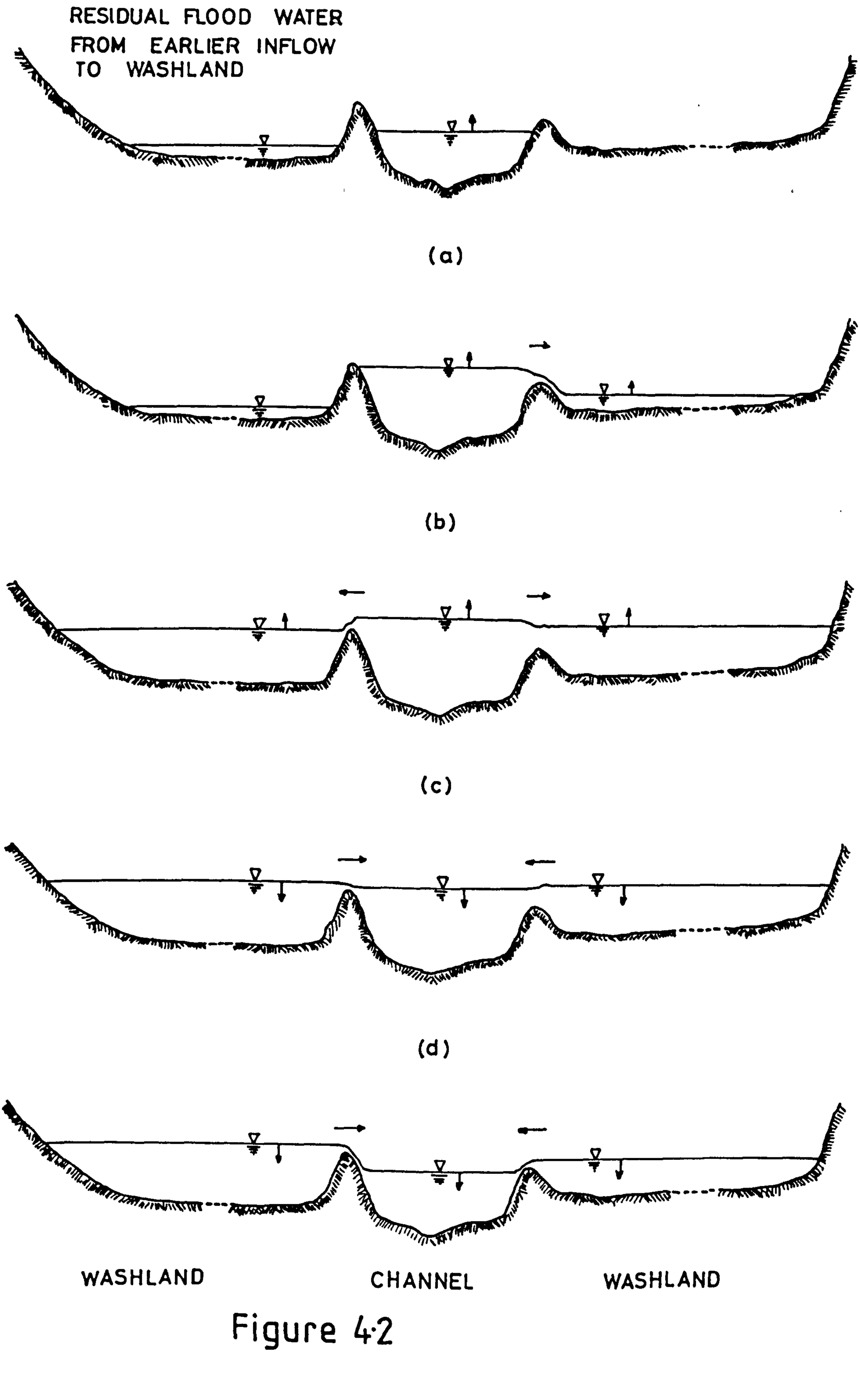
RESIDUAL FLOOD WATER
FROM EARLIER INFLOW
TO WASHLAND
(a)
(b)
(c)
(d)
WASHLAND
CHANNEL
WASHLAND

Figure 4·2

by the main programme and lateral flows are interpolated using the appropriate water levels. Where submerged weir flow is anticipated to occur the submergence ratio (Head downstream/Head upstream) is calculated and a submergence coefficient interpolated from a set of stored values. The actual flow is therefore established from the product of free weir flow and submergence coefficient.

Since individual washland compartments may border an appreciable stretch of river channel it is necessary to be able to accommodate the possibility of simultaneous inflow to and outflow from the washland. Such a circumstance may develop, for example, at a meander loop (Figure 4.3). Upstream of the meander the river level is relatively high and a proportion of the river flow enters the flood plain within the loop of the river. Downstream of the meander the river level is significantly lower due to head losses within the river meander and flow may take place from the flood plain into the river at this point.

4.3 DEVELOPMENT OF A WASHLAND ALGORITHM

Initially, the explicit washland algorithm shown in flow chart 4.1 was tried. This calculates the lateral flows to and from the washland and interpolates the existing washland surface area from stored data. Assuming these to represent average conditions, over the time increment, equation 4.2 is solved for the change in washland water level during the time increment.

Accuracy of this approach depends upon changes in washland water level being small during a time increment, hence not influencing average lateral flows. Numerical

Figure 4·3

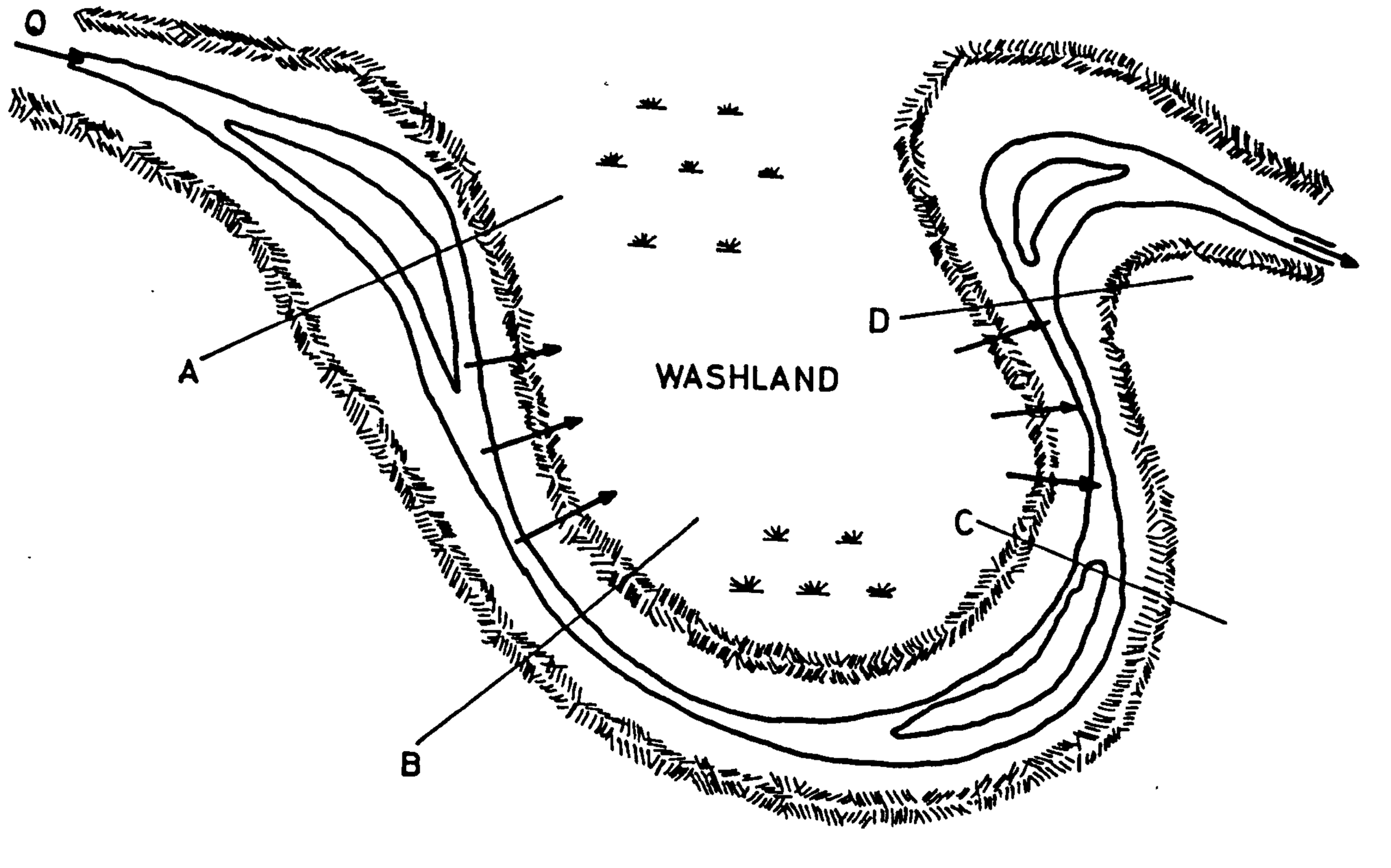

LONGITUDINAL SECTION ON CENTRELINE OF CHANNEL

FLOW CHART 4.1

INITIAL LATERAL STORAGE POND ALGORITHM

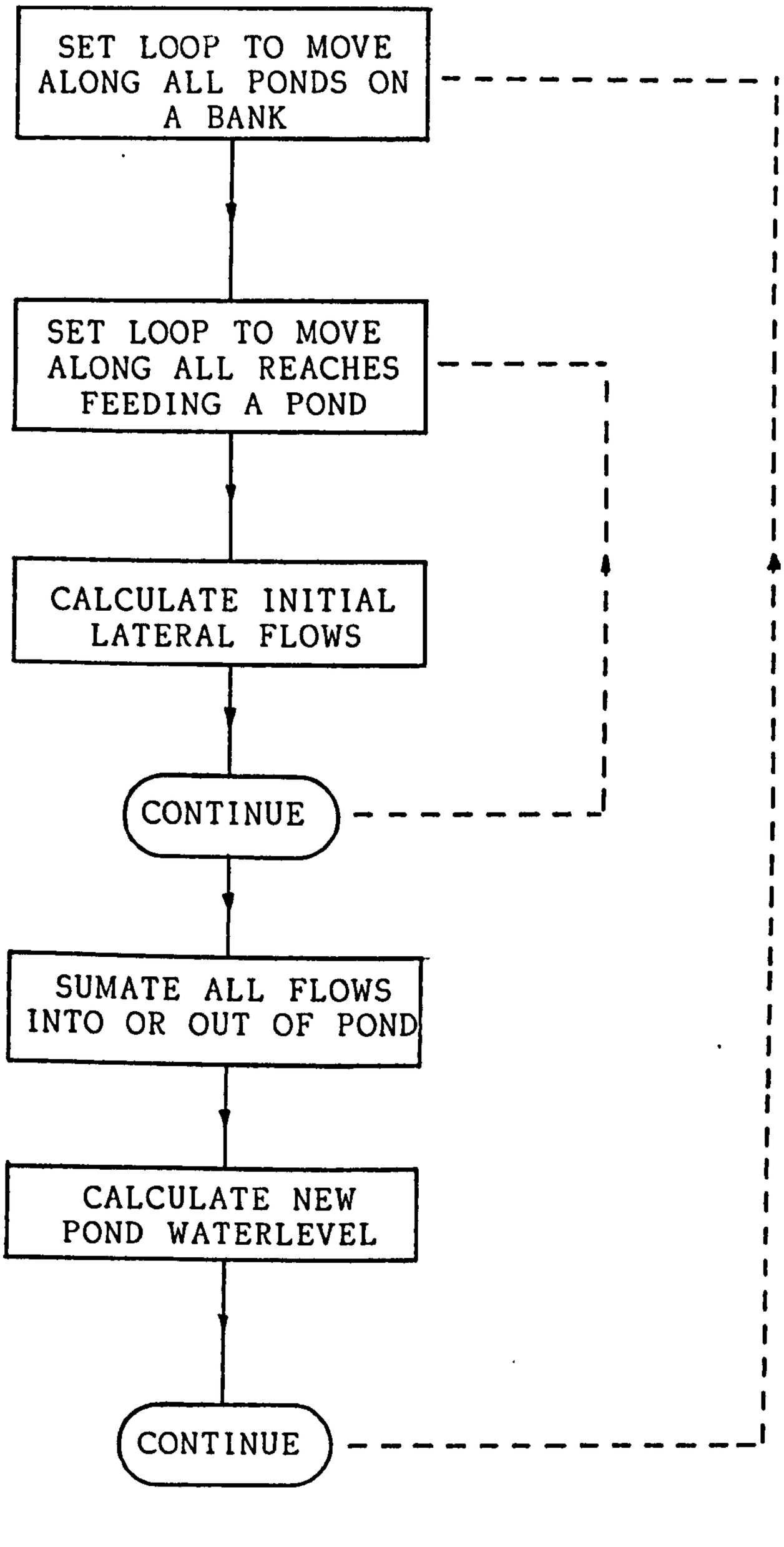

trials showed that this was not the case under certain circumstances, such as where the surface area of any washland was relatively small.

4.4 IMPROVED WASHLAND ALGORITHM

The object of these improvements is to provide better estimates for the average lateral flows, by including in the algorithm the effect that changes in the water levels, during a time increment, have on the initial lateral flows, see Flow Chart 4.2.

4.4.1 OUTFLOWS FROM WASHLANDS

It is obvious that any alteration in the water level within a washland will alter the head available for the production of outflows. To allow for this change the average outflow during a time increment is calculated from:

$$\overline{ql}j = \tfrac{1}{2} \left(ql_j^n + ql_j^n + \Delta qlj\right) \qquad \text{Equation 4.3}$$

where Δql is the change in lateral outflow during a time increment. Now, it can be seen from Figure 4.4 that:

$$\frac{dql}{dWlp} \doteq \frac{\Delta ql}{\Delta Wlp}$$

or,

$$\Delta \overline{ql} \doteq \frac{dql}{dWlp} \Delta Wlp$$

Inserting this in equation 4.3 gives:

$$\overline{ql}j = \tfrac{1}{2} \left(ql_j^n + ql_j^n + \frac{dql}{dWlp} \Delta Wlp\right)$$

Using the above in equation 4.2 and rearranging gives

FLOW CHART 4.2

FINAL LATERAL STORAGE POND ALGORITHM

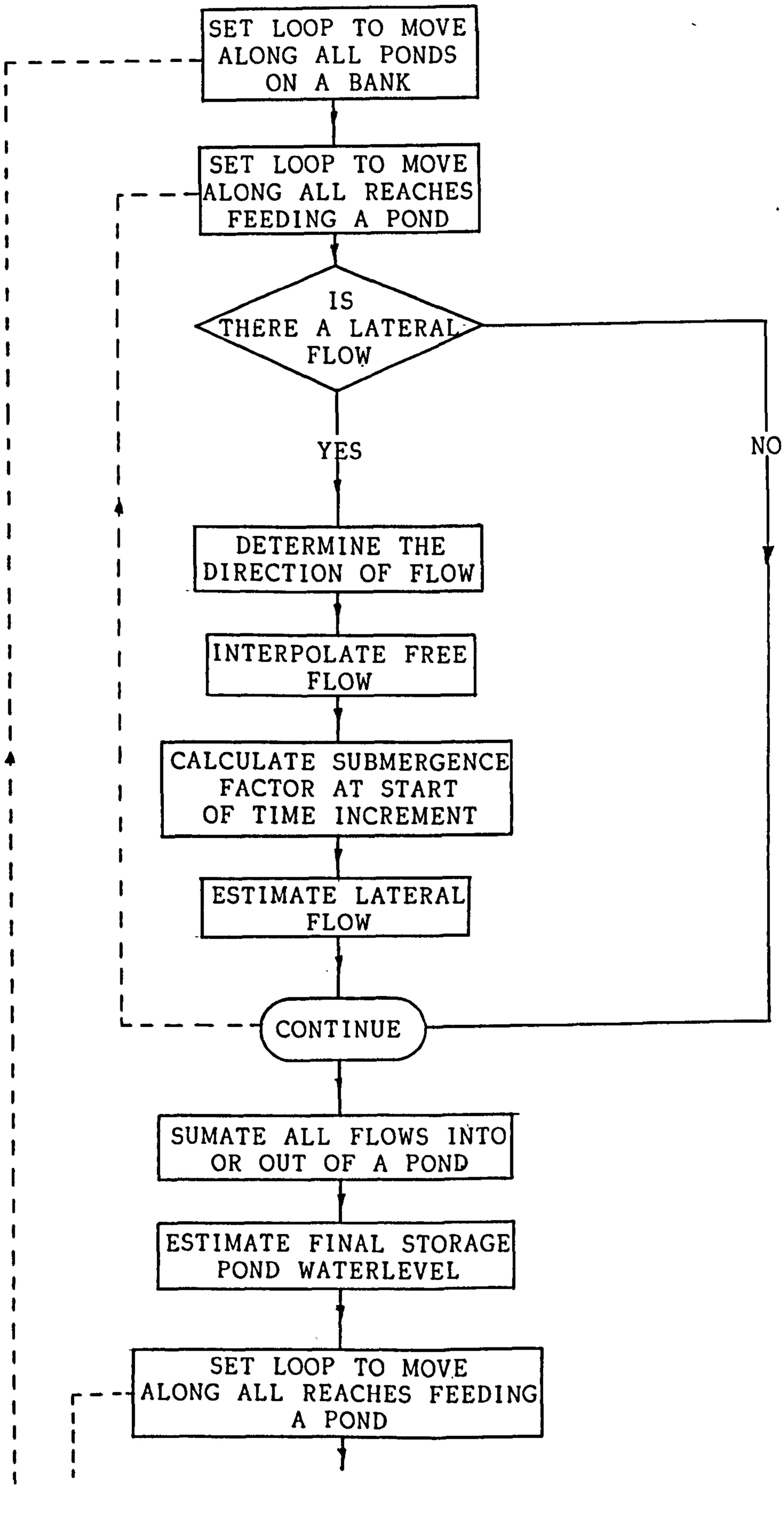

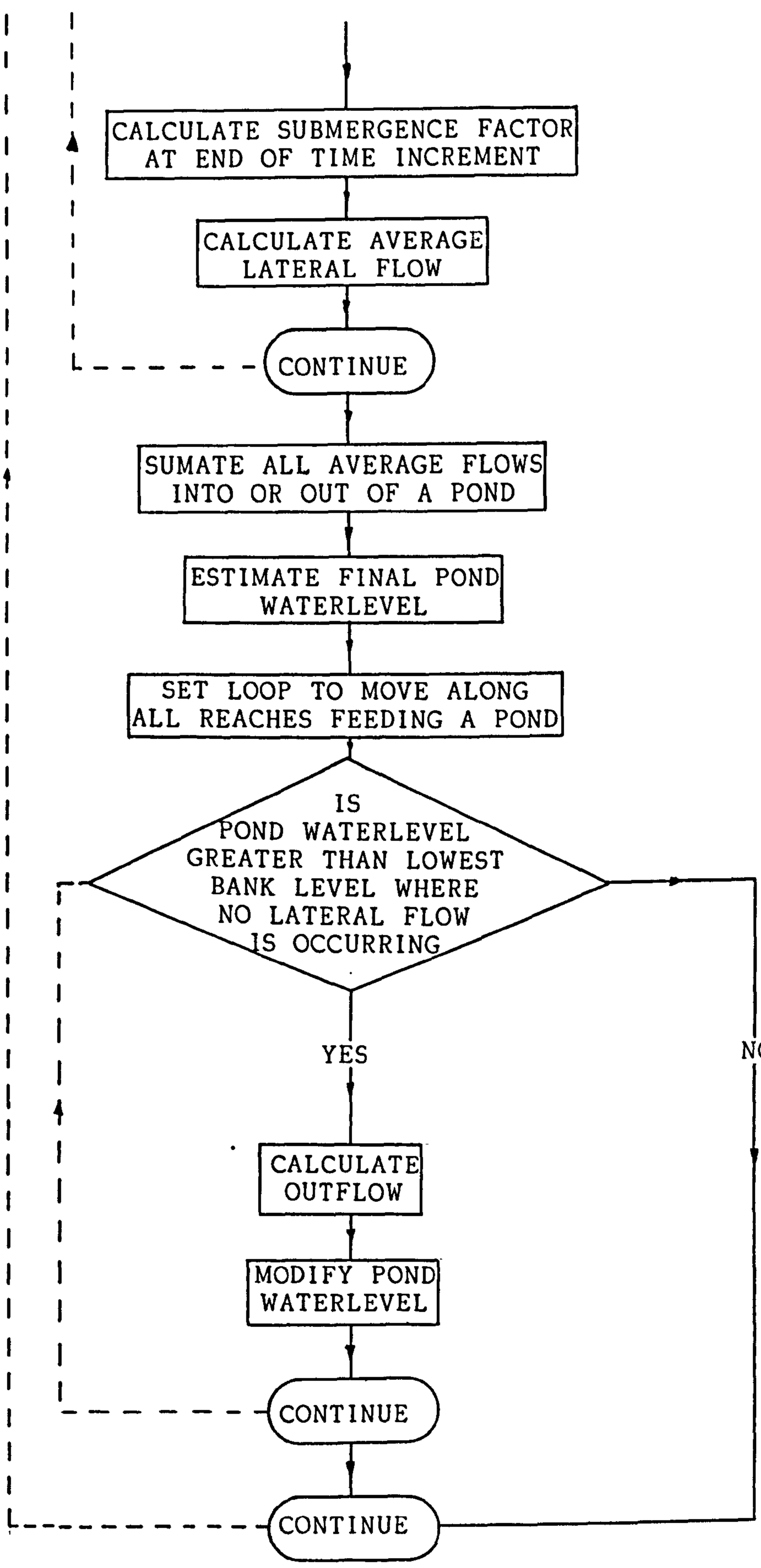
CALCULATE SUBMERGENCE FACTOR AT END OF TIME INCREMENT
CALCULATE AVERAGE LATERAL FLOW
CONTINUE
SUMATE ALL AVERAGE FLOWS INTO OR OUT OF A POND
ESTIMATE FINAL POND WATERLEVEL
SET LOOP TO MOVE ALONG ALL REACHES FEEDING A POND
IS POND WATERLEVEL GREATER THAN LOWEST BANK LEVEL WHERE NO LATERAL FLOW IS OCCURRING
YES
NO
CALCULATE OUTFLOW
MODIFY POND WATERLEVEL
CONTINUE
CONTINUE

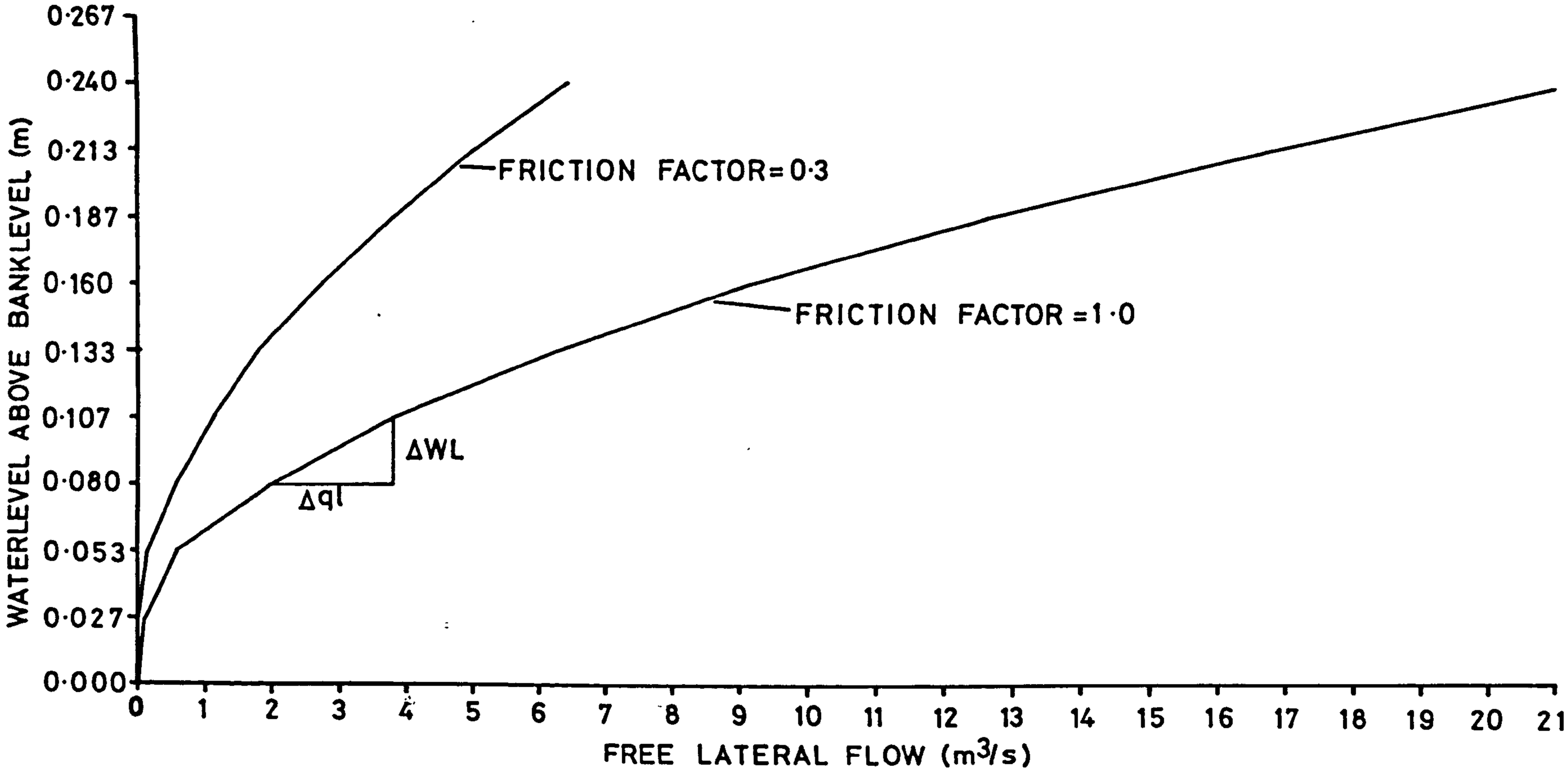

FIGURE 4·4
TYPICAL WATERLEVEL V'S FREE LATERAL FLOW RELATIONSHIP.

the change in washland water level as:

$$\Delta Wlp = \sum_{j=JStart}^{JFinish} qlj / \left(As/\Delta t - \tfrac{1}{2}\sum\left(\frac{dqlj}{dWlp}\right)_{out}\right) \qquad \text{Equation 4.4}$$

where $\left(\frac{dql}{dWlp}\right)_{out}$ represents the gradient of the outflows verses over-bank water level curve and is calculated directly from the curve.

4.4.2 INFLOWS TO WASHLANDS

Changes in washland water level influence lateral inflows through the submergence factor. The assumption that the main channel water levels remain quasi-constant, throughout the time increment, implies that the interpolated free flows will also remain constant. Variations in the true lateral flow depend on the degree of drowning by the washland water level. This is included in the new algorithm by using:

$$\overline{ql}j = \tfrac{1}{2}\left(ql_j^n \,.\, SF_j^n + ql_j^n \,.\, SF_j^{n+1}\right)$$

to calculate the average lateral inflows. The estimate for SF_j^{n+1} is calculated using a first estimate of the final washland water level obtained from applying the initial algorithm.

4.4.3 LATERAL OUTFLOWS STARTING DURING A TIME INCREMENT

During a time increment a washland water level can rise above one or more sections of bank over which no initial lateral flow is occuring. In these circumstances

it is desirable that the lateral outflow over this section, beginning sometime during the time increment, is estimated and its effect on the washland water level calculated.

To accomplish this the final washland water level is estimated, from equation 4.4, using the average lateral flows existing over the whole time increment. The algorithm then compares the estimated washland water level with the lowest dry bank level adjacent to this washland to determine if a new outflow has arisen. This will occur when the estimated washland water level is above the bank level, see Figure 4.5. In these circumstances the resulting free lateral outflow is obtained by interpolating in the water level verses overbank flow curve for the reach in question. The proportion of the time increment over which this flow occurs is required before its effect on the washland water level can be calculated. This is obtained, with reference to Figure 4.5, where it is seen that "TF", the proportion of time increment that the washland water level is above the bank level is defined by:

$$TF = (Wl_{pl}^{n+1} - Bl) \,/\, (Wl_{pl}^{n+1} - Wl_{p}^{n}) \qquad \text{Equation 4.5}$$

The new average lateral outflow can now be calculated from:

$$\overline{ql} = \tfrac{1}{2}\,(0.0 + qlj^{n+1})\,.\,TF$$

and its effect upon the washland water level is given by:

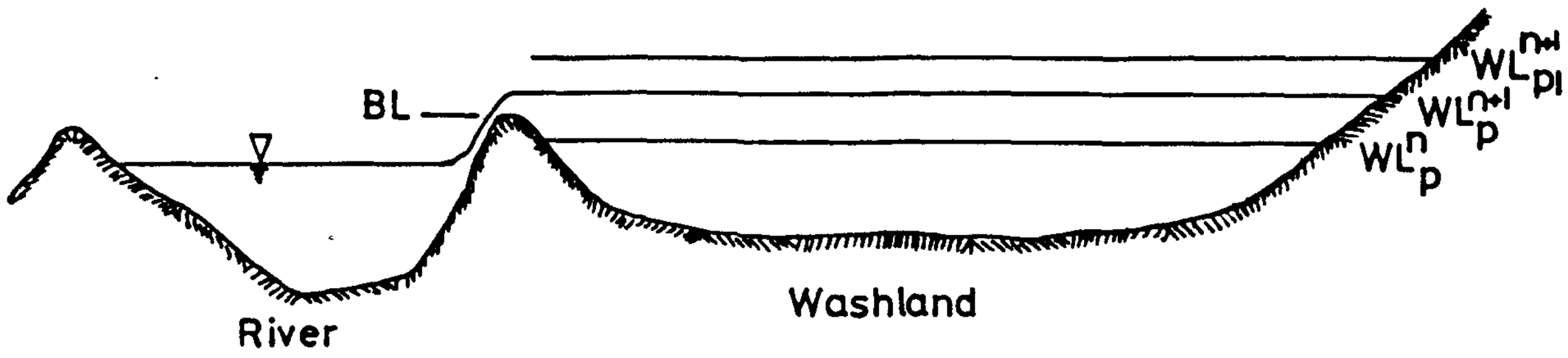

BL=Bank level

WL_{pl}^{n+1}=Estimate of final washland level

WL_{p}^{n+1}=Final washland level

WL_{p}^{n} = Initial washland level

Time factor = $(WL_{pl}^{n+1}-BL)/(WL_{p}^{n+1}-WL_{p}^{n})$

Figure 4·5

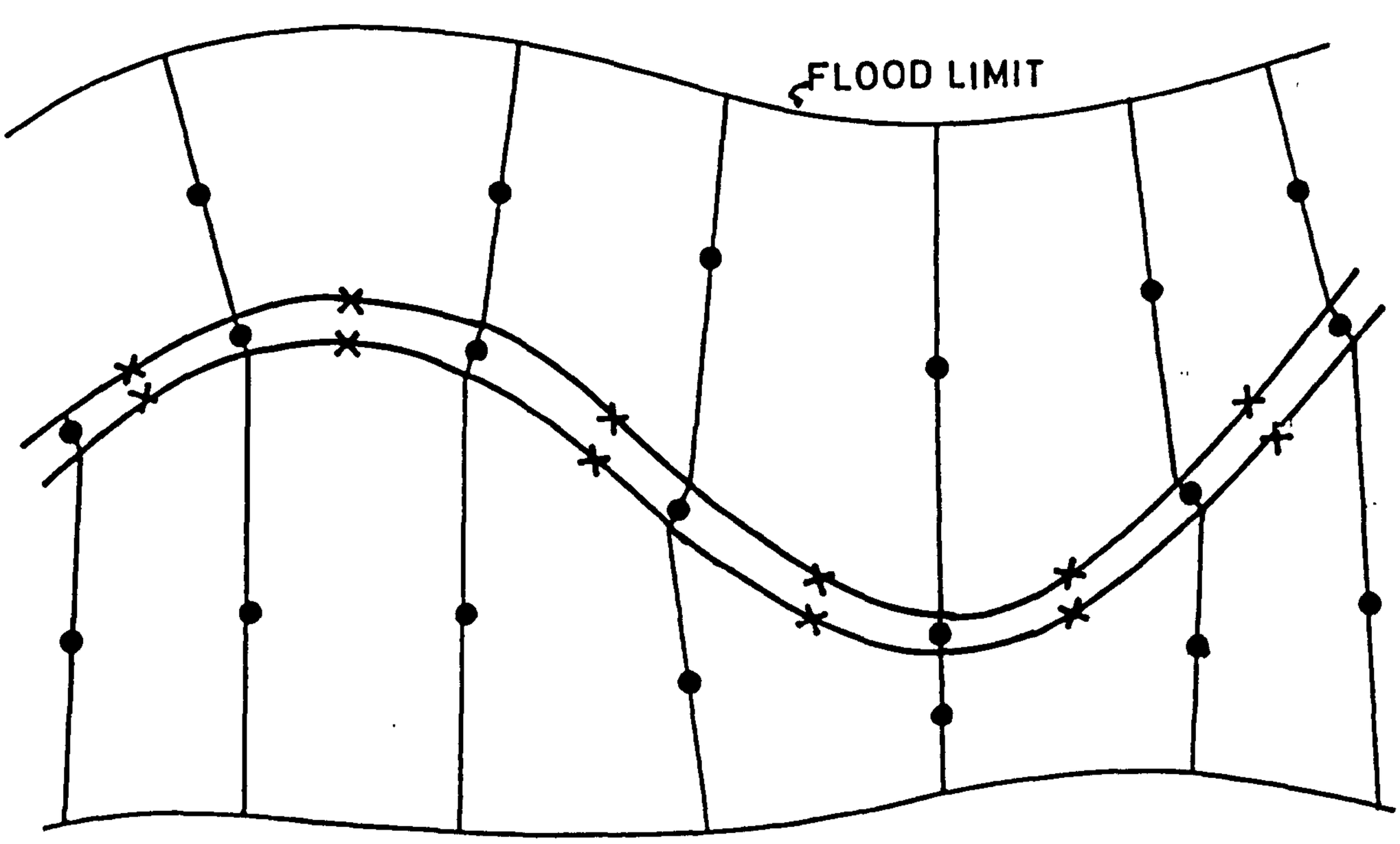

× Weir-type link

● River-type link

Figure 4·6
Flood plain and river schematization after Samuels

$$\Delta Wlp = \overline{ql} \times \Delta t/As \qquad \text{Equation 4.6}$$

Hence, the final lateral storage pond water level is equal to:

$$Wlp^{n+1} = Wlp_1^{n+1} - \Delta Wlp$$

The algorithm continues to compare the remaining dry sections of the bank, in order of increasing elevation, until a bank level above the washland water level is discovered; then all new lateral outflows and their effect on the final lateral storage pond water level will have been accounted for.

4.5 COMPARISON WITH HYDRAULICS RESEARCH EMBER MODEL

The details of a numerical model for simulating flood propagation through a natural river channel and its associated flood plain areas was published by Samuels (1983b). The main channel model used is similar to that described by Price and Samuels (1980). A descriptive comparison between the flood plain algorithm in this model and the current model is given in the following section.

In Samuels' numerical scheme a different schematization of the problem is adopted. Each main channel solution node connects with a storage cell on the left and right bank flood plain and flood plain cells are connected to their neighbours, Figure 4.6. This schematization enables the kinematic modelling of flow along the flood plain.

In the current model individual storage ponds are connected to a number of solution nodes but are considered separate from each other, hence flow along the flood plain cannot

be modelled. In this respect there is scope for further development in the current model.

Samuels reported stability problems arising from the calculated lateral flows over the flood banks a problem also encountered by the author. Different methods have been used to overcome this problem. Samuels outlined his solution procedure as consisting of the following steps for each time increment:

i. Calculate the discharges and levels at the model boundaries from data.

ii. Estimate and store the mean discharge over the banks at each computational cell.

iii. Solve the flow equations for the river channel.

iv. Solve the flow equations for the flood plain.

v. Print results if required.

The stability problems arise at Step ii in obtaining an estimate of the mean lateral discharge over the time increment. Samuels' model calculates the initial lateral disharge at time $n\Delta t$ from the weir flow equation. The estimate of mean lateral flow, over the time increment from $n\Delta t$ to $(n+1)\Delta t$, is obtained using the following steps:

a) force the magnitude of the initial lateral flow not to exceed a global limit.

b) include a proportion of lateral flow of previous time steps by setting $ql^n = \lambda_o ql^n + \lambda_1 ql^{n-1} + \lambda_2 ql^{n-2}$

c) look for possible oscillations in water level and reduce $\overline{ql}^n$ to eliminate these.

d) add a small proportion of ql to the result from step(c).

The limit for step (a) was set to $0.3 m^3/s/m$, and the damping parameters λo, λ_1, λ_2 in step (b) were set to 0.34, 0.33 and 0.33 respectively. Using these the model was successfully applied to the River Trent. A modified version consisting of steps (a), (b), (c), (a) was found to be more appropriate for the River Avon.

The current model solved these stability problems by a different approach. The solution procedure consists of the following steps:

i) calculate the discharges and levels at model boundaries from data.

ii) estimate and store the mean discharge over the banks at each solution node.

iii) solve the washland equations

iv) re-assess the mean discharge over the banks at each solution node.

v) resolve the washland equations

vi) solve equations for the river channel

vii) print results.

A detailed account of each of these steps is given in the preceding sections of this chapter.

It can be seen that the difference between the present model and that of Sam uels is the recomputation of the

lateral discharges and washland levels by what is in effect a single iteration. It is the opinion of the author that the major cause of the stability problems is that insufficient attention is given to changes in washland water levels when operating with a physically realistic time increment. The use of this single iteration is an attempt to solve the stability problem by bringing the numerical procedure closer to the behaviour of the physical prototype.

4.6 INITIAL CALIBRATION AND TESTING

The flood routing model, see Appendix B, was developed with a particular application in mind, that was a flood study of the River Aire in Yorkshire. Before proceeding with this study initial stability tests and calibration runs were undertaken on an upstream section of the River Aire from Kildwick to Stockbridge. A sample of the results obtained is presented below.

4.6.1 SYNTHETIC FLOOD RESULTS

A schematic diagram of the trial channel and its washland system is shown in Figure 4.7. Note that for low flows control sections exist at solution nodes 11 and 16. A synthetic inflow hydrograph rising to a peak flow of $102m^3/s$ from a base flow of $6m^3/s$ in nine hours and decreasing from $102m^3/s$ to $5m^3/s$ in seven hours is shown in Figure 4.8. This can be compared with the two outflow hydrographs obtained for no washland areas and for washland areas with overbank flow calculated using a frictionless

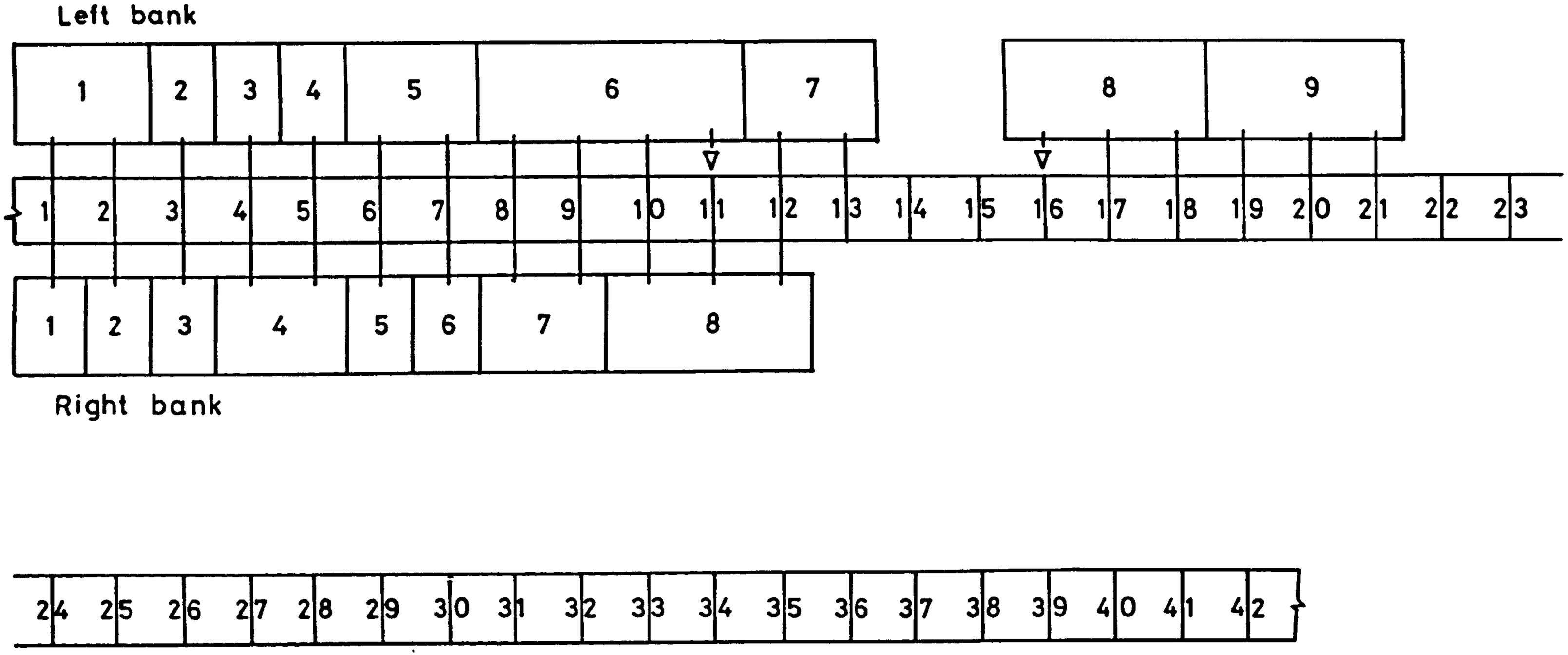

∇ Denotes a potential control.

FIGURE 4.7
SCHEMATIC DIAGRAM OF TEST SECTION OF THE RIVER AIRE.

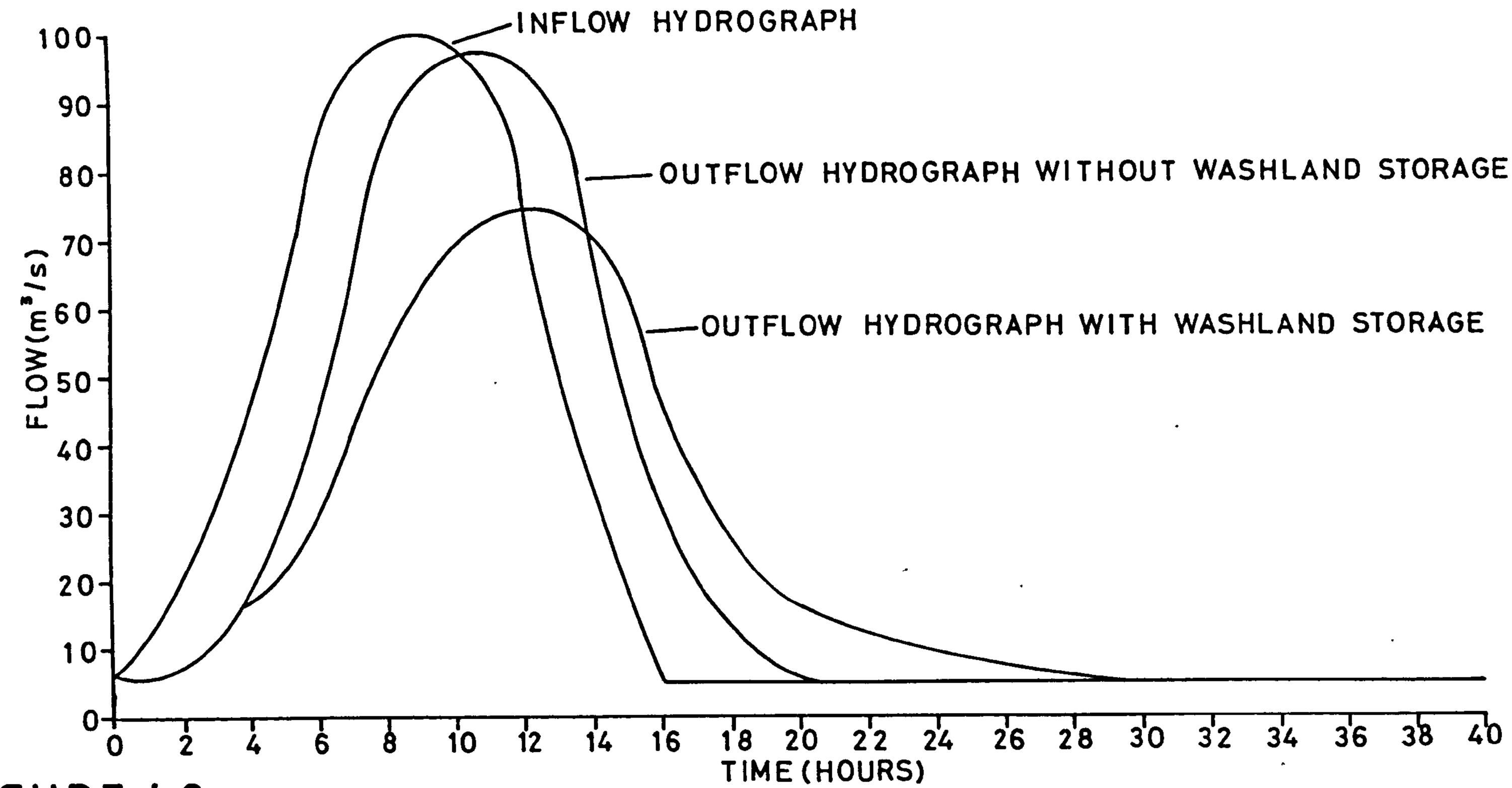

FIGURE 4.8
COMPARISON OF HYDROGRAPHS.

weir flow equation. In both runs theta was equal to 1.0 and a time increment of 900 seconds was used. It can be seen that inclusion of the washland adds significantly to the attenuation of the flood wave.

The behaviour of the washland model was assessed by a detailed examination of the numerical results. Consider first the case of frictionless overbank flow, (Friction factor = 1.0). For illustrative purposes the behaviour of two washlands is discussed. Left bank washland number 2 fed by main channel solution node 3 and left bank washland number 6 fed by main channel solution nodes 8, 9, 10 and 11. The behaviour of washland 2, during the passage of the flood, is shown in Figure 4.9. Figure 4.10 shows the variation of the main channel water level at solution node 3; as it rises above banklevel 3 flow into washland 2 begins, and the water level in washland 2 rises, Figure 4.9. This will be a free lateral lateral flow until approximately six hours when the washland level rises above the bank level. The washland continues to fill until the main channel water level falls below the washland water level at approximately sixteen hours the lateral flow is now reversed and the washland water level begins to drain down. Figures 4.11a to 4.11d illustrate the behaviour of main channel water levels at solution nodes 8, 9, 10 and 11 feeding left bank washland 6. Waterlevels at solution nodes 8, 9 and 10 rise above the left bank levels at around two hours causing flows into washland 6, Figures 4.13a to 4.13c. In this case these flows cause

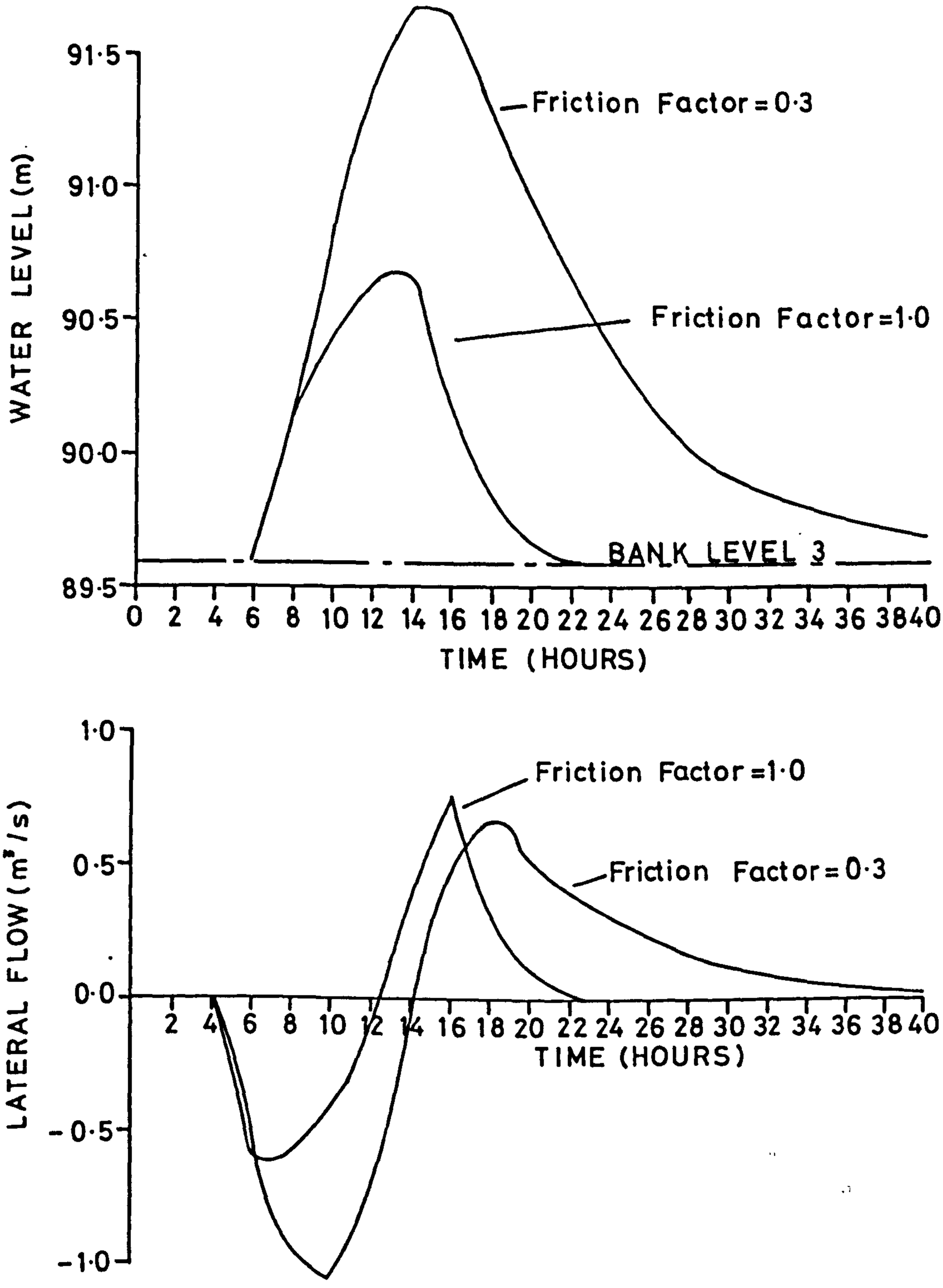

FIGURE 4.9
LEFT BANK WASHLAND NO. 2 .

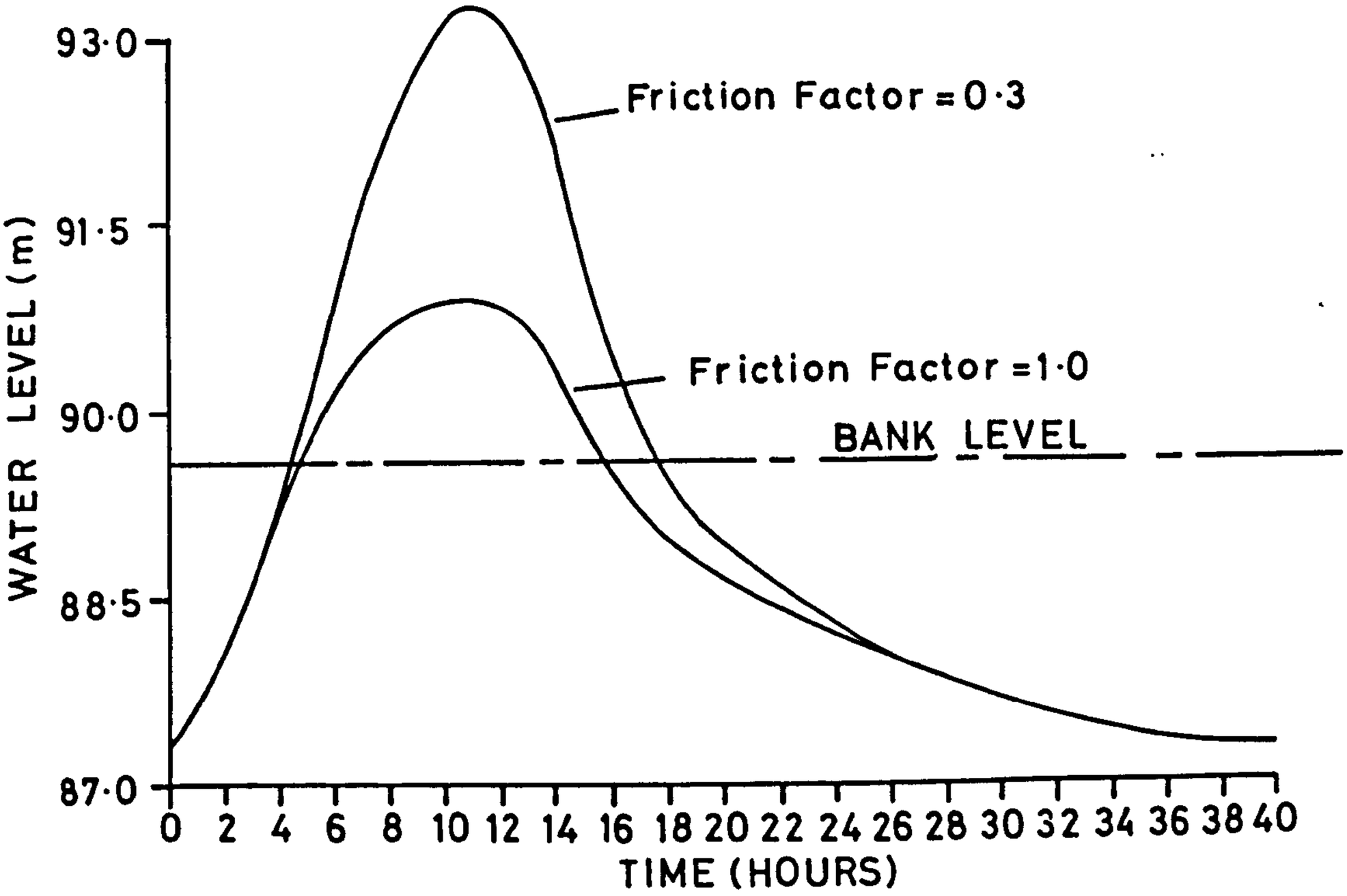

FIGURE 4.10
MAIN CHANNEL WATER LEVELS NODE 3.

washland 6 water level to rise above bank level 11, at eight hours, before the main channel water level at solution node 11, Figures 4.12 and 4.11d. Hence flow takes place out of the washland at solution node 11, Figure 4.13d. This behaviour is undoubtedly enhanced by the presence of the control section at solution node 11, as the restriction to flow imposed by the control will cause high water levels upstream. Part of the flood is bypassing the control by flowing through the washland.

The control section at solution node 11 was a permanent control and operated as such for the duration of the flood. The control at solution node 16 was not and drowned after 5.5 hours. The energy levels during operation and drowning of this control are illustrated in Figure 4.14.

During these initial tests it was discovered that some lateral flows into and out of the washlands were unrealistically large. To reduce these to a more realistic level a percentage reduction factor was introduced to account for frictional resistance to lateral flow over the flood banks. For the purposes of comparison a run was made with all lateral flows reduced by 70% corresponding to the friction factor of 0.3 in Figures 4.9 to 4.13. The expected effect of this was to reduce lateral flows and significantly increase the main channel water levels. This can be seen to be true for the main channel water levels at solution nodes 3, 8, 9, 10 and 11 in Figures 4.10 and 4.11. However, the volume of lateral flow into

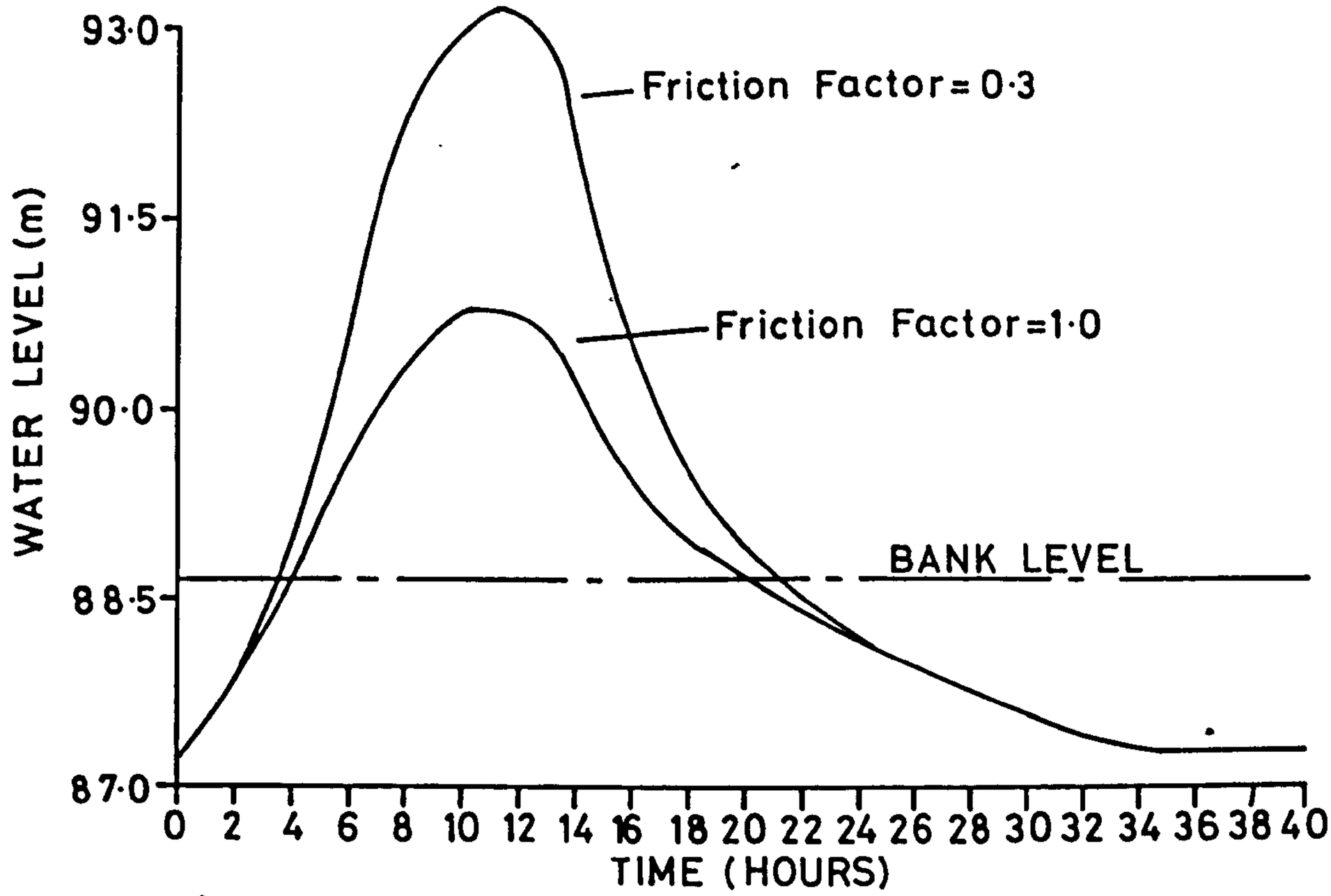

Figure 4.11a
Main channel water levels solution node No. 8

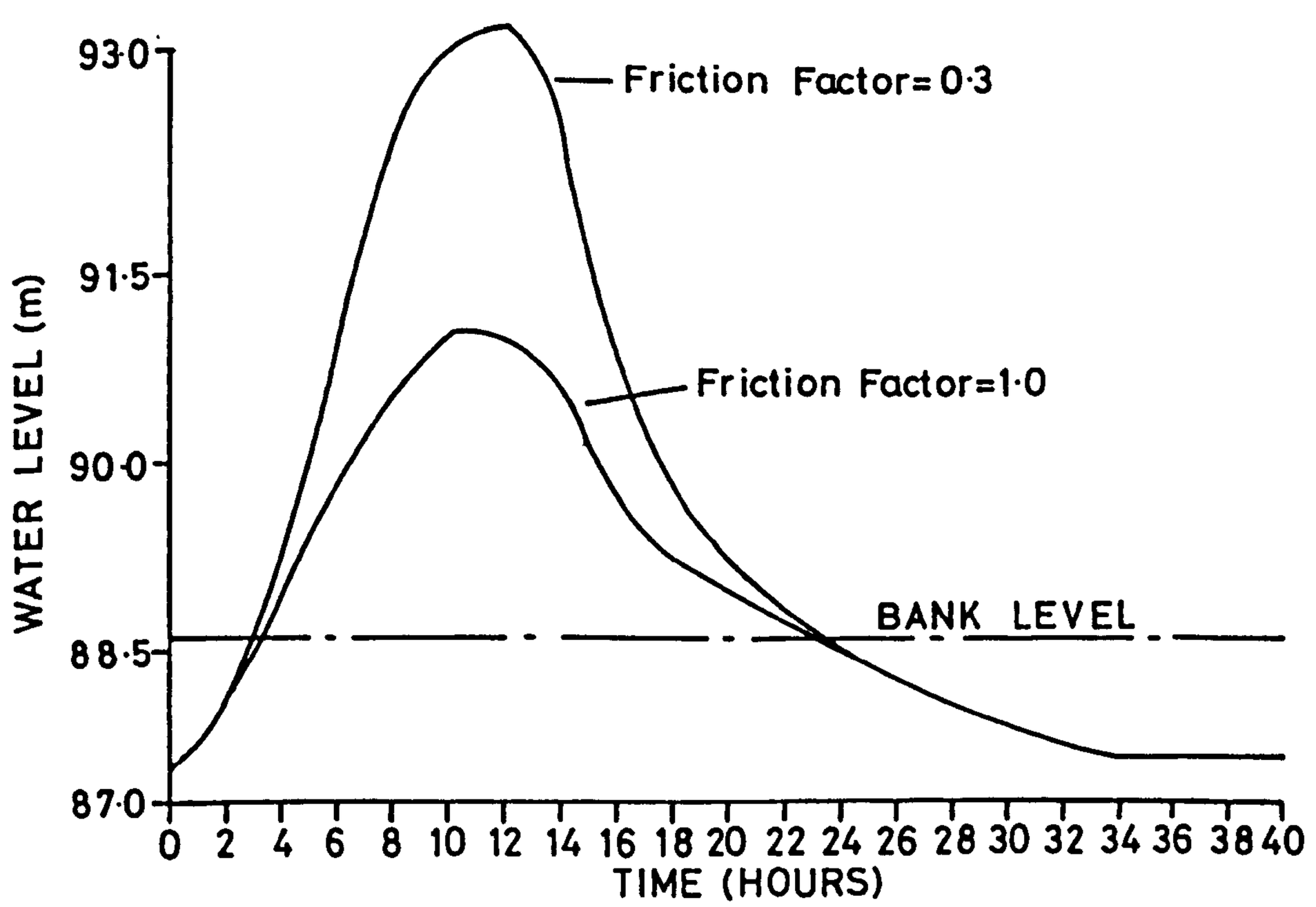

Figure 4.11b
Main channel water levels solution node No. 9

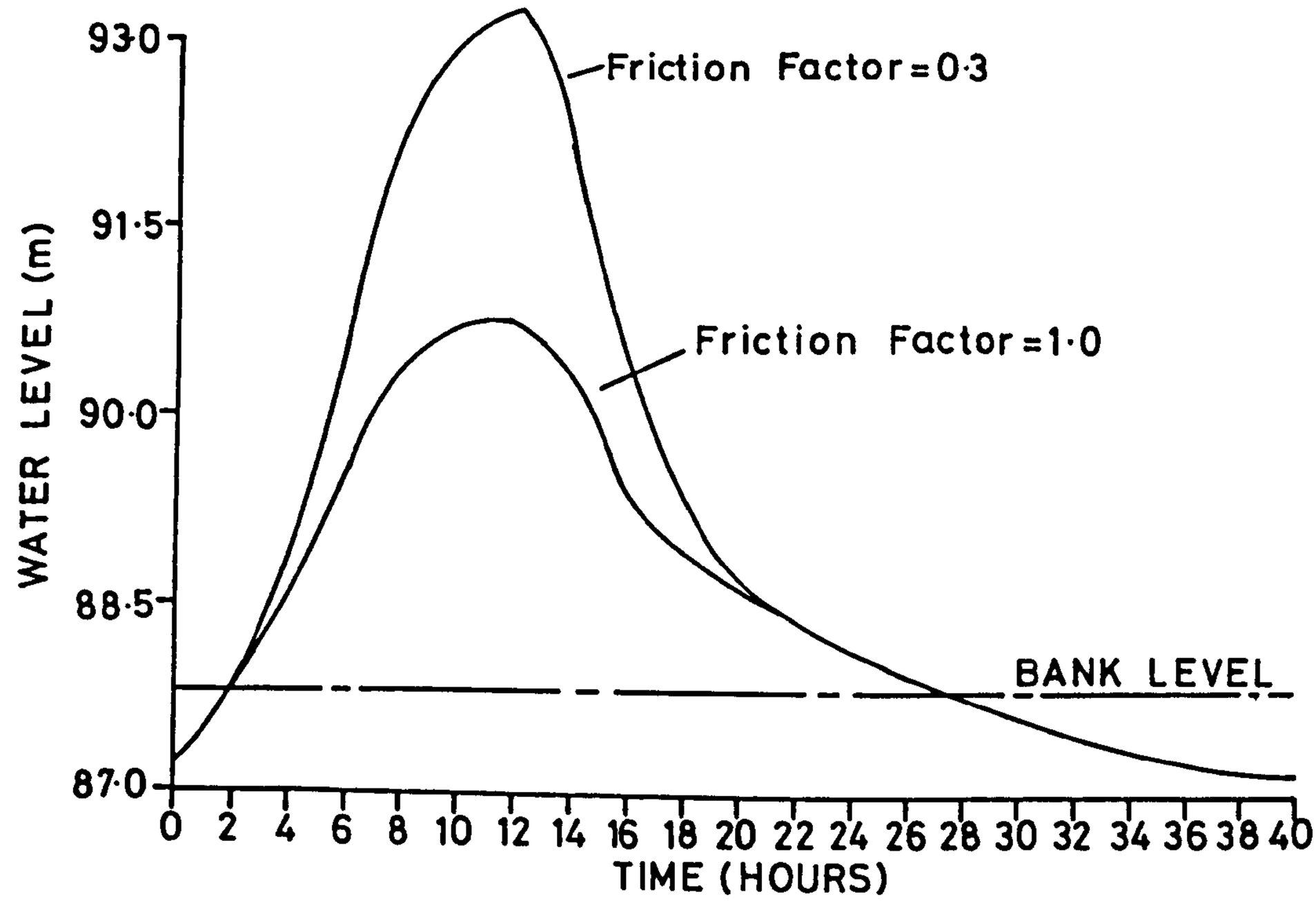

Figure 4.11c
Main channel water levels solution node No.10

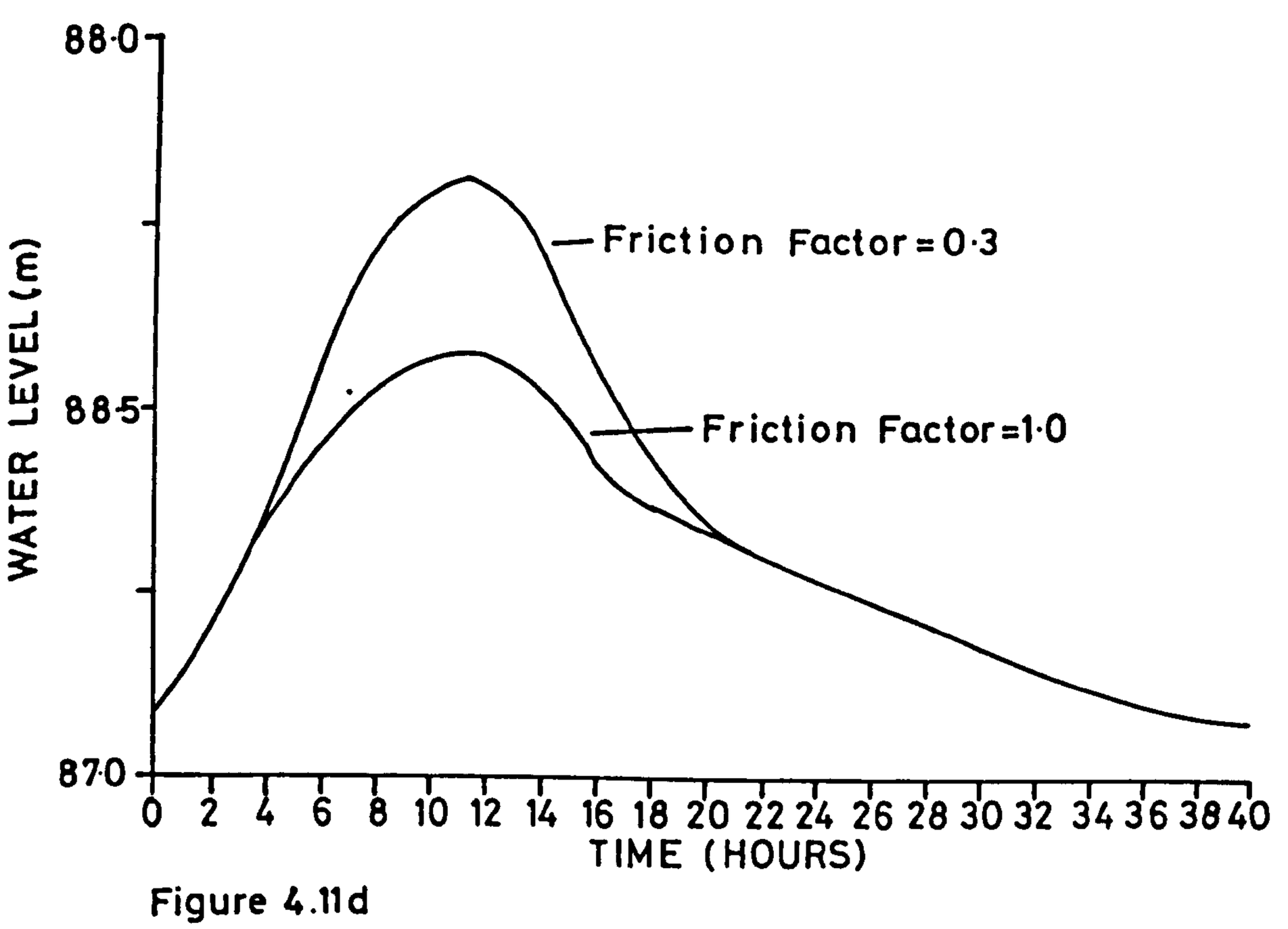

Figure 4.11d
Main channel water level solution node No.11

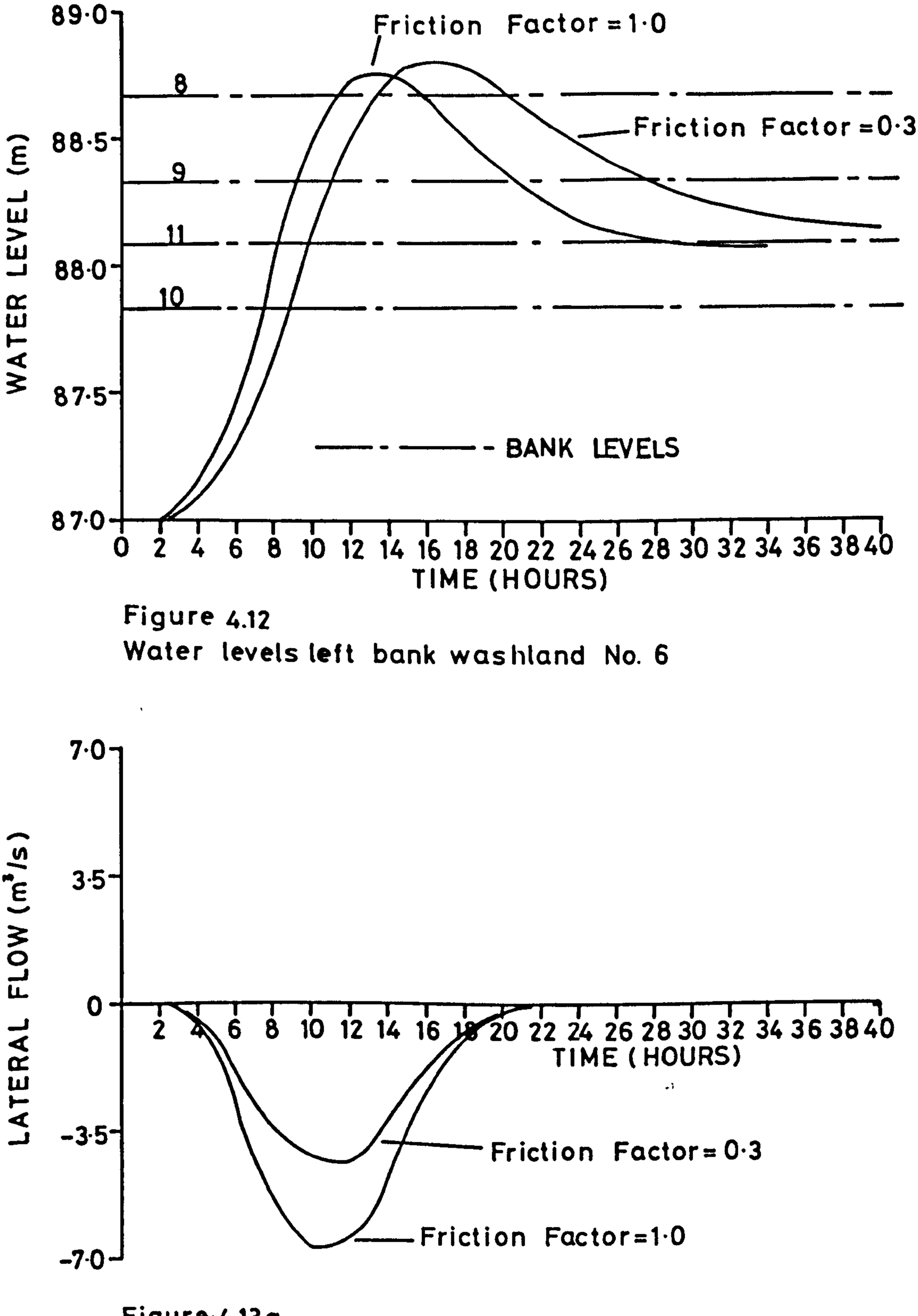

Figure 4.12
Water levels left bank washland No. 6

Figure 4.13a
Lateral flows solution node No. 8.

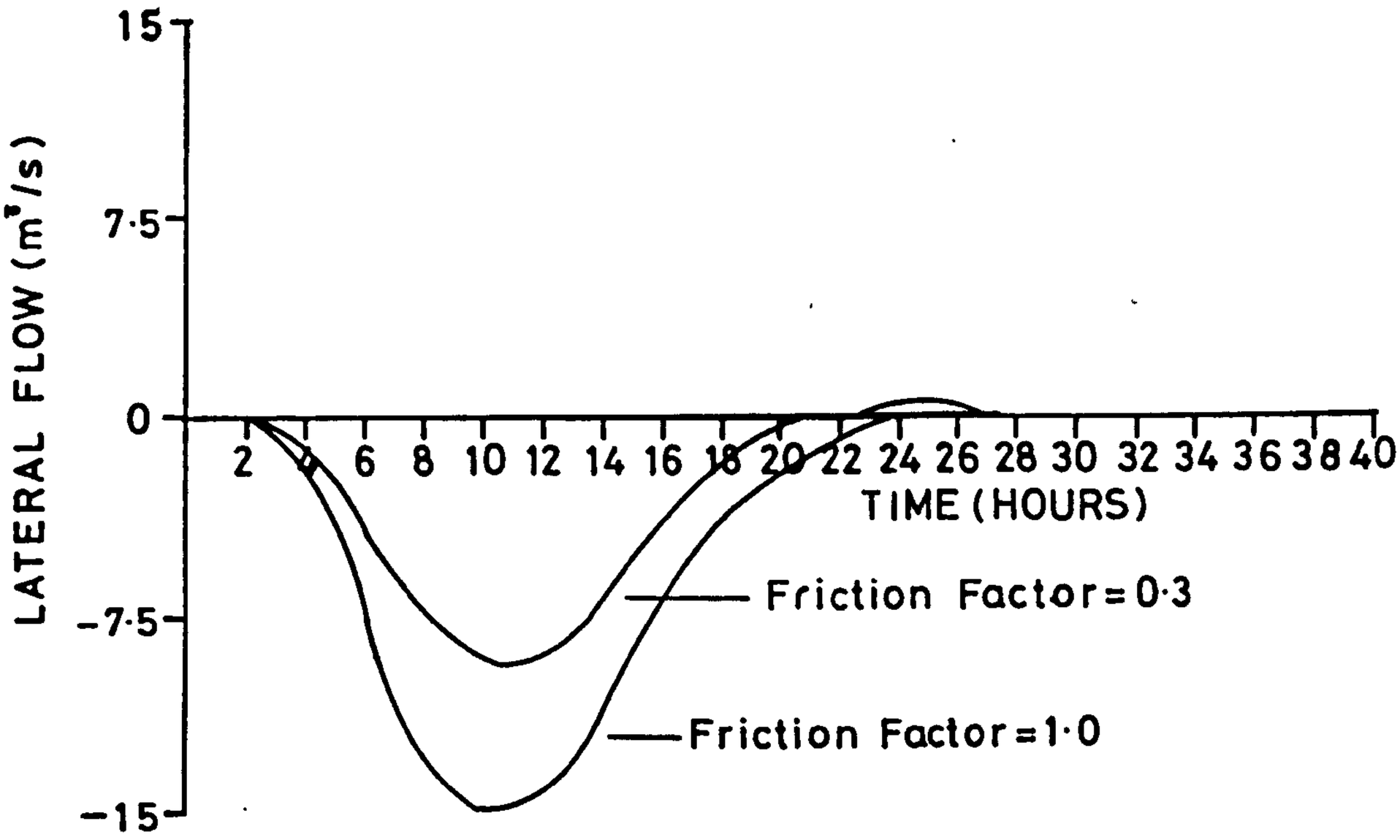

Figure 4.13b
Lateral flows solution node No. 9

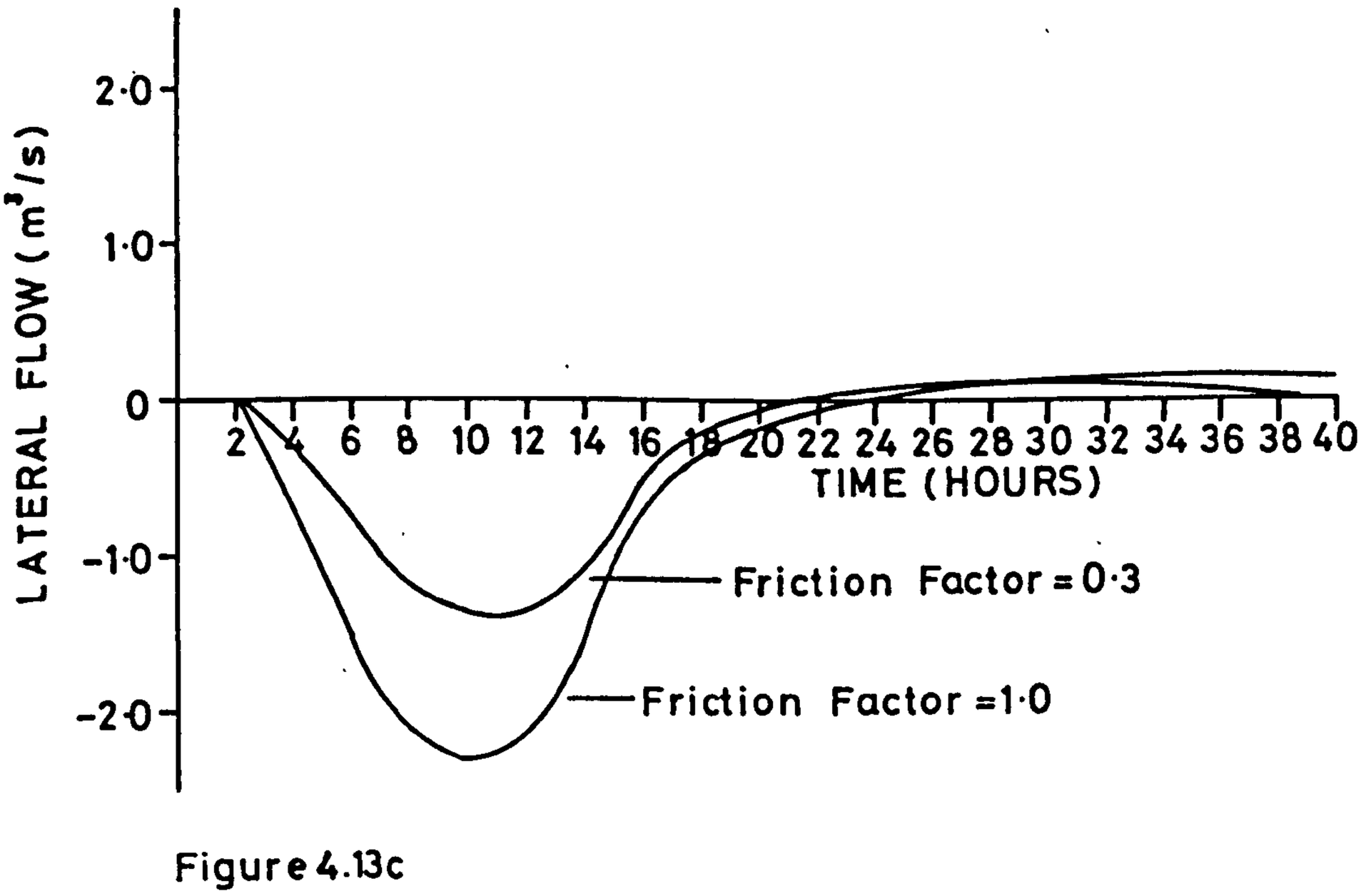

Figure 4.13c
Lateral flows solution node No. 10

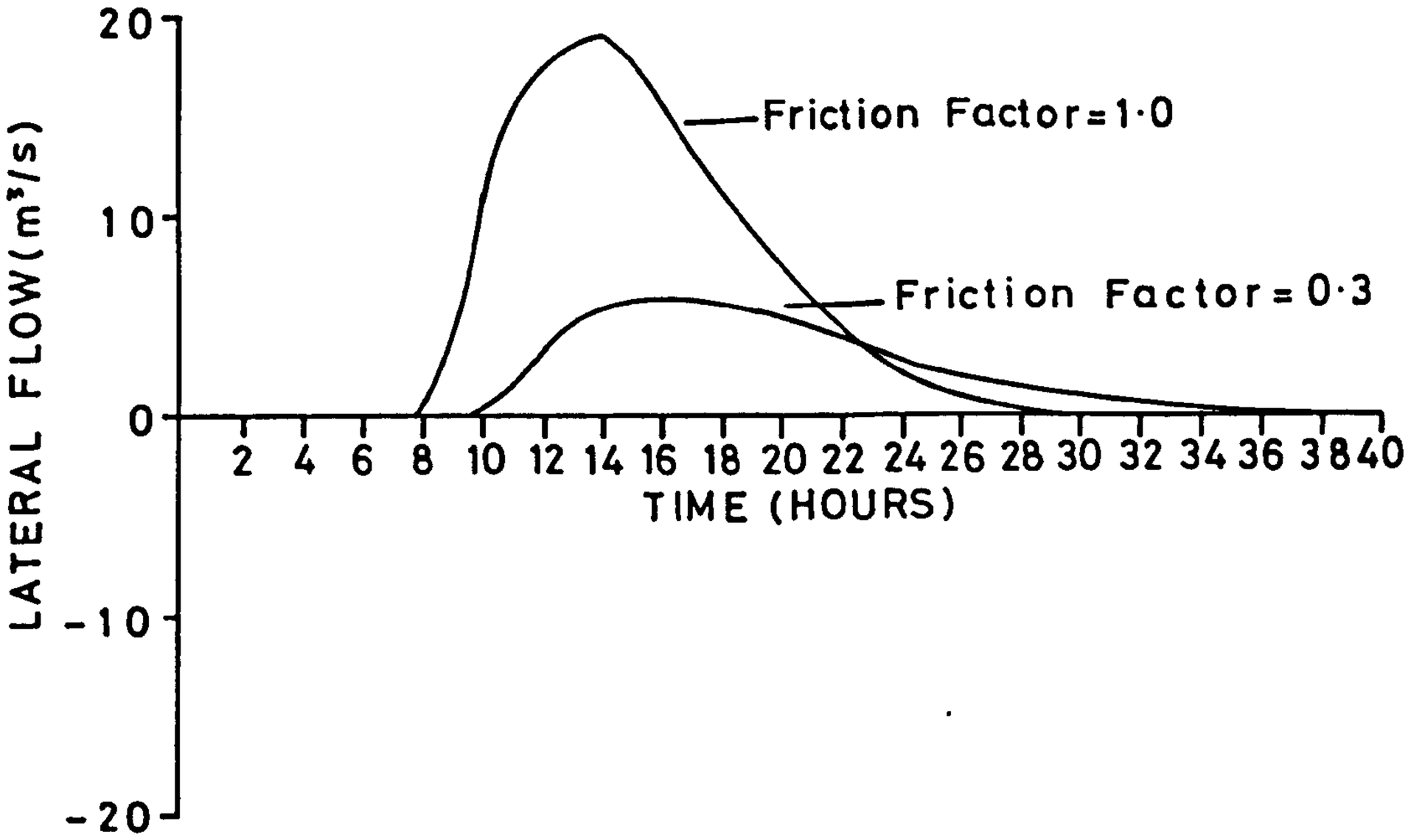

Figure 4.13d
Lateral flows solution node No. 11

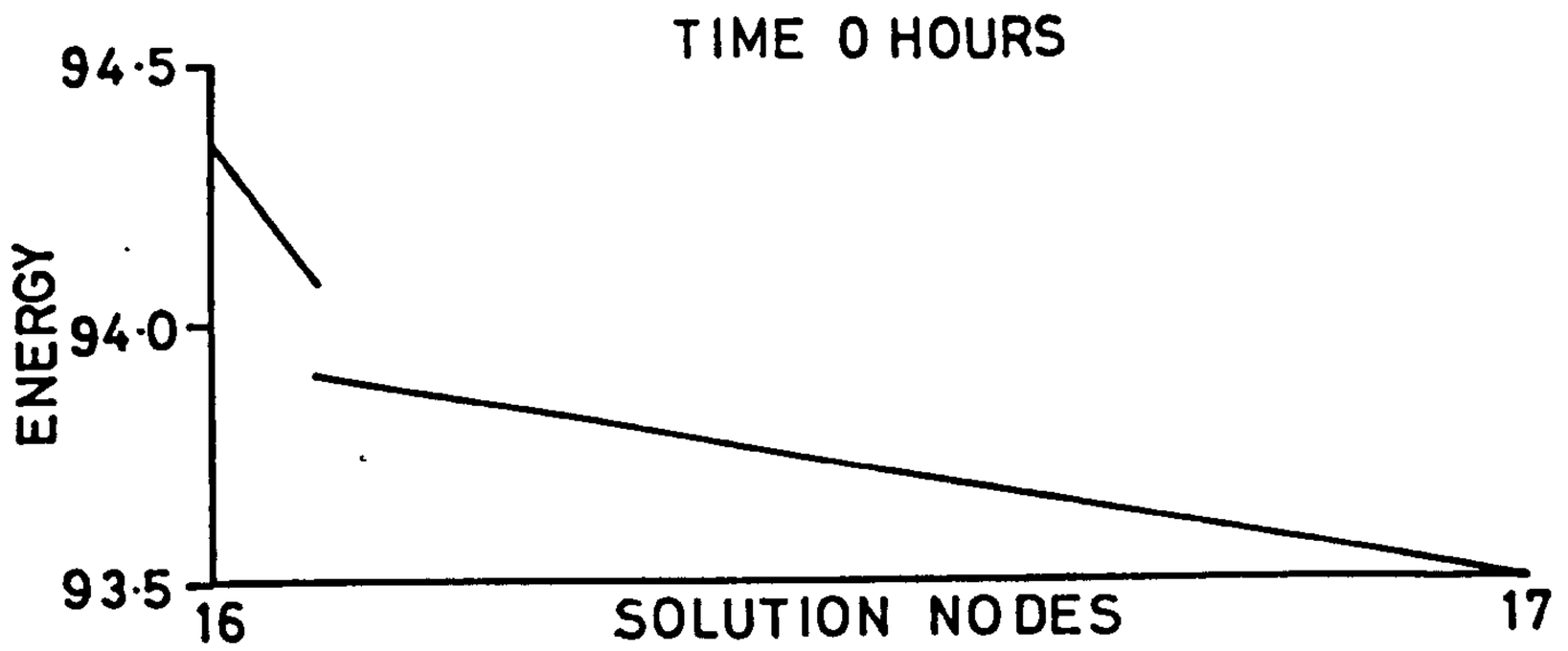

FIGURE 4.14
OPERATION OF CONTROL SECTION.

all the washland areas is not decreased as can be seen in Figure 4.9, for left bank washland 2. The increase in water level at solution node 3 has increased the volume flowing into washland 2 even although the potential for lateral flow has been reduced by 70%. This indicates that each lateral storage pond cannot be calibrated individually but that the system as a whole should be considered during calibration.

4.6.2 INITIAL CALIBRATION CHECKS

In addition to the basic checks on behaviour of the numerical scheme some initial calibration runs to assess the model's ability to reproduce real flow events were undertaken. These used recorded hydrographs at Kildwick as the upstream boundary conditions. Comparisons are made between recorded and simulated hydrographs at Stockbridge. Figure 4.15 shows the comparison between the measured and simulated hydrographs for the flood event of 30th and 31st December, 1981. The model's sensitivity to the value of Manning's 'n' is also illustrated. Hydrographs for the storm events of 22nd to 26th October, 1980 and 26th to 30th October 1980 are shown in Figures 4.16 and 4.17 respectively.

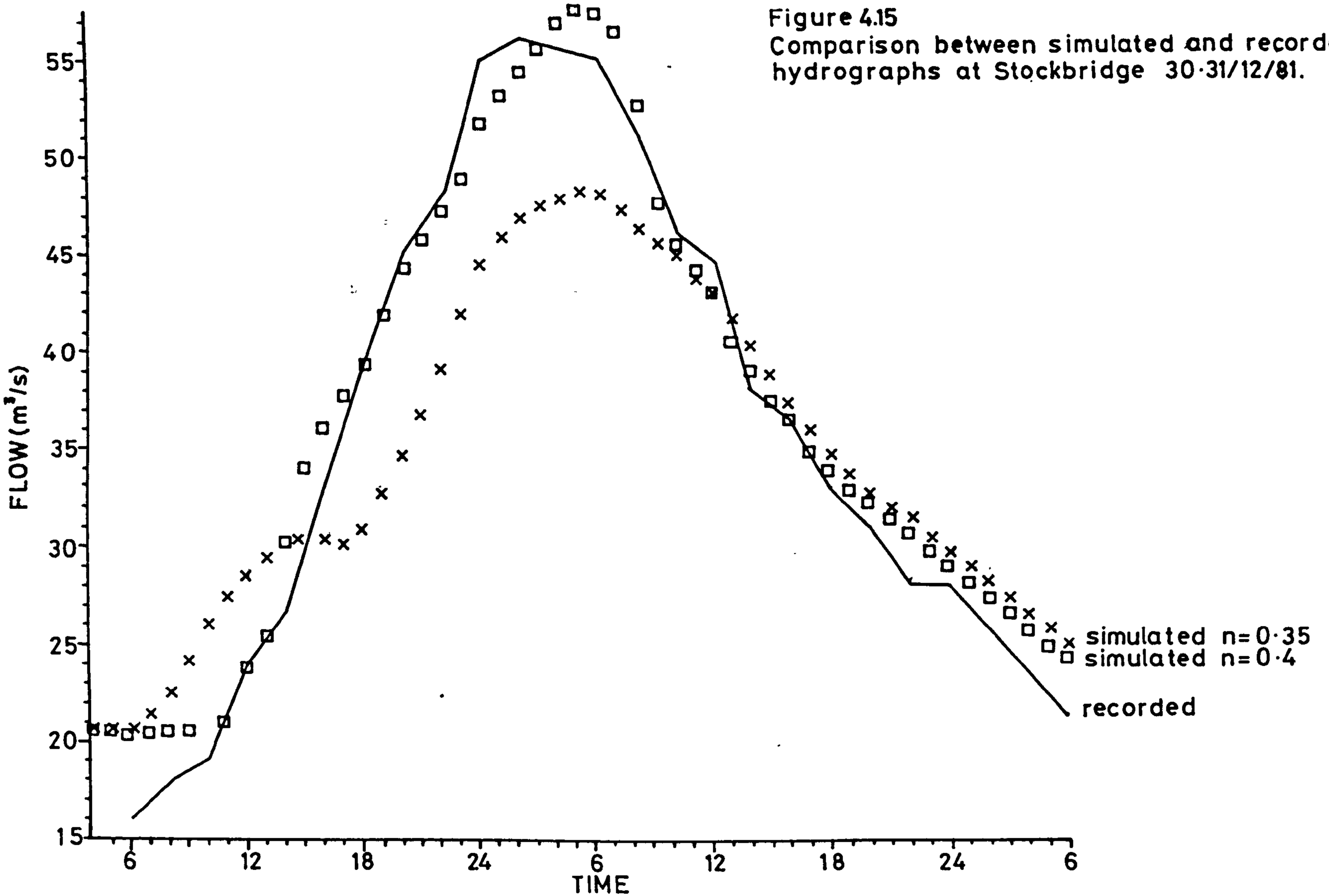

Figure 4.15
Comparison between simulated and recorded hydrographs at Stockbridge 30·31/12/81.

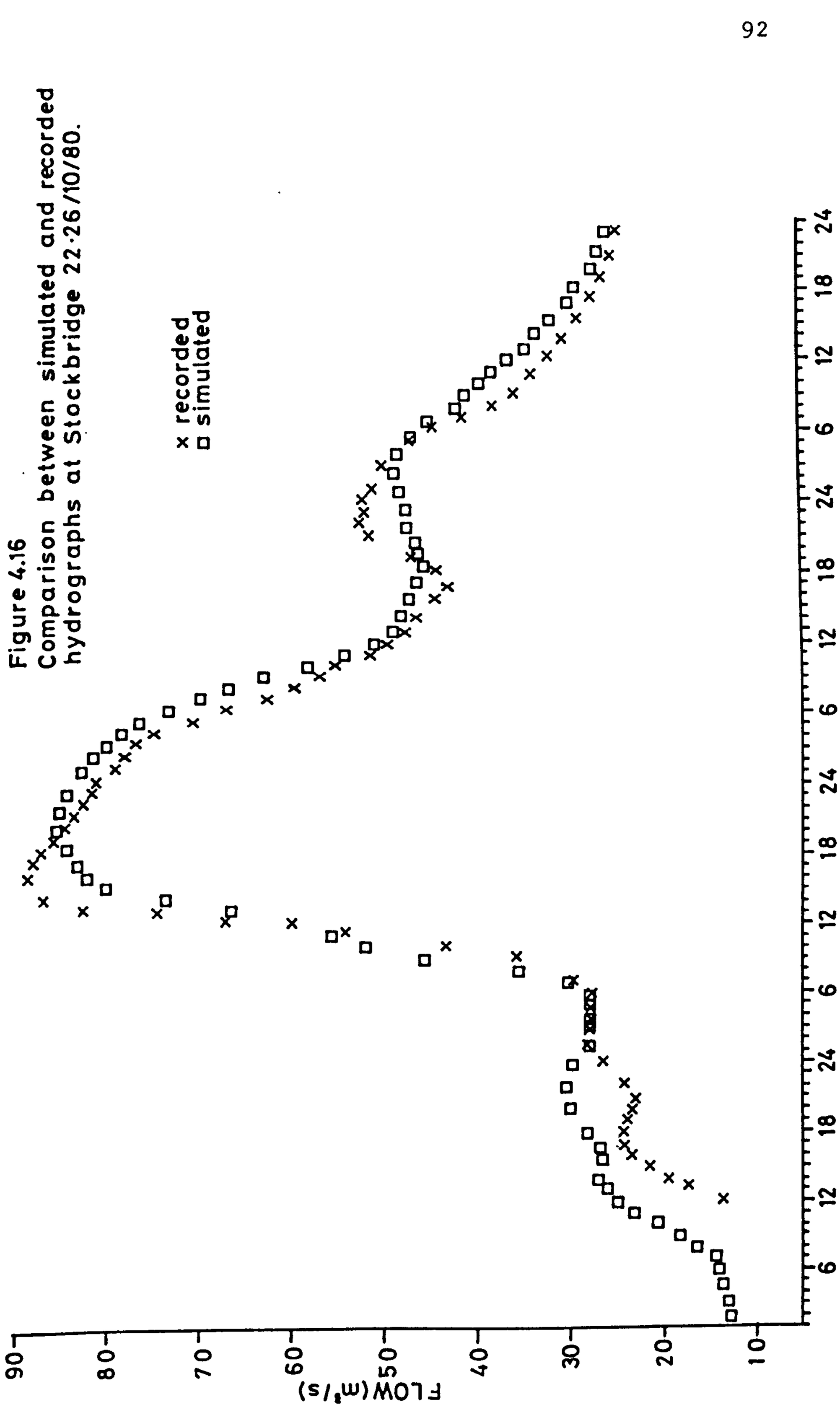

Figure 4.16
Comparison between simulated and recorded hydrographs at Stockbridge 22·26/10/80.

Figure 4.17
Comparison between simulated and recorded hydrographs at Stockbridge 26·30/10/80.

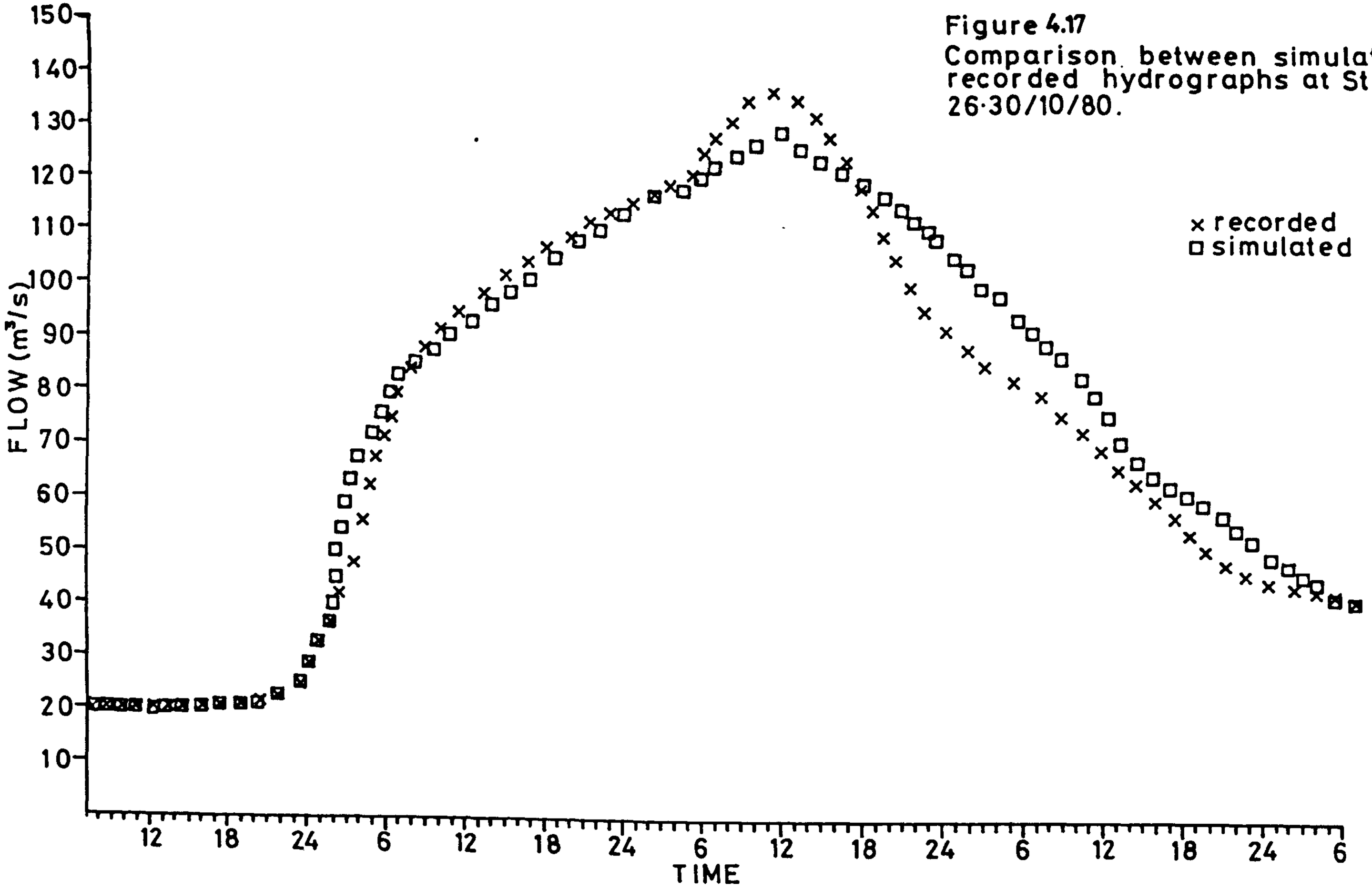

CHAPTER FIVE

NUMERICAL MODELLING OF THE RIVER AIRE WASHLAND SYSTEM

5.1 Introduction

The proposal to construct a new trunk road through Airedale in Yorkshire required that consideration be given to the environmental impact of the route alignment. Alternative routes were the subject of a public enquiry held in 1980 but all are confined to the valley of the River Aire and will occupy part of the river flood plain or washland. In particular the stretch of road between Kildwick and Stockbridge will run almost entirely within the flood plain. To elevate the road above peak flood levels the majority of the road is to be constructed on an embankment. Construction of the new road will, therefore, result in some loss of flood water storage volume either due to direct displacement by the embankment or by divorcing washland storage areas lying behind the new road.

Since flooding from the River Aire into these washlands, Figure 5.1, is of critical importance in protecting areas as far downstream as Leeds from flooding, Yorkshire Water Authority (YWA) expressed the view at the public enquiry that compensatory washland storage should be provided.

It was the opinion of YWA that provision of such compensatory floodwater storage facilities be made prior to road construction in order to avoid the risk of increased severity of flooding both downstream and within the washlands themselves since some of the best agricultural land in

FIGURE 5.1a

Extent of Flooding on 6th January 1982,
Cononley Ings

FIGURE 5.1b

Extent of Flooding on 6th January 1982,
Cononley Ings at Shady Lane

FIGURE 5.1c

Extent of Flooding on 6th January 1982 - Upstream of Kildwick Bridge

FIGURE 5.1d

Extent of Flooding on 6th January 1982 - Upstream of Silsden Bridge

the area lies within the flood plain. The water authority saw the new road as having a potentially serious effect upon flood levels and proposed the use of a mathematical model as a matter of some urgency to establish the effect of the new road construction on the washland system and to examine alternative compensatory schemes. Such a model would also allow the water authority to examine strategies for maintenance and improvement works to the river system and to assess the full extent of any new developments within the valley. As a compensatory scheme could be located upstream of Kildwick, the model would extend from Gargrave to Stockbridge, a distance of 24km, 8km of which will be affected by the proposed trunk road, Figure 5.2.

5.2 THE RIVER VALLEY

The River Aire and its adjoining flood plain or washlands was visualised to respond to flood discharges in a fashion similar to a complex run-of-river regulating reservoir. The river channel is segregated from its washland by a system of flood-banks. Within the washlands, individual compartments are separated from their neighbours by a complex system of cross-banks. Each washland compartment is drained by a system of drainage ditches, many of which have controlled outlets through the embankment. These flood plain elements retain large volumes of flood water which would otherwise increase the severity of flooding downstream.

The catchment has an overall area of 370km^2 above the gauging station at Stockbridge. A further major gauging

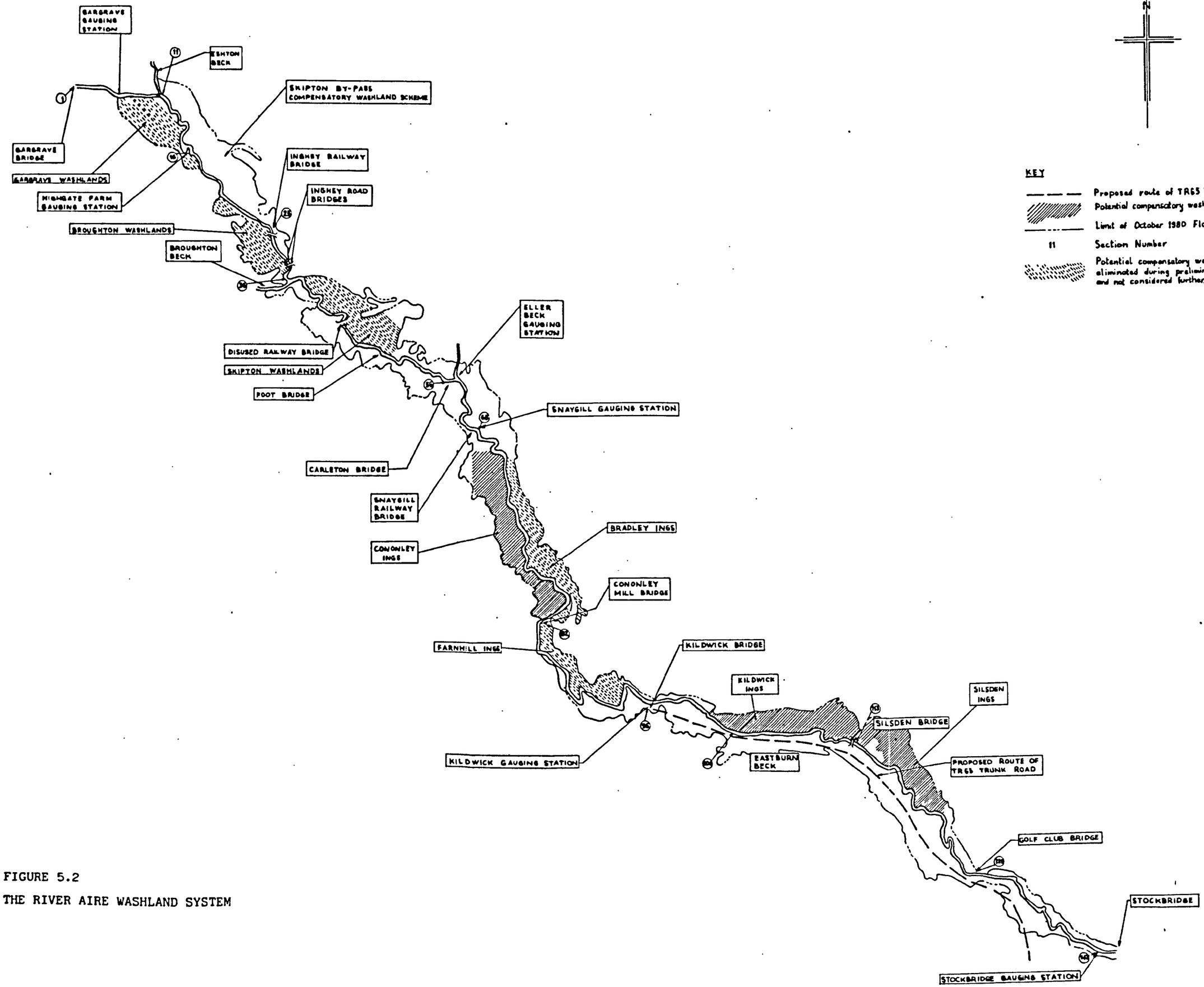

FIGURE 5.2

THE RIVER AIRE WASHLAND SYSTEM

station is located at Kildwick Bridge, the mean flow for this station being 5.4m^3/s. The river channel experiences considerable variations in character over the length of the study area with gradients varying between 1 in 480 and 1 in 25,000. The steeper reaches are generally at the upstream end of the study area between Gargrave and Skipton. A number of important tributaries enter the River Aire and amongst these are Eshton Beck, Broughton Beck, Eller Beck and Eastburn Beck. The river is crossed by both road and rail bridges at several locations, namely at Gargrave, Inghey, Carleton, Snaygill, Cononley, Kildwick, Silsden and Stockbridge.

5.3 MODEL CAPABILITIES

Following an initial visit to the study area the necessary capabilities of the numerical model were identified. The model was required to determine the variations of flow rate and water level with time throughout the length of the defined area of investigation. It was essential that the calculations should include all aspects relating to loss of energy by the flow in passing through the channel. This included the effects of fluid resistance, losses due to irregularities of channel geometry, meanders and the like. Also a means of representing additional head loss at bridge constrictions was required.

The model had to be able to detect and analyse a control section should it arise anywhere within the study area during the course of computations. Control sections may be present throughout the period of flood wave propagation,

such as Gargrave Weir, or a control may be present at low flows and become drowned at higher water levels and flow rates. Since a large proportion of the water entering Airedale derives from tributary inflows all significant tributaries and streams entering the study area were included in the model in the form of inflow hydrographs at the confluence. Exchanges of water between the River Aire and the adjoining washlands were modelled as a series of lateral inflows or outflows from the river. The corresponding variations in washland water level were calculated throughout the period of the flood wave. The influence of the river channel downstream of Stockbridge was represented by the rating curve for the gauging station at that location.

5.4 FIELD SURVEY

Adequate definition of the river channel characteristics and those of its adjoining washland storage areas required a considerable survey effort. River cross-sections were surveyed at intervals of approximately 250 metres, although closer distance increments were used where necessary. The longitudinal profiles of left and right banks of the river were also surveyed. Washland storage areas were defined by ground levels measured throughout the extent of the flood plain by aerial survey. By means of contouring and use of a planimeter the surface area of each storage area was determined as a function of water level in the washland compartment. Dependent upon the size of individual washland compartments it is possible for one compartment to extend over a number of river reaches; a reach being

defined as the length of river between one cross section and the next.

5.5 NUMERICAL DEFINITION OF THE RIVER BASIN

It was considered that computation of the channel properties and overbank flow characteristics, prior to the start of any water surface profile or flood routing calculations, would yield some saving of computer time. Survey data of the river channel was tabulated in the form of co-ordinates spaced around the periphery of the cross-section, Figure 5.3. The co-ordinates 'b' and 'h' defining points on the section were input to the computer together with the location and estimated roughness coefficient of the section. Using a data processing programme the cross-sectional properties were generated using the method described by Smith (1968). These properties were tabulated as a function of water level from the invert of the channel to the highest anticipated water level. Those properties stored for future computations were top width 'B', cross-sectional area 'A', conveyance 'K' and the critical flow 'Qcr'.

River bank characteristics were established by a survey which provided profiles of bank level with distance along the bank, Figure 5.4. These were tabulated in the form of co-ordinates 'b' and 'h' and input to the computer. Assuming the river bank to form an irregular weir, the weir discharge was computed for a range of water levels extending upwards from the lowest point of the bank.

Figure 5·3

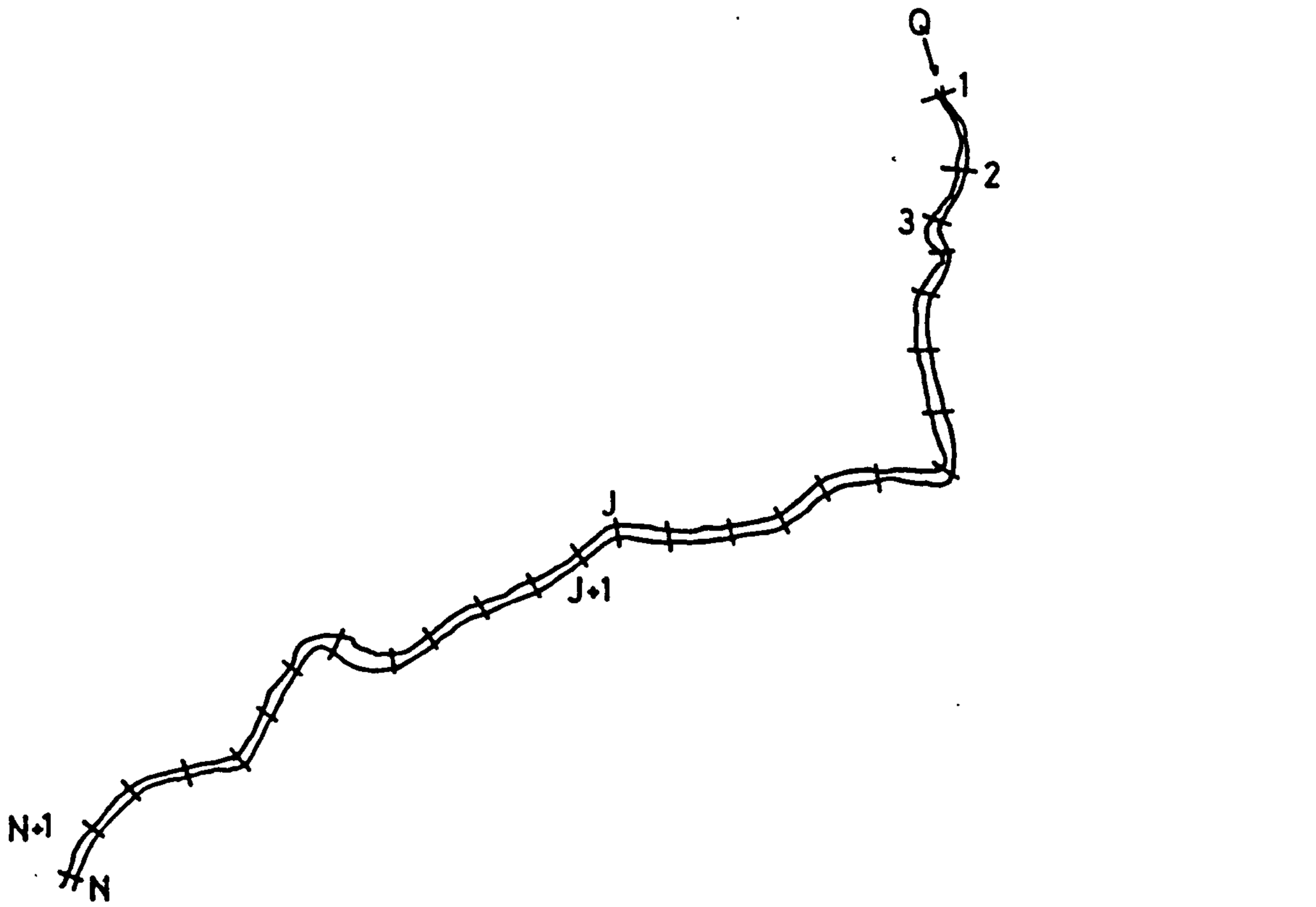

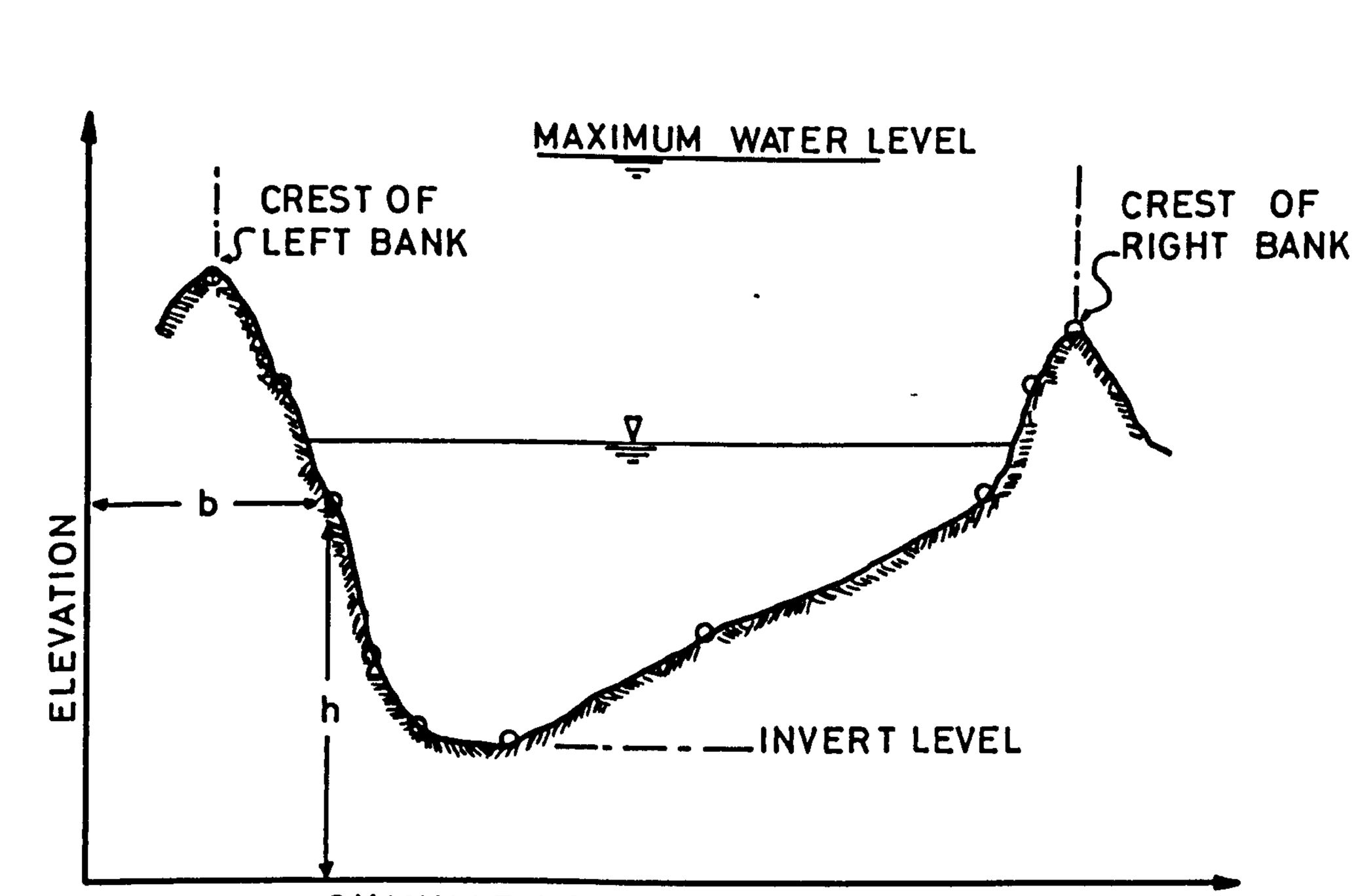

TYPICAL CROSS-SECTION 'J'

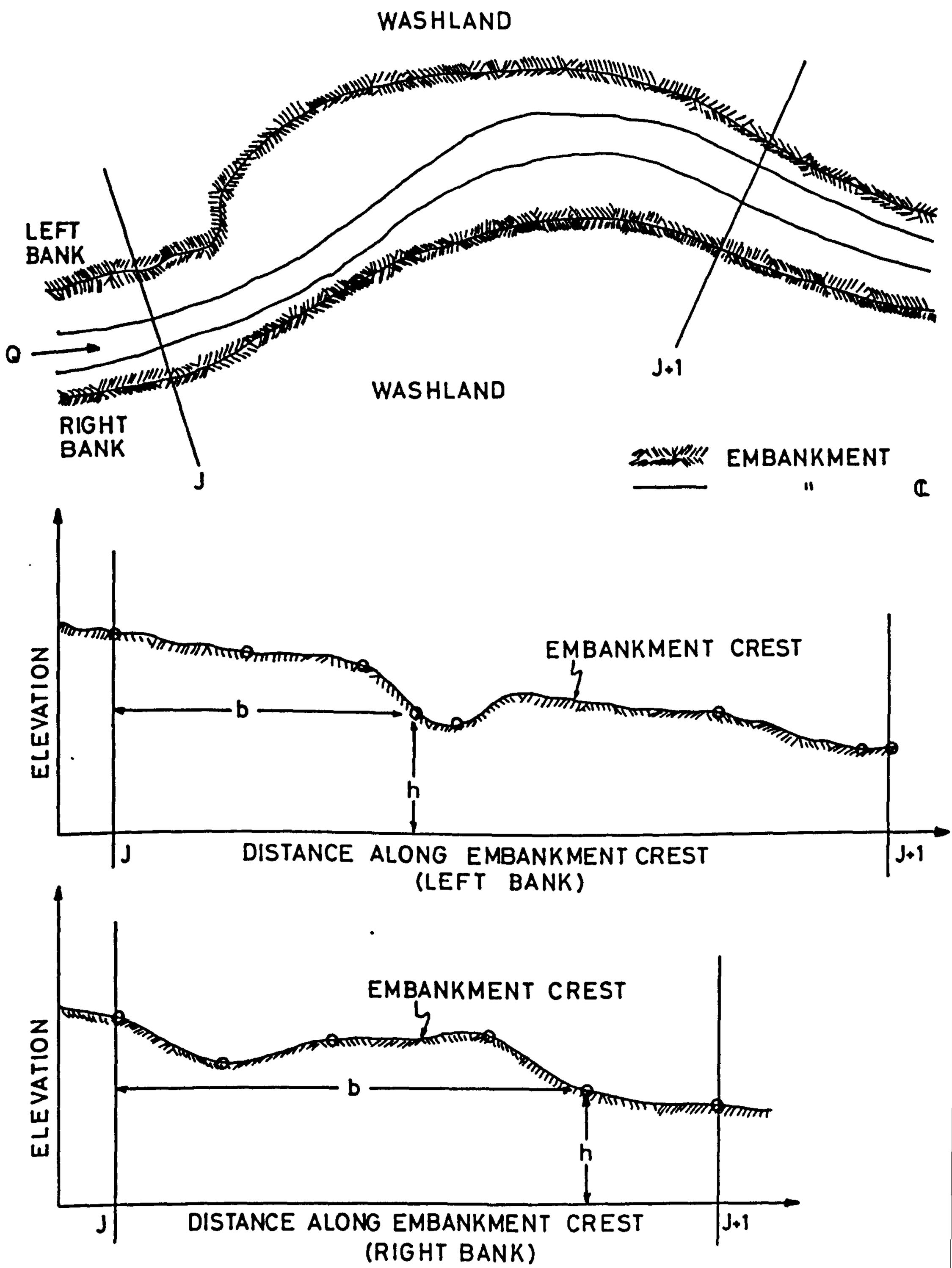
WASHLAND
LEFT BANK
Q
RIGHT BANK
J
J+1
WASHLAND
EMBANKMENT
"
℄
ELEVATION
b
h
EMBANKMENT CREST
J
DISTANCE ALONG EMBANKMENT CREST
(LEFT BANK)
J+1
ELEVATION
EMBANKMENT CREST
b
h
J
DISTANCE ALONG EMBANKMENT CREST
(RIGHT BANK)
J+1

Figure 5·4

The storage capacity of individual washland areas was based on aerial survey information which covered the entire study area. The first step was to schematize washland areas. Washlands were represented as a single tier of storage areas on either side of the river, each storage area covering from one up to a maximum of five river reaches. It was convenient to sub-divide washland areas at natural cross-banks, a tributary, or at a road crossing the valley transversely. In other areas rising ground close to the river means that no washland exists and this forms a natural boundary to adjacent washlands. Fences, walls and hedges were assumed not to act as significant barriers to flow in the washland system. A minimum size of storage area was set such that a compartment would not be completely filled within one time increment. Outflow from a storage compartment would normally be via a river reach immediately adjacent to that compartment. However, it is also possible for outflow to be transferred further downstream or bypass round behind the next downstream storage compartment.

Once the washlands had been schematised on this basis the storage areas on each side were numbered consecutively starting at the storage area farthest upstream. The boundaries of the storage areas were defined on 1:25000 aerial survey plans and within each storage compartment the surface area was measured, using a planimeter, at 0.5m intervals, starting at the lowest contour in the washland and finishing at the contour nearest to the highest expected

flood level. This data was then entered in the washland data file. Where no washland exists this is represented in the file by inserting a zero at the relevant river reaches. Other files could be made up to represent the washland system with the road embankment constructed and compensatory washland schemes under examination inserted. Initial water levels in individual compartments are held in a separate file as some compartments may be partially full at the start of a flood simulation.

5.6 ORGANISATION OF PROGRAMMES AND DATA FILES

Figure 5.5 illustrates the way in which the various data files and programmes are used in the model. In addition to the main flood routing programme (FLOOD) the model uses a suite of programmes for data pre-processing (PROC1 and PROC2), calibration (CALIB, OBANKEDIT and FLAIREDIT) and presentation of results (PEAK and PLOT). The programme (STARTUP) calculates water surface profiles under steady flow conditions and is used to supply initial water surface levels for the main programme and for preliminary calibration. There are a total of eleven data files. Raw channel cross-section data held in the AIRDA file is pre-processed into the PRES file for direct input to the main programme or the STARTUP programme. Bankheight data is similarly pre-processed from the AIREBANK file to the OBANK file. Before a full run is carried out water surface levels at the start of the run are generated using the STARTUP programme together with initial flows (STATQS file), channel data (PRES file), the downstream rating

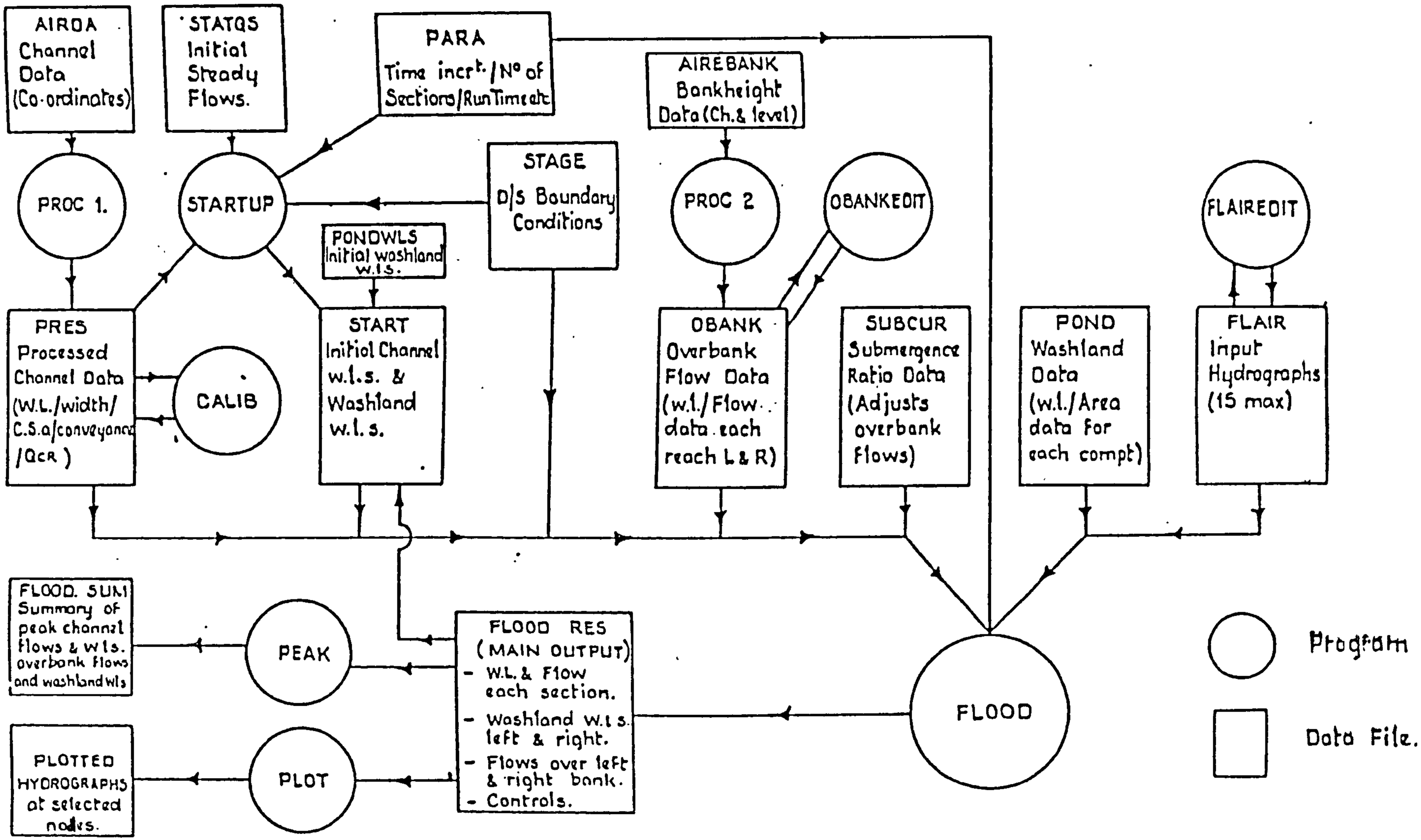

FIGURE 5·5 PROGRAMS AND DATA FILES USED IN MODEL - SCHEMATIC DIAGRAM

curve (STAGE file) and a list of global parameters (PARA file). These initial river levels are merged with initial washland water levels (PONDWLS file) to produce the START file. Each main run uses the PRES, START, STAGE, OBANK and PARA files together with input hydrograph data (FLAIR file), washland data (POND file) and overbank flow submergence data (SUBCUR file). The results can be output for each time increment in terms of river flow, river water level and overbank flow at each section together with water levels in each washland. Alternatively, these results are scanned for peak values or hydrographs plotted at selected points.

5.7 DESCRIPTION OF THE AIREDALE MODEL

The schematic representation of the Airedale Washland system, on which the model is based, is shown in Figure 5.6. The channel is defined by 142 cross sections from Gargrave Bridge to the gauging station at Stockbridge. Provisional values of channel roughness coefficient were based on site observations of the channel characteristics. Mannings 'n' values were generally between 0.03 and 0.035 but values could be increased locally to take account of features such as meanders and bridges. Resulting values of channel conveyance would later be adjusted during calibration, taking account of river stage as well as longitudinal variations in roughness.

The afflux at all of the major bridge crossings had been observed by measuring peak flood levels on either side of the bridge for a number of recorded flood events

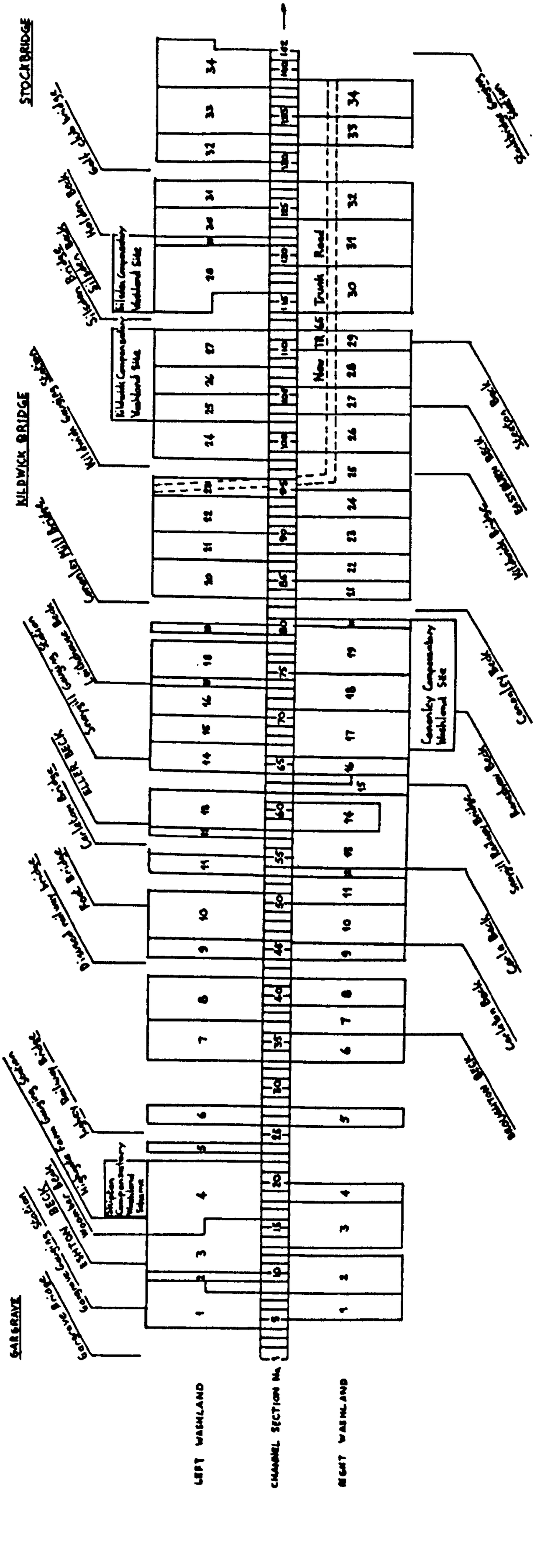

FIGURE 5·6 SCHEMATIC REPRESENTATION OF RIVER CHANNEL AND WASHLANDS

and this data proved very useful in calculating loss coefficients for the bridges. Loss coefficients were expressed as an equivalent value of Mannings 'n' and inserted into the data for the appropriate bridge section. At each bridge location additional cross sections had been surveyed a short distance upstream and downstream of the bridge to allow more accurate modelling of the constriction caused by the bridge.

After pre-processing bank height data a reduction factor was applied to the tables of overbank flows derived. As discussed earlier overbank flows are calculated on the basis of a theoretically perfect, streamlined and friction-less broad-crested weir. The reduction factor which was applied initially takes into account the losses involved in flow over a grassed embankment similar in shape to the flood banks in Airedale. The factor could later be adjusted during calibration.

The washland system is represented by 34 storage compartments along the left bank and 34 along the right bank. The final route of the new trunk road was established in November 1982, and this enabled a series of washland data files to be made up which represented:

i. the existing washland system.

ii. the existing system with the new road embankment constructed and divorced washlands fully connected through the embankment by a system of culverts.

iii. as ii, but with divorced washlands

not reconnected.

In addition, potential compensatory washland schemes could be incorporated by modifying the washland and bank height data files.

In addition to the flow in the River Aire at Gargrave for which flow records were available tributary inflows were also included for the four major tributaries (Eshton Beck, Broughton Beck, Eller Beck and Eastburn Beck) and nine minor tributaries. Rather than model overland flow to the river as a unit flow per metre length of river these relatively small flows were assumed to enter the river at discrete points and were distributed to the nearest tributary inflow.

5.8 FLOOD HYDROGRAPHS

Flood records and rating curves were available for the main gauging stations at Gargrave, Kildwick Bridge and Stockbridge. Records of river stage only were also available for gauges at Highgate Farm and Snaygill. Calibration and prototype runs were based on the following flood events for which a considerable amount of additional data, in the form of peak water levels both in the river and in washlands, had been collected:

Flood Event	Return Period
26th-30th October 1980	50 years
2nd-6th January 1982	7 years
22nd-25th October 1980	2 years

A fourth flood which did not exceed bankfull conditions was also used for initial calibration of channel roughness

coefficient.

The combined catchment areas of the tributaries is 76% of the overall catchment area upstream of Stockbridge. Tributary flows are therefore a major contribution to the total flow in the river. The only tributary which is gauged is Eller Beck but the data for this gauging station was of limited use as it is close to the confluence with the River Aire and becomes drowned out when water levels rise in the main river. It was therefore necessary to synthesise hydrographs for the four main tributaries and nine minor tributaries using recorded rainfall data for the flood events being considered.

A first attempt to synthesise these hydrographs was made using data from the autographic raingauges located within or adjacent to the catchment area and following the Unit Hydrograph Method outlined in Vol 1 of the Flood Studies Report. Problems were however encountered in distributing the rainfall intensities over the individual tributary catchments and it was not possible to obtain any clear idea of the movement of the storm to accurately predict the respective times at which the tributary hydrographs would contribute to the flow in the main river. These problems were overcome by making use of weather radar data available for the events being considered. Comparison of recorded hydrographs with those which had been synthesised for the River Aire at Gargrave showed that a much closer estimate of the tributary hydrographs had been obtained using the radar data.

5.9 CALIBRATION OF THE MODEL

Calibration of the model was based on achieving a reasonable correlation between synthesised and recorded flow hydrographs at the Stockbridge and Kildwick Bridge gauging stations for the three main flood events being considered. Stage hydrographs at Highgate Farm and Snaygill and additional data on peak water levels assisted with calibration.

The following sequence of adjustments to the various data files was adopted for calibration:

i. Using the STARTUP programme runs were carried out under steady flow conditions to check and adjust channel conveyance values using the CALIB programme.

ii. Commencing with the 50 year flood the main FLOOD programme was run and resulting hydrographs and peak flows/water levels compared with recorded data.

iii. The best correlation possible was then obtained by adjusting the reduction factor applied to the overbank flow data and further refining the channel conveyance values.

iv. Calibration of the 50 year flood was then completed by making adjustments to the timing, magnitude and shape of the synthesised tributary hydrographs.

v. Step iv. was then repeated for the other floods being considered.

Whereas adjustment of channel conveyance values had the expected effect of significantly altering channel water levels and the time to peak for a particular hydrograph, it did not significantly affect peak flow values. Variation of the reduction factor applied to overbank flows had a relatively small effect in the range 50% to 70%. In general a factor of 50% gave the best results. Higher reduction factors exceeding 70% had to be applied in some cases, however, where trees, bushes or other obstructions impeded the flow across the flood banks. It was known that for the 50 year flood some of the washlands were partially filled as a result of the preceding 2 year flood. Estimates of initial washland water levels were based on a preliminary run of the 2 year flood but some further adjustment was necessary to obtain a satisfactory final calibration with observed peak washland water levels. For the 7 year and 2 year floods the washlands were assumed to be empty at the start of the flood. Final adjustment of the tributary hydrographs was the most difficult part of the calibration phase as the timing of peak flow and shape of each of the tributary hydrographs, particularly those for the four main tributaries, had significant effect on the overall calibration.

Final calibration of the model resulted in the synthesised hydrographs at Stockbridge and Kildwick Bridge which are shown in Figures 5.7, 5.8 and 5.9. The overall

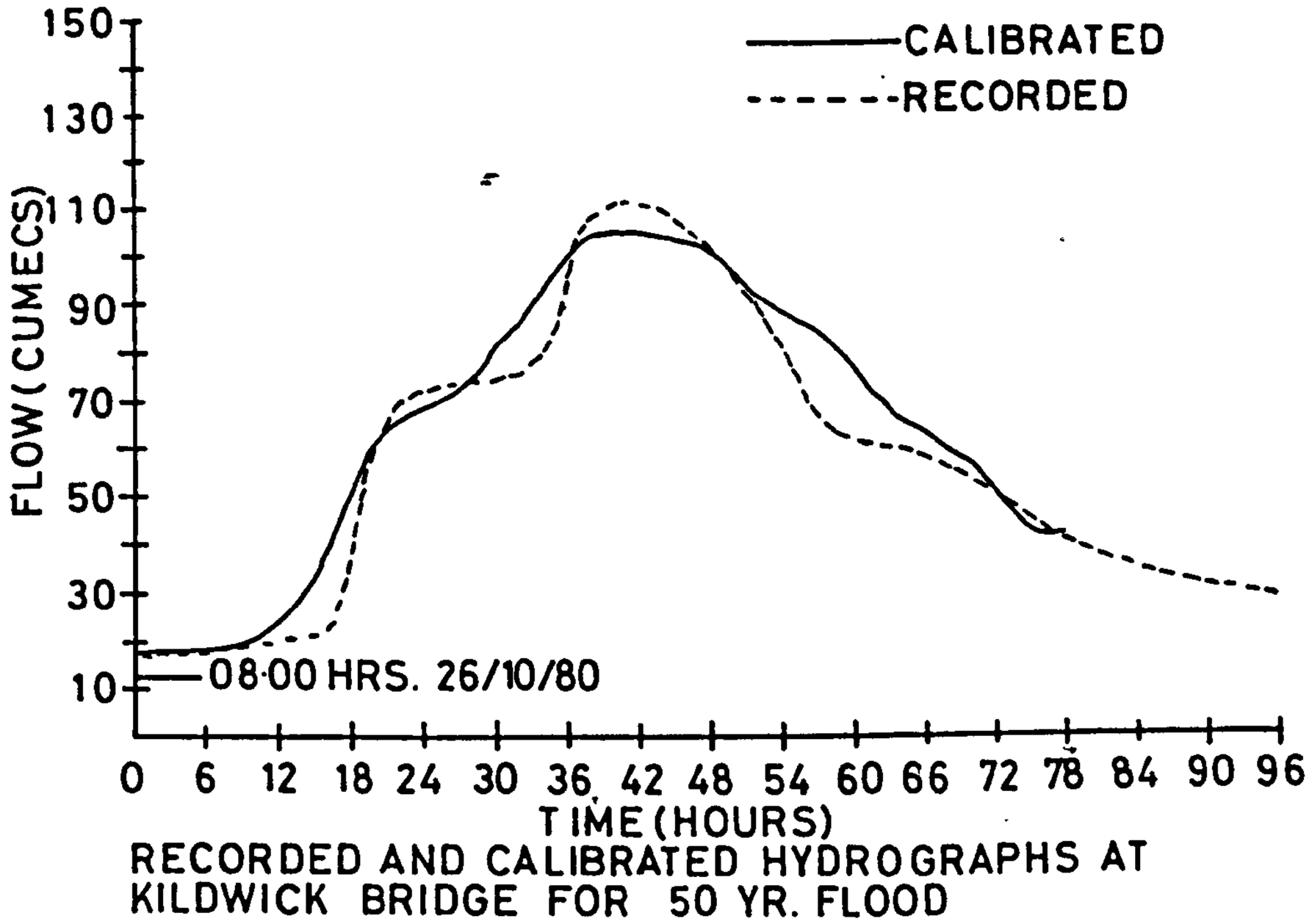

RECORDED AND CALIBRATED HYDROGRAPHS AT KILDWICK BRIDGE FOR 50 YR. FLOOD

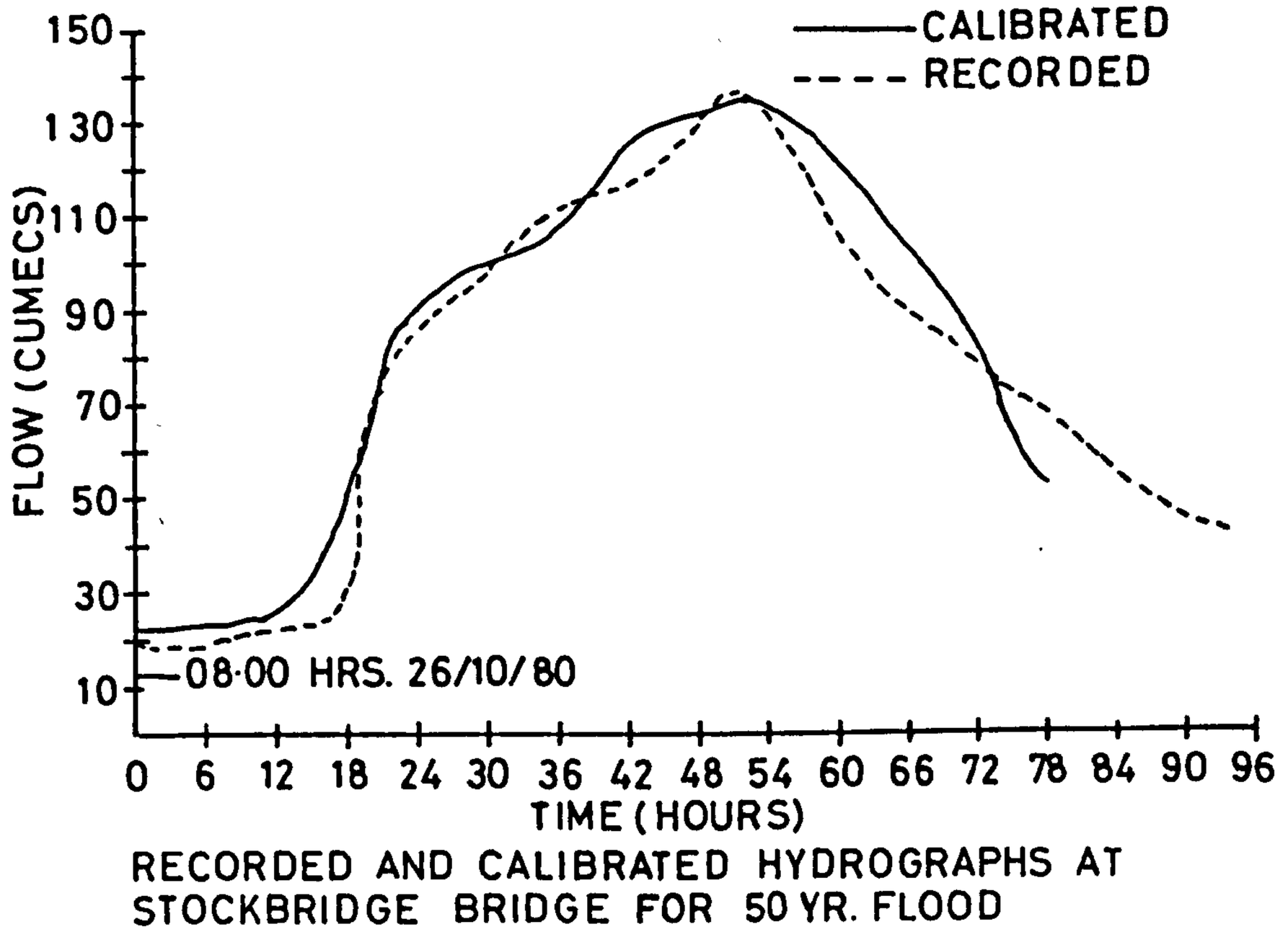

RECORDED AND CALIBRATED HYDROGRAPHS AT STOCKBRIDGE BRIDGE FOR 50 YR. FLOOD

FIGURE 5·7

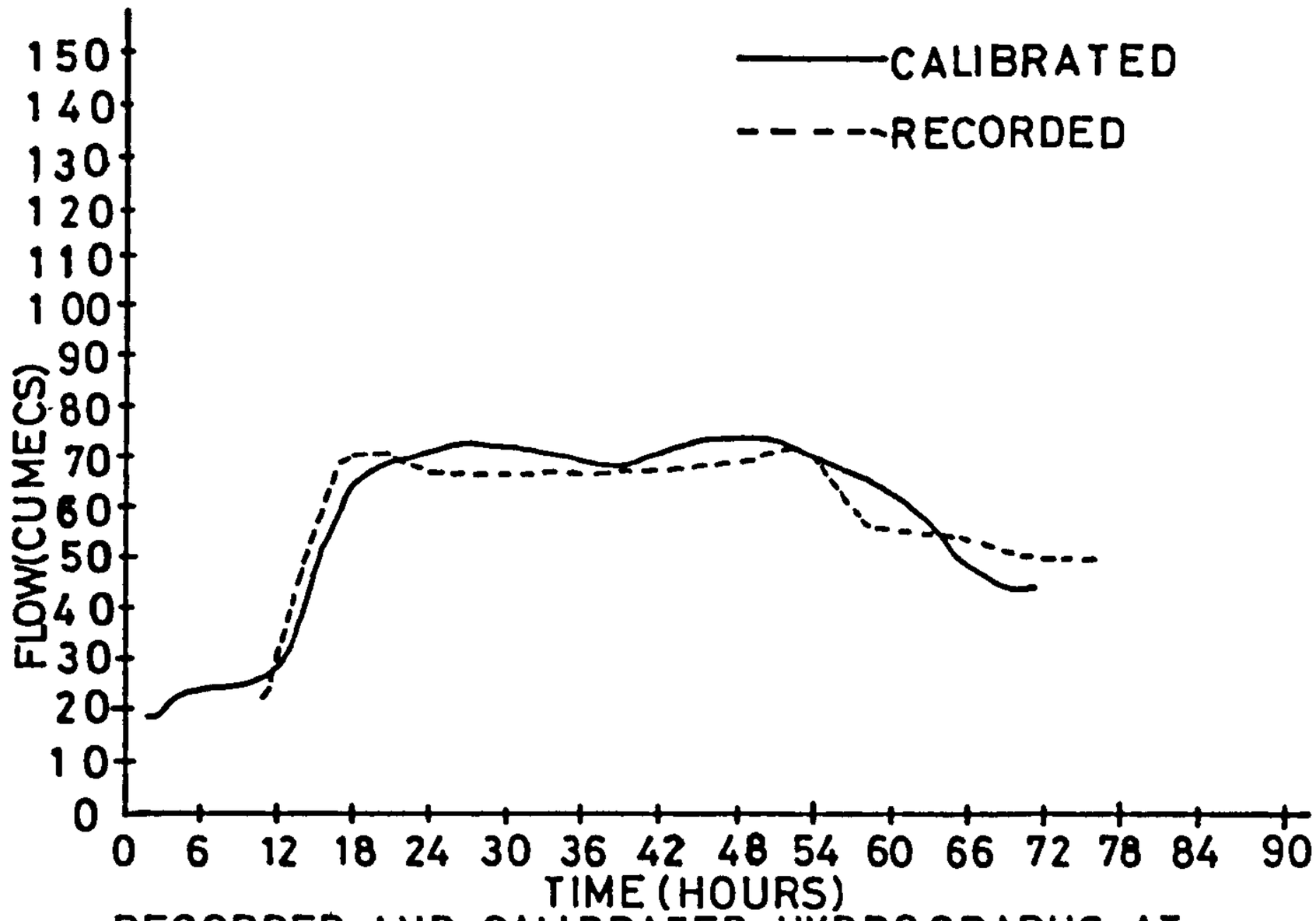

RECORDED AND CALIBRATED HYDROGRAPHS AT KILDWICK BRIDGE FOR 7YR. FLOOD.

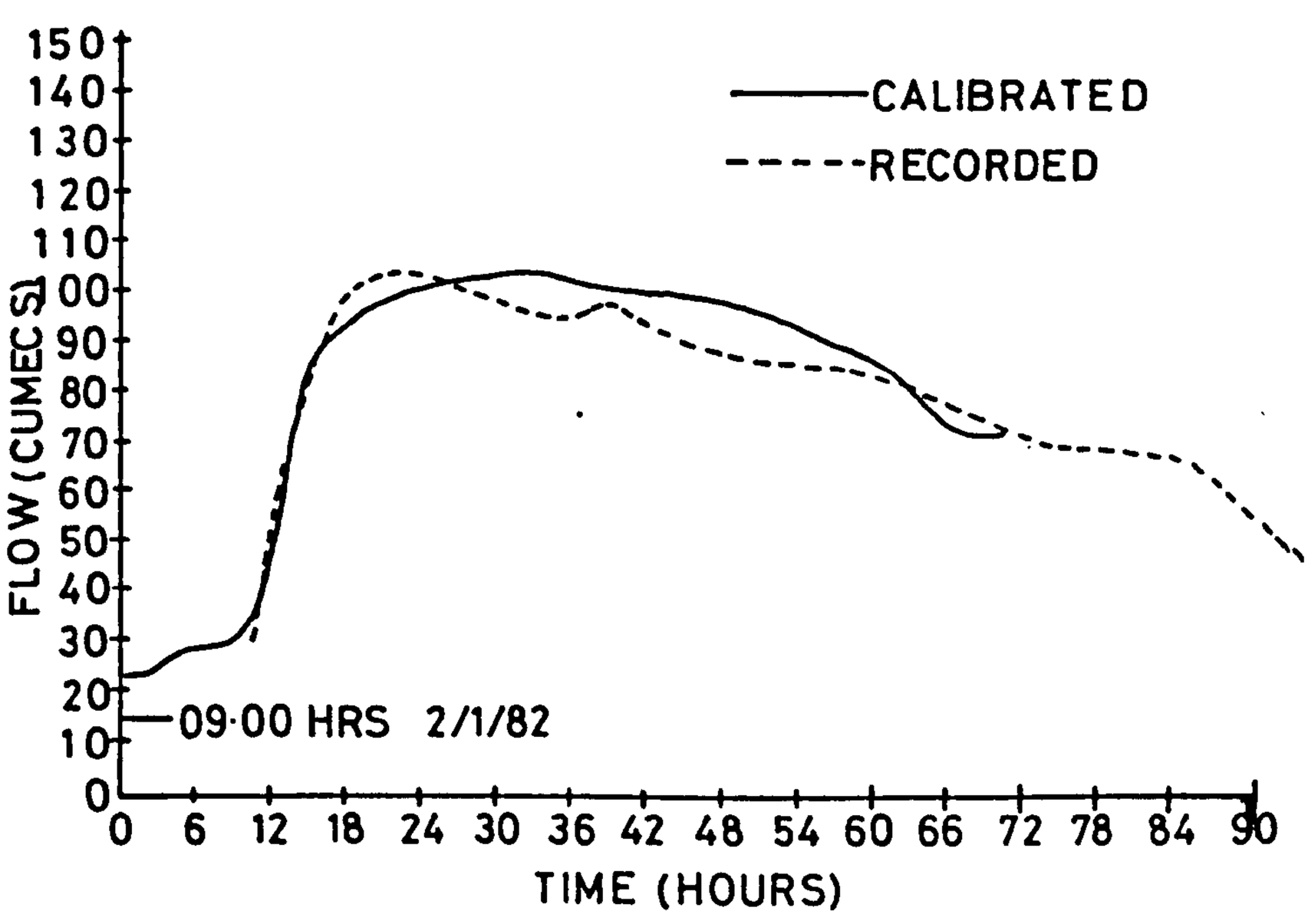

RECORDED AND CALIBRATED HYDROGRAPHS AT STOCKBRIDGE FOR SEVEN YR. FLOOD.

FIGURE 5·8

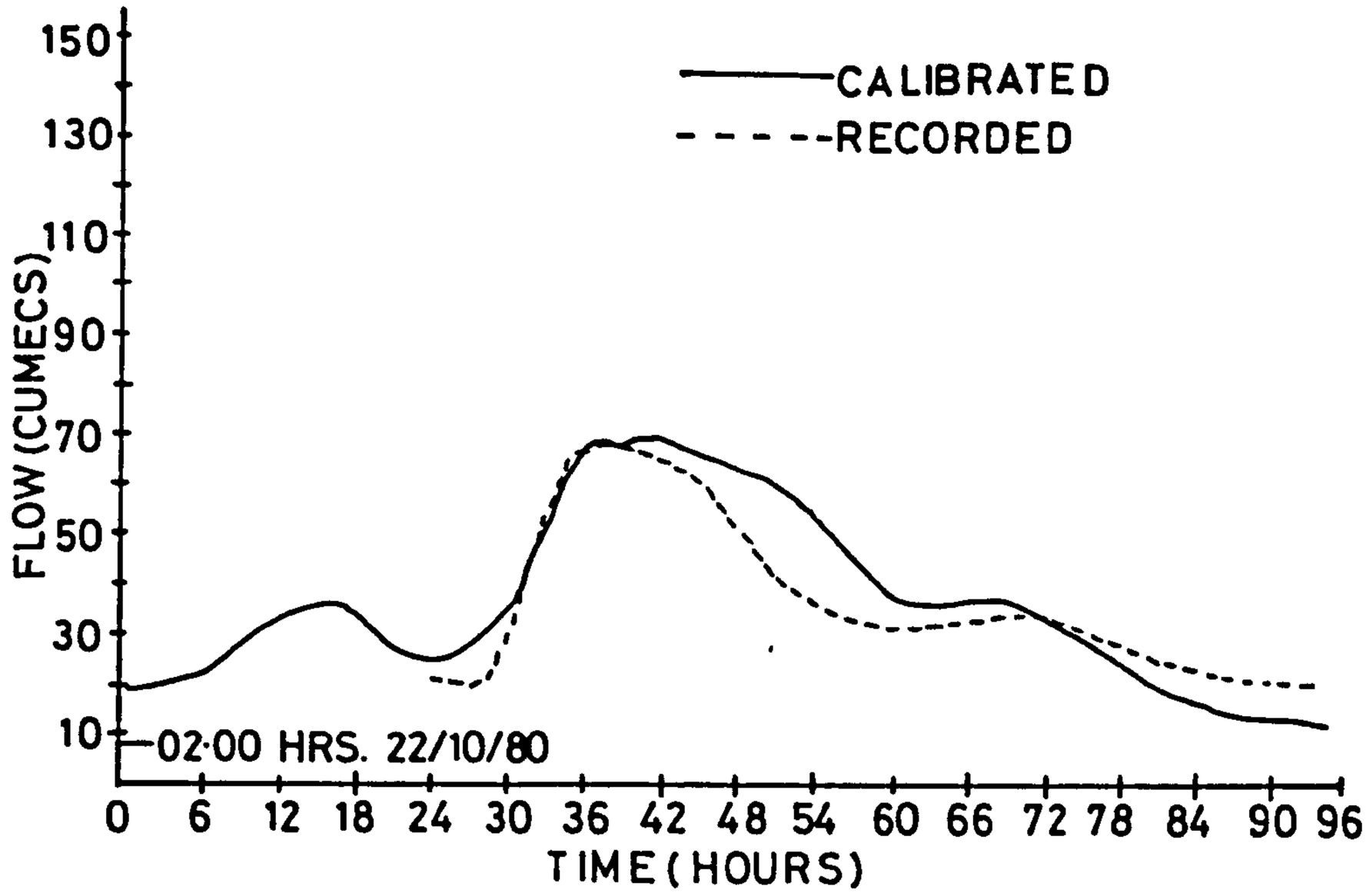

RECORDED AND CALIBRATED HYDROGRAPHS AT KILDWICK BRIDGE FOR 2YR. FLOOD

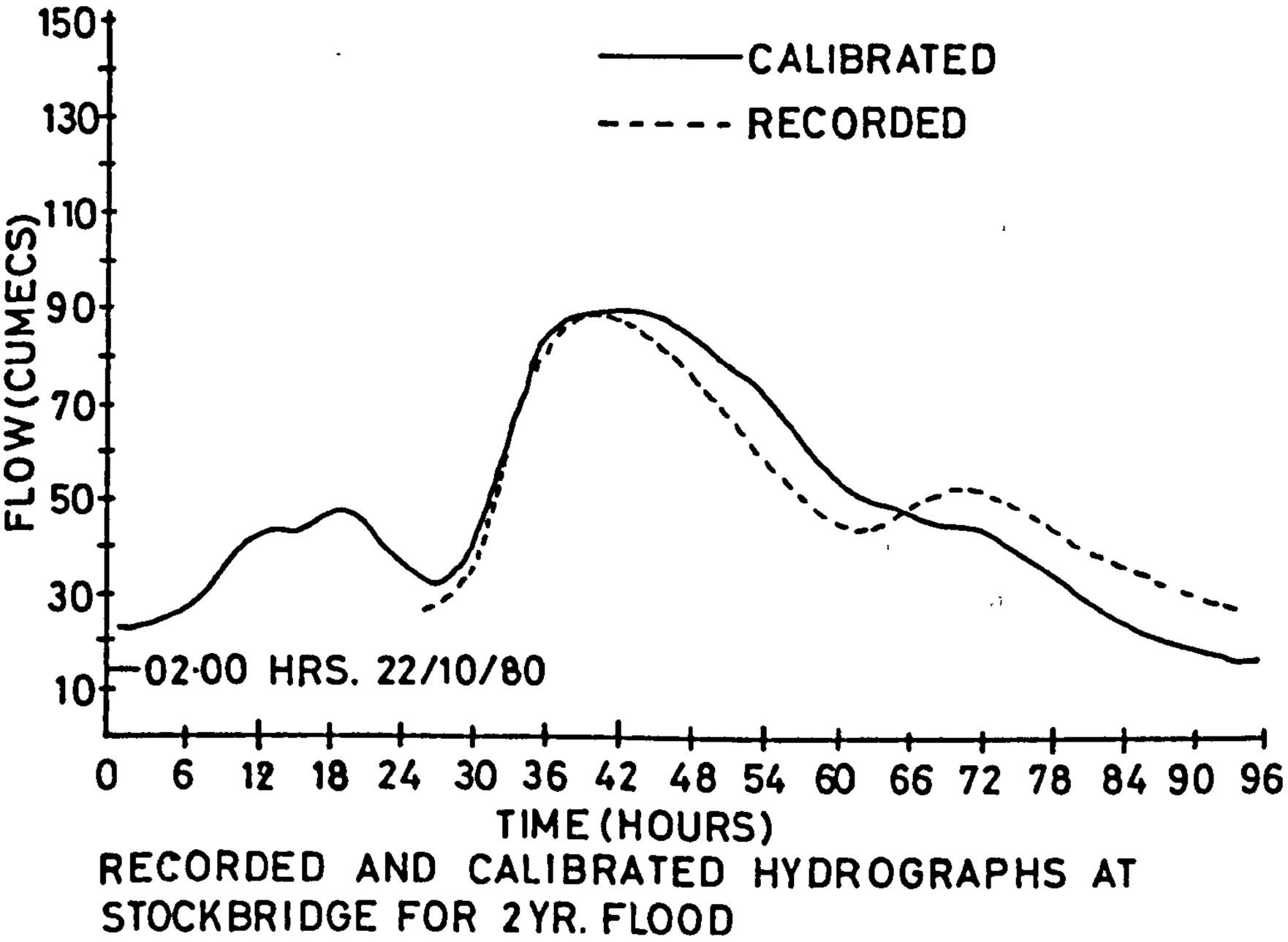

RECORDED AND CALIBRATED HYDROGRAPHS AT STOCKBRIDGE FOR 2YR. FLOOD

FIGURE 59

fit of the hydrographs was generally considered to be good. At Stockbridge the synthesised peak flows are very close to recorded peak flows and the overall shape of the hydrographs was considered to be satisfactory for the purposes of assessing the effect of the new road and examining alternative compensatory schemes.

5.10 EFFECT OF NEW ROAD EMBANKMENT

The criteria adopted for the design of compensatory works stipulated that there should be no detrimental alteration to existing flood hydrographs at Stockbridge. Design would also be to a 50 year flood flow standard. The effect of the new road on the Stockbridge hydrographs, particularly the 50 year flood hydrograph, was therefore of primary interest.

The washland data files were adjusted to model the final alignment of the new road and on the basis that divorced washlands could be fully connected through the road embankment the results sumarised in Table 5.1 were obtained. The corresponding hydrographs at Stockbridge for the 50 year and 7 year floods are shown in Figure 5.10. Although peak flows were increased albeit to a lesser extent than might have been expected, the basic shape of the hydrographs was not significantly alterated by the new road embankments.

Water levels were shown to be influenced as far upstream as Cononley Bridge and peak water levels in the washlands between Cononley and Stockbridge would generally be raised by up to 73mm for the 50 year flood.

Run No.	Description	Flood Event Return Period (in yrs)	Peak Flow at Stockbridge (m^3/s)	Increase in Peak Flow at Stockbridge Relative to Existing System (m^3/s)	Peak W.L. at Stockbridge (m A.O.D.)	Change in Peak W.L. at Stockbridge Relative to Existing System (mm)
G1	Existing System (calibrated)	50	136.98	-	84.919	-
G2	Existing System (calibrated)	7	103.79	-	84.430	-
G3	Existing System (calibrated)	2	88.69	-	84.182	-
G4	New Road Constructed	50	139.83	+2.85	84.962	+43
G5	do do	7	105.44	+1.65	84.455	+25
G6	do do	2	88.74	+0.05	84.183	+1

Table 5.1

SUMMARY OF RESULTS FROM FULL LENGTH MODEL : EFFECT OF NEW ROAD EMBANKMENT
(DIVORCED WASHLANDS CONNECTED)

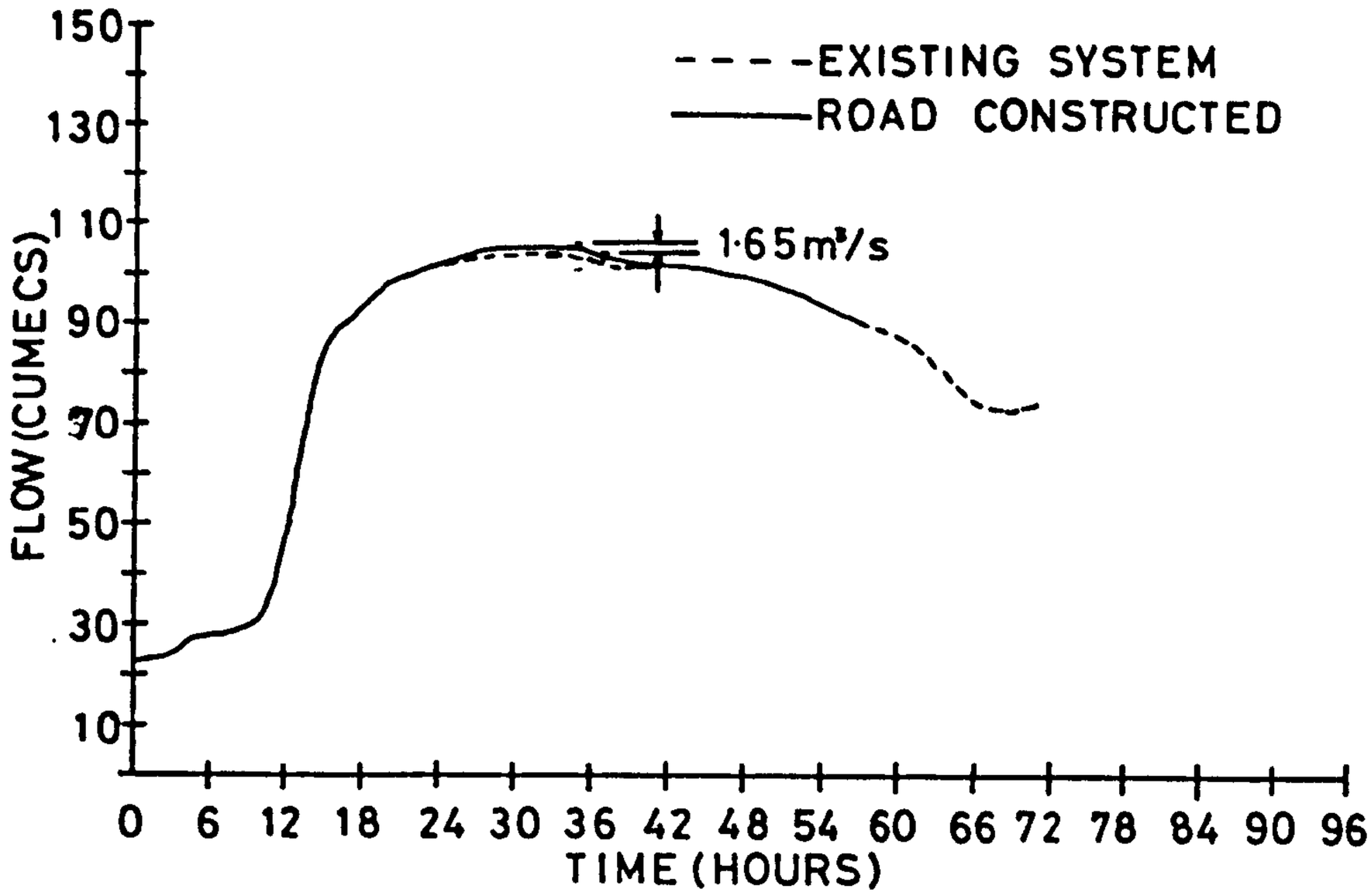

7YR. HYDROGRAPH AT STOCKBRIDGE SHOWING EFFECT OF NEW ROAD

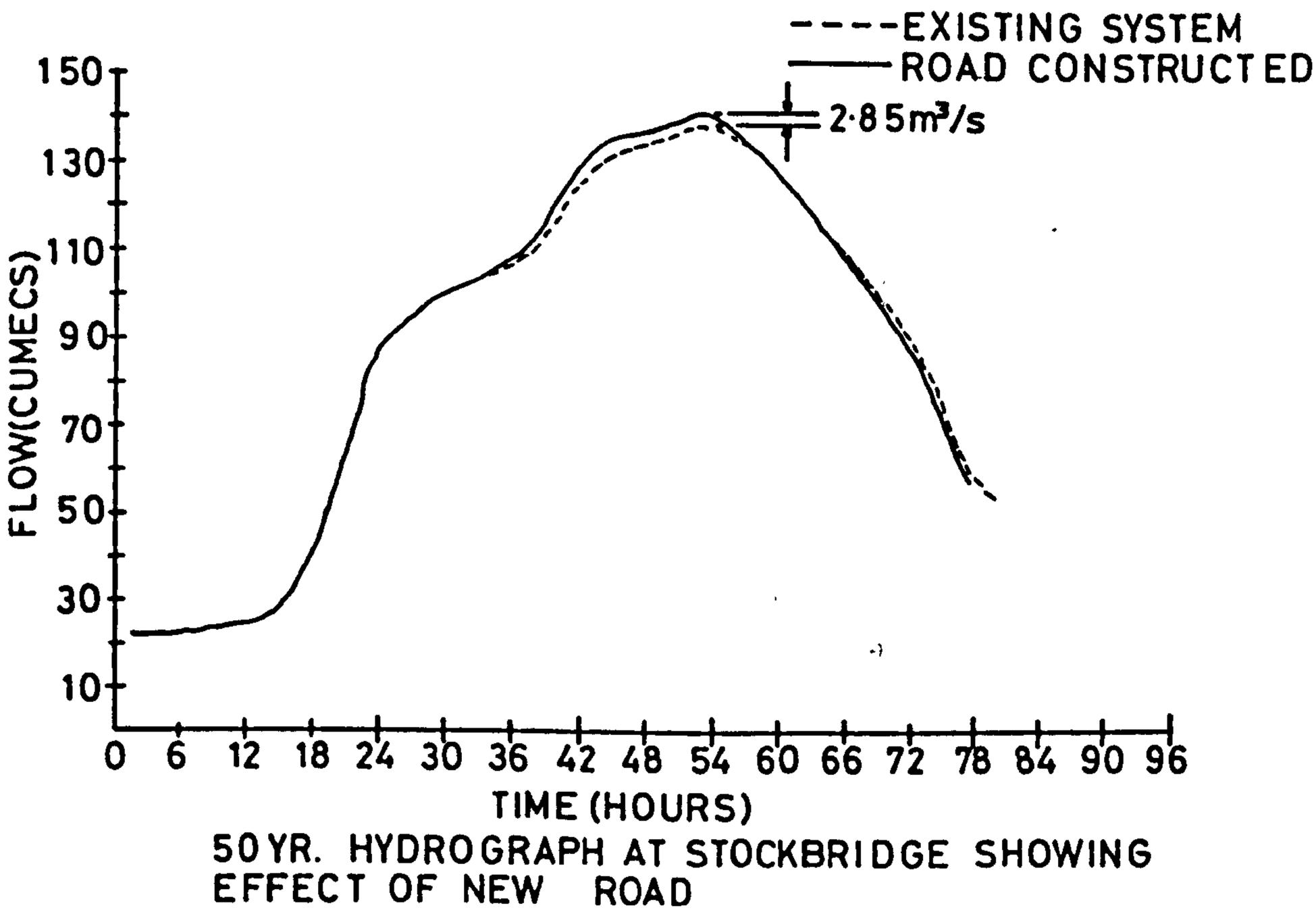

50YR. HYDROGRAPH AT STOCKBRIDGE SHOWING EFFECT OF NEW ROAD

FIGURE 5·10

The average increase in peak water levels was 30mm. The 7 year flood resulted in a slightly higher average increase in peak washland water levels. This may be explained by the fact that some washlands are only partially filled and a relatively small increase in the volume of flood water stored could result in a relatively large increase in water level. With the 50 year flood the increase in water level is generally over the entire washland area. It was however clear that the extent and possibly the frequency of flooding would be significantly increased in the farmlands between Cononley and Stockbridge.

Without further modelling of the river system downstream of Stockbridge the precise effect of the increase in flow and water level obtained at Stockbridge could not be determined for areas further downstream. However, there was little doubt that the flooding of the areas downstream would be adversely affected, although it is unlikely that the rise in water level would be translated as far downstream as Leeds. There was also concern that another 50 year flood of the same level might have a considerably longer duration which would greatly increase the volume of flood water which might overtop defences downstream.

The effect of not reconnecting the washlands which would become divorced by the new road was also examined using a shortened version of the model which commenced at Kildwick Bridge. Runs carried out using this model indicated that the increase in peak flow at Stockbridge would be about 7.50m^3/s for the 50 year flood as opposed to 2.85m^3/s increase if divorced washlands were fully

connected. As a number of culverts are required through road embankment for land and road drainage purposes the necessary increase in the size and distribution of these culverts to provide full connection of divorced washlands was calculated. Bearing in mind that many of the culverts would be dual purpose the cost associated with providing full connection was estimated to be significantly lower than the cost of extra compensatory storage if divorced washlands were not fully connected.

5.11 CONCLUDING REMARKS

The model is currently being used to examine and assess alternative compensatory schemes. It is, however, considered that the usefulness and effectiveness of the model has been proved in allowing comprehensive assessment of the effect of the new TR65 trunk road to be made. As it stands the model may also be used to assess the effect of any other new developments which might affect the storage capacity of the washlands. Examination of strategies for maintenance or improvements to the washland system is also possible.

CHAPTER SIX

NUMERICAL MODEL FOR LONG WAVE PROPAGATION IN TWO-PLAN DIMENSIONS

6.1 ENGINEERING ALTERATIONS TO TIDAL WATERS

Through the ages estuaries and coastal seas have been of social and economic benefit to mankind, providing a source of food, a means of navigation and a medium for the disposal of waste. Thus, it is important that before embarking on any engineering alteration to their geometry its effect on the tidal regime should be fully assessed. Modifications of the geometry of tidal waters may cause mean low tide elevations to be depressed appreciably, thereby decreasing navigable depths; mean high tide elevations or the elevation of surges may be significantly raised causing flooding of property and adversely affecting the discharge of storm and sanitary sewers; currents may be so accelerated that navigation is impeded or possibly made hazardous; or currents may be reduced to such an extent that shoaling is increased, or takes place where there was no shoaling prior to the modification. Changes in the tidal regime may also affect the salinity regime .

The following examples of engineering projects which may have significant effects on the regime of a tidal waterway were given by Harleman (1973):

i. Excavating a channel for navigation in an unimproved waterway

ii. Deepening or enlarging an existing navigation channel

iii. Training works, such as jetties and

dykes.

iv Barriers for power generation, storm surge protection or the prevention of salinity intrusion

v. Projects that increase the area of the waterway subject to the rise and fall of the tide, such as boat basins, lagoons and turning basins

vi. Projects that decrease the area of the waterway subject to the rise and fall of the tide, such as fills resulting from the disposal of dredge spoil, or fills made for the purpose of creating land for development projects.

To predict the effect of geometrical alterations on long wave propagation in a tidal sea some form of approximate analysis must be used. Commonly physical or mathematical modelling of the sea area is necessary. For engineering problems with large capital investment mathematical-physical model combinations are recommended by McDowell and O'Connor (1977). The following chapters are concerned with numerical solutions to the mathematical modelling approach to this problem.

6.2 ECONOMIC CONSIDERATIONS WHEN NUMERICALLY MODELLING TIDAL SEAS

Economic considerations when numerically modelling engineering phenomena have already been discussed in Section 1.2 To recap, these indicate the "design system"

approach described by Abbott (1973, 1976b), to be economically attractive. This approach requires that the model be highly flexible and contain no numerical stability contraints on the choice of time and distance increments. With this in mind a numerical model intended to form the core of such a design project is developed in the following sections.

6.3 ALTERNATIVE NUMERICAL METHODS

Numerical solutions of the long wave equations are obtained from either direct difference methods or characteristic methods. In direct difference methods finite difference approximations to the partial differentials are substituted directly into the differential equations providing finite difference equations that can be solved numerically. With characteristic methods, characteristic equations are obtained from linear combinations of the differential equations, see Section 2.7, before the substitution of finite difference approximations is made.

6.3.1 CHARACTERISTIC METHODS

Characteristic equations are produced through linear combinations of the original hyperbolic equations 2.25 to 2.27. The resulting characteristic equations have the physical significance of defining paths along which disturbances in the solution surface will propagate. In the one-dimensional case these paths will take the form of lines in x-t space, whereas in the two-dimensional case they form a cone in x-y-t space. An approximate solution to the long wave equations can be obtained by numerically integrating the

characteristic equations along these paths. The integration may be performed either on the two-dimensional characteristic equations, Townson (1974), Donald (1981), Chowdhury (1982) or by an alternating direction algorithm applied to a system of one-dimensional, parallel, canalized flows, Balafoutas and Abbott (1977).

When operating a characteristic solution with a rectangular space-time grid, desirable in most fluid flow problems, numerical stability depends on the interpolation scheme used to determine initial conditions on the characteristics, Goldberg and Wylie (1983). If Hartree spatial interpolations shown in Figure 6.1a are employed, Hartree (1958), then the stability criterion is that a Courant number less than or equal to one must be used. This is identical to an explicit scheme. These restrictions may be overcome by adoption of the Vardy spatial interpolations shown in Figure 6.1b, Vardy (1977). In effect this scheme adjusts the Δx increment to operate at $Cr=1$ for each solution point. Alternatively, the time interpolation, shown in Figure 6.1c, Ellis (1979) and Wylie (1980), can be adopted to produce an implicit characteristic solution. If the Vardy spatial interpolations or the implicit time line interpolations are used an unconditionally stable characteristic method can be developed.

The major disadvantage of the characteristic method however, is its nonconservative nature, Roach (1972, pp 33). This is especially evident if it is applied to areas where large changes in channel geometry occur, Ellis (1970).

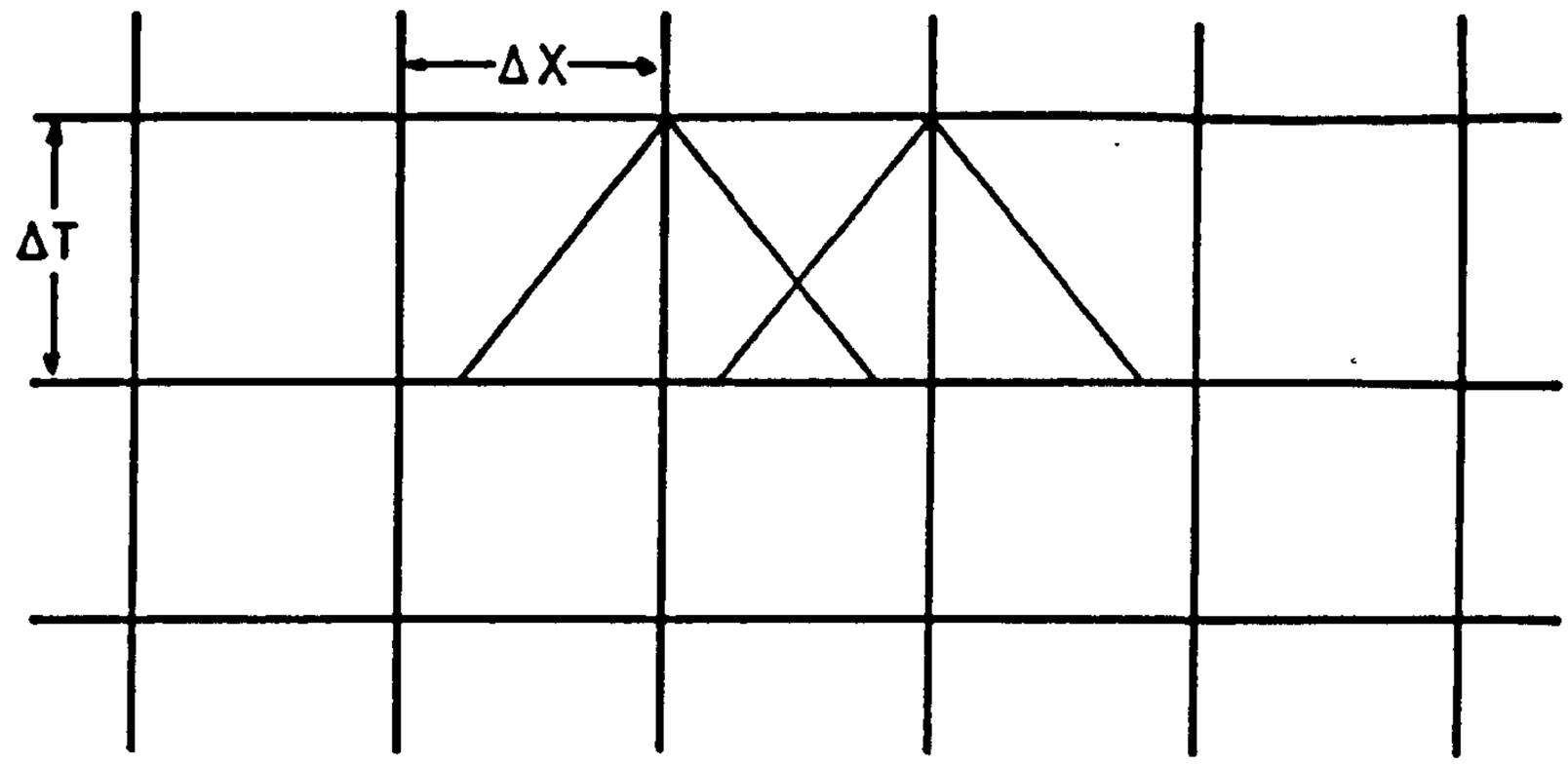

a Hartree Spatial Interpolations

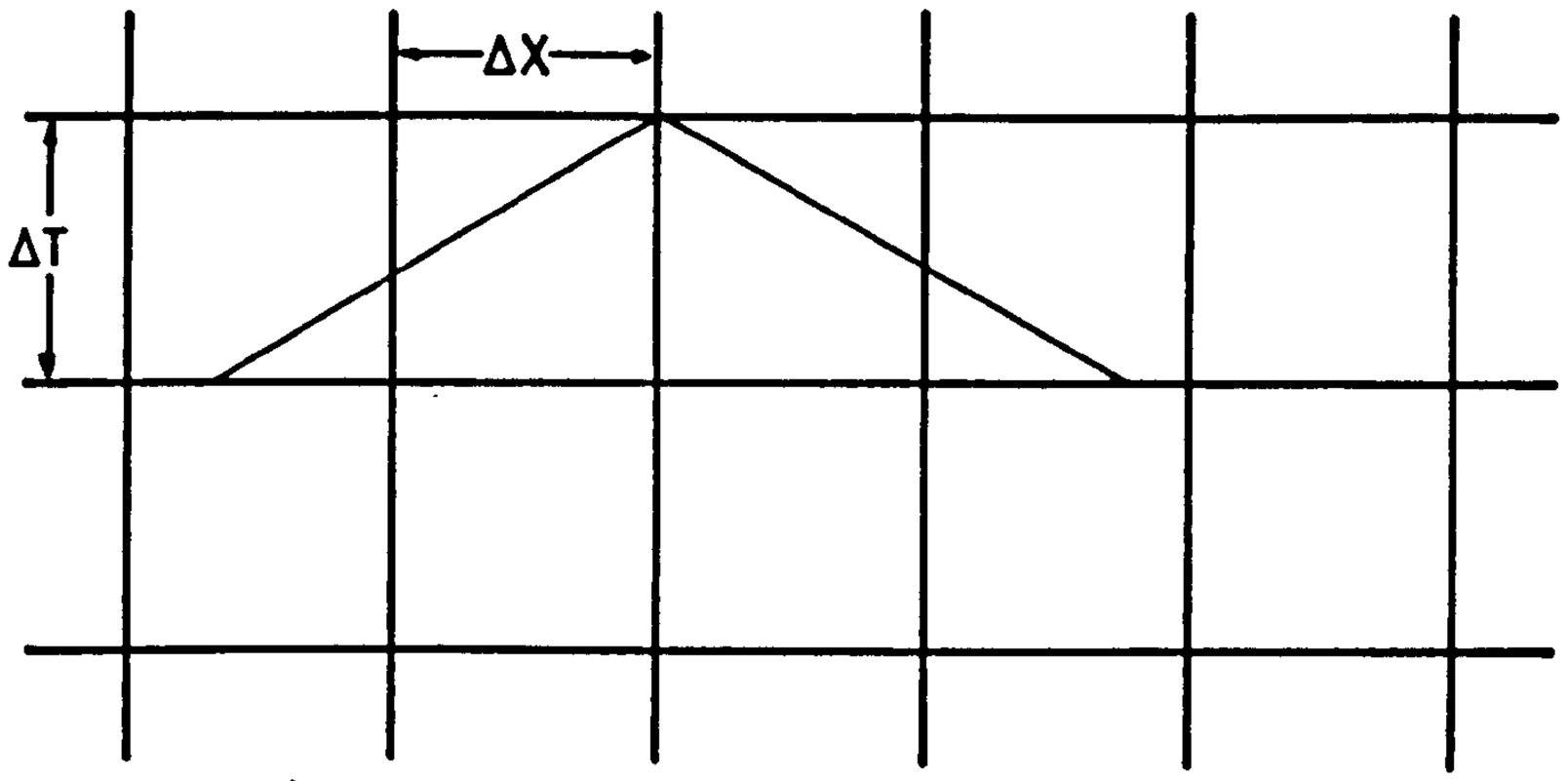

b Vardy Spatial Interpolations

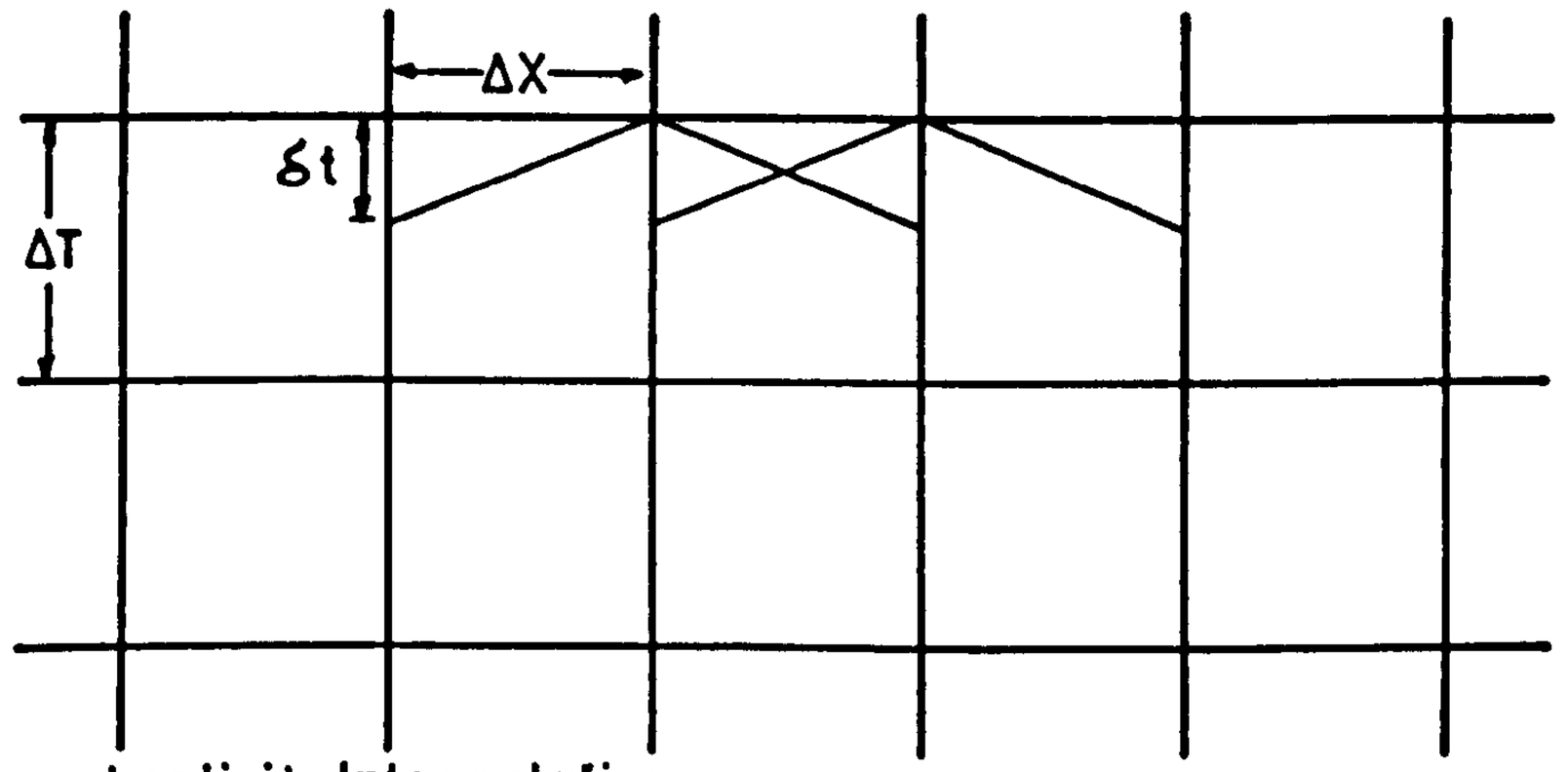

c Implicit Interpolations

Figure 6·1

6.3.2 DIRECT EXPLICIT METHODS

In explicit finite difference schemes, such as that used by Reid and Bodine (1968), Heaps (1969), Flather and Heaps (1975), the value of dependent variables at one time can be expressed as an explicit function of the values of the dependent variables at an earlier time. Time steps used in these models are defined by strict stability criterion, generally necessitating the use of small time steps whenever a fine space grid is required by the model.

6.3.3 ALTERNATING DIRECTION IMPLICIT METHODS

Alternating direction implicit methods or ADI methods, were first introduced in companion papers by Peaceman and Rachford (1955) and Douglas (1955). Later they were applied to two-dimensional long wave equations in the multi-operational models of Leendertse (1967) and Abbott (1968). The Leendertse scheme solves equations 2.5 to 2.7 by the application of implicit and explicit finite difference schemes alternated in direction over two half time increments, whereas Abbott's scheme uses two implicit solutions alternated in direction over a time increment. By analysis of amplification factors and phase errors Sobey (1970) showed the two schemes to be identical.

To enhance computational efficiency both these schemes utilize the tridiagonal algorithm, described by Abbott (1979), to solve the implicit finite difference equations. Adoption of this algorithm necessitates that values of

velocity and depth be defined at alternate grid points as shown in Figure 6.2. This data layout has disadvantages at model boundaries especially if the boundary condition is given as a waterlevel versus flow relationship. This, however, has not prevented the schemes being used widely in engineering practice, being successfully applied to tidal problems by Abbott, Damsgaard and Rodenhuis (1972), Grubert (1976) and Liu and Leendertse (1978), among others.

More recently, the method has been applied to two-dimensional flood plain flow by Vreugdenhil and Wijbenga (1982).

6.4 DEVELOPMENT OF AN ALTERNATING DIRECTION IMPLICIT MODEL

In the present work it was decided to investigate the possibility of improving model flexibility by solving for flow and water level at every grid point; a desirable feature if variable distance increments or rating curve relationships were required in a model application. Such features are of use when modelling flooding and drying of low lying areas or where over topping of sand bars and spits is possible.

The implicit scheme for one-dimensional long wave propagation, described in Section 3.4, is adopted as the basis of a fractioned step two-dimensional plan numerical model for long wave propagation. Originally it was intended that the implicit scheme would solve the continuity and one dynamic equation, say in the x-direction to give water levels and x-flows at the intermediate time step. An

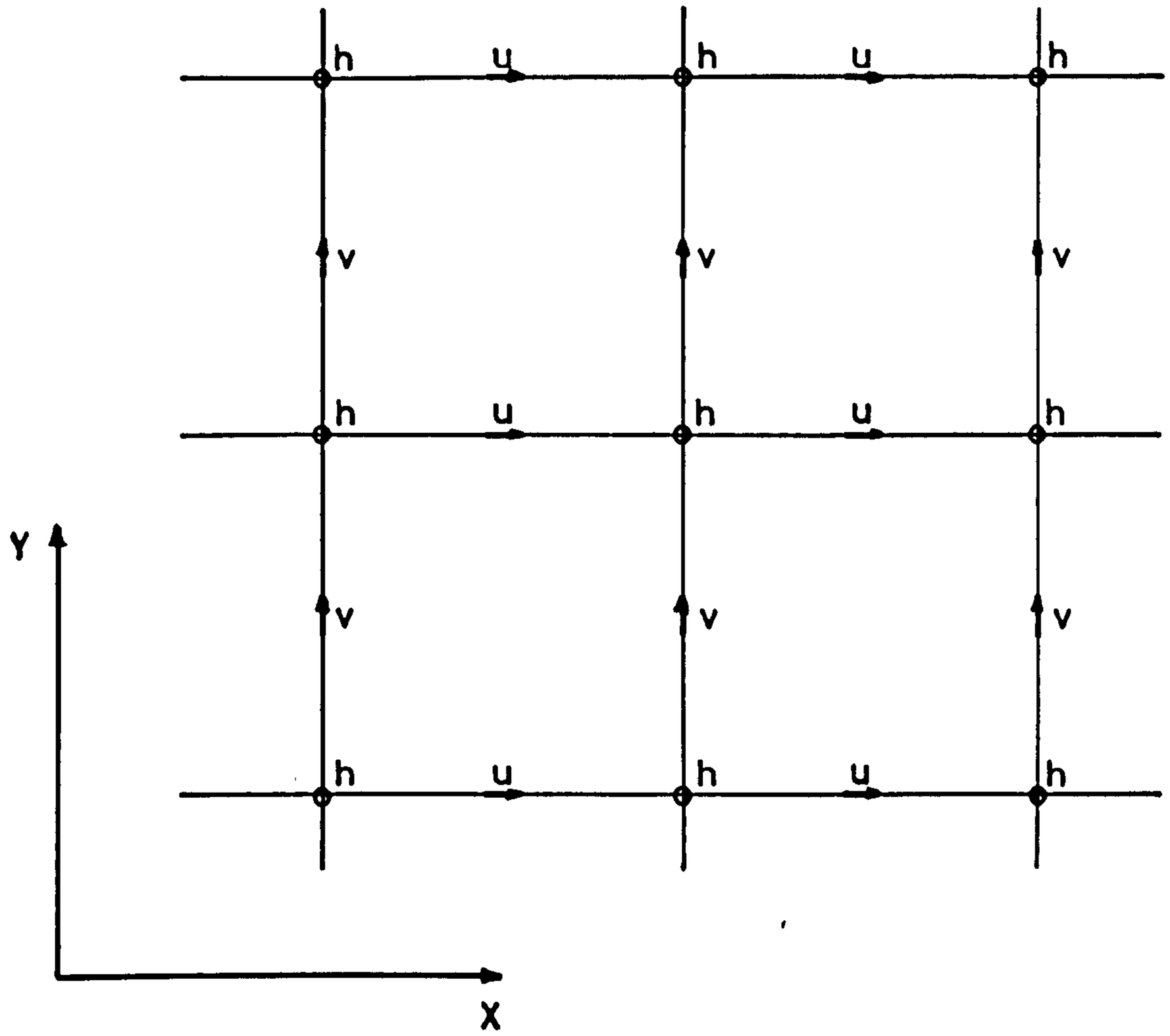

Figure 6·2

Data layout for two-dimension implicit schemes of the Leendertse(1967) type and Abbott(1968) type.

explicit solution of the y-direction dynamic equation would then advance y-flows over the same half time increment.

In the following half time increment the implicit scheme would be employed in the y-direction solving for final water levels and y-flows, the explicit scheme would be used in the x-direction to solve for x-flows. In numerical tests the resulting scheme proved unstable when used with a physically realistic time increment.

In an attempt to overcome this stability problem the explicit scheme was replaced by a characteristic scheme, using Vardy spatial interpolations. By adopting this method it was hoped that the advantages of the characteristic method in modelling wave propagation speeds could be utilized, while retaining overall conservation of mass through the implicit scheme. The model operated well in cases where estuary beds were approximately level or shelfing linearly. However, in areas where large changes in bed elevations occurred the failure of the characteristic model to conserve volume caused it to be incompatible with the conservative implicit stage. The incompatibility took the form of large fluctuations in flows which eventually destroyed the solution.

Finally, a double application of the implicit scheme was adopted for each solution of equations 2.25, 2.26 and 2.27, giving a total of four applications of the implicit scheme to advance the solution forward one full time increment..

6.5 ADI MODEL DESCRIPTION

The solution procedure is based on the idea of dividing the two-dimensional computational field into parallel channels and of approximating the two-dimensional flow by two series of one-dimensional canalized flows parallel to the x and y axes.

The following four step alternating direction implicit algorithm, shown in Figure 6.3, is employed to advance the solution from time $n\Delta t$ to $(n+1)\Delta t$, using the finite difference scheme described in the next section.

Firstly, flows in the x-direction are advanced from time $(n)\Delta t$ to time $(n+\frac{1}{2})\Delta t$ and a first estimate is made for the waterlevels at time $(n+\frac{1}{2})\Delta t$; by applying the implicit finite difference scheme of equations 2.25 and 2.27 along each row in the x-direction, with an explicit evaluation of the $\partial qy/\partial y$ term in the continuity equation.

Secondly, flows in the y-direction are advanced from time $n\Delta t$ to $(n+\frac{1}{2})\Delta t$ and the values of water levels at time $(n+\frac{1}{2})\Delta t$ improved; by applying the implicit finite difference scheme of equations 2.26 and 2.27 along each row in the y-direction using a time centred evaluation of the $\partial qx/\partial x$ term in the continuity equation.

Thirdly, flows in the y-direction are advanced from time $(n+\frac{1}{2})\Delta t$ to $(n+1)\Delta t$ and a first estimate for water levels at $(n+1)\Delta t$ is obtained; by applying the implicit finite difference scheme of equations 2.26 and 2.27 along each row in the y-direction with an explicit evaluation of the $\partial qx/\partial x$ term in the continuity equation based on

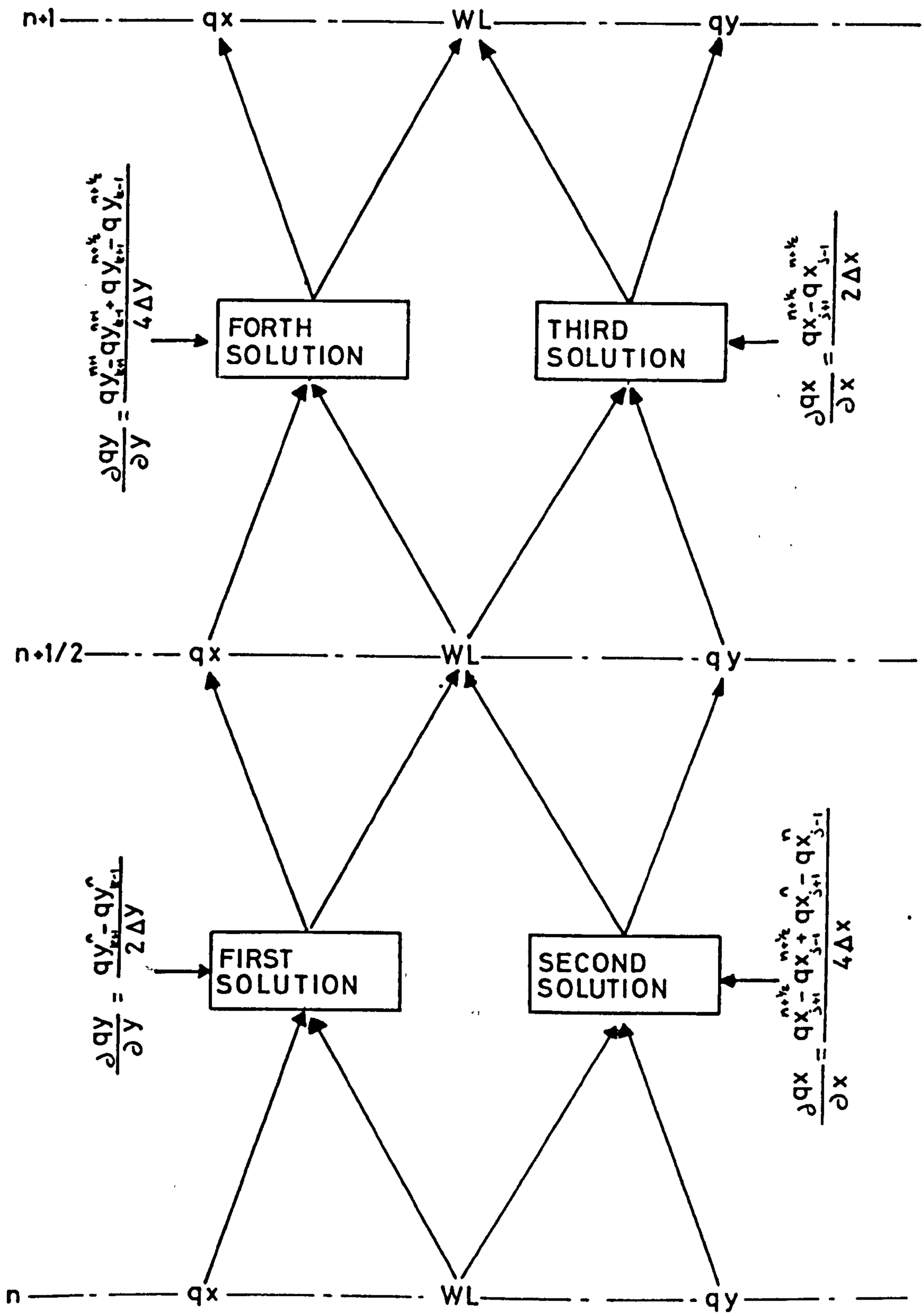
n+1
qx
WL
qy
FORTH SOLUTION
THIRD SOLUTION
n+1/2
qx
WL
qy
FIRST SOLUTION
SECOND SOLUTION
n
qx
WL
qy

Figure 6.3

conditions at time $(n+\frac{1}{2})\Delta t$.

Finally, flows in the x-direction are advanced from time $(n+\frac{1}{2})\Delta t$ to $(n+1)\Delta t$ and the value of water levels at time $(n+1)\Delta t$ are finalized; by applying the implicit finite difference scheme of equations 2.25 and 2.27 along each row in the x-direction with a time centred evaluation of the $\partial qy/\partial y$ term in the continuity equation.

6.6 FINITE DIFFERENCE REPRESENTATION OF THE TWO-DIMENSIONAL LONG WAVE EQUATIONS

The finite difference equations are again based on the Preissmann scheme discussed in section 3.4 It should be remembered that in the present case the scheme is applied over two half time increments as opposed to the one time increment in the one-dimensional case. Superscript n denotes the number of time increments which have elapsed since the initial conditions, while subscripts j and k denote x and y ordinates respectively. The symbols used are as defined in Chapter Three.

No linear stability analysis was undertaken as it was expected that stability properties and wave deformation characteristics for this ADI scheme would be similar to those for the one-dimensional scheme, see section 3.5. This was later confirmed by numerical experiments.

In the following the application of the scheme to solutions in the x-direction is described. Solutions in the y-direction are identical under interchange of x and y.

6.6.1 CONTINUITY EQUATION

For the first application of the implicit solution in the x-direction, replacing the partial differential operators in equation 2.27 by the following finite difference operators:

$$\partial Wl/\partial t = (Wl^{n+\frac{1}{2}}_{j,k} - Wl^{n}_{j,k} + Wl^{n+\frac{1}{2}}_{j+1,k} - Wl^{n}_{j+1,k})/4\Delta t$$

$$\partial qx/\partial x = (qx^{n+\frac{1}{2}}_{j+1,k} - qx^{n+\frac{1}{2}}_{j,k} + qx^{n}_{j+1,k} - qx^{n}_{j,k})/2\Delta t$$

$$\partial qy/\partial y = (qy^{n}_{j,k+1} - qy^{n}_{j,k-1} + qy^{n}_{j+1,k+1} - qy^{n}_{j+1,k-1})/4\Delta y$$

gives the finite difference continuity equation:

$$(Wl^{n+\frac{1}{2}}_{j,k} + Wl^{n+\frac{1}{2}}_{j+1,k})/4\Delta t - (Wl^{n}_{j,k} + Wl^{n}_{j+1,k})/4\Delta t + (qx^{n+\frac{1}{2}}_{j+1,k} - qx^{n+\frac{1}{2}}_{j,k})/2\Delta x$$

$$+ (qx^{n}_{j+1,k} - qx^{n}_{j,k})/2\Delta x + (qy^{n}_{j,k+1} - qy^{n}_{j,k-1} + qy^{n}_{j+1,k+1} -$$

$$qy^{n}_{j+1,k-1})/4\Delta y = 0.$$

rearranging,

$$Wl^{n+\frac{1}{2}}_{j,k}/4\Delta t + Wl^{n+\frac{1}{2}}_{j+1,k}/4\Delta t + qx^{n+\frac{1}{2}}_{j+1,k}/2\Delta x - qx^{n+\frac{1}{2}}_{j,k}/2\Delta x = Gj \quad \text{Equation 6.1}$$

where

$$Gj = (Wl^{n}_{j,k} + Wl^{n}_{j+1,k})/4\Delta t - (qx^{n}_{j+1,k} - qx^{n}_{j,k})/2\Delta x - (qy^{n}_{j,k+1} -$$

$$qy^{n}_{j,k-1} + qy^{n}_{j+1,k+1} - qy^{n}_{j+1,k-1})/4\Delta y \quad \text{Equation 6.2}$$

In the second application in the x-direction the finite difference operators are:

$$\partial Wl/\partial t = (Wl^{n+1}_{j,k} - Wl^{n+\frac{1}{2}}_{j,k} + Wl^{n+1}_{j+1,k} - Wl^{n+\frac{1}{2}}_{j+1,k})/4\Delta t$$

$$\partial qx/\partial x = (qx^{n+1}_{j+1,k} - qx^{n+1}_{j,k} + qx^{n+\frac{1}{2}}_{j+1,k} - qx^{n+\frac{1}{2}}_{j,k})/2\Delta x$$

$$\partial qy/\partial y = (qy^{n+1}_{j,k+1} - qy^{n+1}_{j,k-1} + qy^{n+\frac{1}{2}}_{j,k+1} - qy^{n+\frac{1}{2}}_{j,k-1} + qy^{n+1}_{j+1,k+1} -$$

$$qy^{n+1}_{j+1,k-1} + qy^{n+\frac{1}{2}}_{j+1,k+1} - qy^{n+\frac{1}{2}}_{j+1,k-1})/8\Delta y$$

giving the finite difference continuity equation as:

$$Wl^{n+1}_{j,k}/4\Delta t + Wl^{n+1}_{j+1,k}/4\Delta t + qx^{n+1}_{j+1,k}/2\Delta x - qx^{n+1}_{j,k}/2\Delta x = G_j \quad \text{Equation 6.3}$$

where

$$Gj = (Wl^{n+\frac{1}{2}}_{j,k} + Wl^{n+\frac{1}{2}}_{j+1,k})/4\Delta t - (qx^{n+\frac{1}{2}}_{j+1,k} - qx^{n+\frac{1}{2}}_{j,k})2\Delta x - (qy^{n+1}_{j,k+1} -$$

$$qy^{n+1}_{j,k-1} + qy^{n+\frac{1}{2}}_{j,k+1} - qy^{n+\frac{1}{2}}_{j,k-1} + qy^{n+1}_{j+1,k+1} - qy^{n+1}_{j+1,k-1} + qy^{n+\frac{1}{2}}_{j+1,k+1}$$

$$qy^{n+\frac{1}{2}}_{j+1,k-1})/8\Delta y \quad \text{Equation 6.4}$$

6.6.2 X-DIRECTION DYNAMIC EQUATION

Leaving aside barometric pressure, coriolis, bottom and surface friction terms for the present, the remaining differential operators in equation 2.25 can be replaced by the following finite difference operators:

6.6.2.1 ACCELERATION TERM

$$\partial(qx/h)/\partial t = (qx^{n+\frac{1}{2}}_{j+1,k}/h^{n}_{j+1,k} - qx^{n}_{j+1,k}/h^{n}_{j+1,k} + qx^{n+\frac{1}{2}}_{j,k}/h^{n}_{j,k} -$$

$$qx^{n}_{j,k}/h^{n}_{j,k})/4\Delta t.$$

6.6.2.2. SURFACE GRADIENT

$$\partial Wl/\partial x = [\Theta(Wl^{n+\frac{1}{2}}_{j+1,k} - Wl^{n+\frac{1}{2}}_{j,k}) + (1-\Theta)(Wl^{n}_{j+1,k} - Wl^{n}_{j,k})]/\Delta x.$$

6.6.2.3 CONVECTIVE ACCELERATION

Rewriting the partial differential convective acceleration in the

x-direction as $\frac{1}{2g}\frac{\partial u^2}{\partial x}$ the finite difference term is expressed as:

$$\frac{1}{2g\Delta x}\left[\ \Theta\left(qx^{n+\frac{1}{2}}_{j+1,k}\ qx^{n}_{j+1,k}/\left(h^{n}_{j+1,k}\right)^2 - qx^{n+\frac{1}{2}}_{j,k}\ qx^{n}_{j,k}/\left(h^{n}_{j,k}\right)^2\right) +\right.$$

$$\left.(1-\Theta)\ \left(\left(qx^{n}_{j+1,k}\right)^2/\left(h^{n}_{j+1,k}\right)^2 - \left(qx^{n}_{j,k}\right)^2/\left(h^{n}_{j,k}\right)^2\right)\right]$$

Convective acceleration in the y-direction is expressed as:

$$\frac{qy}{2h}\frac{\partial(qx/h)}{\partial y} = \frac{1}{4g\Delta y}\left[(qy^{n}_{j,k}/h^{n}_{j,k})(qx^{n}_{j,k+1}/h^{n}_{j,k+1} - qx^{n}_{j,k-1}/h^{n}_{j,k-1})\right.$$

$$\left. + (qy^{n}_{j+1,k}/h^{n}_{j+1,k})(qx^{n}_{j+1,k+1}/h^{n}_{j+1,k+1} - qx^{n}_{j+1,k-1}/h^{n}_{j+1,k-1})\right]$$

6.6.2.4 Inserting the above terms in the partial differential equation gives the x-direction finite difference dynamic equation as:

$$\frac{1}{4g\Delta t}\ (qx^{n+\frac{1}{2}}_{j+1,k}/h^{n}_{j+1,k} - qx^{n}_{j+1,k}/h^{n}_{j+1,k} + qx^{n+\frac{1}{2}}_{j,k}/h^{n}_{j,k} - qx^{n}_{j,k}/h^{n}_{j,k})$$

$$+\frac{1}{2g\Delta x}\left[\ \Theta\ (qx^{n+\frac{1}{2}}_{j+1,k}\ qx^{n}_{j+1,k}/\left(h^{n}_{j+1,k}\right)^2 - qx^{n+\frac{1}{2}}_{j,k}\ qx^{n}_{j,k}/(h^{n}_{j,k})^2)\right.$$

$$\left.+\ (1-\Theta)\ \left(\left(qx^{n}_{j+1,k}\right)^2/\left(h^{n}_{j+1,k}\right)^2 - \left(qx^{n}_{j,k}\right)^2/\left(h^{n}_{j,k}\right)^2\right)\ \right]$$

$$+\frac{1}{4g\Delta y}\left[(qy^{n}_{j,k}/h^{n}_{j,k})(qx^{n}_{j,k+1}/h^{n}_{j,k+1} - qx^{n}_{j,k-1}/h^{n}_{j,k-1}) +\right.$$

$$\left.(qy^{n}_{j+1,k}/h^{n}_{j+1,k})(qx^{n}_{j+1,k+1}/h^{n}_{j+1,k+1} - qx^{n}_{j+1,k-1}/h^{n}_{j+1,k-1})\ \right]$$

$$+\frac{1}{\Delta x}\left[\ \Theta\ (Wl^{n+\frac{1}{2}}_{j+1,k} - Wl^{n+\frac{1}{2}}_{j,k}) + (1-\Theta)\ (Wl^{n}_{j+1,k} - Wl^{n}_{j,k})\right] = 0.$$

Rearranging gives:

$$\left(\frac{1}{4g\Delta th^{n}_{j+1,k}} + \frac{\Theta qx^{n}_{j+1,k}}{2g\Delta x(h^{n}_{j+1,k})^{2}}\right) qx^{n+\frac{1}{2}}_{j+1,k} + \left(\frac{1}{4g\Delta th^{n}_{j,k}} - \frac{\Theta qx^{n}_{j,k}}{2g\Delta x(h^{n}_{j,k})^{2}}\right)$$

$$qx^{n+\frac{1}{2}}_{j,k} + \frac{\Theta}{\Delta x} Wl^{n+\frac{1}{2}}_{j+1,k} - \frac{\Theta}{\Delta x} Wl^{n+\frac{1}{2}}_{j,k} = Hj \qquad \text{Equation 6.5}$$

Where:

$$Hj = \frac{1}{g4\Delta t}(qx^{n}_{j+1,k}/h^{n}_{j+1,k} + qx^{n}_{j,k}/h^{n}_{j,k}) - \frac{1}{2g\Delta x}(1-\Theta)\left[(qx^{n}_{j+1,k})^{2}/(h^{n}_{j+1,k})^{2}\right.$$

$$\left. - (qx^{n}_{j,k})^{2}/(h^{n}_{j,k})^{2}\right] - \frac{1}{4g\Delta x}\left[\, qy^{n}_{j,k}/h^{n}_{j,k}\,(qx^{n}_{j,k+1}/h^{n}_{j,k+1} -\right.$$

$$qx^{n}_{j,k-1}/h^{n}_{j,k-1}) + qy^{n}_{j+1,k}/h^{n}_{j+1,k}\,(qx^{n}_{j+1,k+1}/h^{n}_{j+1,k+1} -$$

$$\left. qx^{n}_{j+1,k-1}/h^{n}_{j+1,k-1})\,\right] - \frac{(1-\Theta)}{\Delta x}(Wl^{n}_{j+1,k} - Wl^{n}_{j,k}) \qquad \text{Equation 6.6}$$

6.6.3 FINITE DIFFERENCE REPRESENTATION OF BOTTOM FRICTION, WIND STRESS, CORIOLIS ACCELERATION AND BAROMETRIC PRESSURE

The following terms are represented explicitly and can be taken directly to the right hand side of equation 6.5 to modify the value of Hj.

6.6.3.1 BOTTOM FRICTION

The use of the empirical Chezy equation to represent the dissipation of energy in tidal flow is discussed in section 2.5.4. The resulting expression for frictional resistance in the x-direction is:

$$Sfx = U\,(V^2 + U^2)^{\frac{1}{2}} / C^2 h$$

An explicit finite difference formulation of this term is used in equation 2.25. Namely,

$$Sfx = \tfrac{1}{2}\Big[(qx^n_{j+1,k}/h^n_{j+1,k})\,[(qy^n_{j+1,k})^2/(h^n_{j+1,k})^2 + (qx^n_{j+1,k})^2/(h^n_{j+1,k})^2]^{1/2} / C^2 h^n_{j+1,k}$$

$$+ (qx^n_{j,k}/h^n_{j,k})\,[(qy^n_j)^2/(h^n_{j,k})^2 + (qx^n_{j,k})^2/(h^n_{j,k})^2]^{1/2} / C^2 h^n_{j,k}\Big]$$

Equation 6.7

6.6.3.2 WIND STRESS

For the present applications the areas over which the model is applied are sufficiently small for wind speed and direction to be considered constant over the model area during a time increment. Wind stress in the x-direction is represented by:

$$Swx = K\rho a\, W^{n^2}\, \mathrm{Cos}\ \beta\ / g\rho h^n_j$$

If at a later date the model were applied to larger sea areas it would be little trouble to modify the programme to include a number of meteorological sub-areas, such as used by Heaps (1969).

6.6.3.3 CORIOLIS ACCELERATION

The coriolis acceleration in the x-direction is represented in finite difference form by:

$$\Omega\ V = \Omega \tfrac{1}{2}\ (qy^n_{j+1,k}/h^n_{j+1,k} + qy^n_{j,k}/h^n_{j,k}) \qquad \text{Equation 6.8}$$

6.6.3.4 BAROMETRIC PRESSURE VARIATION

In the storm surge events modelled in the present study barometric pressure variations contribute little to the total surge amplitude. It was, therefore, possible to represent the variations of barometric pressure in the x and y directions as gradients, changing in time, over the whole model area giving a barometric pressure term of the form:

$$\partial Pa/\partial x = (\Delta Pa/\quad (jj-1)\,\Delta x)^n \qquad \text{Equation 6.9}$$

6.6.4 The above finite difference x-direction dynamic equation is used to advance the dependent variables of qx and Wl from time $n\Delta t$ to $(n+\frac{1}{2})\Delta t$. The finite difference x-direction dynamic equation for time $(n+\frac{1}{2})\Delta t$ to $(n+1)\Delta t$ is identical with superscripts n and $n+\frac{1}{2}$ replaced by $n+\frac{1}{2}$ and n+1 respectively.

6.7 SOLUTION OF THE FINITE DIFFERENCE EQUATIONS

Given appropriate boundary conditions application of the finite difference scheme to each row of the four step solution algorithm results in a set of simultaneous equations. The format of these equations is identical to those of the one dimensional model, i.e. the coefficient matrix is banded with a band width of four. Hence each set of simultaneous equations can be solved using the modified Gaussian elimination routine described in Appendix A. As with the flood routing model the scheme was applied without iteration.

6.8 BOUNDARY CONDITIONS

One of the major advantages of the finite difference scheme described previously is its flexibility in handling boundary conditions. The current model can utilize open boundaries, fixed shore line boundaries, moving shore line boundaries and possible "weir flow" type boundaries. Open boundaries refer to areas on the extremities of the numerical model where either flow or water level is known as a function of time. All natural shore line boundaries can move in that no matter what the elevation of the surrounding land it can always be flooded by an extreme event. For the purposes of the numerical model, however, the shore line boundaries are sub-divided into fixed shore line boundaries which maintain the same position irrespective of the adjacent water level and moving shore line boundaries which expand and contract with the rise and fall of the tide, such boundaries enable modelling of flooding and drying of sand flat areas. "Weir" type boundaries are considered to exist wherever a natural or manmade barrier with a width considerably less than the grid scale protrudes above the low water level. This boundary condition allows overtopping of natural barriers, such as: sand spits and bars, or manmade structures such as: causeways and jetties, to be modelled.

6.8.1 OPEN BOUNDARIES

Open boundaries can be sub-divided into those in

which flow is expressed as a function of time or in which water level is given as a function of time. In each case the value of q or Wl at the boundary is either given to the model or calculated from some arithmetic expression. For flow as a function of time the model calculates the boundary water level and with water level as a function of time the flow per unit width across the model boundary is calculated. In both circumstances the component of velocity along the boundary is neglected. The effect of this is discussed in section 7.9.

6.8.2 FIXED SHORE LINE BOUNDARIES

At fixed shore line boundaries the flow perpendicular to the boundary is taken as zero and free slip conditions along the boundary are assumed. The value of water level at the boundary is calculated. This type of boundary is sometimes referred to as a reflecting boundary.

6.8.3 MOVING SHORE LINE BOUNDARIES

If the near-shore area is fairly flat then the rise and fall of water level associated with tides or storm surges will produce a large lateral fluctuation of the shore line position. Numerical simulation of this feature is possible by allowing the model to adjust the grid point system accordingly.

A survey of models incorporating this feature was undertaken by Chowdhury (1982). He reported that the methods used may be broadly divided into two categories. In one, the coastal boundary is moved across the calculation

grid in discrete grid-size steps. The excursion is envisaged in terms of a series of discrete movements as if the fluid in the last grid-cell accumulates against an imaginary vertical barrier. The velocity is assumed to be zero normal to this barrier which is then moved simply according to the calculated depth of water. Evidently this is a kinematic approach. In the second category, no lateral boundary condition of zero normal velocity is imposed and the dynamic equations are solved to compute the velocity components. The shore line is located by extrapolating the water level from the last two underwater grid points. Chowdhury's own characteristic model uses this method. In the present model the first of these two methods is employed. The details of the operation are described in the following.

For the flooding stage water accumulates against an imaginary barrier until the water level at the last under water point is at least equal to some predetermined level above the adjacent dry invert level, Figure 6.4. The boundary then expands by one distance increment to the position shown. The depth at the new solution point is assumed equal to the old boundary water level minus the new invert level for the first implicit calculation at the new boundary. The use of this approximation is to prevent excessively high velocities at the front of the wave during the flooding stage. No significant error in timing of flooding will occur provided the invert level is set below its true value by an amount equal to the

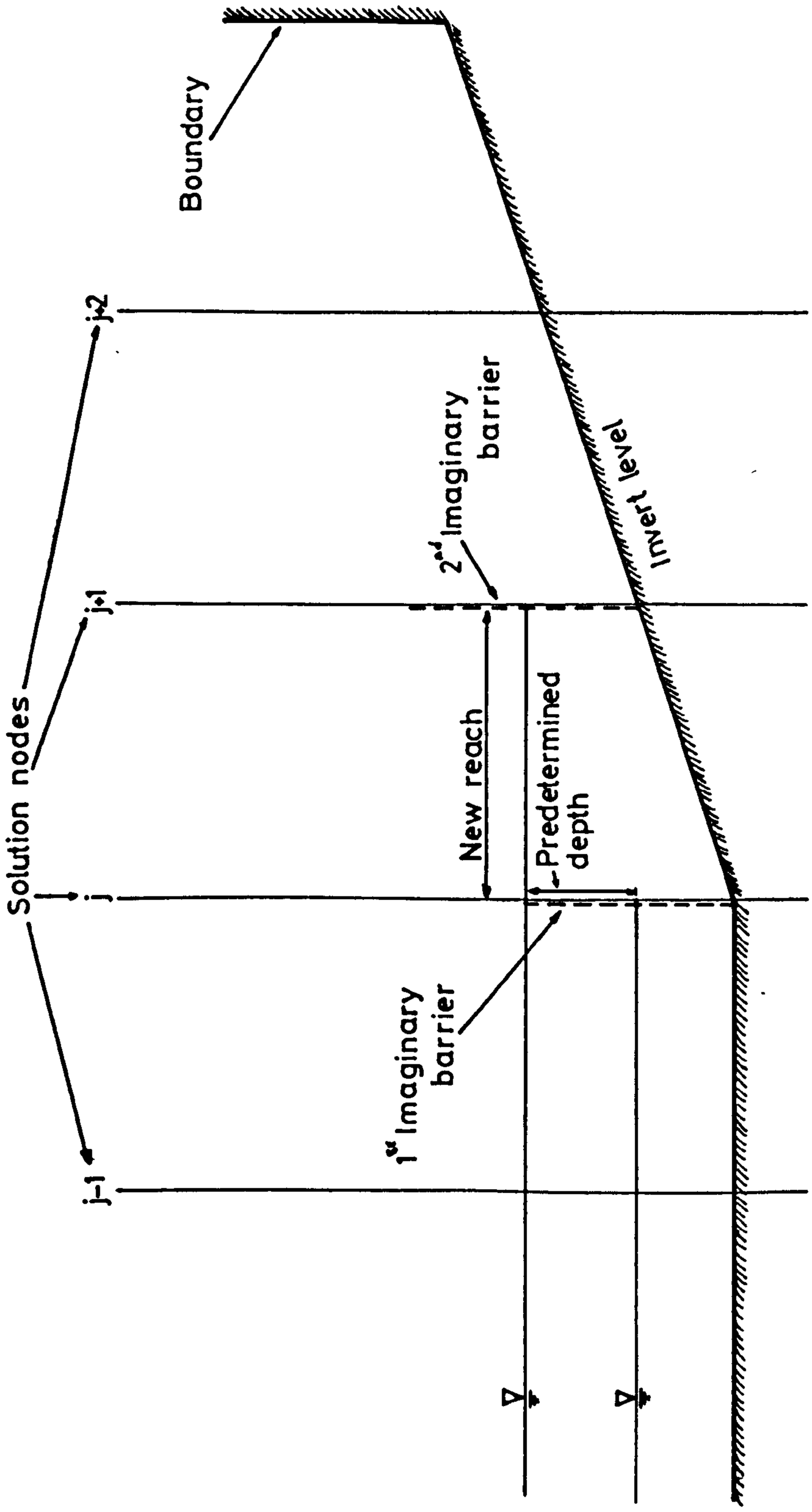
Boundary
j+2
j+1
Solution nodes
j
j-1
2nd Imaginary barrier
1st Imaginary barrier
New reach
Predetermined depth
Invert level

Figure 6.4

depth at which flooding is assumed to occur. Likewise no continuity error will occur provided the sand flat is considered dry at the same depth above the invert level.

It would seem logical to handle the drying phase in an analogous fashion. That is, the boundary contracts by one distance increment when the depth at the boundary drops below a predetermined value. However, if the sand flat is approximately level the water level may draw down faster at interior points than at the boundary; this implies that an interior depth will drop below the chosen value before the boundary depth. If the first method alone were employed not only would there be the possibility of a continuity error occurring but critical flow could arise at interior points. Therefore, in addition to the boundary depth check it is necessary to test the depth at the low water boundary. If this drops below the selected value that section is considered to be dry and the section from the low water boundary to the present boundary is excluded from further implicit calculations.

Any remaining water on the sand flat could be permitted to drain off through the use of a rating curve boundary at the low water level. In the following applications this proved to be unnecesary as the volume retained on the sand flat was not significant, compared to the total fluid volume crossing the boundaries during a tidal cycle.

It should be remembered that in a two-dimensional

model as the wetted area expands and contracts in one direction new reaches are created and destroyed in the other direction. A book-keeping routine is incorporated in the model to account for these changes automatically.

6.8.4 "WEIR FLOW" BOUNDARIES

In certain circumstances barriers with widths considerably less than the numerical distance increment protrude above the low water level in an estuary. These barriers can be natural, e.g. sand spits and bars, or manmade, e.g. causeways and jetties. In most circumstances they will be above normal high water, however, they may be overtopped during extreme meteorological events. It was considered desirable that a facility for modelling such features be included at the development stage of the model. A similar boundary condition was used by Reid and Bodine (1968) for their explicit numerical model of hurricane events in Galveston Bay, Texas. Here inclusion of the condition in an ADI method is discussed. It is analogous to the control section condition used in the one-dimensional model, Chapter Three.

Currently, provision is made for one barrier in both the x and y directions; however, there is no reason why the number of barriers cannot be increased if the need should arise. The position and mean elevation of a barrier is stored in a two-dimensional array. This permits the barrier to be defined at an angle other than along the numerical grid. The mean barrier elevation

can be constant or vary along the length of the barrier; Figure 6.5 shows the flood tide condition of flow over the barrier from reach (a) to reach (b). Reach (a) is therefore solved first. Reach (b) is the downstream reach and its upstream boundary condition is the flow out of reach (a) over the barrier. On the ebb tide this will be reversed. A check for the order of solution of reaches separated by a barrier is carried out by the programme. When the upstream water level adjacent to the barrier is greater than the barrier elevation and the downstream water level is less than the barrier elevation flow over the barrier is calculated explicitly from:

$$q_b = \pm Co\ h \sqrt{gh} \qquad \text{Equation 6.10}$$

Where h is the depth of water upstream of the barrier and Co is an appropriate non-dimensional overflow coefficient.

In the case where the water level on both sides of the barrier exceeds the barrier-crest elevation discharge is taken as that for a submerged weir, namely

$$q_b = \pm Cs\ h \sqrt{g\ |Wl_1 - Wl_2|} \qquad \text{Equation 6.11}$$

In which h is the depth of water over the crest of the barrier, Wl_1 and Wl_2 are the water levels on the two sides of the barrier (both of which exceed zb) and Cs is an appropriate non-dimensional discharge coefficient for the submerged barrier.

6.9 DATA REQUIREMENTS

Finite difference equations 6.3 and 6.5 provide a

Figure 6·5

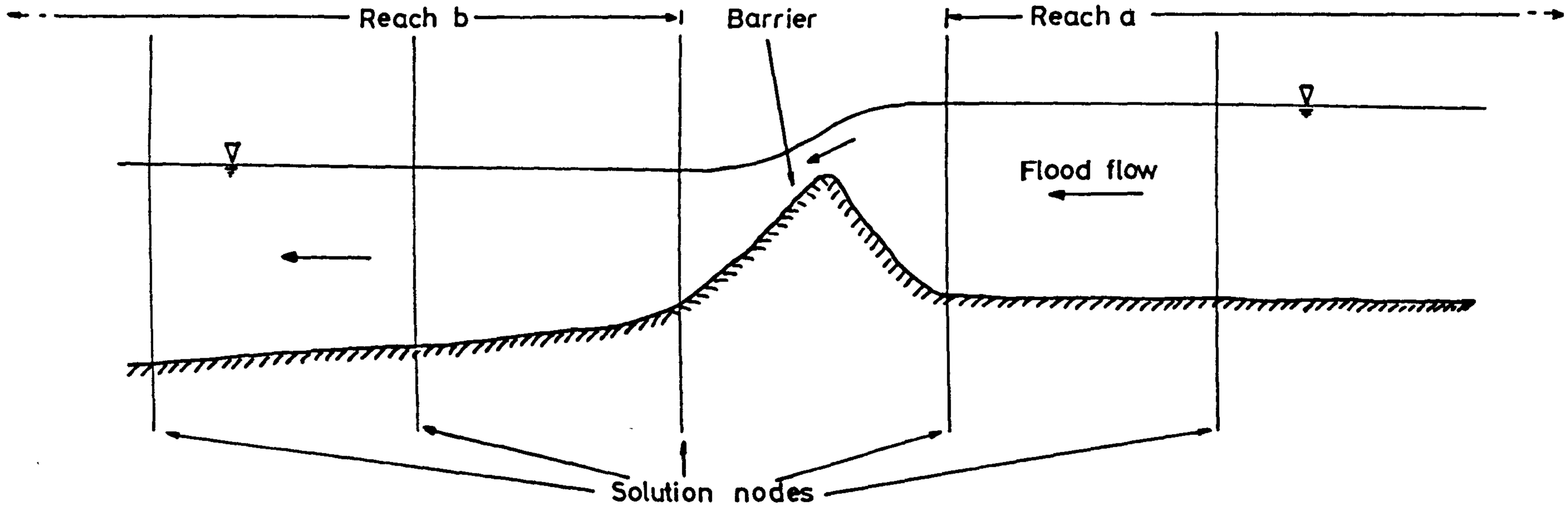

set of simultaneous equations, which given appropriate data will describe the variation in flows and water levels with time resulting from the influence of tides and storm surges. Data requirements include: a bathymetrical description of the sea area, initial conditions, boundary data and storm surge data.

6.9.1 BATHYMETRICAL DATA

A bathymetrical description of an estuary for use in the ADI model is obtained in two stages.

Firstly, a finite difference grid is laid on a topographical map of the model area and the position of open boundaries, fixed shore boundaries, moveable shore boundaries and possible "weir flow" boundaries are established. This information is read into the programme by using two integer arrays, one defining reaches and boundaries in the x-direction, the other in the y-direction. Integer arrays for the Firth of Clyde are shown in Figures 6.6a and 6.6b. The integers used to define each type of boundary condition are as follows: (1) and (2) water level given as a function of time, (3) flow given as a function of time. This value is used for both fixed shore boundaries and specified flow boundaries. (4) moveable shore boundaries "Weir flow" boundaries are stored independently; their position and crest level are read into a weir boundary array. A preprocessing stage of the main programme processes this data and stores the number of x-reaches to be solved in each y-row and the number of y-reaches to be solved in each x-row. Also stored is the integer value indicating the type of boundary at the extremities

```
0 0 3 0 3 0 0 0 0 0 0 0 0 3 3 3 3 0 0
0 0 3 0 3 0 0 0 0 0 0 0 3 0 0 0 0 3 0
0 0 3 0 3 0 0 0 0 0 0 0 3 0 0 0 0 3 0
0 0 0 3 3 0 0 0 0 0 0 0 3 3 0 0 0 0 0
0 0 0 3 0 3 0 0 0 0 0 3 0 3 0 0 0 0 0
0 0 0 3 0 0 3 3 3 0 3 0 0 3 0 0 0 0 0
0 0 0 0 3 0 0 0 3 0 3 0 0 3 0 0 0 0 0
0 0 0 0 0 3 0 0 3 0 3 0 0 3 0 0 0 0 0
0 0 0 0 3 0 0 0 0 3 0 3 0 3 0 0 0 0 0
0 0 0 3 0 0 0 0 0 0 3 3 0 3 0 0 0 0 0
0 0 3 0 0 0 0 0 0 0 0 0 0 3 0 0 0 0 0
0 0 3 0 0 3 0 3 0 0 0 0 0 3 0 0 0 0 0
0 0 3 0 3 0 0 0 3 0 0 0 0 0 3 0 0 0 0
0 0 3 3 0 0 0 0 3 0 0 0 0 0 0 0 3 0 0
0 0 3 0 3 0 0 0 3 0 0 0 0 0 0 0 0 3 0
0 3 0 0 3 0 0 0 3 0 0 0 0 0 0 0 0 3 0
0 3 0 0 3 0 0 0 0 3 0 0 0 0 0 0 0 0 3
0 3 0 0 3 0 0 0 0 3 0 0 0 0 0 0 0 0 3
0 3 0 0 0 3 0 0 0 3 0 0 0 0 0 0 0 0 3
3 0 0 0 0 3 0 0 0 3 0 0 0 0 0 0 0 0 3
3 0 0 0 0 0 0 0 0 0 0 0 0 0 0 0 0 3 0
3 0 0 0 0 0 0 0 0 0 0 0 0 0 0 0 3 0 0 0
0 3 0 0 0 0 0 0 0 0 0 0 0 0 0 0 3 0 0 0
0 3 0 0 0 0 0 0 0 0 0 0 0 0 0 3 0 0 0 0
0 1 0 0 0 0 0 0 0 0 0 0 0 0 3 0 0 0 0 0
0 1 0 0 0 0 0 0 0 0 0 0 0 3 0 0 0 0 0 0
0 1 0 0 0 0 0 0 0 0 0 0 3 0 0 0 0 0 0 0
0 1 0 0 0 0 0 0 0 0 0 0 3 0 0 0 0 0 0 0
0 1 0 0 0 0 0 0 0 0 0 0 3 0 0 0 0 0 0 0
0 1 0 0 0 0 0 0 0 0 0 3 0 0 0 0 0 0 0 0
0 1 0 0 0 0 0 0 0 0 0 3 0 0 0 0 0 0 0 0
0 1 0 0 0 0 0 0 0 0 3 0 0 0 0 0 0 0 0 0
0 1 0 0 0 0 0 0 0 0 3 0 0 0 0 0 0 0 0 0
0 1 0 0 0 0 0 3 0 3 0 3 0 0 0 0 0 0 0 0
0 1 0 0 0 0 0 3 0 3 0 3 0 0 0 0 0 0 0 0
0 1 0 0 0 0 0 3 0 0 3 3 0 0 0 0 0 0 0 0
0 1 0 0 0 0 0 3 0 0 0 0 0 0 0 0 0 0 0 0
0 1 0 0 0 0 0 3 0 0 0 0 0 0 0 0 0 0 0 0
```

Figure 6.6a

Array Defining Reaches in the x-direction
For the Firth of Clyde Model

0	0	3	3	3	0	0	0	0	0	0	0	0	3	3	3	3	0	0
0	0	0	0	0	0	0	0	0	0	0	0	3	0	0	0	0	3	0
0	0	3	0	0	0	0	0	0	0	0	0	0	0	3	3	3	3	0
0	0	0	0	0	0	0	0	0	0	0	0	0	0	0	0	0	0	0
0	0	0	0	0	3	0	0	0	0	0	3	0	0	0	0	0	0	0
0	0	0	3	0	0	3	3	3	0	3	0	0	0	0	0	0	0	0
0	0	0	0	3	0	0	0	0	0	0	0	0	0	0	0	0	0	0
0	0	0	0	0	0	0	0	0	0	3	0	0	0	0	0	0	0	0
0	0	0	0	3	0	0	0	0	3	0	0	0	0	0	0	0	0	0
0	0	0	3	0	0	0	0	0	0	3	0	0	0	0	0	0	0	0
0	0	3	0	0	0	3	0	0	0	0	0	0	0	0	0	0	0	0
0	0	0	0	0	3	0	3	0	0	0	0	0	0	0	0	0	0	0
0	0	0	0	3	0	0	0	0	0	0	0	0	0	3	0	0	0	0
0	0	0	0	0	0	0	0	0	0	0	0	0	0	0	3	3	0	0
0	0	0	0	3	0	0	0	0	0	0	0	0	0	0	0	0	3	0
0	3	0	0	0	0	0	0	3	0	0	0	0	0	0	0	0	0	0
0	0	0	0	0	0	0	0	0	0	0	0	0	0	0	0	0	0	3
0	0	0	0	0	0	0	0	0	0	0	0	0	0	0	0	0	0	0
0	0	0	0	0	3	0	0	0	0	0	0	0	0	0	0	0	0	0
3	0	0	0	0	0	0	0	0	0	0	0	0	0	0	0	0	0	3
0	0	0	0	0	0	3	3	3	3	0	0	0	0	0	0	3	3	0
3	0	0	0	0	0	0	0	0	0	0	0	0	0	0	0	0	0	0
0	0	0	0	0	0	0	0	0	0	0	0	0	0	0	3	0	0	0
0	3	0	0	0	0	0	0	0	0	0	0	0	0	0	0	0	0	0
0	3	0	0	0	0	0	0	0	0	0	0	0	0	0	0	0	0	0
0	0	0	0	0	0	0	0	0	0	0	0	0	0	3	0	0	0	0
0	0	0	0	0	0	0	0	0	0	0	0	0	0	0	0	0	0	0
0	0	0	0	0	0	0	0	0	0	0	0	0	0	3	0	0	0	0
0	0	0	0	0	0	0	0	0	0	0	0	0	0	0	0	0	0	0
0	0	0	0	0	0	0	0	0	0	0	0	3	0	0	0	0	0	0
0	0	0	0	0	0	0	0	0	0	0	0	0	0	0	0	0	0	0
0	0	0	0	0	0	0	0	0	0	0	3	0	0	0	0	0	0	0
0	0	0	0	0	0	0	0	0	0	0	0	0	0	0	0	0	0	0
0	0	0	0	0	0	0	0	0	0	0	0	0	0	0	0	0	0	0
0	0	0	0	0	0	0	0	3	0	0	0	0	0	0	0	0	0	0
0	0	0	0	0	0	0	0	0	0	0	3	0	0	0	0	0	0	0
0	0	0	0	0	0	0	0	0	3	0	0	0	0	0	0	0	0	0
0	0	0	0	0	0	0	0	0	0	3	3	0	0	0	0	0	0	0
0	0	0	0	0	0	0	0	0	0	0	0	0	0	0	0	0	0	0
0	1	1	1	1	1	1	1	0	0	0	0	0	0	0	0	0	0	0

Figure 6.6b

Array Defining Reaches in the y-direction
For the Firth of Clyde Model

of each reach.

Secondly, invert levels at each grid point are obtained from a hydrographic chart. In choosing invert levels it should be remembered that the point is representative of conditions over an area $\Delta x \times \Delta y$ centred on the grid point. Hence, a mean level for this area should be adopted. Invert levels are given even for permanently dry areas as they determine the position at which moving shore boundaries cease to expand.

The bathmetry of the sea area is now defined as shown for the Firth of Clyde in Figure 7.1.

6.9.2 INITIAL CONDITIONS

The nature of tidal flow is such that numerical calculations are not heavily dependent upon initial conditions. Experience has shown, Harleman (1973), that if initial conditions of mean tidal level and zero flows are used, only three to eight tidal cycles are required before the solution converges to a quasi-steady state condition. This property of calculation can be used to generate realistic initial conditions for transient studies.

6.9.3 BOUNDARY DATA

Water level variation as a function of time is the more commonly used of the open boundary conditions as information is readily available in the form of the Admiralty Tide Tables and Co-tidal Charts, e.g. Chart No 5058 for the British Isles and surrounding sea areas. Flather and Heaps (1975) successfully used depth mean current

as the open boundary condition for their numerical model of Morecombe Bay. A considerable data collection effort was required and problems were encountered in ensuring the model contained the correct volume of water. It is noteworthy that in their conclusions they stress the advantages of using a large scale encompassing model to generate boundary conditions for a smaller scale model.

If a numerical model is used to examine the effect of proposed geometrical alterations on the tidal regime care must be taken with open boundary conditions, as input boundary data consists of incoming and reflected waves. When estuary geometry is altered the reflected wave and hence the boundary conditions will also be altered, Liu and Leendertse (1978).

6.9.4 SURGE DATA

When modelling storm surge propagation additional information is required. This includes increases in water level at the model's open sea boundaries, resulting from an external surge, together with information on wind speed, wind direction and barometric pressure variations over the model area. Collection of external surge data requires the installation of tidal gauges at open sea boundaries. For the British Isles surge data, i.e. wind and barometric pressure variations can be obtained at six hourly intervals from daily weather charts published by the Meteorological Office. Should these intervals prove too long for simulation purposes more detailed weather

station records can be obtained from the Meteorological Office.

CHAPTER SEVEN

NUMERICAL SIMULATION OF TIDE AND STORM SURGE PROPAGATION IN THE FIRTH OF CLYDE

7.1 CHOICE OF THE FIRTH OF CLYDE

The Firth of Clyde was chosen to test the numerical scheme's ability to model tide and storm surge phenomena for the following reasons:

i. Although providing only a modest tidal range (approximately 3.1m) the area provides a stern test of the model's capability to handle highly variable bathymetry, see Figure 7.1.

ii. Tide Tables provide data at coastal locations, in sufficient quantity to verify the model's performance.

iii. To capitalize on the efforts of Donald (1981) in collecting wind, pressure and surge data in the Firth.

iv. A comparison could be made between the results from the ADI method and those from Donald's x-y-t characteristic model.

7.2 PHYSICAL DESCRIPTION OF THE FIRTH OF CLYDE

The extent of the Firth of Clyde encompassed by the numerical model is shown in Figure 7.2 The seaward limit is defined by a line from Portpatrick to Sanda Island. A distance increment of 3000m was considered to provide a suitable representation of the bathymetry from Portpatrick in

FIGURE 7·1
FIRTH OF CLYDE BATHYMETRY.

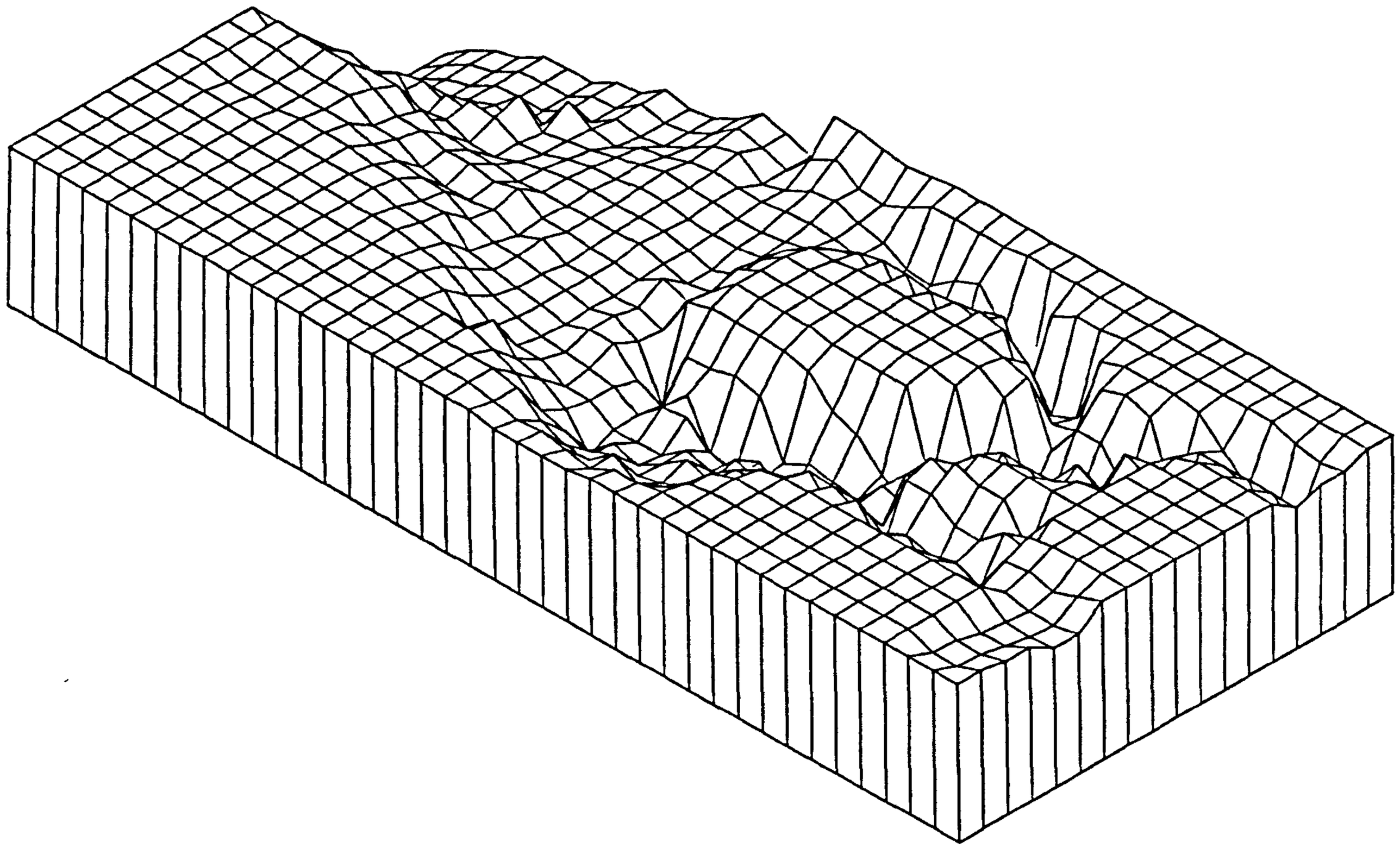

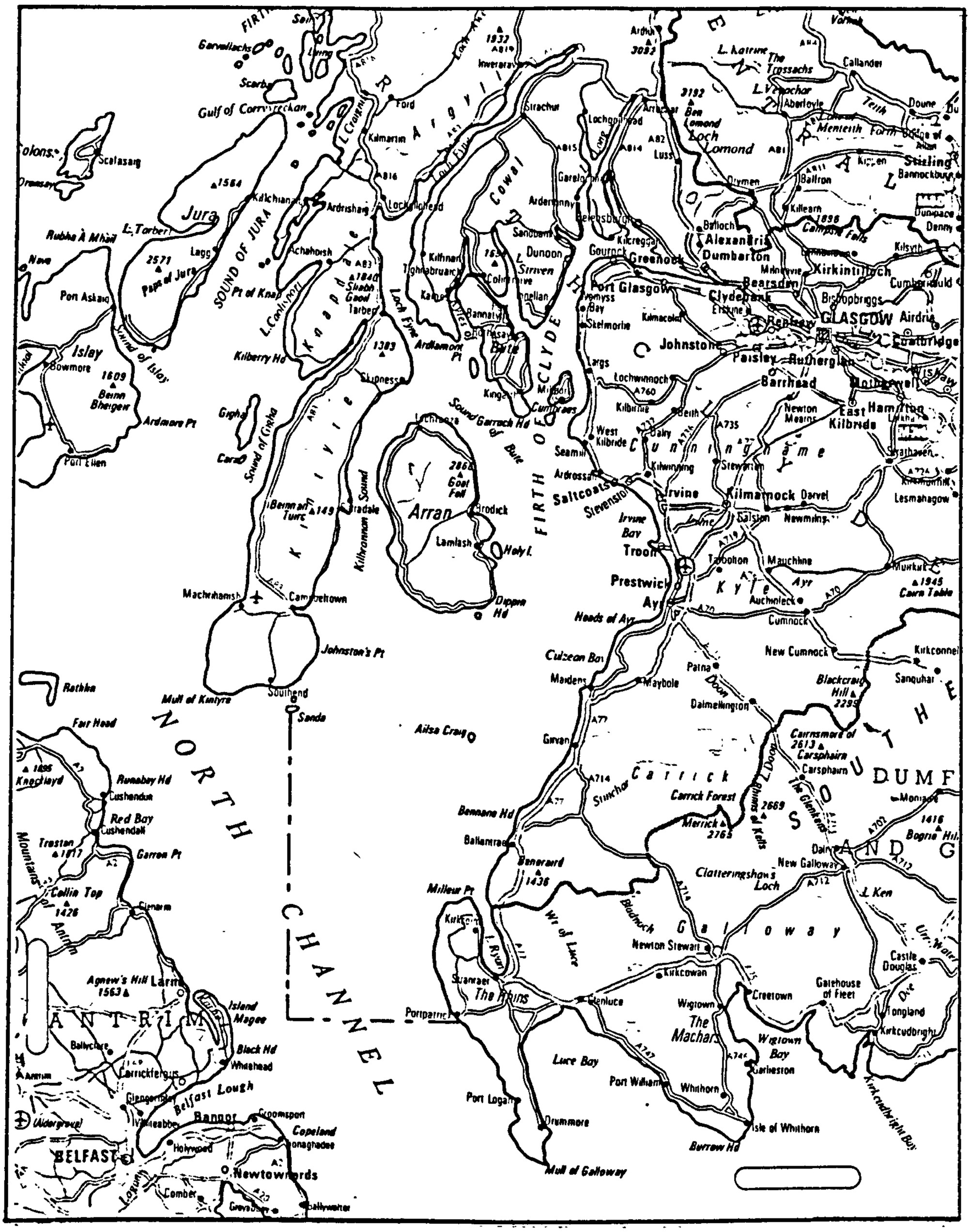

FIGURE 7·2
THE FIRTH OF CLYDE.

the south to the mouths of the River Clyde and Loch Fyne in the north. Further north, however, the fjordic nature of Loch Fyne and Loch Long and the length of the River Clyde mean that tidal influences propagate a considerable distance upstream in channels with a breadth less than that resolvable by the numerical grid. As the primary interest in the present study lies in modelling tide and storm surge propagation in the main body of the Firth, rather than flow details at the upstream extremities Loch Fyne, Loch Long and the River Clyde were represented within the numerical grid as equivalent water surface areas.

7.3 TIDE PROPAGATION IN THE FIRTH OF CLYDE AND SURROUNDING SEAS

Donald (1981) placed tidal motion in the Firth of Clyde in context with the tidal oscillations occurring in the surrounding seas. The area is shown in Figure 7.3, together with the co-range and co-phase lines for the M_2 tide as computed by Doodson and Corkan (1932).

The progression of the co-phase lines in the North Channel indicate that the Firth of Clyde tides are determined by tidal propagation across the coast of Northern Ireland from the Atlantic Ocean. Hence, the Firth of Clyde tides are in co-oscillation with those in an area of the Atlantic, west of the Clyde. This is an interesting feature since the orientation of the Firth of Clyde is north-southwards and so is more exposed, yet apparently less influenced by the tidal oscillations in the Irish Sea. This feature

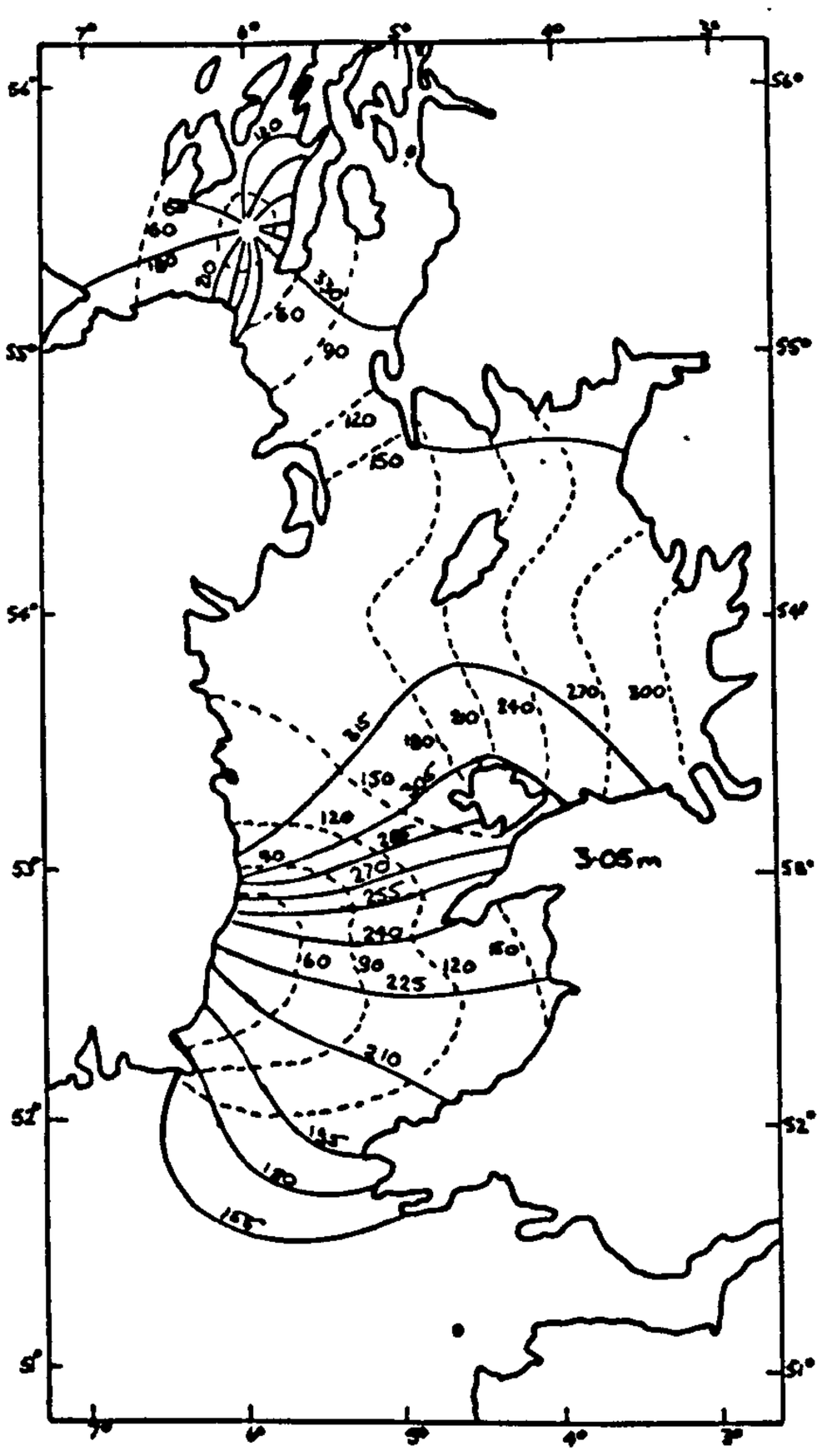

Co-tidal and co-range lines of the M_2 tide in the Irish Sea.
—, phase in degrees referred to upper culmination of the moon in Greenwich
---, amplitude in cm.

FIGURE 7·3

is also evident in the tidal streams shown later in section 7.9.

The tidal propagation in the Firth of Clyde itself is straight-forward since it is a converging estuary which communicates with the North Channel through only one open sea boundary. The average spring range varies from 2.5 metres at the mouth to 3.1 metres at the head of the estuary while the phase difference along its length is around thirty minutes.

7.4 PAST NUMERICAL STUDIES IN THE FIRTH OF CLYDE

Previous numerical modelling efforts in the Firth of Clyde include those of Ellis (1970, 1972), who employed a one-dimensional characteristic scheme to model tide propagation in the River Clyde, the Gareloch, Loch Long and Loch Goil.

More recently, Donald (1981) used a two-dimensional characteristic model, based on work of Townson (1974) to model tide and storm surge propagation in the Firth of Clyde. Discretization of the present model is similar to Donald's model 3. The intention was to draw conclusions regarding the relative merits of characteristic and ADI methods when applied to tide and storm surge propagation problems in coastal seas.

7.5 BOUNDARY CONDITIONS

Fresh water inflows and variations in surface areas from flooding of sand flats were considered unimportant

in the Firth of Clyde. Two boundary conditions are therefore required. One relates the normal component of flow at the land water boundaries to zero:

$$qy = 0$$

or

$$qx = 0$$

and the other defines boundary water levels as a function of time. The open boundary is considered to extend from Portpatrick to Sanda Island, see Figure 7.2. Data concerning the spring tide ranges along this boundary was taken from Admiralty Chart No 5058. Variations between high and low water are considered to be of cosine form. Range and phase data are read in by the model and the water level variations on the boundary are calculated automatically.

7.6 INITIAL CONDITIONS

Initial conditions for the first tidal period were taken as: zero flows and water levels corresponding to mean tidal level. After a run of three tidal cycles, a periodic variation of water level in the estuary had been attained. At this point the calculation was terminated and the final conditions used as initial conditions for all subsequent runs.

7.7 WAVE DEFORMATION CHARACTERISTICS

Before proceeding with the calibration process the model's sensitivity to choice of time increment and theta value was tested.

Plots of water level verses time at selected positions

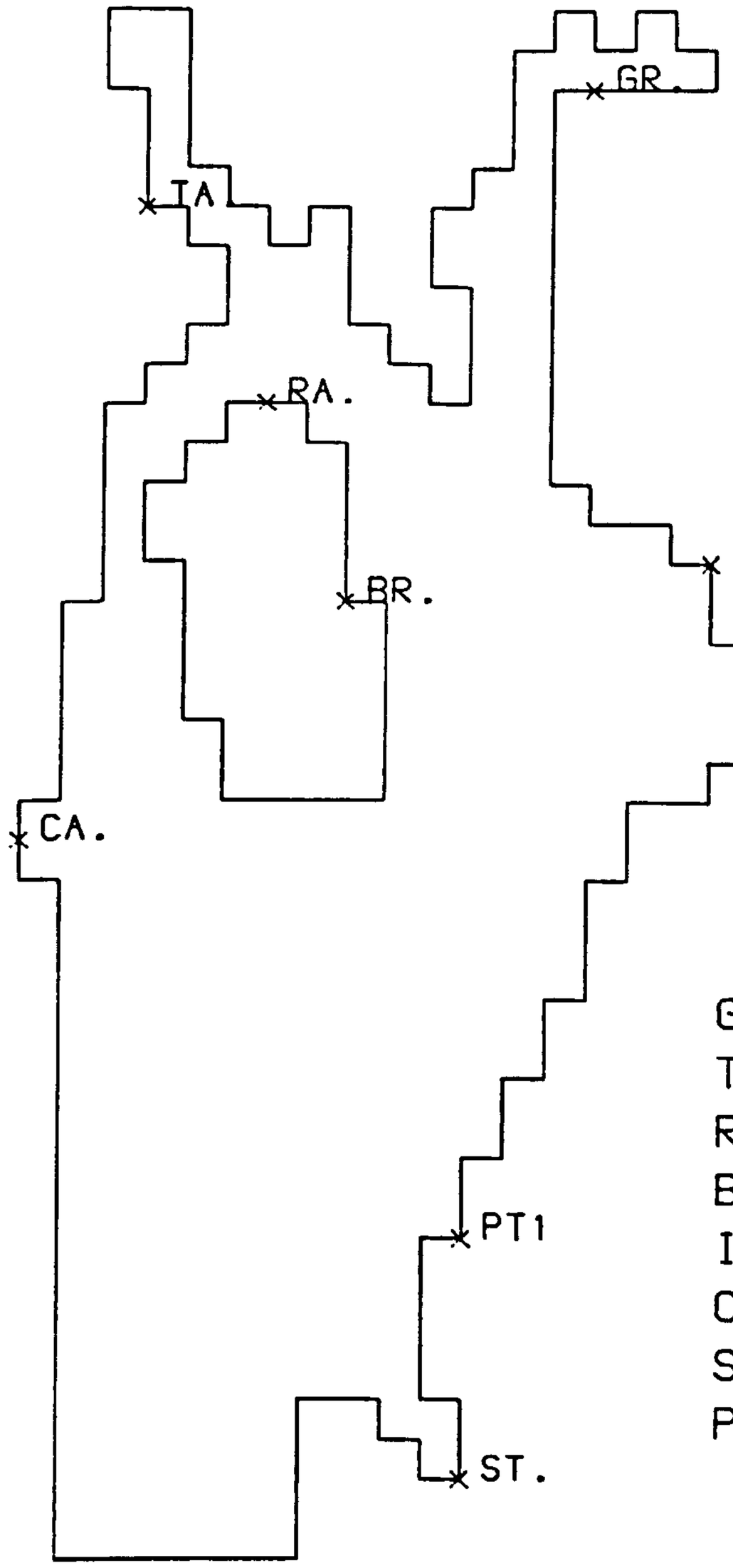

FIGURE 7·4 a
POSITION OF WATERLEVEL HISTORYS

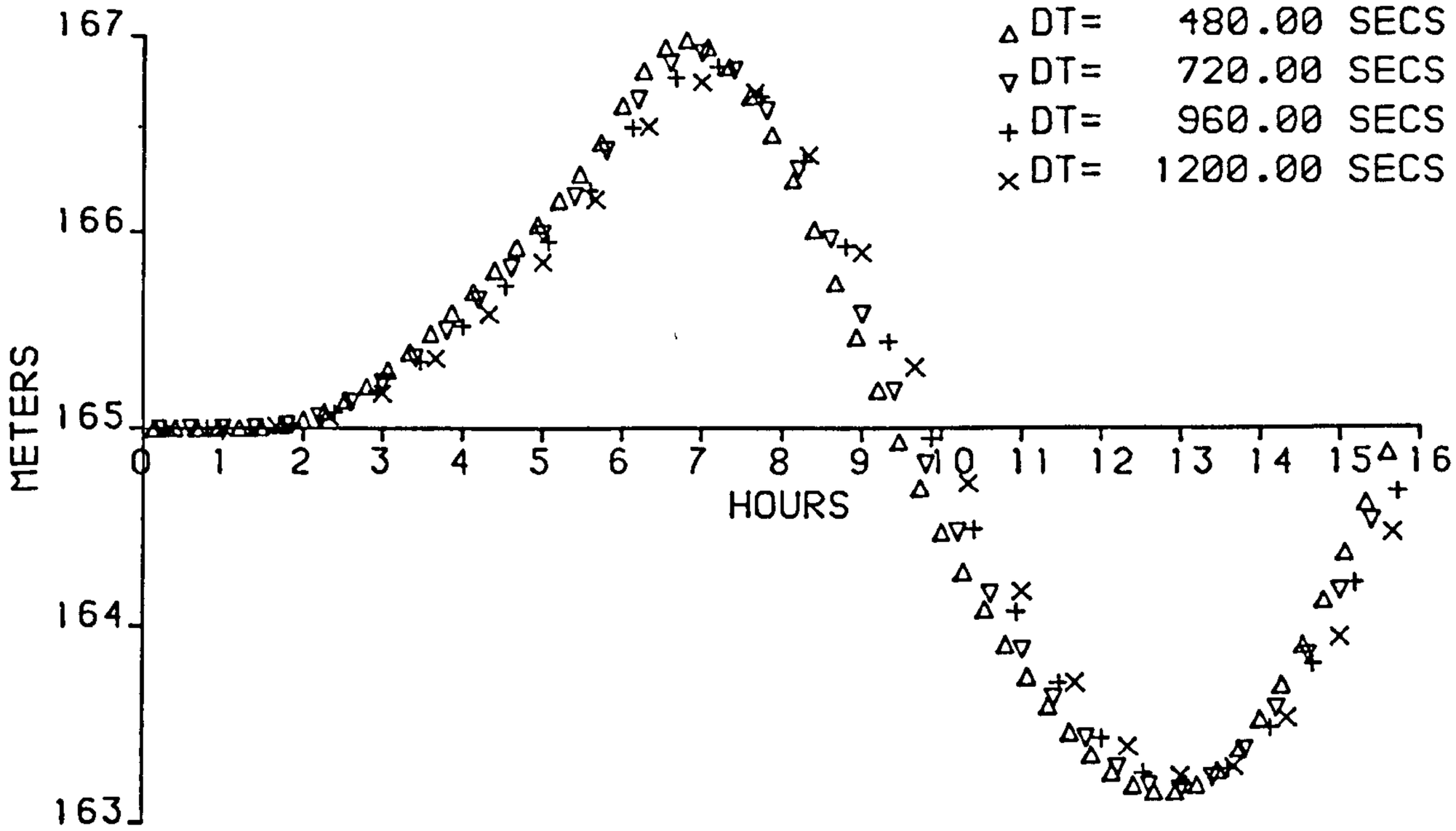

FIGURE 7·4 b

TIME HISTORY OF WATERLEVELS AT GREENOCK

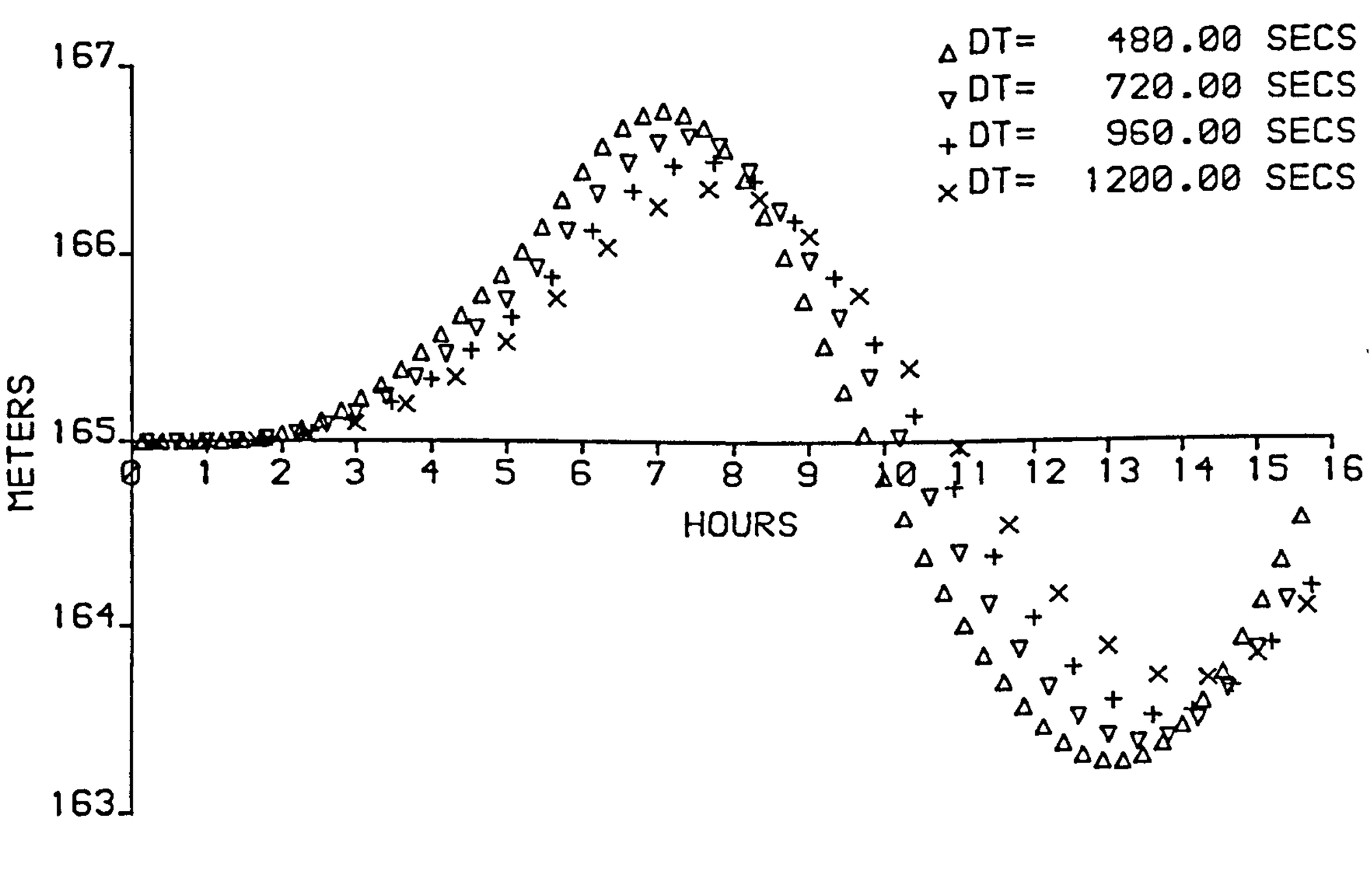

FIGURE 7·4 c

TIME HISTORY OF WATERLEVELS AT EAST LOCH TARBERT

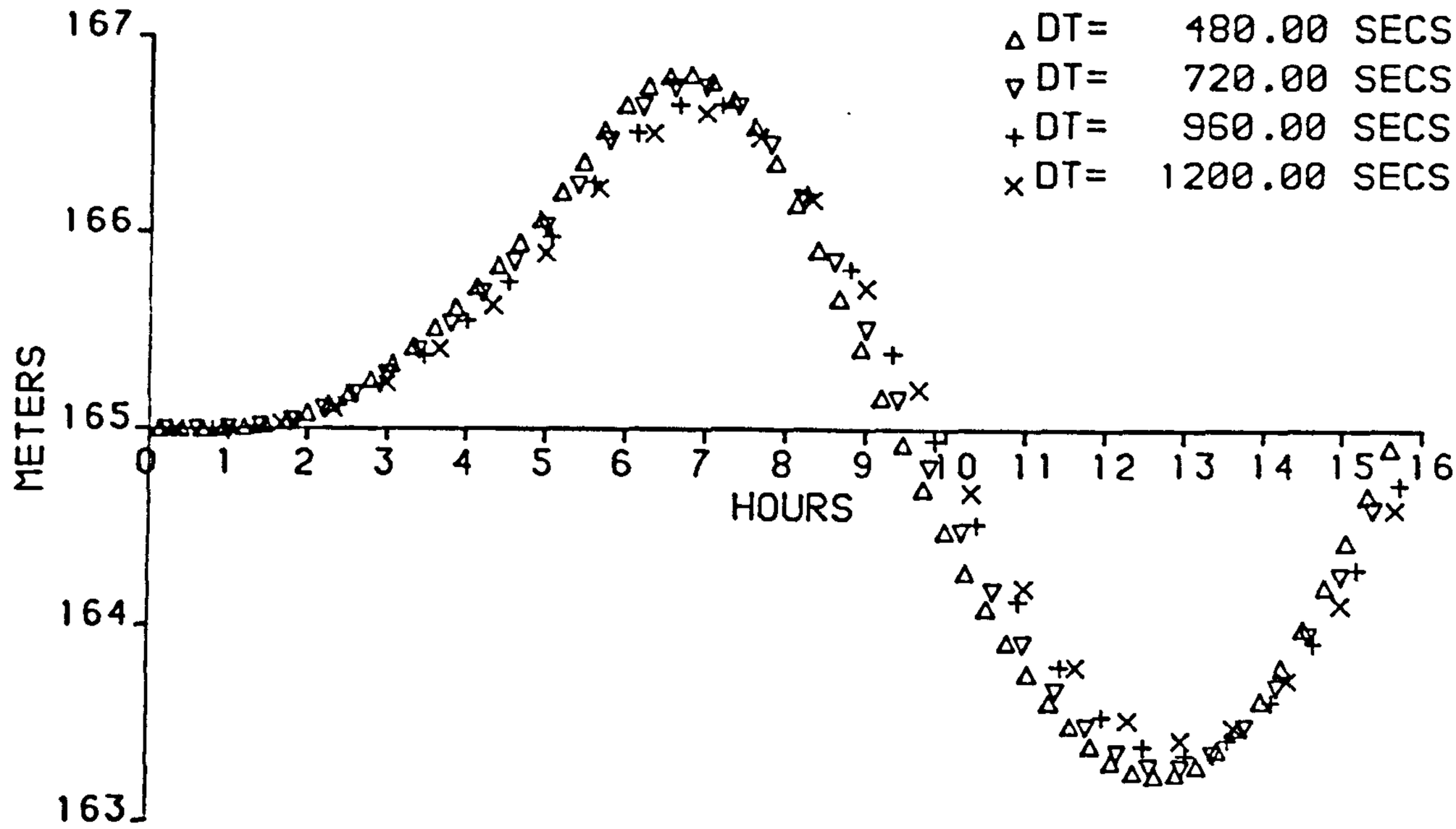

FIGURE 7·4 d

TIME HISTORY OF WATERLEVELS AT LOCH RANZA

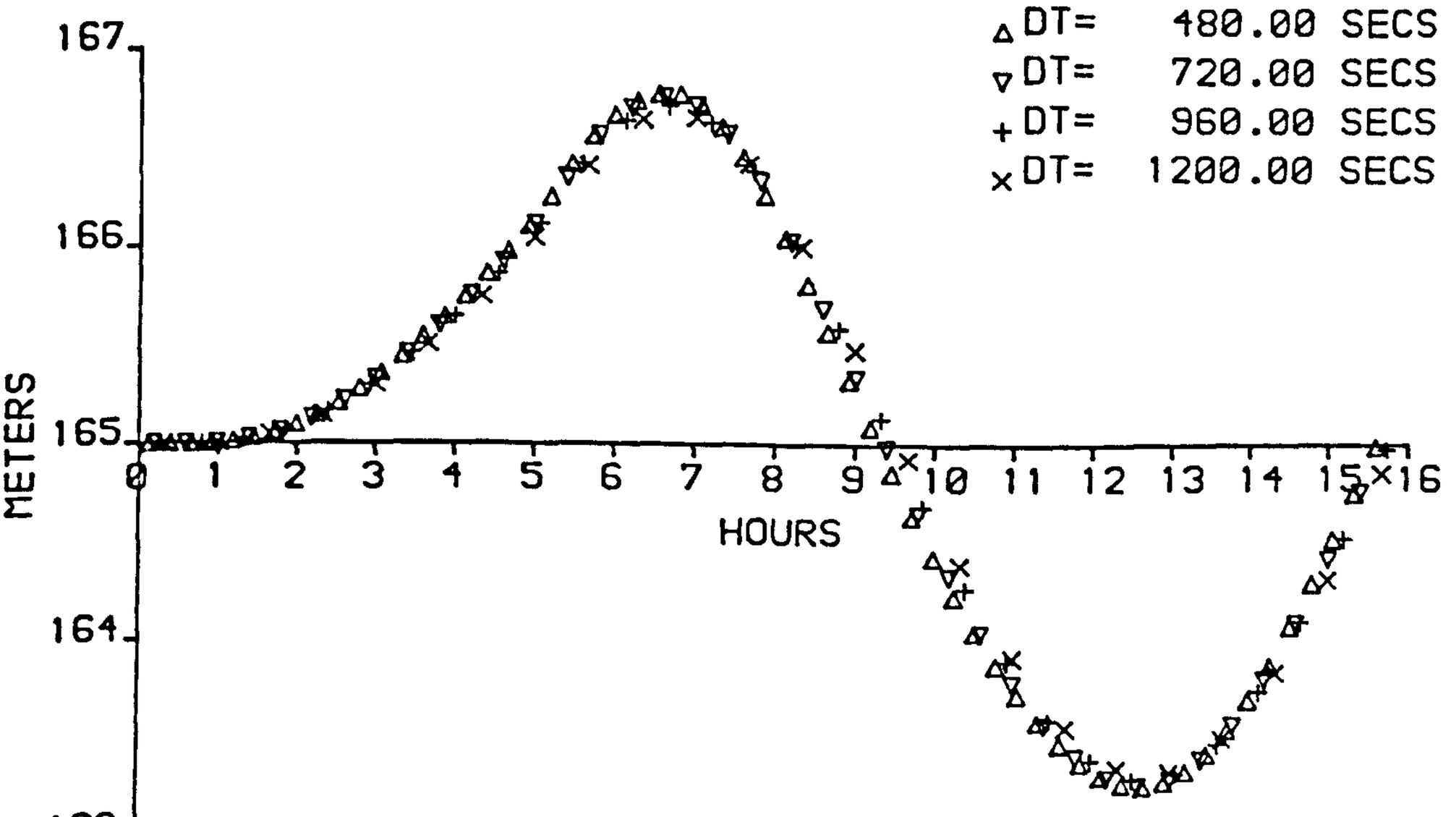

FIGURE 7·4e

TIME HISTORY OF WATERLEVELS AT BRODICK BAY

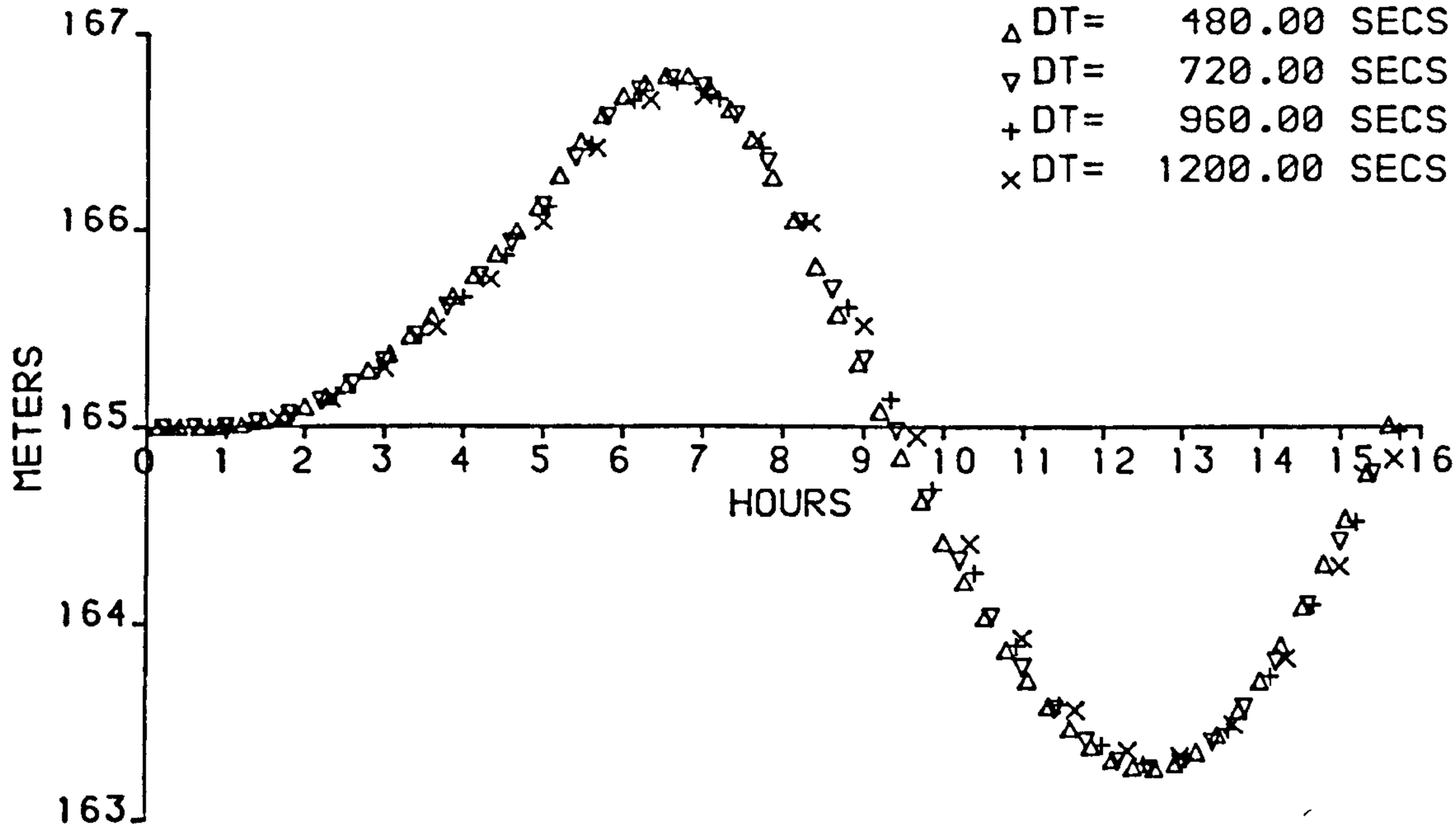

FIGURE 7·4 f

TIME HISTORY OF WATERLEVELS AT IRVINE

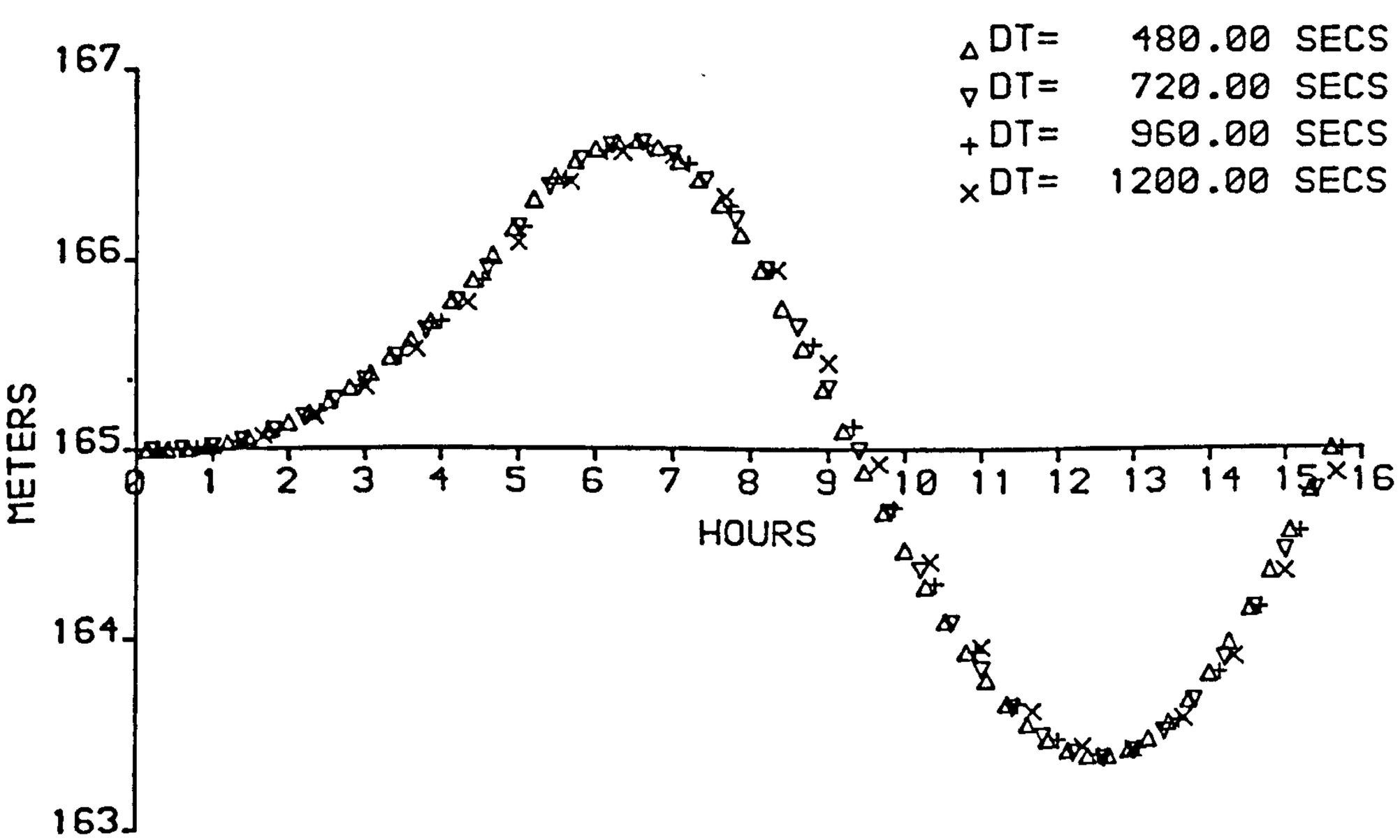

FIGURE 7·4g

TIME HISTORY OF WATERLEVELS AT CAMPBELTOWN

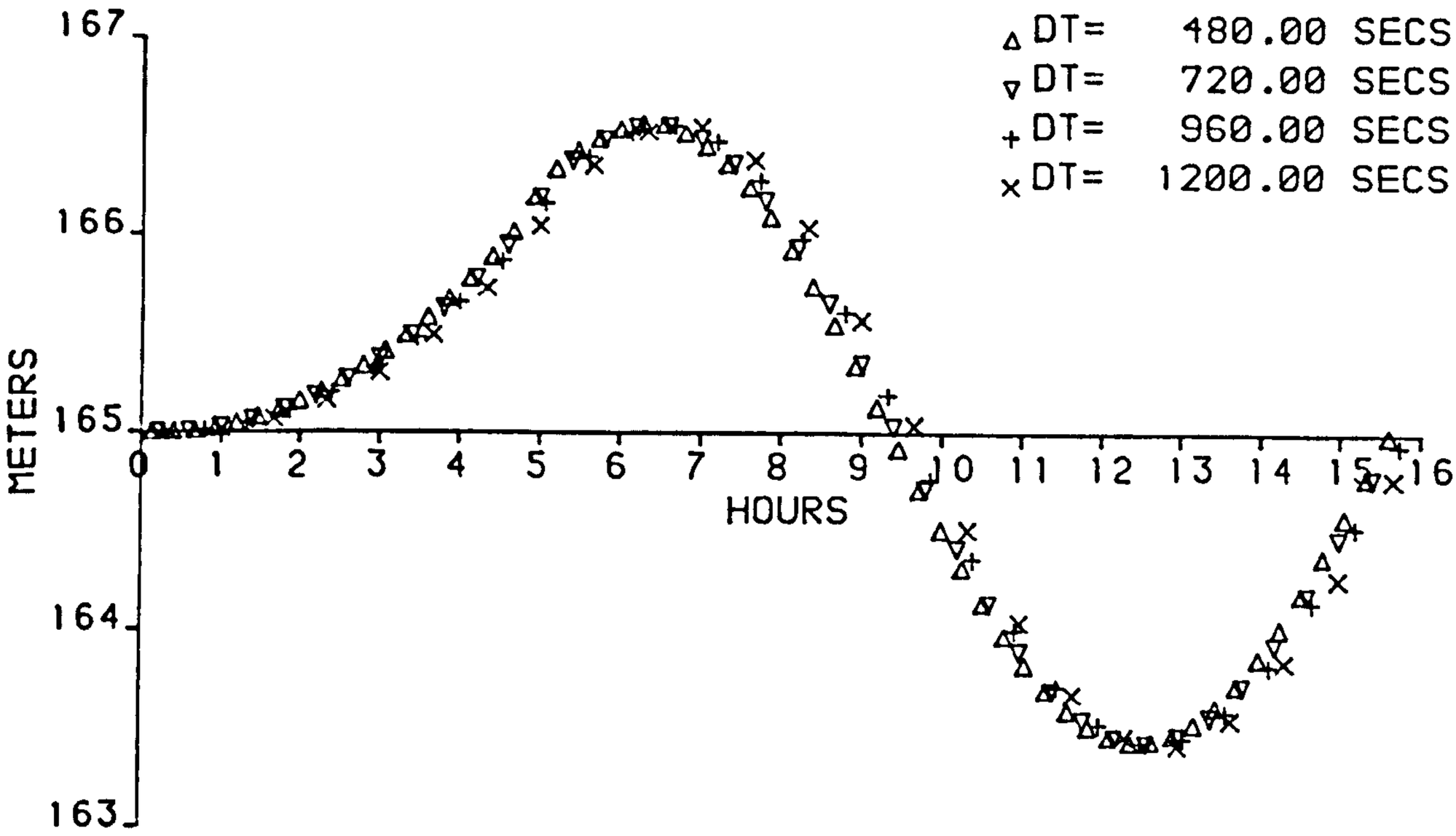

FIGURE 7·4h

TIME HISTORY OF WATERLEVELS AT STRANRAER

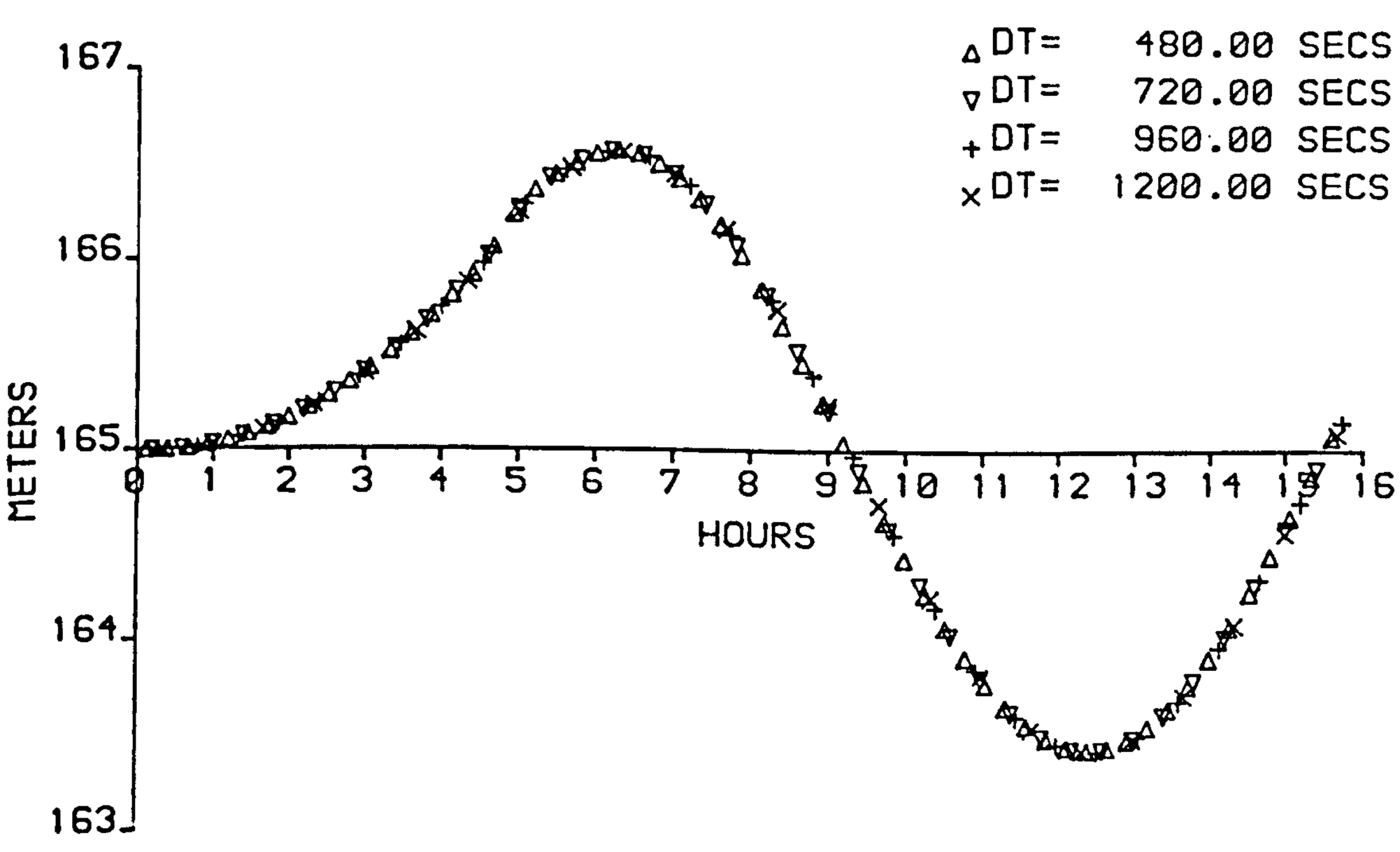

FIGURE 7·4i

TIME HISTORY OF WATERLEVELS AT POINT ONE

in the Firth are shown in Figures 7.4a to 7.4i. Four values of time increment were used corresponding to average Courant numbers of 4, 5, 7 and 9. The results show that although the numerical scheme remains stable for high Courant numbers the accuracy of the results is reduced in areas of the model. This numerical damping is most pronounced in the East Loch Tarbert region, Figure 7.4c, where 28% reduction in the computed range is recorded by using a Courant number of 9.

The reason behind this numerical damping can be seen from examining the schematization of the Firth in Figure 7.4a. In the East Loch Tarbert area the centreline of Loch Fyne runs at 45° to the numerical grid. This necessitates use of an irregular closed boundary to schematize the banks of the loch. The effect of such a feature on ADI solutions of the long wave equations has been studied by Weare (1979). Weare showed that by using this type of schematization effectively a no-slip condition is imposed along the model walls. He concluded that care should be taken in the application of ADI schemes to ensure that the economic advantages of operating at high Courant numbers do not override accuracy considerations.

Using a Courant number of four the influence of theta on computed results was assessed by varying its value between 1.0 and 0.6. Figures 7.5a to 7.5m show comparisons of computed tidal records at selected locations within the Firth. It is evident from these that variations

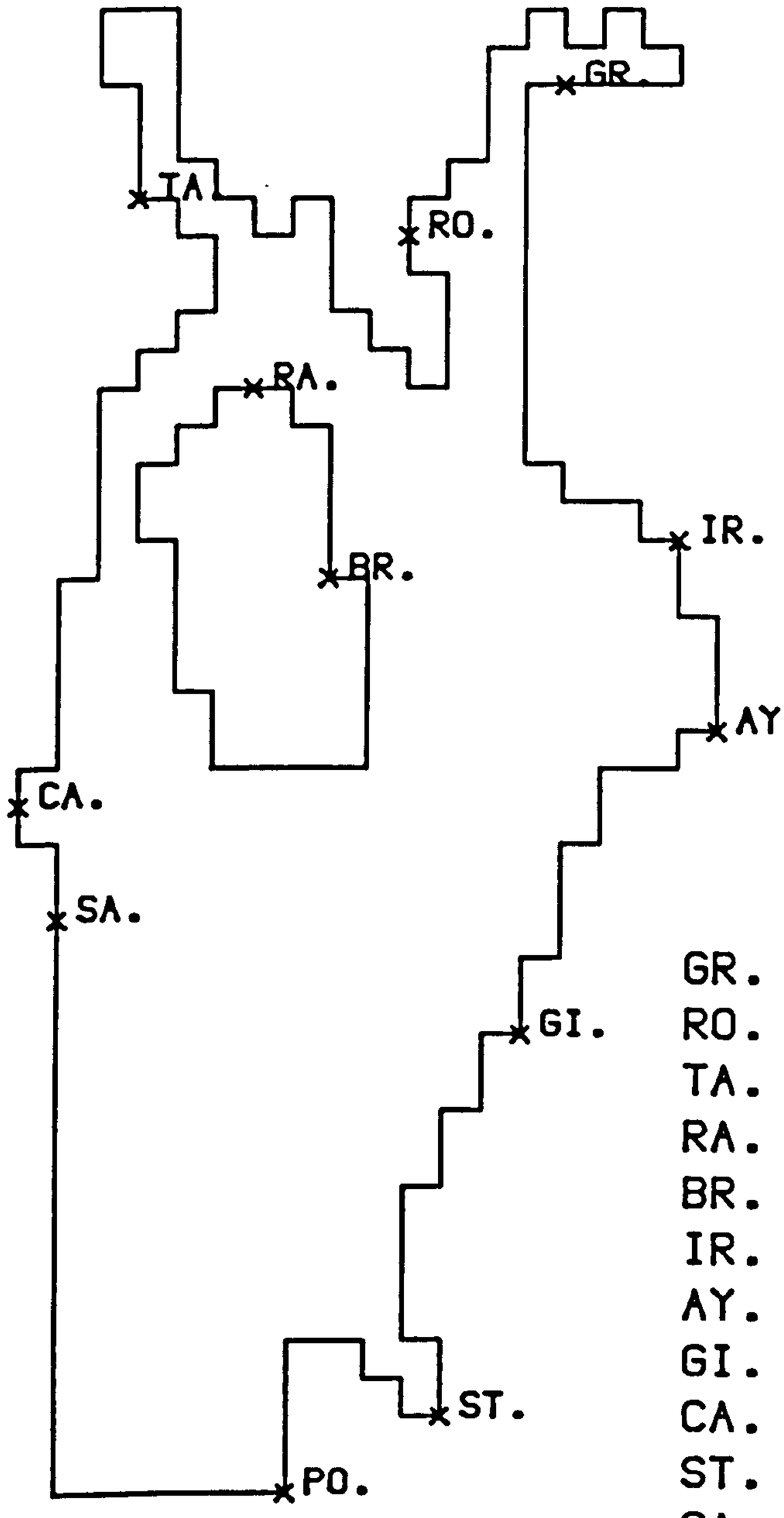

GR. GREENOCK
RO. ROTHESAY BAY
TA. EAST LOCH TARBERT
RA. LOCH RANZA
BR. BRODICK BAY
IR. IRVINE
AY. AYR
GI. GIRVAN
CA. CAMPBELTOWN
ST. STRANRAER
SA. SANDA ISLAND
PO. PORTPATRICK

FIGURE 7·5a
POSITION OF WATER LEVEL HISTORYS

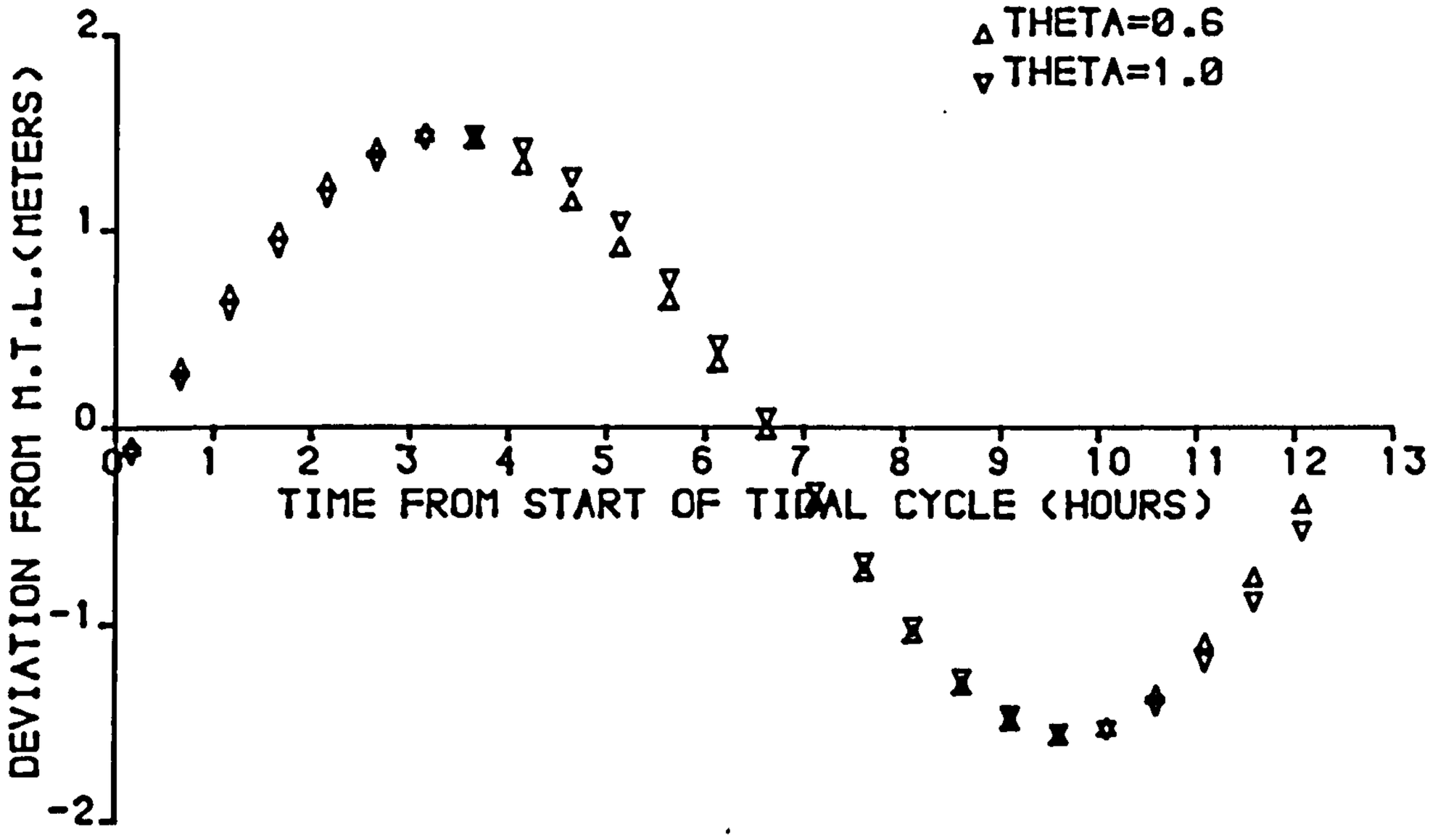

FIGURE 7.5 b

SPRING TIDE WATER LEVELS AT GREENOCK

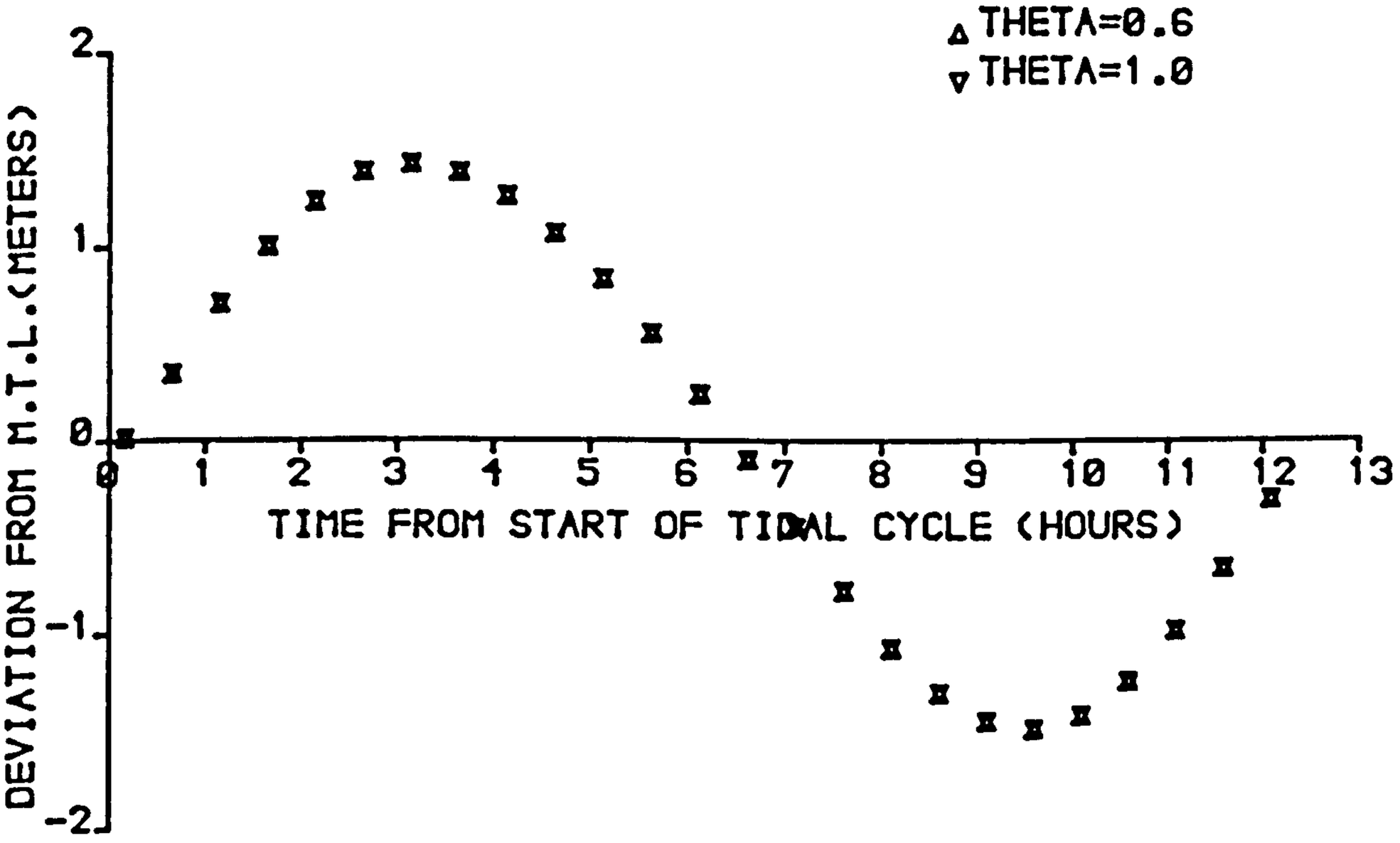

FIGURE 7.5c

SPRING TIDE WATER LEVELS AT ROTHESAY BAY

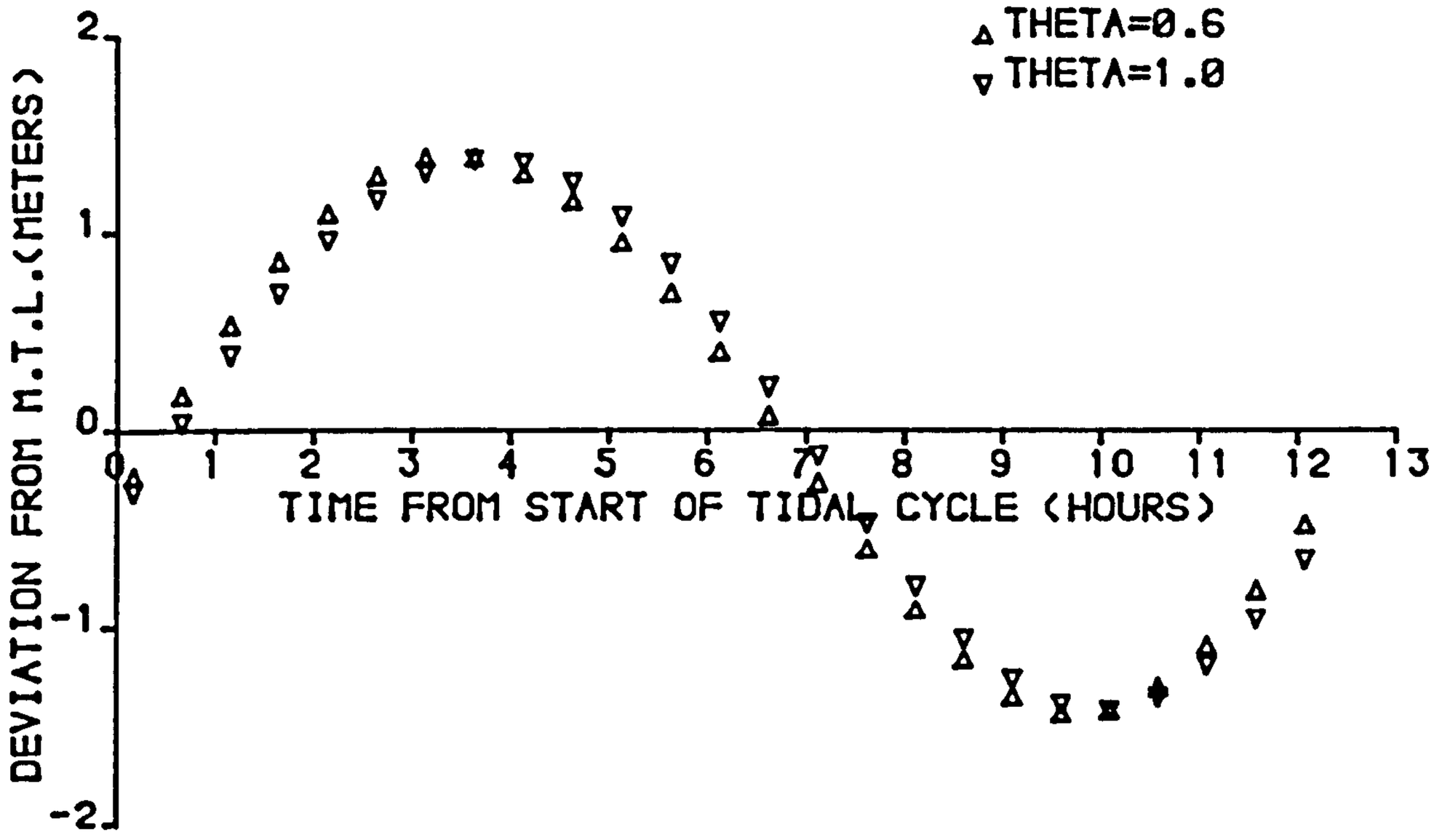

FIGURE 7·5d

SPRING TIDE WATER LEVELS AT EAST LOCH TARBERT

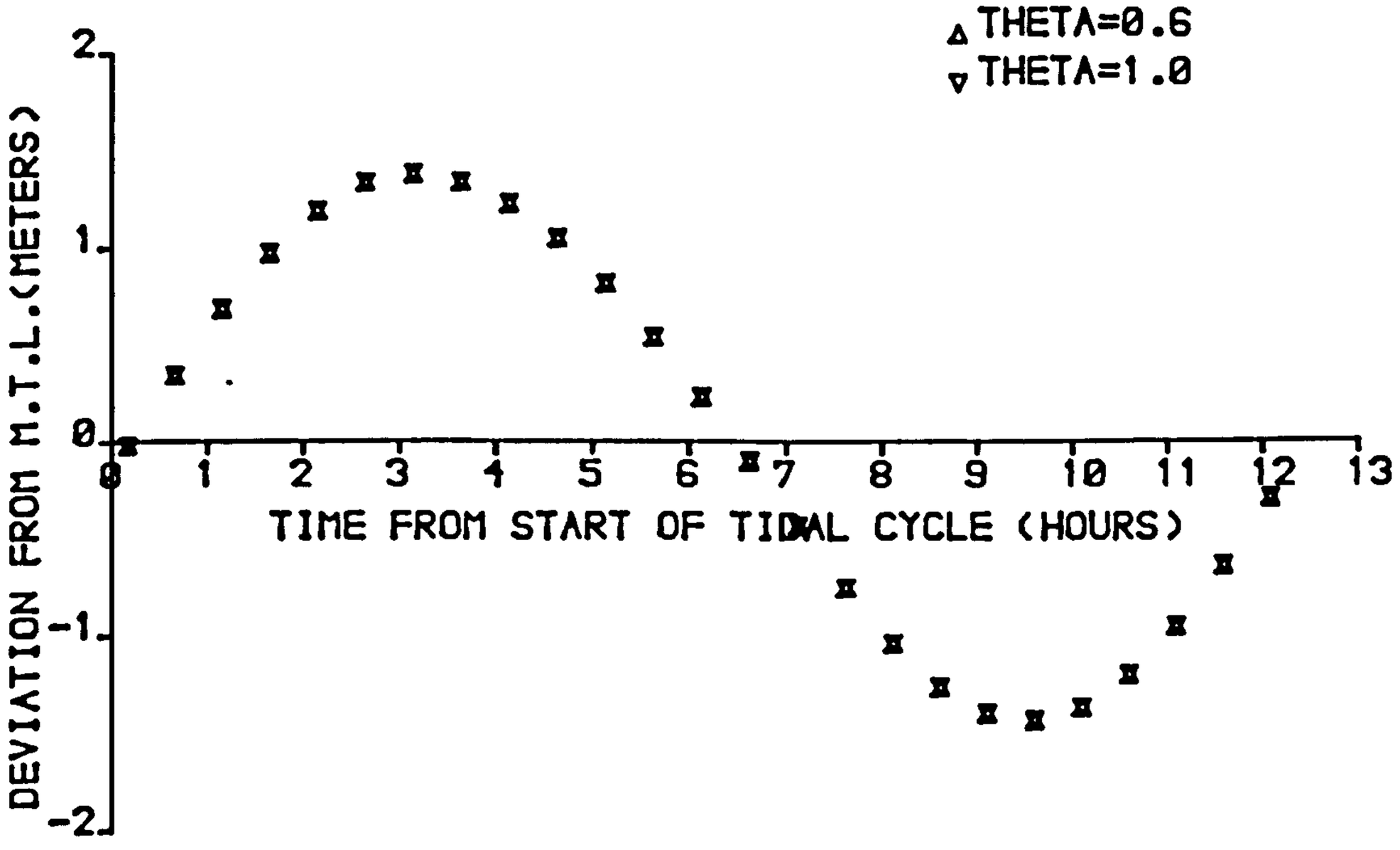

FIGURE 7·5e

SPRING TIDE WATER LEVELS AT LOCH RANZA

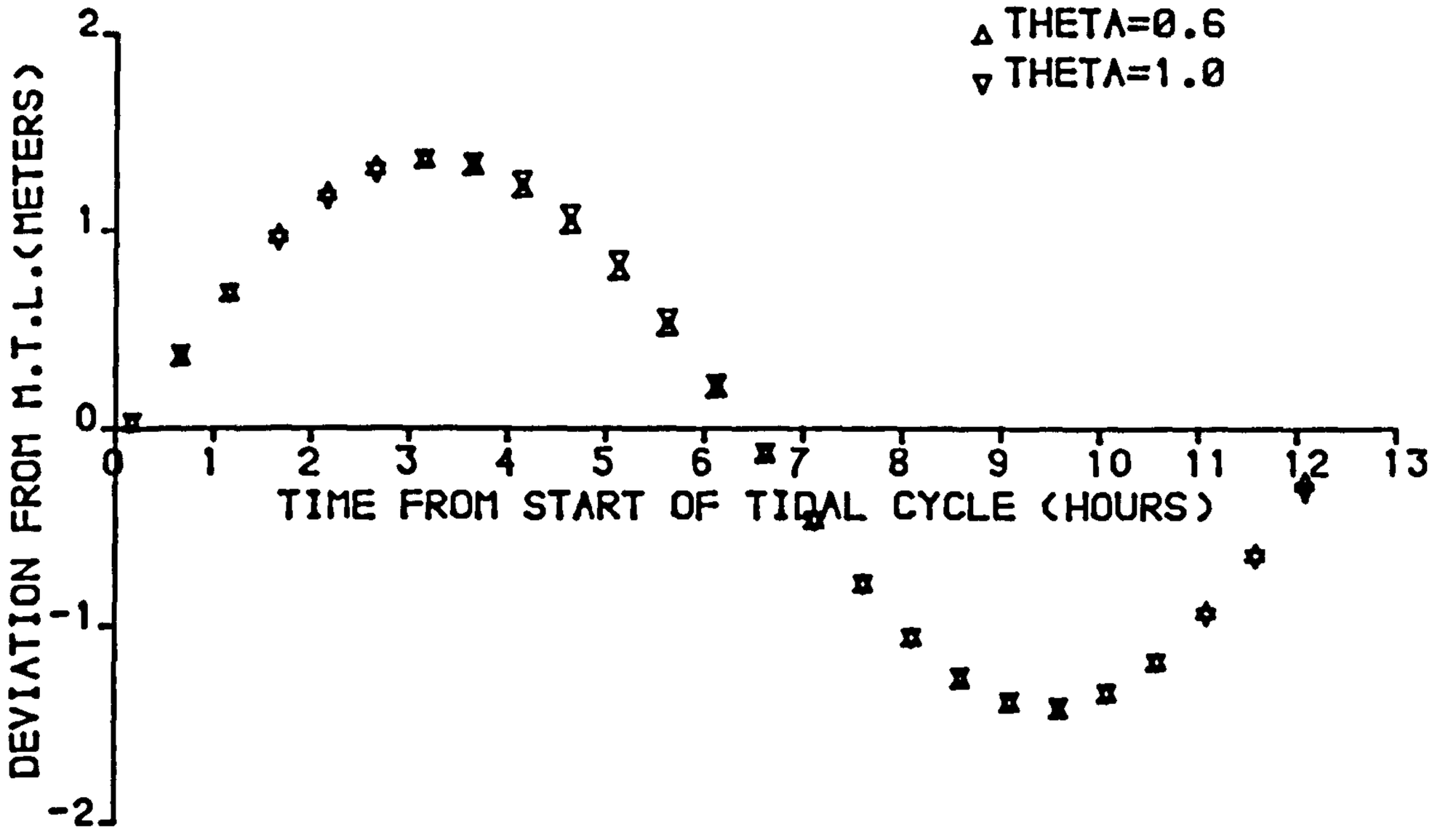

FIGURE 7·5f

SPRING TIDE WATER LEVELS AT BRODICK BAY

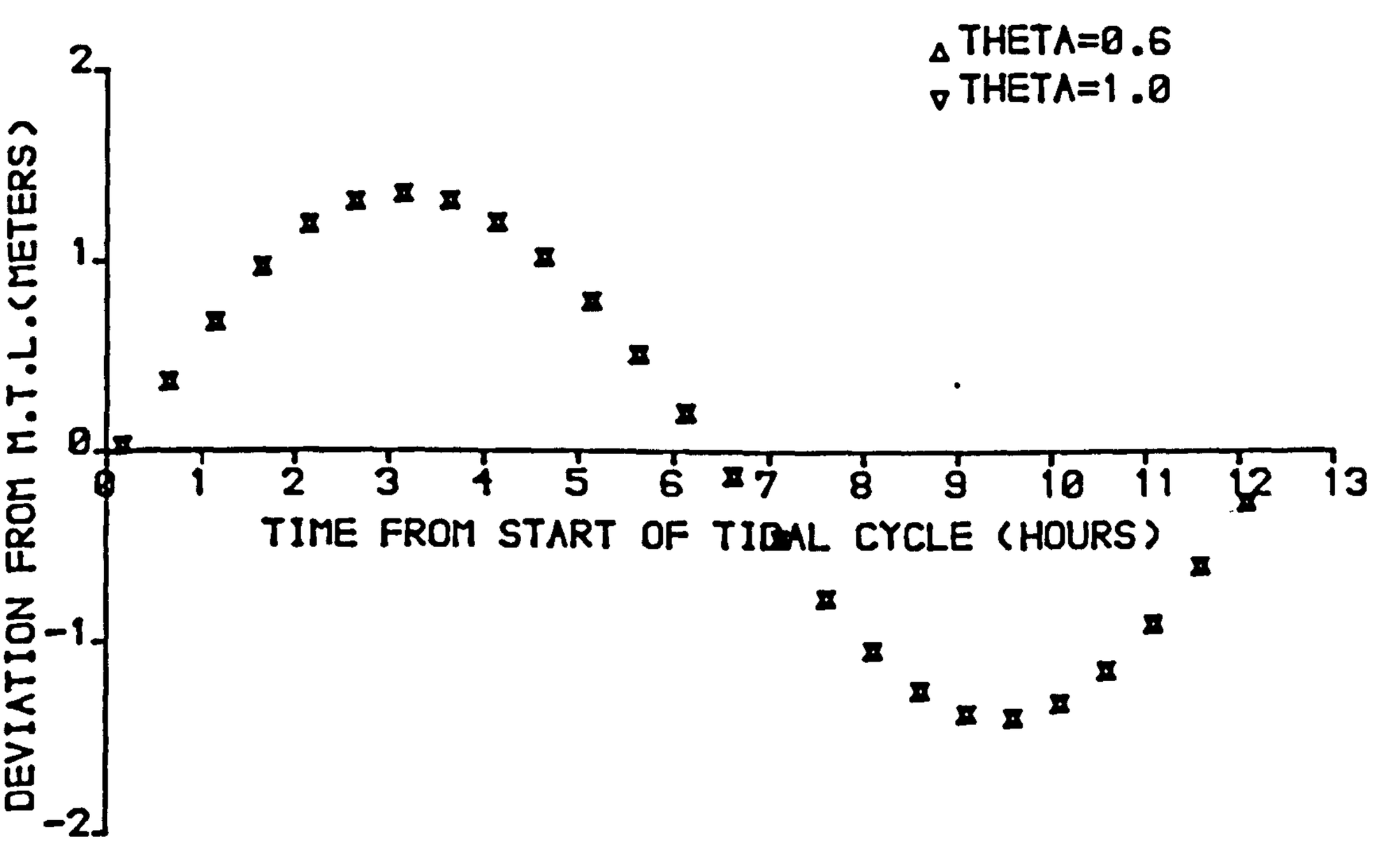

FIGURE 7·5g

SPRING TIDE WATER LEVELS AT IRVINE

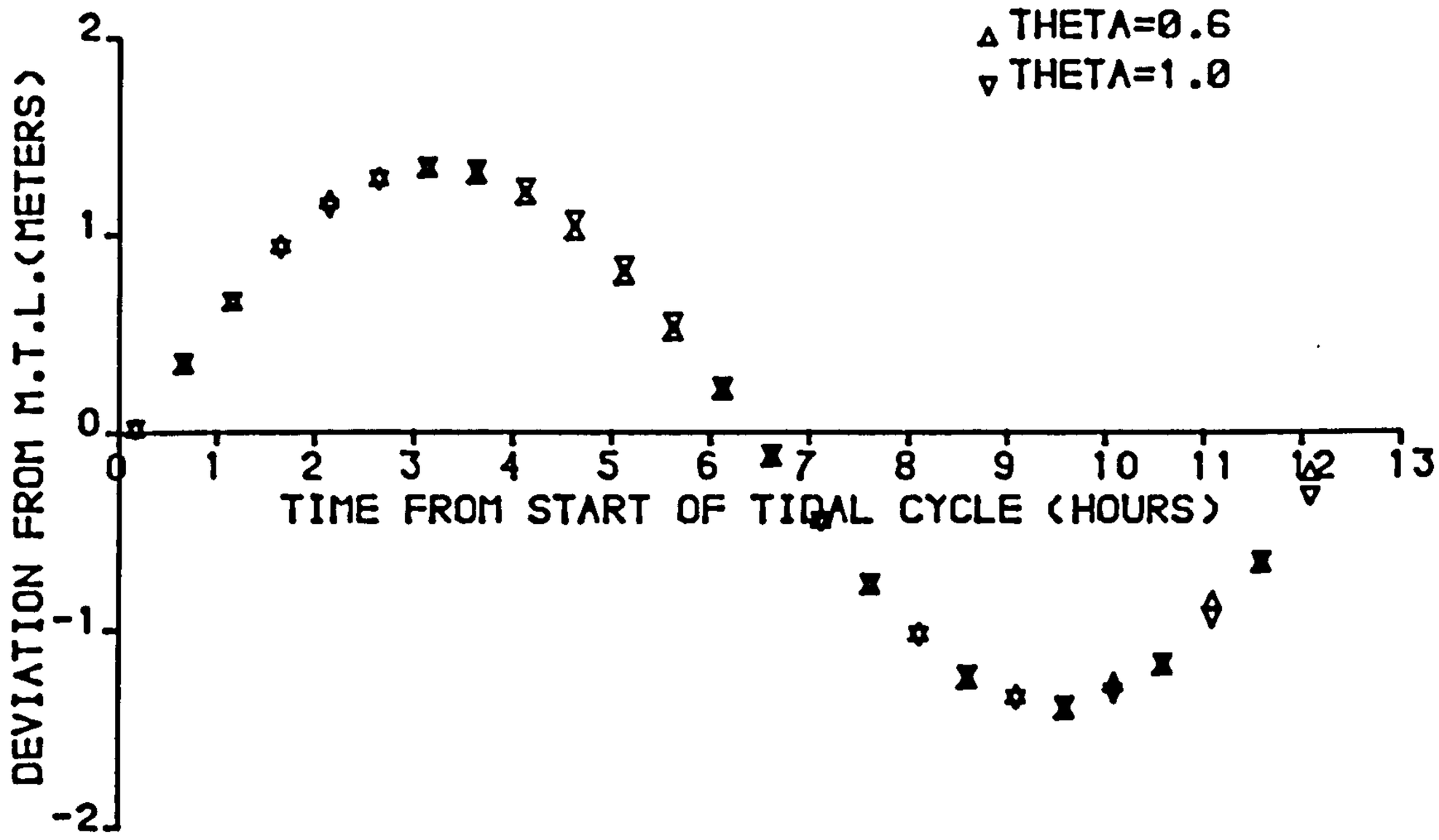

FIGURE 7·5h

SPRING TIDE WATER LEVELS AT AYR

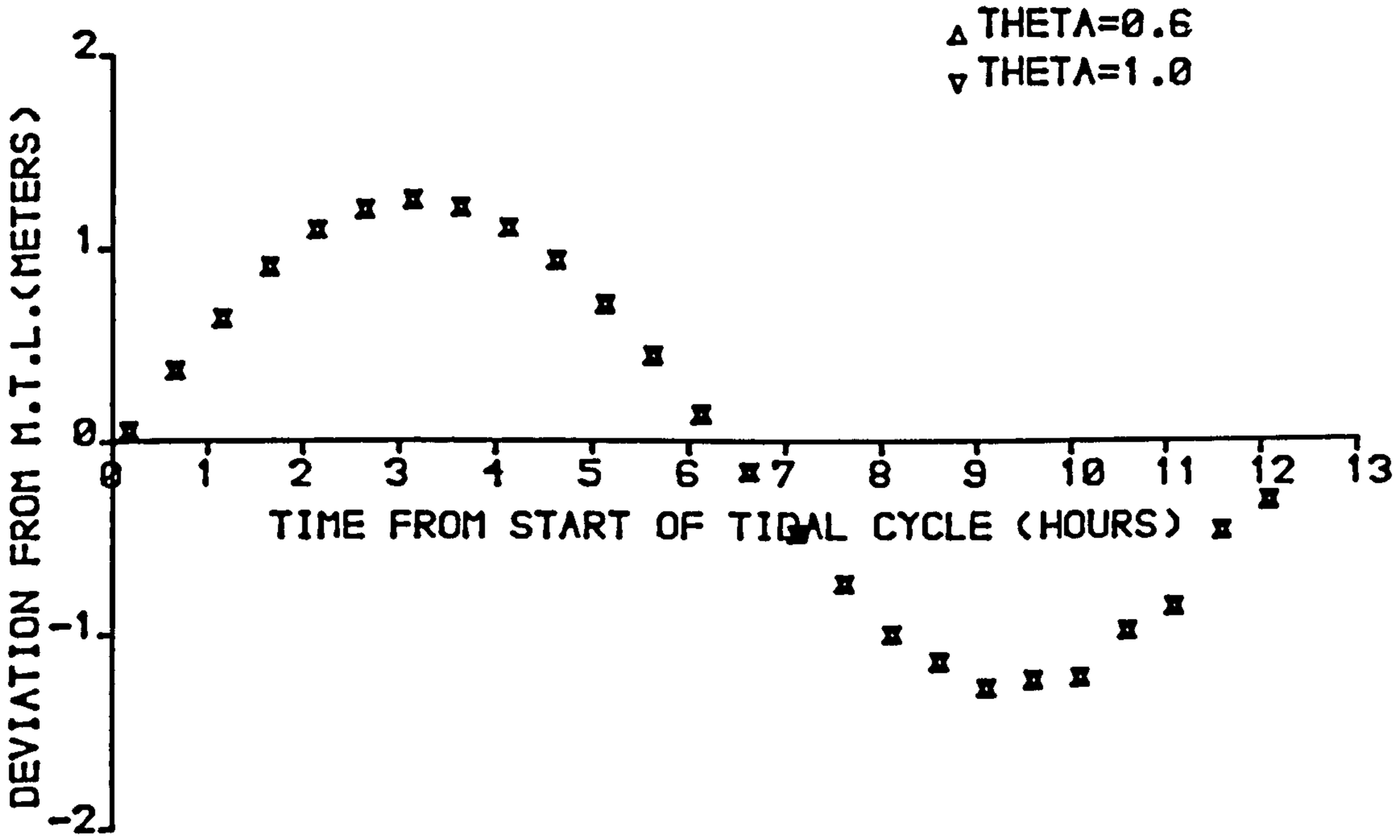

FIGURE 7·5i

SPRING TIDE WATER LEVELS AT GIRVAN

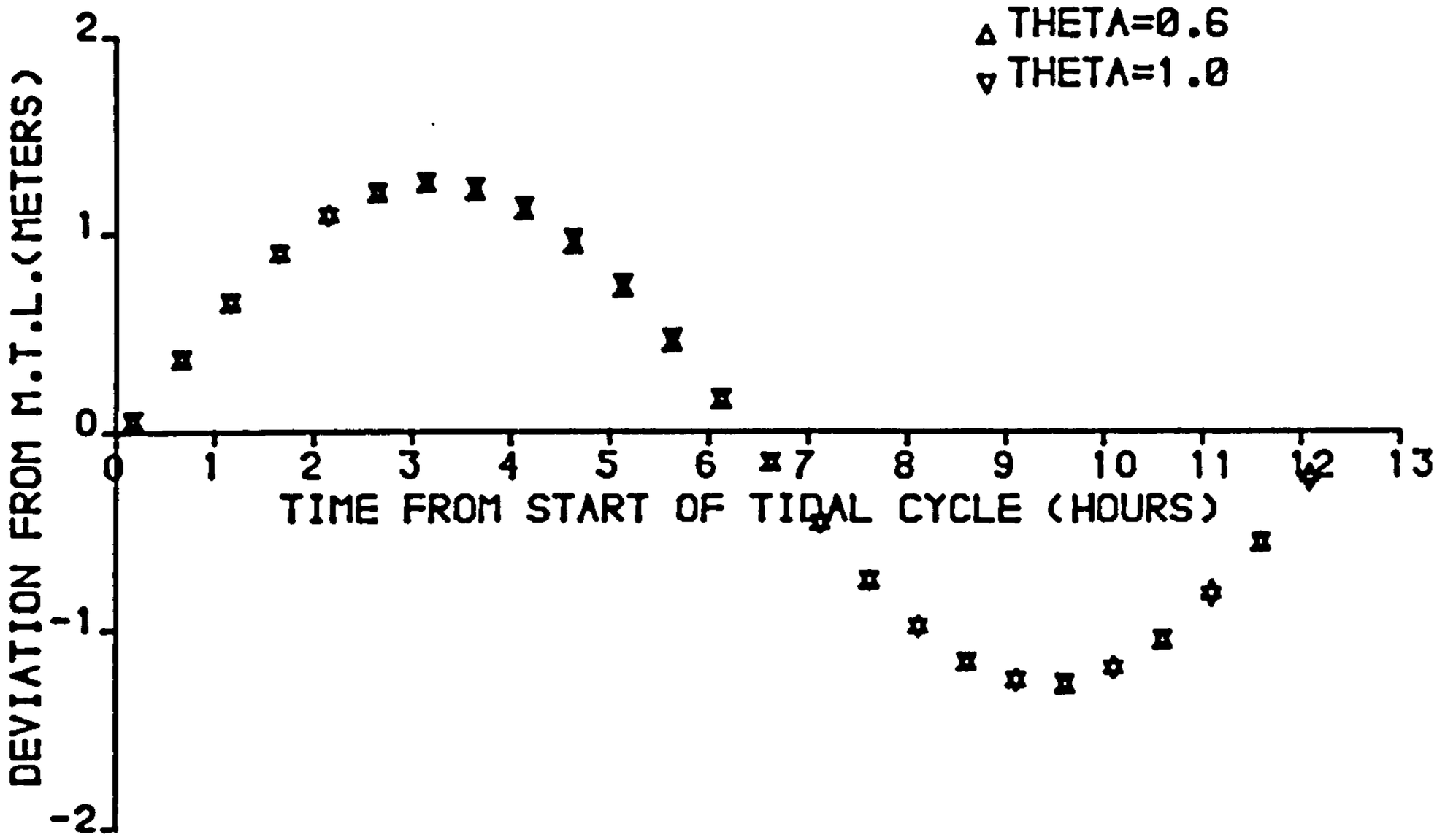

FIGURE 7·5j

SPRING TIDE WATER LEVELS AT CAMPBELTOWN

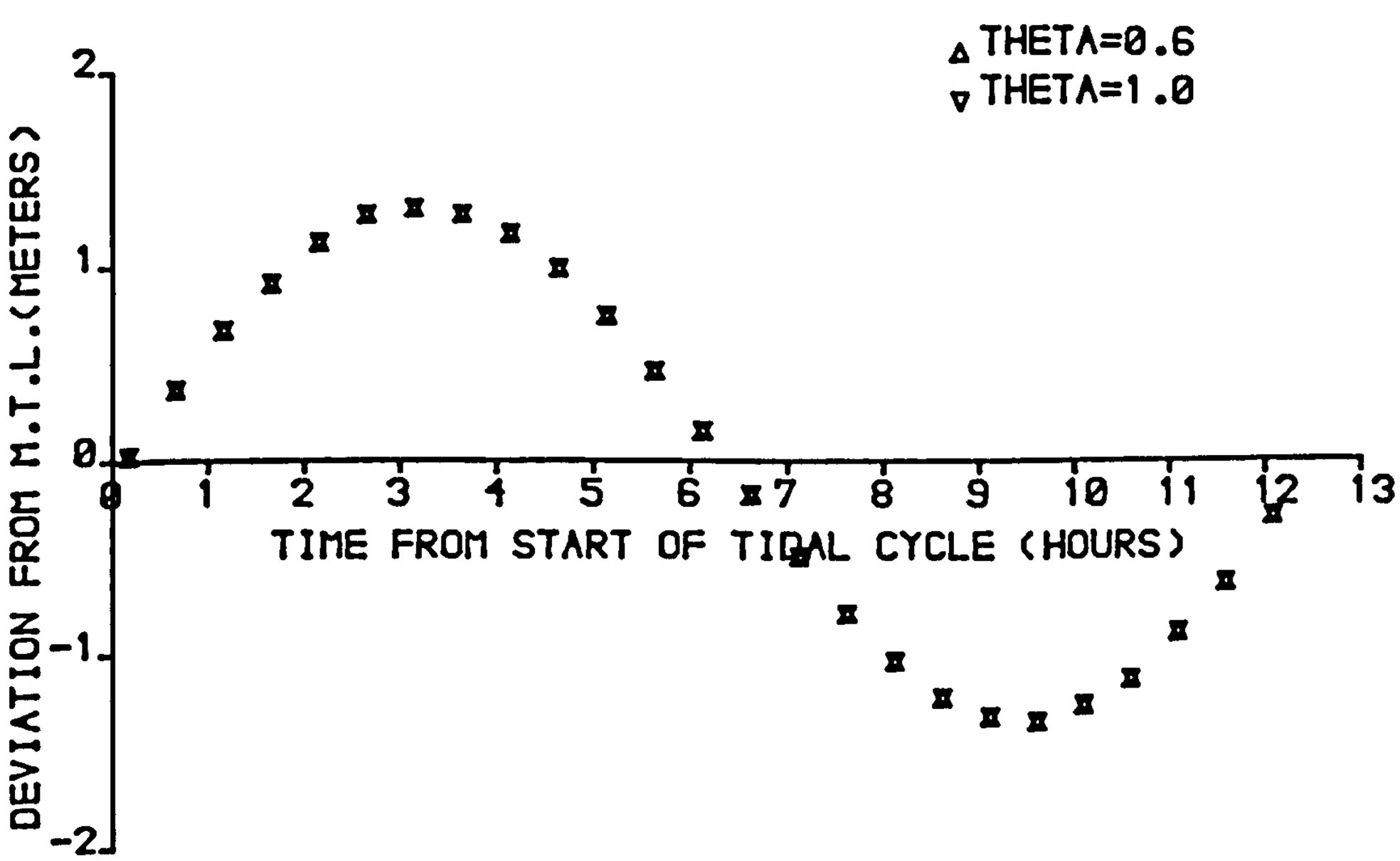

FIGURE 7·5k

SPRING TIDE WATER LEVELS AT STRANRAER

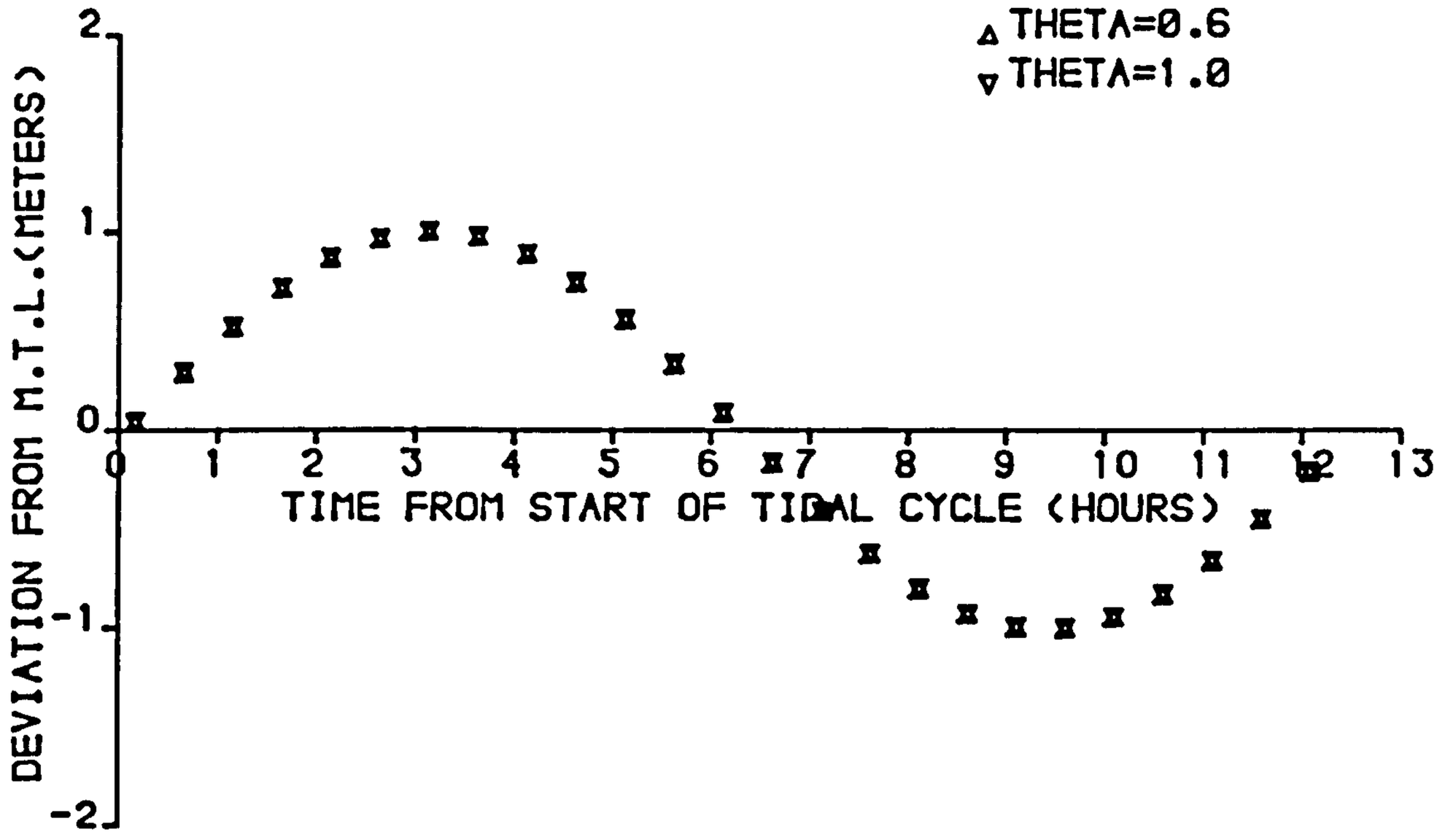

FIGURE 7·5l

SPRING TIDE WATER LEVELS AT SANDA ISLAND

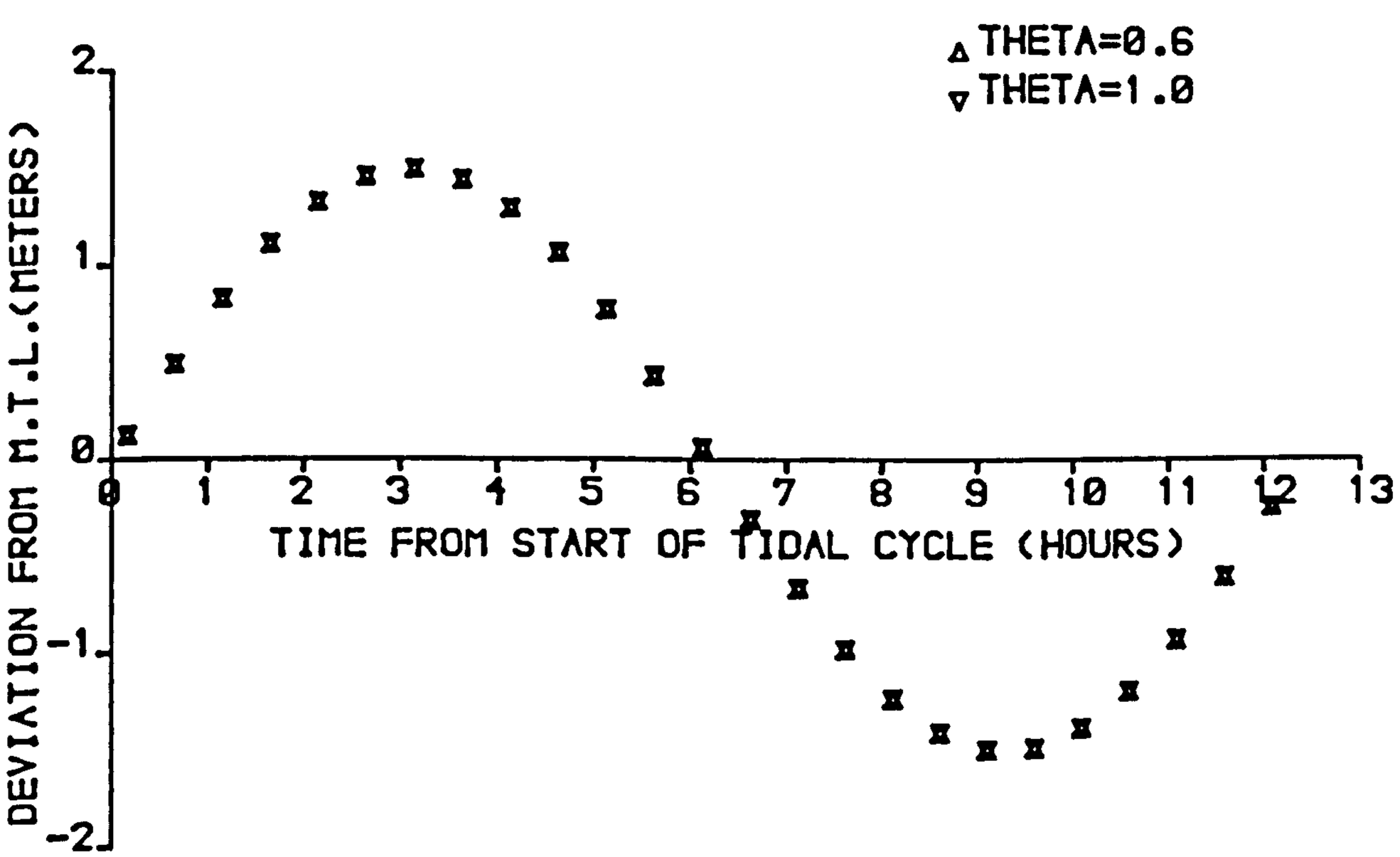

FIGURE 7·5m

SPRING TIDE WATER LEVELS AT PORTPATRICK

have little effect in the present application. Thus, in the Clyde sea area a distance increment of 3000m gives a sufficiently high number of grid points per tidal wave length to prevent numerical damping at high theta values.

7.8 CALIBRATION

The Firth of Clyde is a relatively deep inland sea area. In the numerical model the depths corresponding to mean tidal level are no where less than five metres. This implies that long wave propagation in the Firth is effected little by friction and that the numerical model will be insensitive to variation of the Chezy coefficient. This effect was confirmed by numerical experiments. A summary of these results is presented in tables 7.1 and 7.2. Table 7.1 shows a modest variation in range as the Chezy coefficient is varied between $100m^{\frac{1}{2}}/s$ and $50m^{\frac{1}{2}}/s$. Variations in the time of high water relative to Greenock are given in table 7.2. On first inspection changes in the times of high water at Sanda Island and Portpatrick suggest that the wave speed is sensitive to changes in the Chezy coefficient, however, it is important that this is placed in context with the rate of change of water levels in the Firth. Figure 7.6 shows that the twenty minute variation in the timing of high water is negligable when translated to differences in water levels.

Ultimately, a Chezy coefficient of $100m^{\frac{1}{2}}/s$ was chosen to represent turbulent energy losses in the Firth. This value being in the range of $60m^{\frac{1}{2}}/s$ to $100m^{\frac{1}{2}}/s$ suggested

LOCATION	RANGES						
	Predicted	Computed (Chezy Coefficient)					
	1979	100	90	80	70	60	50
GREENOCK	3.08	3.04	3.03	3.02	3.01	3.00	3.00
ROTHESAY BAY	3.08	2.91	2.91	2.90	2.89	2.88	2.87
EAST LOCH TARBERT	3.08	2.78	2.77	2.77	2.77	2.76	2.75
LOCH RANZA	2.65	2.81	2.80	2.80	2.80	2.79	2.79
BRODICK BAY	2.83	2.77	2.77	2.77	2.76	2.76	2.76
IRVINE	2.77	2.76	2.76	2.76	2.75	2.75	2.74
AYR	2.56	2.72	2.72	2.72	2.71	2.71	2.71
GIRVAN	2.68	2.54	2.54	2.54	2.54	2.54	2.53
CAMPBELTOWN	2.56	2.53	2.53	2.53	2.53	2.53	2.53
STRANRAER	2.77	2.65	2.64	2.64	2.64	2.64	2.63
SANDA ISLAND	-	2.00	2.00	2.00	2.00	2.00	2.00
PORTPATRICK	3.44	3.00	3.00	3.00	3.00	3.00	3.00

Table 7.1

LOCATION	TIME OF HIGH WATER						
	Predicted	Computed (Chezy Coefficient)					
	1979	$100m^{\frac{1}{2}}/s$	90	80	70	60	50
GREENOCK	0	0	0	0	0	0	0
ROTHESAY BAY	+5	-10	-10	-10	-10	-10	-20
EAST LOCH TARBERT	-10	+20	+20	+20	+10	+10	+10
LOCH RANZA	-10	-10	-10	-5	-10	-10	-20
BRODICK BAY	0	-10	-10	-10	-20	-20	-20
IRVINE	-15	-10	-10	-10	-20	-20	-20
AYR	-20	-10	-10	-10	-20	-15	-20
GIRVAN	-20	-10	-15	-15	-20	-20	-30
CAMPBELTOWN	-15	-10	-10	-10	-20	-20	-30
STRANRAER	-15	-10	-10	-10	-20	-20	-30
SANDA ISLAND	-40(-35)	-20	-20	-20	-30	-30	-40
PORTPATRICK	-59(-40)	-20	-20	-20	-30	-30	-40

Table 7.2

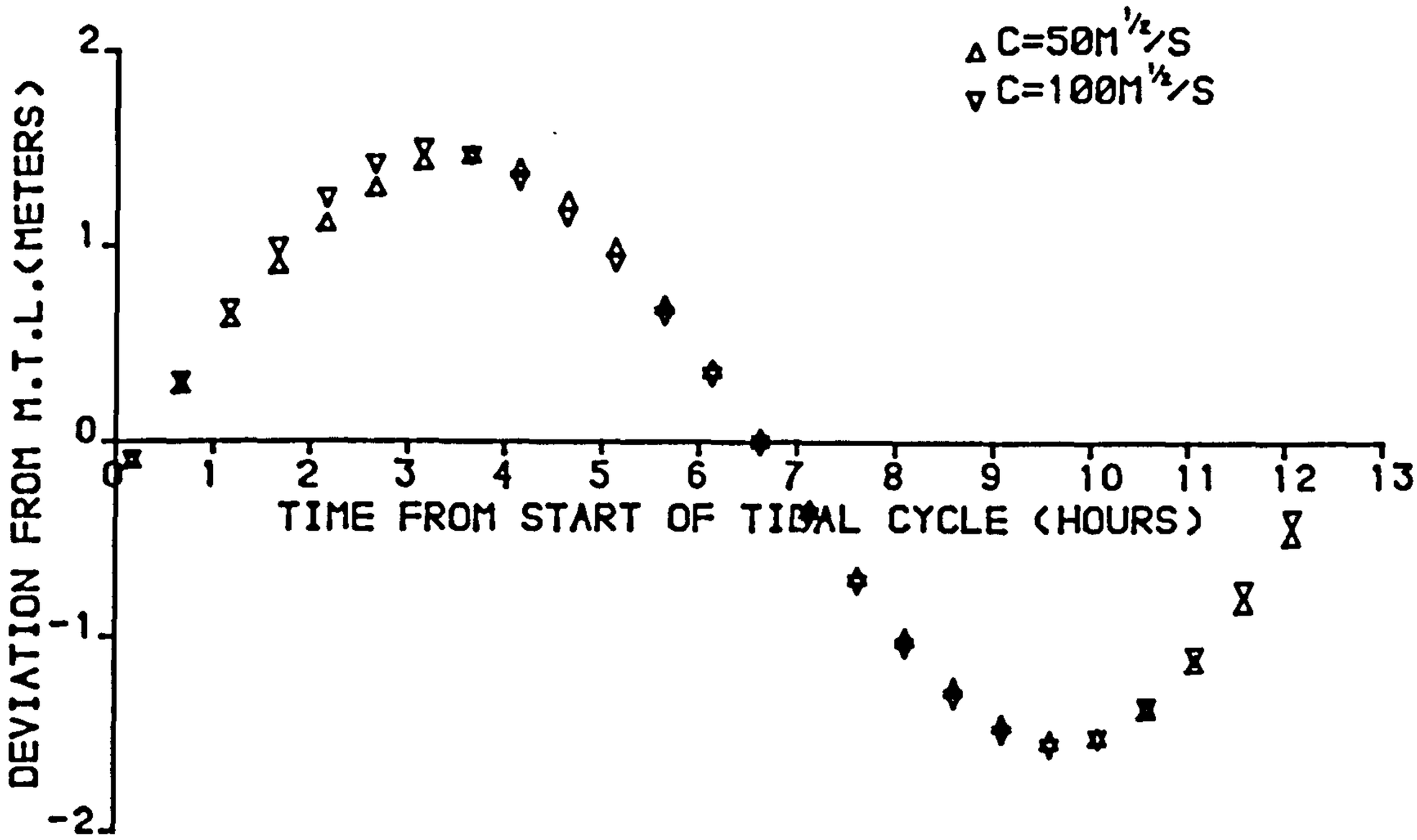

FIGURE 7·6a

SPRING TIDE WATER LEVELS AT GREENOCK

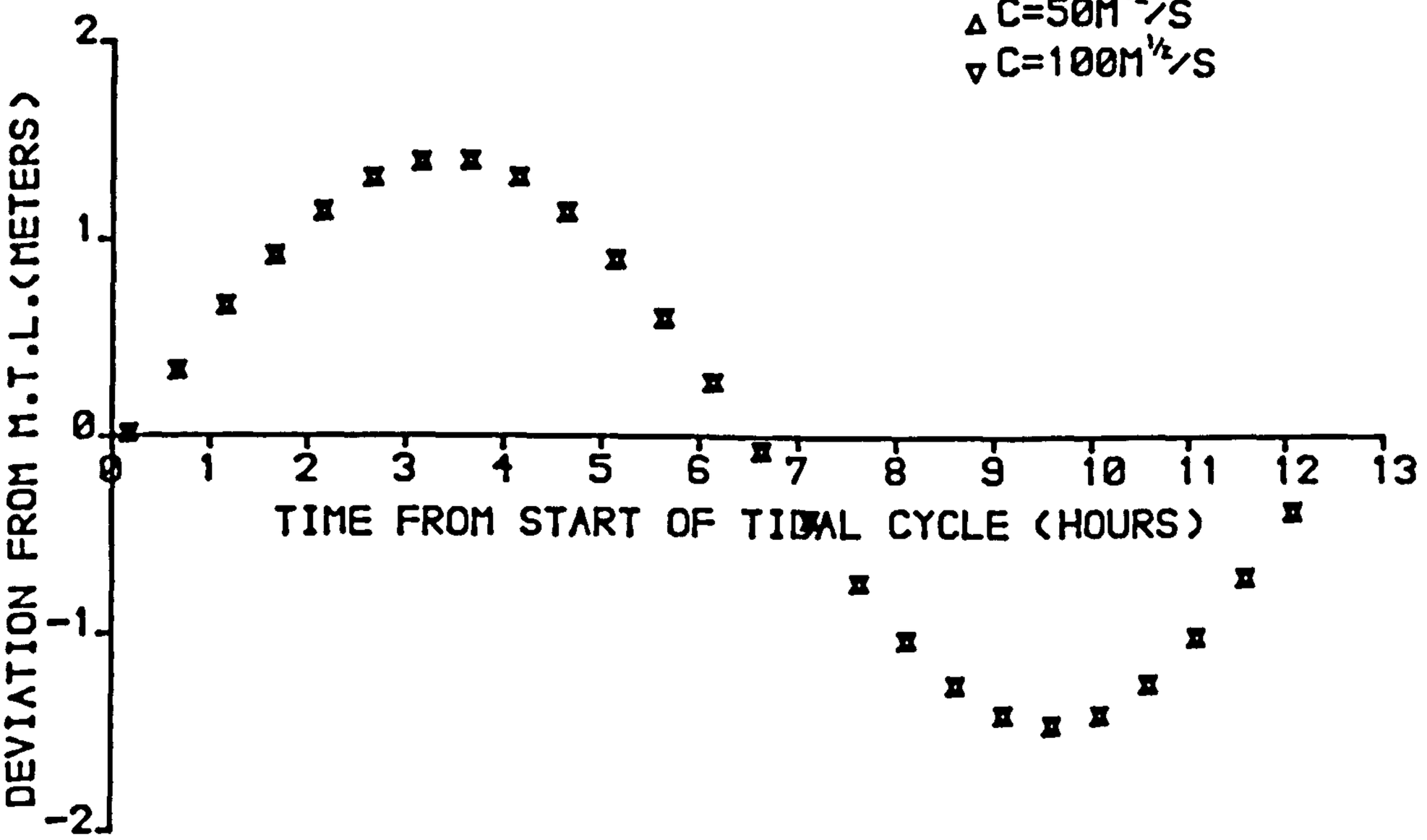

FIGURE 7·6b

SPRING TIDE WATER LEVELS AT ROTHESAY BAY

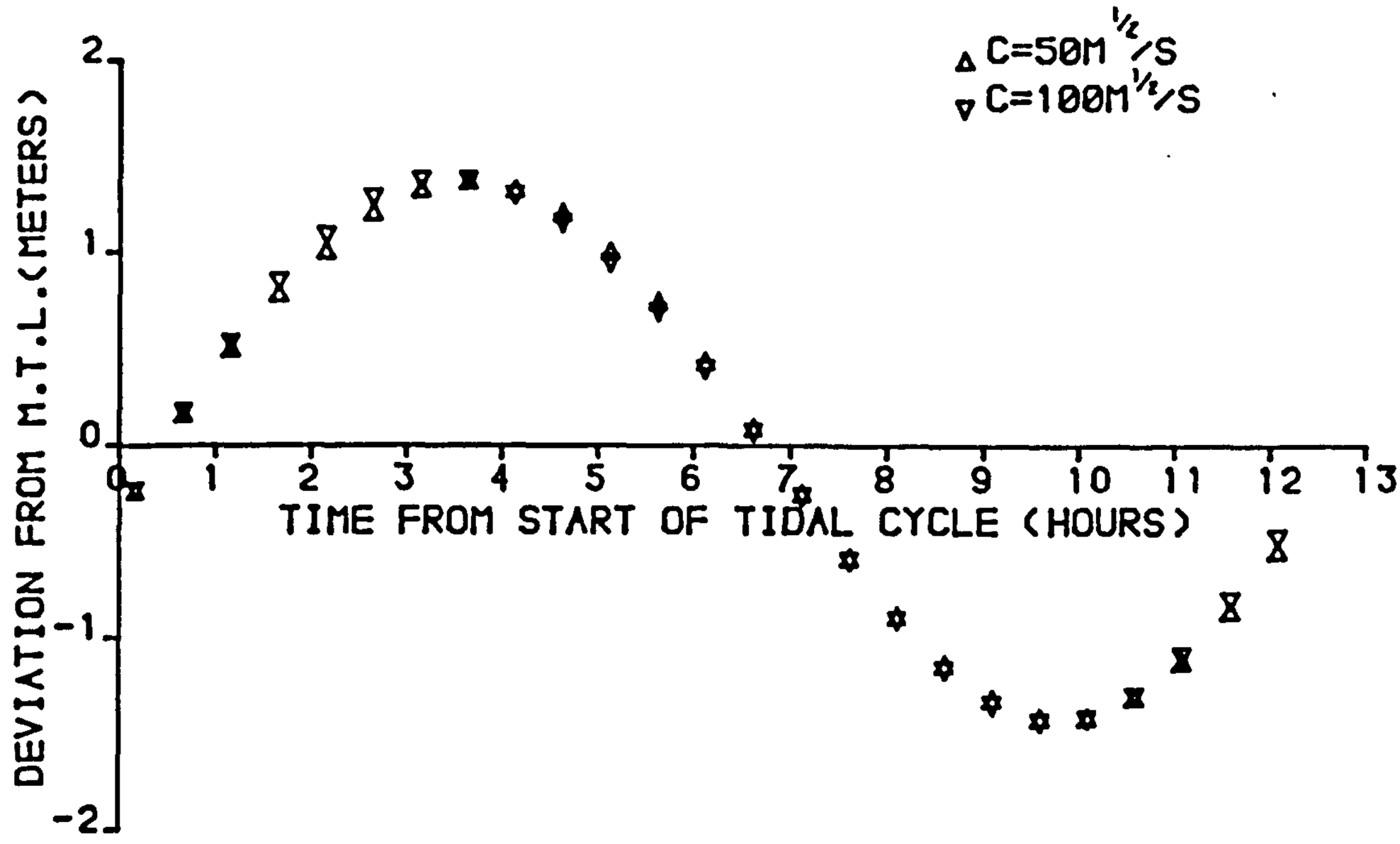

FIGURE 7·6c

SPRING TIDE WATER LEVELS AT EAST LOCH TARBERT

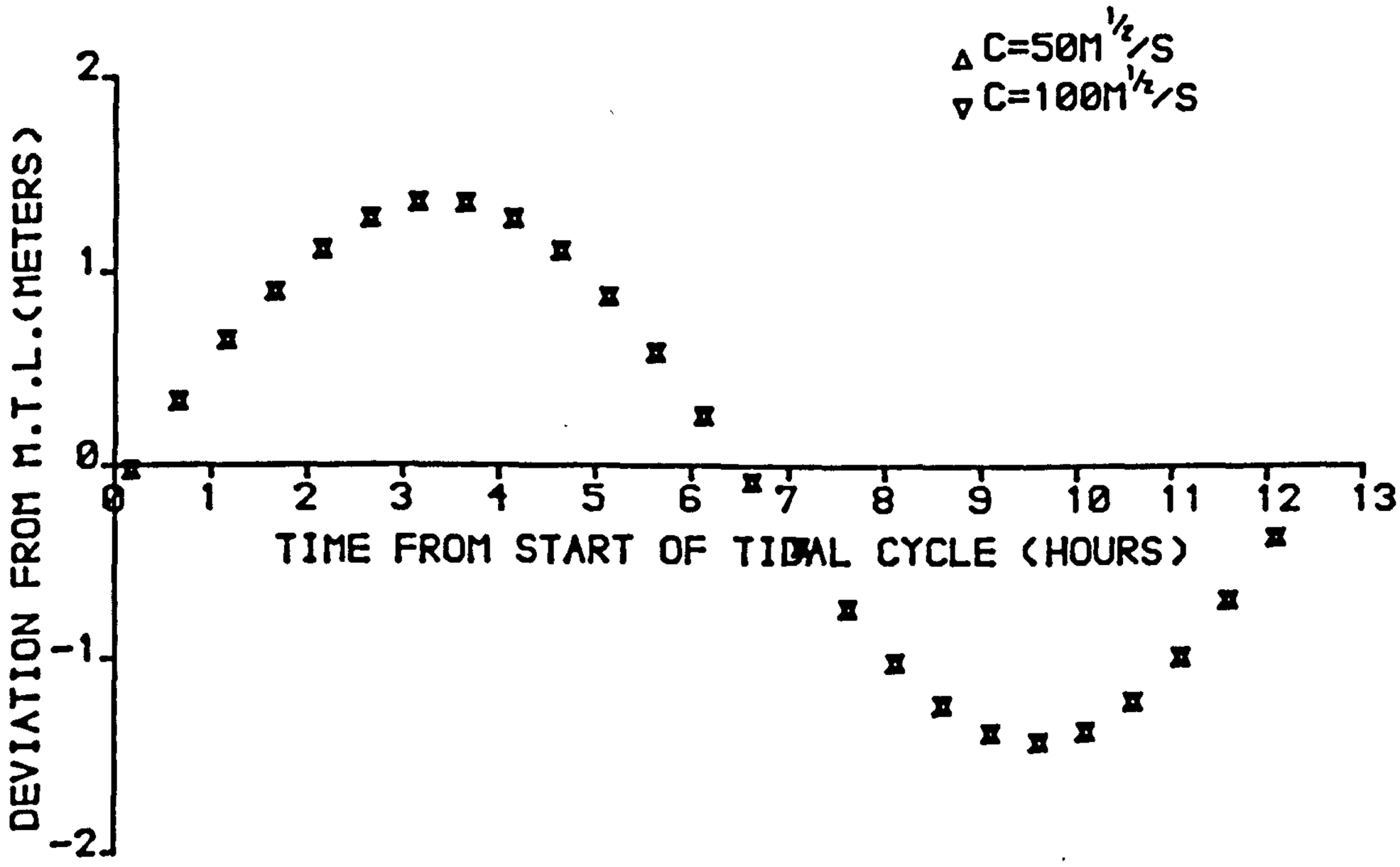

FIGURE 7·6d

SPRING TIDE WATER LEVELS AT LOCH RANZA

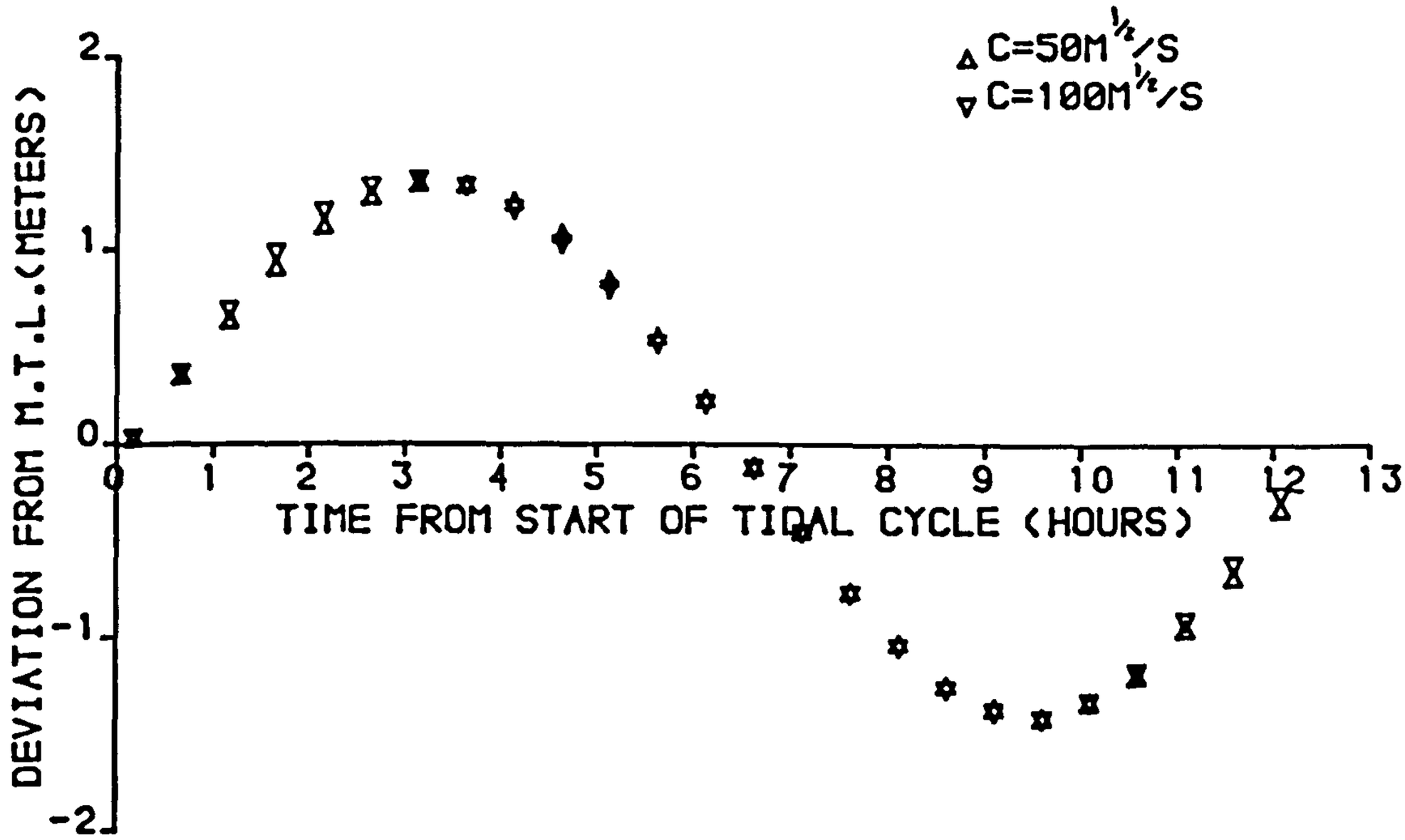

FIGURE 7·6e

SPRING TIDE WATER LEVELS AT BRODICK BAY

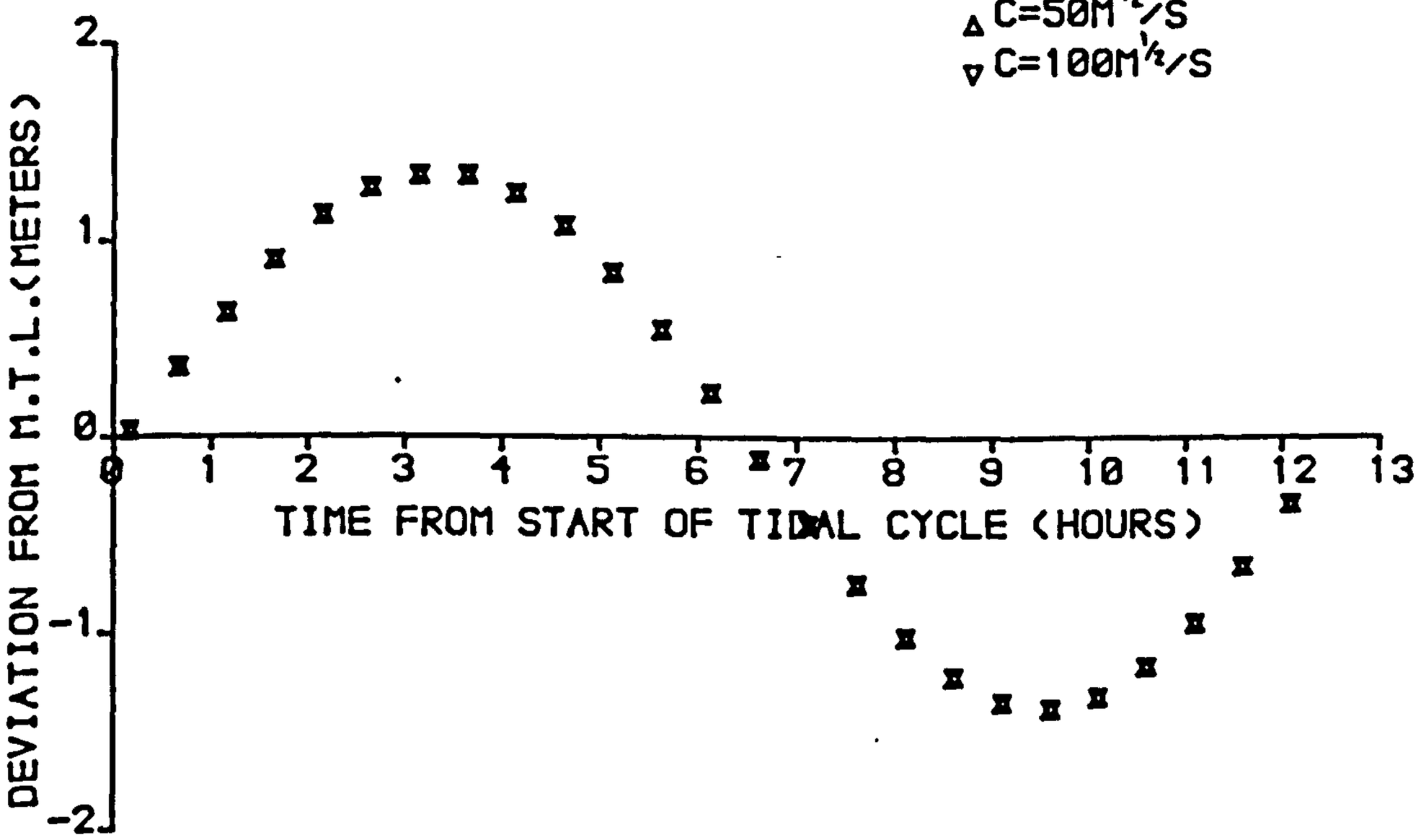

FIGURE 7·6f

SPRING TIDE WATER LEVELS AT IRVINE

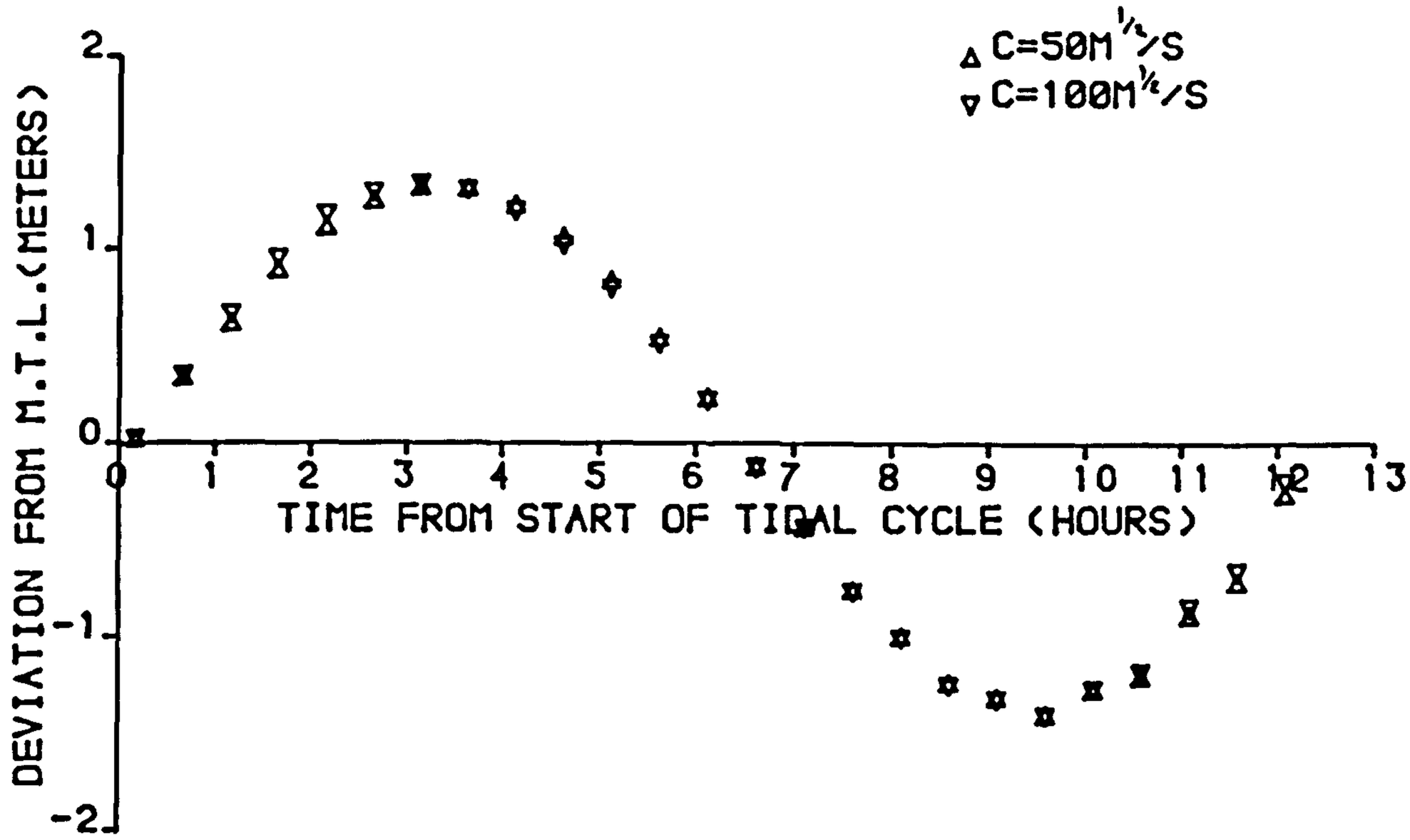

FIGURE 7·6g

SPRING TIDE WATER LEVELS AT AYR

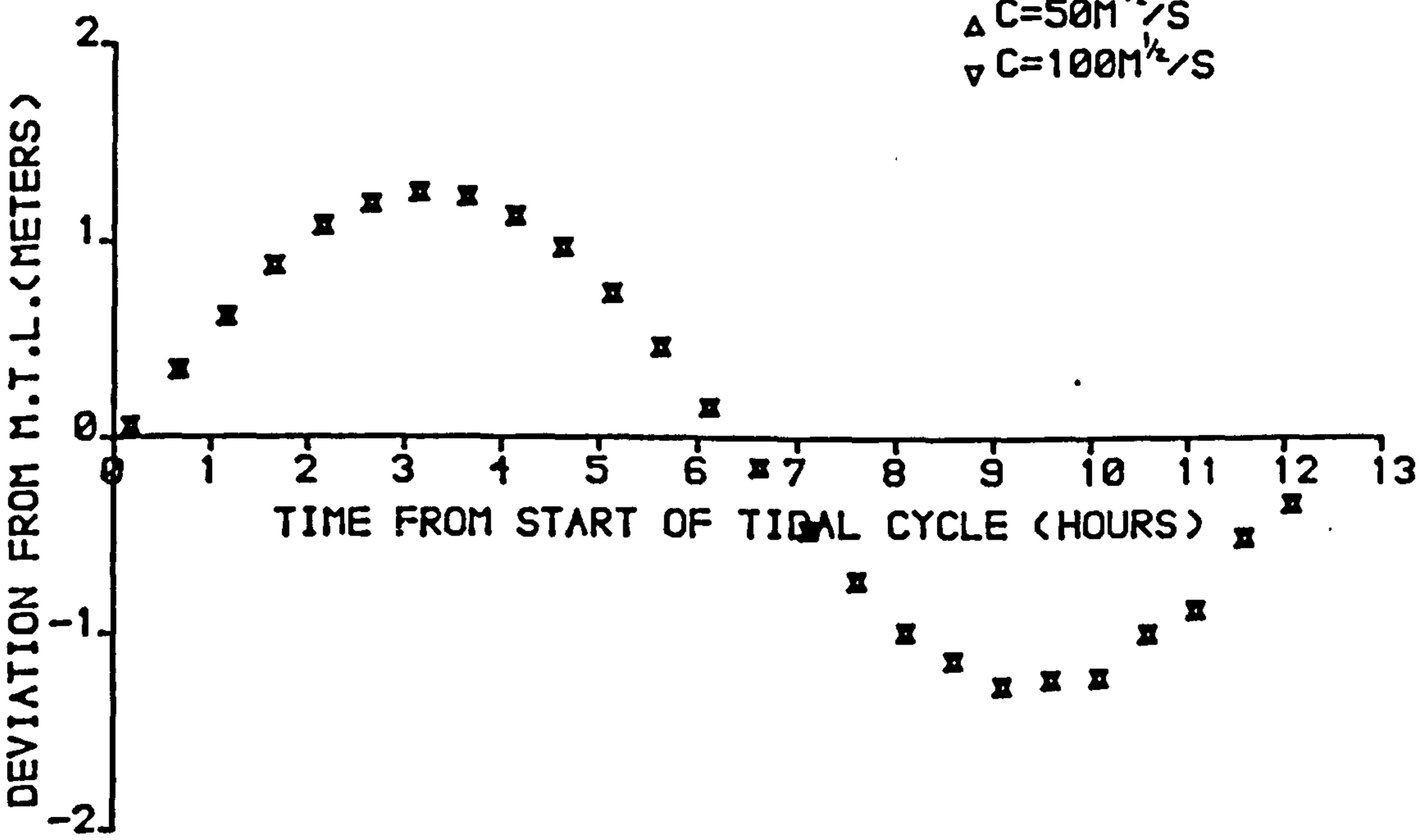

FIGURE 7·6h

SPRING TIDE WATER LEVELS AT GIRVAN

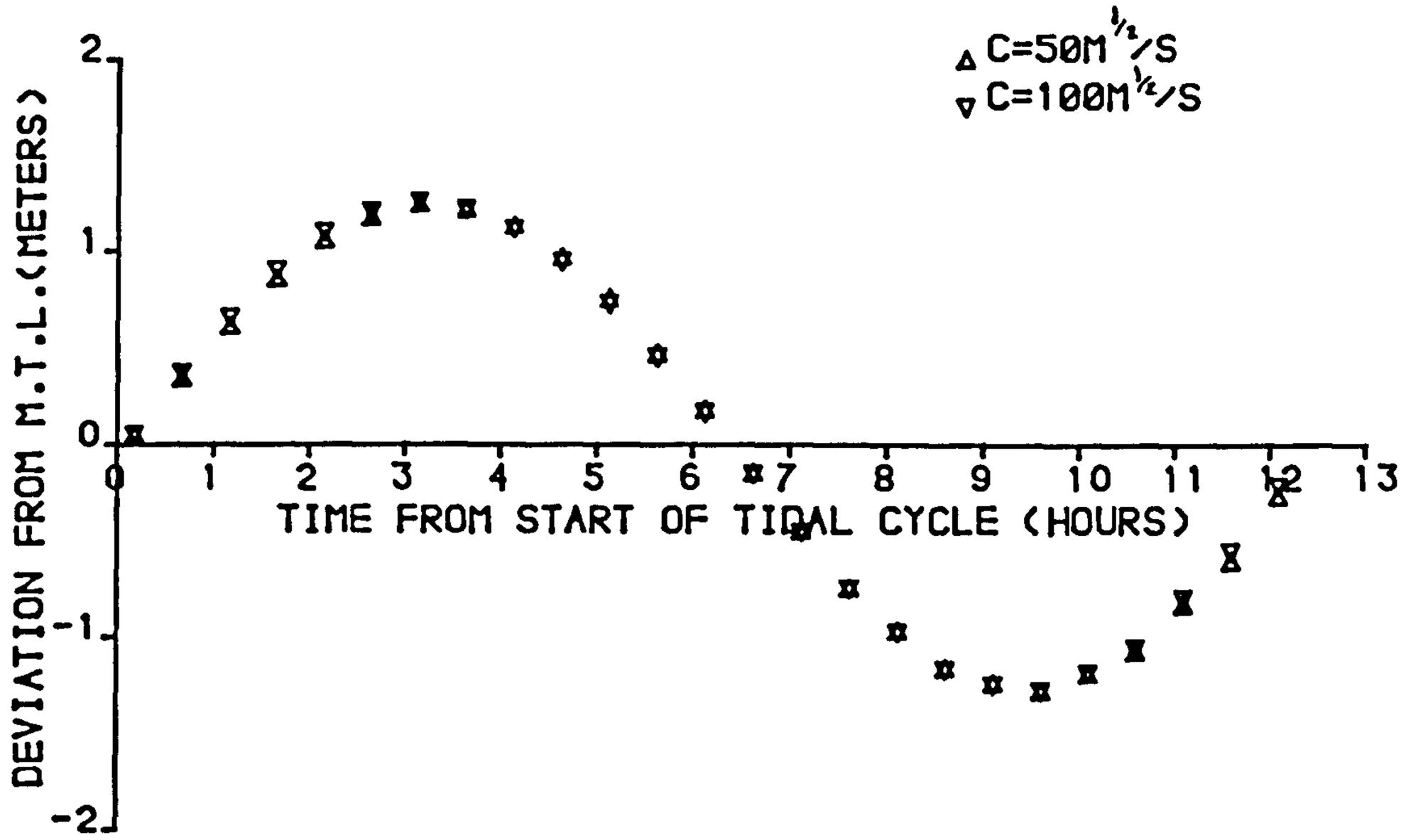

FIGURE 7·6i

SPRING TIDE WATER LEVELS AT CAMPBELTOWN

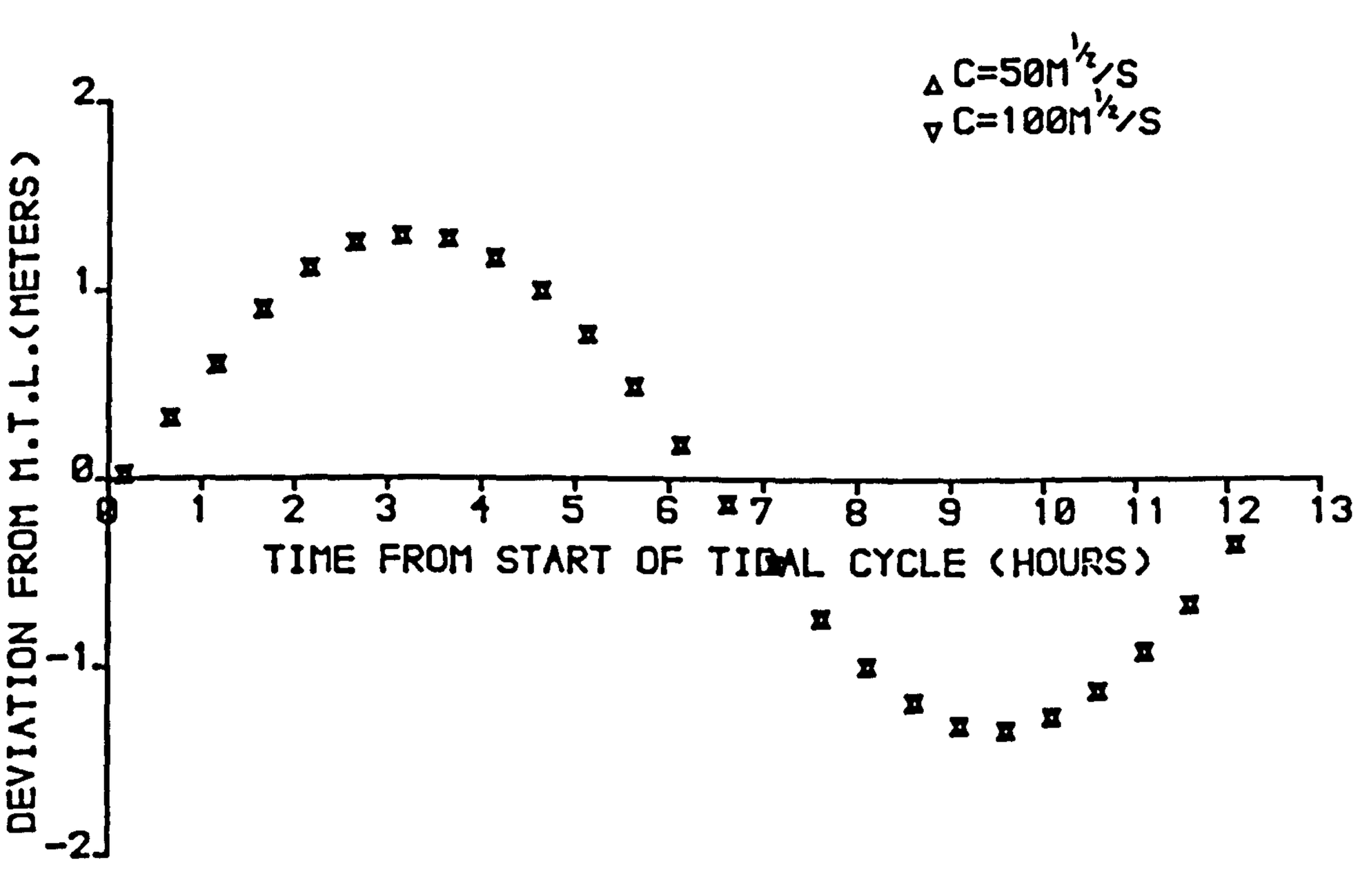

FIGURE 7·6j

SPRING TIDE WATER LEVELS AT STRANRAER

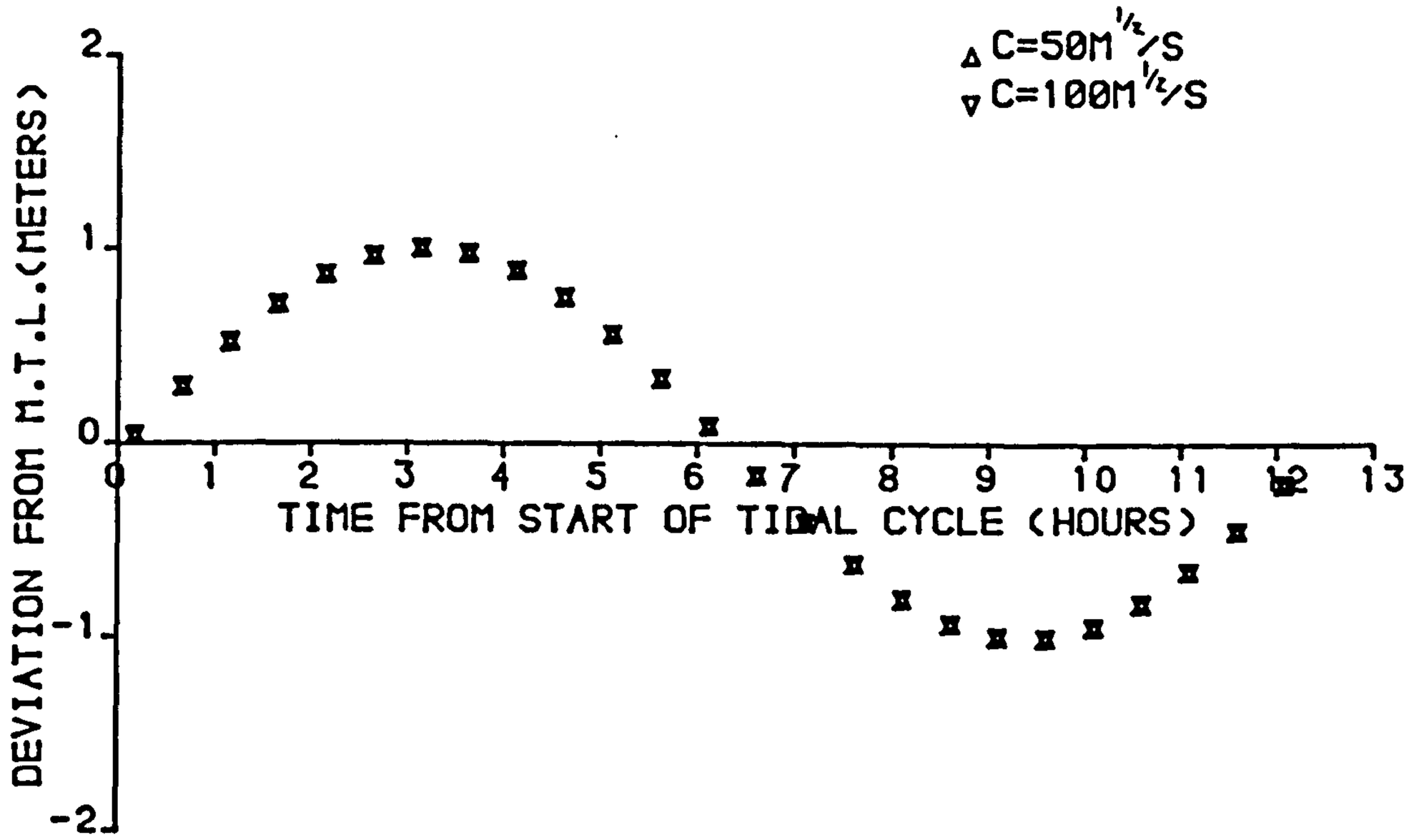

FIGURE 7·6k

SPRING TIDE WATER LEVELS AT SANDA ISLAND

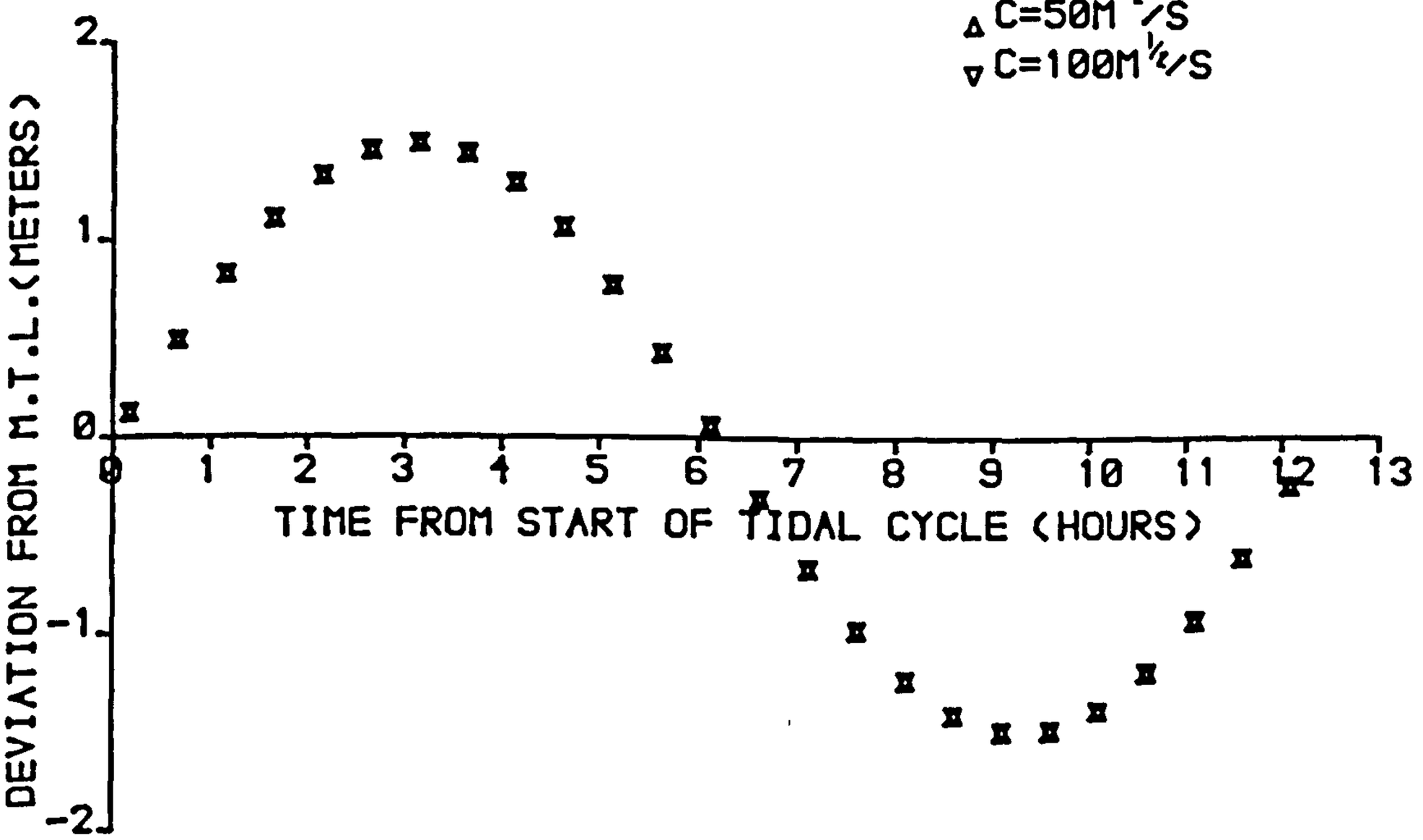

FIGURE 7·6l

SPRING TIDE WATER LEVELS AT PORTPATRICK

by Dronkers (1964) for typical estuaries.

7.9 SIMULATED SPRING TIDES IN THE FIRTH OF CLYDE

The results from modelling spring tide propagation in the Firth of Clyde are shown Figures 7.7a to 7.9. Frictional and coriolis effects were included in the numerical simulation. A Chezy coefficient of $100m^{\frac{1}{2}}/s$ was used. The time increment was 596.0 seconds giving an average Courant number of 4. The theta value was set at 1.0.

Comparisons between computed water levels and predicted ranges and phases taken from the Admiralty Tide Tables (1983) are shown in Figures 7.7a to 7.71. A harmonic cosine function was used to provide the variation between high and low water for the predicted values. Figure 7.5a shows the position of each of these points within the estuary. It can be seen that in general a good agreement is achieved between the computed and predicted values, the exceptions being East Loch Tarbert where some numerical dissipation is evident a 12% reduction in predicted tidal range, see section 7.7, and Campbeltown where a phase error of thirty-five minutes is recorded. Consulting earlier editions of the Admiralty Tide Tables showed that the timing of the predicted spring tide at Campbeltown is some twenty-five minutes later in the 1983 edition than those published in previous editions. If comparisons had been made with say the 1979 edition this phase error would be reduced to ten minutes. This is considered an acceptable error in the present application.

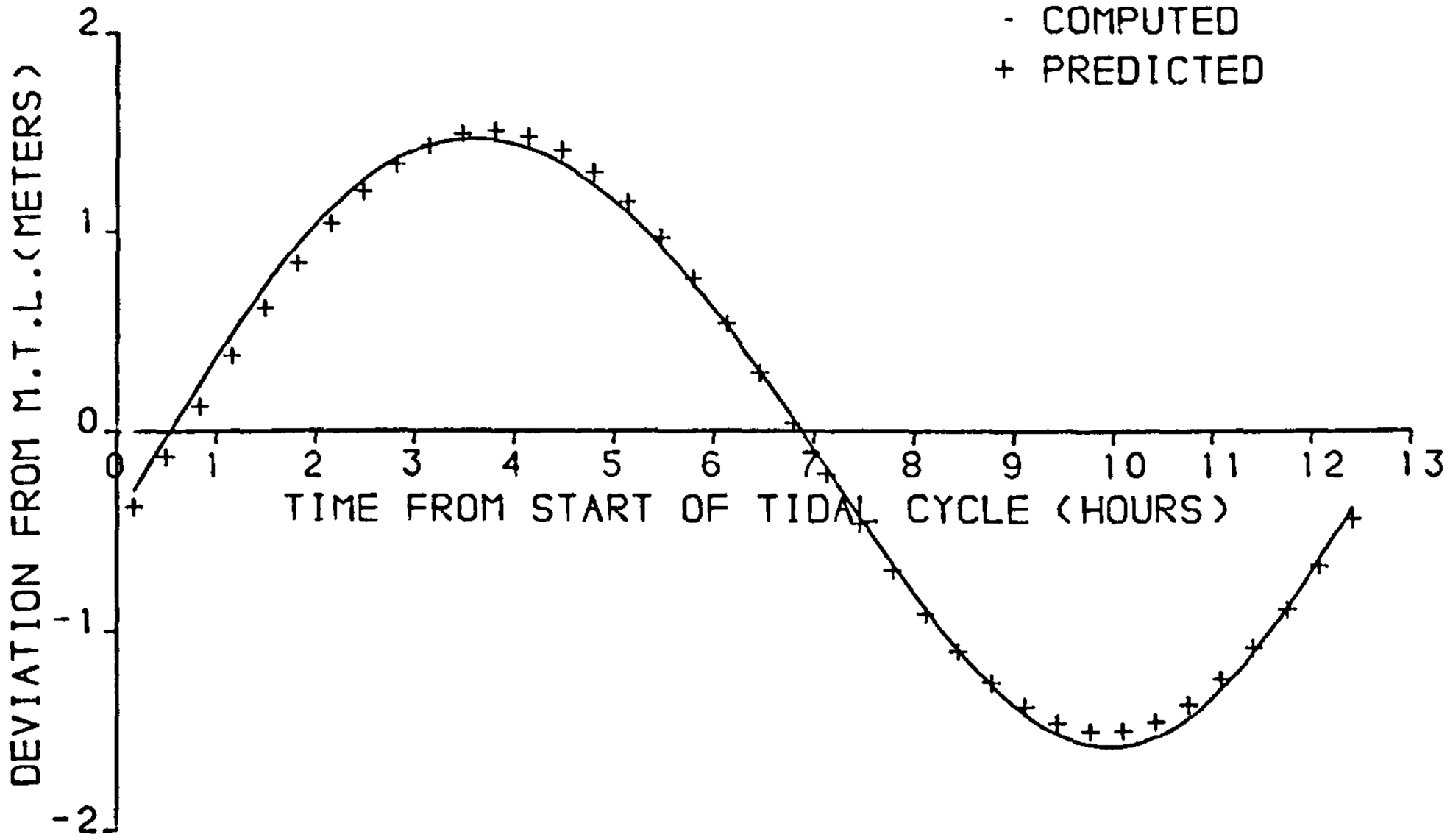

FIGURE 7.7a

SPRING TIDE WATER LEVELS AT GREENOCK

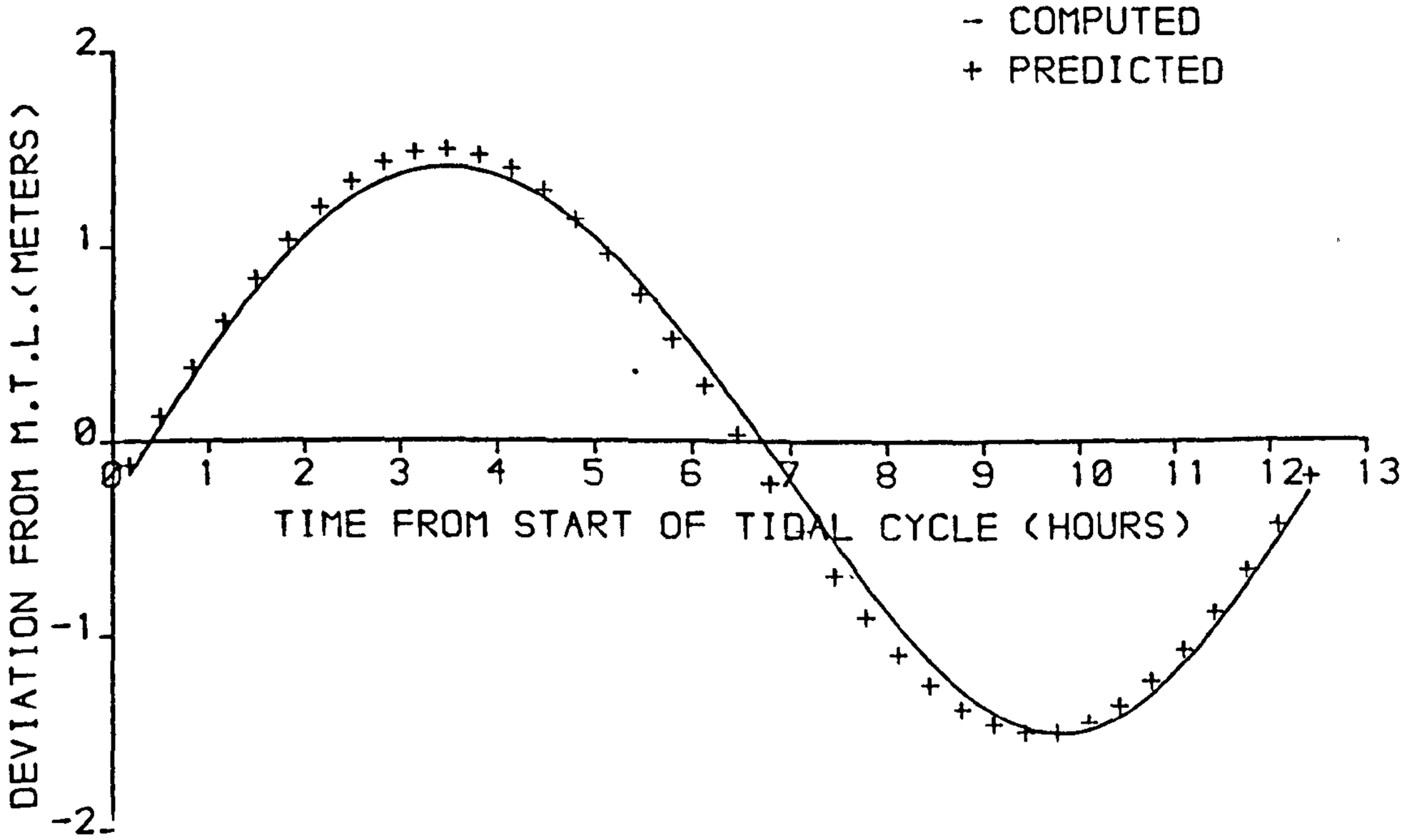

FIGURE 7.7b

SPRING TIDE WATER LEVELS AT ROTHESAY BAY

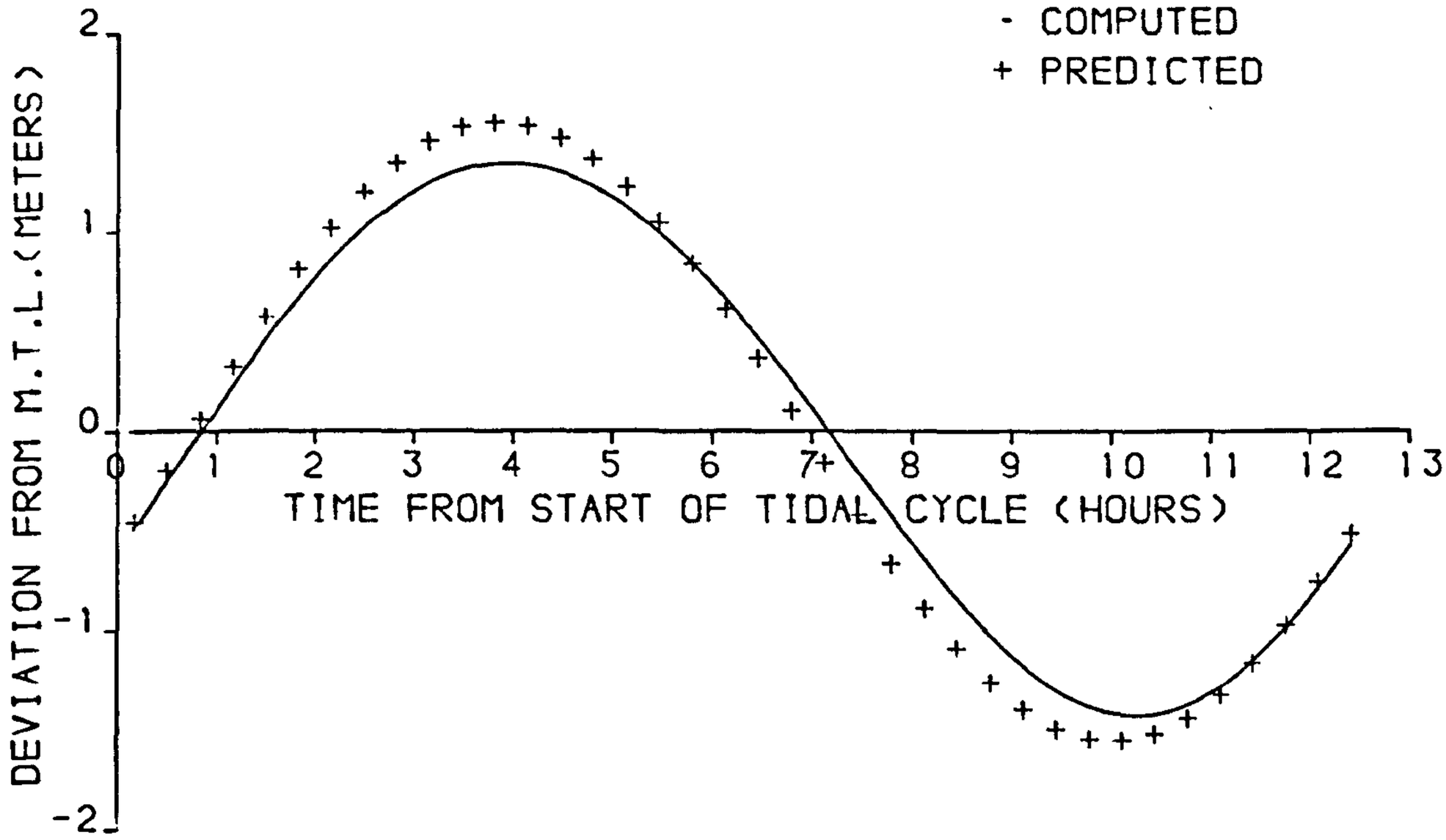

FIGURE 7·7c

SPRING TIDE WATER LEVELS AT EAST LOCH TARBERT

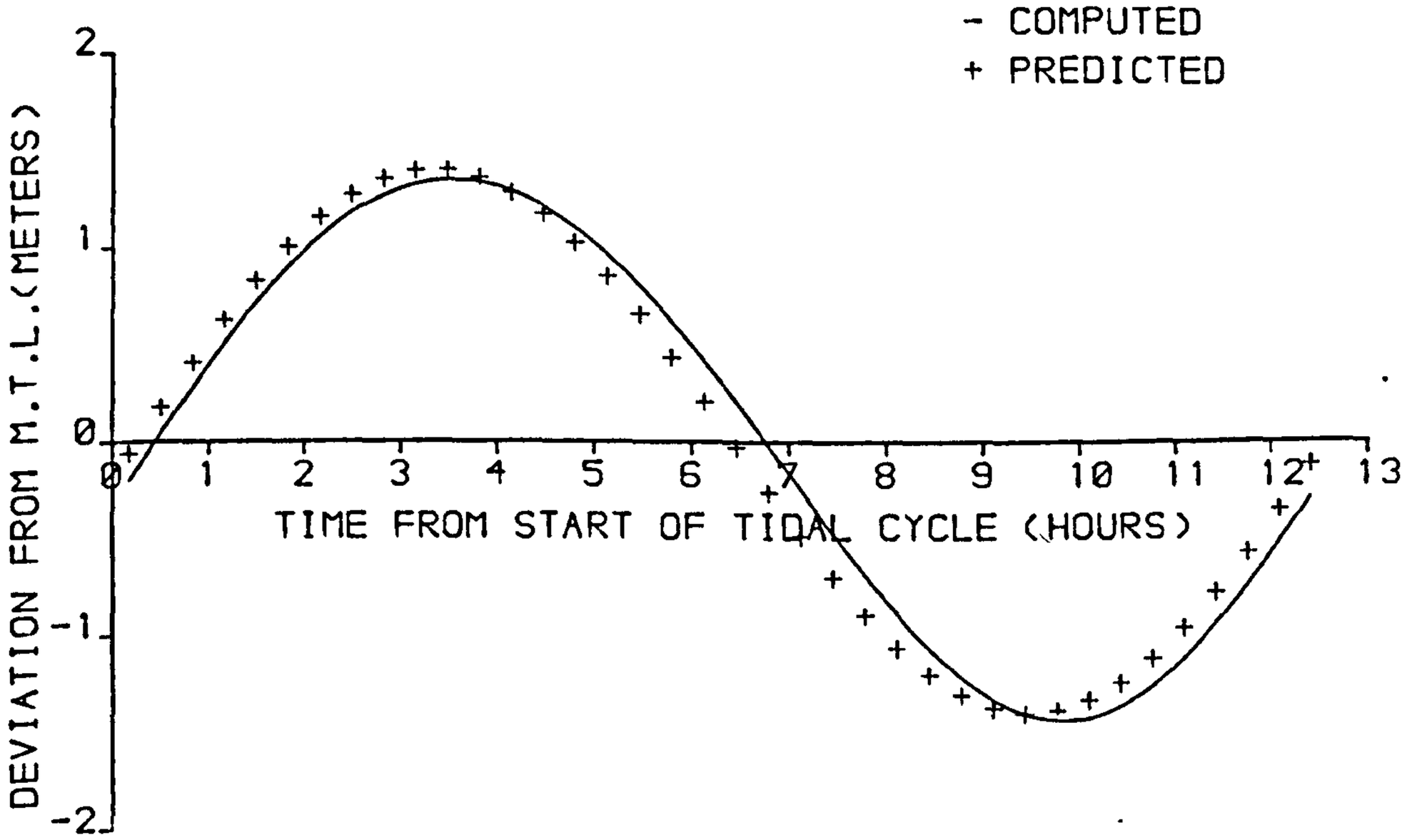

FIGURE 7·7d

SPRING TIDE WATER LEVELS AT LOCH RANZA

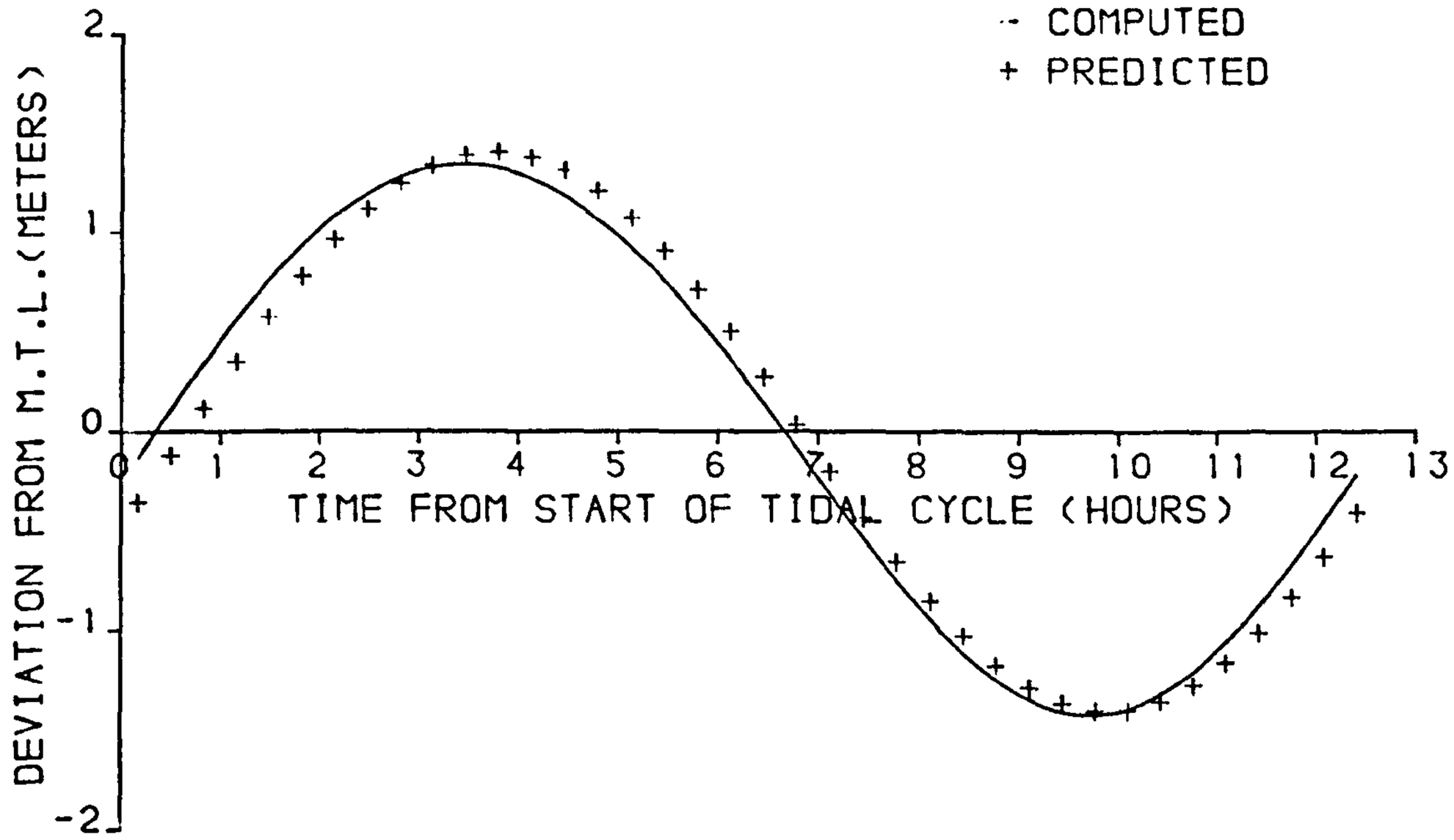

FIGURE 7.7e

SPRING TIDE WATER LEVELS AT BRODICK BAY

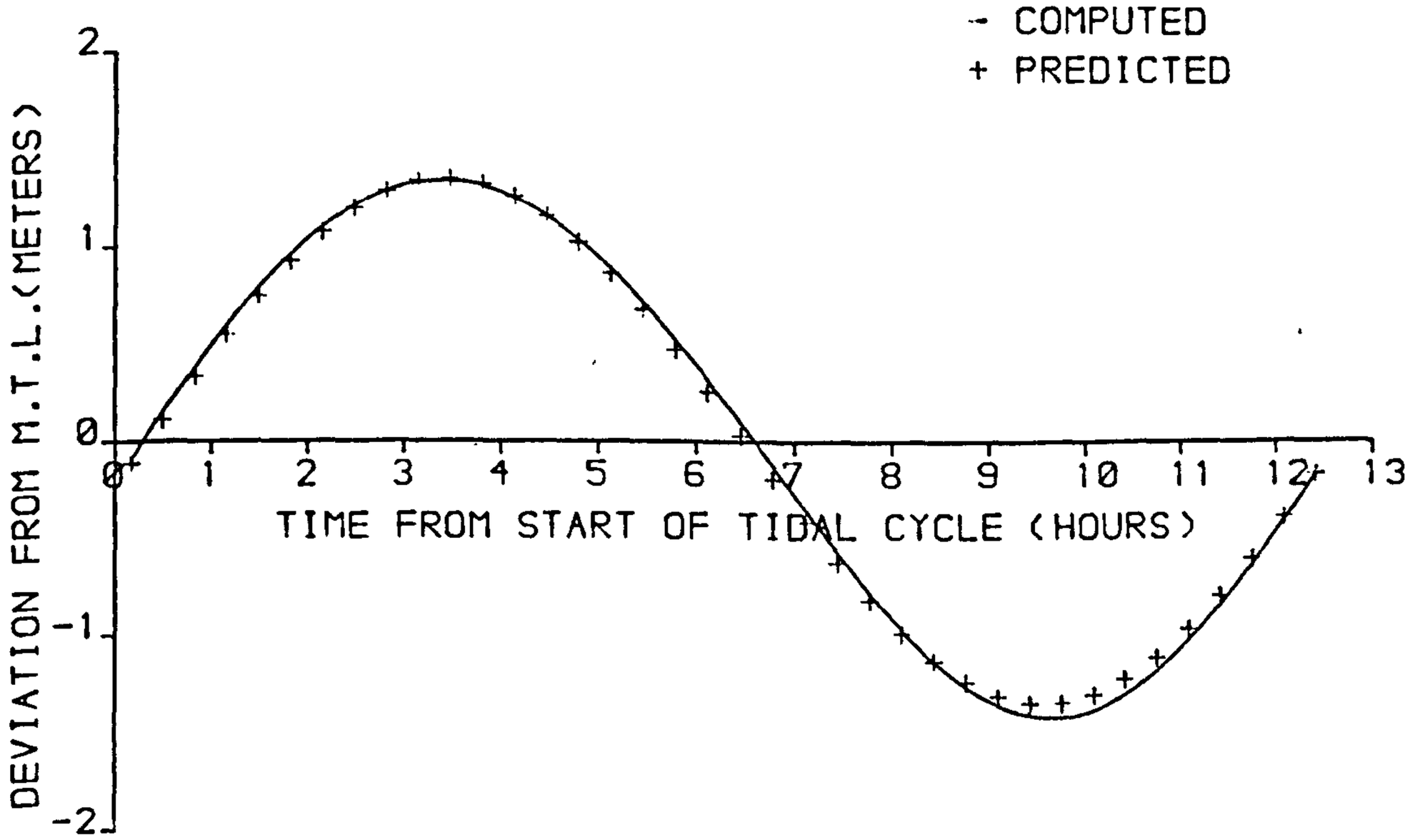

FIGURE 7.7f

SPRING TIDE WATER LEVELS AT IRVINE

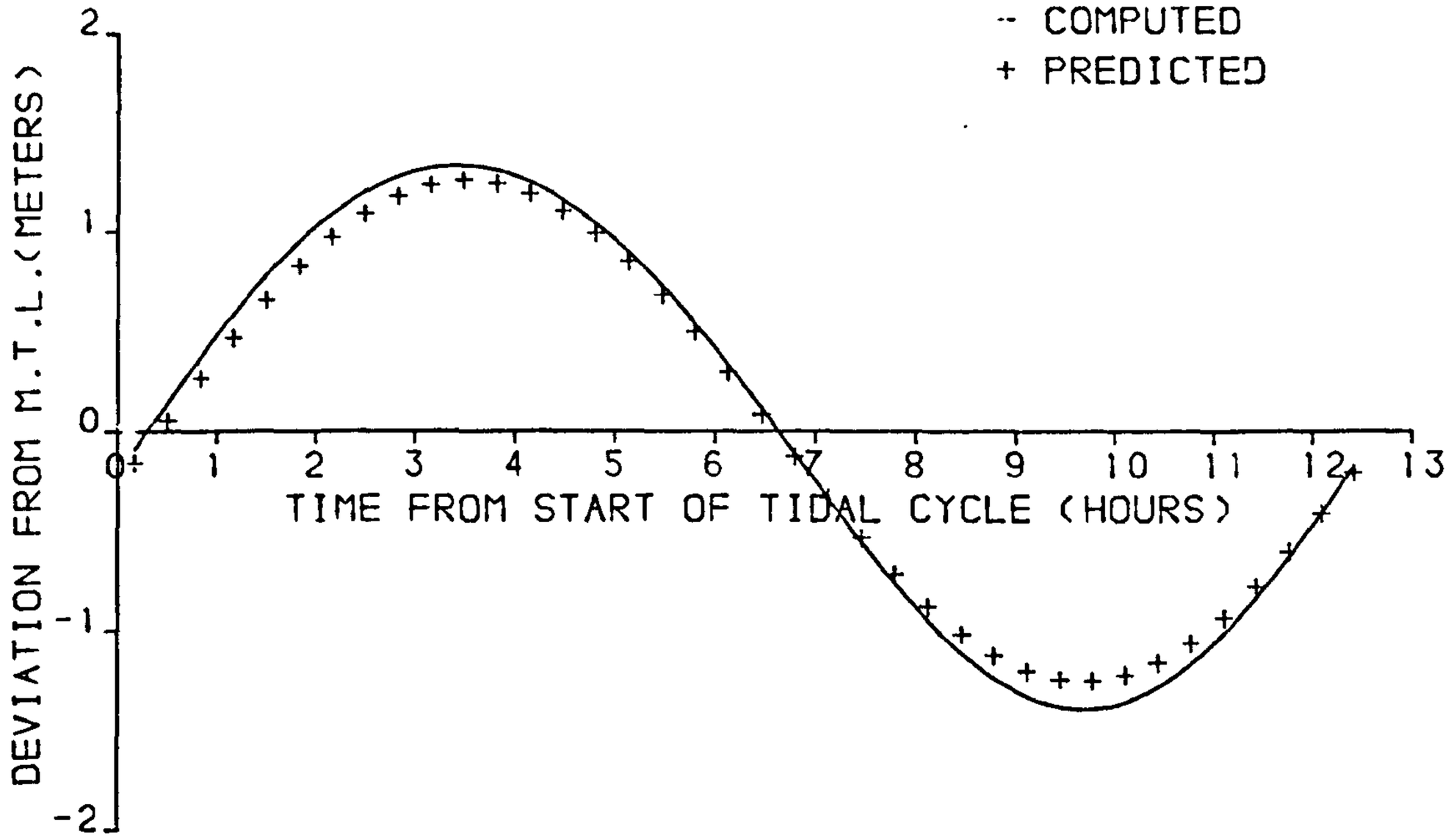

FIGURE 7.7g

SPRING TIDE WATER LEVELS AT AYR

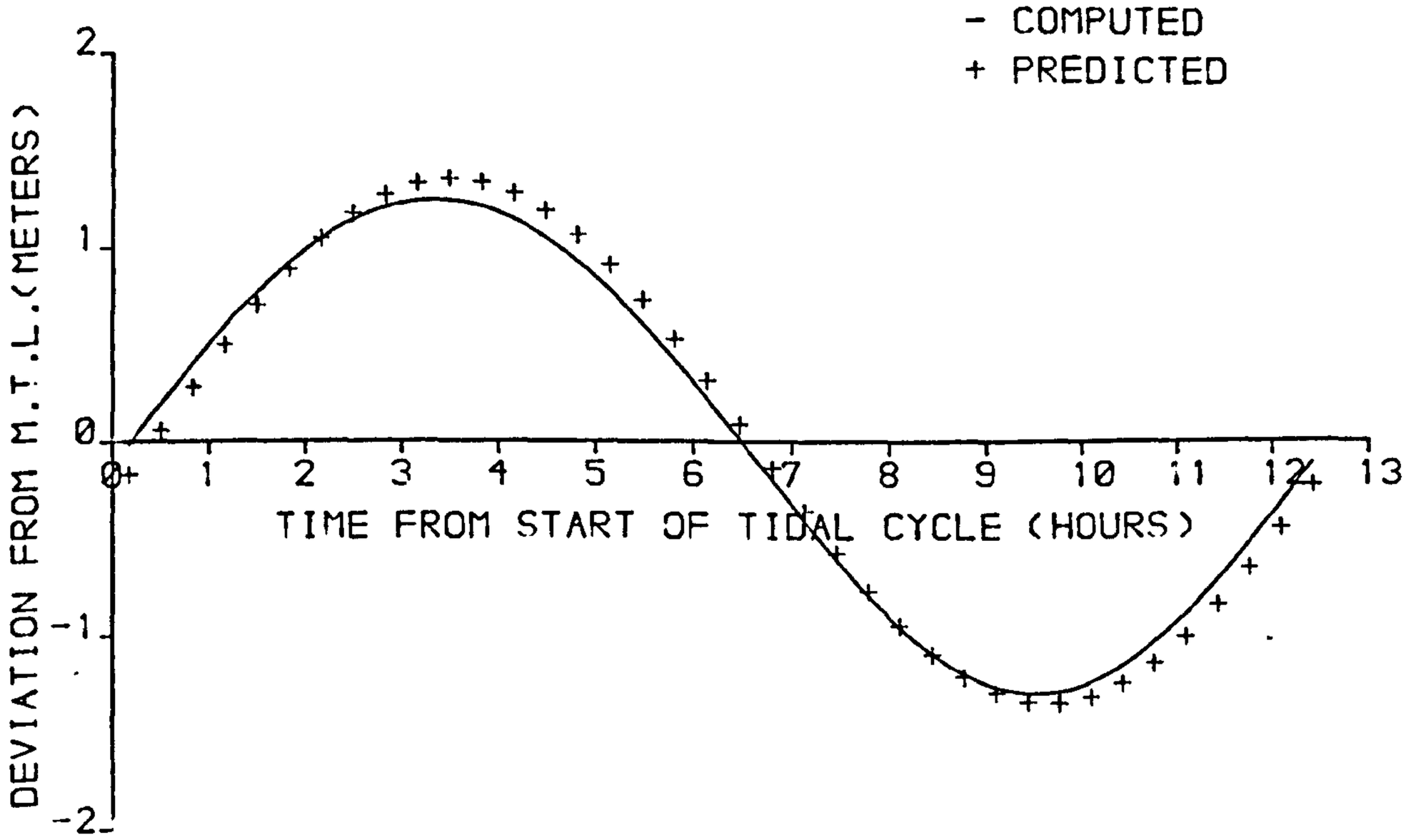

FIGURE 7.7h

SPRING TIDE WATER LEVELS AT GIRVAN

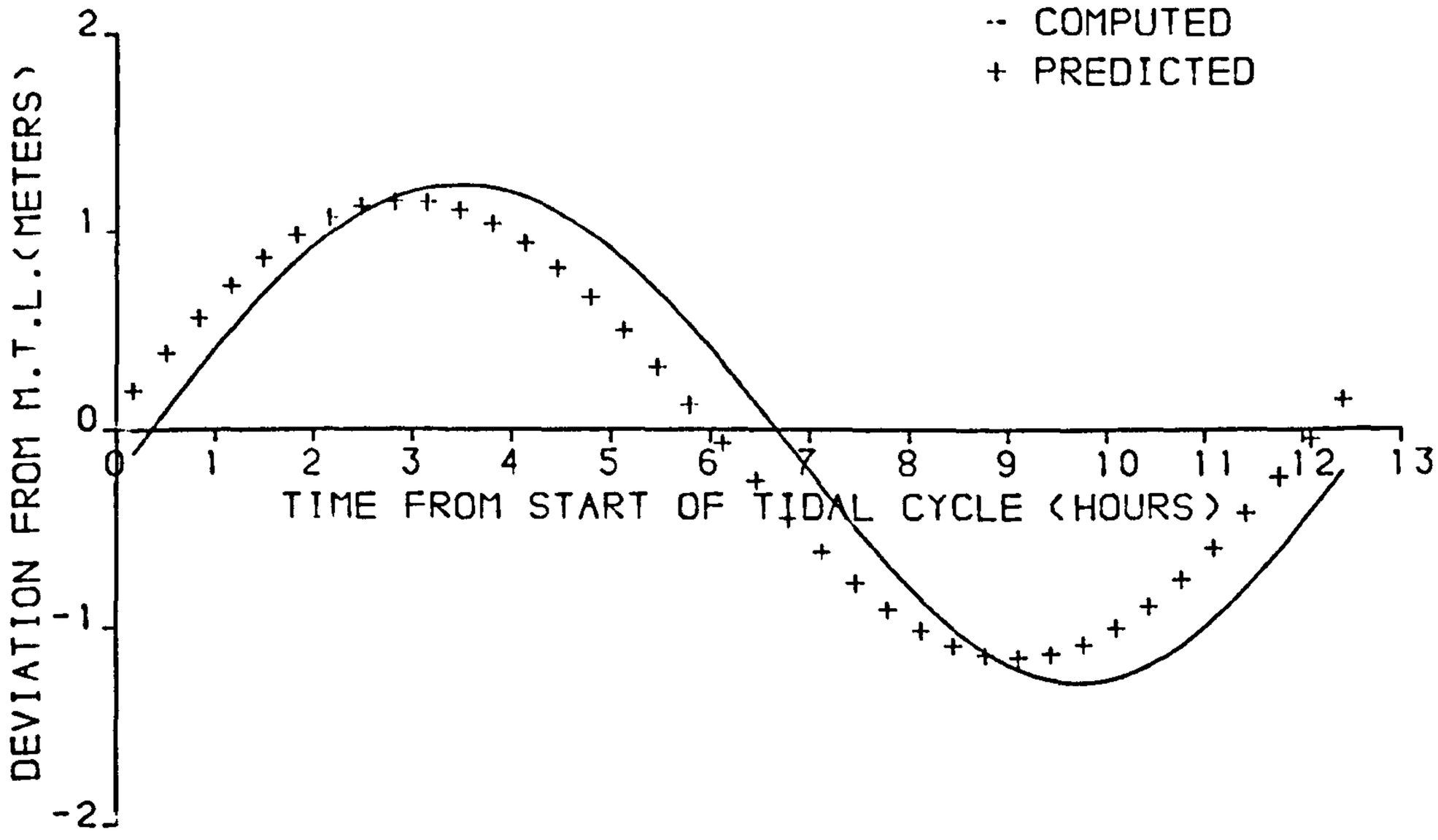

FIGURE 7·7i

SPRING TIDE WATER LEVELS AT CAMPBELTOWN

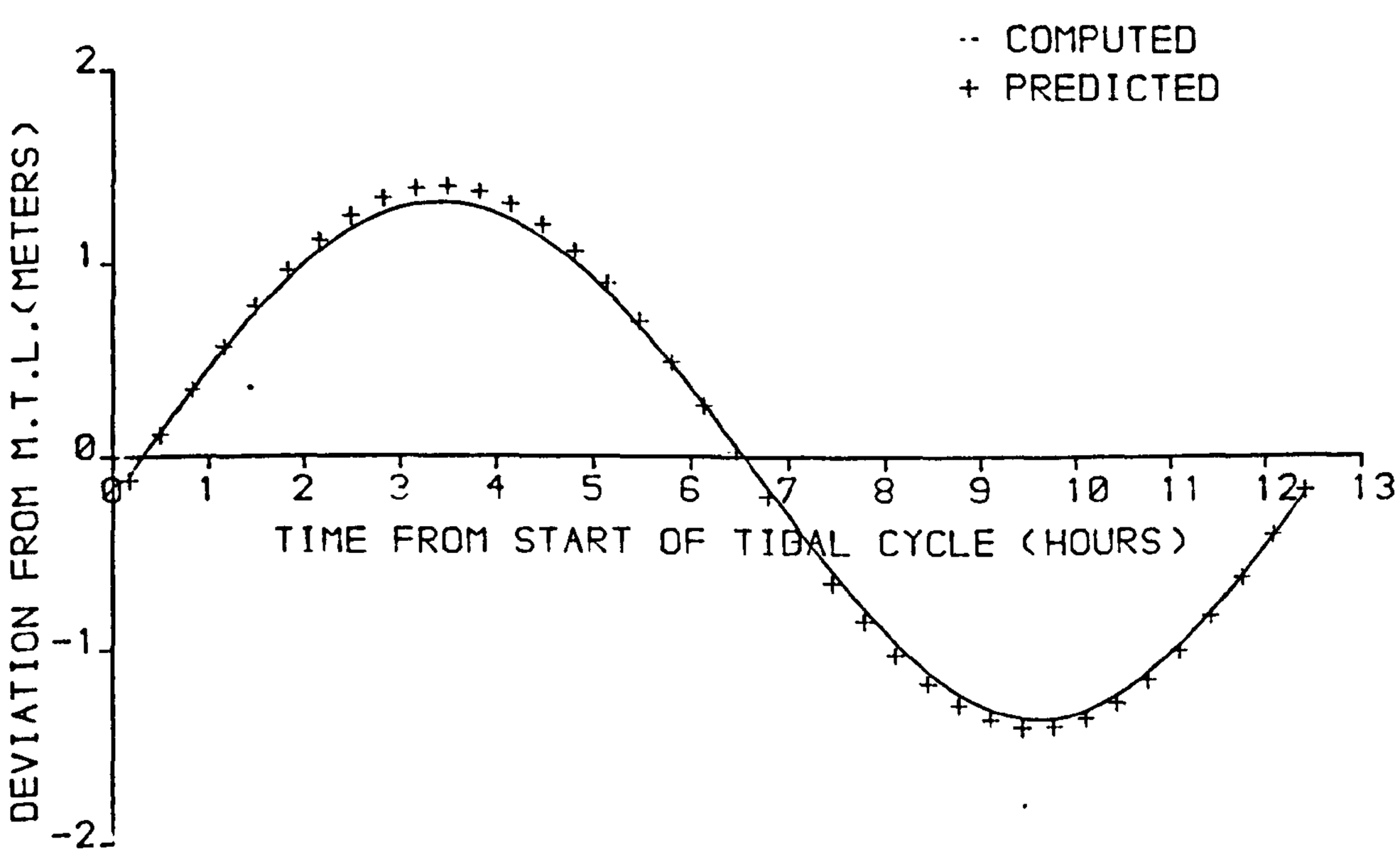

FIGURE 7·7j

SPRING TIDE WATER LEVELS AT STRANRAER

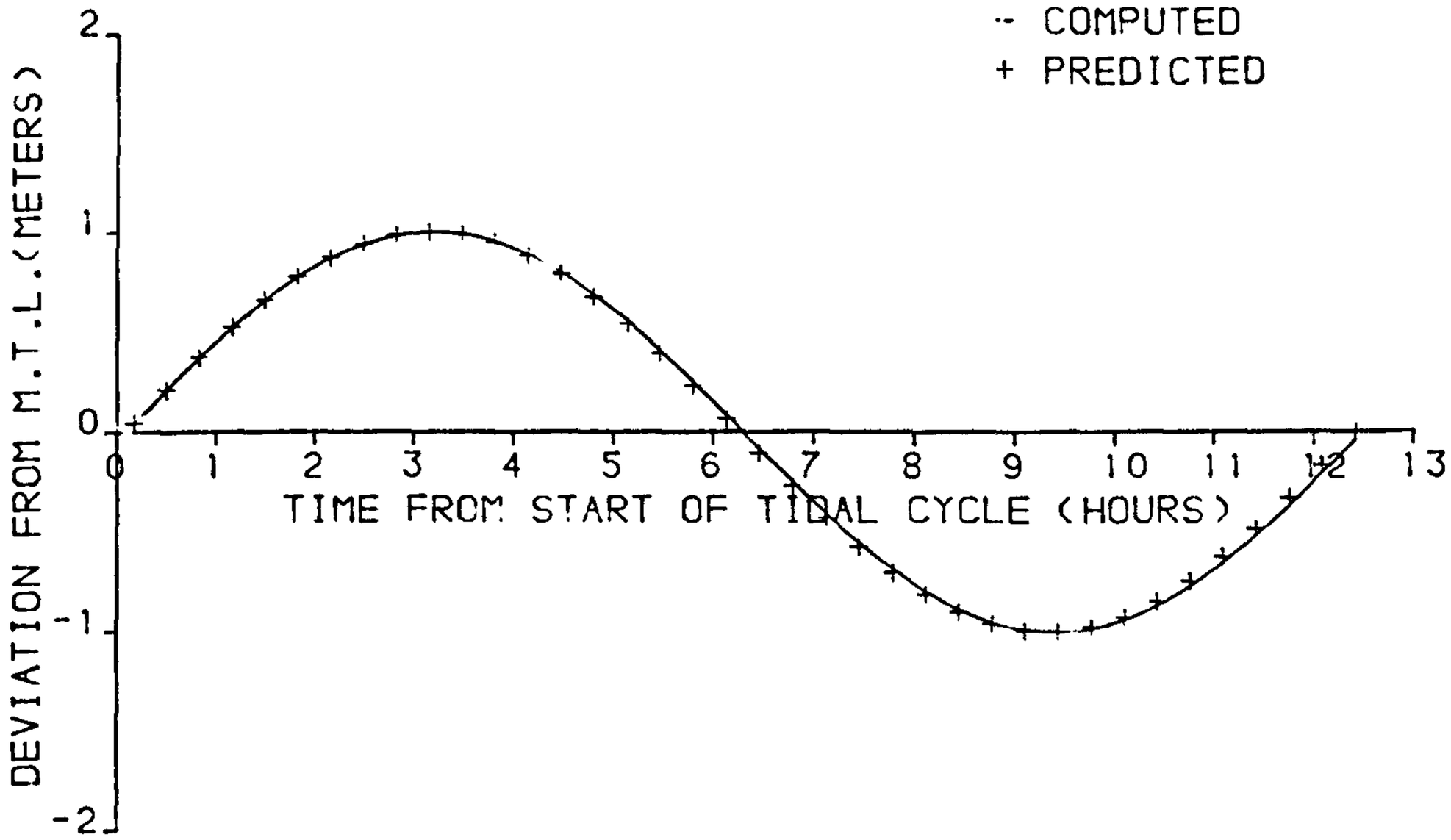

FIGURE 7·7k

SPRING TIDE WATER LEVELS AT SANDA ISLAND

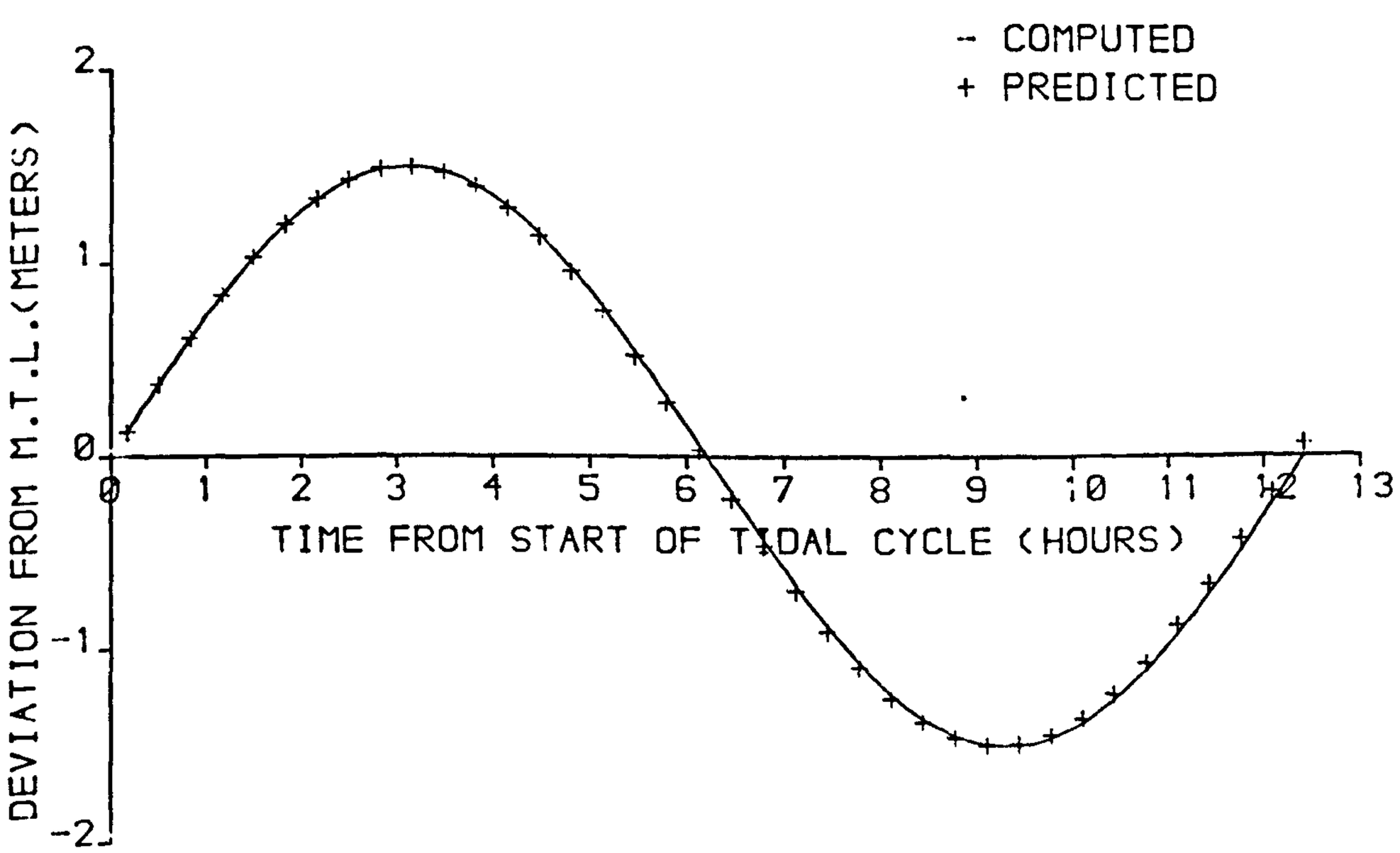

FIGURE 7·7l

SPRING TIDE WATER LEVELS AT PORTPATRICK

Velocity vectors in the Firth are shown at 2.98 hourly intervals throughout the tidal cycle in Figures 7.8a to 7.8e. These can be compared with the velocity vectors for the Clyde sea area, taken from the Admiralty Tidal Stream Atlas, shown in Figure 7.9. The latter have been converted from their published time relative to high water Dover to model time. Note that the timings do not coincide exactly. A fair agreement is obtained between the directions and magnitudes of the computed and measured velocities. In general computed velocities are slightly less than the measured ones. This could be attributed to the computed values being depth averaged while the measured values are surface velocities. A further point evident from Figure 7.8 is the co-oscillation of the Firth of Clyde with an area of Atlantic Ocean rather than the Irish Sea, a feature already described in Section 7.3. Also noticeable in the velocity vector diagrams is the effect of solving for one velocity component at the open boundaries. The effect of this artificial condition appears to be dissipated by the second or third solution point. Therefore, provided one is not interested in results in close proximity to the boundary this condition should not severely restrict the model's use.

Figures 7.10a to 7.10c show the global variation of water level in the Firth. It is stressed that the vertical scale in the figures varies, by virtue of the plotting routine, and that the figures serve only to illustrate the nature of tidal propagation in the Firth of Clyde.

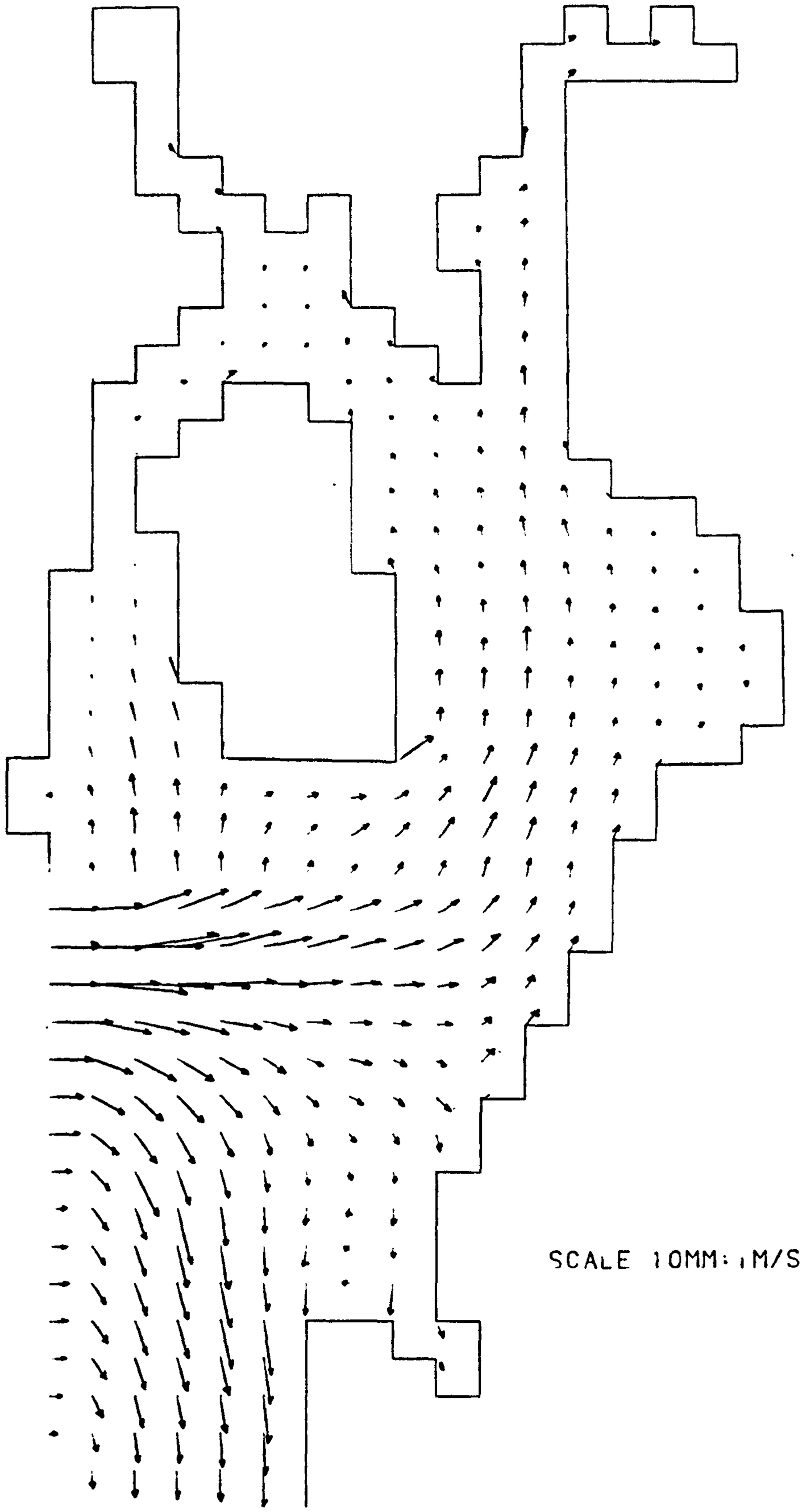

FIGURE 7·8a
SPRING TIDE VELOCITIES IN CLYDE ESTUARY.
TIME FROM START OF TIDAL CYCLE HOURS= .00

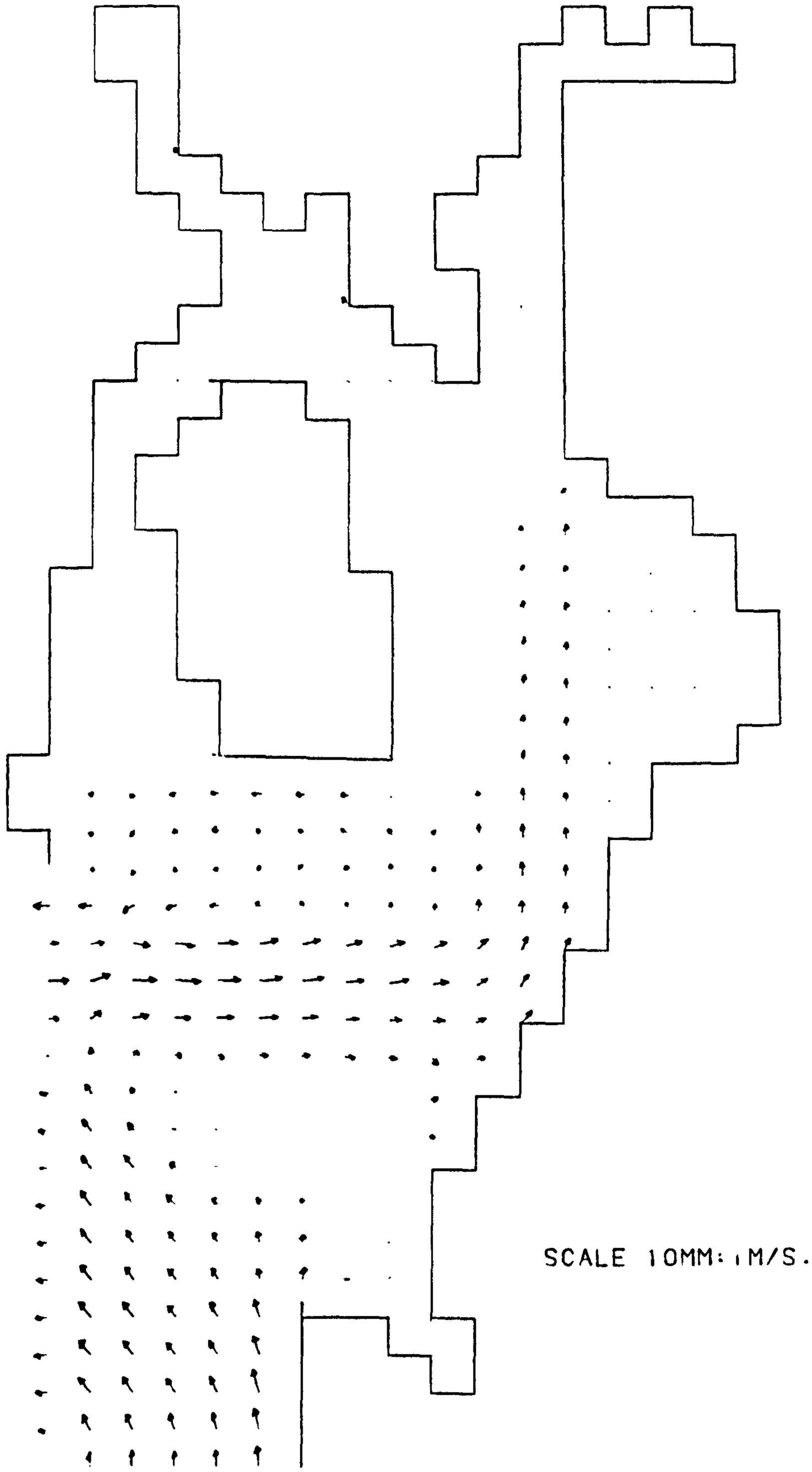

FIGURE 7·8b
SPRING TIDE VELOCITIES IN CLYDE ESTUARY.
TIME FROM START OF TIDAL CYCLE HOURS= 2.98

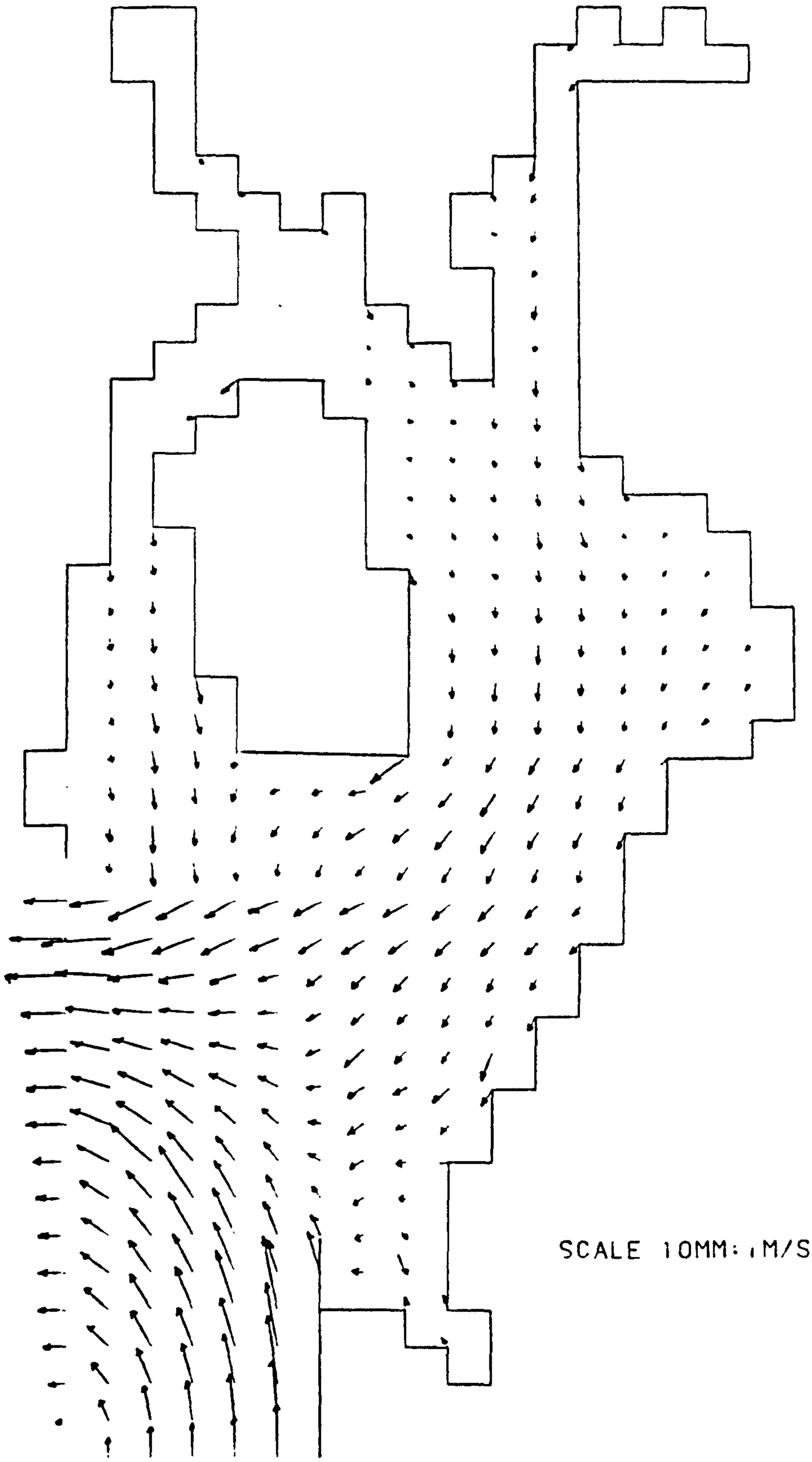

FIGURE 7·8c
SPRING TIDE VELOCITIES IN CLYDE ESTUARY.
TIME FROM START OF TIDAL CYCLE HOURS= 5.96

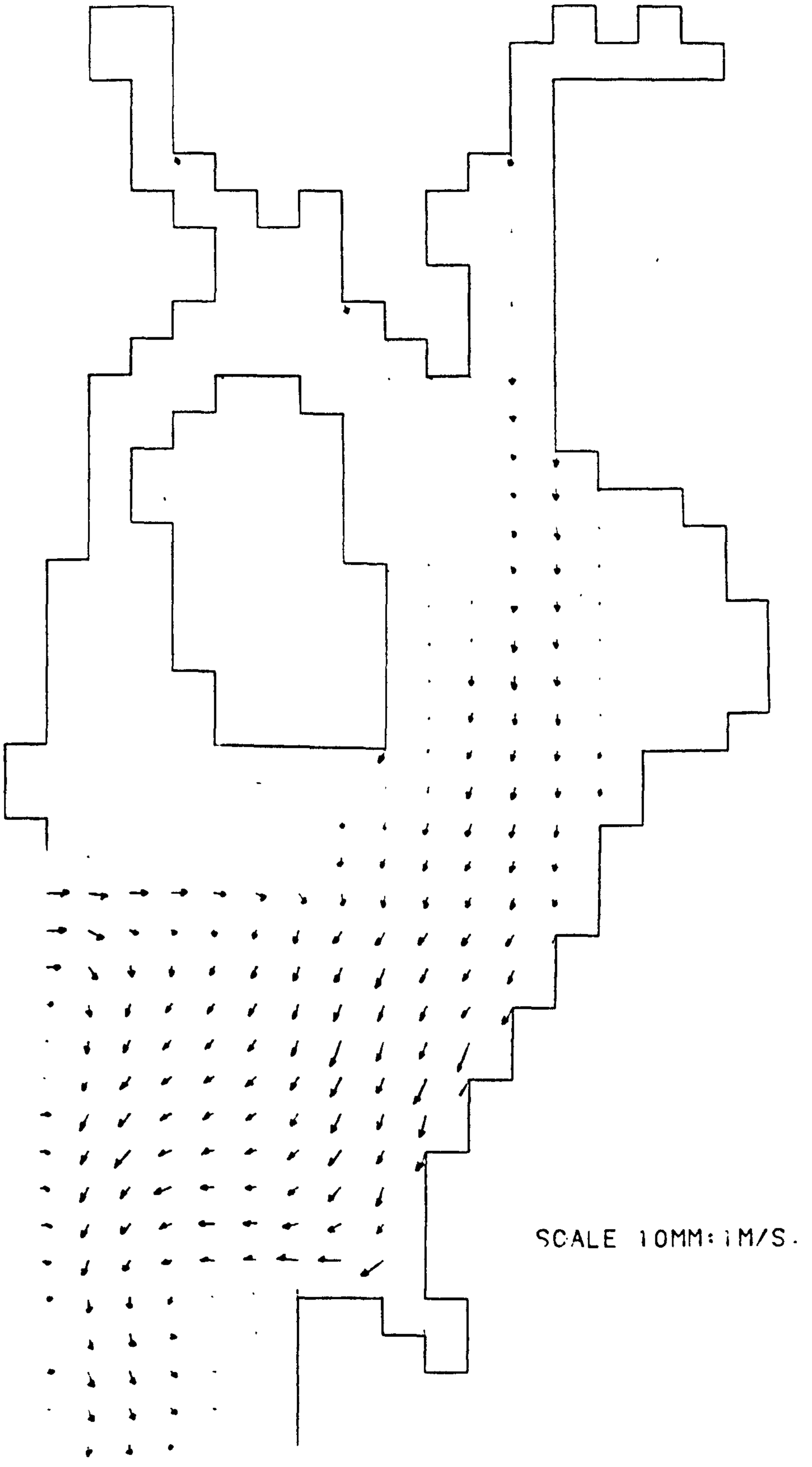

FIGURE 7·8 d
SPRING TIDE VELOCITIES IN CLYDE ESTUARY.
TIME FROM START OF TIDAL CYCLE HOURS= 8.94

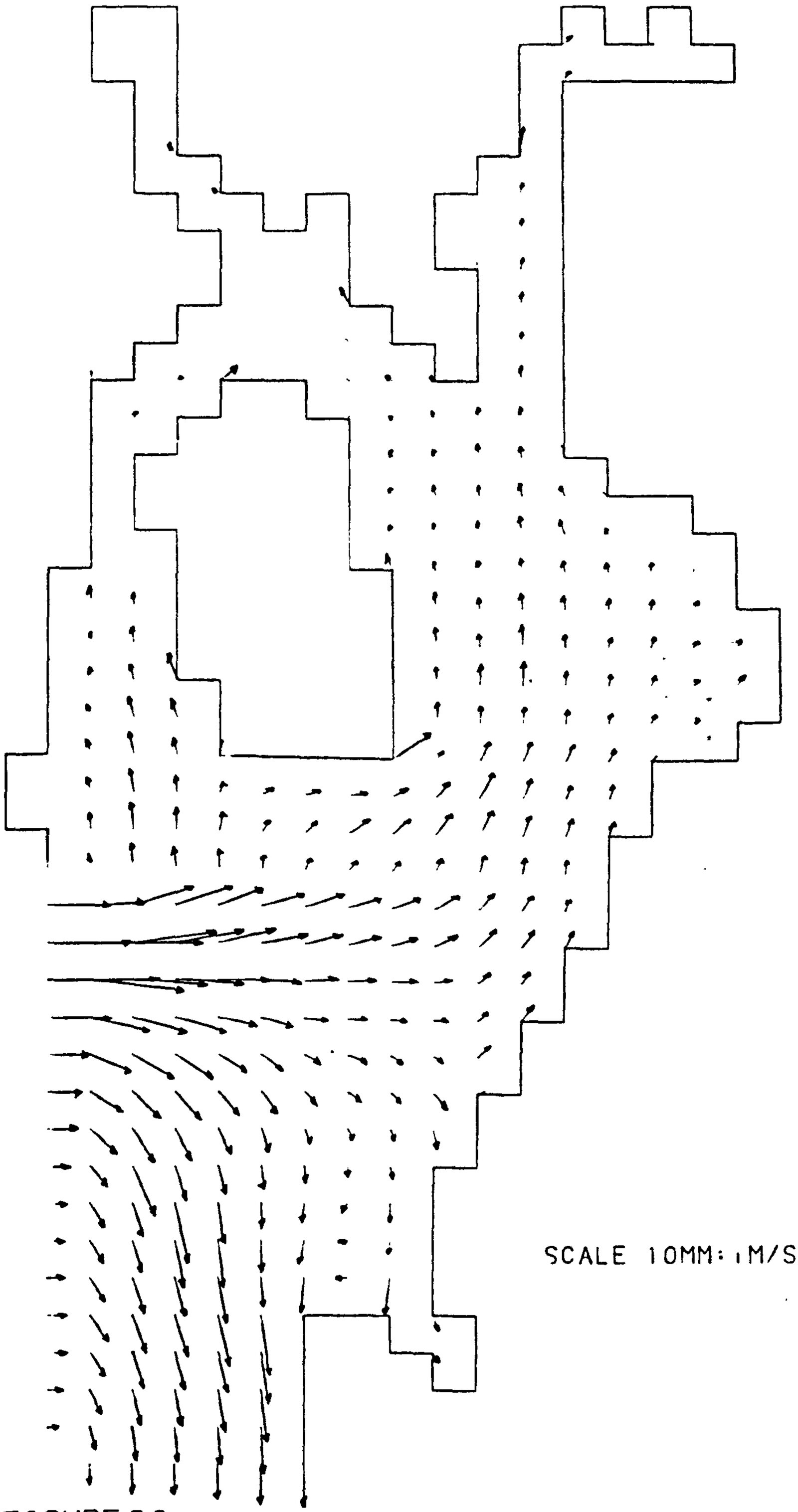

FIGURE 7·8e

SPRING TIDE VELOCITIES IN CLYDE ESTUARY.
TIME FROM START OF TIDAL CYCLE HOURS= 11.92

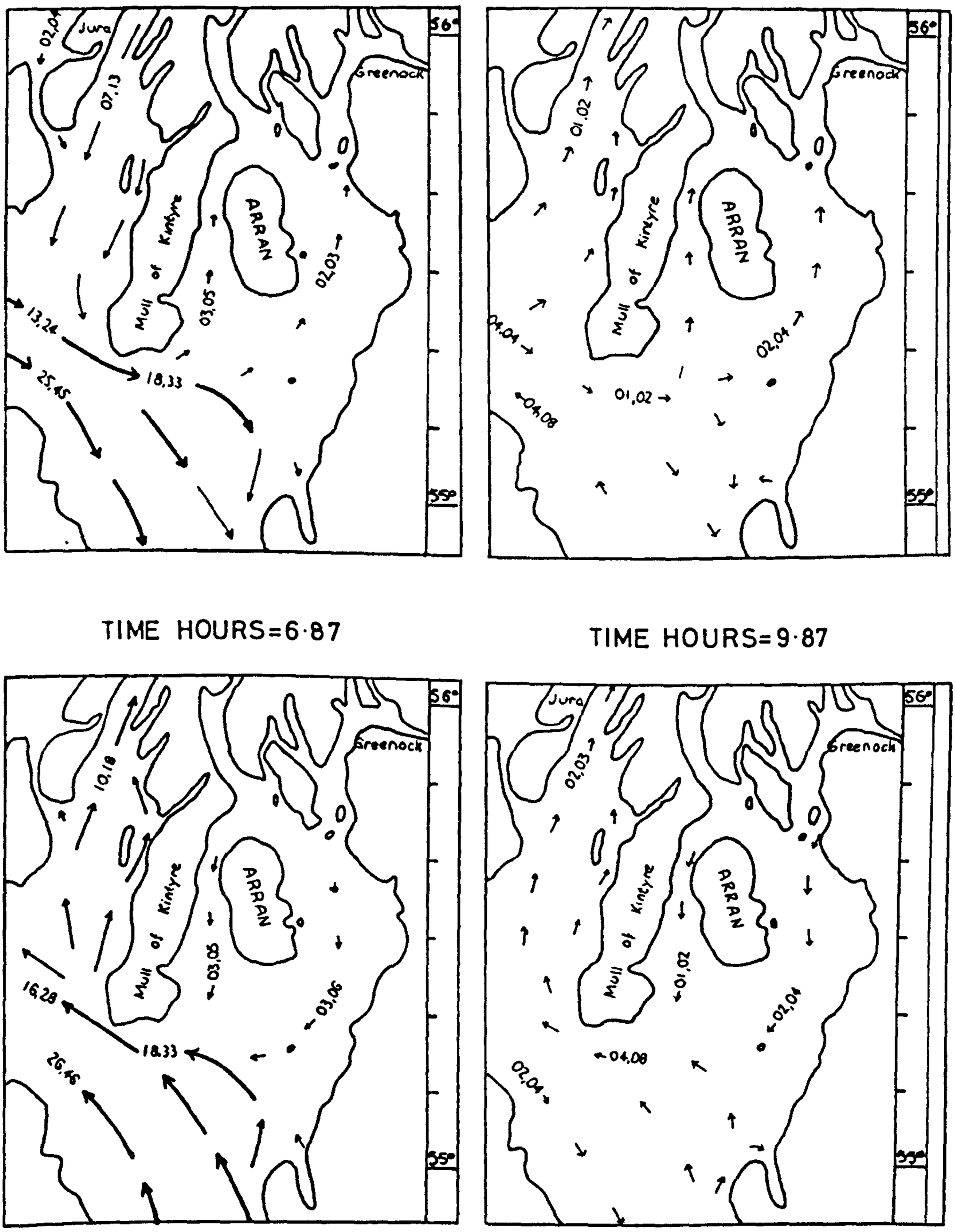

The figures against the arrows give the mean neap and spring rates in tenths of a knot, thus 19,34 indicates a mean neap rate of 1·9 knots and a mean spring rate of 3·4 knots.

FIGURE 79
TIDAL STREAMS IN THE FIRTH OF CLYDE.

FIGURE 7.10 a
SPRING TIDE PROPAGATION IN THE CLYDE ESTUARY.
TIME FROM START OF TIDAL CYCLE HOURS = .00

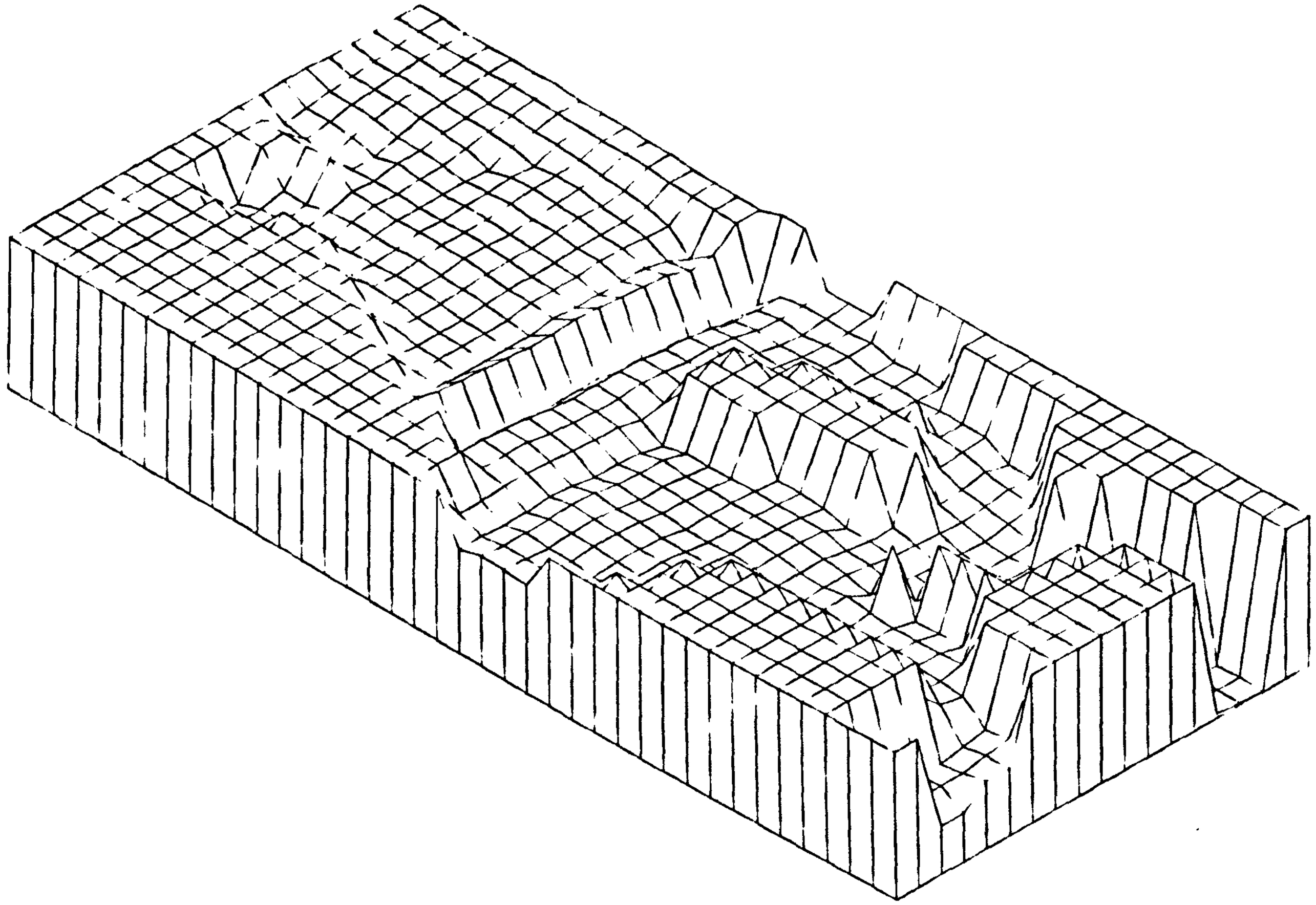

FIGURE 7.10 b
SPRING TIDE PROPAGATION IN THE CLYDE ESTUARY.
TIME FROM START OF TIDAL CYCLE HOURS= 4.99

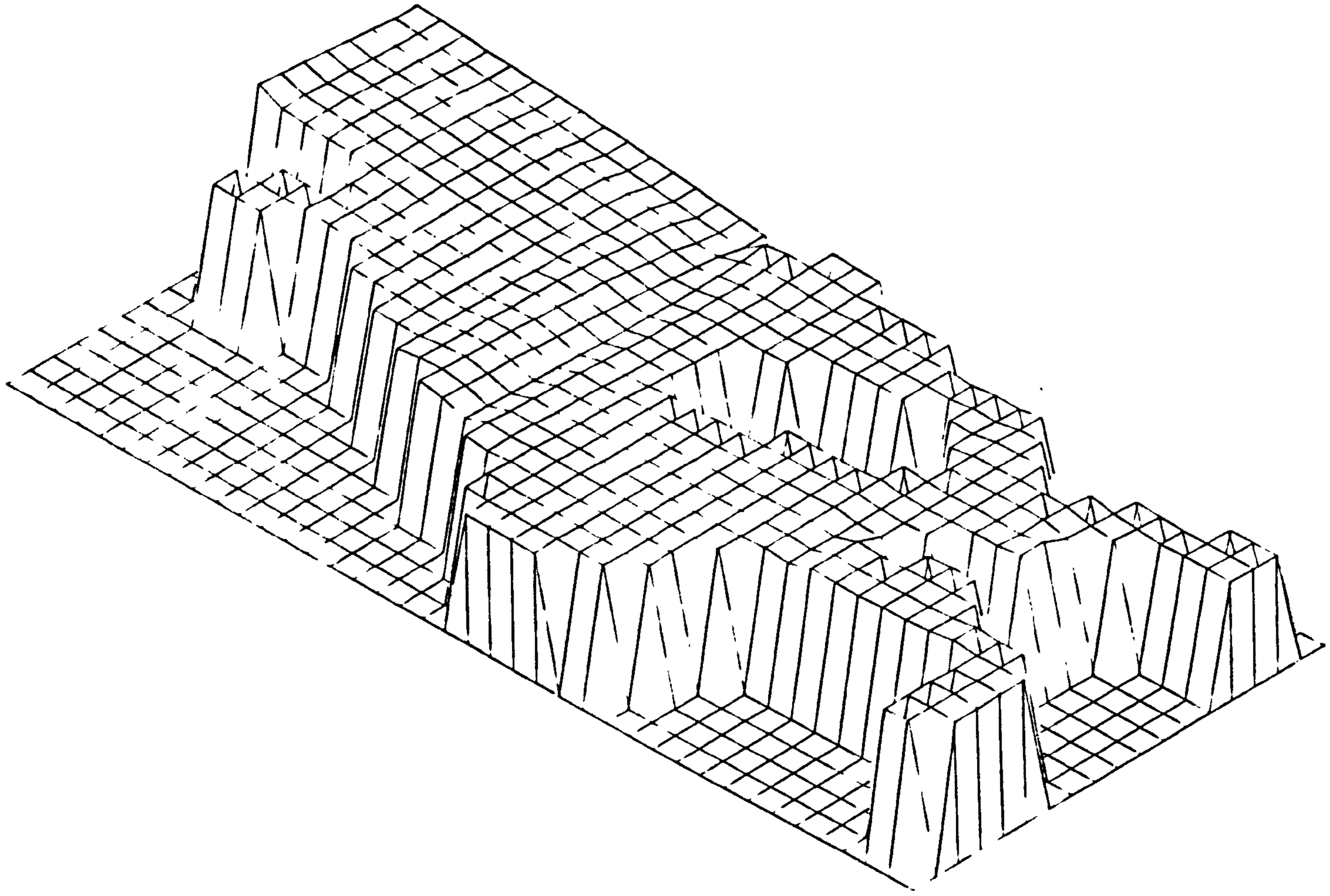

FIGURE 7·10c
SPRING TIDE PROPAGATION IN THE CLYDE ESTUARY.
TIME FROM START OF TIDAL CYCLE HOURS= 7.33

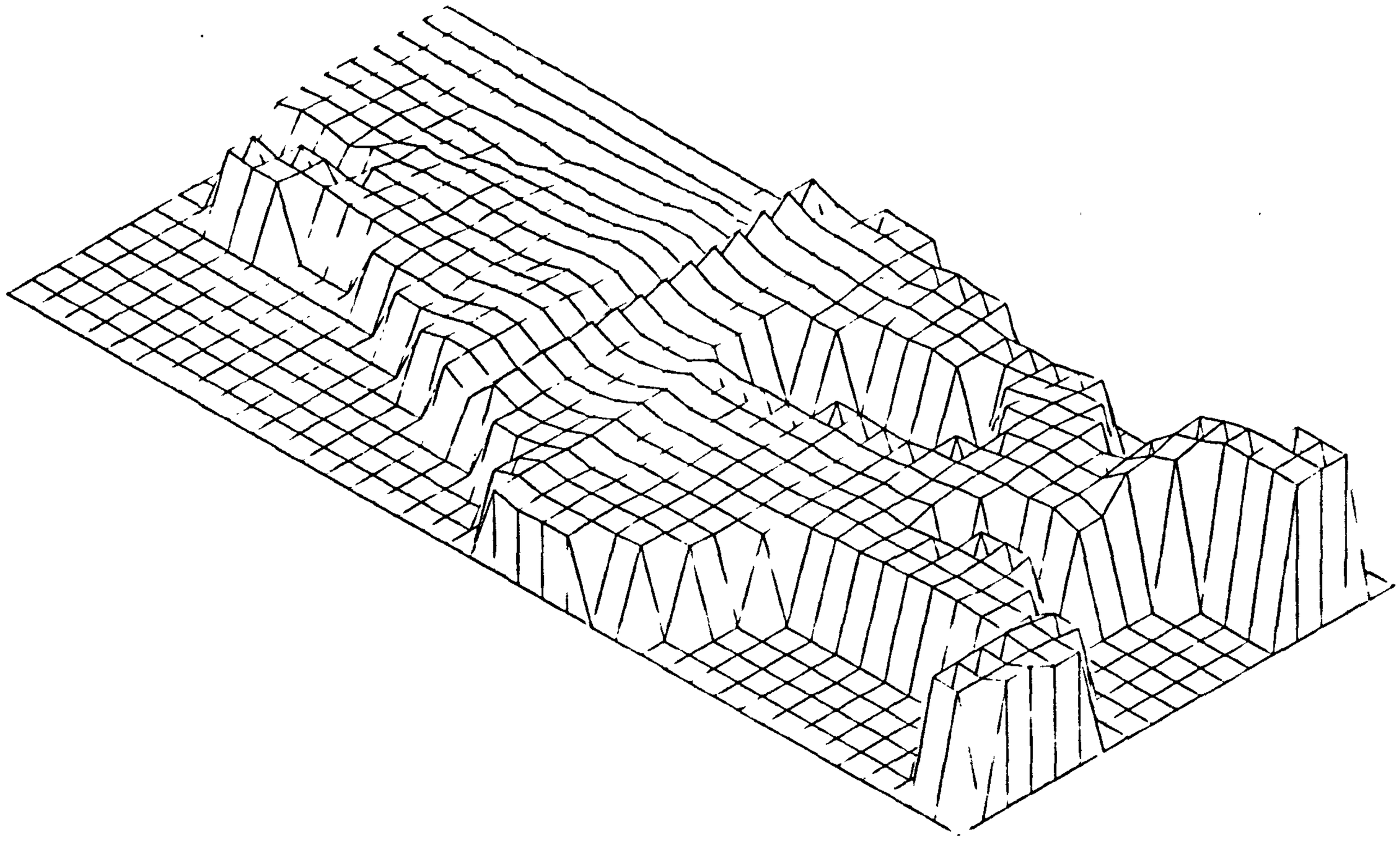

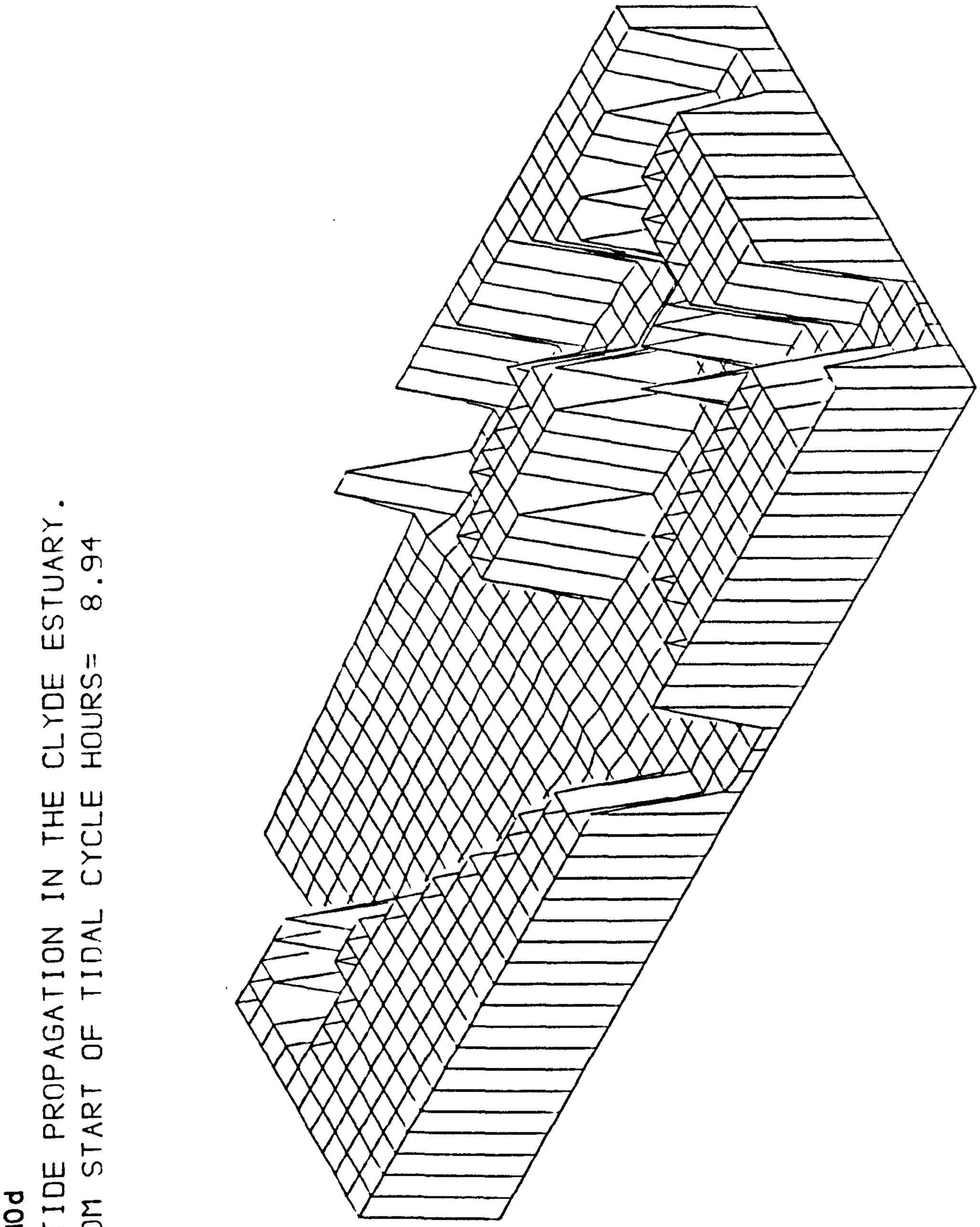

FIGURE 7.10d
SPRING TIDE PROPAGATION IN THE CLYDE ESTUARY.
TIME FROM START OF TIDAL CYCLE HOURS= 8.94

FIGURE 7·10 e
SPRING TIDE PROPAGATION IN THE CLYDE ESTUARY.
TIME FROM START OF TIDAL CYCLE HOURS= 11.92

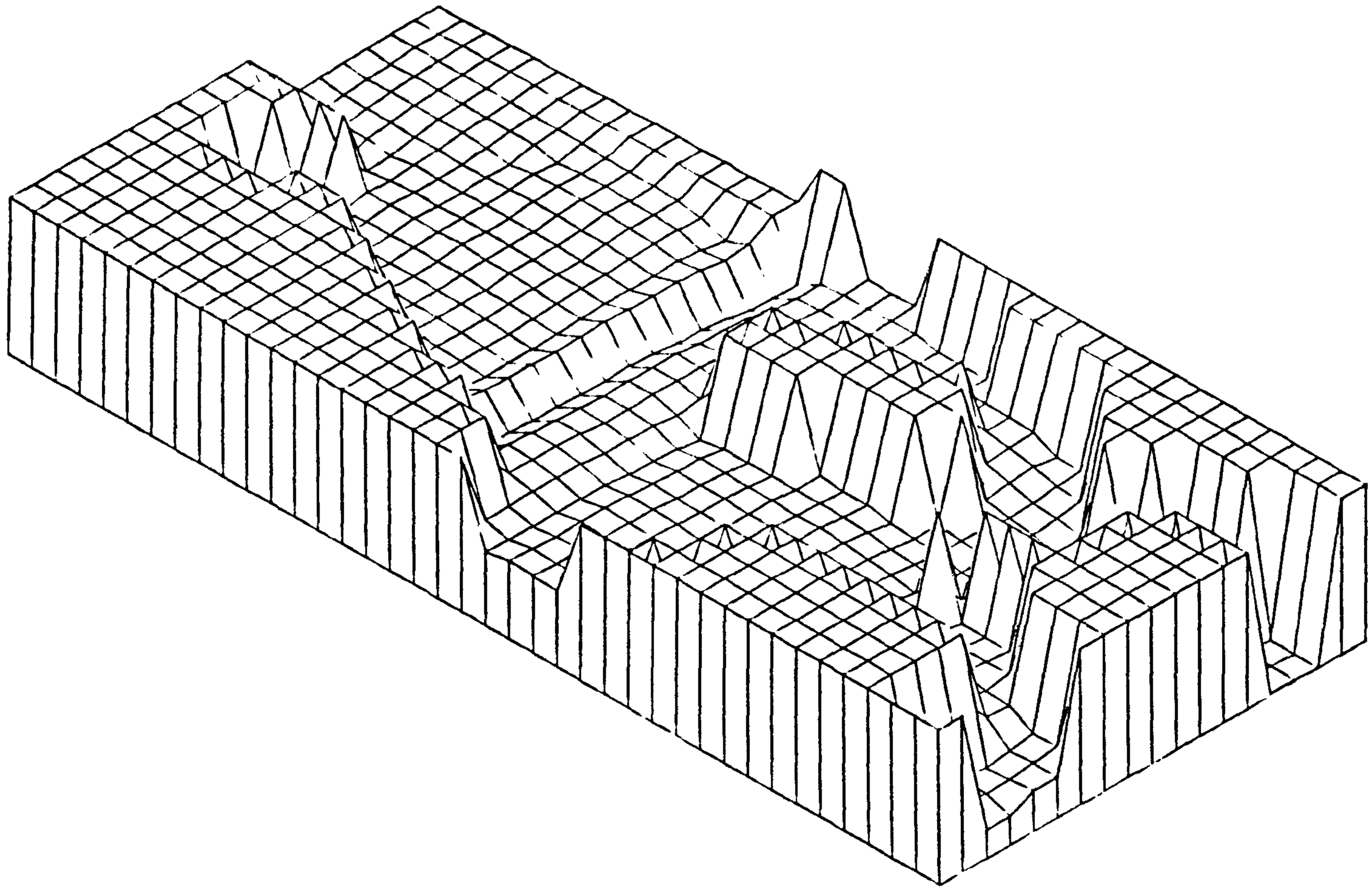

7.10 STORM SURGE PROPAGATION IN THE FIRTH OF CLYDE

7.10.1 DEFINITION OF A STORM SURGE

Storm surges are sometimes referred to as meteorological tides since they are caused by unusually high or low barometric pressures and associated strong or prolonged wind speeds. When these conditions differ from the norm there are corresponding differences between the actual and predicted tides which, if recorded, become a measure of the storm surge. In this way a positive surge is associated with a net transport of water towards the shore resulting in an increase in tidal level. Naturally enough, previous studies have been more concerned with low pressure distributions and in simulating positive surges because of their importance in flood prediction.

7.10.2 THE WEATHER CONDITIONS ASSOCIATED WITH MAJOR STORM SURGES ALONG THE WEST COAST OF THE BRITISH ISLES

The intensity of the storm has been found by Harris (1966) to be the most important parameter for estimating the storm surge produced. The central pressure, the pressure gradient across the depression and the maximum wind speed are all valid indices of the storm intensity. The central pressure being the most stable of these parameters. The location of the peak surge is largely determined from the track of the storm and the area affected depends on both its track near the coast and its size.

An analysis similar to that of Harris was performed by Lennon (1968) for surge events along the west coast

of the British Isles. He analysed seven depressions at both Liverpool and Avonmouth and noted the similarity of features in the depressions which were responsible for producing surges at either or both these parts. He concluded that a major surge could be expected along the west coast when four meteorological conditions occurred, namely if:

i. a deepening and well developed secondary depression approaches the country from the Atlantic Ocean such that its right-rear quadrant acts upon the water surface en route to the ports. Hence, the ports experiencing the greatest surge, lie to the right of the path of the depression.

ii. the speed of approach of the depression is of the order of 40 knots.

iii. a radius of depression up to 150 to 200 nautical miles is well defined by roughly concentric isobars.

iv. the depression reaches a depth of 50mb over the country and is associated with a pressure gradient of approximately 30mb in 250 nautical miles in its right-rear quadrant.

Lennon further concluded that of these four conditions, the first pair are more important than the second pair. The occurrence of these features in the recorded Scottish west coast surge on 7th-9th March 1979 is discussed later.

7.11 THE STORM SURGE OF 7th-9th MARCH 1979

During 7th March a depresion (Low C) to the northwest of Scotland moved away northeastwards and a new shallow depression (Low S) formed on the frontal trough between Scotland and Norway. On 8th March a small but deep depression (Low R) close to southwest Norway moved steadily northeast while another deep depression (Low L) to the west of Iceland moved slowly east. Accompanying frontal troughs moved close to northern Britain later in the day. During the next twenty-four hours the Icelandic depression intensified, moving slowly northeast between Scotland and Iceland. During 9th to 10th March this depression (Low L) moved north, away from east of Iceland, while its associated fronts over Britain moved away eastwards. During this period pressure remained low north of Scotland.

As a result of the presence of Low L, a positive surge occurred during 8th and 9th March 1979 on the west coast of Scotland. The parameters defining the storm are as follows, and are comparable with those presented by Lennon, discussed previously.

i. The maximum surge occurred during 1800 G.M.T. on 8th till 0800 G.M.T. on 9th March. During this time the centre of the depression was about three hundred nautical miles north of the Orkneys.

ii. During a thirty-hour time interval the depression travelled 820 nautical miles

therefore its average speed was 27 knots.

iii. The radius of depression was measured as 100 nautical miles.

iv. The maximum depth of the depression below standard atmospheric pressure was 57 millibars.

7.12 WIND, PRESSURE AND SURGE DATA

Donald (1981) collected and analysed wind, pressure and surge data for his model which encompassed the Firth of Clyde and its surrounding sea area for the period 7th to 9th March 1979. The present numerical model is concerned with surge propagation in the Firth of Clyde alone. Hence, the relevant data has been extracted from Donald's work and is presented in the following section.

The wind records at Abbotsinch, shown in Figure 7.11, were taken as being representative of those over the model area. A wind stress coefficient, K, of 2.0×10^{-3} was used and assumed to remain constant over the whole range of wind speeds, Abbott (1979, pp 38). Pressure differences between Machrahanish and Prestwick and Abbotsinch, table 7.3, were taken as representative of the $d\,Pa/dx$ and $d\,Pa/dy$ terms respectively. A more sophisticated approach evaluating these terms was considered unnecessary in the present case, as Donald's conclusions state that the main factor influencing storm surge propagation in the Firth of Clyde is the external surge input at the boundary. The external surge elevations used at the

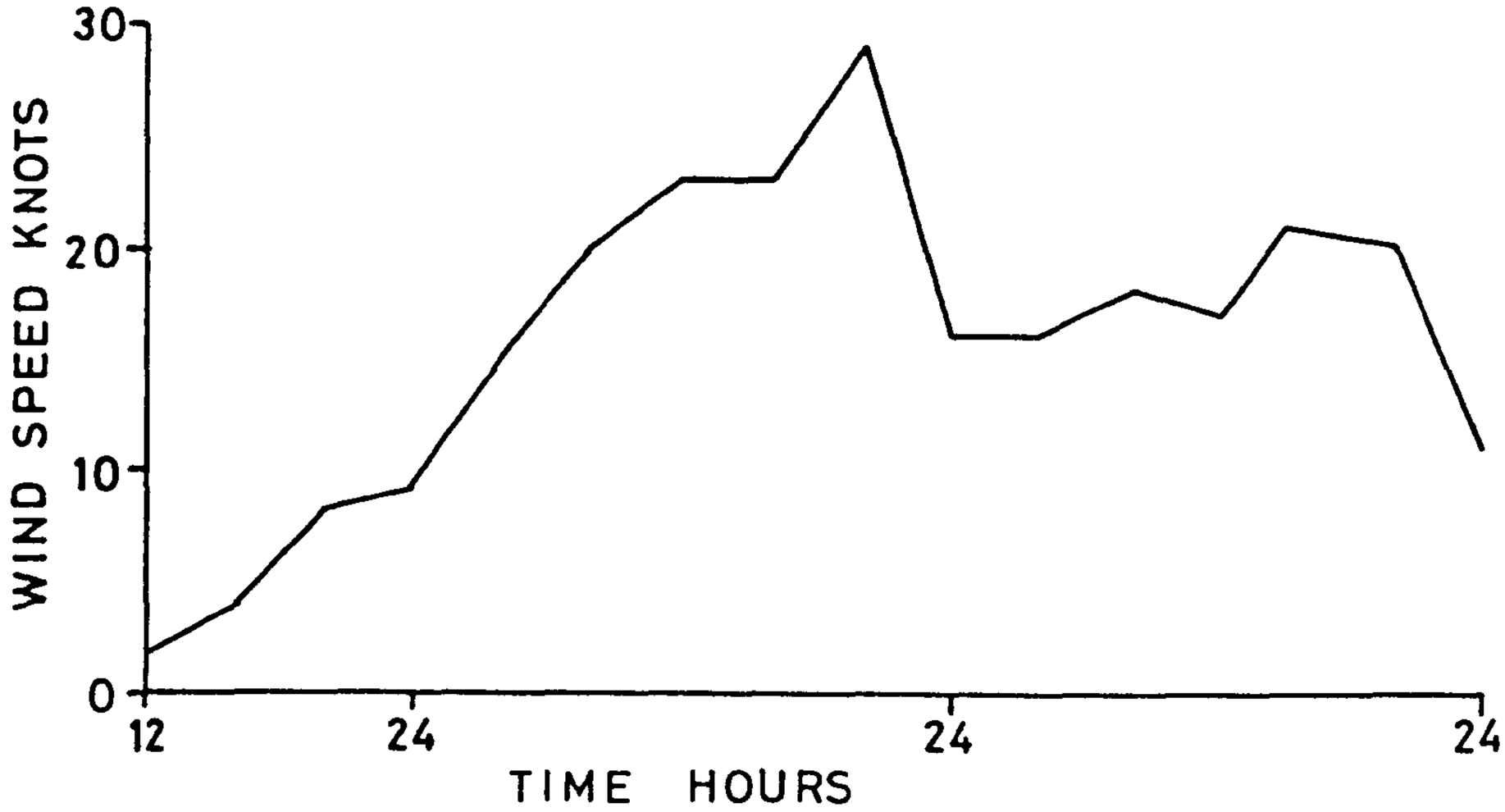

FIGURE 7·11a
WIND SPEEDS IN THE FIRTH OF CLYDE ON THE 7th – 9th OF MARCH 1979.

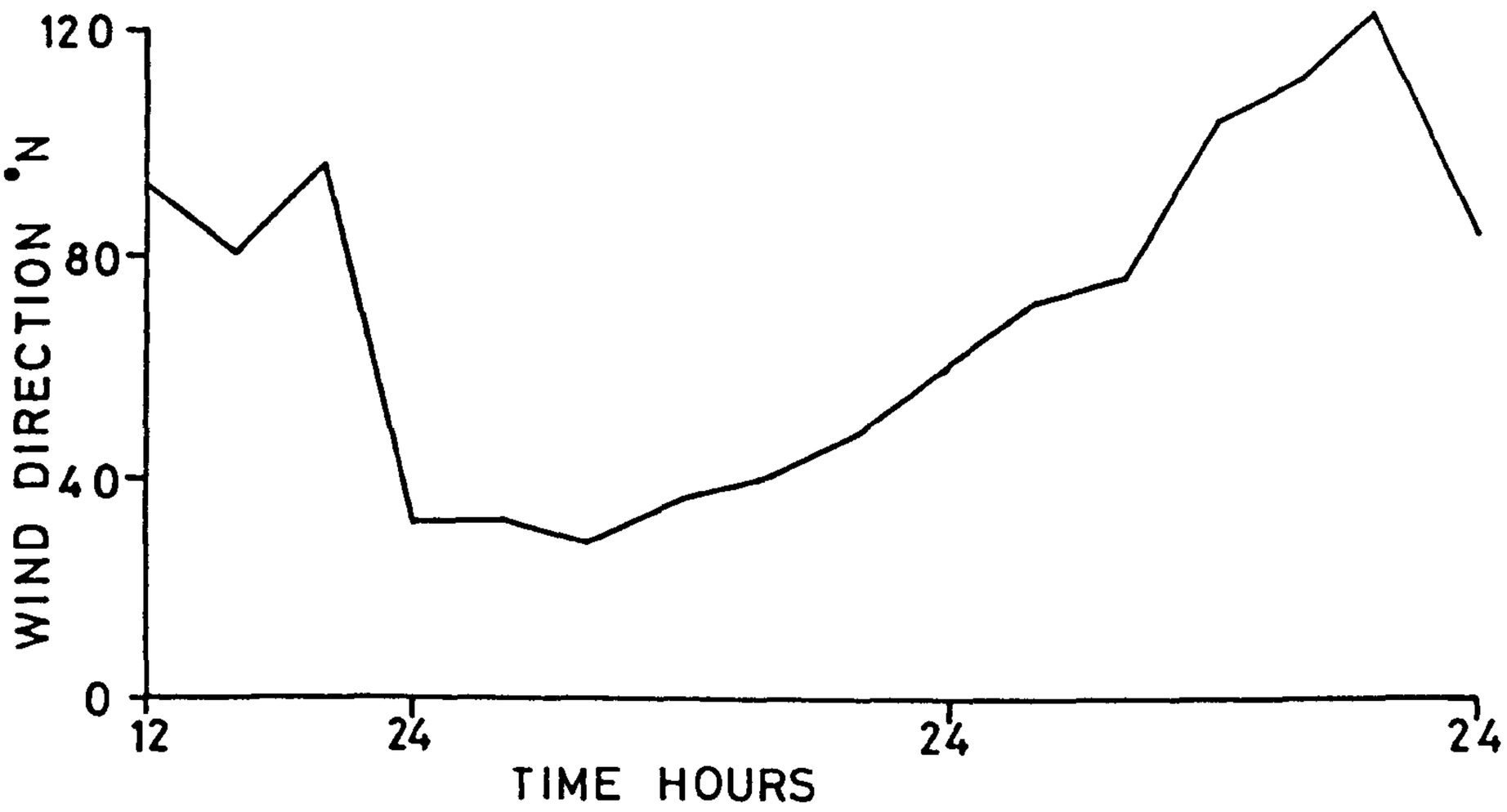

FIGURE 7·11b
WIND DIRECTION IN THE FIRTH OF CLYDE ON THE 7th – 9th OF MARCH 1979.

TIME	ABBOTSINCH	PRESTWICK	MACHRAHANISH
7th			
1200	1003.0	1003.0	1000.0
1800	1006.0	1007.4	1007.7
8th			
0000	1009.0	1010.3	1009.7
0600	1005.0	1006.7	1005.1
1200	999.2	1006.0	1002.4
1800	989.0	990.9	990.1
9th			
0000	982.0	983.5	983.6
0600	980.9	983.1	983.3
1200	983.1	984.4	985.0
1800	991.8	993.9	995.2
0000	1004.5	1001.6	1001.8

Table 7.3

THE VARIATION OF BAROMETRIC PRESSURE WITH TIME AT WEATHER STATIONS IN THE FIRTH OF CLYDE DURING 7th to 9th MARCH 1979

(Pressure in Millibars)

extremities of the open sea boundary were those measured by Donald's tidal survey at Portpatrick and Campbeltown. Between these coastal locations elevations were obtained by interpolation.

These external surge boundary conditions were assumed to be independent of conditions in the Firth. As such, they were superimposed upon the predicted elevations (taken from the Admiralty Tide Tables 1979) at the open sea boundary.

7.13 COMPARISON OF SIMULATED RESULTS WITH RECORDED DATA

An evaluation of the model's ability to reproduce storm surge conditions was made at certain locations corresponding to the availability of tide records. The records from tide gauges situated at Millport and Greenock were used for this purpose. Millport and Greenock are located at the head of the Firth, see Figure 7.12a.

Computed tide plus surge elevations are compared with the predicted tides in Figures 7.12b to 7.12e. It is noted that the storm surge is of insufficient magnitude to radically modify the tidal oscillations, as during the period of positive surge the phases of recorded and predicted tides are very similar. A comparison between the computed tide plus surge and the measured tide plus surge is shown in Figures 7.13a to 7.13d. It can be seen that a good agreement is achieved between the two curves, tide plus surge peak water levels being over estimated by around 0.2m The accuracy of the computed surge can be properly assessed by comparing it with the recorded surge as shown

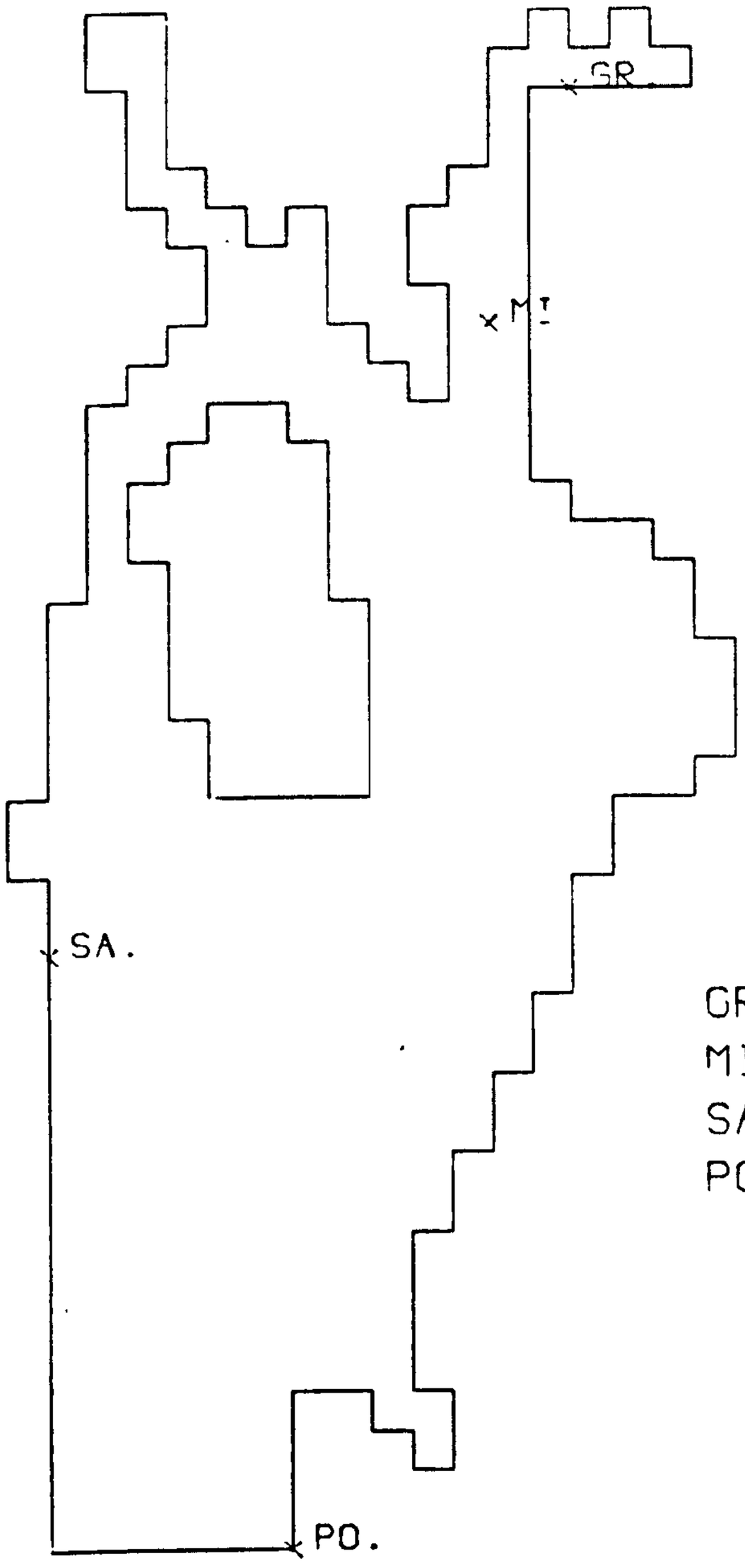

GR. GREENOCK
MI. MILLPORT
SA. SANDA ISLAND
PO. PORTPATRICK

FIGURE 7·12a
POSITION OF WATER LEVEL HISTORYS

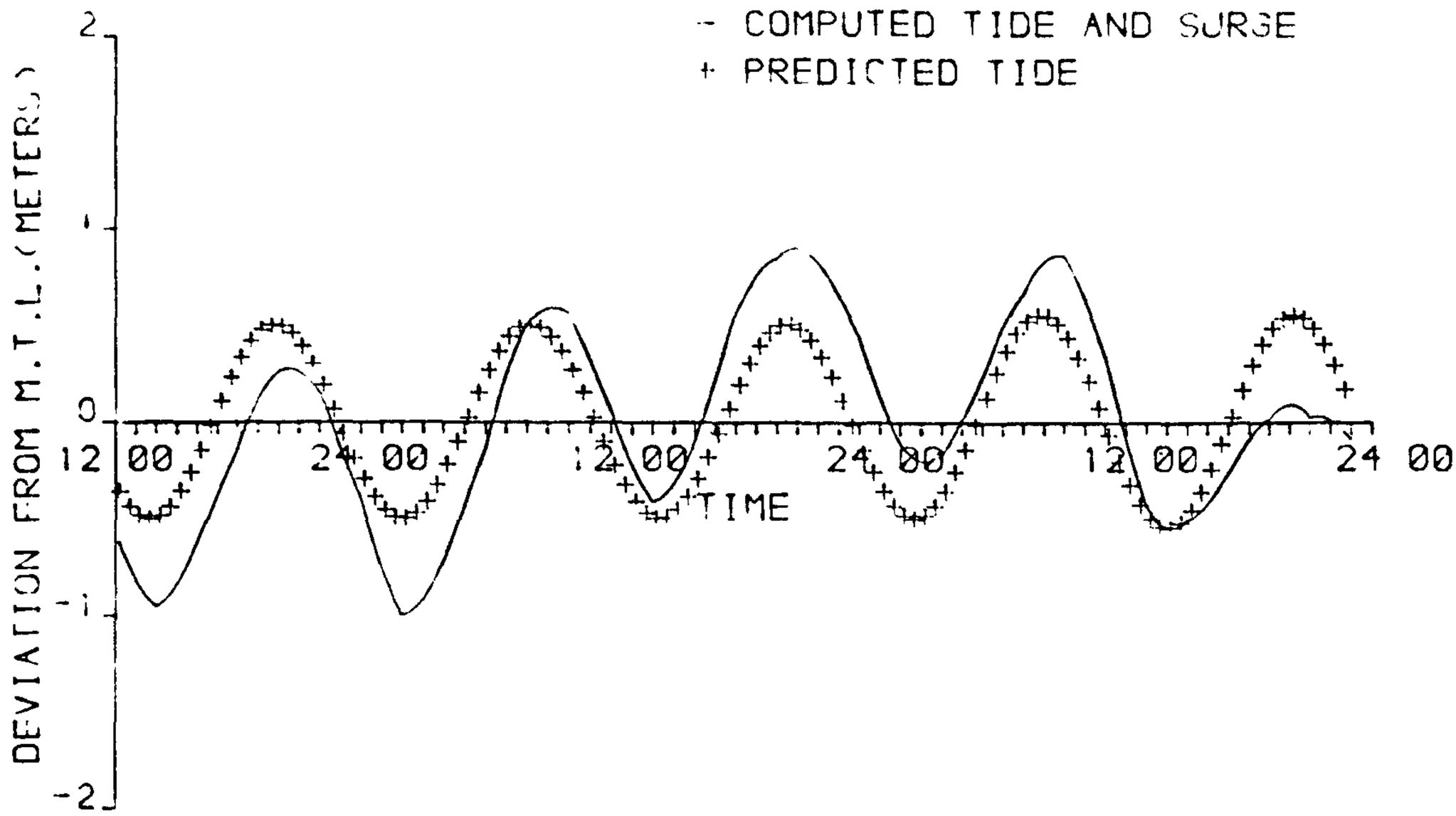

FIGURE 7·12 b
STORM SURGE WATER LEVELS AT SANDA ISLAND
ON THE 7TH TO 9TH OF MARCH 1979

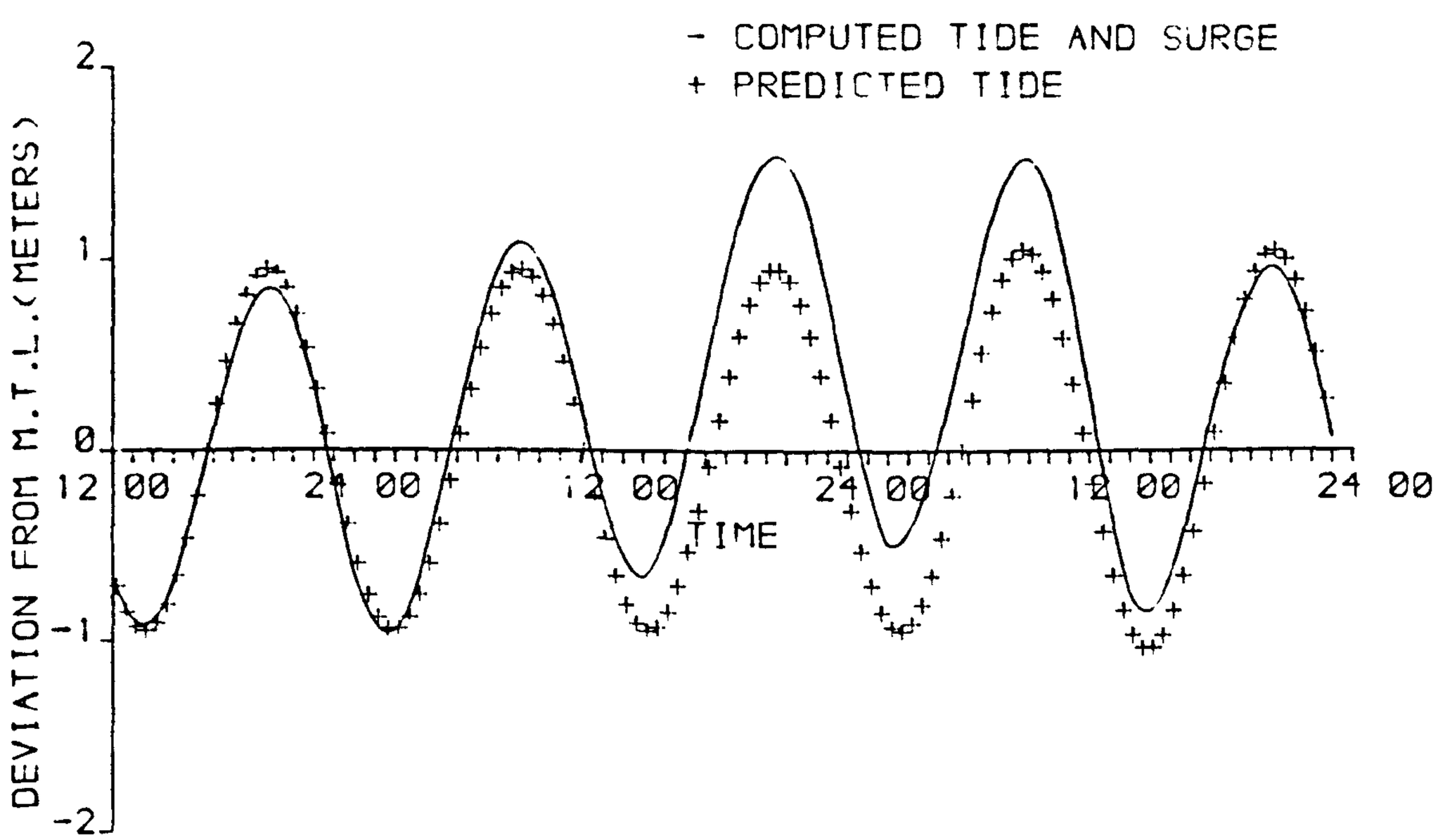

FIGURE 7·12 c
STORM SURGE WATER LEVELS AT PORTPATRICK
ON THE 7TH TO 9TH OF MARCH 1979

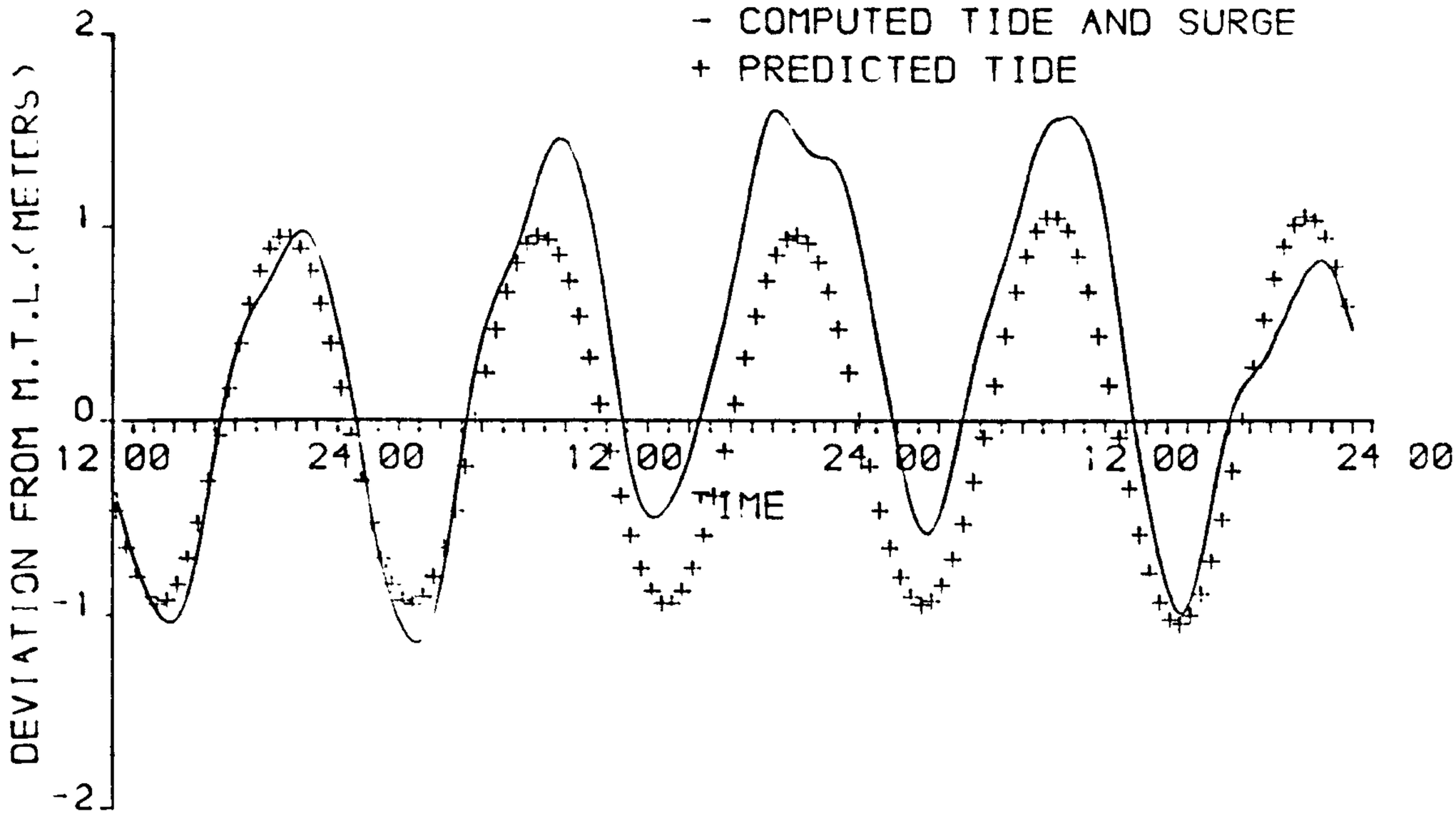

FIGURE 7·12 d
STORM SURGE WATER LEVELS AT GREENOCK
ON THE 7TH TO 9TH OF MARCH 1979

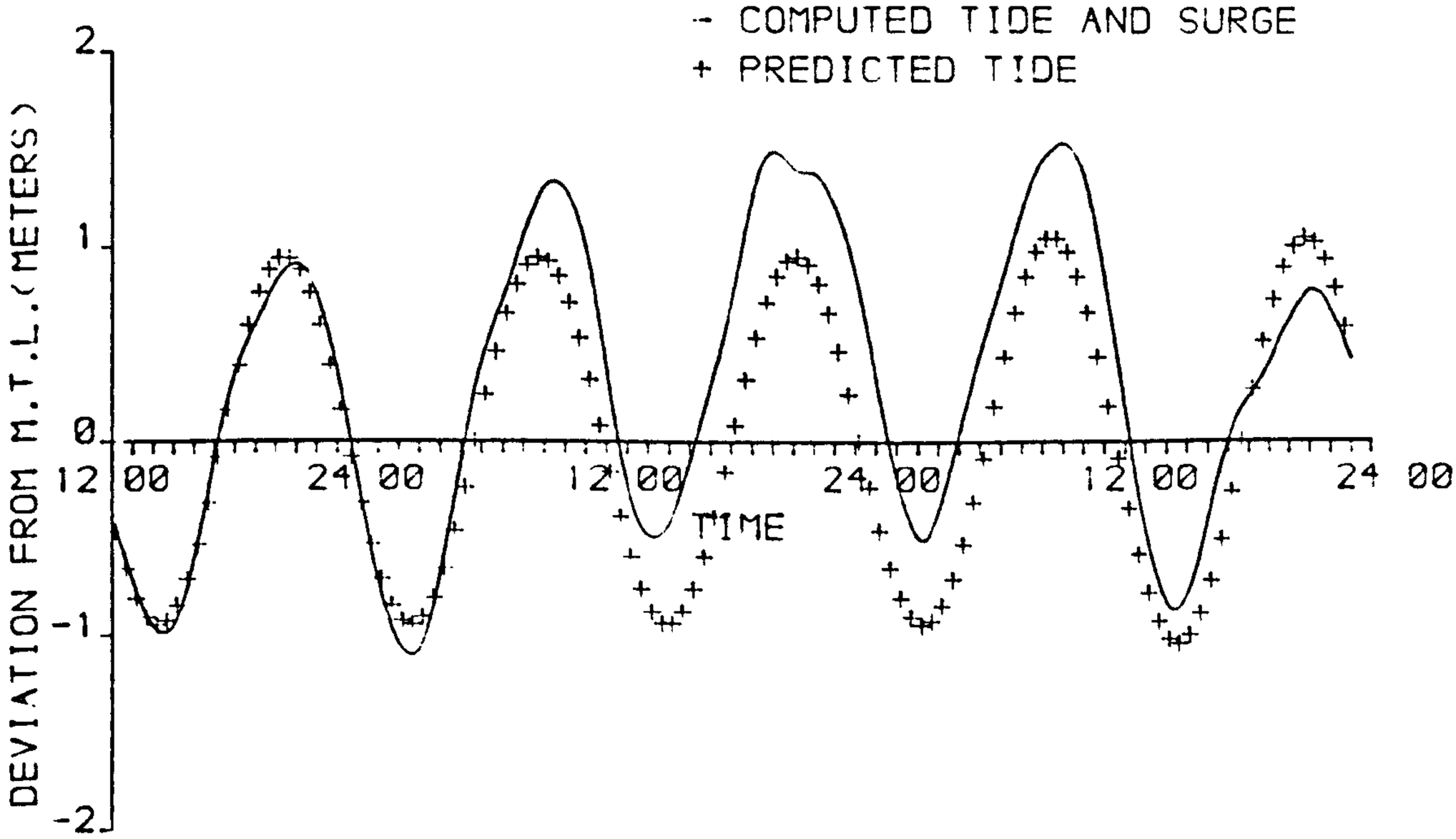

FIGURE 7·12 e
STORM SURGE WATER LEVELS AT MILLPORT
ON THE 7TH TO 9TH OF MARCH 1979

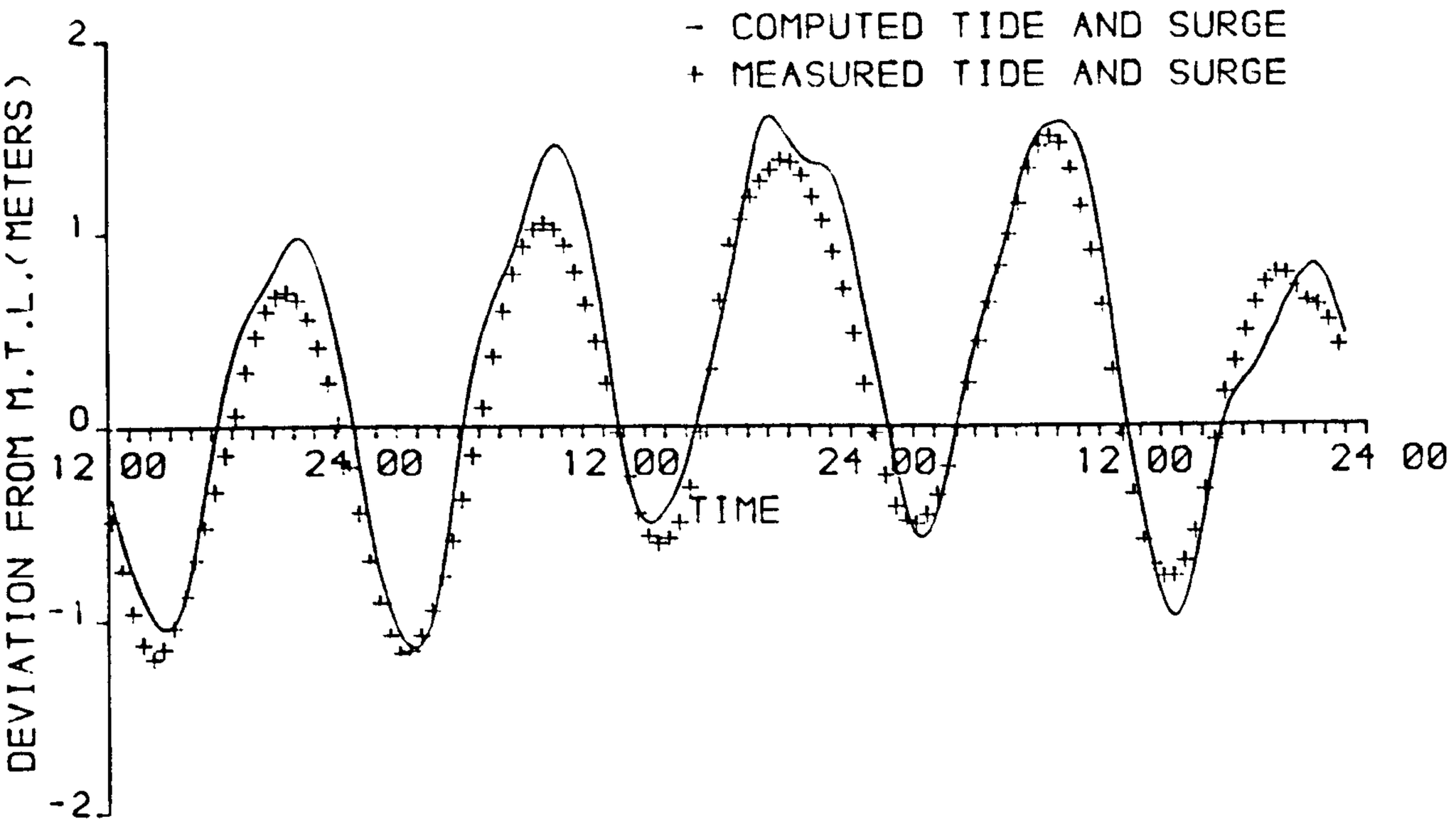

FIGURE 7·13a
STORM SURGE WATER LEVELS AT GREENOCK
ON THE 7TH TO 9TH OF MARCH 1979

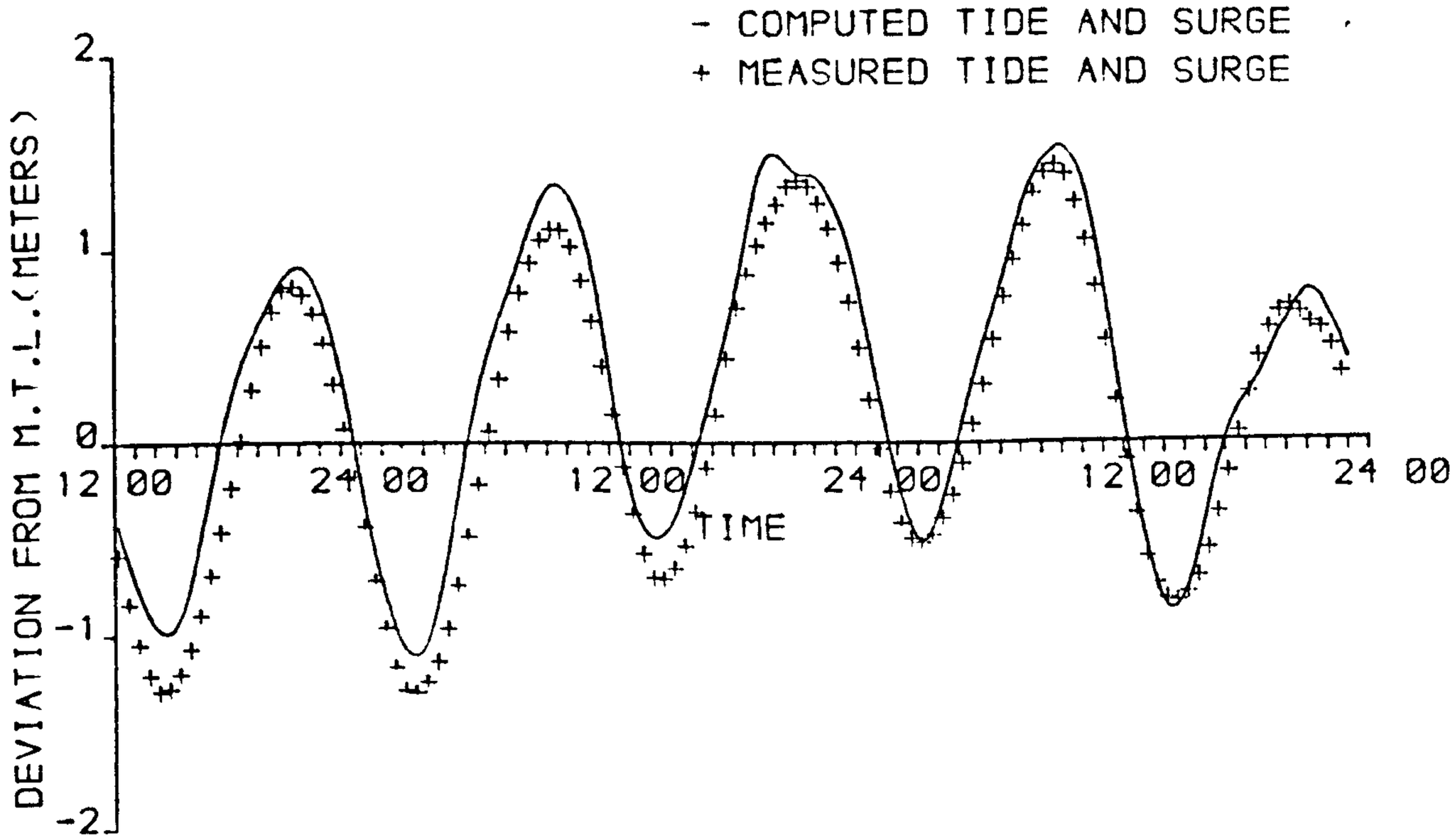

FIGURE 7·13b
STORM SURGE WATER LEVELS AT MILLPORT
ON THE 7TH TO 9TH OF MARCH 1979

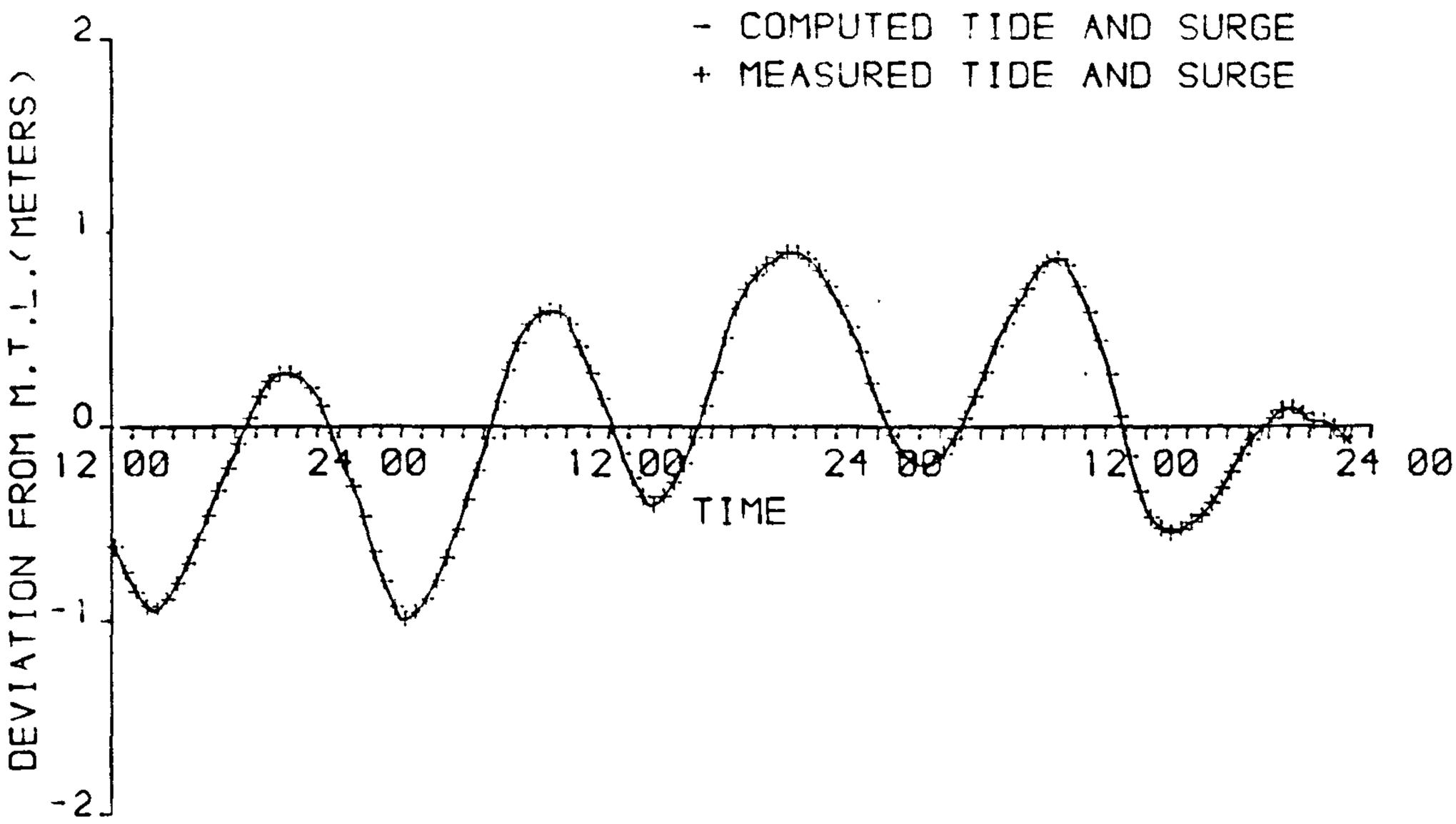

FIGURE 7·13c
STORM SURGE WATER LEVELS AT SANDA ISLAND
ON THE 7TH TO 9TH OF MARCH 1979

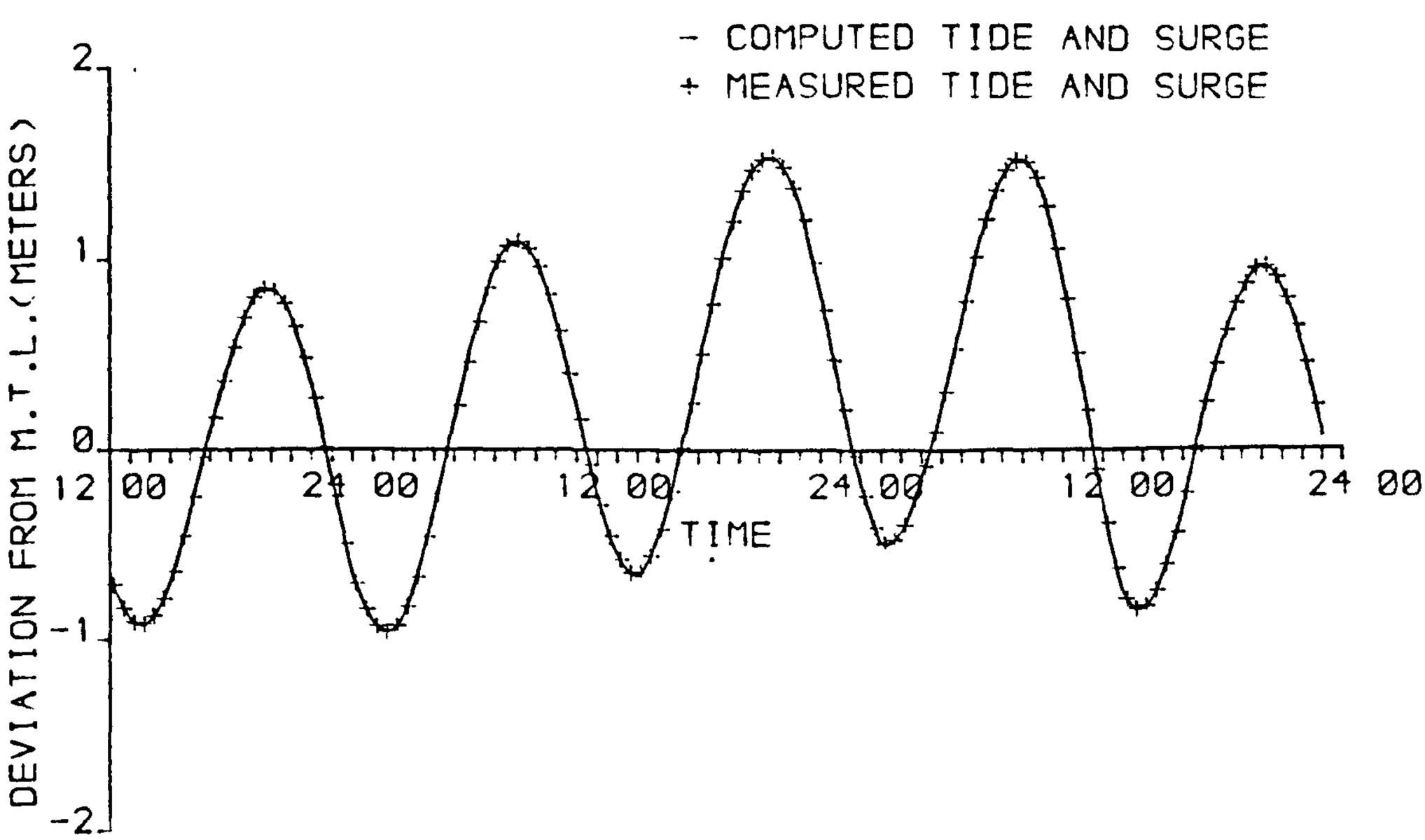

FIGURE 7·13d
STORM SURGE WATER LEVELS AT PORTPATRICK
ON THE 7TH TO 9TH OF MARCH 1979

in Figures 7.14a and b. From these figures it is evident the computed surge is more active than the measured surge. Most of this discrepancy is probably due to insufficient external surge data at the model boundaries. As the numerical model assumed surge information at Campbeltown to be representative of that at Sanda Island and assumed external surge elevations to vary linearly between Sanda Island and Portpatrick.

It is considered that these results demonstrate the model's ability to simulate storm surges in a near shore environment, where wind and pressure variations have a minimal effect on surge elevations. However, it is stressed that the method of simulation is strongly dependent on prior knowledge of the external surge elevations.

7.14 COMPARISON OF AN ALTERNATING DIRECTION IMPLICIT METHOD AND A X-Y-T CHARACTERISTIC METHOD IN THE FIRTH OF CLYDE

Advocates of the method of characteristics often stress the method's ability to model the physical properties of the hyperbolic continuum equations. Namely, the reproduction of domains of dependence and regions of influence. However, it should be remembered that the inclusion of non-linear terms and an interpolation scheme presents discretization problems in a finite difference approximation to the characteristic equations on a regular x-y-t grid. These can introduce volume conservation errors and a degree of numerical damping. Further, the characteristic conditions are inherent

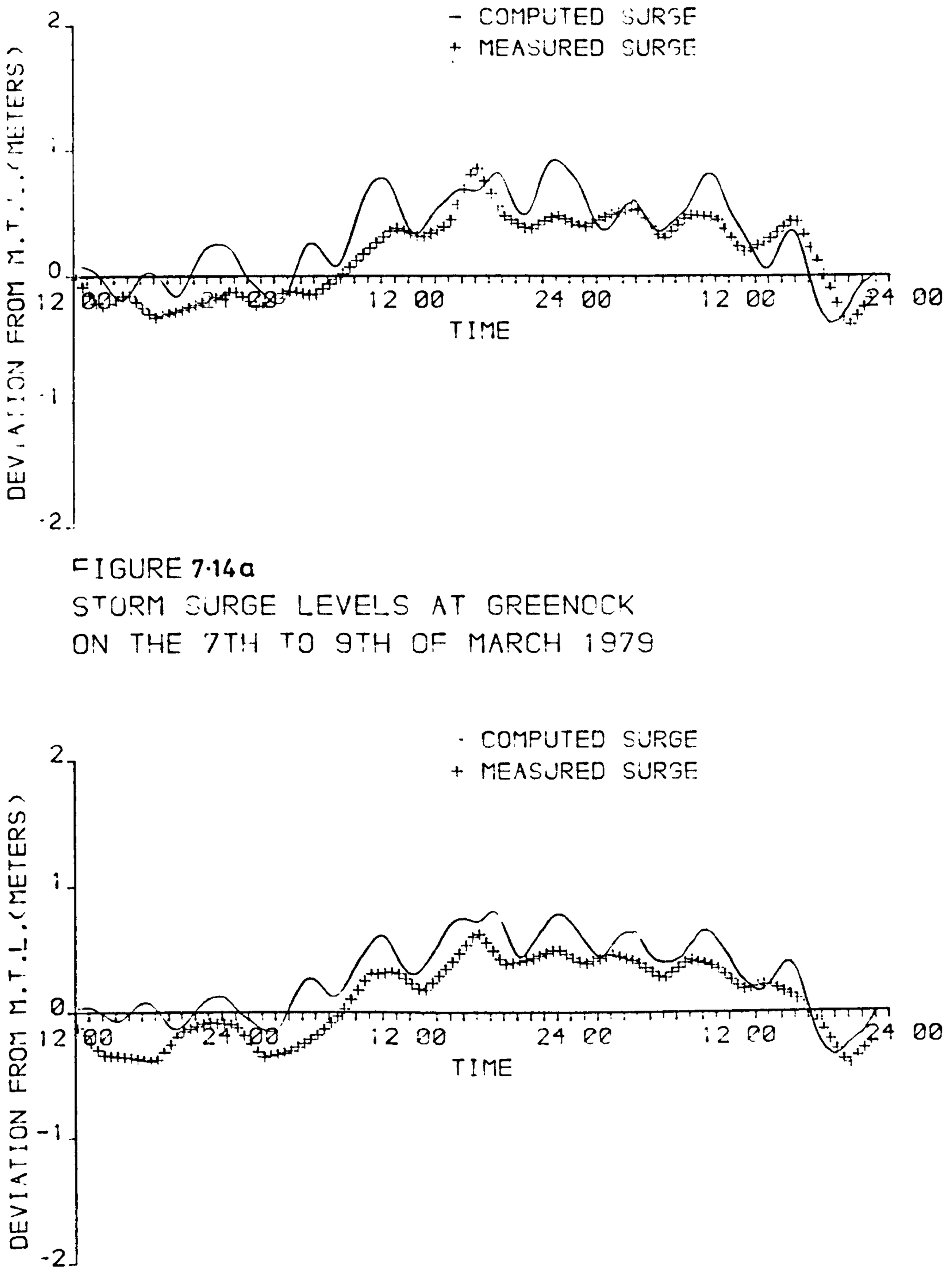

FIGURE 7·14a
STORM SURGE LEVELS AT GREENOCK
ON THE 7TH TO 9TH OF MARCH 1979

FIGURE 7·14b
STORM SURGE LEVELS AT MILLPORT
ON THE 7TH TO 9TH OF MARCH 1979

in direct finite difference approximations to the finite difference equations and some schemes, for example, the Preissmann scheme, will furnish the exact solution to the fully linearized flow equations for a special choice of Δx and Δt. The above points indicate that whatever physical advantages the method of characteristics appears to possess in its differential form these may be lessened in the realization of a numerical solution. The following sections examine to what extent this is true by comparing the results of Donald's model three run fourteen with those of the author's alternating direction implicit model.

7.14.1 BASIS OF COMPARISON

Both models use a similar schematization of the Firth of Clyde area, any differences occurring along the open sea boundary. Variations of water level with time, taken from the Admiralty Co-tidal Chart 5058, are used as boundary conditions. Discrepancies in these boundary conditions can be seen in table 7.4. Donald's ranges at Portpatrick being some 200mm greater than the current model ranges. This difference is considered to have negligable effect as the Firth is not greatly influenced by tidal oscillations in the Irish Sea, see section 7.3. Of greater concern is the difference of 150mm at Sanda Island. Donald's use of 2.15m as the range at this point would appear to be incorrect as his own Figure 6.6 clearly shows the range to be 2m. The error, however, does not appear to significantly influence results in the interior of the model. Possibly aided by the use of a Chezy coefficient

LOCATION	TIDE TABLES 1979	PENDER 1983	DONALD 1981
GREENOCK	3.08	3.04	3.17
ROTHESAY BAY	3.08	2.91	2.96
EAST LOCH TARBERT	3.08	2.78	2.71
LOCH RANZA	2.65	2.81	2.73
BRODICK BAY	2.83	2.77	2.78
IRVINE	2.77	2.76	2.83
AYR	2.56	2.72	2.82
GIRVAN	2.68	2.54	2.70
CAMPBELTOWN	2.56	2.53	2.49
STRANRAER	2.77	2.65	2.81
SANDA ISLAND	-	2.00	2.15
PORTPATRICK	3.44	3.00	3.20

Table 7.4

COMPARISON OF RANGES

of $35m^{\frac{1}{2}}/s$ in the characteristic model. The alternating direction implicit model uses a Chezy coefficient of $100m^{\frac{1}{2}}/s$.

7.14.2 COMPARISON OF RANGES

Table 7.4 shows the ranges at a selection of ports in the Firth of Clyde from the two numerical models and the Admiralty Tide Tables (1979). A good comparison is obtained from both models. It is interesting to note that for both sets of simulated results the maximum negative error occurs at East Loch Tarbert and that the maximum positive error occurs at Ayr. These errors are probably due to schematization effects. Indeed, this is certainly the case for the alternating direction implicit model at East Loch Tarbert, see section 7.7.

7.14.3 COMPARISONS OF TIMES OF HIGH WATER

Comparisons of the times of high water, relative to Greenock, are shown for both numerical models and the Admiralty Tide Tables (1979) in table 7.5. It can be seen that the models produce a similar scatter of results at interior points. However, the maximum differences occur at Sanda Island and Portpatrick with the alternating direction implicit model. In assessing the severity of these differences it should be remembered that:

i. the current model can only predict high water to the nearest ten minutes.

ii. the rate of change of water levels in the Firth of Clyde is relatively modest with a variation of the order of 10mm

LOCATION	TIDE TABLES 1979	PENDER 1983	DONALD 1981
GREENOCK	0	0	0
ROTHESAY BAY	0	-10	-5
EAST LOCH TARBERT	+5	+20	+33
LOCH RANZA	-10	-10	+9
BRODICK BAY	0	-10	-2
IRVINE	-15	-10	-14
AYR	-20	-10	-12
GIRVAN	-20	-15	-32
CAMPBELTOWN	-15	-15	-22
STRANRAER	-15	-10	-26
SANDA ISLAND	-40	-20	-40
PORTPATRICK	-59	-20	-44

Note : All Time in Minutes

Table 7.5

COMPARISON OF HIGH WATER TIMES
RELATIVE TO HIGH WATER GREENOCK

occurring over a forty minute period at high water.

iii. the time difference between high water at the open boundary and at Greenock is an area where the Tide Tables and the Co-tidal Chart disagree. The Co-tidal Chart gives the difference as thirty-five minutes between Sanda Island and Greenock at forty minutes between Portpatrick and Greenock.

In the light of the above considerations it is felt that the current model has reproduced the time differences between high waters with reasonable accuracy.

7.14.4 CO-TIDAL CHARTS

A co-tidal chart of the alternating direction implicit model results is shown in Figure 7.15. This can be compared with Figure 7.16, where the co-range and co-phase lines from Admiralty Chart No 5058 are drawn on the numerical representation of the Firth of Clyde, and the co-tidal chart from Donald's model three run fourteen, shown in Figure 7.17. Similarities between the three figures are evident.

7.14.5 CONCLUSIONS REGARDING COMPARATIVE ACCURACY AND EFFICIENCY

From the previous discussion it is clear that the two numerical models are comparable with regard to their ability to simulate two-dimensional long wave propagation and that the physical significance of the method of

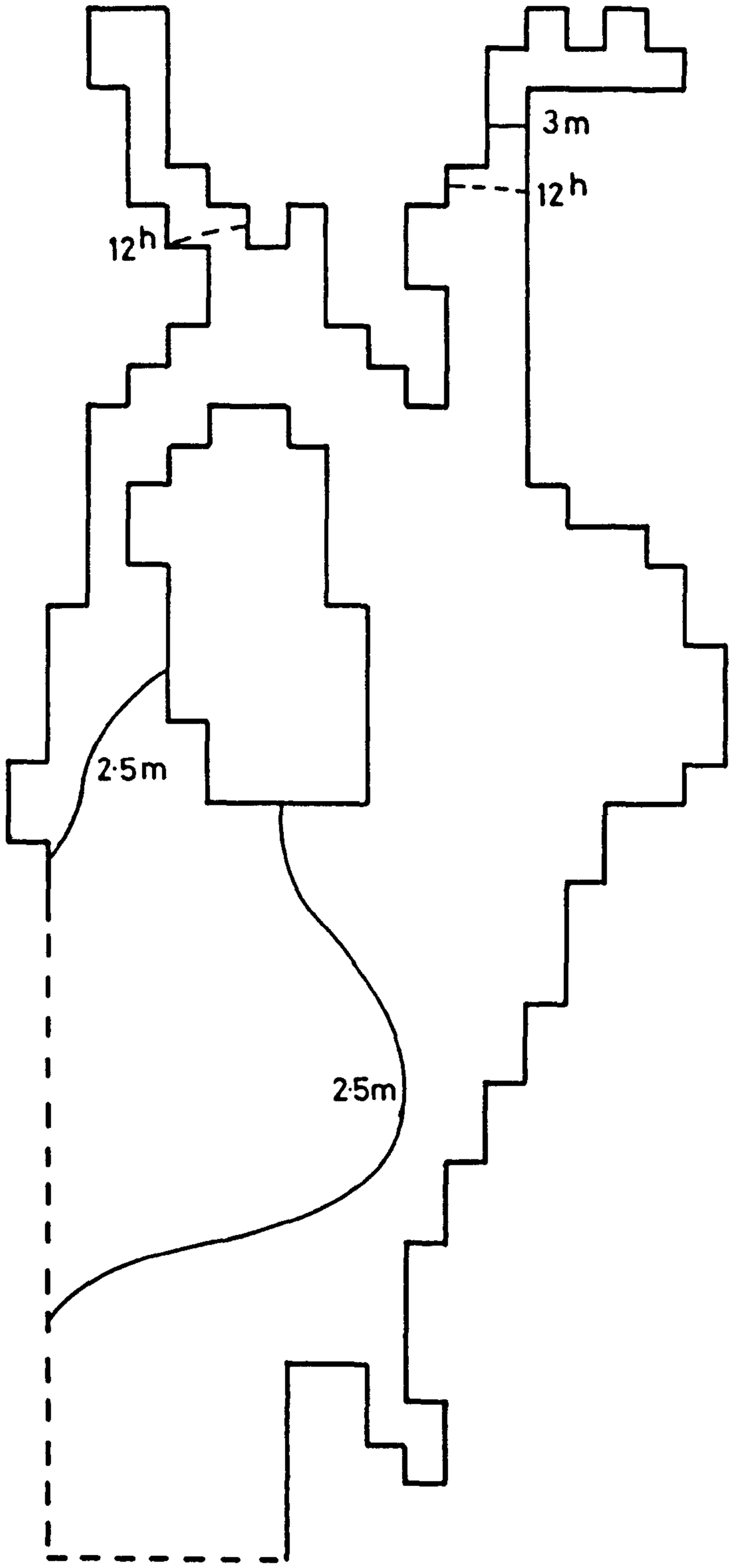

FIGURE 7·15
SPRING TIDE CO-RANGE AND CO-PHASE LINES IN THE FIRTH OF CLYDE.

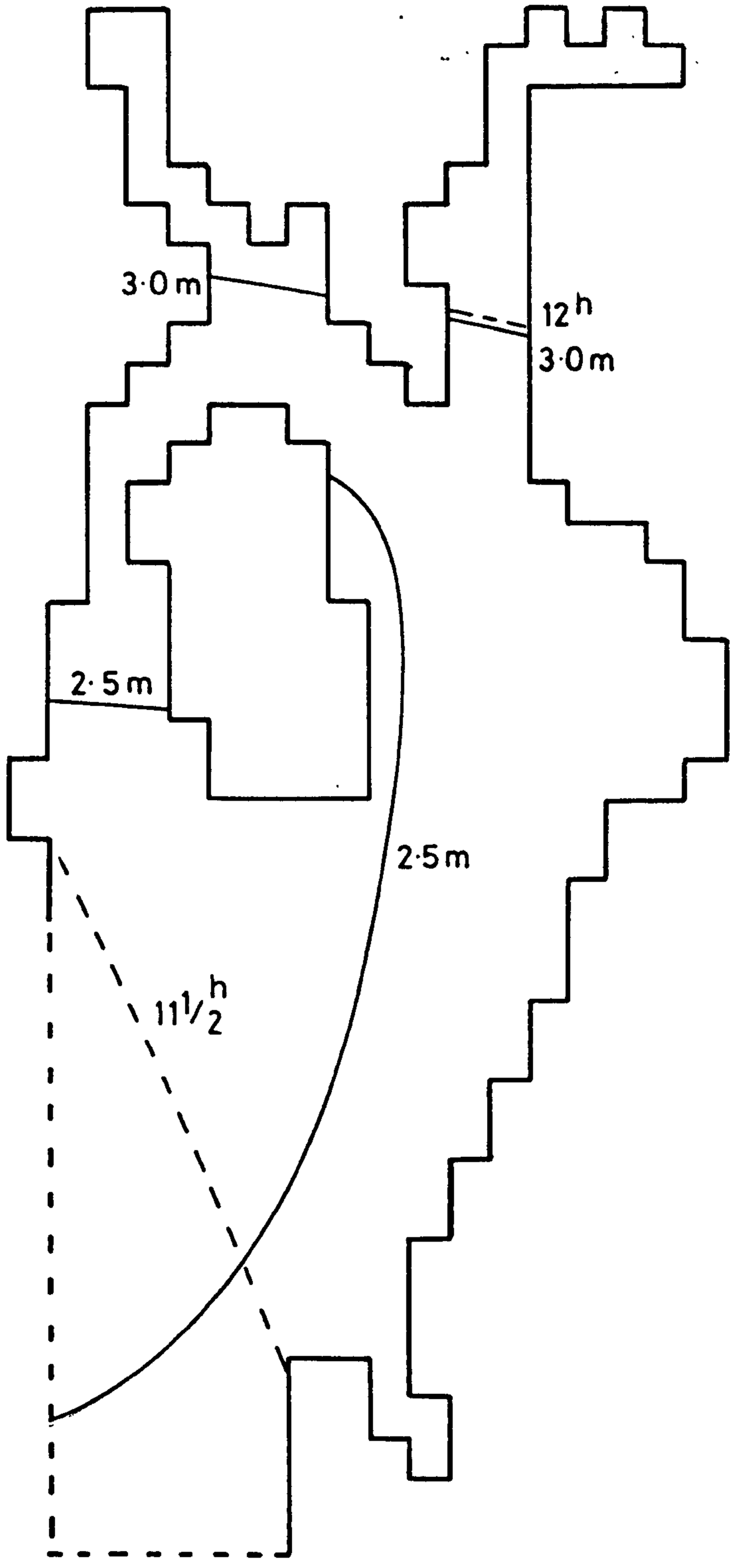

FIGURE 7·16
SPRING TIDE CO-RANGE AND CO-PHASE LINES IN THE FIRTH OF CLYDE TAKEN FROM ADMIRALTY CHART 5058.

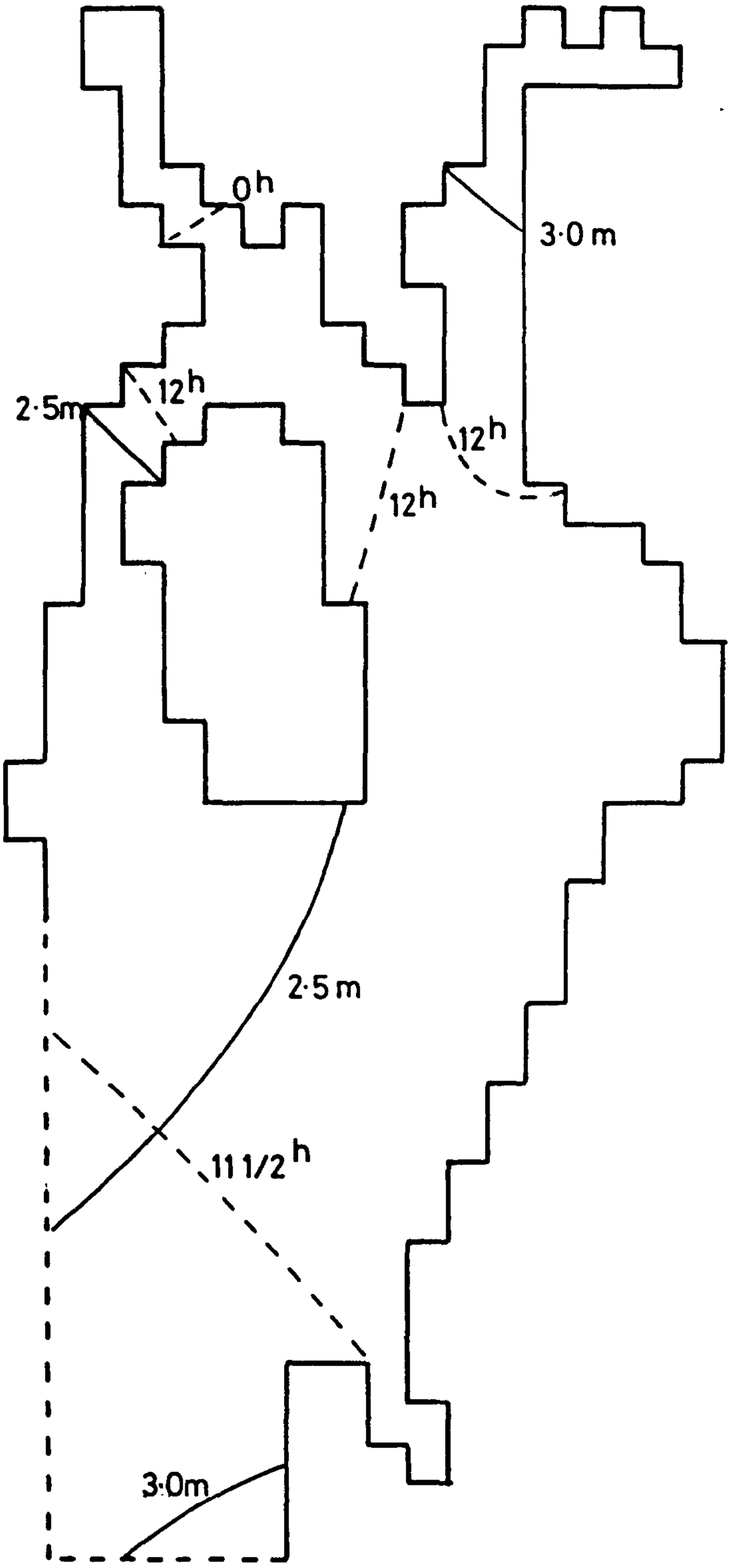

FIGURE 7·17
SPRING TIDE CO-RANGE AND CO-PHASE LINES IN THE FIRTH OF CLYDE TAKEN FROM DONALD (1981).

characteristics is not a dominant factor when modelling two-dimensional tidal wave propagation in an inland sea area.

However, there are considerable differences regarding the relative efficiency of each scheme. The time step used in characteristic model is restricted to forty-eight seconds by a stability criterion; Donald reported that twenty minutes of computer time per tidal cycle was required to run this model on the ICL 1904S machine at the University of Strathclyde. With the alternating direction implicit model the time step is limited by accuracy considerations to five hundred and ninety-six seconds. Using this time step the alternating direction implicit model required six minutes of computer time per tidal cycle on the ICL 1904S. Therefore, the alternating direction implicit model is of the order of three times faster than the characteristic model for this particular case.

Donald gives no figures as to the storage requirements of the characteristic model; the alternating direction implicit model required around 50k computer words of storage for the Firth of Clyde simulation.

CHAPTER EIGHT

NUMERICAL MODELLING OF THE HUMBER ESTUARY

8.1 Introduction

The Humber Estuary is one of the major inlets along the east coast of England, serving the ports of Hull, Immingham, Grimsby and Goole. Its use for shipping, waste disposal and fishing is of great importance to the economic welfare of the region. Annual trade through the estuary is very substantial. In 1973 the total was about 34 million tonnes, about half of which (18 million tonnes) was crude oil and oil refined products. To help visualise the scale of this trade, these annual tonnages are about two thirds of the corresponding amounts for the Thames Estuary.

In the early sixties increases in the size of ships and accelerating development along the banks of the Humber, particularly the building of oil refineries, led to proposals for a dredged channel through the middle shoal. This channel would permit the passage of fully laden oil tankers across the shoal to Immingham at neap tides.

In 1964 the Hydraulics Research Station began a detailed investigation of the tidal regime on behalf of the Humber Conservancy Board. The object was to discover whether the proposed dredged channel could be maintained economically with a reasonable amount of maintenance dredging and whether this channel would have detrimental effects on the approaches to Grimsby Docks. The choice

of deposit site was also investigated. Experimental dredging, followed by regular surveys, was used to determine the extent of siltation and to provide information as to the cost of maintaining a full-sized dredged channel. The last in a series of reports by the Hydraulics Research Station, on the subject, was published in 1968.

During the period 1964-68 a data collection programme for the verification of a physical model of the estuary, being built at the British Transport Docks Research Station, Hull, was initiated. The information collected during this survey was published by the Humber Estuary Research Committee in 1974. Among other things the model was used to estimate the recirculation performance of cooling water works and to predict surface flow patterns for the Killingholme Power Station, Hydraulics Research Station, 1970 and 1974. Recently, increased operating costs have led to replacement of the physical model by a numerical model developed by Hydraulics Research Limited.

In 1972 the Humber Advisory Group was formed. Its aim was to increase collaboration between various organisations concerned with the Estuary. Representatives include County and District Councils, River Authorities, the North Eastern Sea Fisheries Committee, industries including the CBI, the University of Hull, Chambers of Commerce, Shipping and Trade, Industrial Water Users Association, Yorkshire and Humberside Economic Planning Council and the Sports Council. Its terms of reference are:

a) The reduction of pollution of the Estuary and its contribution to pollution of the North Sea.

b) The programme to be prepared by the Humber Consultative Committee to monitor flows and quality conditions of the Estuary.

c) The protection of the Estuary for the passage of migratory fish and as a fishery in its own right.

d) The effect on the Estuary of future development on both banks of the Humber, including the effect of provision of the Humber Bridge.

e) The function of the Estuary in respect of land drainage.

f) The use of the estuary for amenity purposes.

In 1973 a symposium was held in an attempt to assess understanding of the physical, biological and sociological features of the Estuary and the way in which these inter-relate. The proceedings of this meeting were published by the Natural Environment Research Council in 1975.

8.2 SCOPE OF THE NUMERICAL STUDY

As may be determined from the prece ding section, considerable resources have been spent to fully assess the hydraulic behaviour and development potential of the

Humber Estuary. The following numerical study is not an attempt to provide any new information regarding these aspects of the Estuary. The intentions are: firstly, to provide a further test of the numerical model of Chapter Six by using it in a relatively shallow estuary with a greater tidal range than that provided by the Firth of Clyde; secondly, to test the flexible boundary condition on shoals such as Spurn Bight, Foul Holme Sand and Haile Sand Flats; and, thirdly, to test the "weir" flow boundary condition by modelling flow over Spurn Head sand spit.

8.3 PHYSICAL DESCRIPTION OF THE HUMBER ESTUARY

Figure 8.1 shows the channel configuration in the lower Humber and adjoining area of the North Sea. The deep water channel approaches the Humber through New Sand Hole where depths generally exceed 18m below low water of a spring tide and in places exceed 30m.

South of Spurn Head the approach channel divides into two channels and sometimes three separate channels, namely, Hawke Road to the north, Haile Channel to the south and Bull Channel in the centre. Depths in these channels vary between 9m and 17m at low water.

North of Grimsby these channels encounter "The Middle" where natural depths shallow to approximately 8m. In 1969 a channel was dredged through Sunk Road to give a depth of 9m at low water.

West of Grimsby a single channel system is re-established for approximately two miles, with depths greater than 12m and, in places, 20m at low water springs. The Immingham

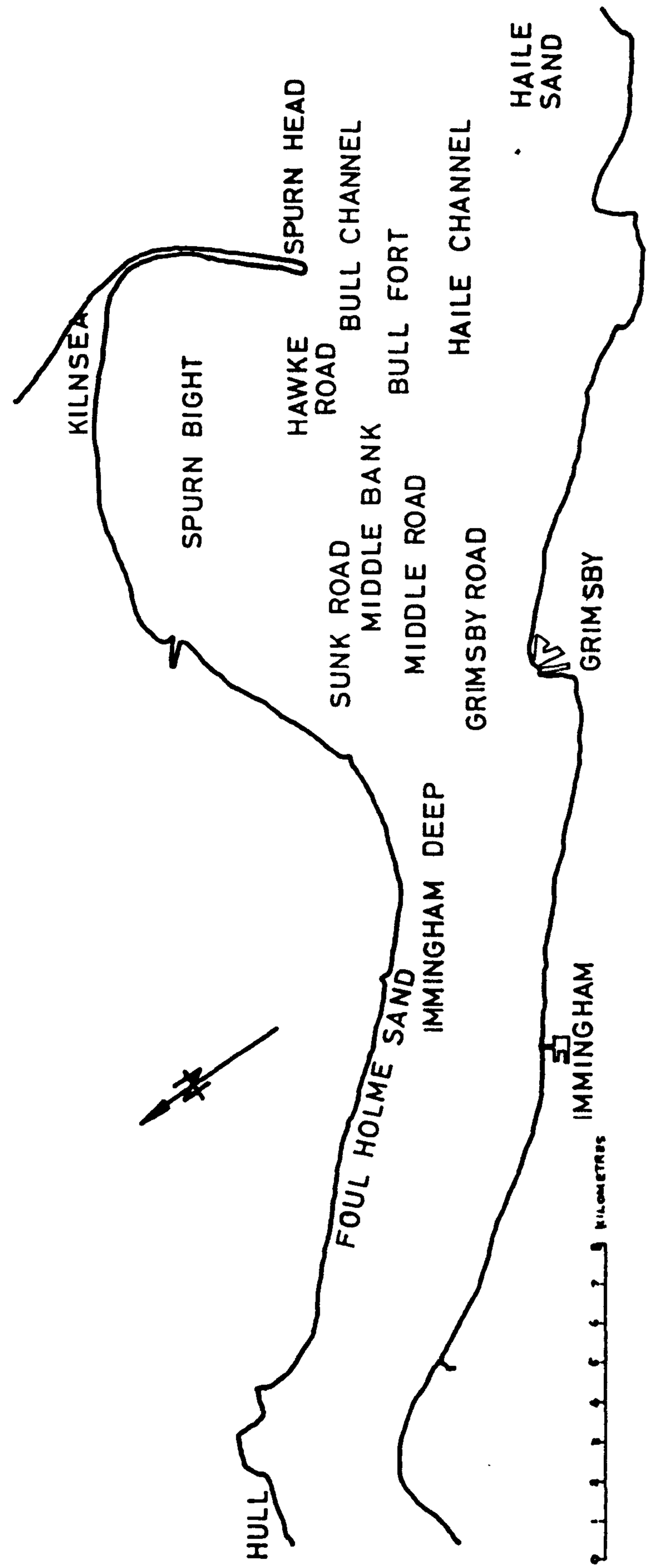

FIGURE 8·1
LOWER HUMBER ESTUARY

Oil Terminal has taken advantage of the natural deep just east of Immingham Dock Entrance. Opposite the dock, the channel is again split into two separate arms by Foul Holme Spit - a sand bank which dries at low water springs.

The channel to the north of the spit has formed since the early part of this century. Previously, Foul Holme Sand was broader and encompassed Foul Holme Spit; as the channel developed through the sand bank so depths were reduced in the main channel to the south of the spit.

Further west the navigation channel swings across the Estuary to the Hull water front where low water depths of 9m or more are found. South of Hull Road lies Hull middle, a broad sand bank which dried at low tide.

The above description of the lower Humber and adjoining North Sea area was given by N.E. Denman (1973).

8.4 NUMERICAL REPRESENTATION OF THE HUMBER ESTUARY

Three numerical representations of the Humber Estuary were used in the study. Successive models contain refinements of the numerical representation of the physical system.

Figure 8.2 shows the extent of the lower Humber estuary included in model one. The model is terminated above Hull with a closed boundary. This approximation was desirable to reduce computer storage requirements and enhance turn round time during the early stages of model development.

A numerical grid with a distance increment of 1000m is used. Bathymetry is represented by a series of average

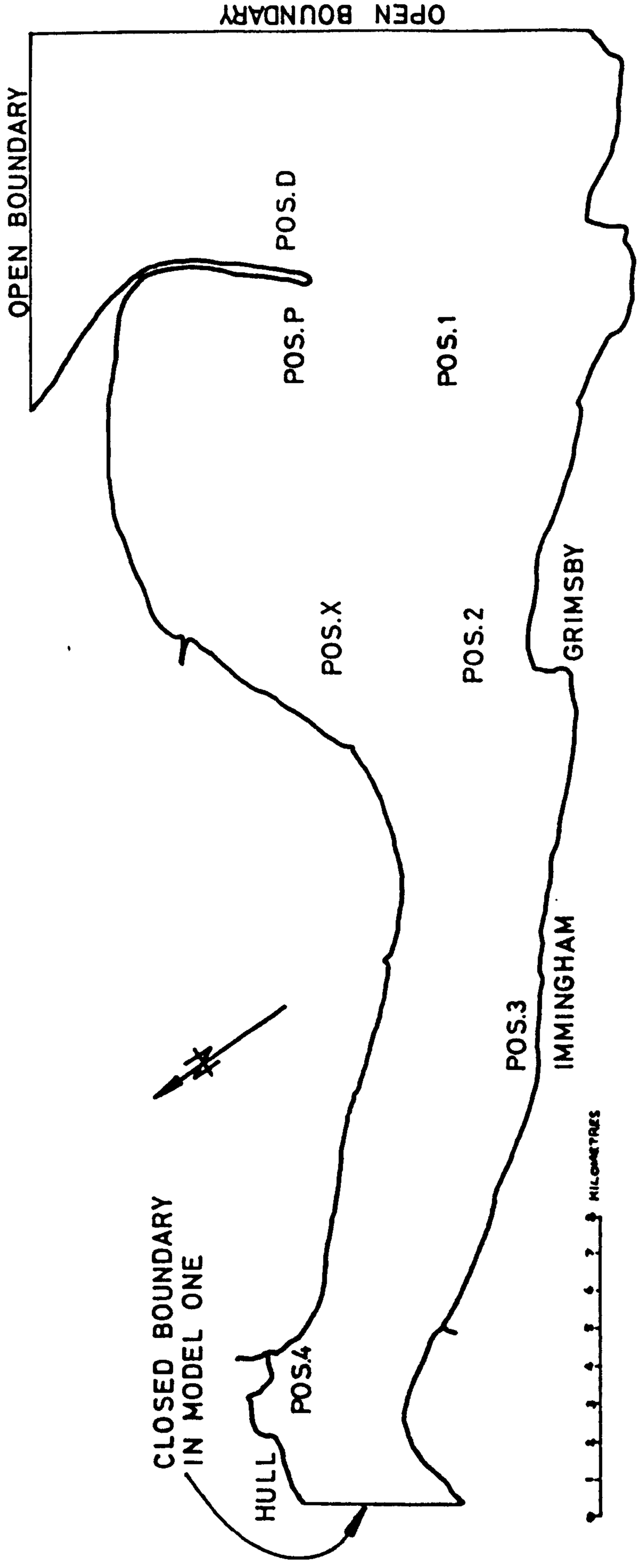

FIGURE 8·2
POSITION OF VELOCITY OBSERVATIONS

depths, taken from Admiralty Chart 109, at each solution node.

The numerical grid is rotated from the normal west-east and south-north arrangement to align the physical boundaries with the numerical ones. By doing this it was hoped to alleviate the time increment restrictions imposed by using irregular boundaries, section 7.7.

Expanding boundary conditions were used to model the flooding and drying of the three major sand flat regions. These were Spurn Bight, Haile Sand and Foul Holme Sand. Chart 109 gave insufficient information regarding sand flat levels to permit modelling of the slope. Hence each sand flat was modelled as a level area using an approximate average level taken from the chart. Smaller sand flat areas such as Foul Holme Spit and Hull Middle were considered too small to be included in the numerical discretization. They were represented as permanently wet areas having a depth of around 1m at low water springs.

Open boundary conditions for model one were taken from Admiralty Chart No 5058, a cosine variation was assumed between high and low water level. These conditions were applied along the two legs of the open boundary, see Figure 8.2.

8.5 PARAMETER CHOICE

It was stated in the previous section that in order to prevent numerical damping from irregular boundaries the numerical grid for the Humber Estuary was aligned

along the natural estuary boundaries. Before calibrating the model it was thought necessary to test if this had been successful and to chose a suitable time increment for further calculations. Figures 8.3a to 8.3d show water level verses time curves computed using time increments varying from 300 seconds to 1200 seconds. These curves were computed without sand flat areas. It can be seen that variations in time increments have little effect on the amplitude of the computed wave. Therefore, aligning the numerical grid in this way allows greater freedom in the choice of time increment.

For subsequent calculations flooding and drying of sand flat areas will be incorporated in the numerical estuary representation. In order that the numerical model should provide details of this behaviour a time increment of 600 seconds was thought to be suitable.

A theta value of 1.0 was used in all model applications. A reasonable choice, as this value did not produce significant numerical damping in the Firth of Clyde model using a distance increment of 3000 m, and therefore is unlikely to cause problems in the Humber Estuary where a distance increment of 1000m is used.

Initial calibration was made by varying the value of the Chezy coefficient. A comparison of ranges taken from simulations using different friction coefficients is given in Table 8.1. Referring to these a Chezy coefficient of $100 m^{\frac{1}{2}}/s$ is considered to provide a good first estimate of friction losses in the Humber Estuary.

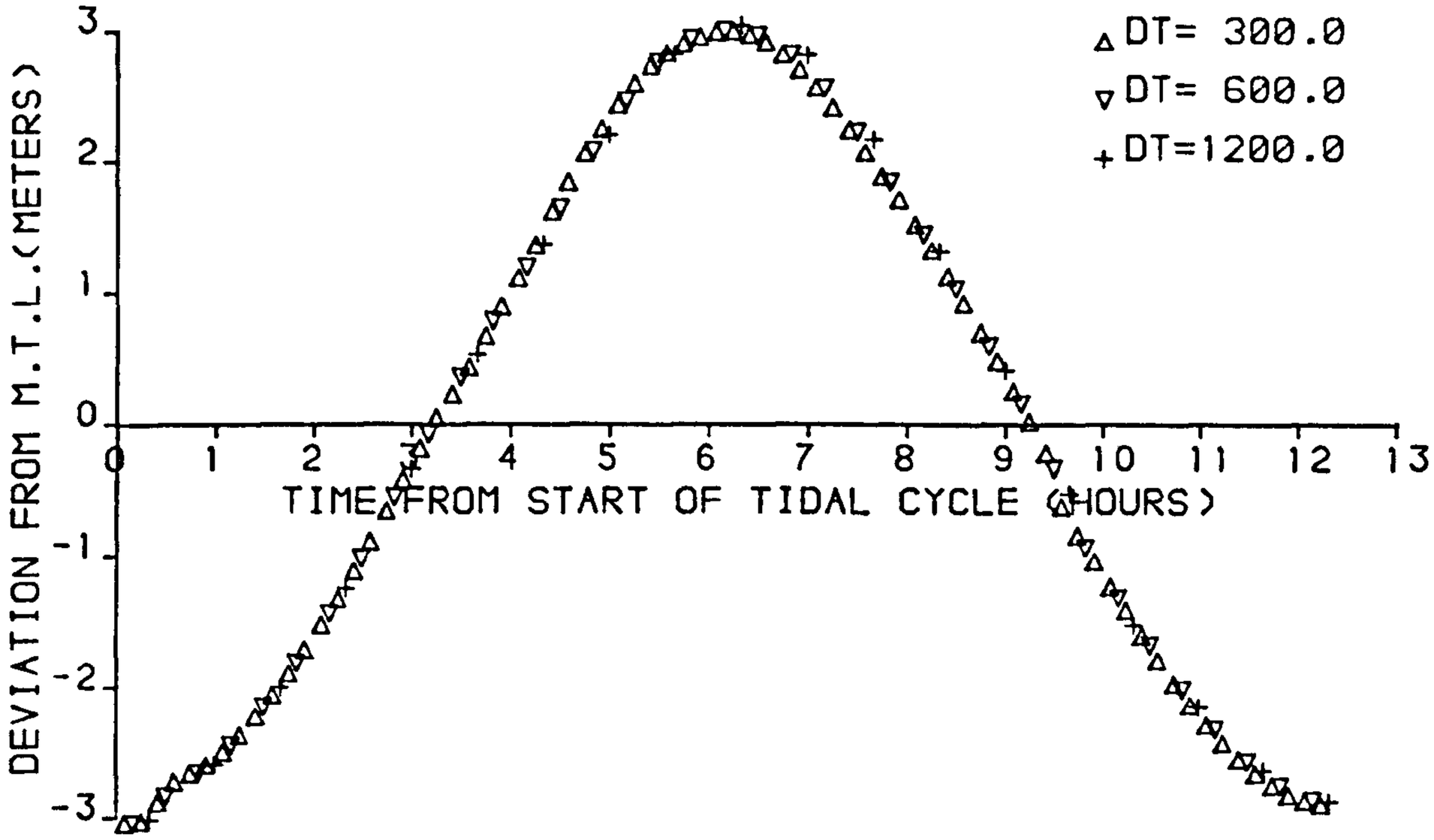

FIGURE 8·3a

COMPARISON OF WATER LEVELS AT BULL SAND

USING DIFFERENT COURANT NUMBERS

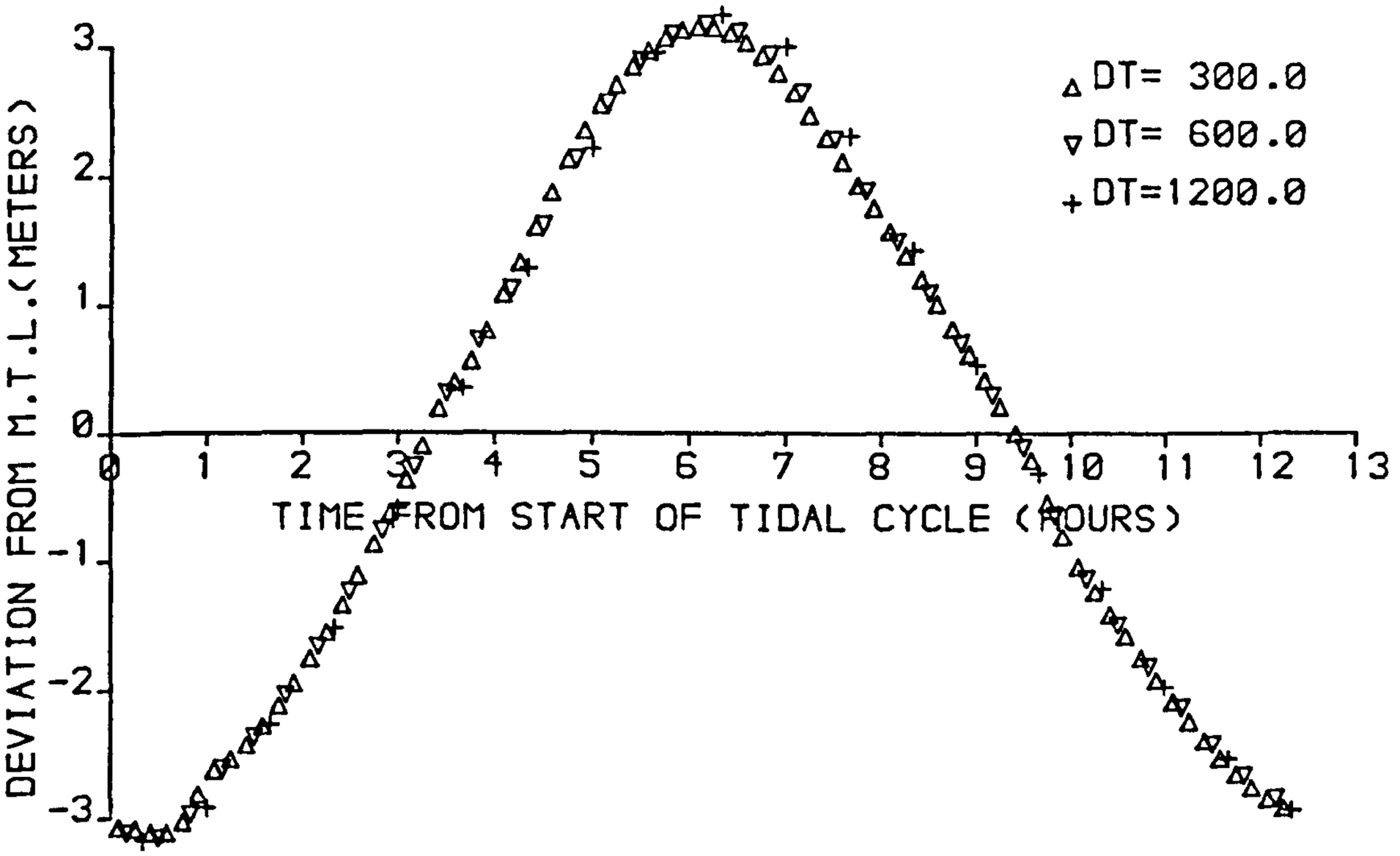

FIGURE 8·3 b

COMPARISON OF WATER LEVELS AT GRIMSBY

USING DIFFERENT COURANT NUMBERS

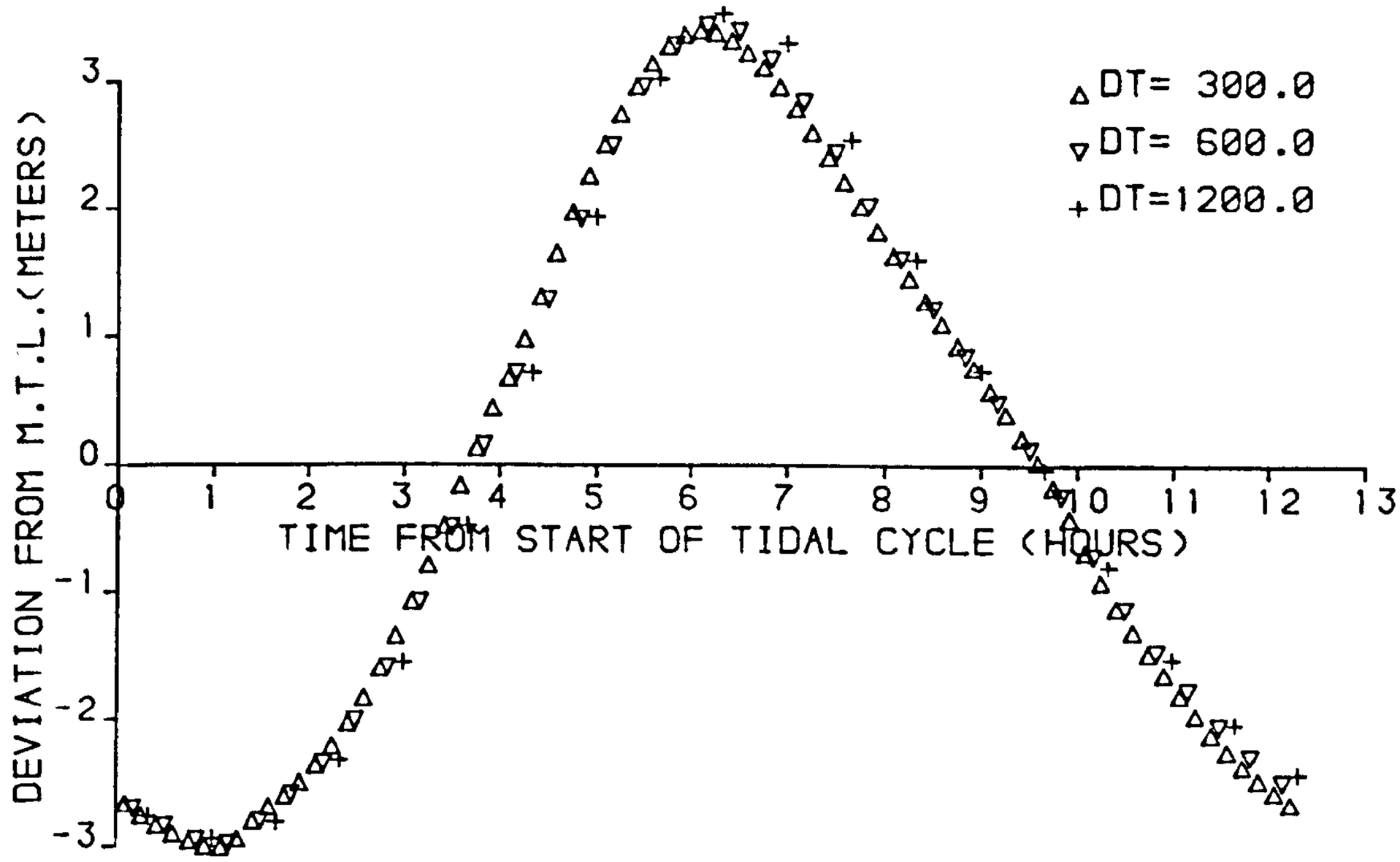

FIGURE 83c

COMPARISON OF WATER LEVELS AT IMMINGHAM

USING DIFFERENT COURANT NUMBERS

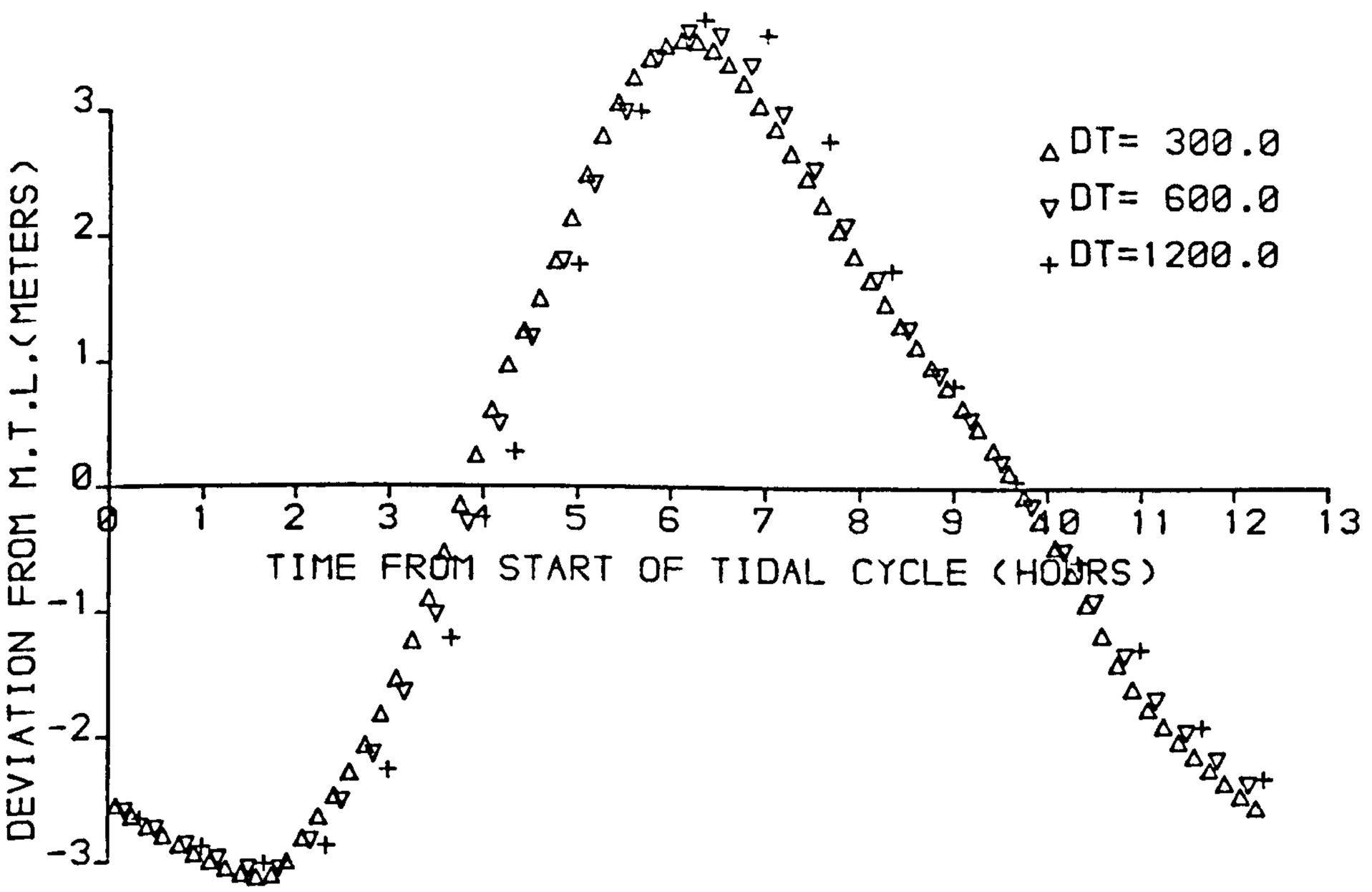

FIGURE 83d

COMPARISON OF WATER LEVELS AT HULL

USING DIFFERENT COURANT NUMBERS

LOCATION	PREDICTED 1983	COMPUTED RANGES FOR VARYING CHEZY COEFFICIENTS				
		80	90	100	110	120
BULL SAND	5.8	5.84	5.86	5.87	5.91	5.93
GRIMSBY	6.3	6.13	6.14	6.13	6.19	6.20
IMMINGHAM	6.4	6.25	6.29	6.34	6.39	6.40
HULL	6.6	6.52	6.57	6.65	6.70	6.73

Table 8.1a

RANGE COMPARISONS

LOCATION	PREDICTED 1983	COMPUTED HIGH WATER TIMINGS VARYING CHEZY COEFFICIENTS 80	90	100	110	120
BULL SAND	-20	-10	0	0	0	0
GRIMSBY	-3	-10	0	0	0	0
IMMINGHAM	0	0	0	0	0	0
HULL	+5	0	0	+10	0	0

Table 8.1b

COMPARISON OF HIGH WATER TIMES

8.6 MODEL ONE RESULTS

Figures 8.4b to 8.4e show comparisons of predicted and computed water levels at locations in the Estuary. The position of these locations is shown in Figure 8.4a. A cosine variation of water level has been used to represent the predicted tidal curves. It can be seen that a good comparison of tide curves at Bull Sand and Grimsby has been achieved. At Immingham and Hull, however, discrepancies between the computed and predicted curves are evident. The major difference between the curves is that the predicted curves are assumed symmetrical while the computed curve is influenced by shallow water effects. That is, the speed of the tidal wave is significantly faster at high water than at low water. More information on the shape of tidal curves at Immingham and Hull was required before further conclusions regarding these comparisons could be drawn.

Velocity vectors at hourly intervals during a tidal cycle are presented in Figures 8.5a to 8.5m. Velocities over the sand flat areas can be seen in Figures 8.5e to 8.5j. These confirm that the method of including flooding and drying of sand flats described in Section 6.8.3 provides stable results over one tidal cycle. The magnitude of the velocities over the shallow area will, however, be affected by the assumption of a minimum depth, computed velocities being less than those in the prototype on these areas.

The global variation of water level in the Estuary is shown in Figures 8.6a to 8.6m. As with the similar

BS. BULL SAND
GR. GRIMSBY
IM. IMMINGHAM
HU. HULL
——— HIGH WATER BOUNDARY
_ _ LOW WATER BOUNDARY
_ . _ OPEN BOUNDARY

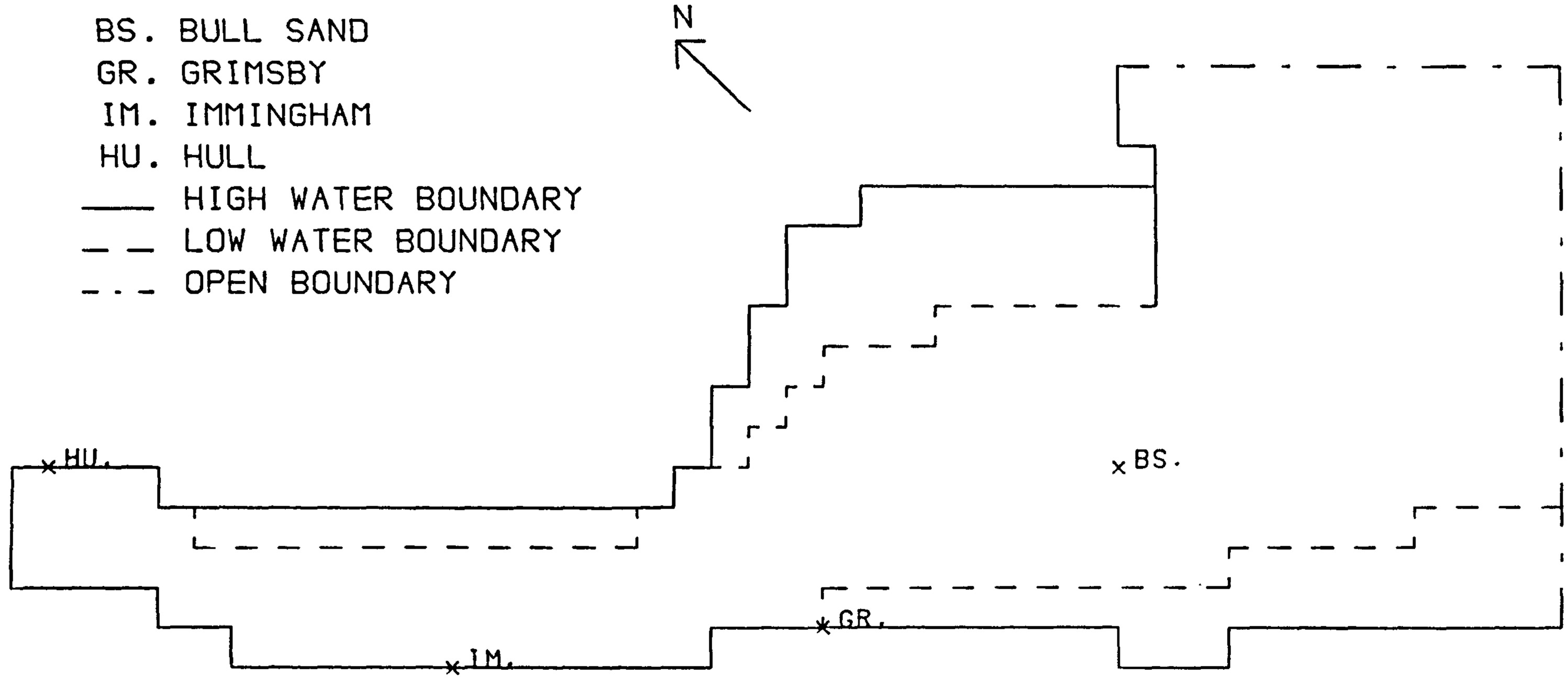

FIGURE 8·4a
POSITION OF WATER LEVEL HISTORYS IN THE HUMBER ESTUARY.

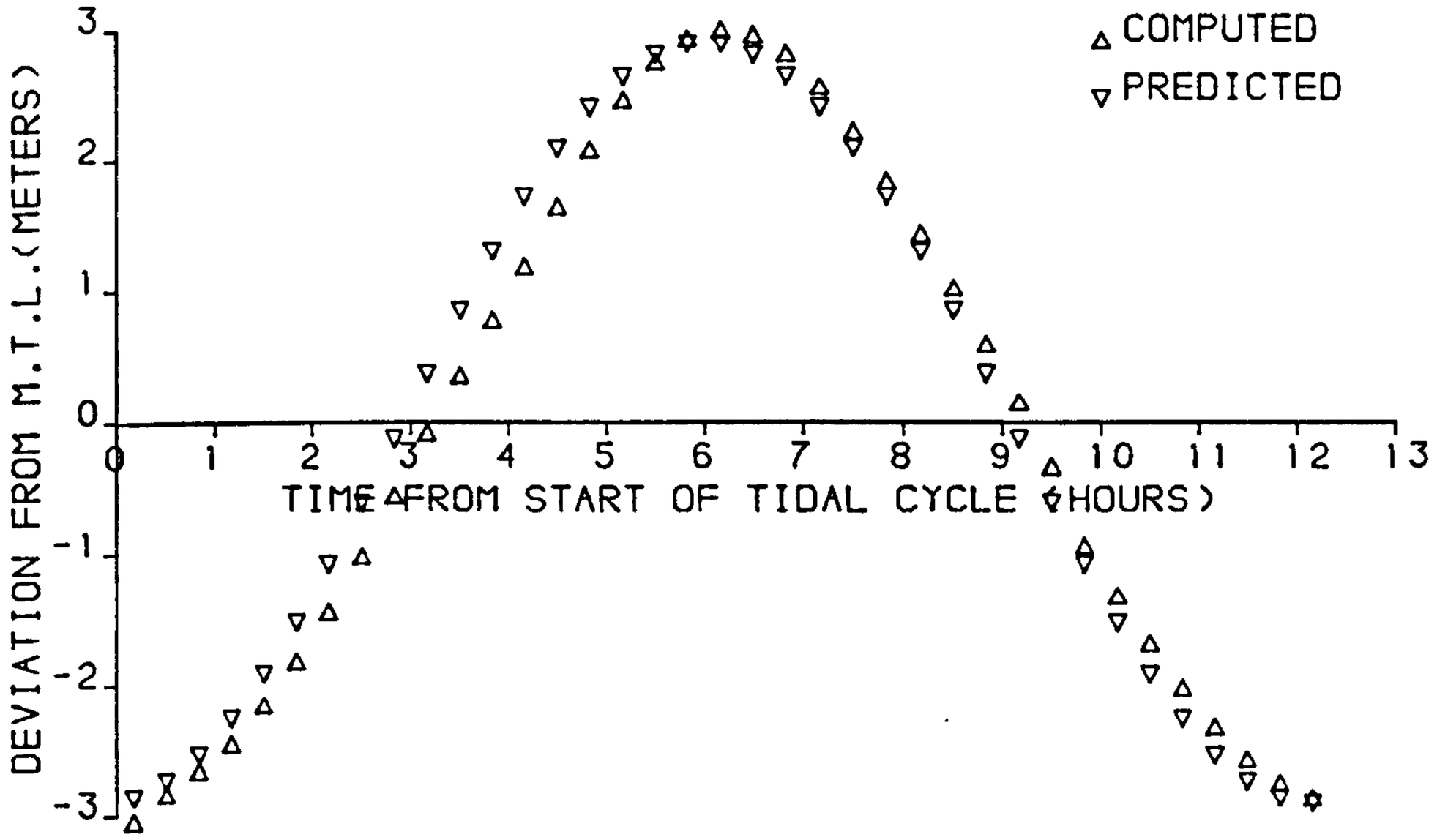

FIGURE 8·4 b

SPRING TIDE WATER LEVELS AT BULL SAND

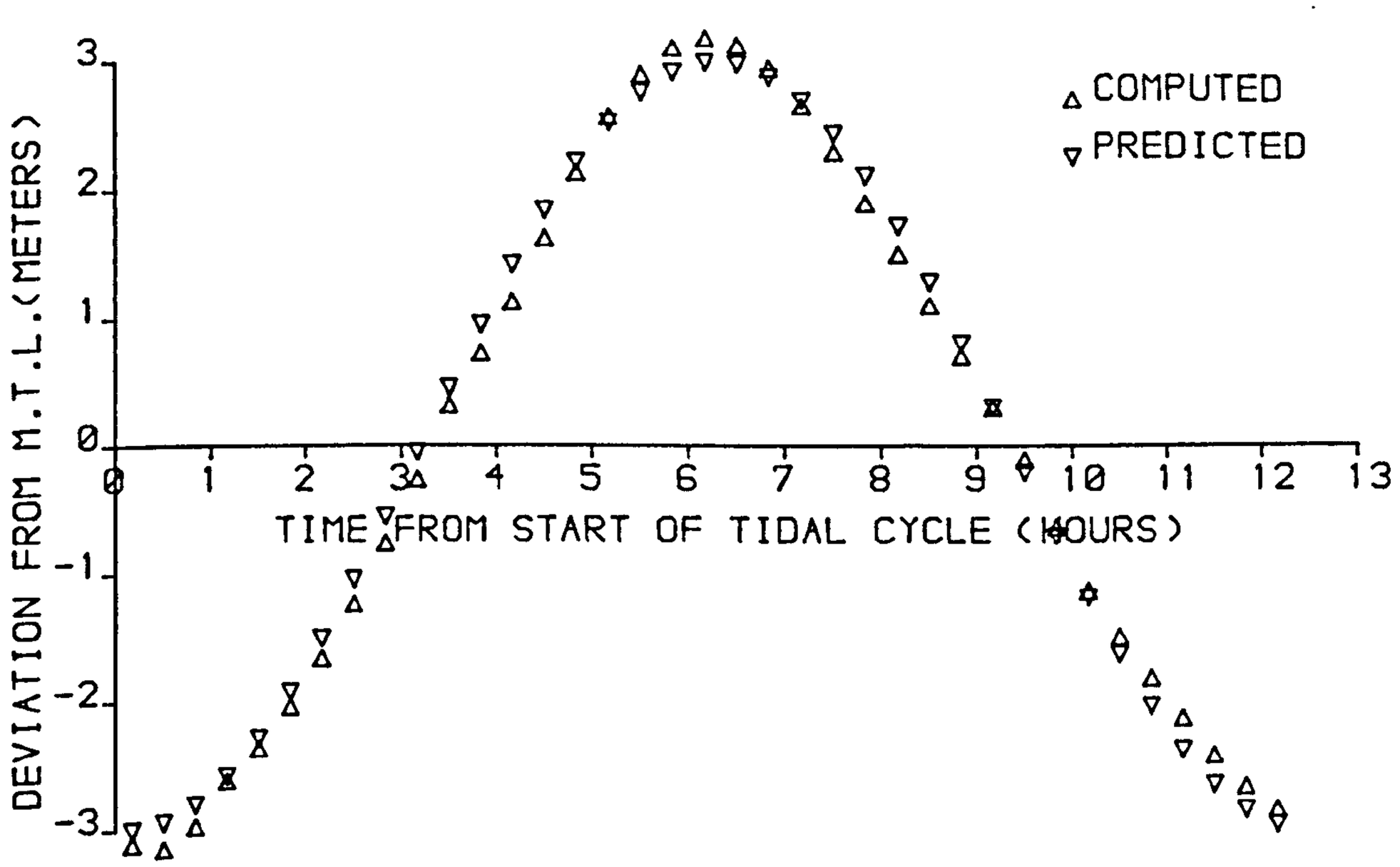

FIGURE 8·4 c

SPRING TIDE WATER LEVELS AT GRIMSBY

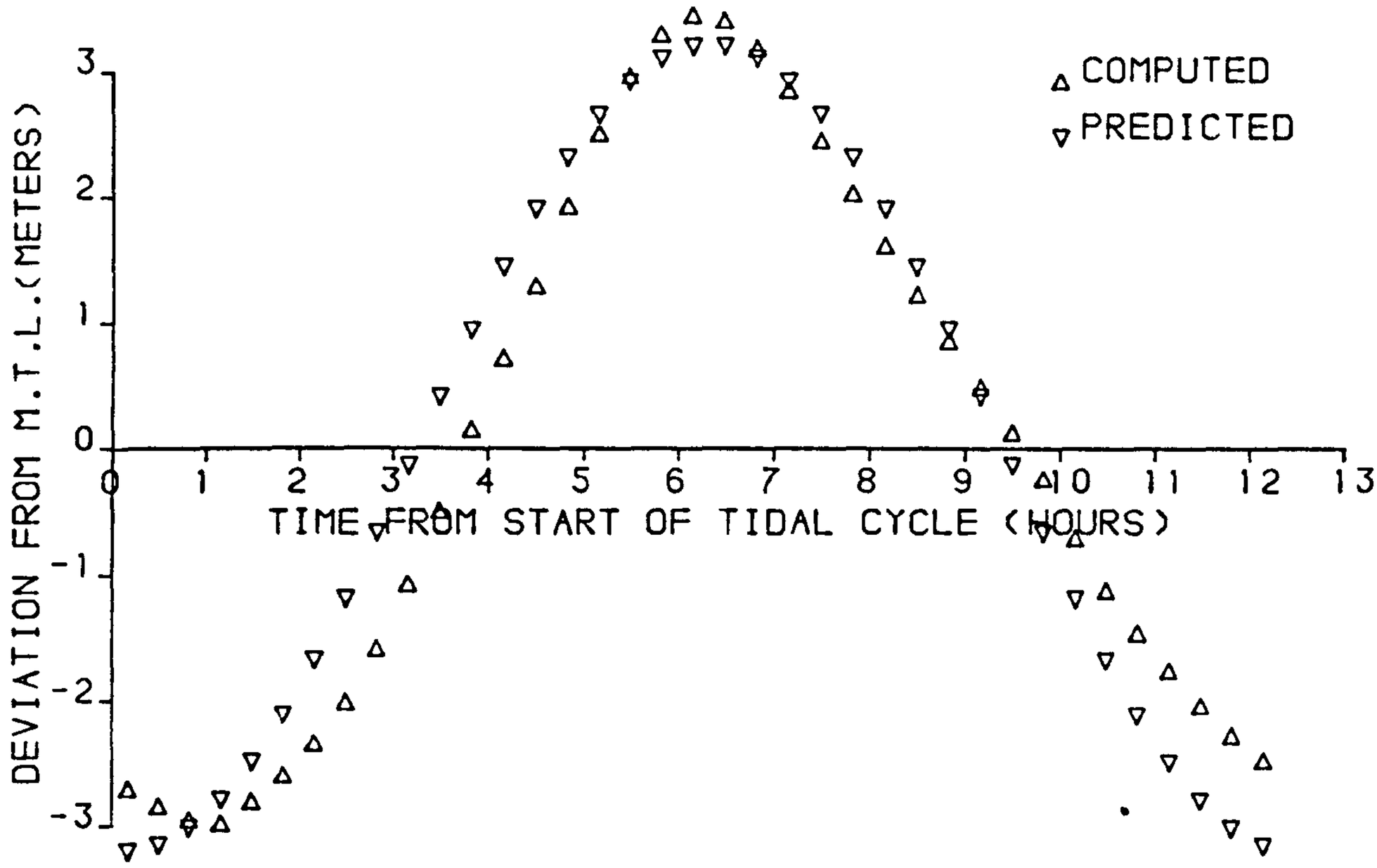

FIGURE 8·4d

SPRING TIDE WATER LEVELS AT IMMINGHAM

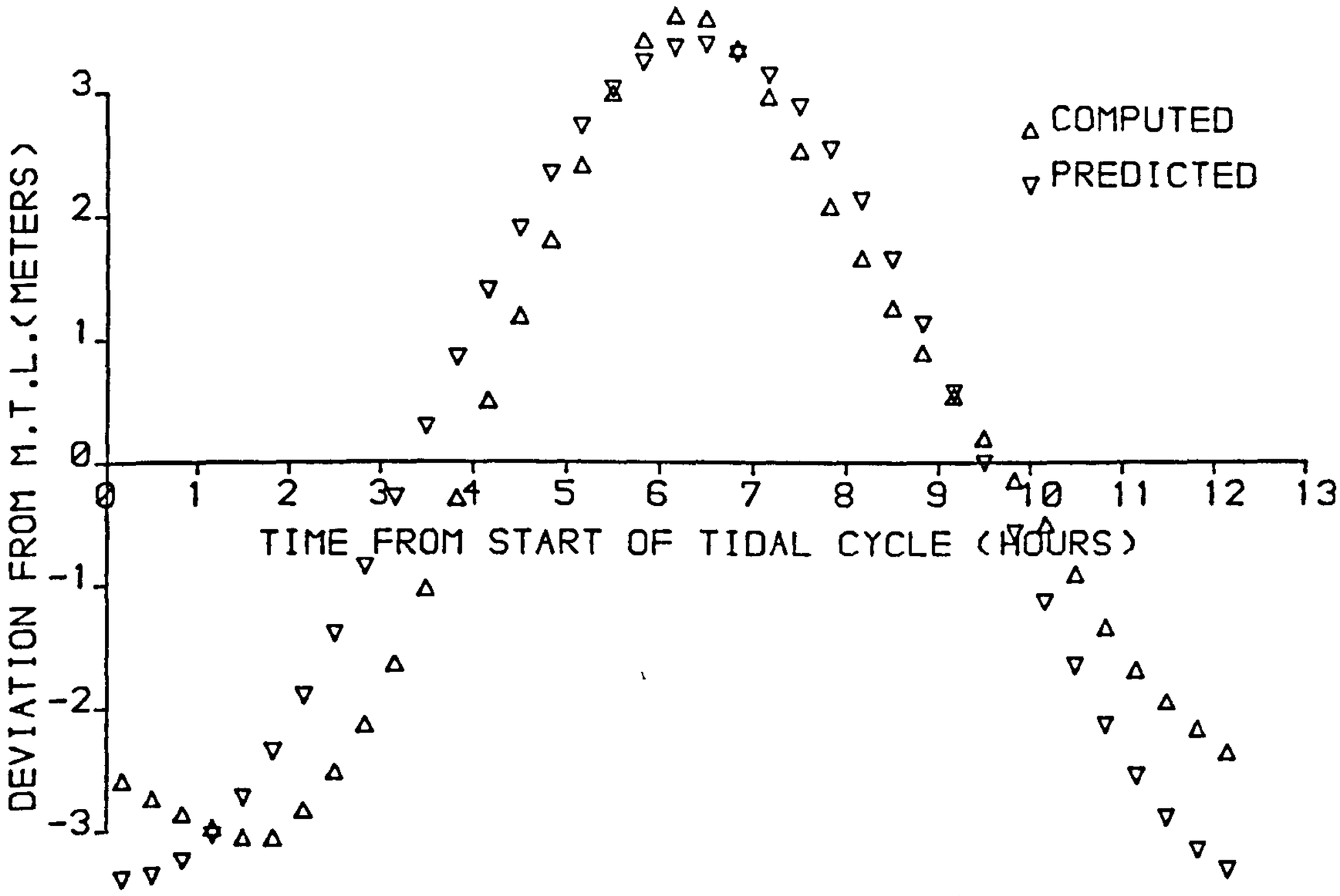

FIGURE 8·4e

SPRING TIDE WATER LEVELS AT HULL

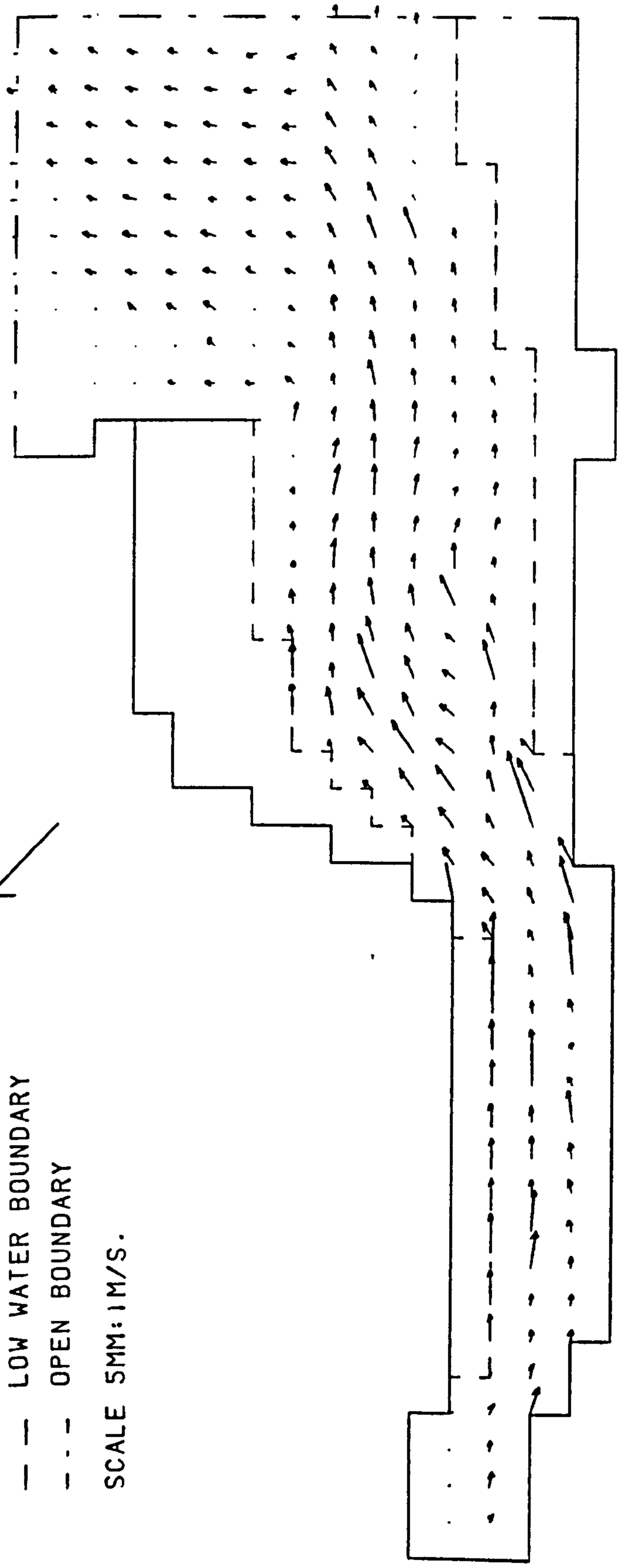

FIGURE 8.5a TIDE VELOCITIES IN THE HUMBER ESTUARY.
SPRING TIDE
TIME FROM START OF TIDAL CYCLE HOURS= .00

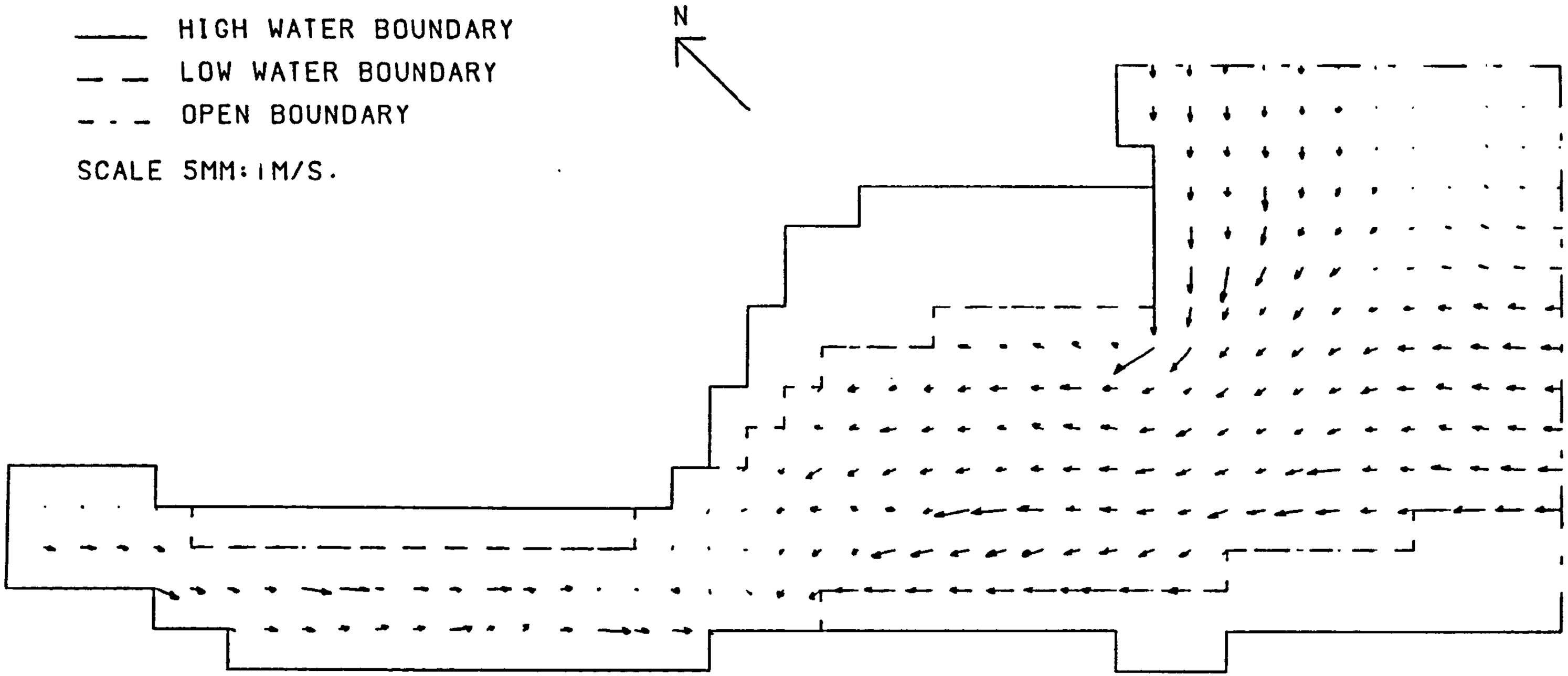

FIGURE 8·5b
SPRING TIDE VELOCITIES IN THE HUMBER ESTUARY.
TIME FROM START OF TIDAL CYCLE HOURS= 1.00

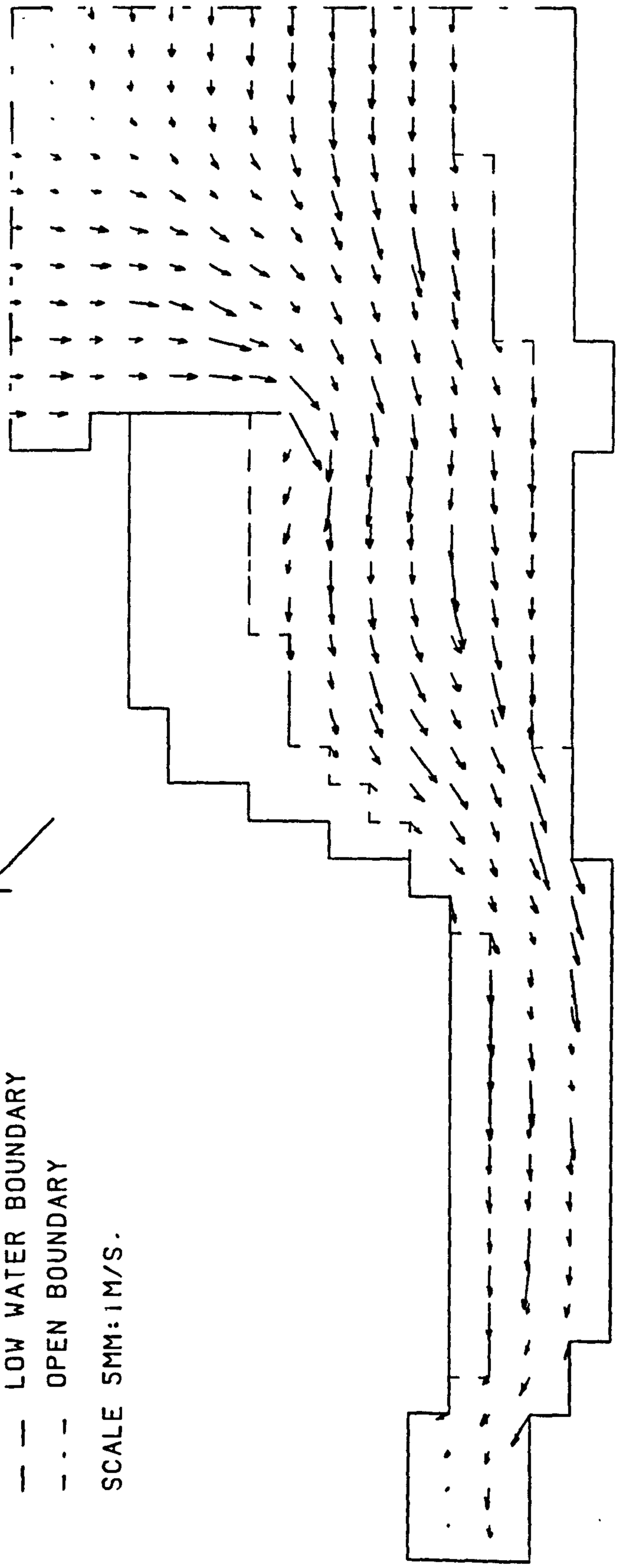

N

HIGH WATER BOUNDARY

LOW WATER BOUNDARY

OPEN BOUNDARY

SCALE 5MM:1M/S.

FIGURE 8.5c
SPRING TIDE VELOCITIES IN THE HUMBER ESTUARY.
TIME FROM START OF TIDAL CYCLE HOURS= 2.00

HIGH WATER BOUNDARY

LOW WATER BOUNDARY

OPEN BOUNDARY

SCALE 5MM: 1M/S.

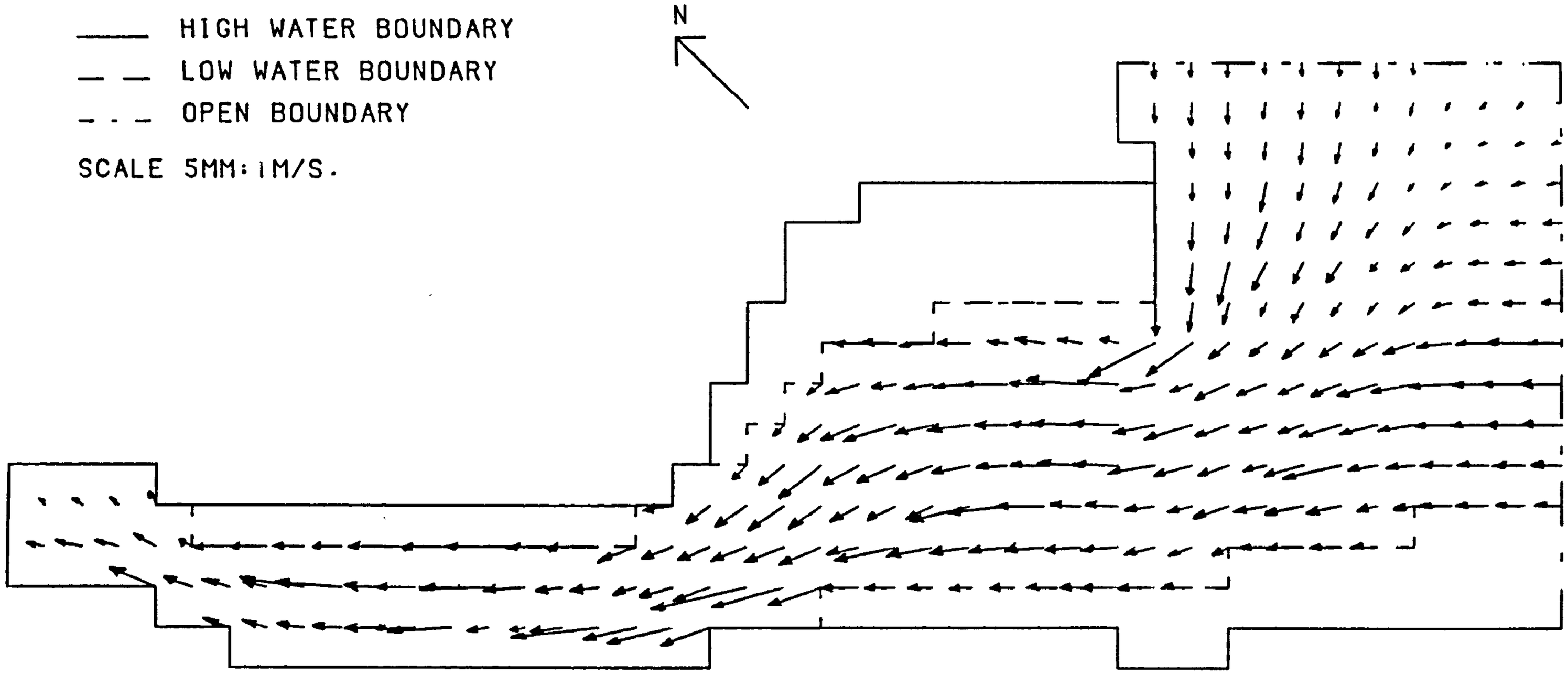

FIGURE 8·5d
SPRING TIDE VELOCITIES IN THE HUMBER ESTUARY.
TIME FROM START OF TIDAL CYCLE HOURS= 3.00

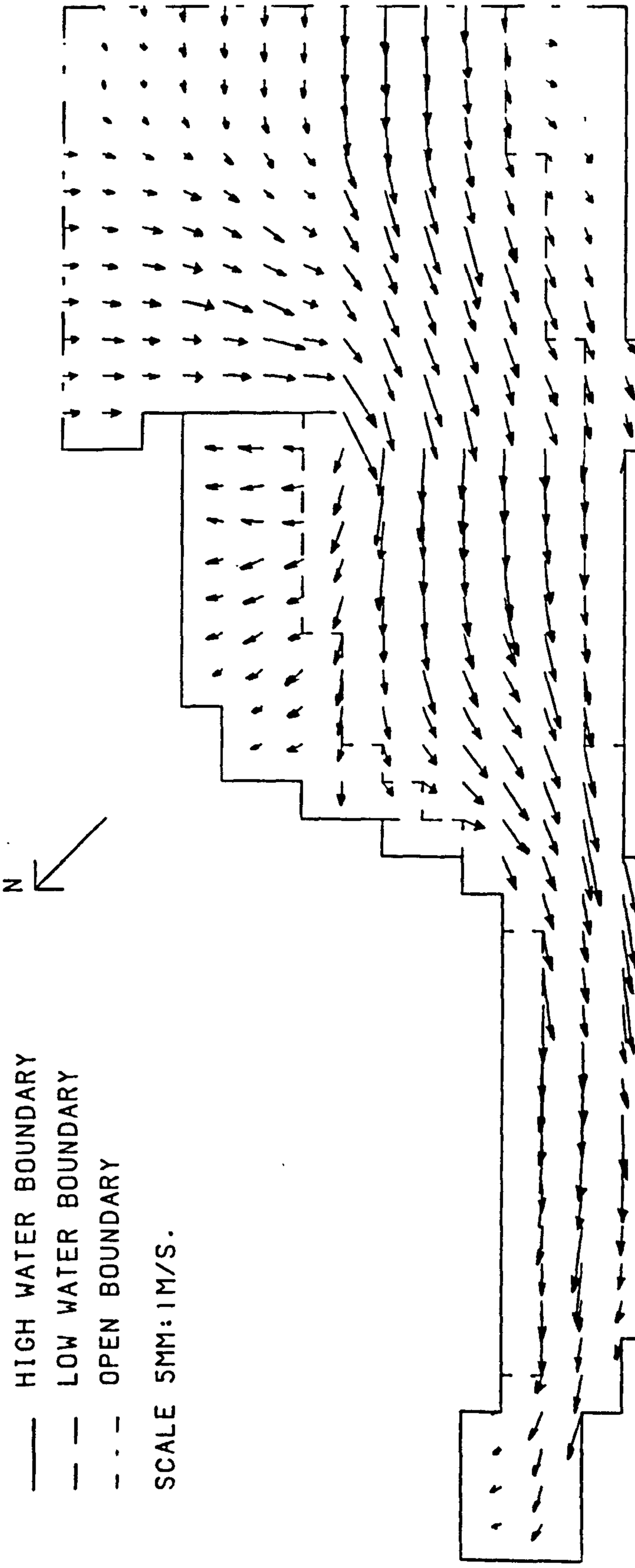

FIGURE 8.5e SPRING TIDE VELOCITIES IN THE HUMBER ESTUARY.
TIME FROM START OF TIDAL CYCLE HOURS= 4.00

HIGH WATER BOUNDARY

LOW WATER BOUNDARY

OPEN BOUNDARY

SCALE 5MM: 1M/S.

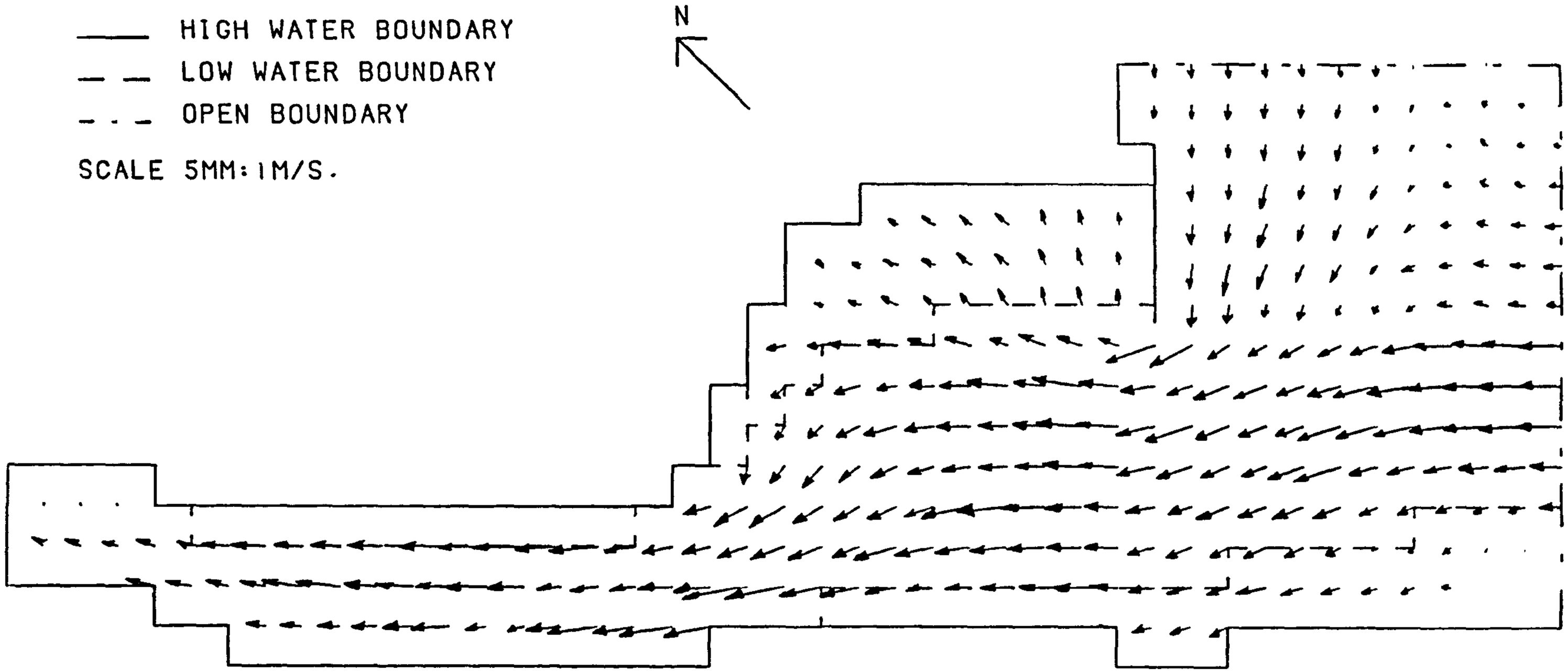

FIGURE 85f
SPRING TIDE VELOCITIES IN THE HUMBER ESTUARY.
TIME FROM START OF TIDAL CYCLE HOURS= 5.00

HIGH WATER BOUNDARY

LOW WATER BOUNDARY

OPEN BOUNDARY

SCALE 5MM:1M/S.

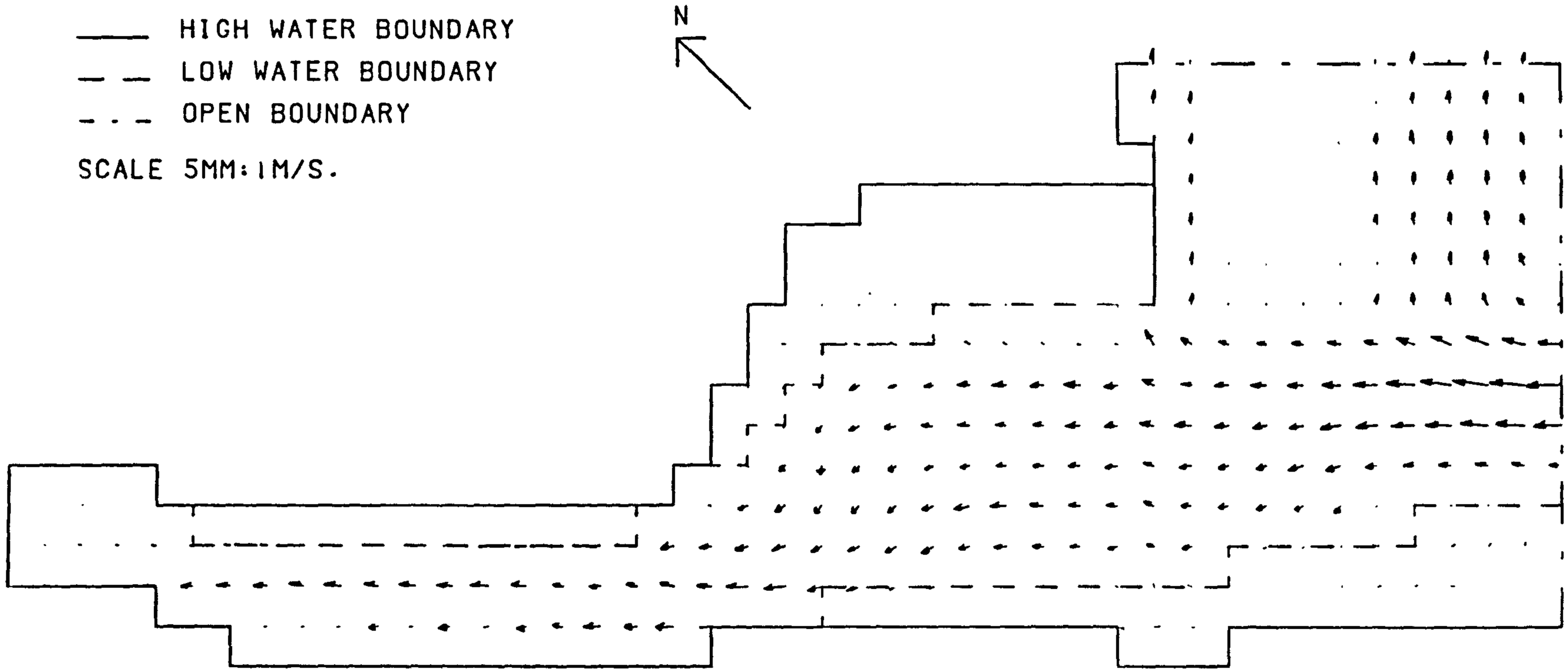

FIGURE 85g
SPRING TIDE VELOCITIES IN THE HUMBER ESTUARY.
TIME FROM START OF TIDAL CYCLE HOURS= 6.00

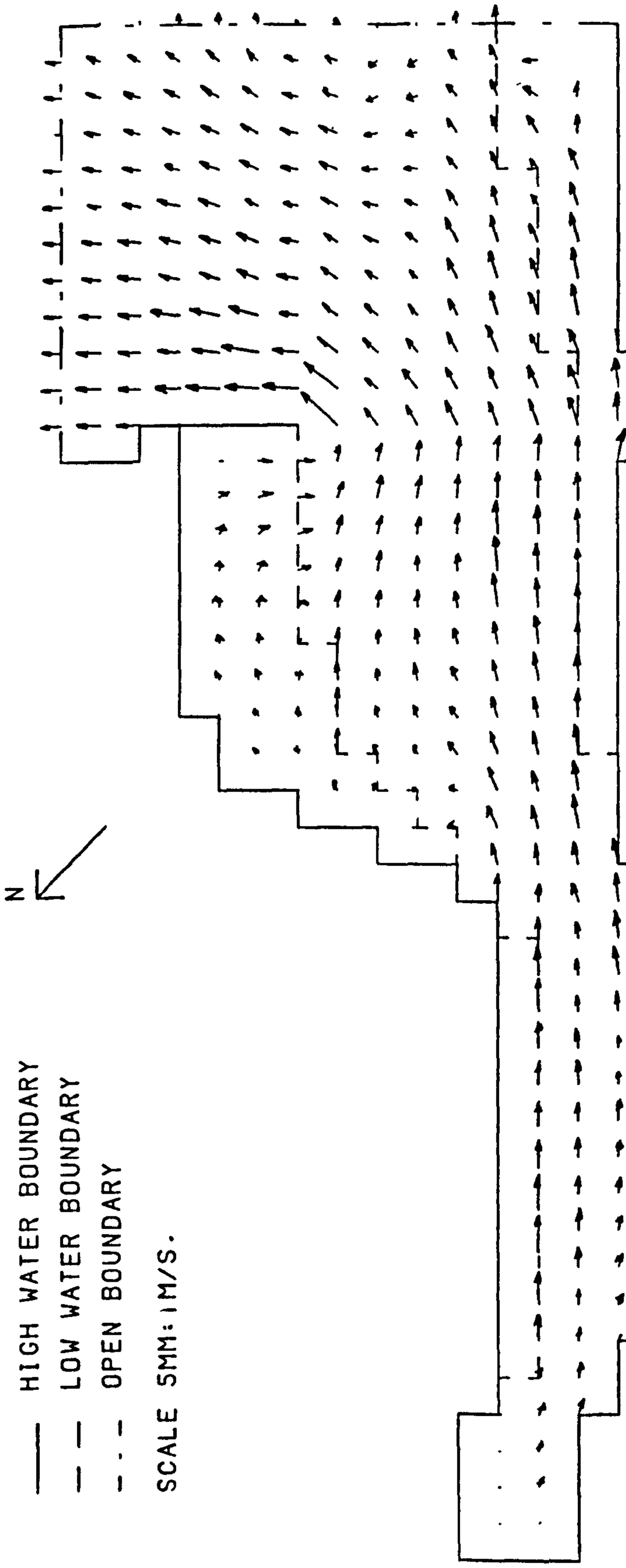

FIGURE 8.5h PREDICTED VELOCITIES IN THE HUMBER ESTUARY.
SPRING TIDE. TIME FROM START OF TIDAL CYCLE HOURS= 7.00

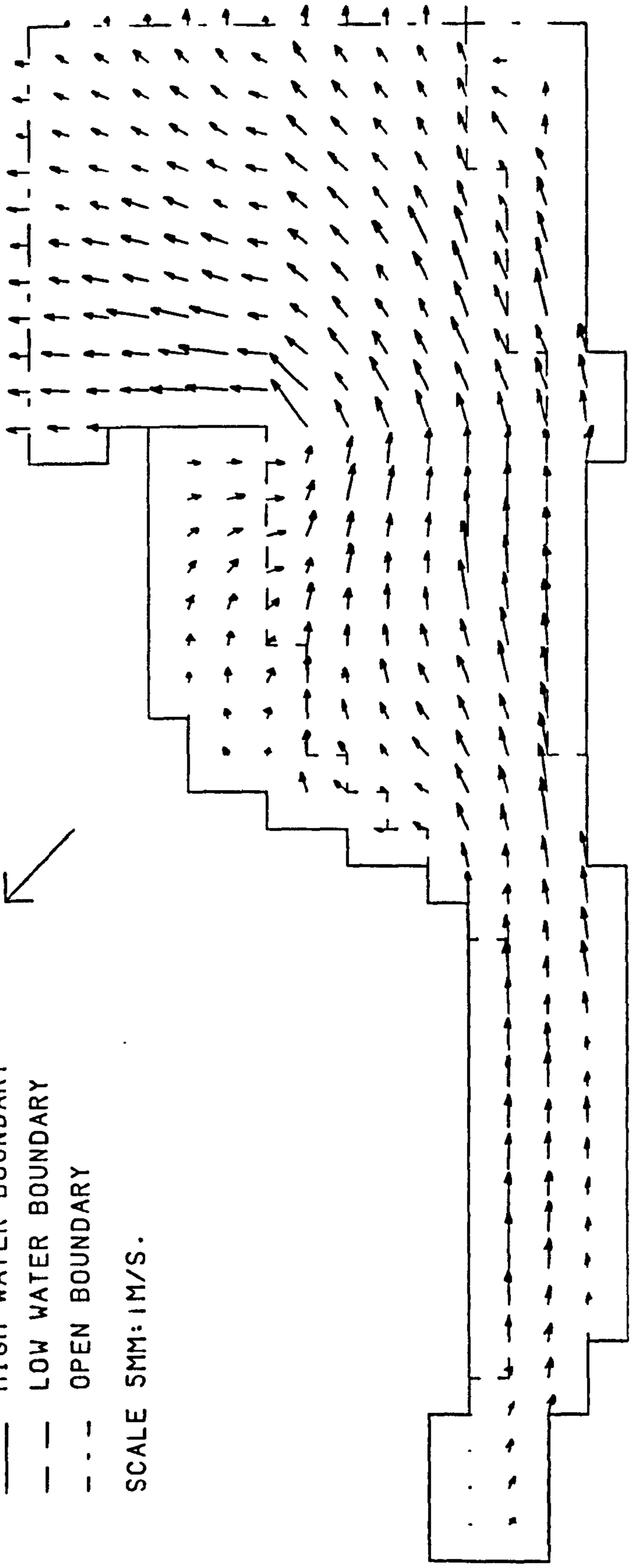

FIGURE 8.5i
SPRING TIDE VELOCITIES IN THE HUMBER ESTUARY.
TIME FROM START OF TIDAL CYCLE HOURS= 8.00

HIGH WATER BOUNDARY

LOW WATER BOUNDARY

OPEN BOUNDARY

SCALE 5MM:1M/S.

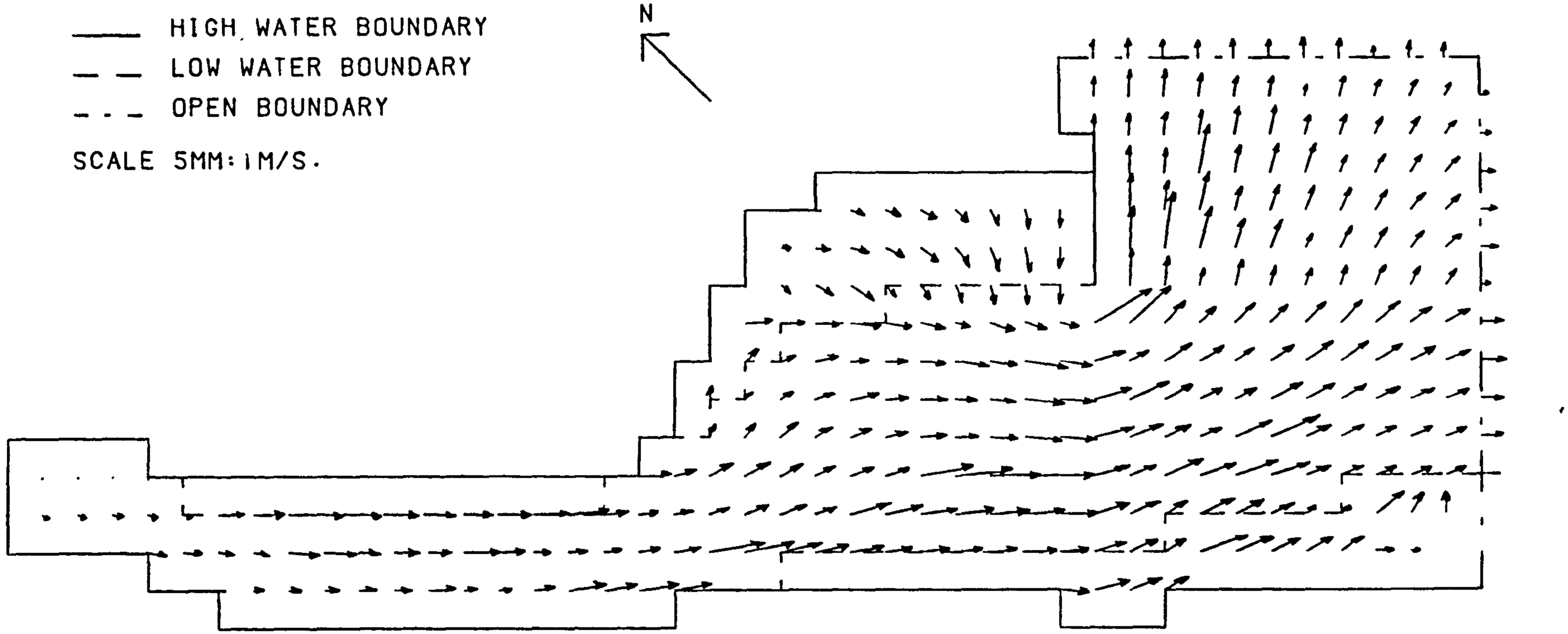

FIGURE 8·5j
SPRING TIDE VELOCITIES IN THE HUMBER ESTUARY.
TIME FROM START OF TIDAL CYCLE HOURS= 9.00

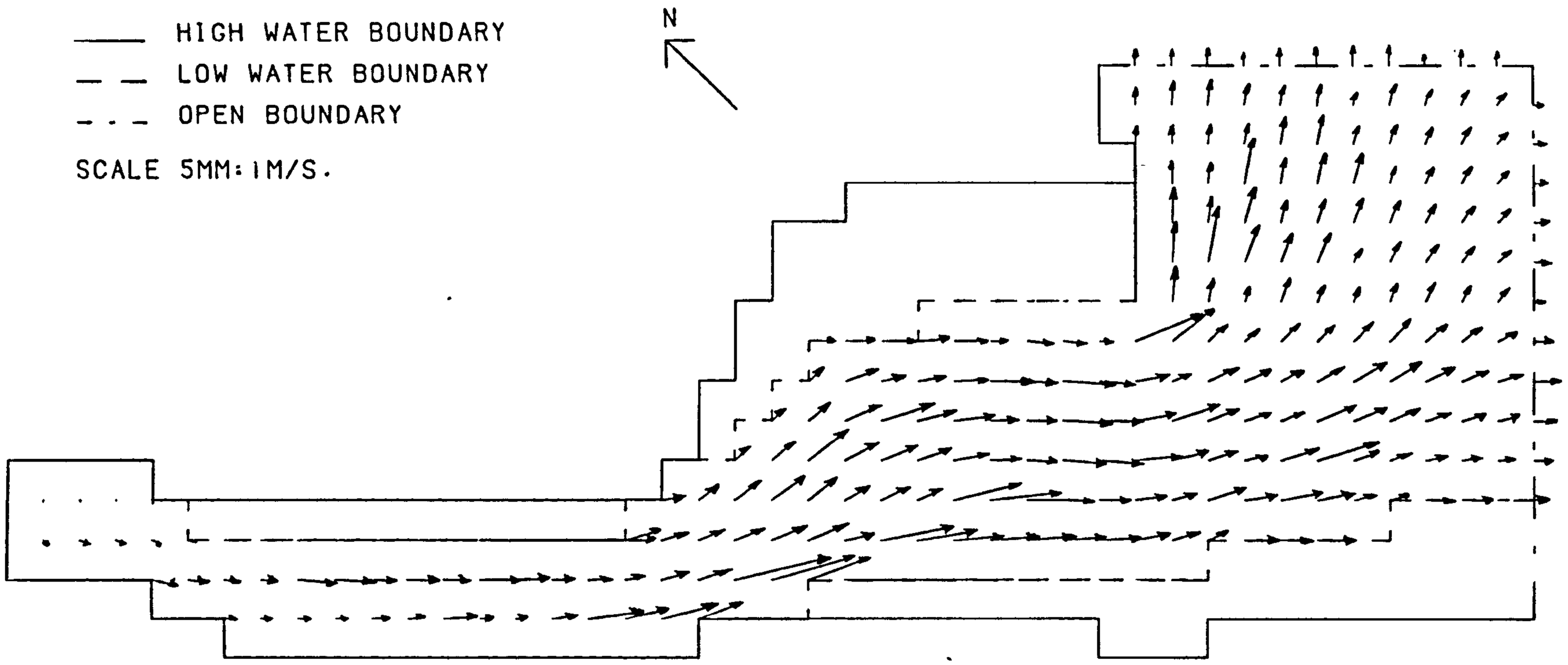

FIGURE 8·5k
SPRING TIDE VELOCITIES IN THE HUMBER ESTUARY.
TIME FROM START OF TIDAL CYCLE HOURS= 10.00

HIGH WATER BOUNDARY

LOW WATER BOUNDARY

OPEN BOUNDARY

SCALE 5MM:1M/S.

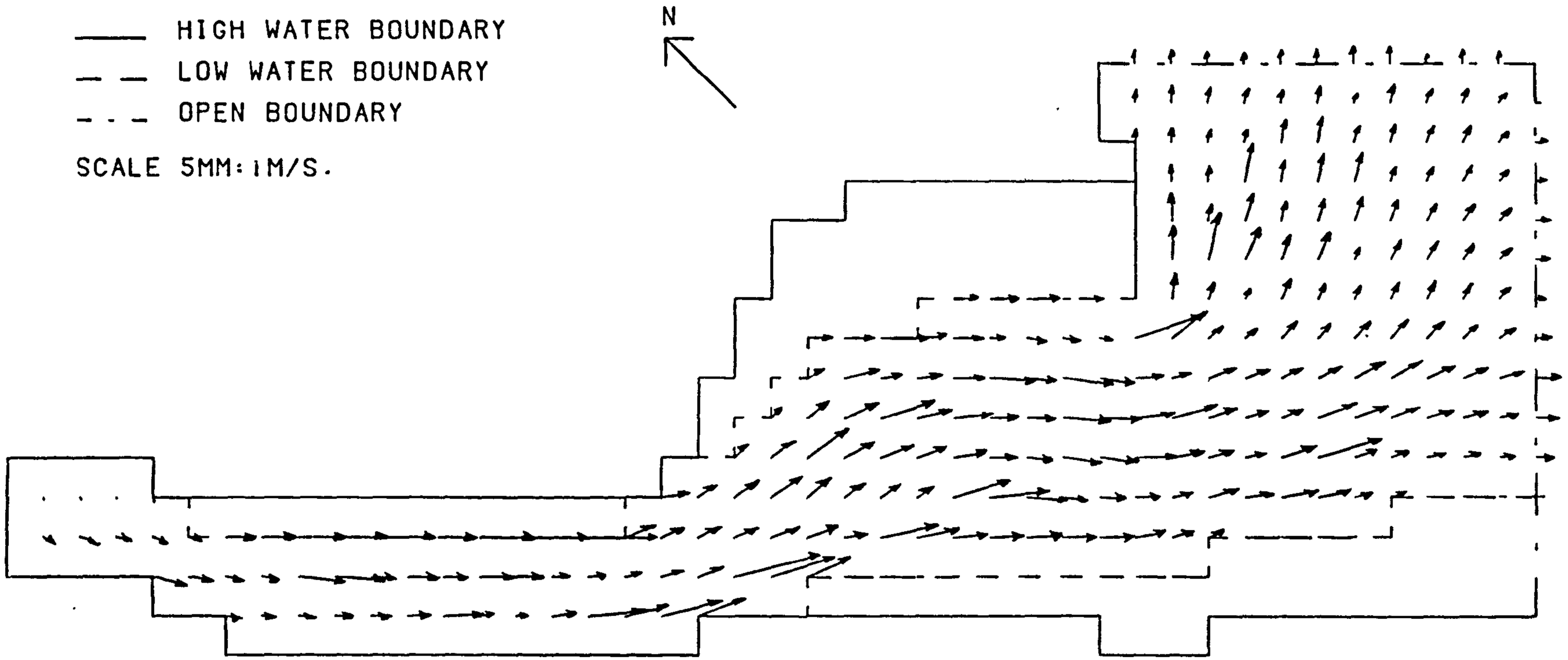

FIGURE 8.51
SPRING TIDE VELOCITIES IN THE HUMBER ESTUARY.
TIME FROM START OF TIDAL CYCLE HOURS= 11.00

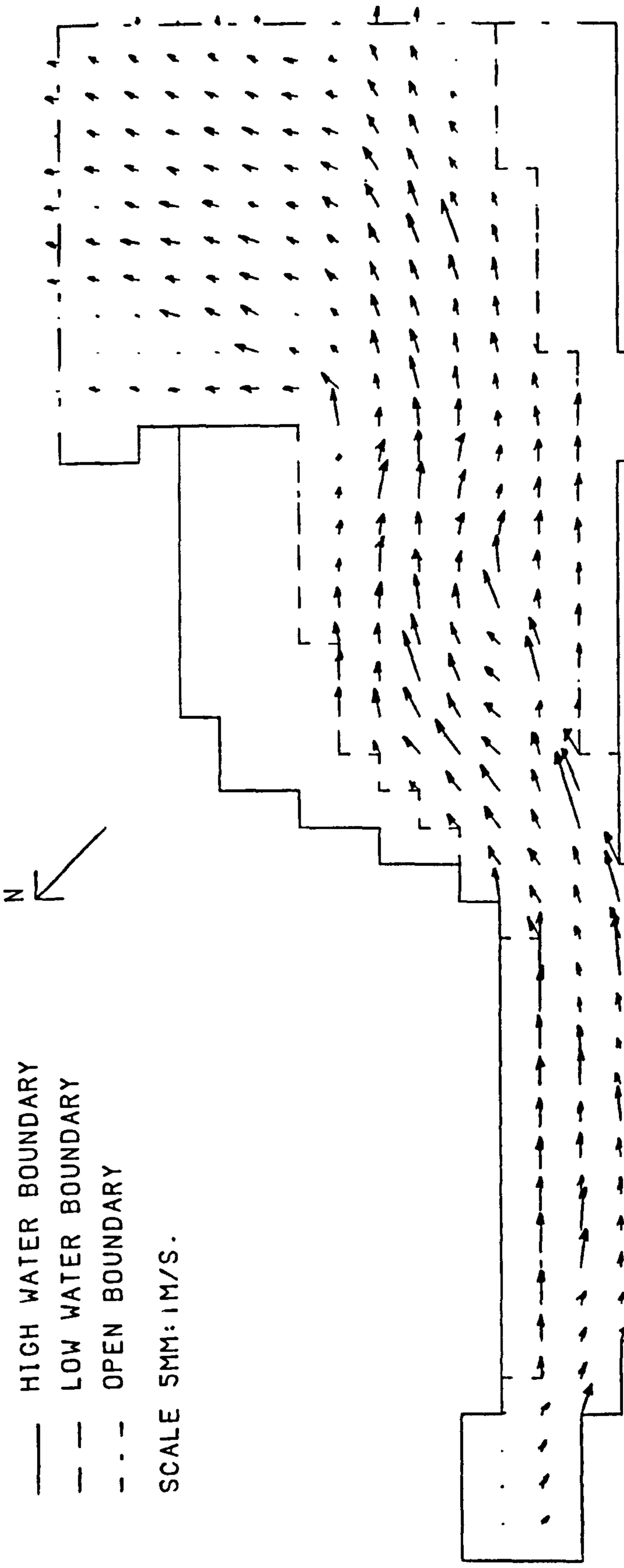

FIGURE 8.5 TIDE VELOCITIES IN THE HUMBER ESTUARY.
SPRING TIDE. MEAN RANGE 8.5m
TIME FROM START OF TIDAL CYCLE HOURS= 12.00

FIGURE 8·6a
SPRING TIDE PROPAGATION IN THE HUMBER ESTUARY.
TIME FROM START OF TIDAL CYCLE HOURS= .00

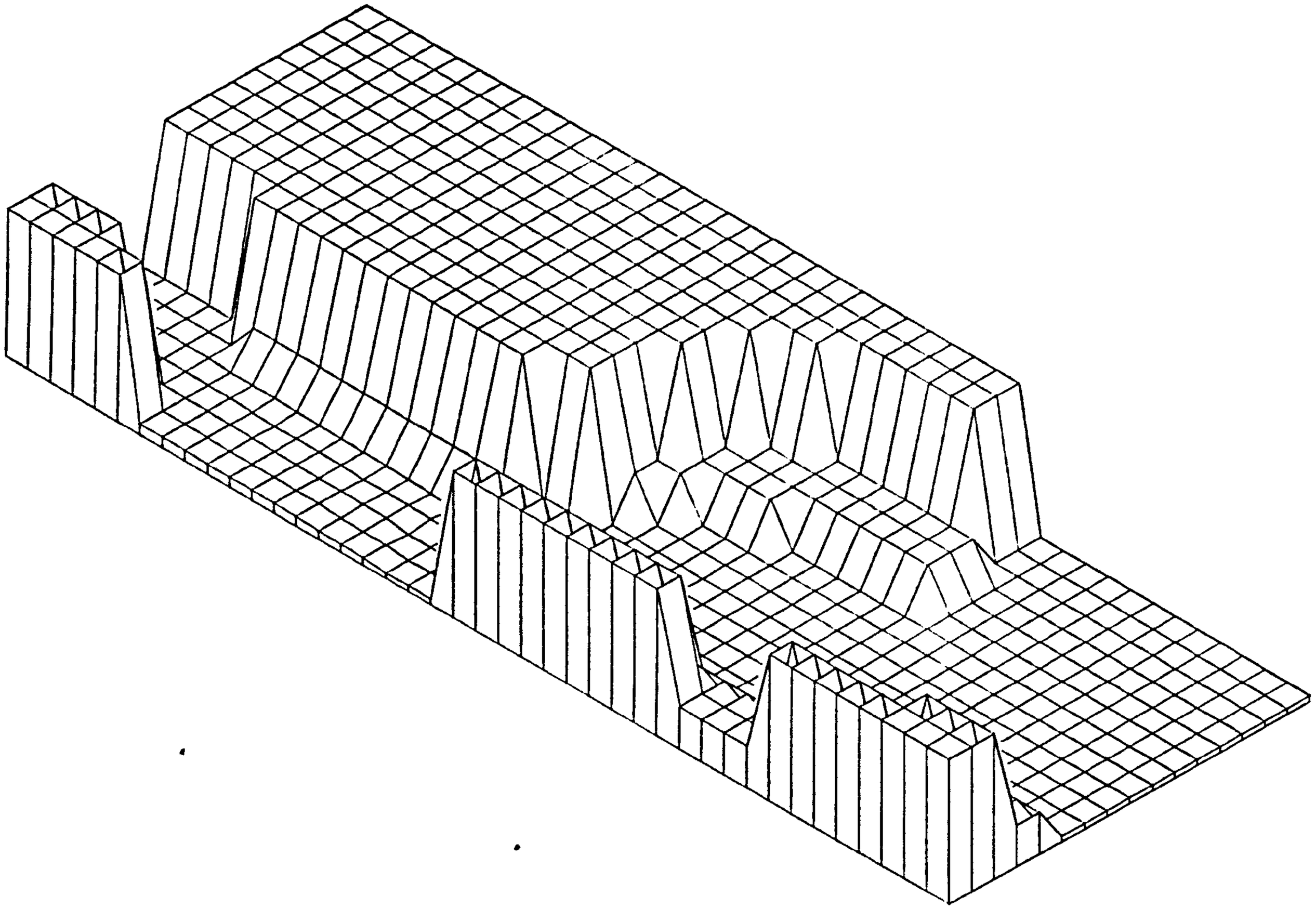

FIGURE 8·6 b
SPRING TIDE PROPAGATION IN THE HUMBER ESTUARY.
TIME FROM START OF TIDAL CYCLE HOURS= 1.00

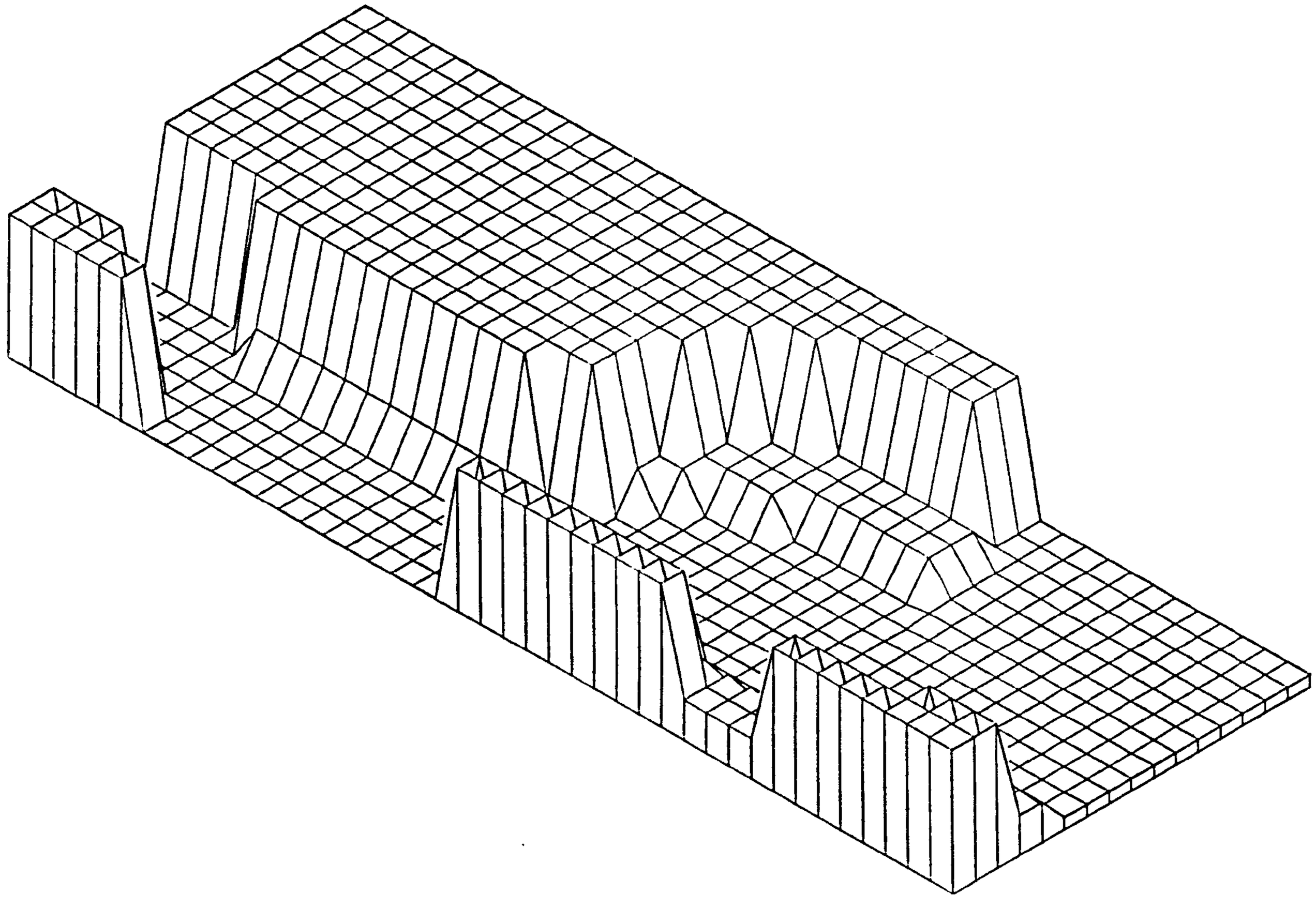

FIGURE 8·6c
SPRING TIDE PROPAGATION IN THE HUMBER ESTUARY.
TIME FROM START OF TIDAL CYCLE HOURS= 2.00

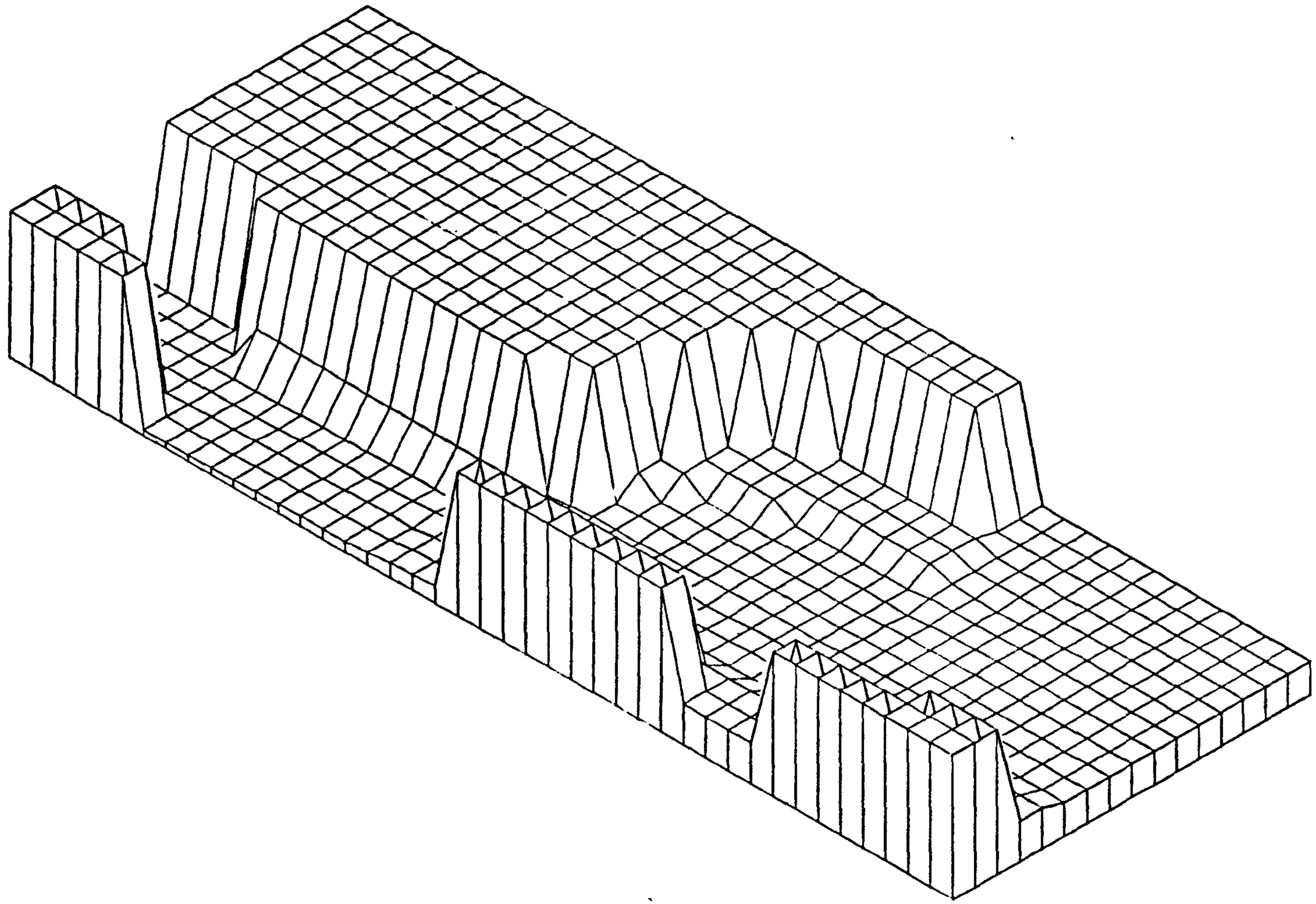

FIGURE 8.6d
SPRING TIDE PROPAGATION IN THE HUMBER ESTUARY.
TIME FROM START OF TIDAL CYCLE HOURS= 3.00

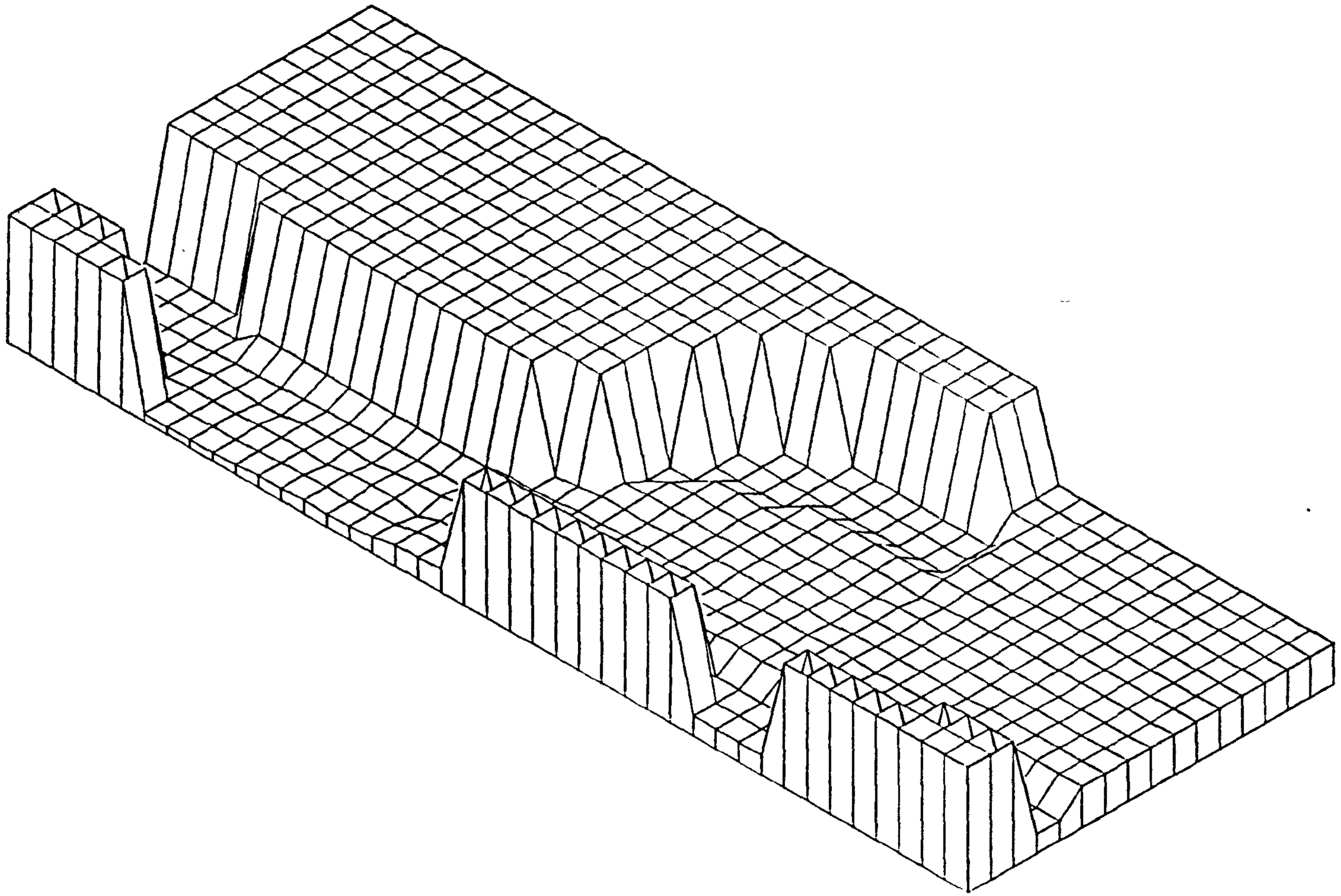

FIGURE 8.6e
SPRING TIDE PROPAGATION IN THE HUMBER ESTUARY.
TIME FROM START OF TIDAL CYCLE HOURS= 4.00

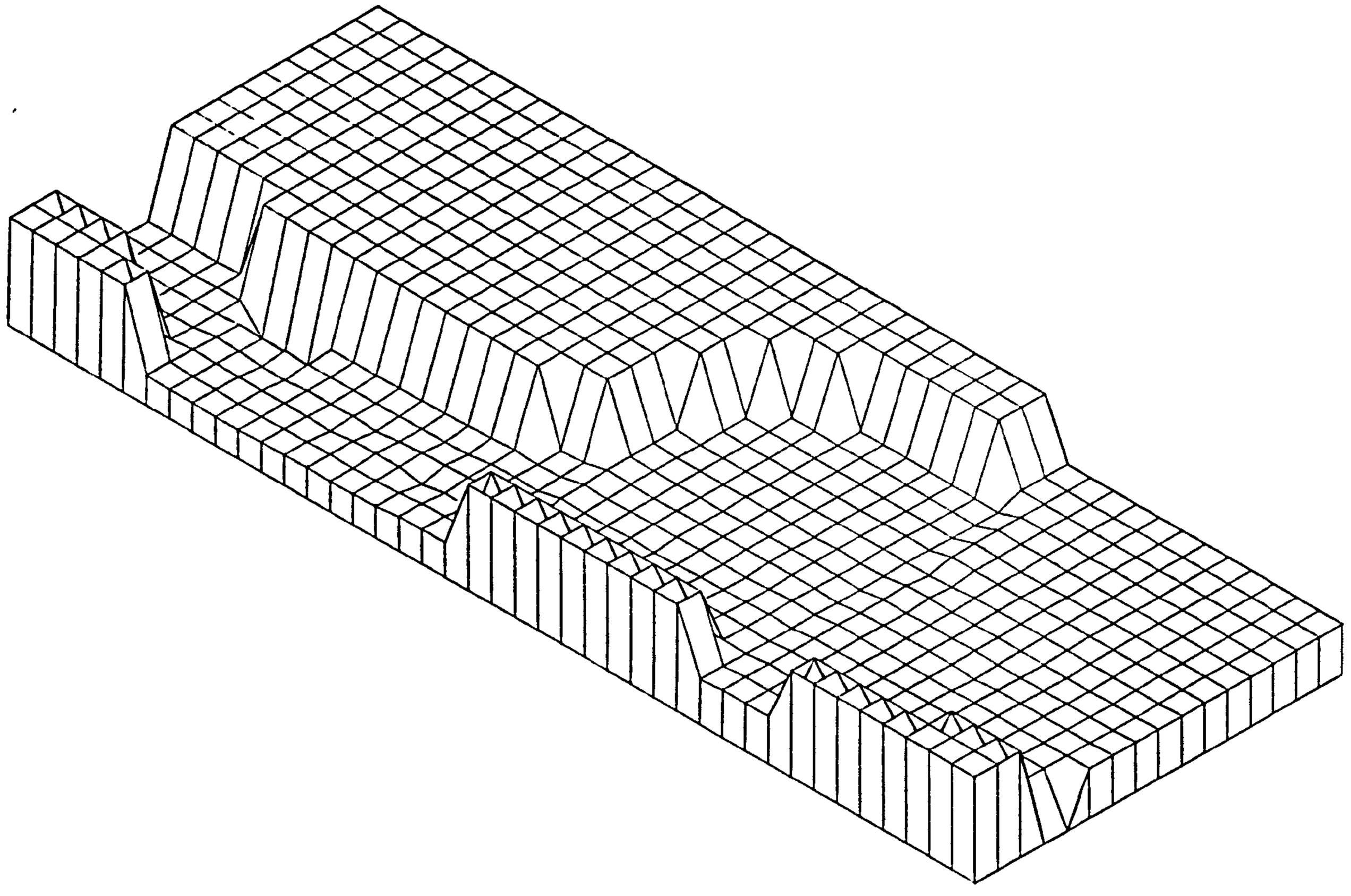

FIGURE 8.6f
SPRING TIDE PROPAGATION IN THE HUMBER ESTUARY.
TIME FROM START OF TIDAL CYCLE HOURS= 5.00

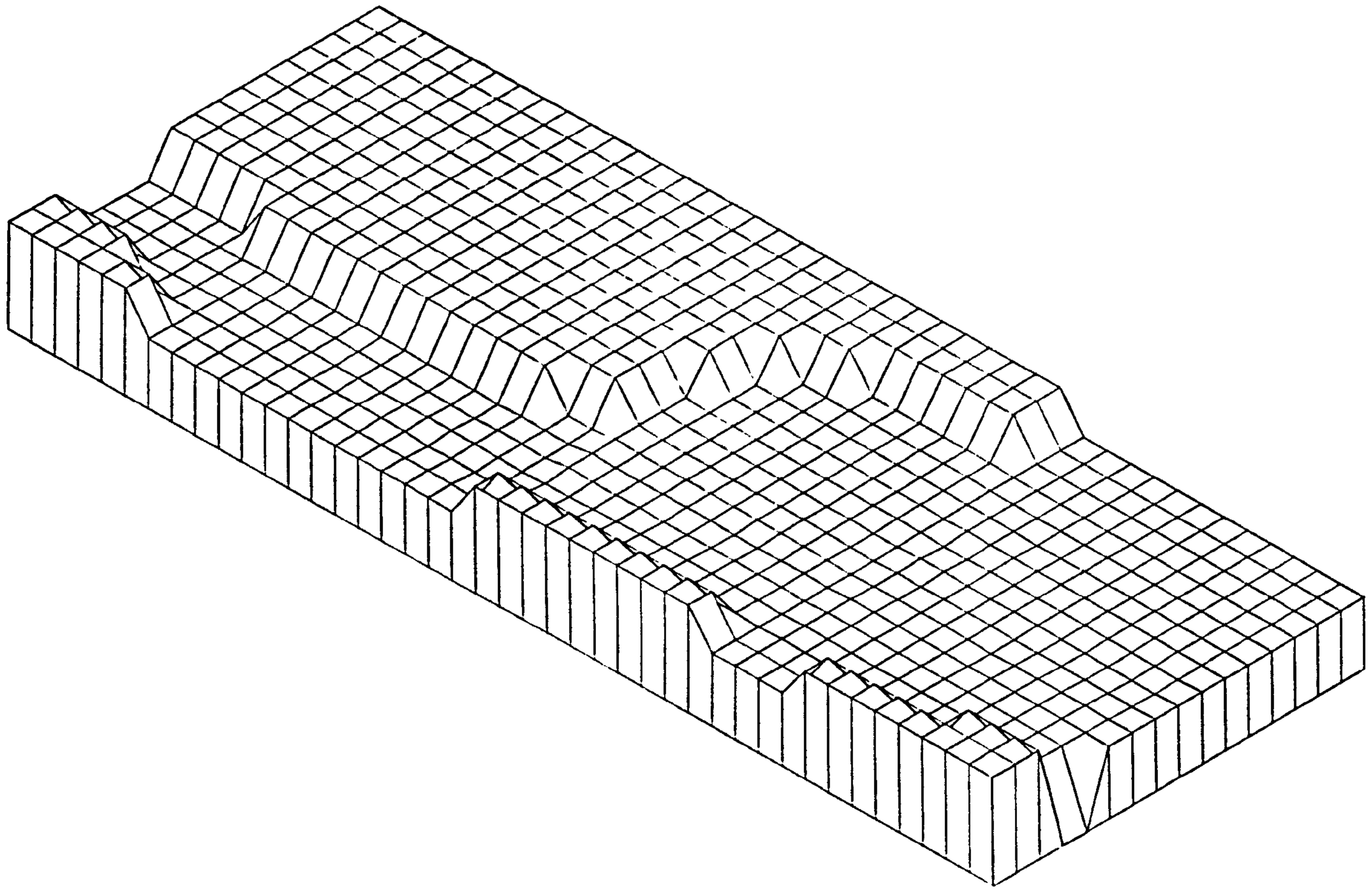

FIGURE 8·6g
SPRING TIDE PROPAGATION IN THE HUMBER ESTUARY.
TIME FROM START OF TIDAL CYCLE HOURS= 6.00

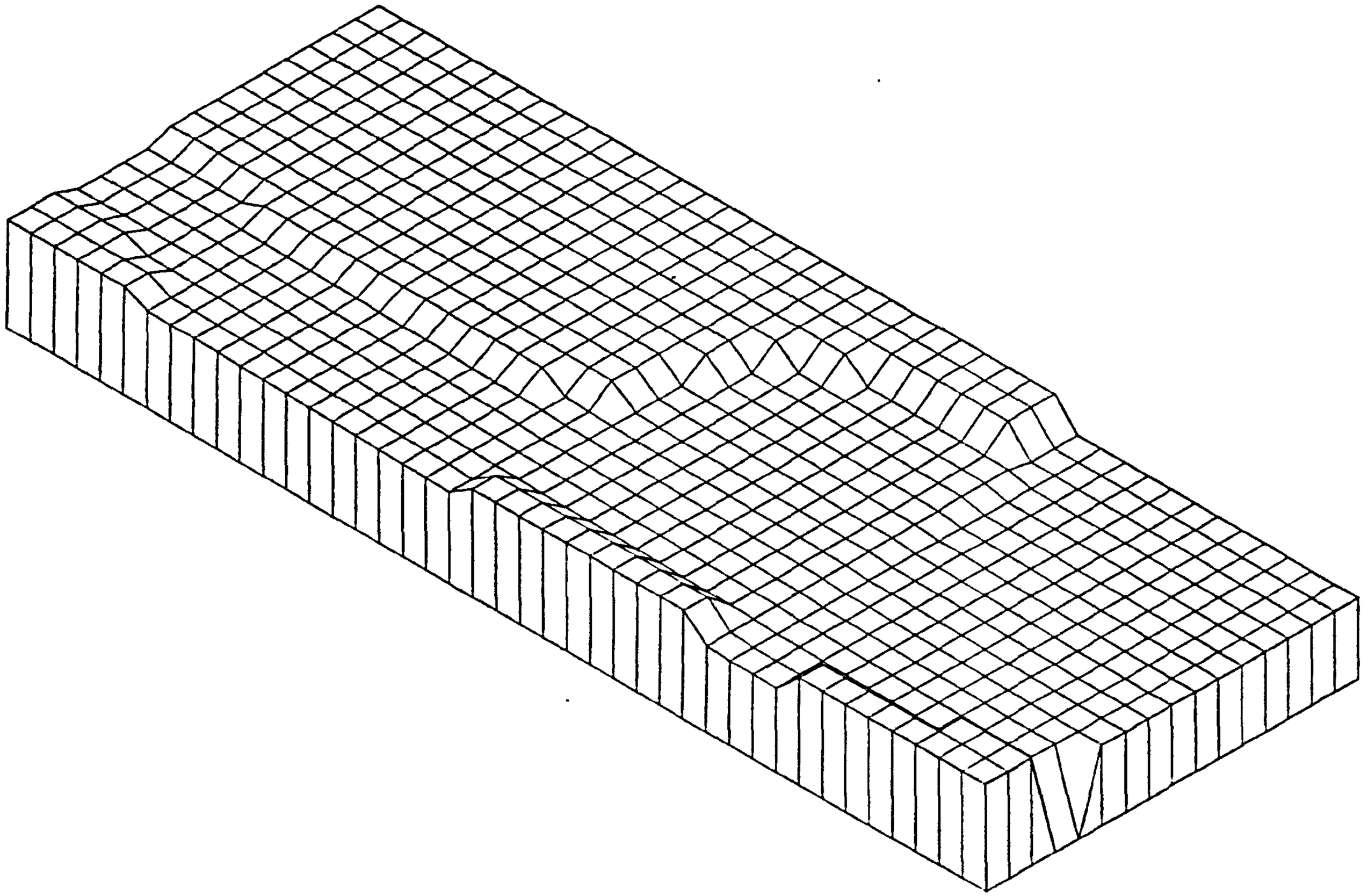

FIGURE 8.6h
SPRING TIDE PROPAGATION IN THE HUMBER ESTUARY.
TIME FROM START OF TIDAL CYCLE HOURS= 7.00

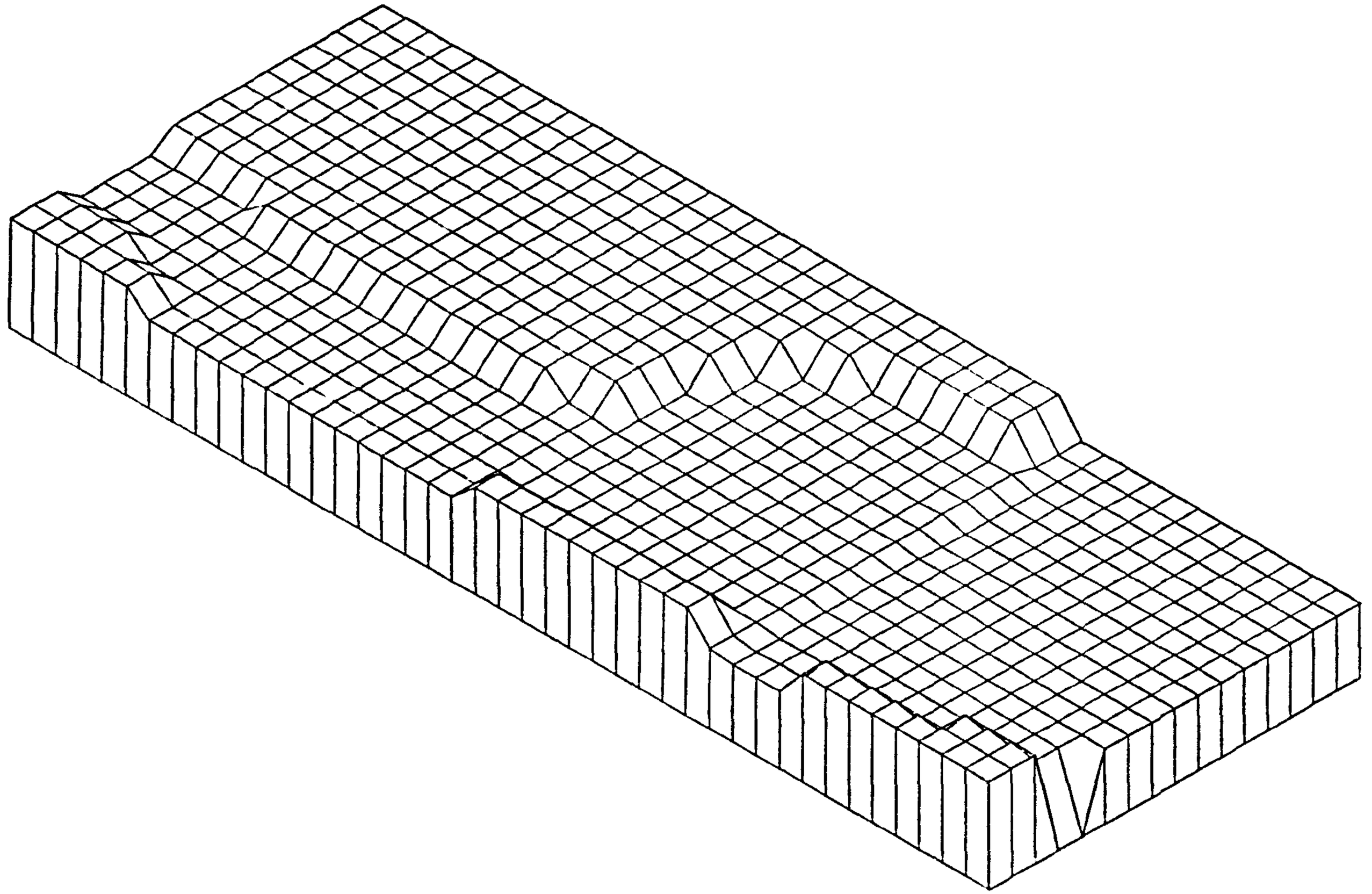

FIGURE 8.6i
SPRING TIDE PROPAGATION IN THE HUMBER ESTUARY.
TIME FROM START OF TIDAL CYCLE HOURS= 8.00

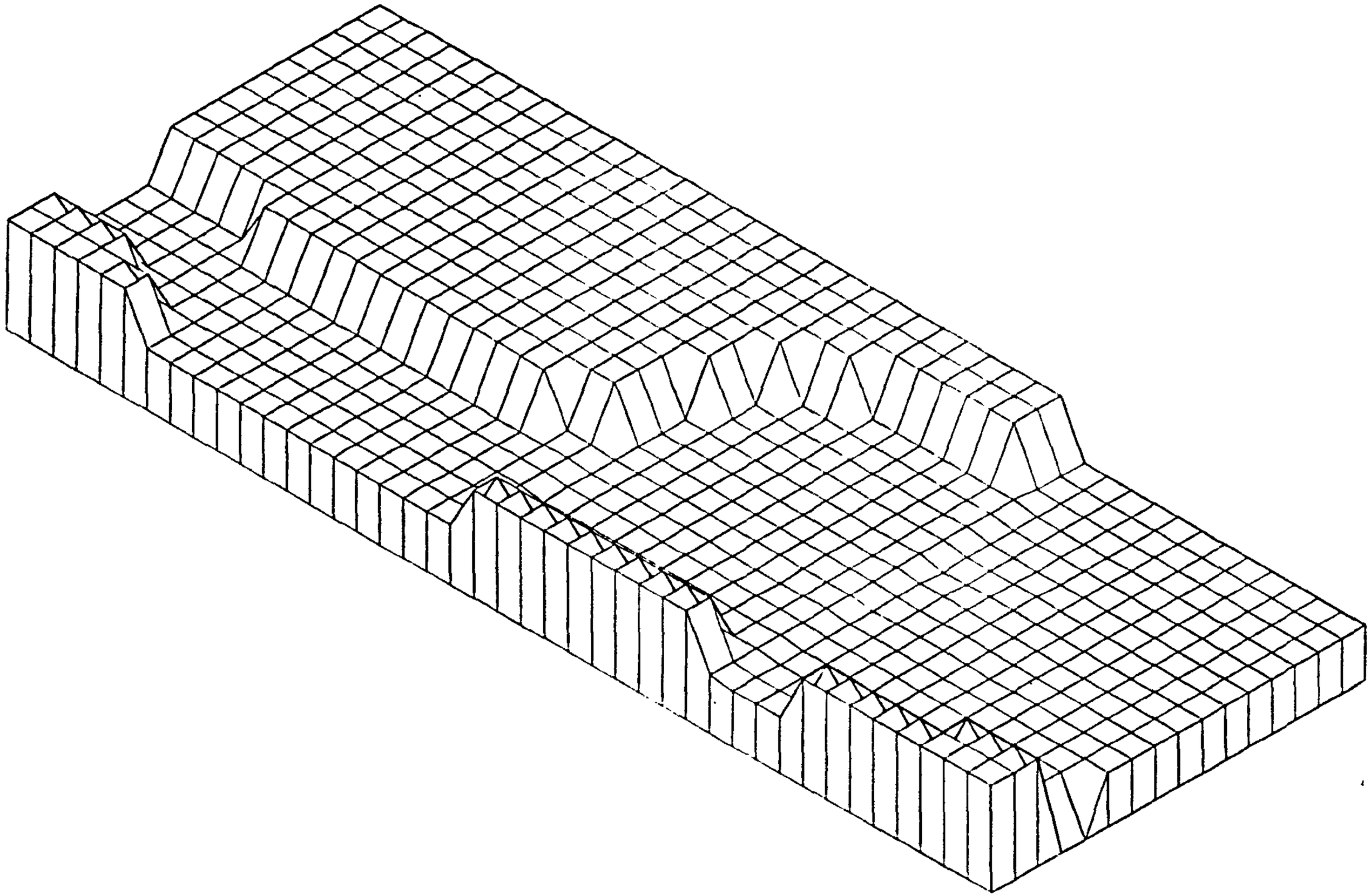

FIGURE 8·6j
SPRING TIDE PROPAGATION IN THE HUMBER ESTUARY.
TIME FROM START OF TIDAL CYCLE HOURS= 9.00

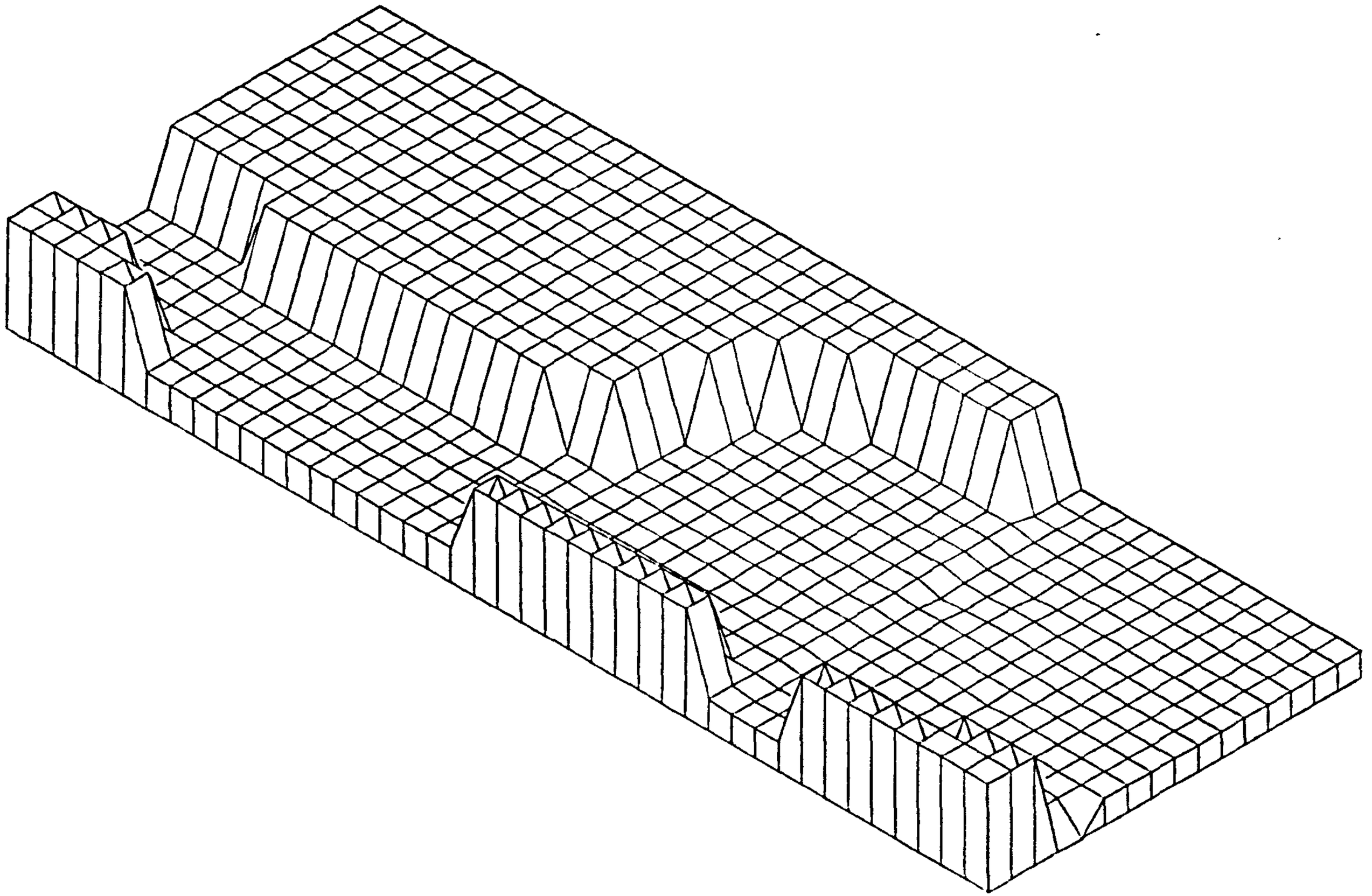

FIGURE 8·6k
SPRING TIDE PROPAGATION IN THE HUMBER ESTUARY.
TIME FROM START OF TIDAL CYCLE HOURS= 10.00

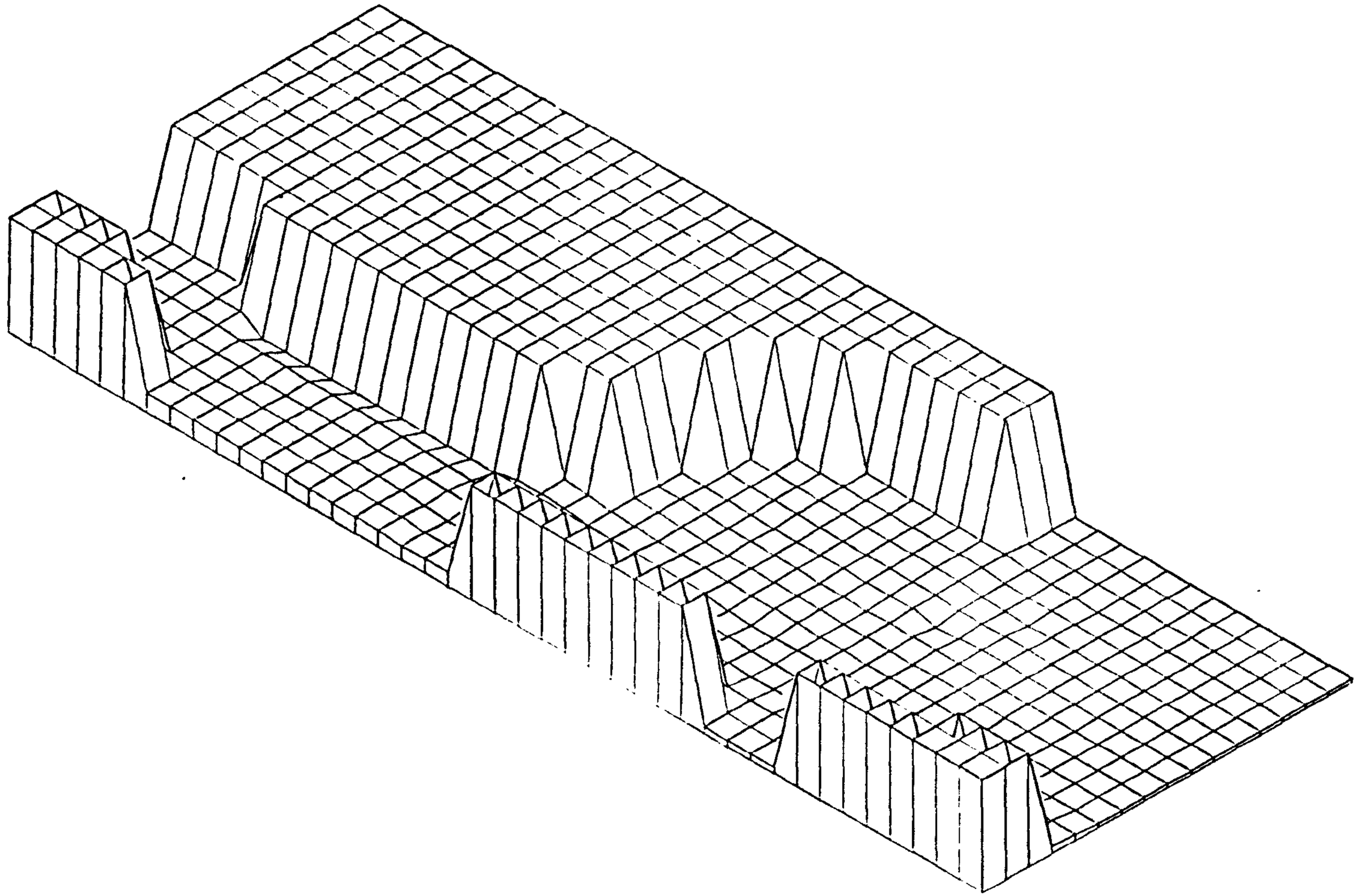

FIGURE 8·61
SPRING TIDE PROPAGATION IN THE HUMBER ESTUARY.
TIME FROM START OF TIDAL CYCLE HOURS= 11.00

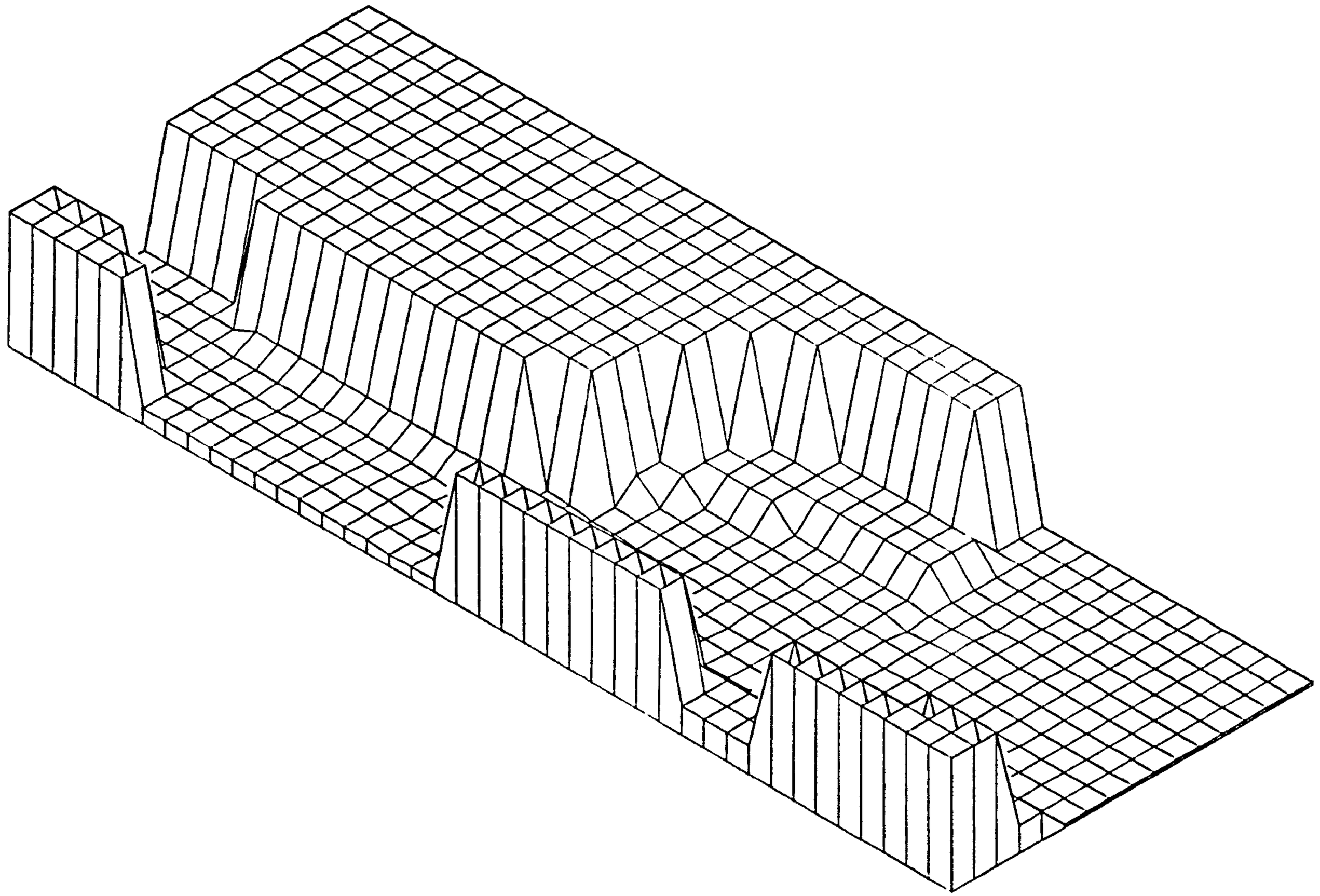

FIGURE 8·6m
SPRING TIDE PROPAGATION IN THE HUMBER ESTUARY.
TIME FROM START OF TIDAL CYCLE HOURS= 12.00

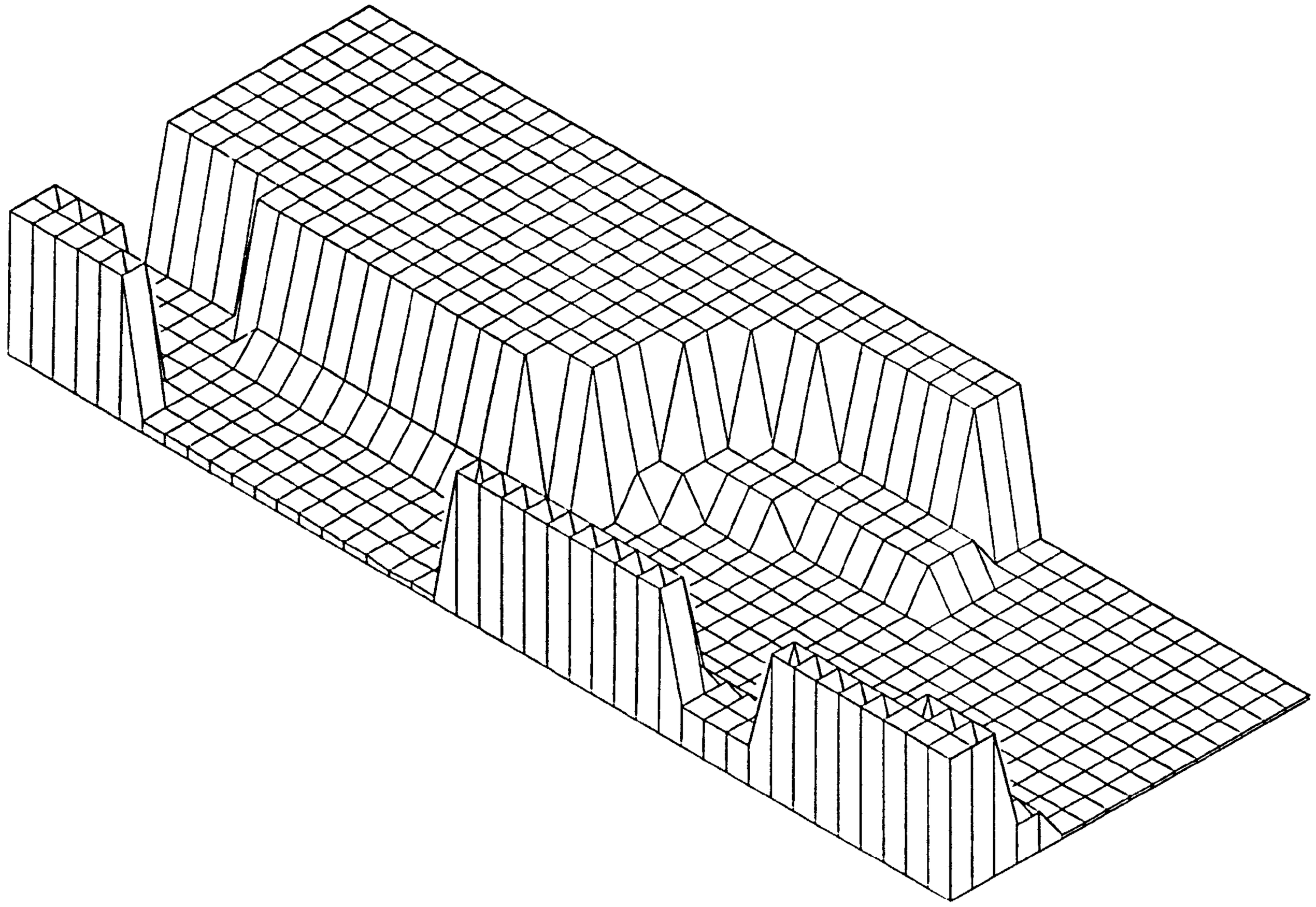

drawings for the Firth of Clyde it is stressed that the vertical scale varies from figure to figure and that the drawings serve only to illustrate the nature of tidal propagation in the Estuary. Figure 8.6d shows the wave front propagating over the sand flats.

8.7 FIELD OBSERVATIONS

The existence of comprehensive field measurements in the Humber Estuary provided the opportunity for a rigorous examination of numerical model results. Four comparisons were used as the basis of the examination. These were:

i. Observed and computed tide curves.

ii. Observed and computed velocity magnitudes.

iii. Observed and computed velocity directions.

iv. Observed and computed cubature.

Observed data was obtained from the following sources:

i. Hydraulics Research Station, Reports Ex 386, Ex 495 and Ex 670.

ii. Humber Estuary Research Committee, Report H1, 1974.

iii. Humber Advisory Group, Symposium, 1973.

8.8 COMPARISON OF MODEL ONE RESULTS WITH OBSERVED DATA

Initial examination of observed tidal curves suggested that tides at Immingham and Saltend were not significantly influenced by shallow water effects as were the numerical results from model one. This deduction is reinforced by the results of a harmonic analysis of the tides in

the lower estuary undertaken by the Hydraulics Research Station. This showed the tide in the lower estuary to be dominated by the semi-diurnal constituent having two nearly equal high and low waters each lunar day. The amplitude of the fourth diurnal component for a spring tide on 5th April 1966 was less than 0.12m at all observed stations seawards of Saltend, compared with a 3.05m amplitude of the semi-diurnal component, showing that tide levels in the lower estuary are hardly affected by shallow water effects.

Examination of computed velocities from model one showed them to be high, while the computed cubature at Spurn Head, Grimsby and Immingham was too small. These discrepancies were considered to be the result of inadequate numerical representation of the bathymetry rather than a failure of the numerical scheme.

8.9 ADJUSTMENT OF THE NUMERICAL BATHYMETRY

A number of adjustments were made to the numerical bathymetry of model one in an attempt to improve the above comparisons. The resulting bathymetry constitutes model two. Firstly, depths within the model were increased by 2m. This was considered to be a reasonable correction as chart depths are given relative to the lowest astronomical tide and some allowance should be added to bring these up to low water spring tide level. Secondly, the estuary area west of Hull was included as an equivalent water surface area. This was estimated as 49km^2 and is too large to be omitted from the calculation. Thirdly, sand

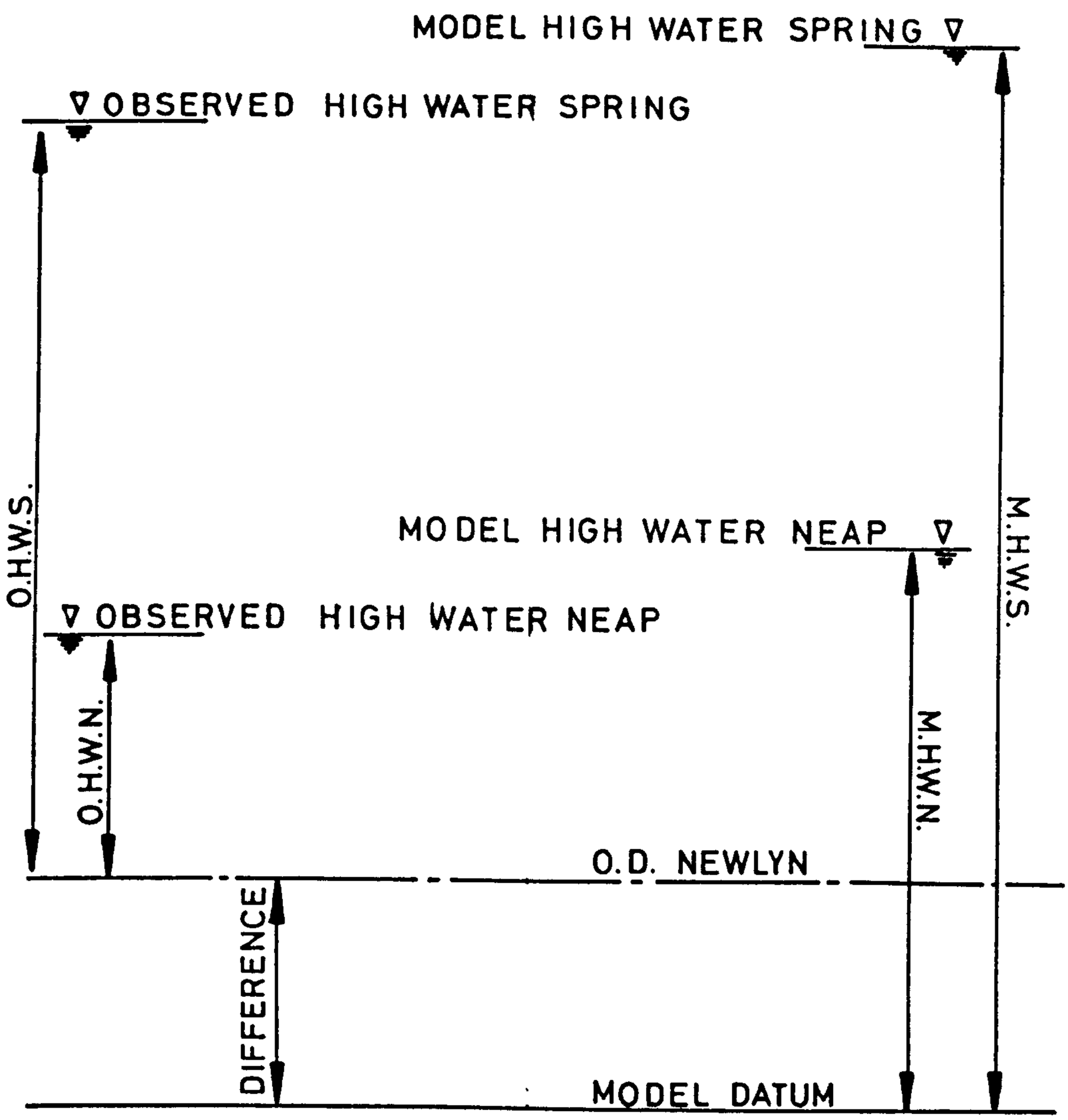

DIFFERENCE = (M.H.W.S. − O.H.W.S. + M.H.W.N. − O.H.W.N.) / 2

FIGURE 8·7

flat levels were adjusted to improve cubature comparisons particularly at Spurn Head. The level adjustments were of the order of 0.5m; a realistic adjustment considering the difficulty in assessing a mean level and the approximation involved in modelling the sand flats as level as opposed to sloping shoals.

8.10 MODEL TWO COMPARISONS

8.10.1 BASIS OF COMPARISONS

For the purpose of the following comparisons model times and levels were related to prototype times and levels in the following way. Time comparisons were obtained by assuming computed high water and observed high water at Bull Sand to be coincidental. Model datum level was related to Ordnance Datum Newlyn by the procedure shown in Figure 8.7.

8.10.2 WATER LEVELS

Comparisons between computed and observed water levels for the spring tide of 5th April 1966 are shown in Figures 8.8 to 8.11.

8.10.3 VELOCITY MAGNITUDES

Computed and observed velocities are shown in Figures 8.12a to 8.18a. The location of these comparisons is shown in Figure 8.2. Velocity observations were made on a number of different days and may be influenced by meteorological conditions. To assist in assessing the degree of any such influence simultaneous tide curves for the nearest port are shown on the figures. When

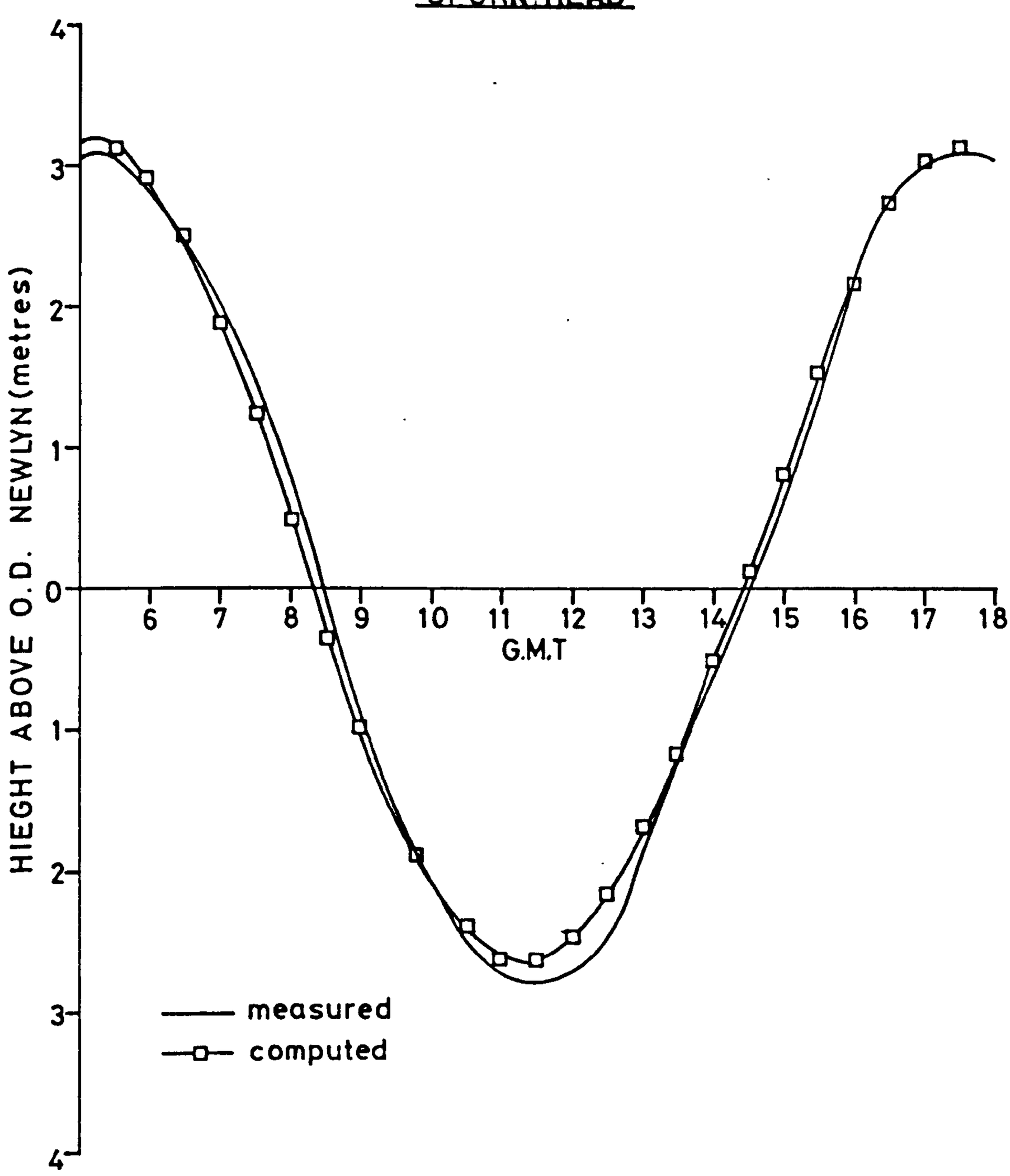

FIGURE 8·8
COMPARISON OF SPRING TIDE CURVES

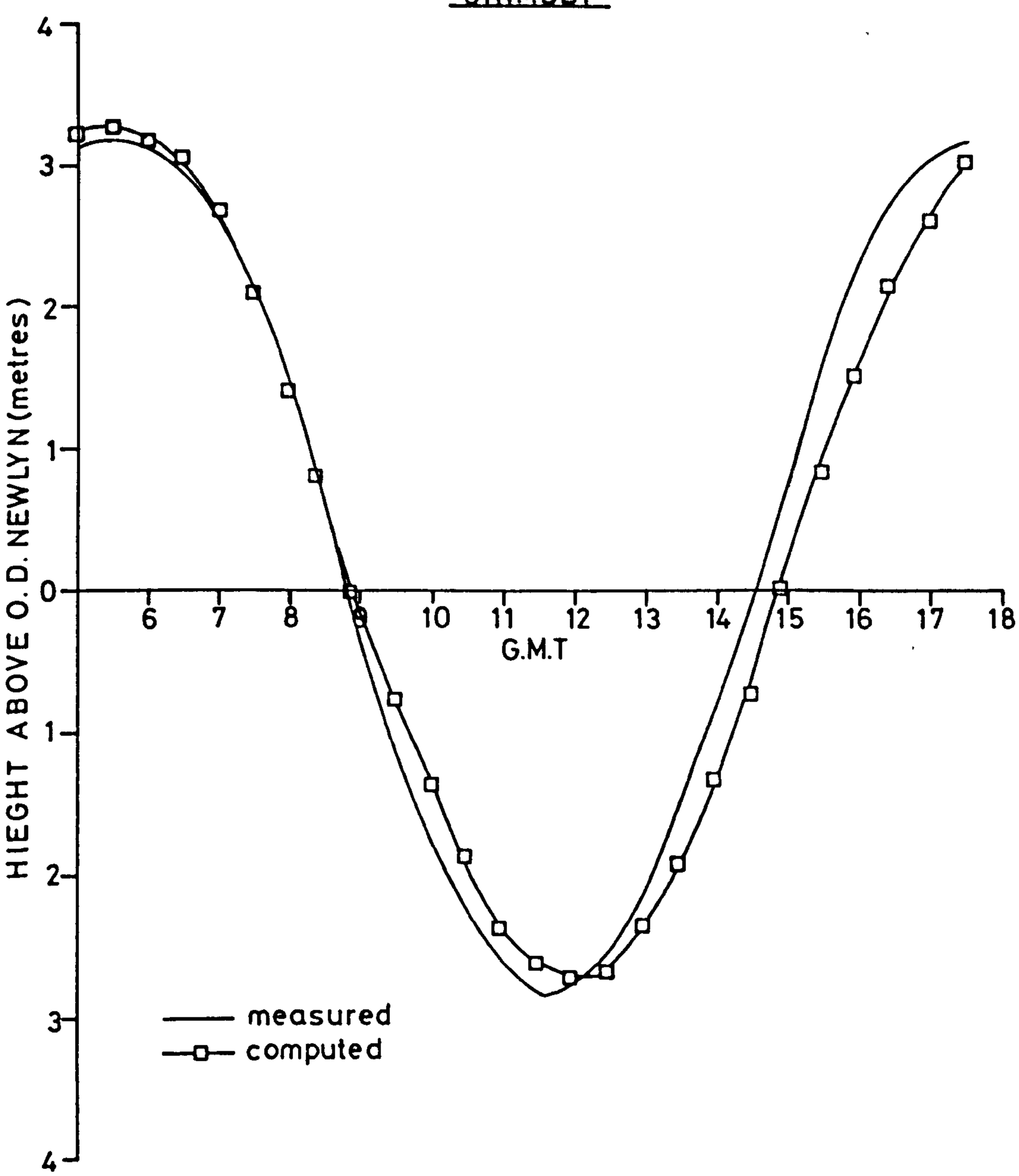

FIGURE 8·9

COMPARISON OF SPRING TIDE CURVES

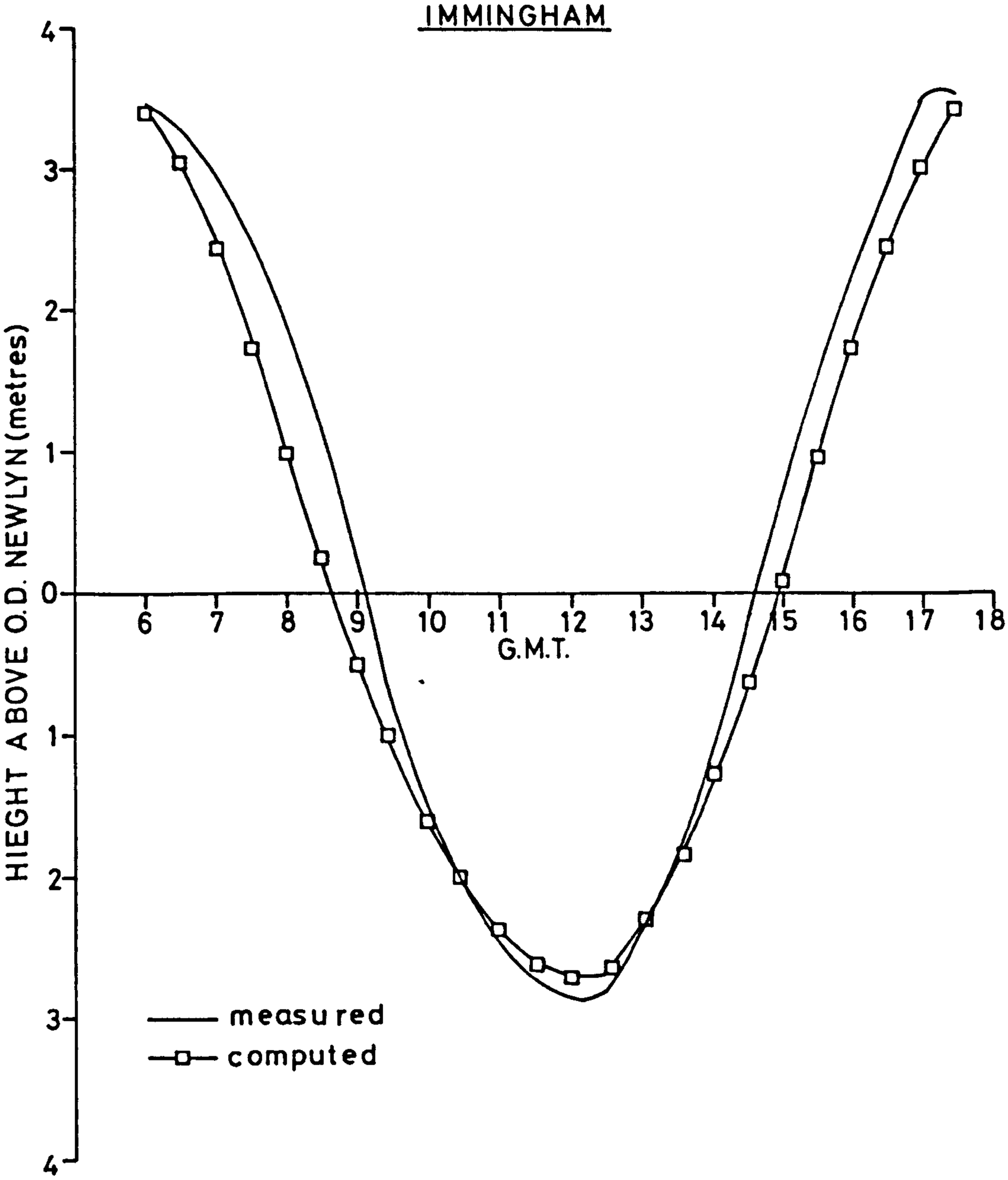

FIGURE 8·10
COMPARISON OF SPRING TIDE CURVES

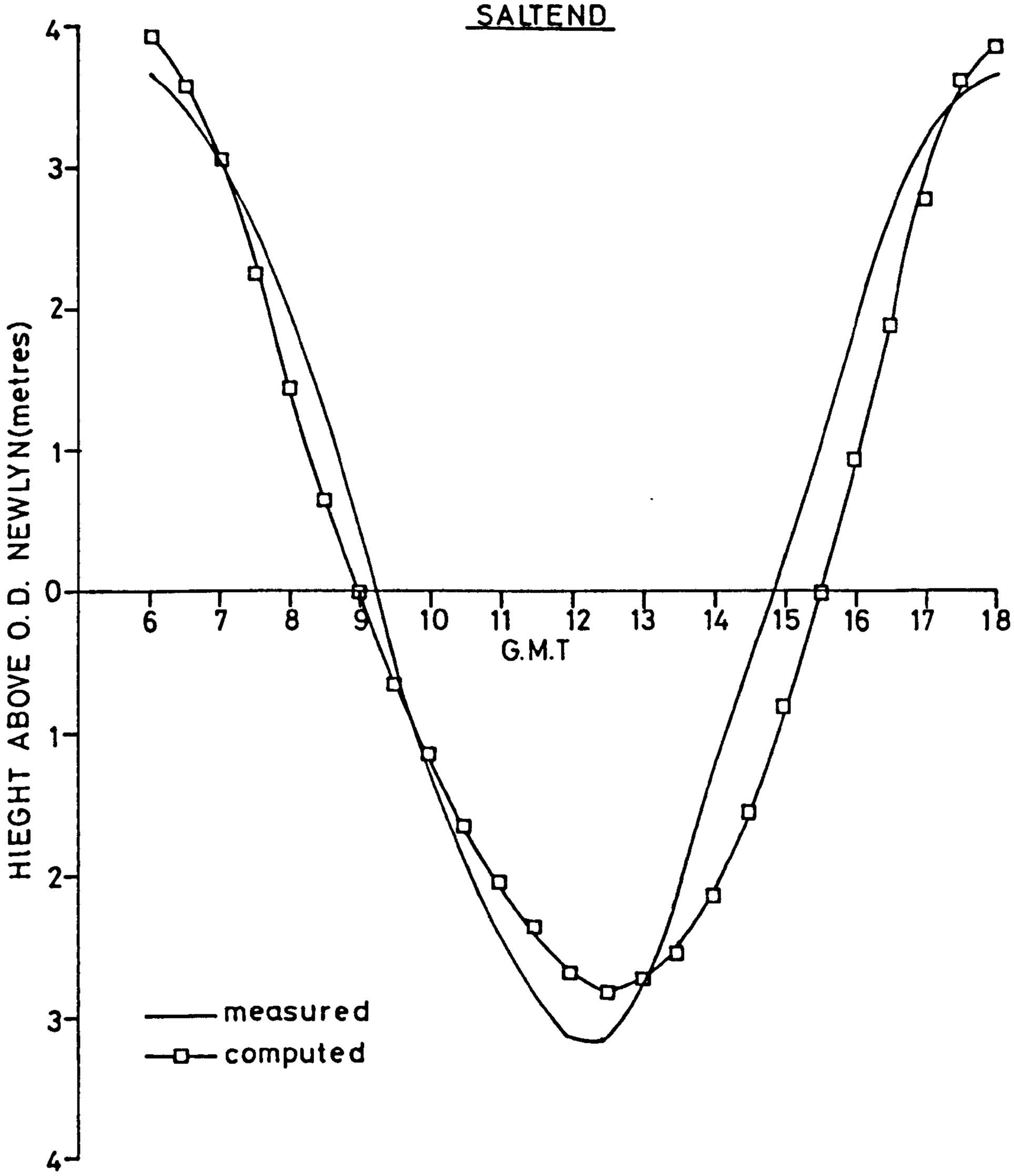

FIGURE 8·11

COMPARISON OF SPRING TIDE CURVES

VELOCITY COMPARISONS

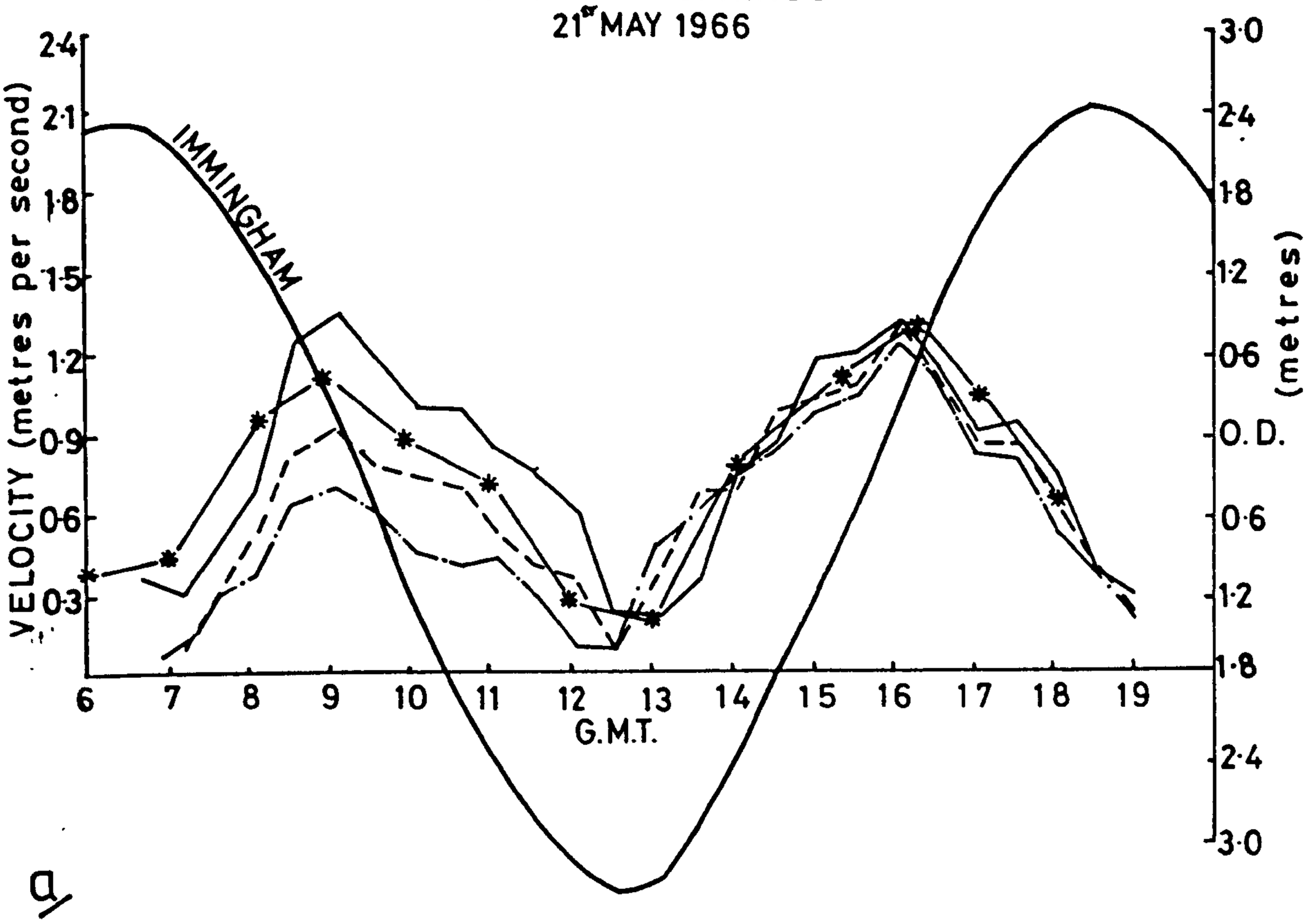

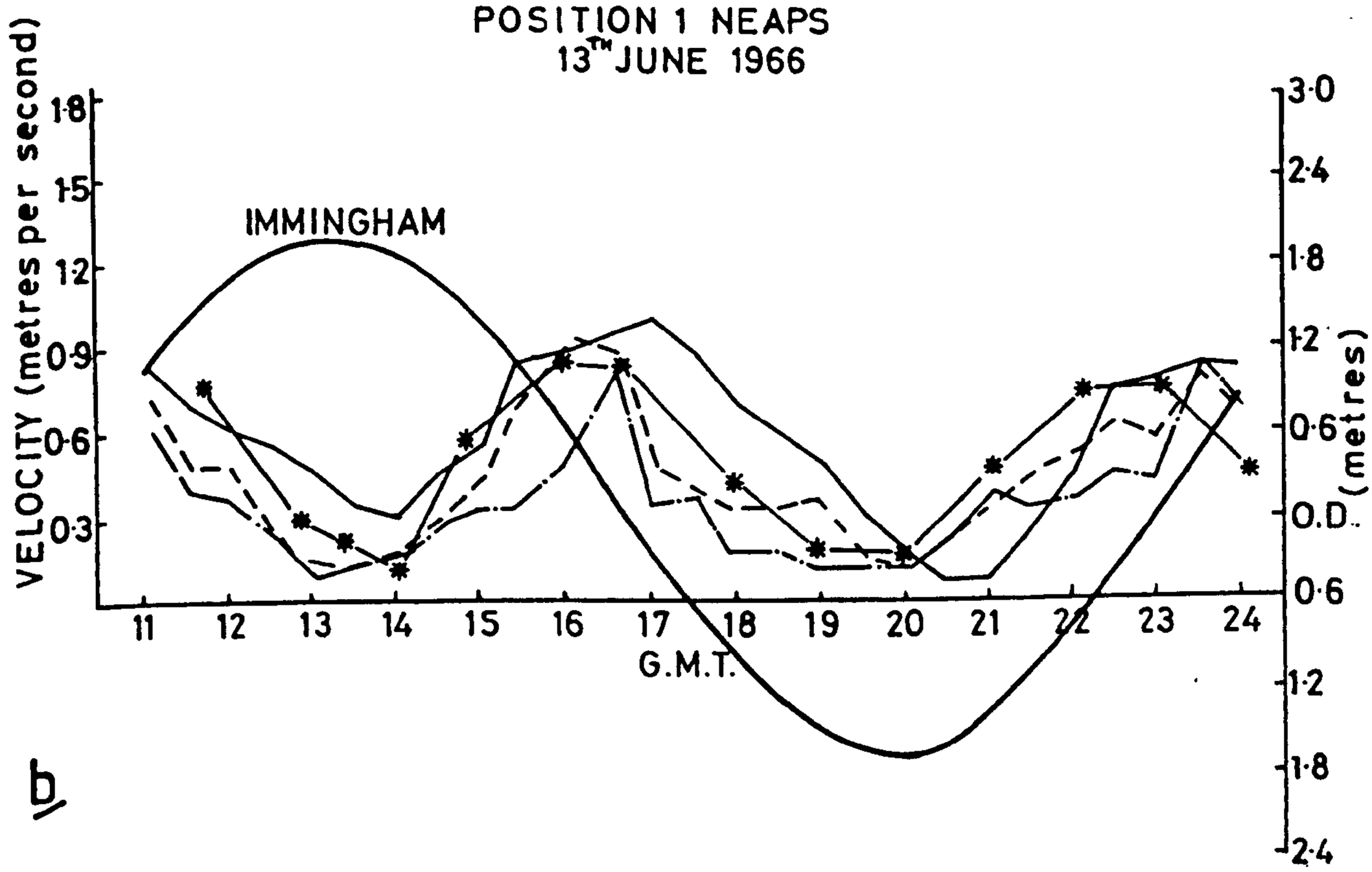

SURFACE—— MID DEPTH-·· 0·75 DEPTH—·— COMPUTED —*—

FIGURE 8·12

VELOCITY COMPARISONS

POSITION 2 SPRINGS
1st JUNE 1966

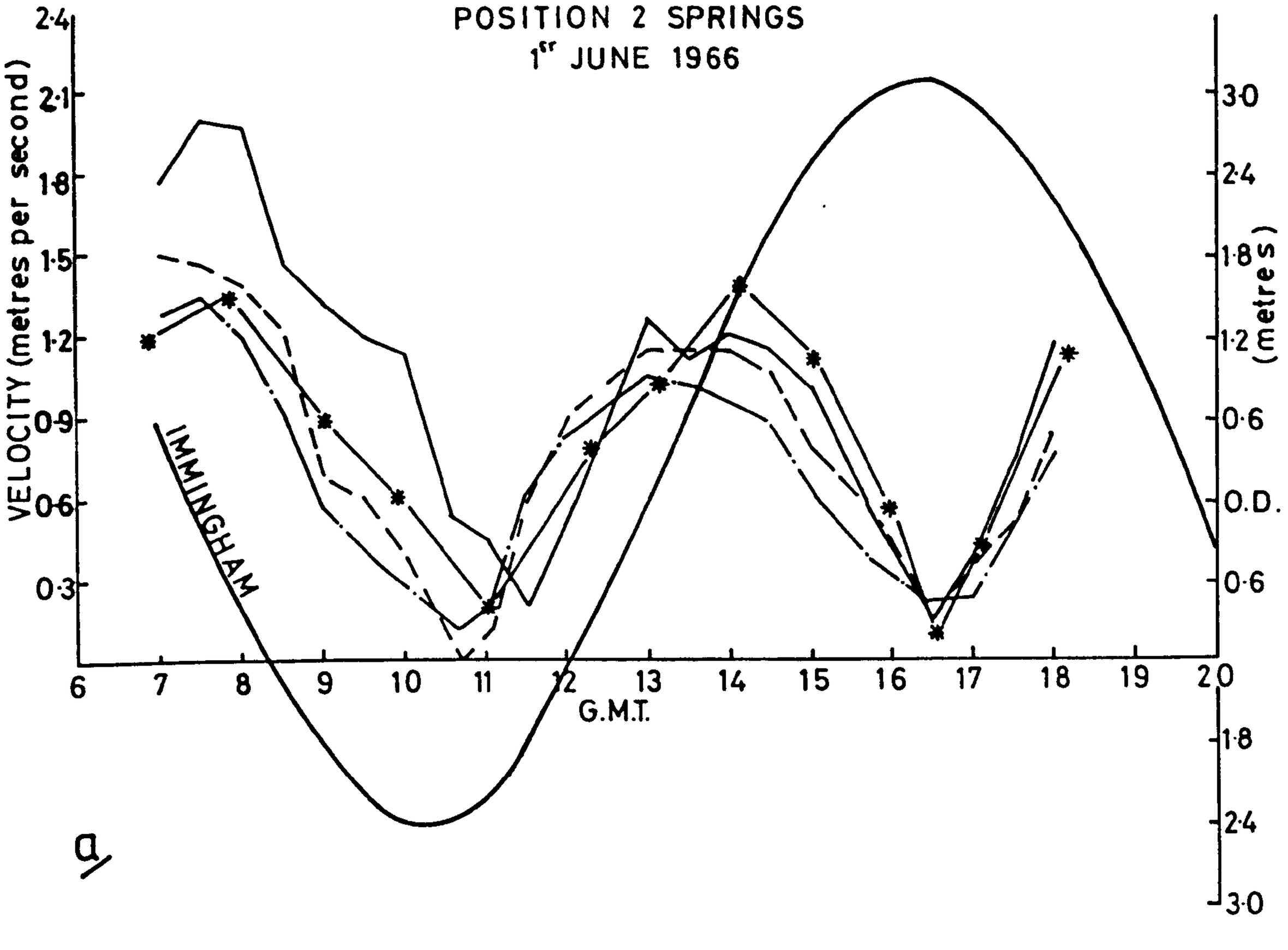

a/

POSITION 2 NEAPS
12th JUNE 1966

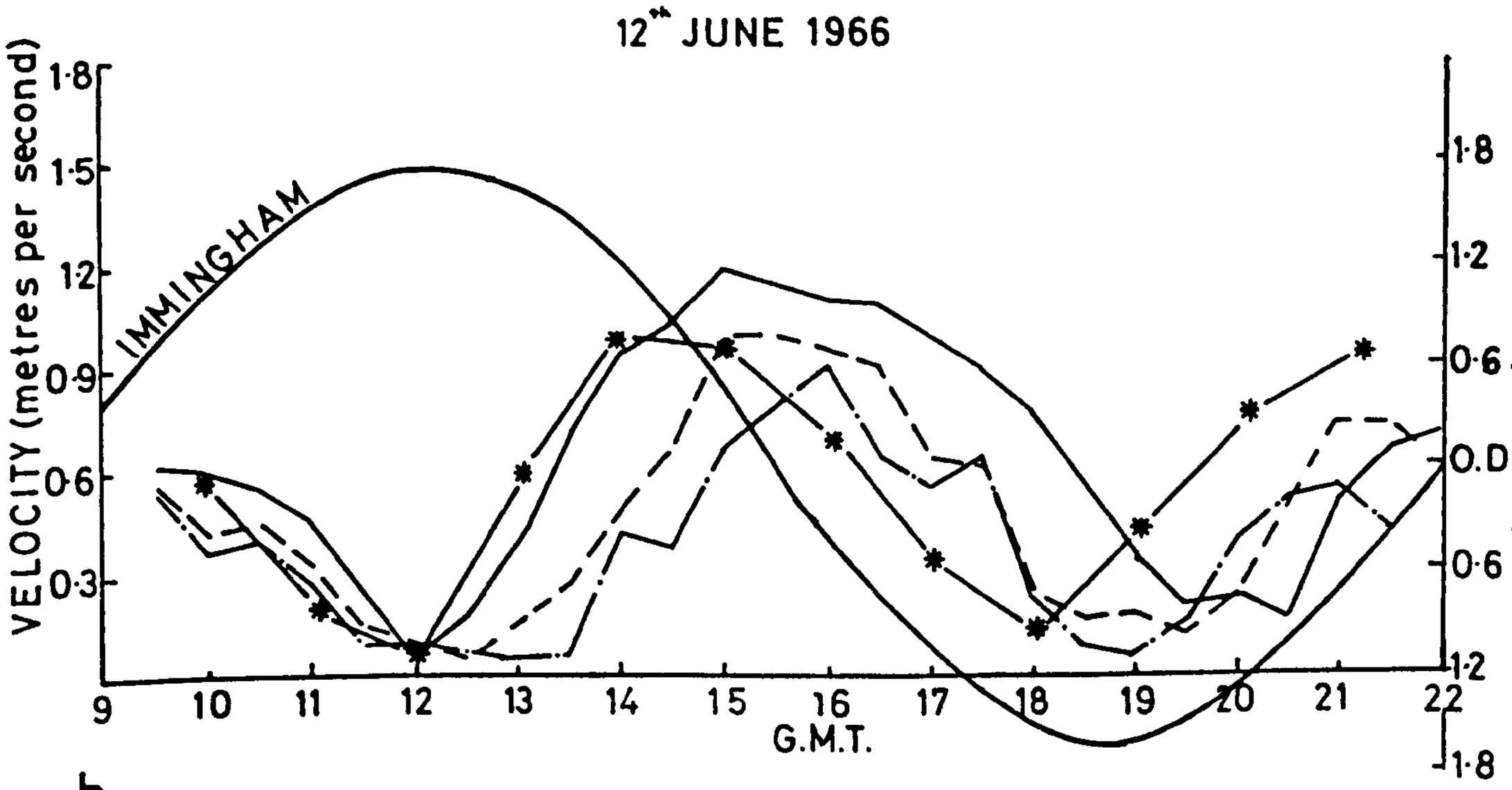

b/

SURFACE —— MID DEPTH- - - - 0·75 DEPTH —·— COMPUTED — * —

FIGURE 8·13

VELOCITY COMPARISONS

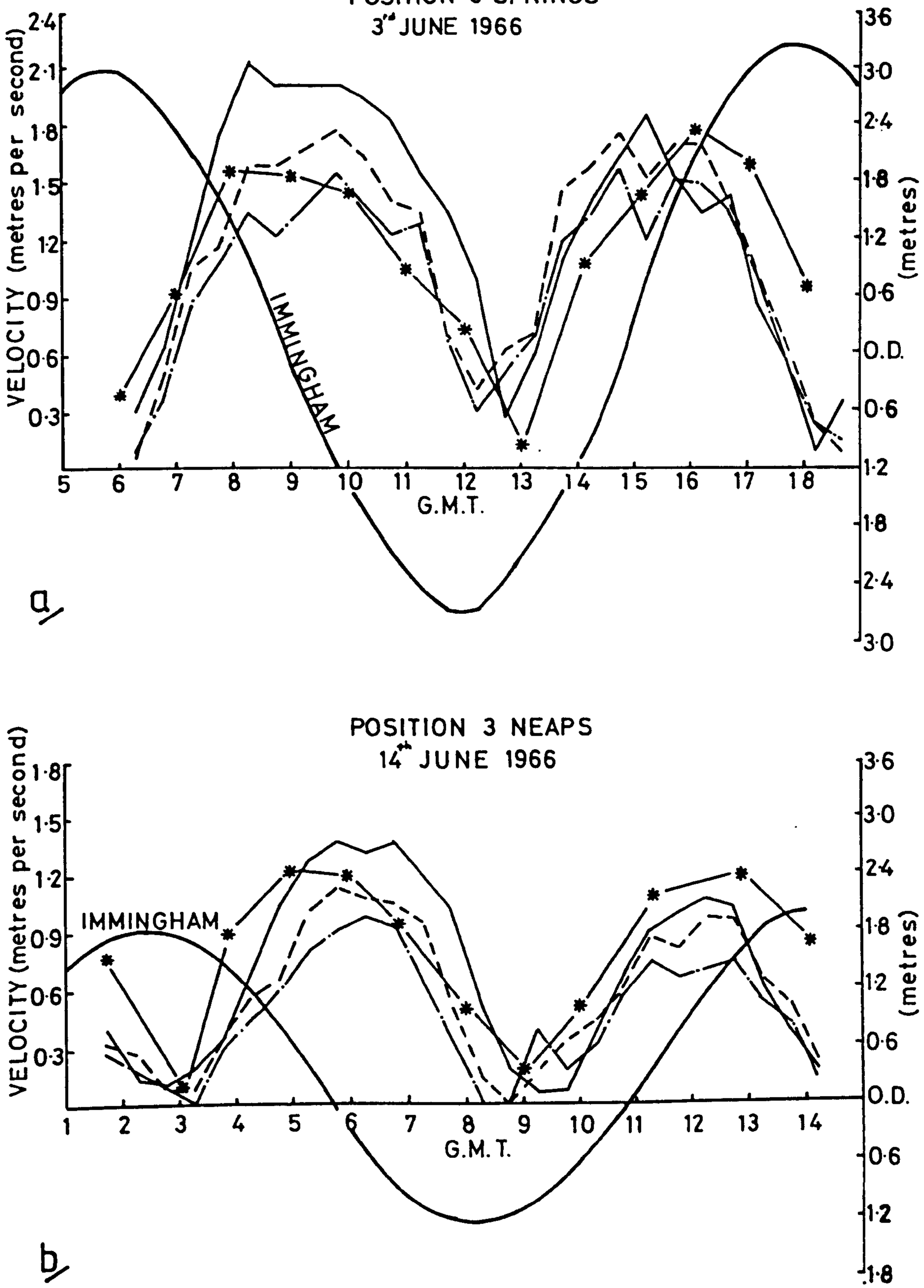

FIGURE 8·14

VELOCITY COMPARISONS

POSITION 4 SPRINGS
5th JUNE 1966

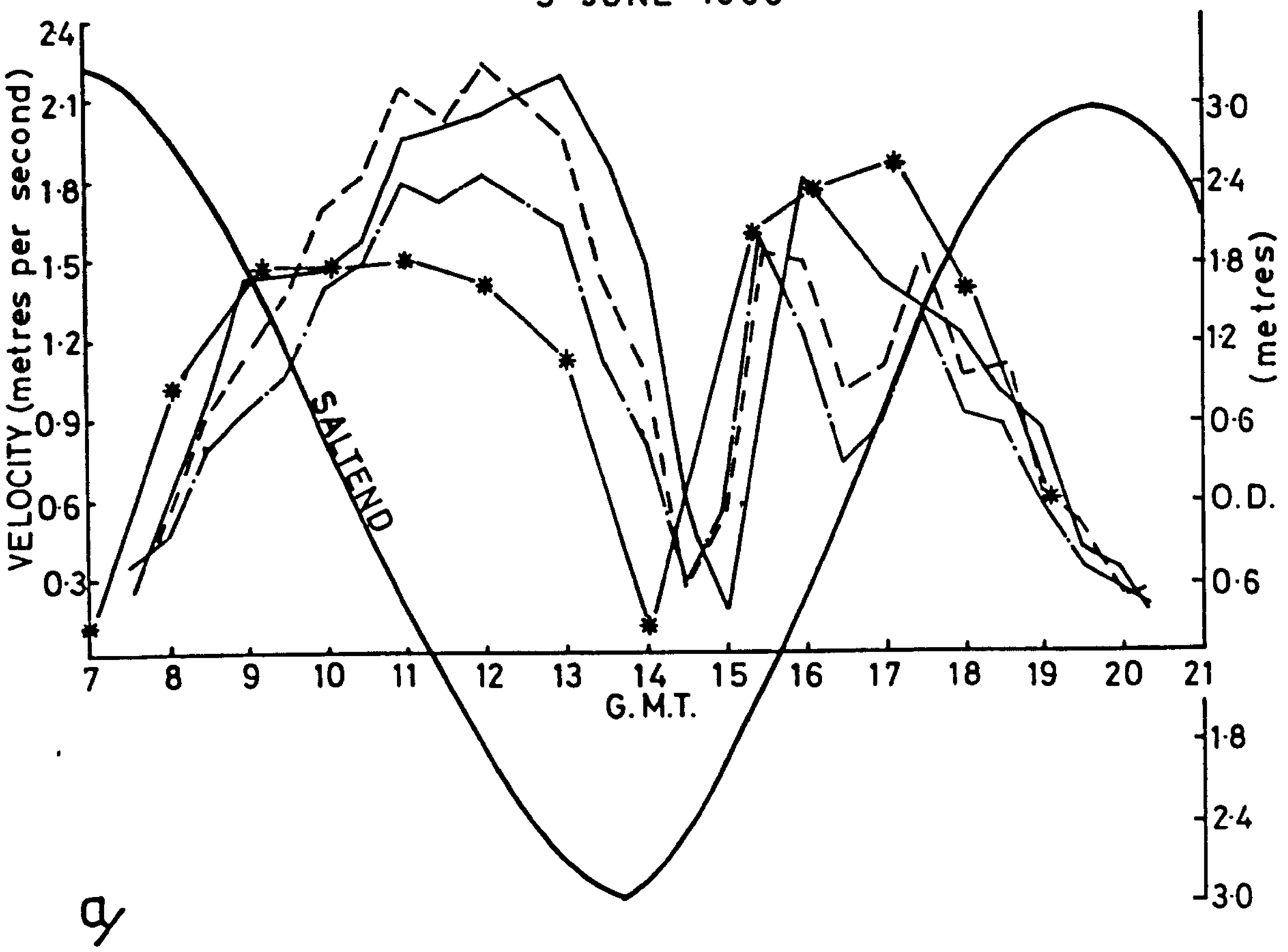

a/

POSITION 4 NEAPS
11th JUNE 1966

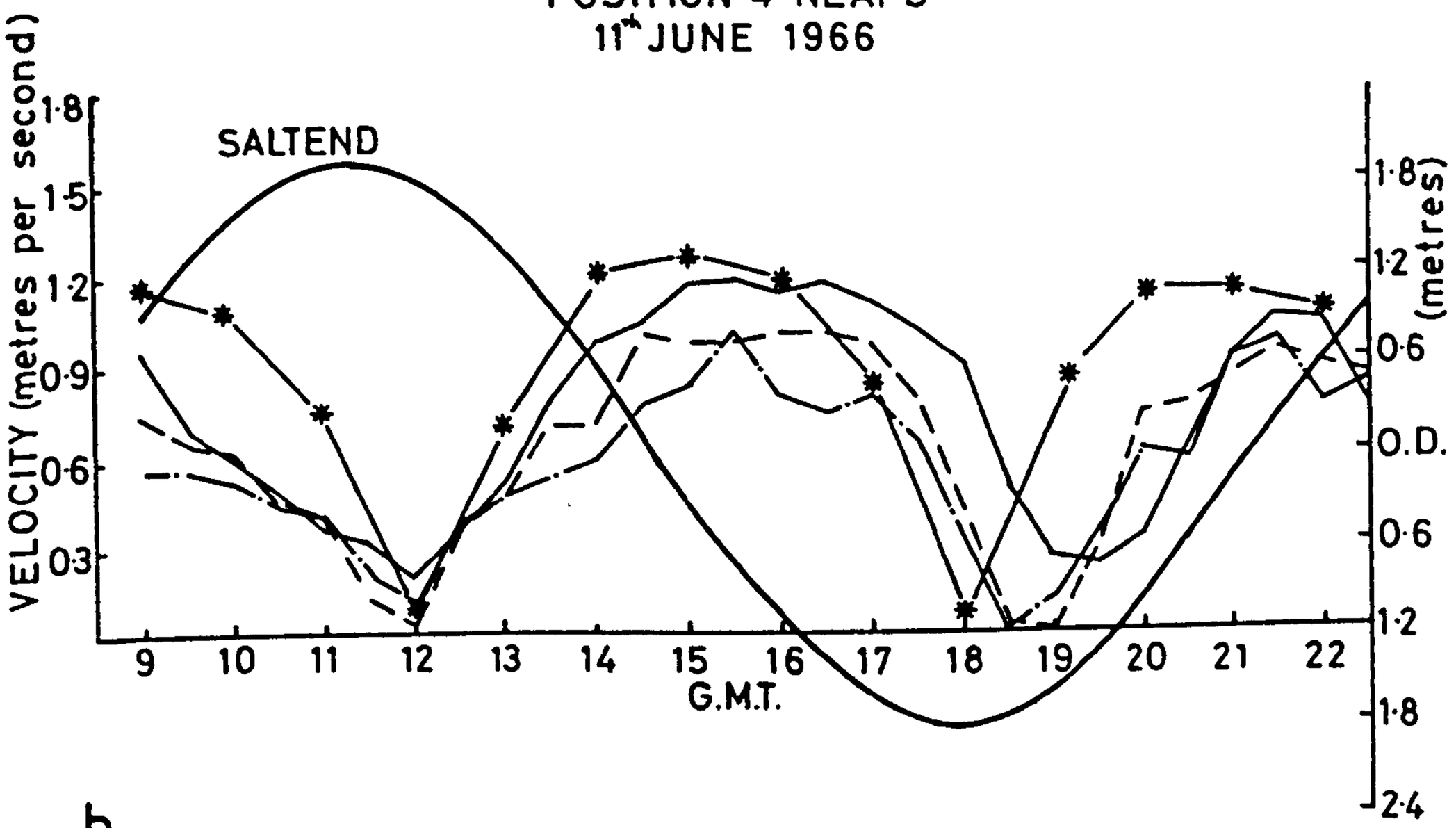

b/

SURFACE—— MID DEPTH---- 0·75 DEPTH—·— COMPUTED —*—

FIGURE 8·15

VELOCITY COMPARISONS

POSITION D SPRINGS
11th NOVEMBER 1966

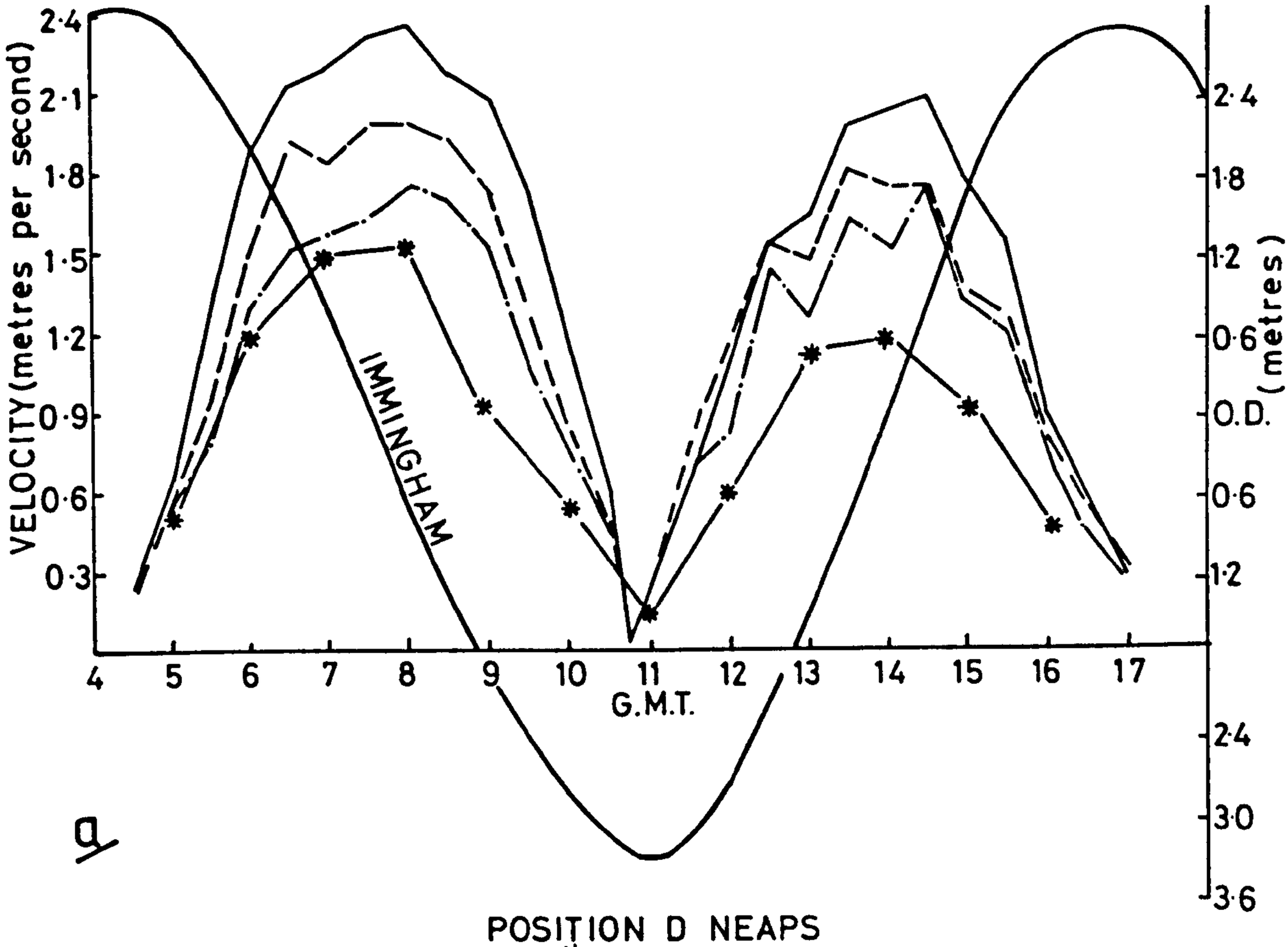

a

POSITION D NEAPS
29th JUNE 1967

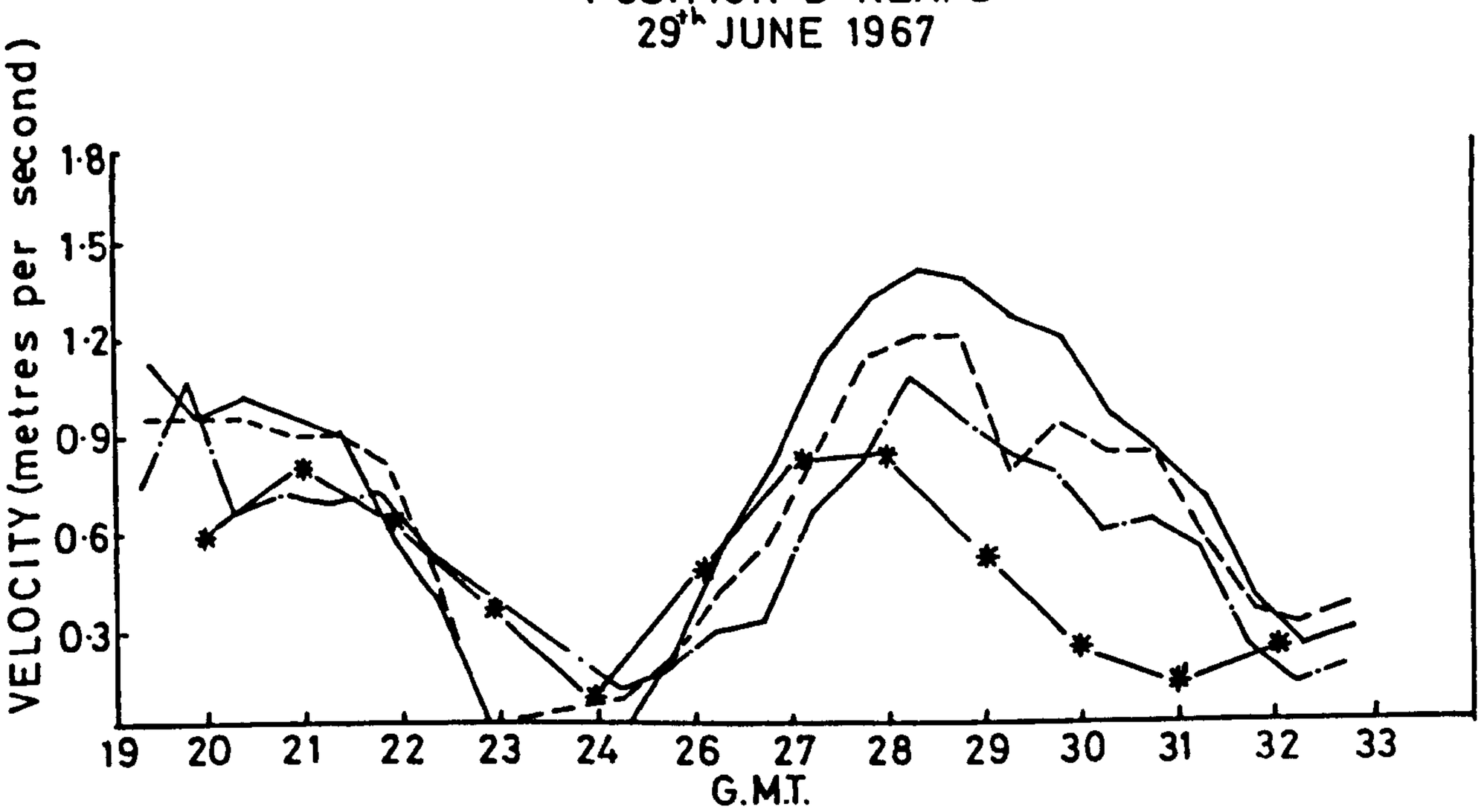

b

SURFACE —— MID DEPTH ---- 0·75 DEPTH —·— COMPUTED —*—

FIGURE 8·16

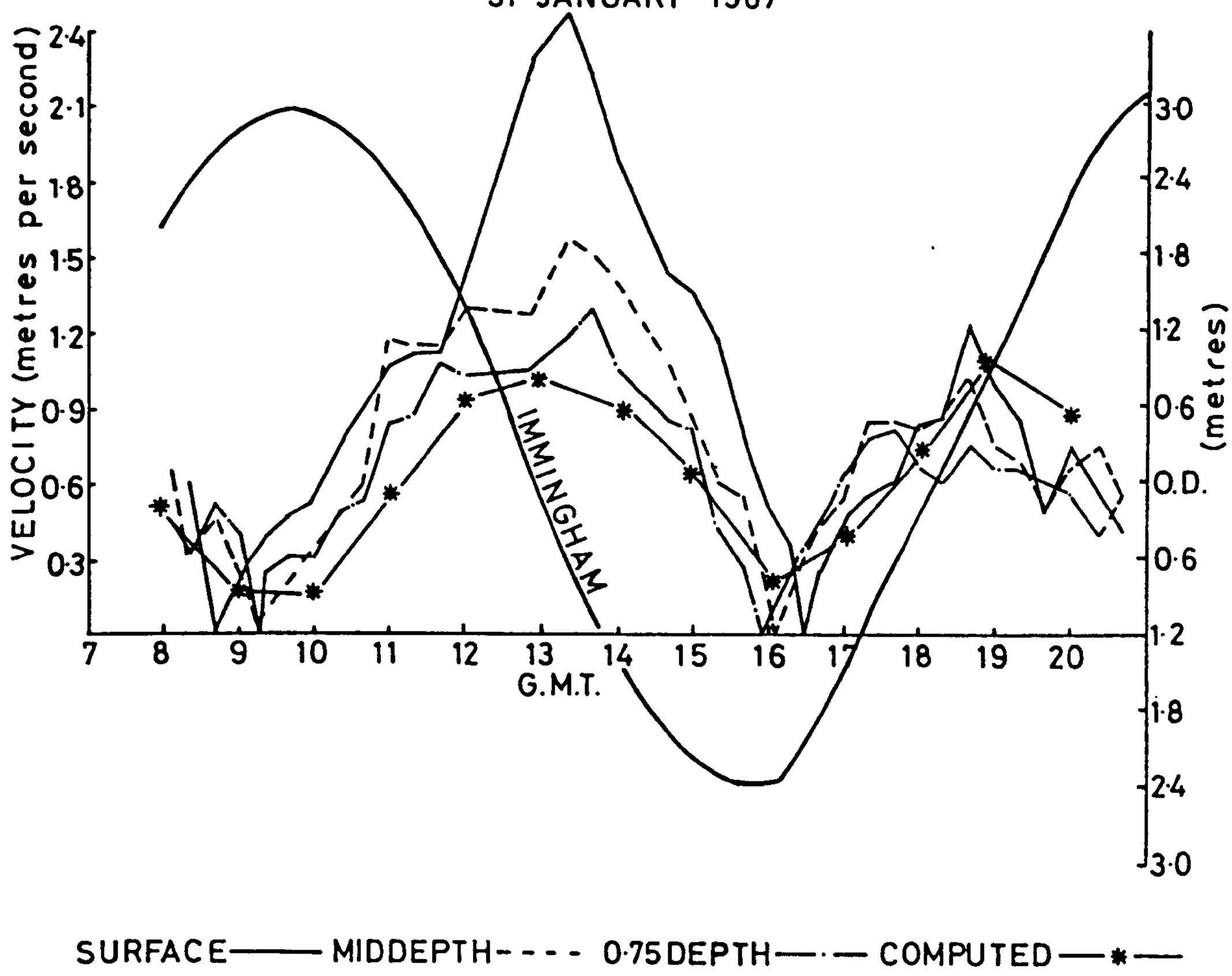
VELOCITY COMPARISONS
POSITION P SPRINGS
31ST JANUARY 1967
VELOCITY (metres per second)
2·4
2·1
1·8
1·5
1·2
0·9
0·6
0·3
IMMINGHAM
7
8
9
10
11
12
13
14
15
16
17
18
19
20
G.M.T.
3·0
2·4
1·8
1·2
0·6
O.D.
0·6
1·2
1·8
2·4
3·0
(metres)
SURFACE—— MIDDEPTH- - - - 0·75DEPTH—·— COMPUTED —*—

FIGURE 8·17

VELOCITY COMPARISONS

POSITION X SPRINGS
29th NOVEMBER 1966

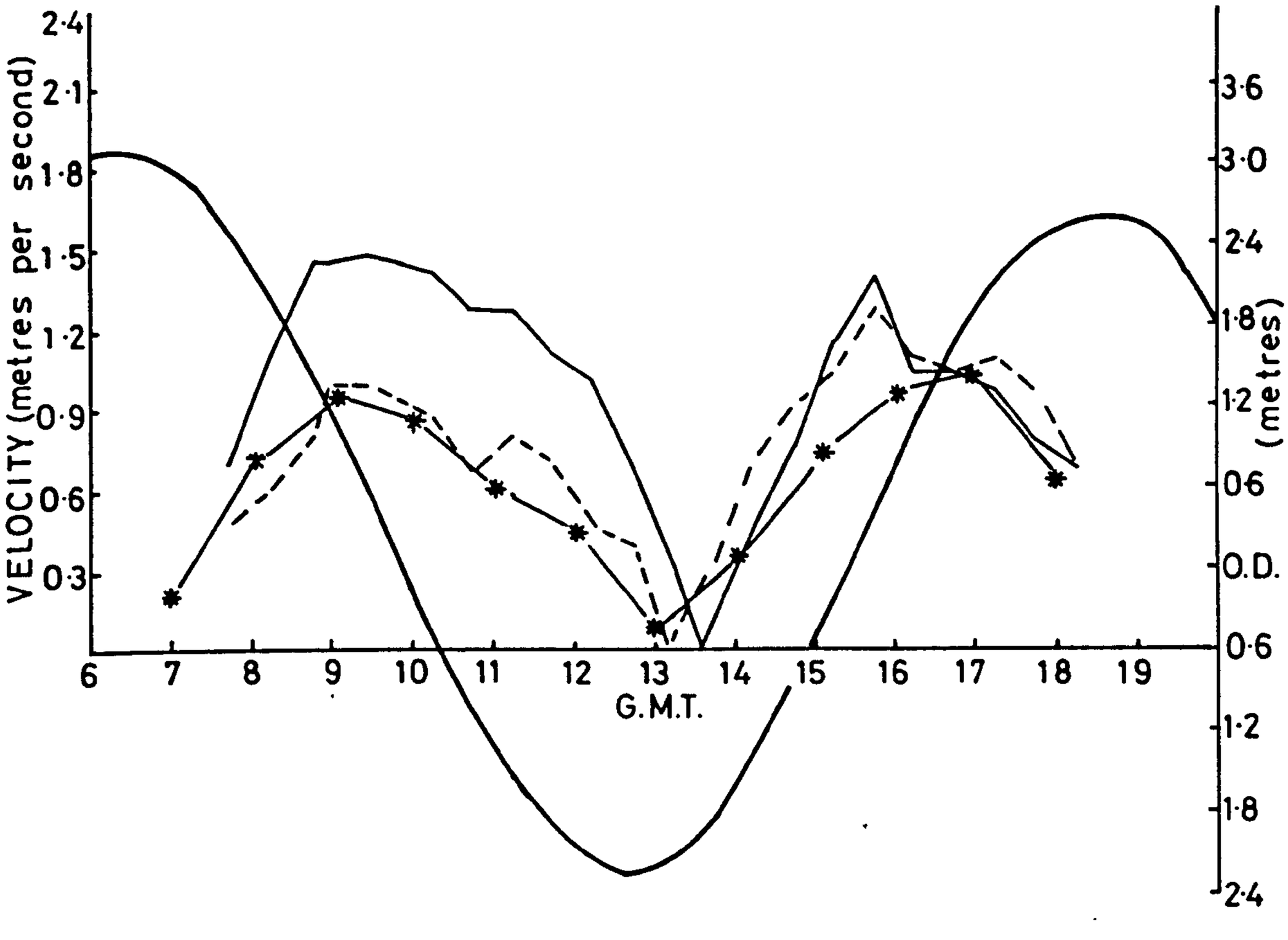

SURFACE—— MIDDEPTH- - - - COMPUTED —*—

FIGURE 8·18

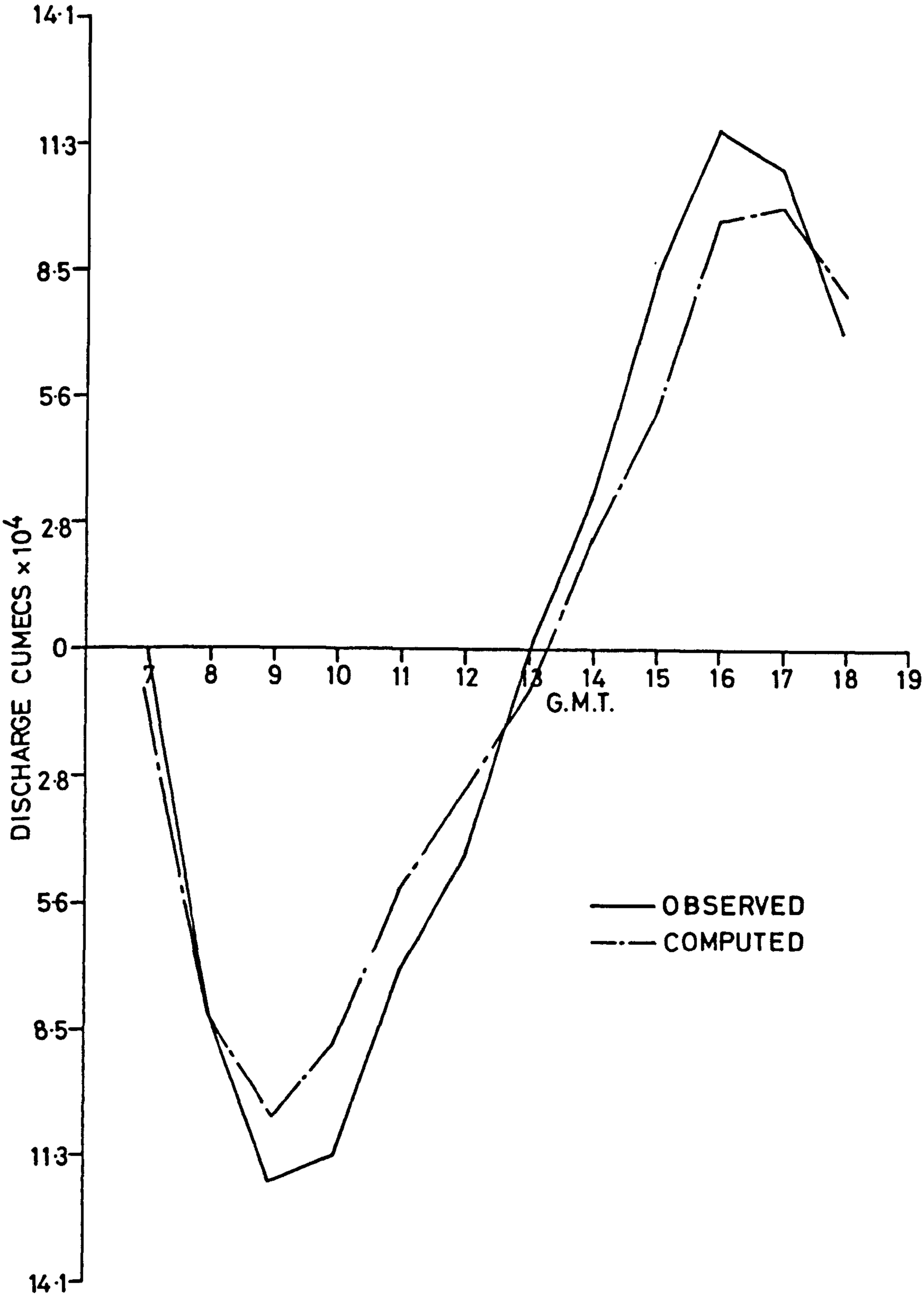

FIGURE 8·19
SPRING TIDE CUBATURE AT SPURN HEAD.

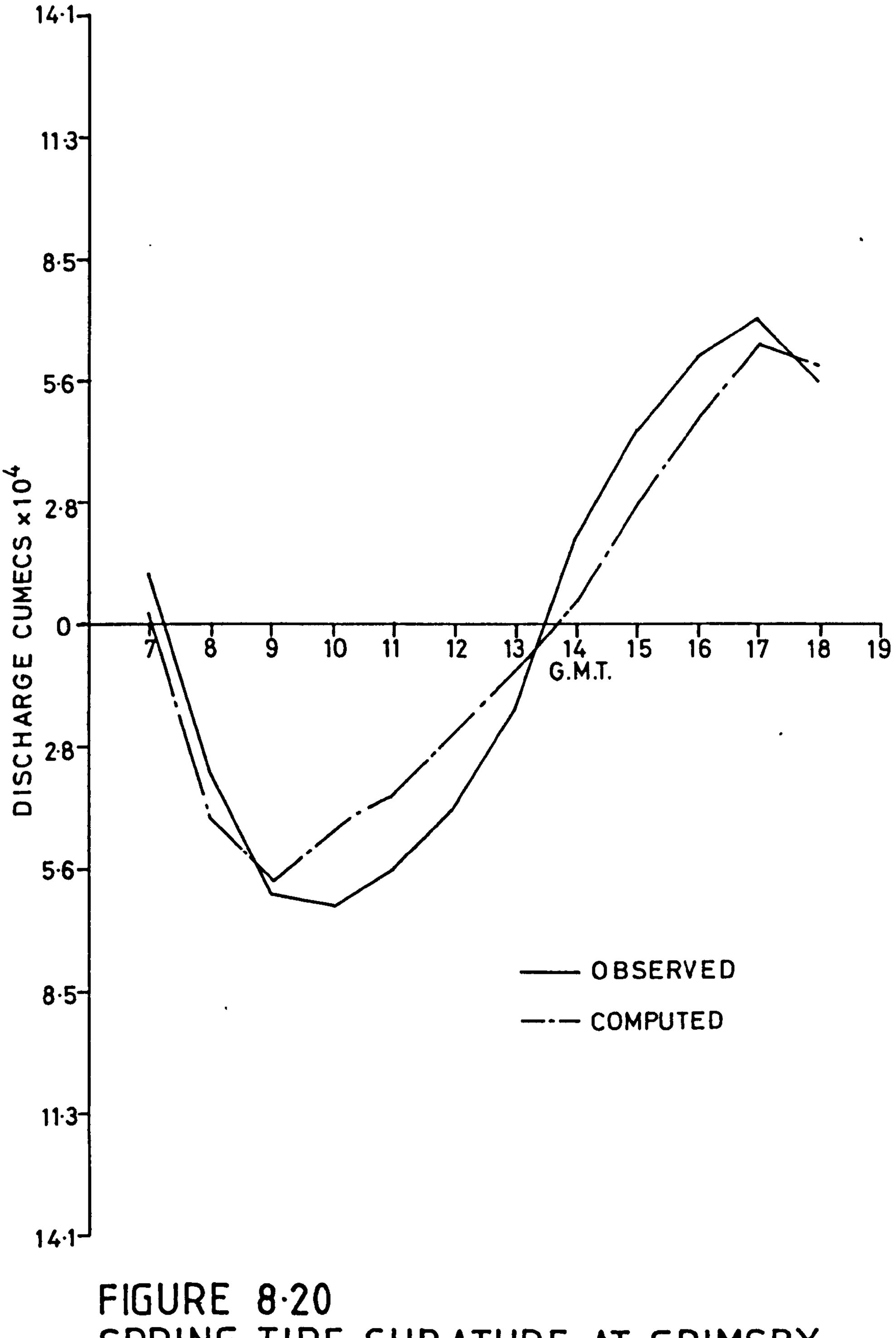

FIGURE 8·20
SPRING TIDE CUBATURE AT GRIMSBY

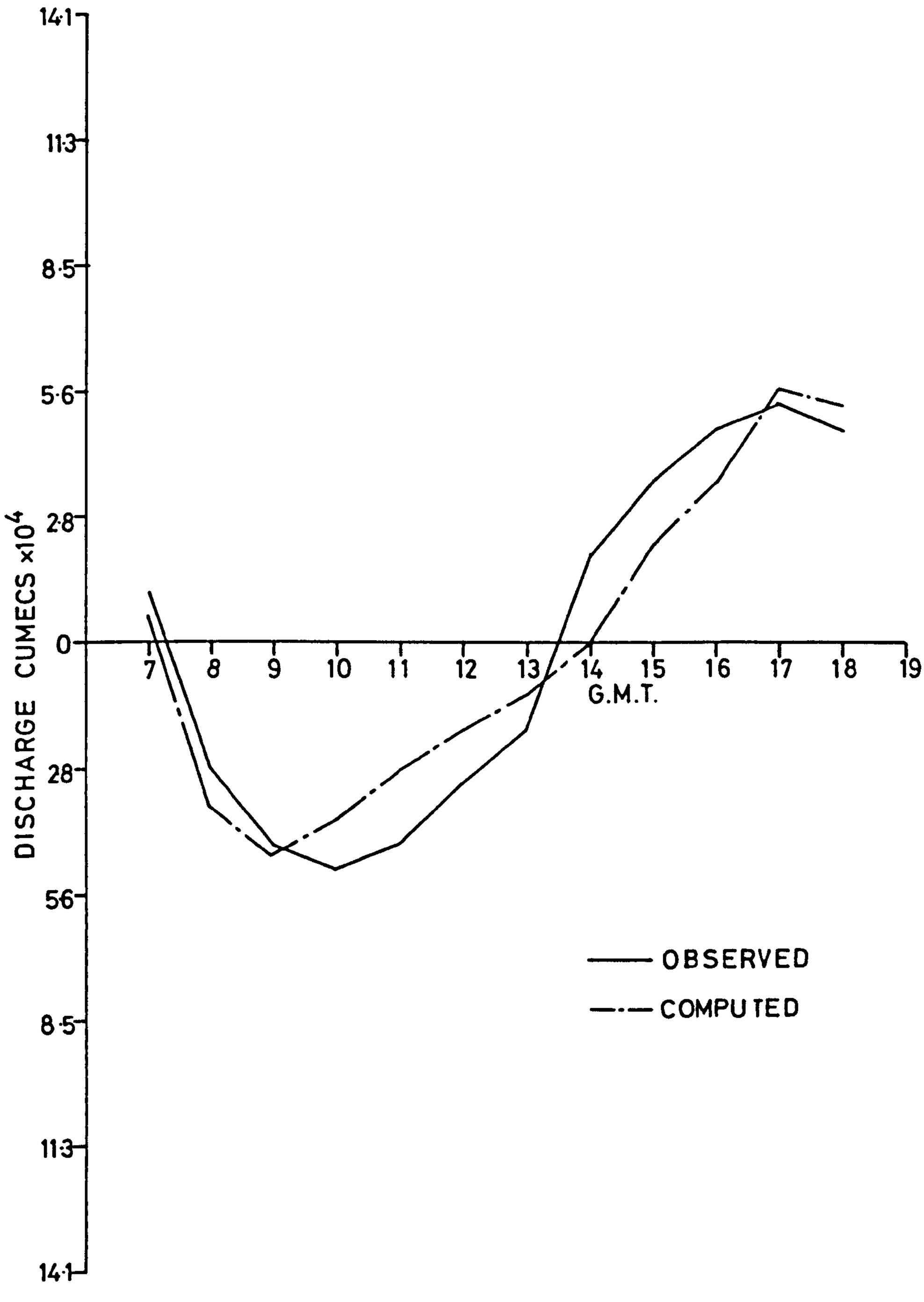

FIGURE 8·21
SPRING TIDE CUBATURE AT IMMINGHAM.

comparing computed and observed velocity magnitudes it should be remembered that the computed velocities are depth averaged and calculated using an average depth for the area around the solution node. The largest discrepancy between computed values occurs at position P and is due to the way Spurn Bight drains, see Section 8.12.

8.10.4 CUBATURE COMPARISONS

Total volumes of flow past Spurn Head, Grimsby and Immingham calculated by the numerical model are compared with the values published by the Hydraulics Research Station in Report Ex 386, see Figures 8.19 to 8.21. A reasonable agreement is obtained. It is difficult to draw further conclusions without knowledge of how the Hydraulics Research Station arrived at their estimates.

8.10.5 NEAP TIDE COMPARISONS

Further verification of the calibration and bathymetrical adjustments was gained by neap tide comparisons. Figures 8.22a to 8.22d show computed tide curves compared to observed neap tide curves on 27th July 1966. Velocity magnitudes are compared in Figures 8.12b to 8.16b. Computed neap cubatures are shown in Figure 8.23.

8.11 MODEL THREE

The results from model two were considered to show a good agreement between computed and observed values; however, three further refinements were made to the numerical model, Figure 8.24. The first of these was to provide

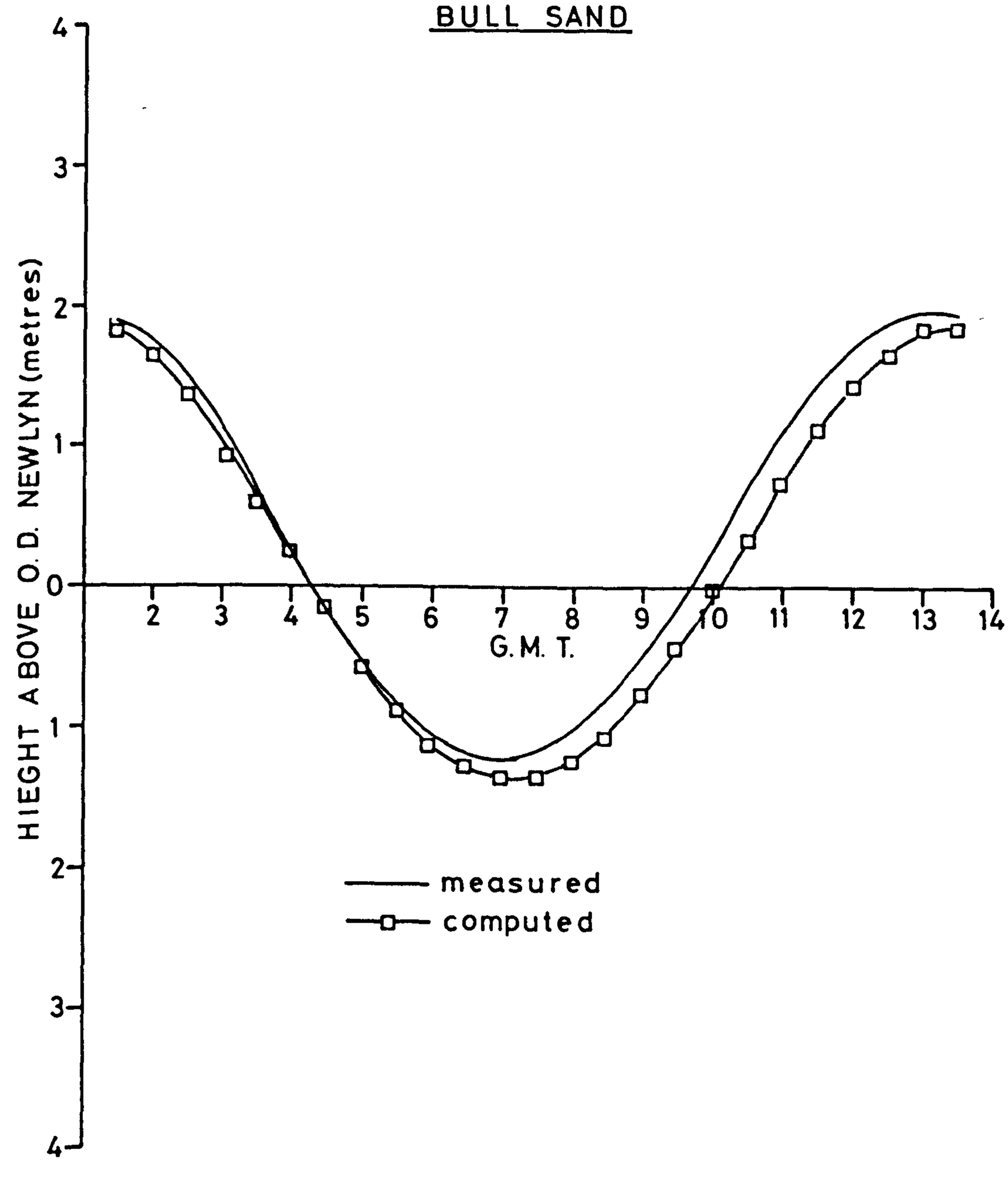

FIGURE 8·22a
COMPARISON OF NEAP TIDE CURVES

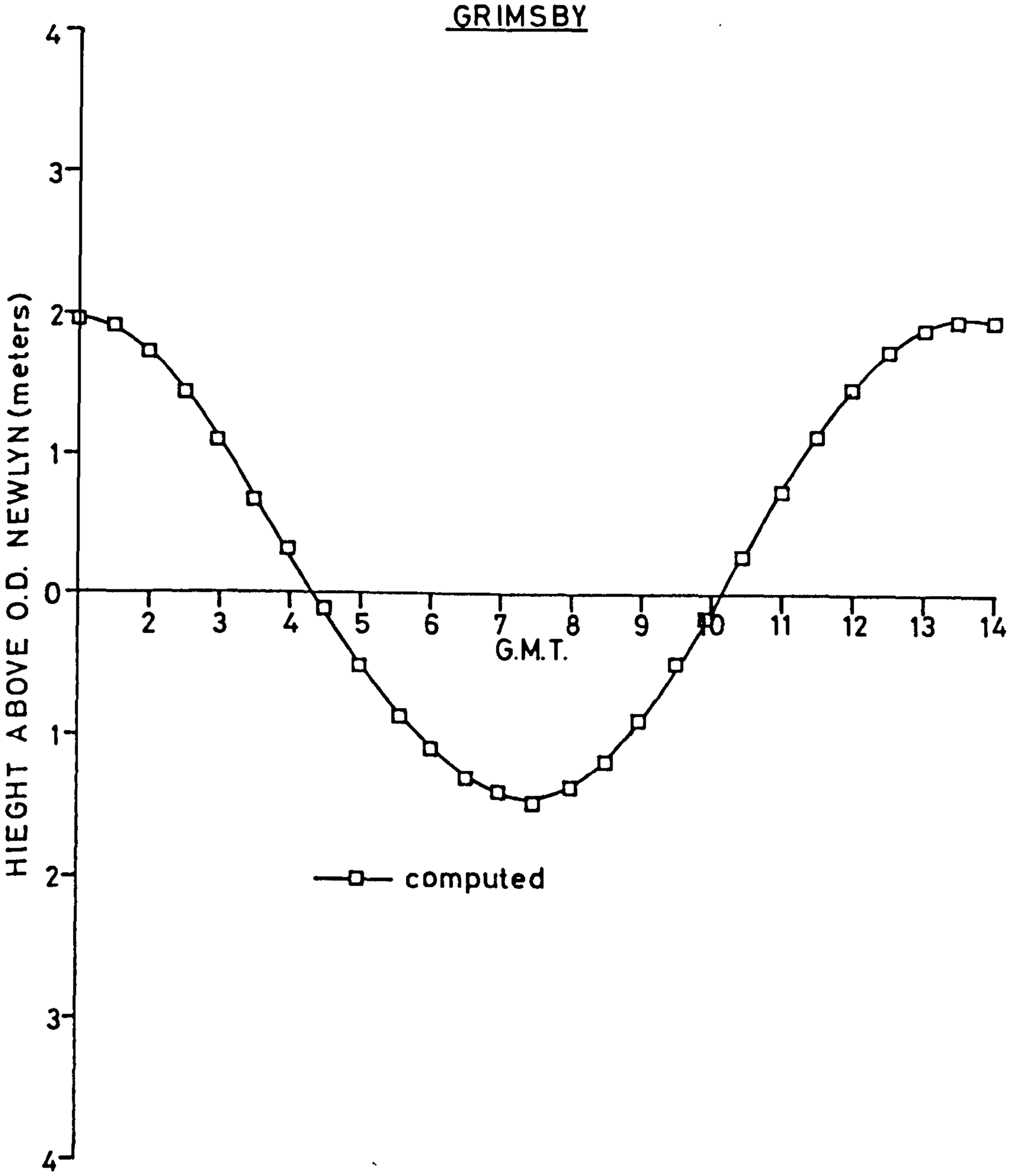

FIGURE 8·22 b
COMPUTED NEAP TIDE

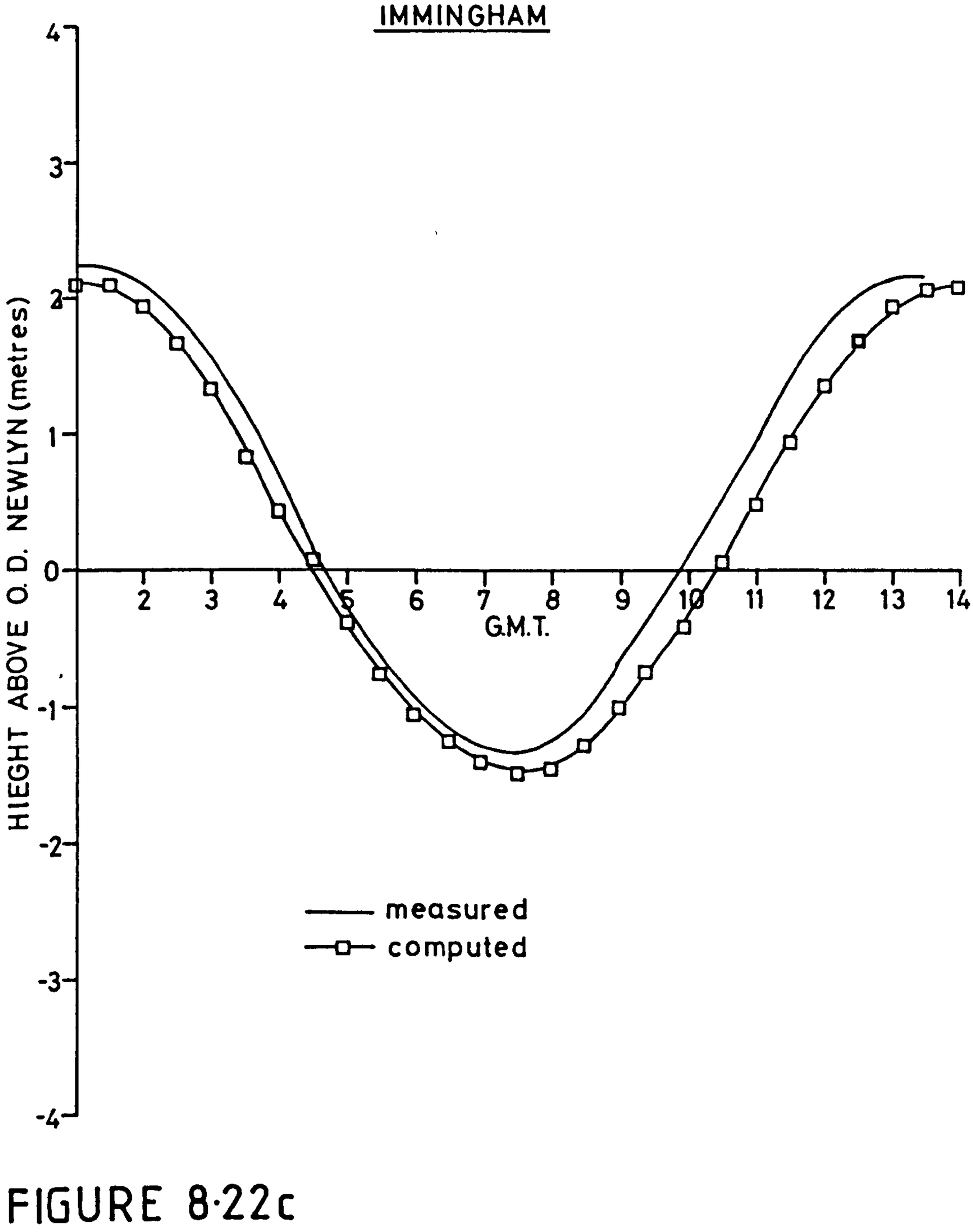

FIGURE 8·22c
COMPARISON OF NEAP TIDE CURVES

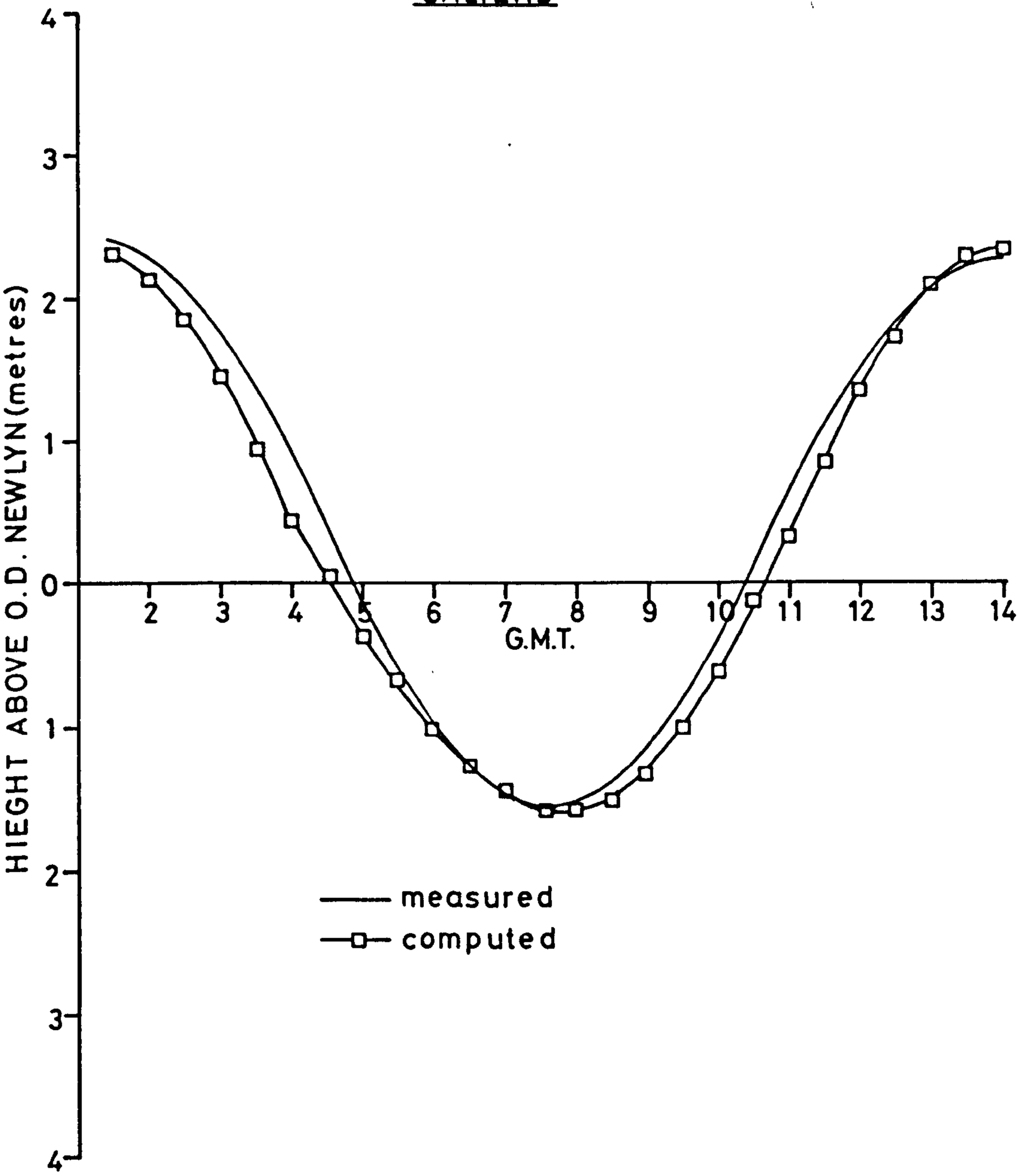

FIGURE 8·22d

COMPARISON OF NEAP TIDE CURVES

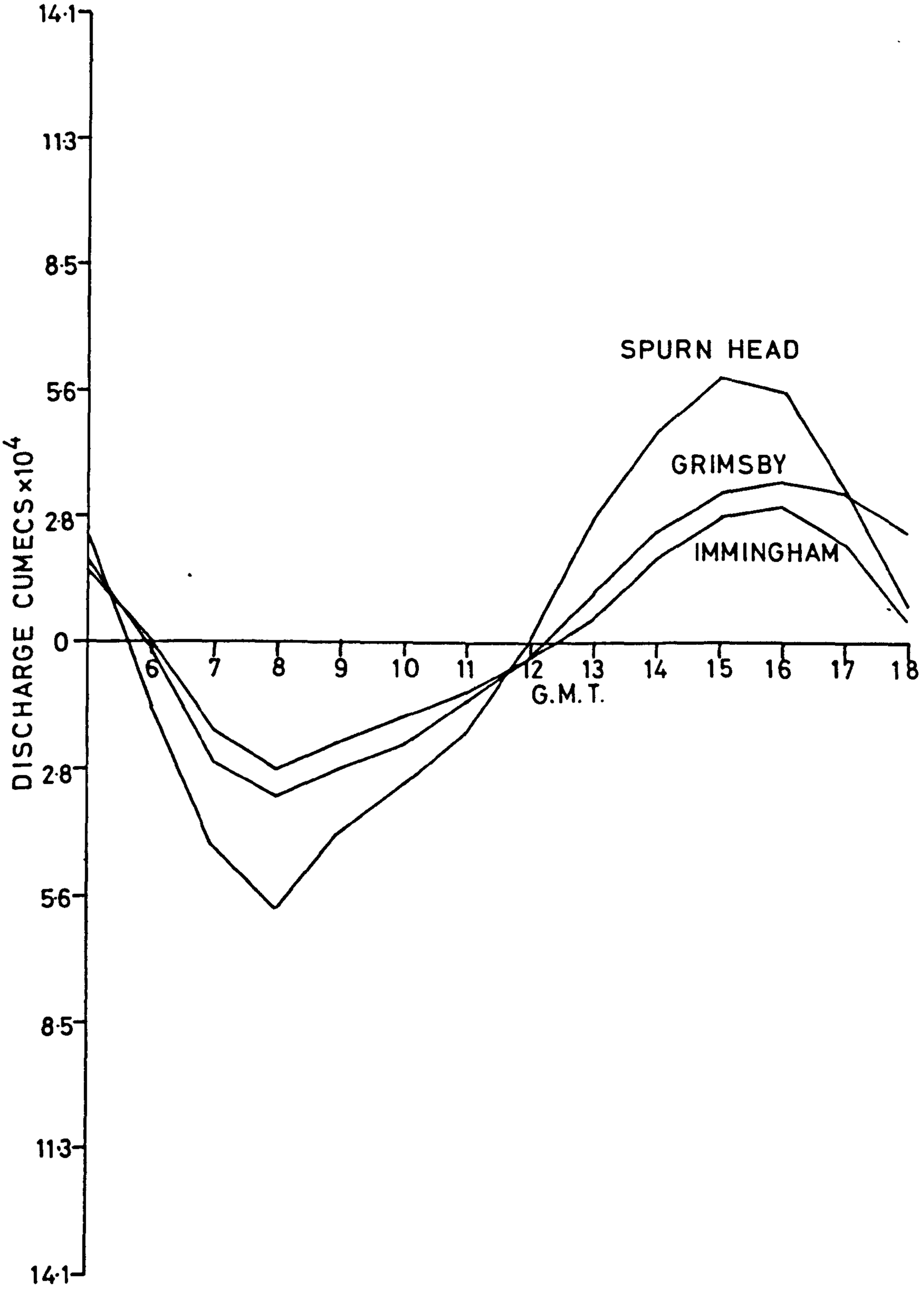

FIGURE 8·23
COMPUTED NEAP TIDE CUBATURE

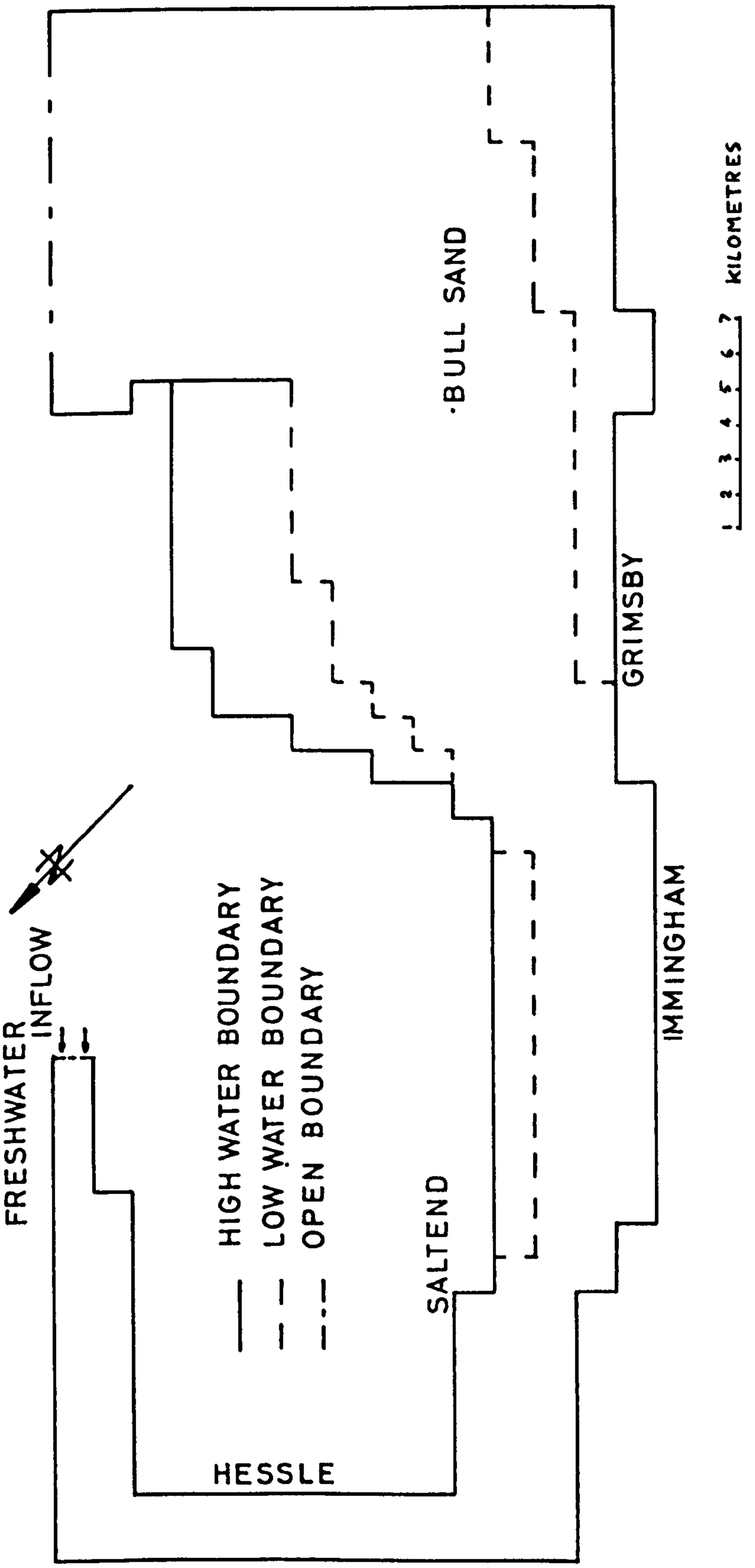
FRESHWATER INFLOW
HESSLE
BULL SAND
SALTEND
GRIMSBY
IMMINGHAM
HIGH WATER BOUNDARY
LOW WATER BOUNDARY
OPEN BOUNDARY
1 2 3 4 5 6 7 KILOMETRES

FIGURE 8·24

a more realistic representation of channel dimensions upstream of Hull. This was achieved by retaining the same equivalent free surface area but in a longer and narrower channel. Secondly, a freshwater inflow boundary condition was used at the upstream limit of the model. Average daily mean flows taken from the Humber Estuary Research Committee, Report H1, 1974, were used, see Table 8.2. The object of these refinements was to test the numerical scheme's ability to reproduce shallow water modifications to a tidal wave. Finally, the open boundary conditions were altered. As discussed in Section 8.4 models one and two used known water level conditions along two legs, Figure 8.1. In real life the nature of tide propagation in the North Sea means that currents sweep down the coast and into the mouth of the Humber in a wide arc. Haile Sand is the dividing line between this flow and the main tidal stream going down the coast. It was thought this could be better represented in the numerical model by closing the second leg of the boundary, Figure 8.24. This is similar to the open boundary condition used in the British Transport Docks Board physical model where a pneumatic tide generator along this leg of the open boundary was used to simulate tidal rise and fall.

8.12 RESULTS FROM MODEL THREE

In the main body of the Estuary from Spurn Head to Hull results from model three were little different from those of model two, shown in Figures 8.11 to 8.23.

RIVER	AVERAGE DAILY MEAN	TYPICALLY HIGH FLOW	EXTREME HIGH FLOW
TRENT	98	851	1787
YORKSHIRE OUSE	54	198	482
AIRF	37	198	326
DERWENT	17	57	114
DON	16	113	284
WHARFE	19	170	434
HULL	4	14	23

Table 8.2

FRESHWATER FLOWS INTO THE HUMBER (CUMECS)

However, velocity magnitudes at position D were increased by 21% on the flood tide. This increase brings the computed velocities closer to the observed values shown in Figure 8.16.

Although the numerical representation of the upstream portion of the Estuary has been improved it is still fairly crude; a false alignment and estimated depth are used. Even with these restrictions model three gave a reasonable reproduction of the tidal range at Hessle, Figure 8.25, the computed range being 0.114m greater than the observed range. Shallow water distortion of the wave has been successfully reproduced; the rising limb of the computed tidal curve taking a period of 5 hours the same as the observed tidal curve, the computed falling limb takes 7 hours 20 minutes compared with 7 hcurs for the observed. The distortion of the tidal wave as it moves up the Estuary can be seen from the simultaneous computed tidal curves shown in Figure 8.26.

Comparing model three velocity vectors in Figures 8.27a to 8.27m with those of model one, Figures 8.5a to 8.5m, the changes in flow patterns seaward of Spurn Head are evident. The model three flow pattern at times 2 hours and 9 hours can be compared with the flow patterns, obtained from float tracking experiments carried out by the Hydraulics Research Station, Report Ex 386, 1968, for peak flow patterns on the flood and ebb tide, Figures 8.28a and 8.28b. The general trend of the tidal streams has been faithfully reproduced. An area of disagreement

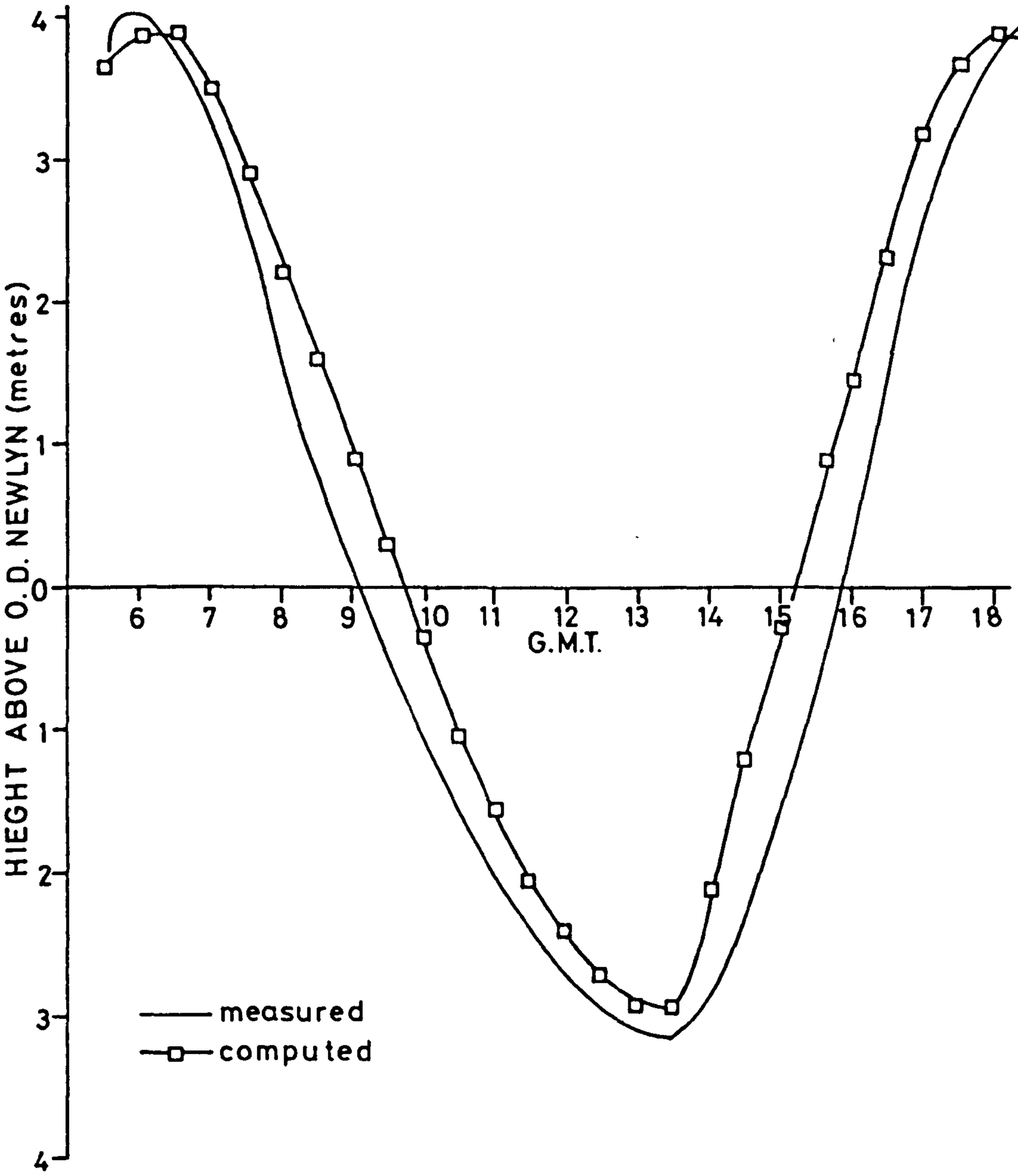

FIGURE 8·25
COMPARISON OF SPRING TIDE CURVES

FIGURE 8·26
SIMULTANEOUS COMPUTED TIDE CURVES

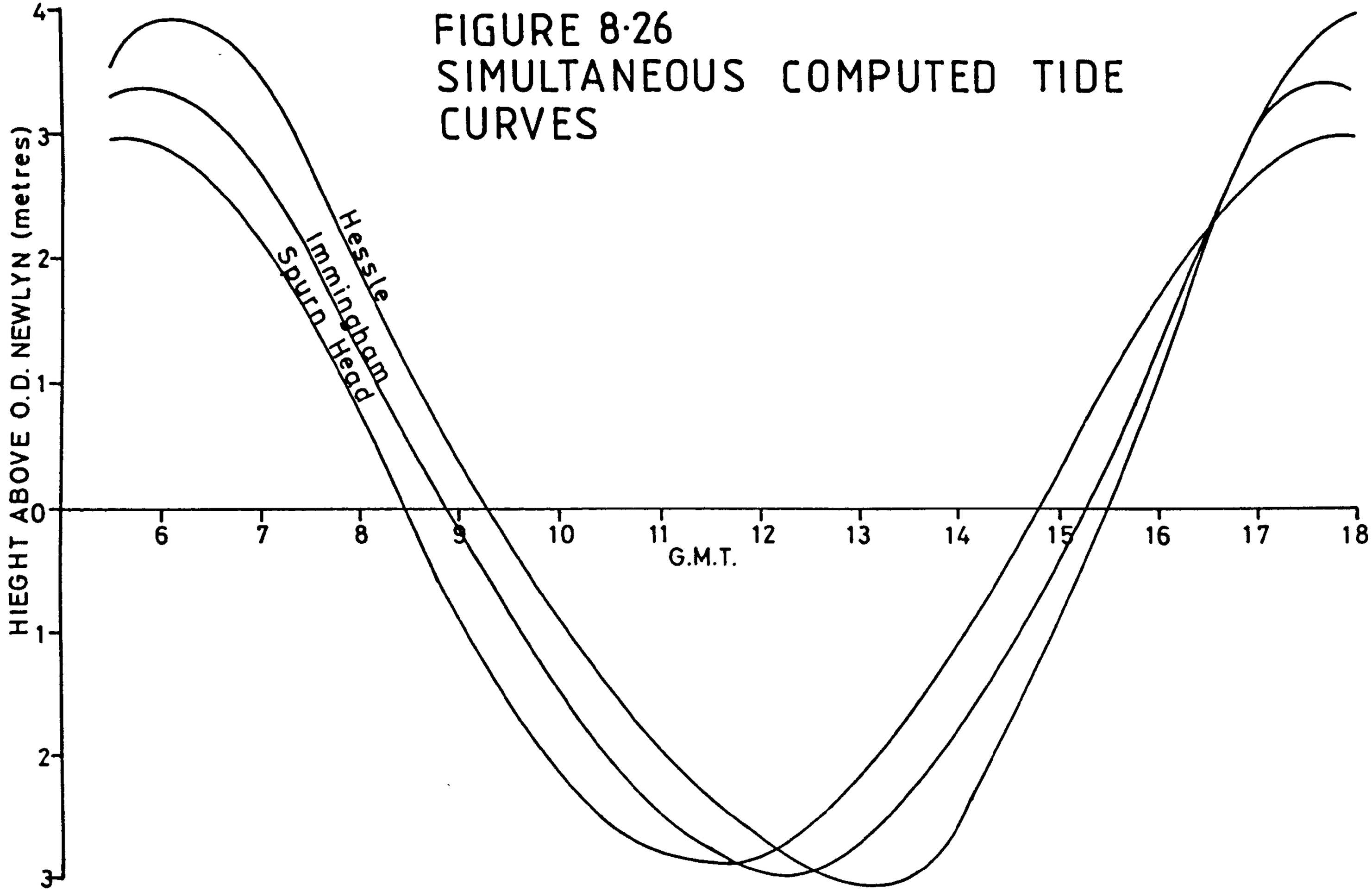

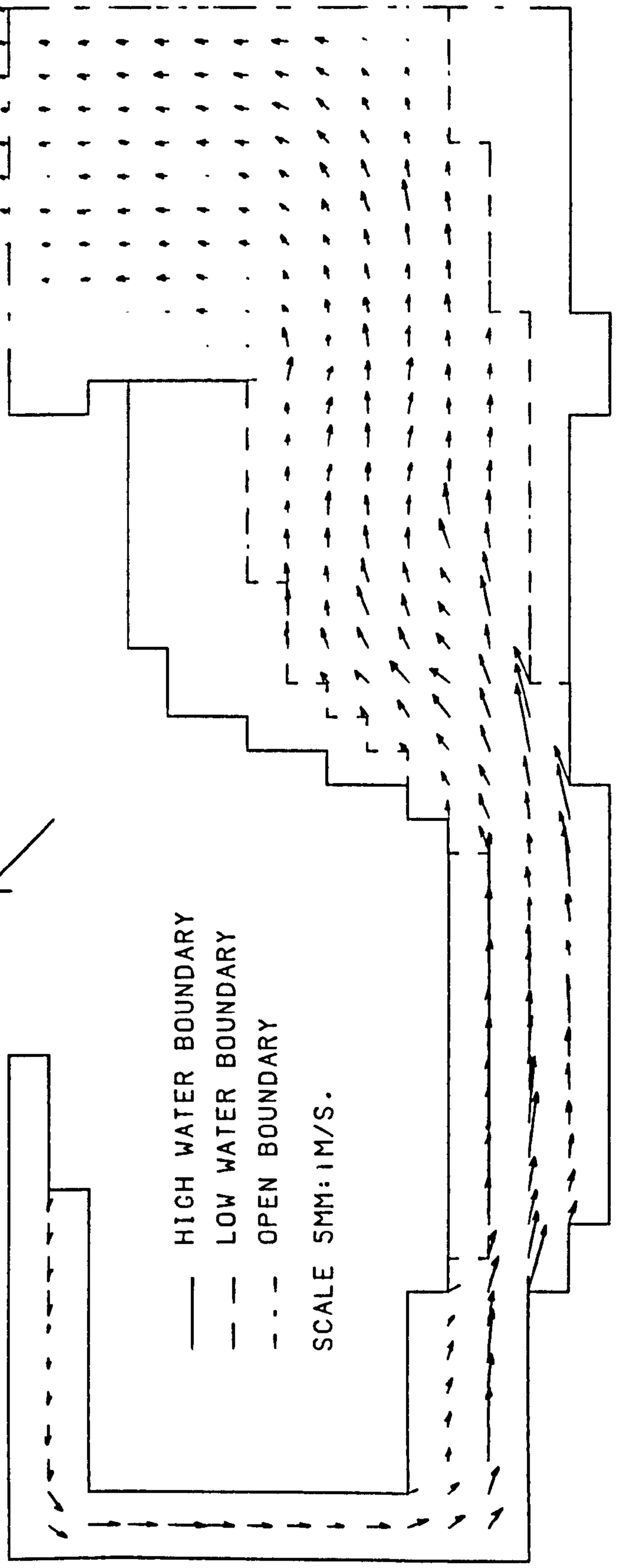

FIGURE 8·27a
SPRING TIDE VELOCITIES IN THE HUMBER ESTUARY.
TIME FROM START OF TIDAL CYCLE HOURS= 0.00

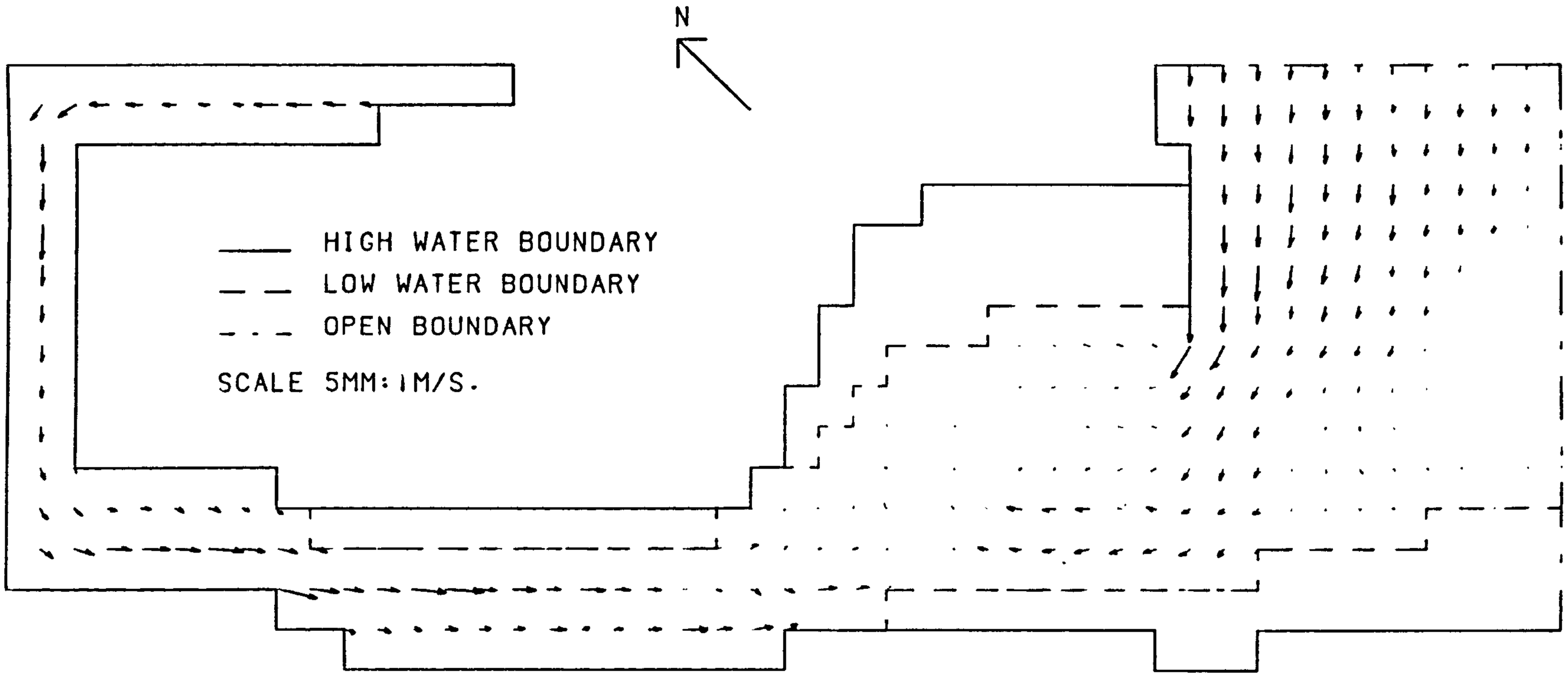

FIGURE 8·27b
SPRING TIDE VELOCITIES IN THE HUMBER ESTUARY.
TIME FROM START OF TIDAL CYCLE HOURS= 1.00

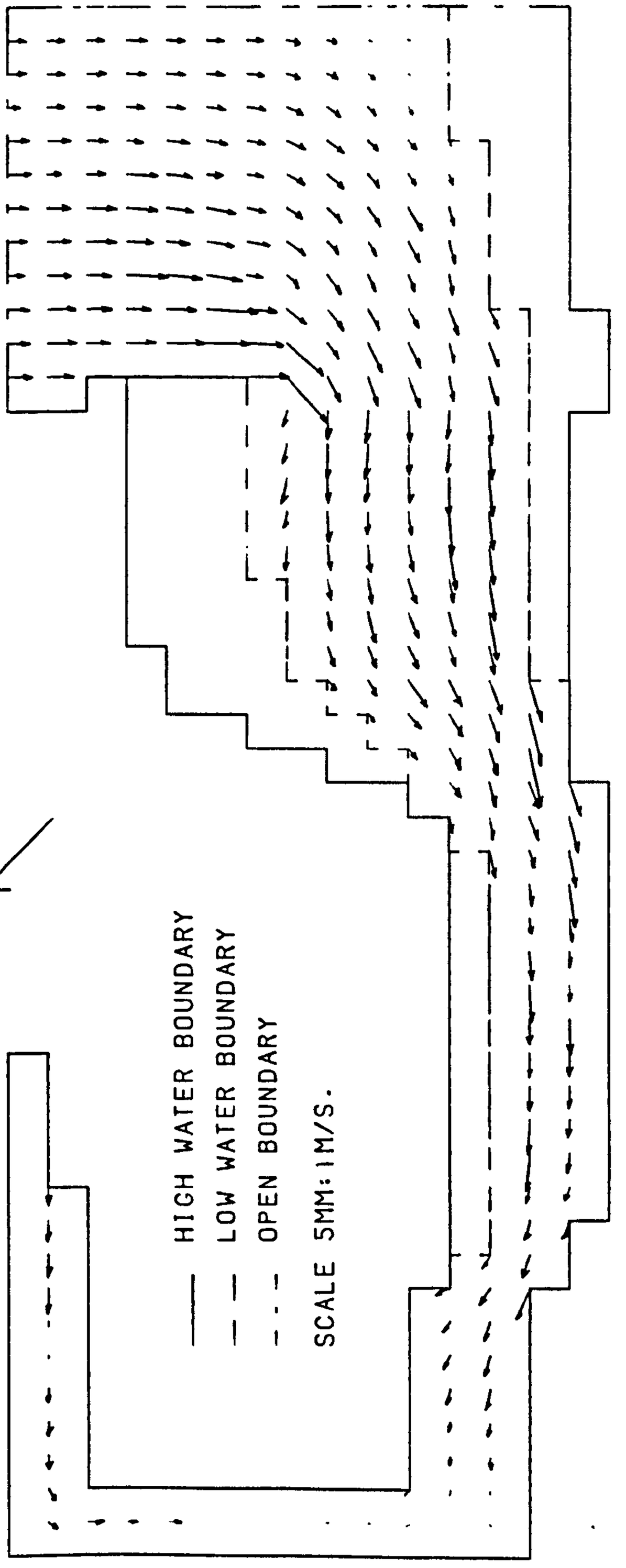

FIGURE 8.27c
SPRING TIDE VELOCITIES IN THE HUMBER ESTUARY.
TIME FROM START OF TIDAL CYCLE HOURS= 2.00

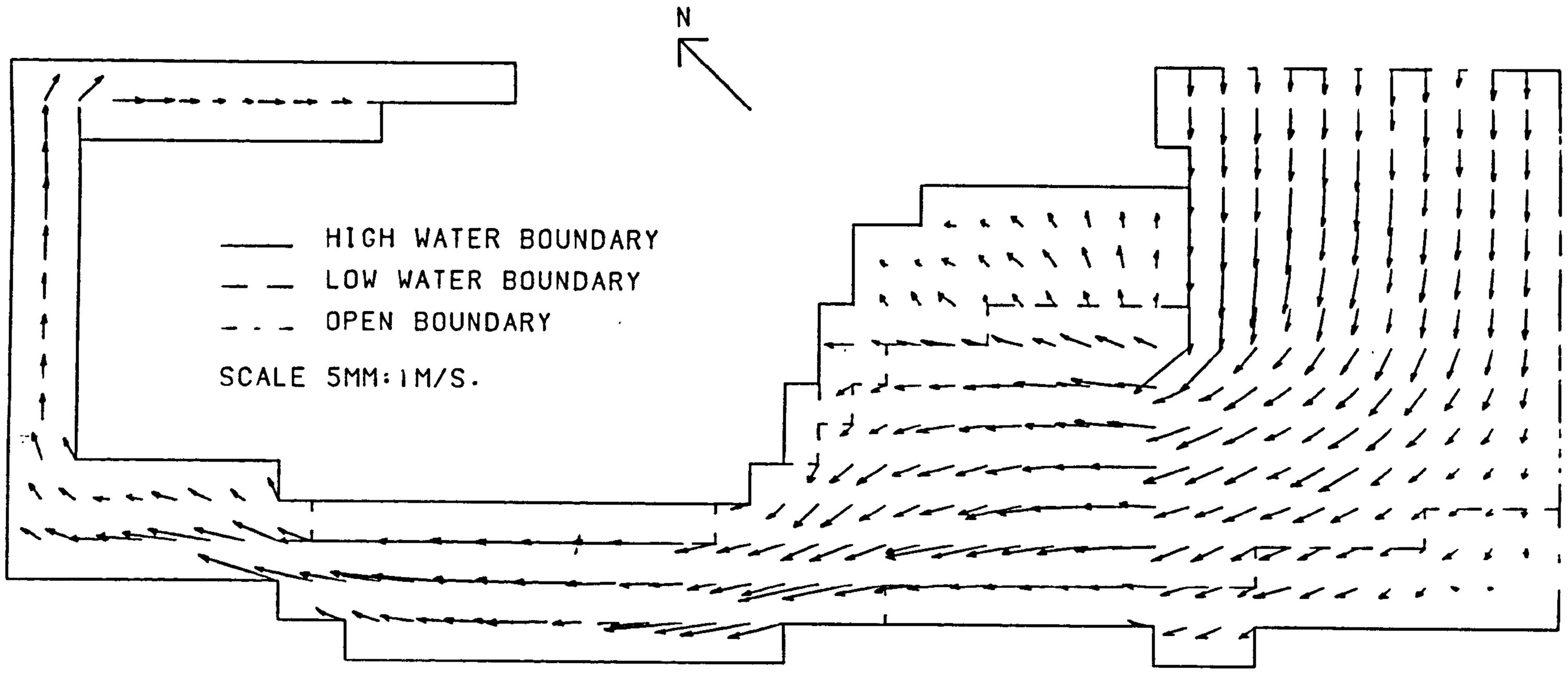

FIGURE 8·27d
SPRING TIDE VELOCITIES IN THE HUMBER ESTUARY.
TIME FROM START OF TIDAL CYCLE HOURS= 3.00

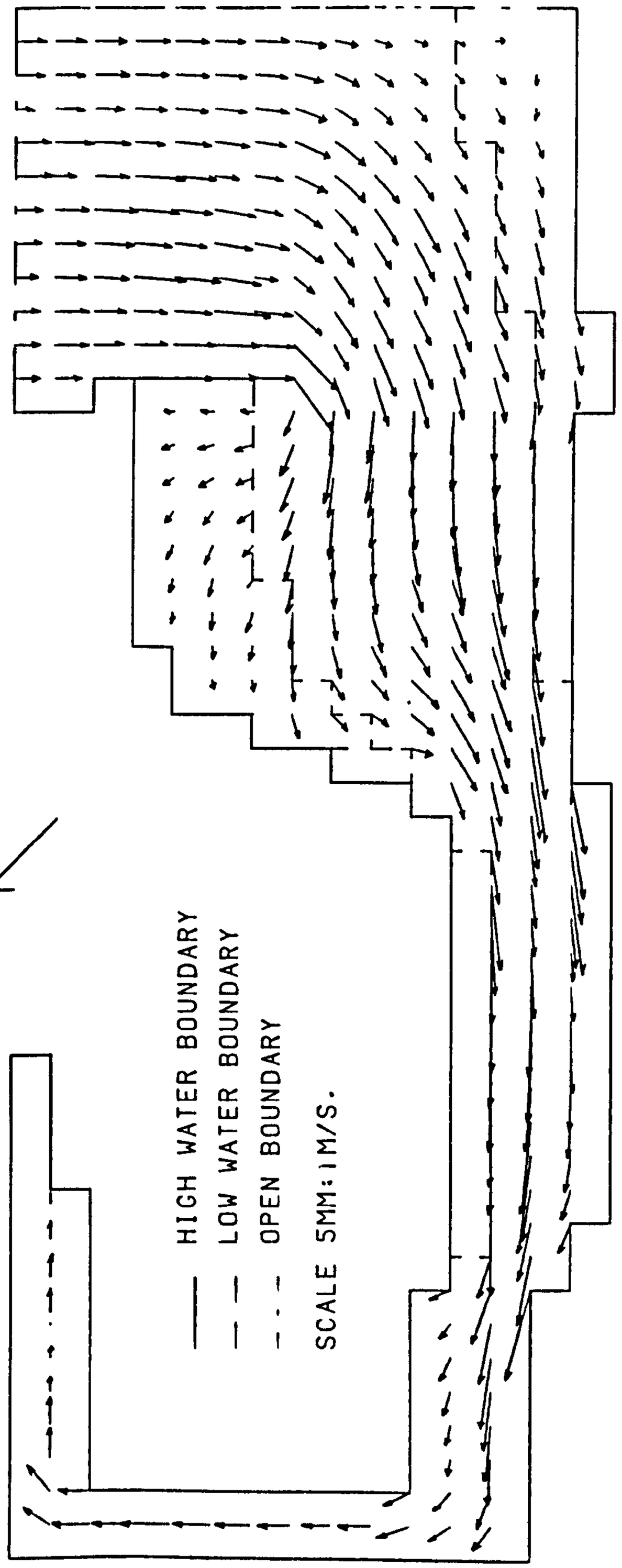

FIGURE 8·27e
SPRING TIDE VELOCITIES IN THE HUMBER ESTUARY.
TIME FROM START OF TIDAL CYCLE HOURS= 4.00

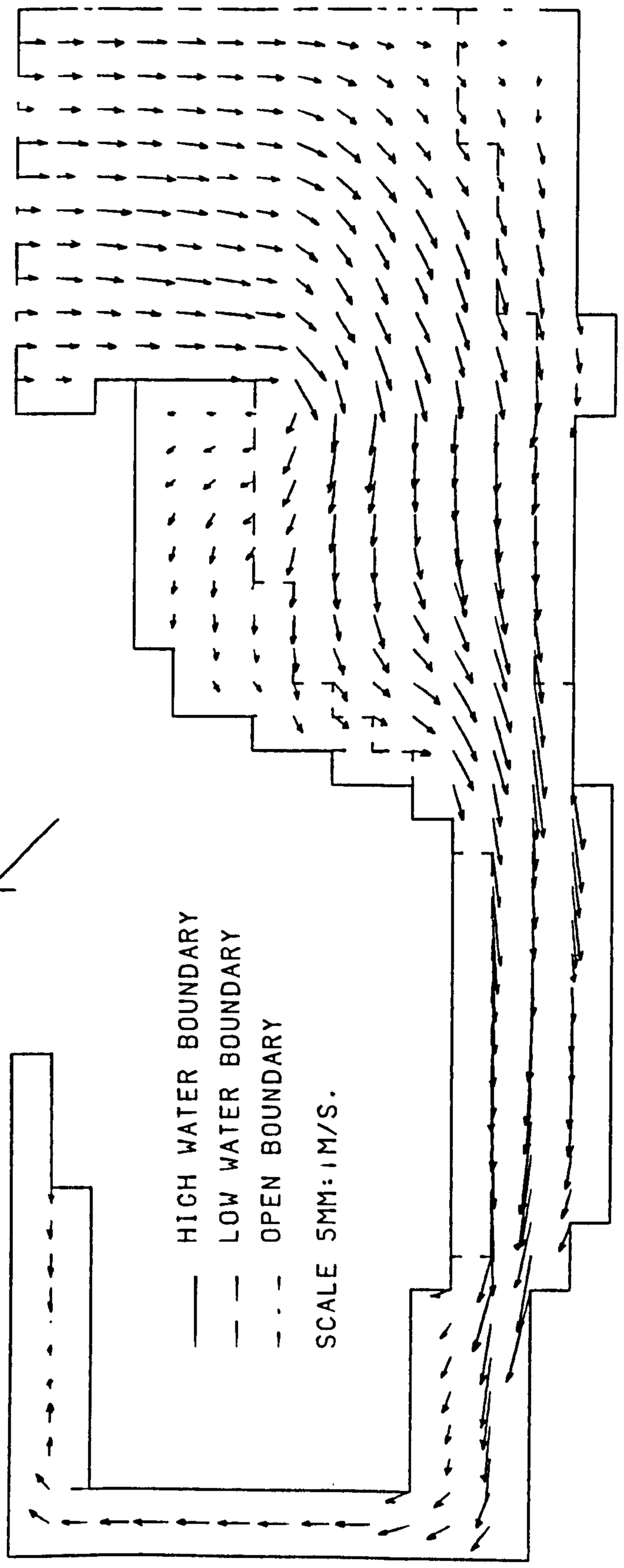

FIGURE 8.27
SPRING TIDE VELOCITIES IN THE HUMBER ESTUARY.
TIME FROM START OF TIDAL CYCLE HOURS= 5.00

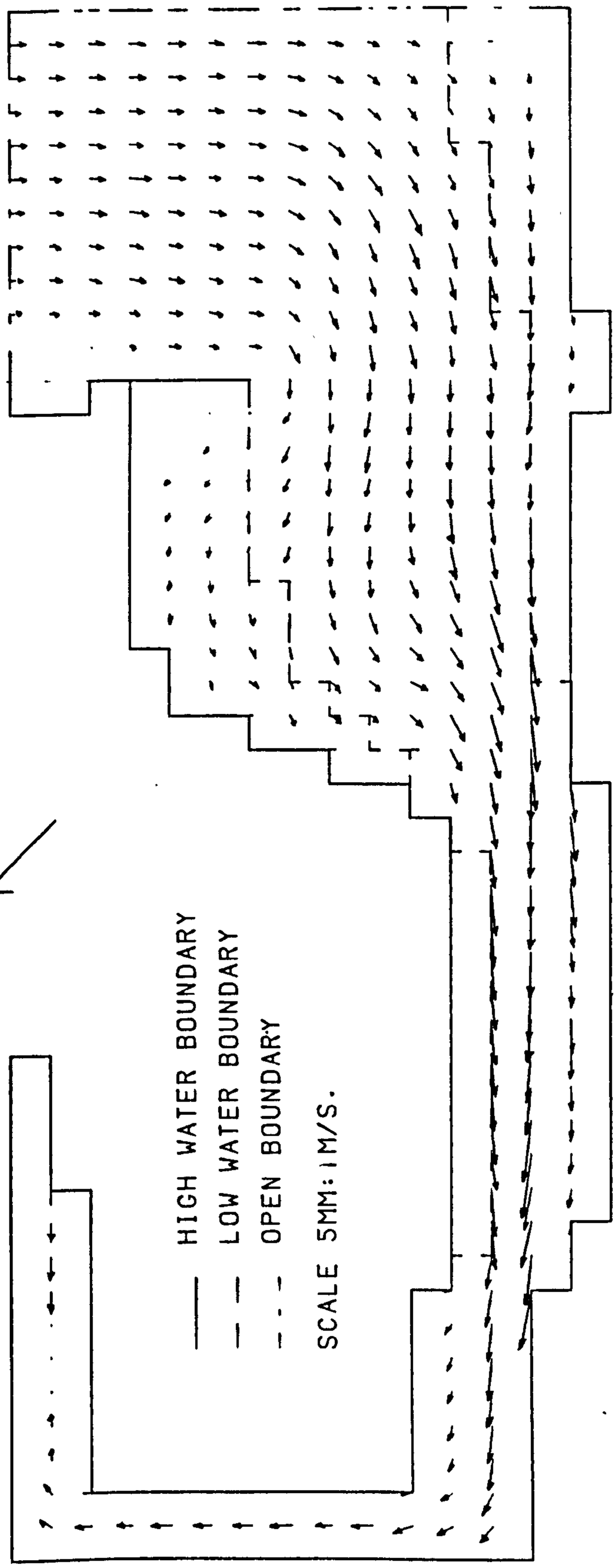

FIGURE 8·27g
SPRING TIDE VELOCITIES IN THE HUMBER ESTUARY.
TIME FROM START OF TIDAL CYCLE HOURS= 6.00

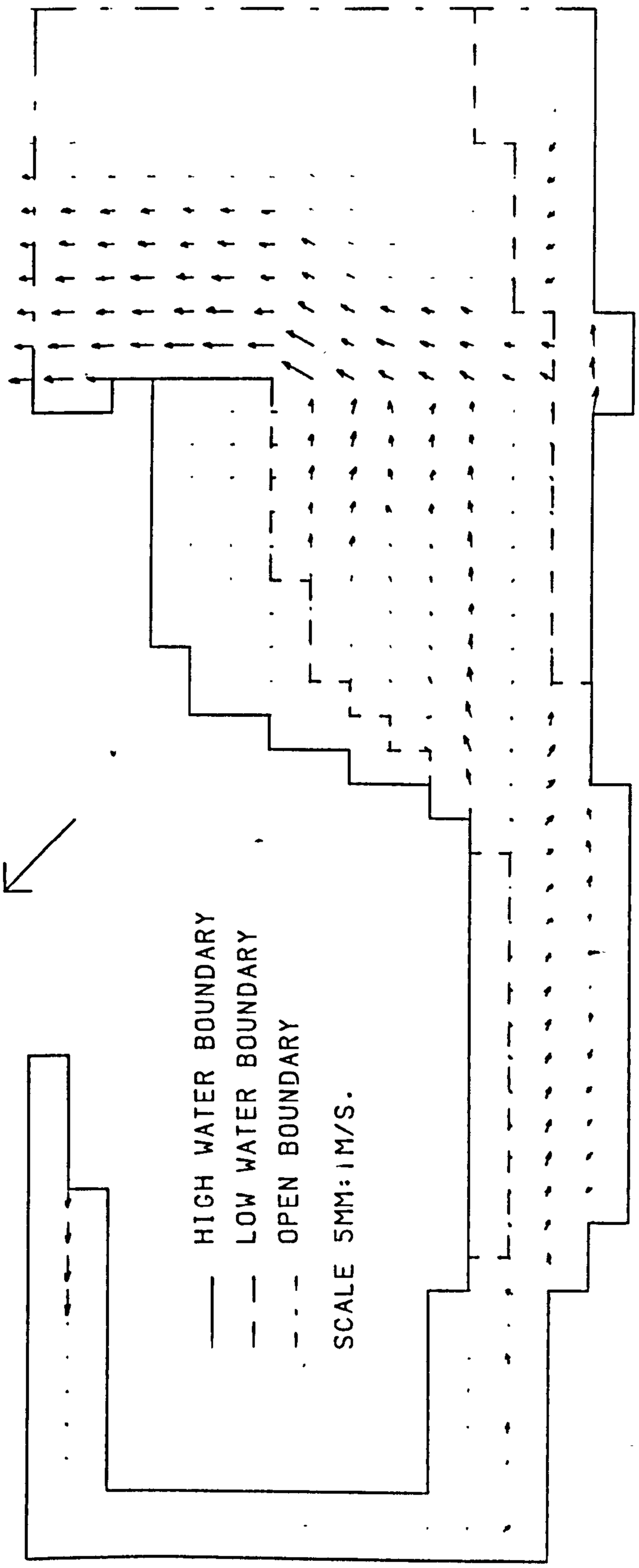

FIGURE 8.27 h
SPRING TIDE VELOCITIES IN THE HUMBER ESTUARY.
TIME FROM START OF TIDAL CYCLE HOURS= 7.00

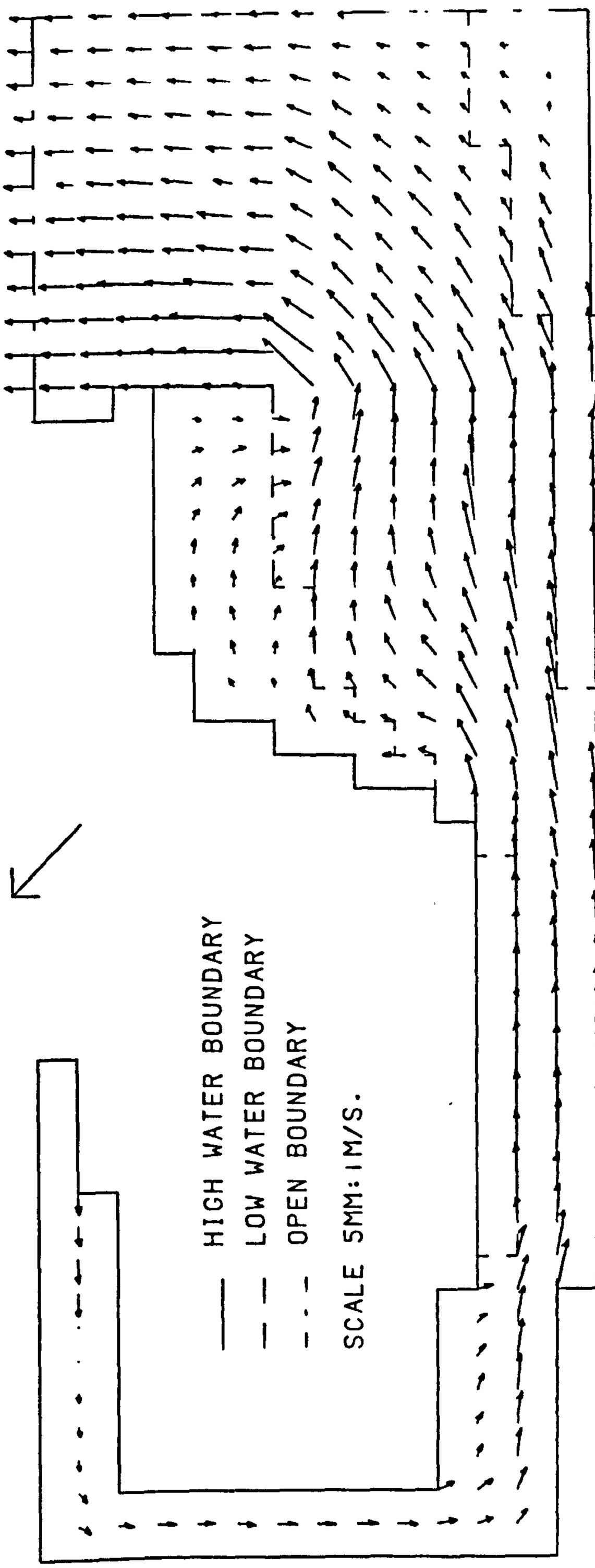

FIGURE 8.27i
SPRING TIDE VELOCITIES IN THE HUMBER ESTUARY.
TIME FROM START OF TIDAL CYCLE HOURS= 8.00

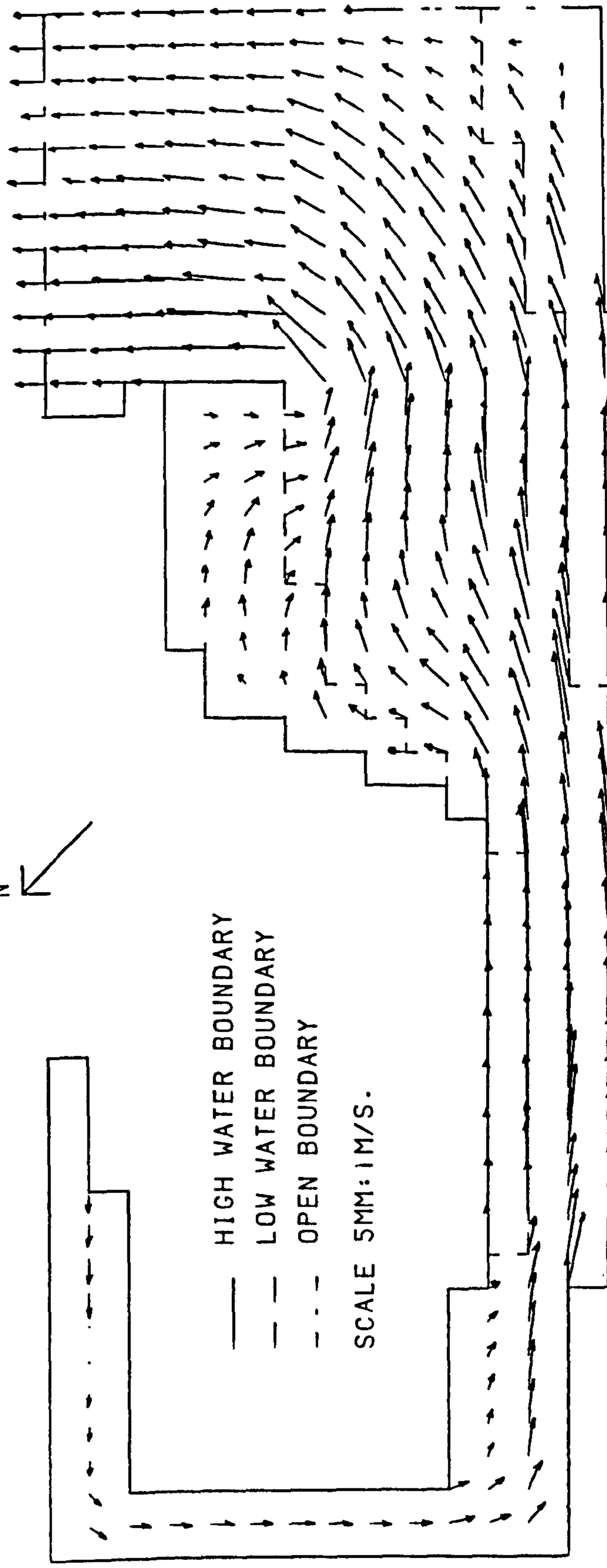

FIGURE 8·27j HUMBER ESTUARY.
SPRING TIDE VELOCITIES IN THE HORIZONTAL PLANE
TIME FROM START OF TIDAL CYCLE HOURS= 9.00

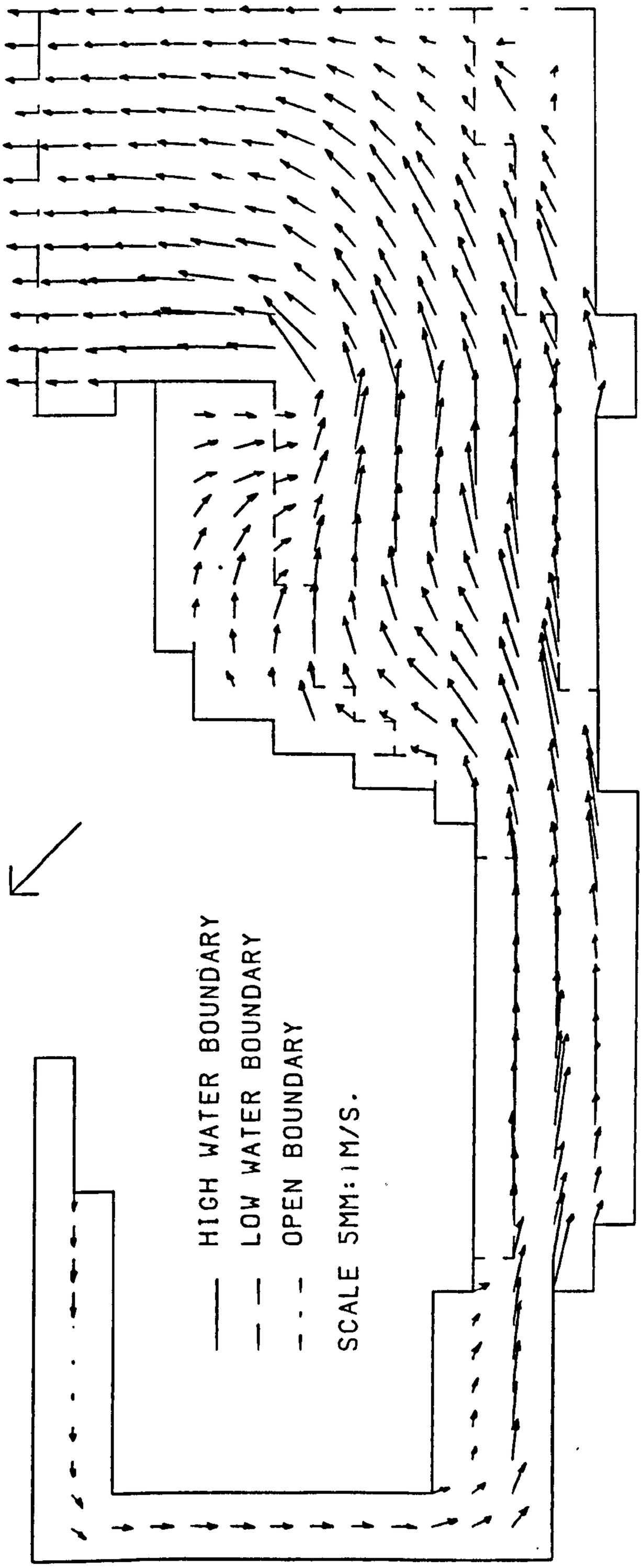

FIGURE 8.27 k
SPRING TIDE VELOCITIES IN THE HUMBER ESTUARY.
TIME FROM START OF TIDAL CYCLE HOURS= 10.00

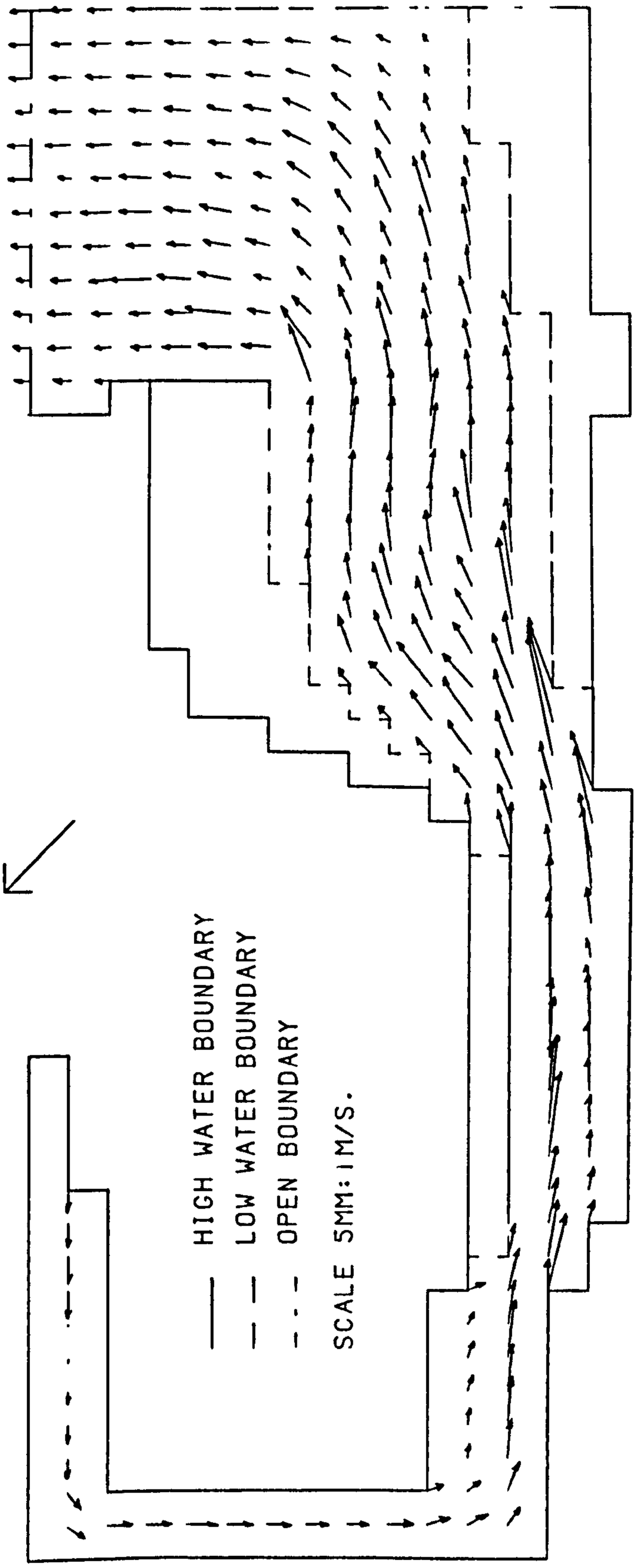

FIGURE 8·27
SPRING TIDE VELOCITIES IN THE HUMBER ESTUARY.
TIME FROM START OF TIDAL CYCLE HOURS= 11.00

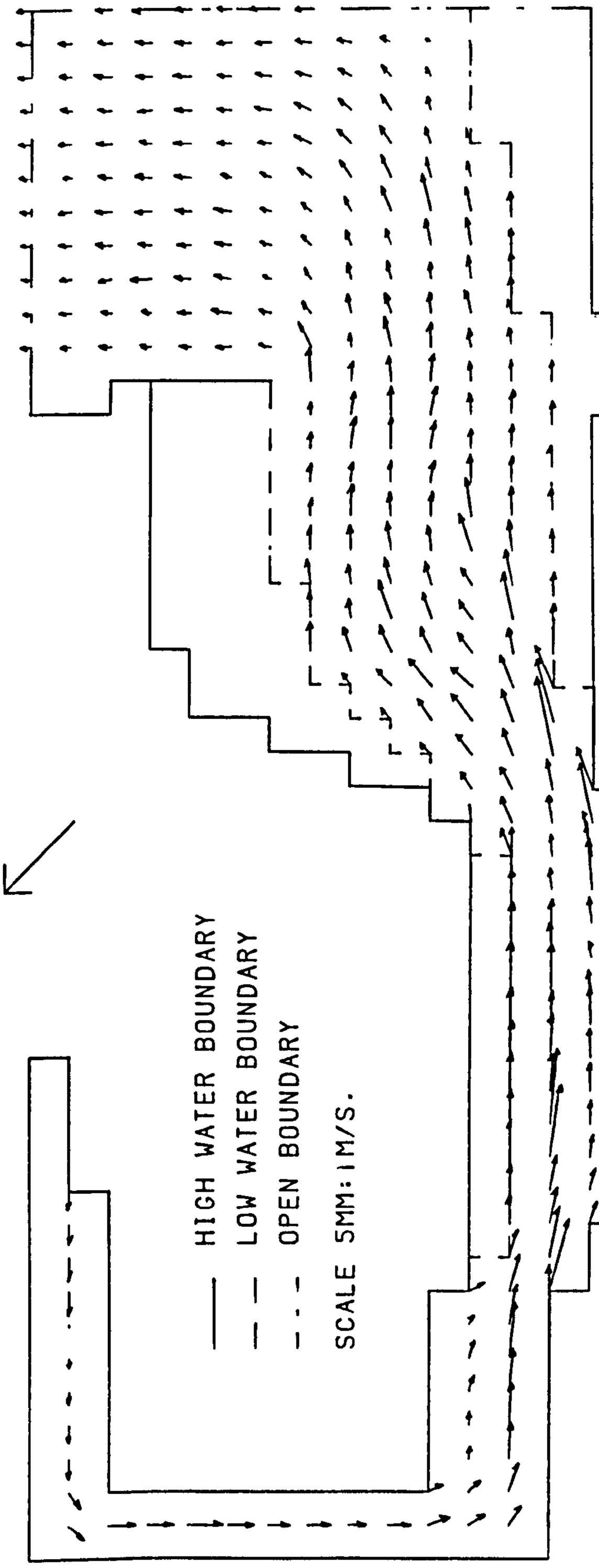

FIGURE 8·27m
SPRING TIDE VELOCITIES IN THE HUMBER ESTUARY.
TIME FROM START OF TIDAL CYCLE HOURS= 12.00

FIGURE 8·28a
GENERL FLOW PATTERN DURING PEAK CURRENTS ON THE FLOOD TIDE
TAKEN FROM H.R.S. REPORT EX 386

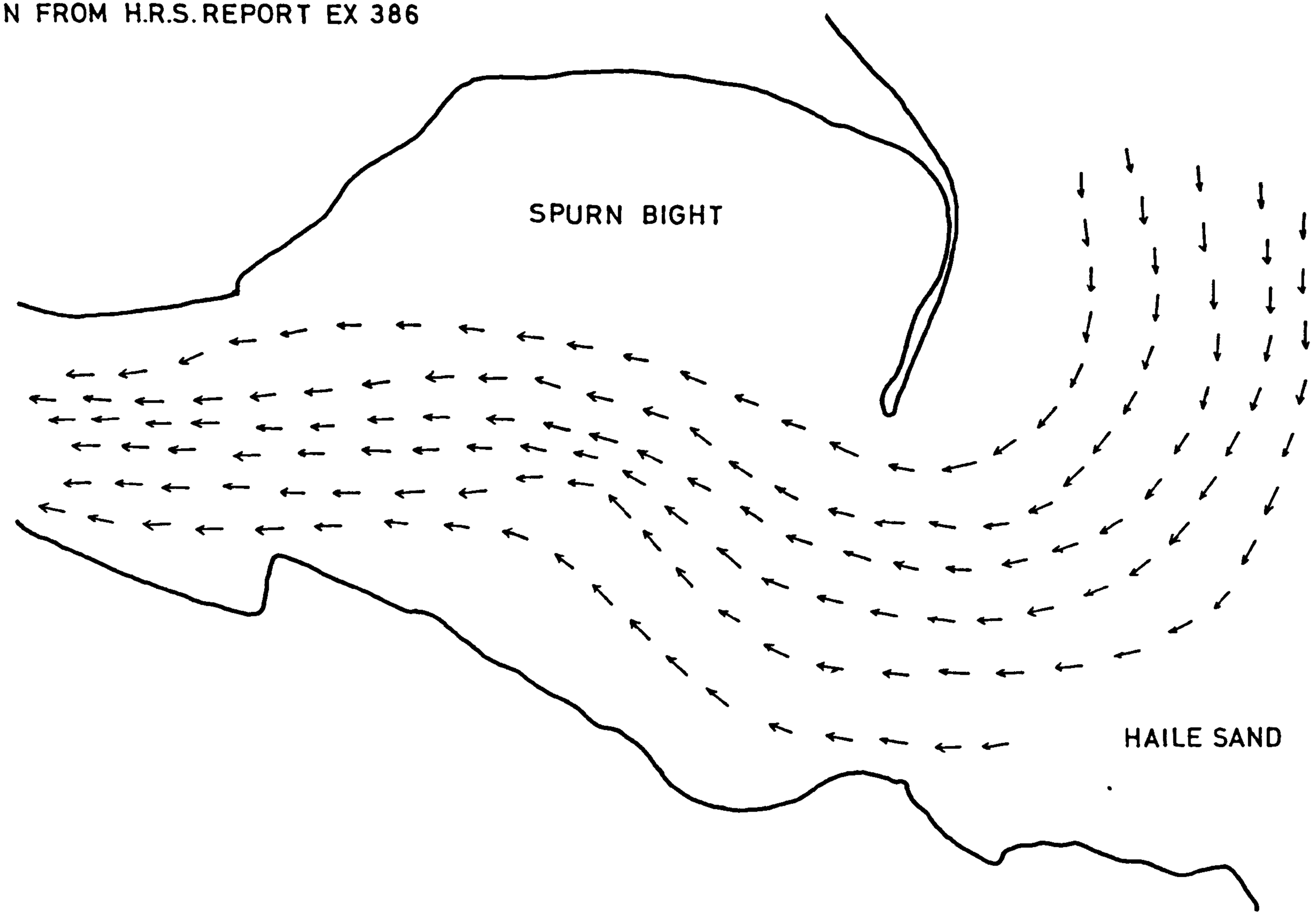

FIGURE 8.28b
GENERAL FLOW PATTERN DURING PEAK CURRENTS ON THE EBB TIDE
TAKEN FROM H.R.S. REPORT EX 386

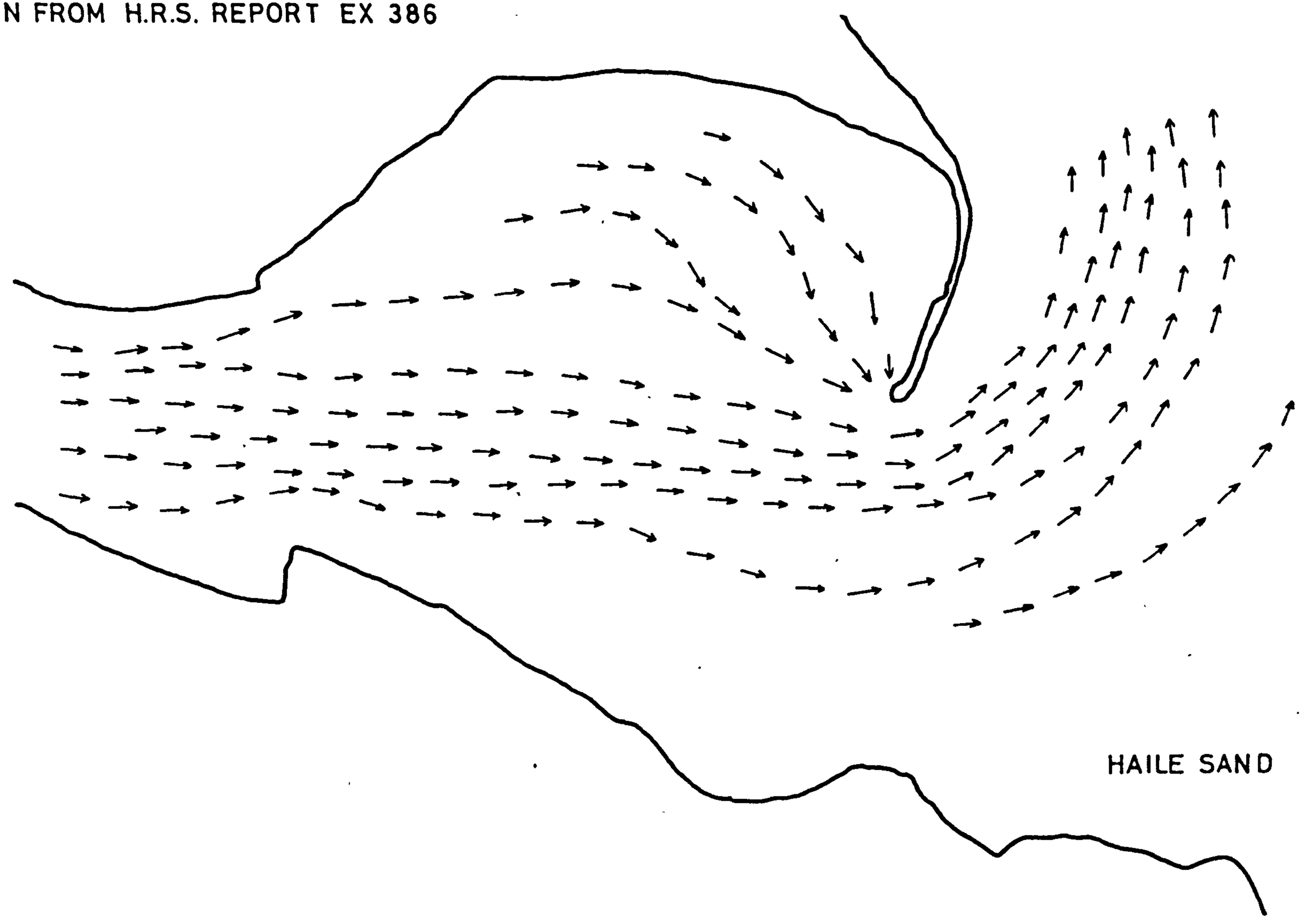

occurs during the draining of Spurn Bight. The float-tracking experiments show that water tends to leave the Bight via a channel close to Spurn Head. The numerical model, however, permits the Bight to drain along its full length. This effect is also evident in Figure 8.17 for velocity magnitudes at position P. The numerical modelling of this effect could be improved by a more sophisticated representation of the energy gradient over the sand flats than used at present.

During the alterations for models two and three the choice of Chezy's C was continually reassessed. Table 8.3 shows the ranges, times of high and times of low water for values of C, ranging from $60m^{\frac{1}{2}}/s$ to $120m^{\frac{1}{2}}/s$. The table confirms the value of $100m^{\frac{1}{2}}/s$ as providing the best estimate of energy losses in the Humber Estuary. Figure 8.29 shows the extent to which friction affects the numerical results at Hessle.

8.13 ASSESSMENT OF MODEL PERFORMANCE

The foregoing results are considered to show a good agreement with the observed values within the bounds of approximation of the numerical model. Some obvious improvements could be made. Firstly, a better estimate of mean sea level could be obtained. Secondly, were greater computer storage readily available the model could be extended upstream in a more realistic manner, i.e. using the correct channel alignment. The advantages of this are debatable as upstream of Hull the channel configuration is better suited to one plan dimension numerical modelling.

LOCATION	OBSERVED	RANGES COMPUTED (VARYING CHEZY C)						
		120	110	100	90	80	70	60
SPURN HEAD	5.8	5.923	5.985	5.868	5.836	5.797	5.749	5.687
GRIMSBY	6.0	6.174	6.132	6.089	6.035	5.958	5.865	5. 739
IMMINGHAM	6.3	6.524	6.442	6.352	6.230	6.076	5.863	5.598
HULL	6.8	7.091	6.978	6.839	6.655	6.431	6.145	5.768
HESSLE	7.0	7.368	7.260	7.114	6.937	6.706	6.413	6.029

LOCATION	OBSERVED	TIME TO HIGH WATER COMPUTED (VARYING CHEZY C)						
		120	110	100	90	80	70	60
SPURN HEAD	0.0	0.0	0.0	0.0	0.0	0.0	0.0	0.0
GRIMSBY	+0.30	0.10	0.10	0.10	0.10	0.10	0.10	0.10
IMMINGHAM	+0.45	0.20	0.20	0.20	0.30	0.30	0.30	0.40
HULL	+0.45	0.30	0.40	0.40	0.50	0.50	1.00	1.10
HESSLE	+1.00	0.30	0.40	0.40	0.50	1.00	1.10	1.20

LOCATION	OBSERVED	TIME TO LOW WATER COMPUTED (VARYING CHEZY C)						
		120	110	100	90	80	70	60
SPURN HEAD	+6.00	6.00	6.10	6.10	6.10	6.10	6.10	6.10
GRIMSBY	+6.20	6.10	6.20	6.20	6.20	6.20	6.30	6.30
IMMINGHAM	+6.40	6.40	6.50	6.50	6.50	7.00	7.10	7.10
HULL	+7.00	7.20	7.30	7.30	7.40	7.40	7.50	8.00
HESSLE	+7.50	7.50	8.00	8.00	8.10	8.10	8.20	8.30

Table 8.3

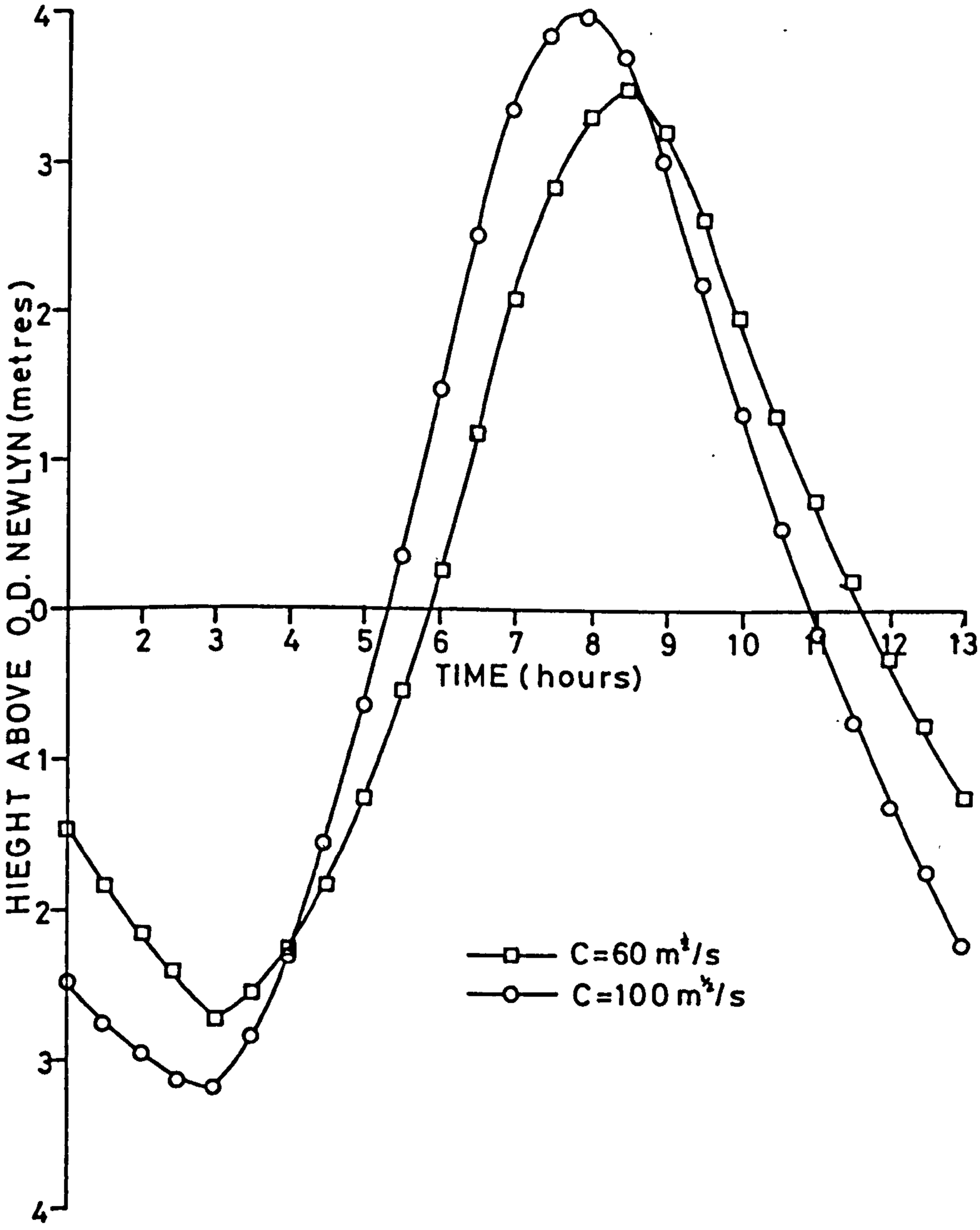

FIGURE 8·29

COMPUTED TIDE CURVES AT HESSLE

Thirdly, more detailed knowledge of sand flat behaviour could be included. Knowledge of levels and the rate of flooding and drying would be of advantage in enabling correct sand flat storage to be modelled.

8.14 NUMERICAL MODELLING OF A STORM SURGE IN THE HUMBER ESTUARY

It was considered desirable to test the scheme's ability to simulate events with a duration longer than one tidal cycle in an estuary such as the Humber. Of particular interest was the long term numerical stability with extreme water levels and a number of successive floodings and dryings of the sand flats. The event modelled was the so called "Hamburg" surge on 15th to 17th February 1962.

Conditions in the North Sea leading to this event were described by Heaps (1968) as follows:

"This event may be regarded as representing the class of 'major' North Sea surges. The weather charts of Figure 8.30 show that a large deep depression approached the west coast of Norway from the direction of Iceland and then past south-eastwards over Scandinavia into the Baltic. Gale force westerly to north-westerly winds associated with the depression, extended over most parts of the North Sea impelling water towards its southern and south-eastern coasts. As a result, large rises in sea level occurred along these boundaries, particularly in the German Bight which was directly exposed to the most violent winds."

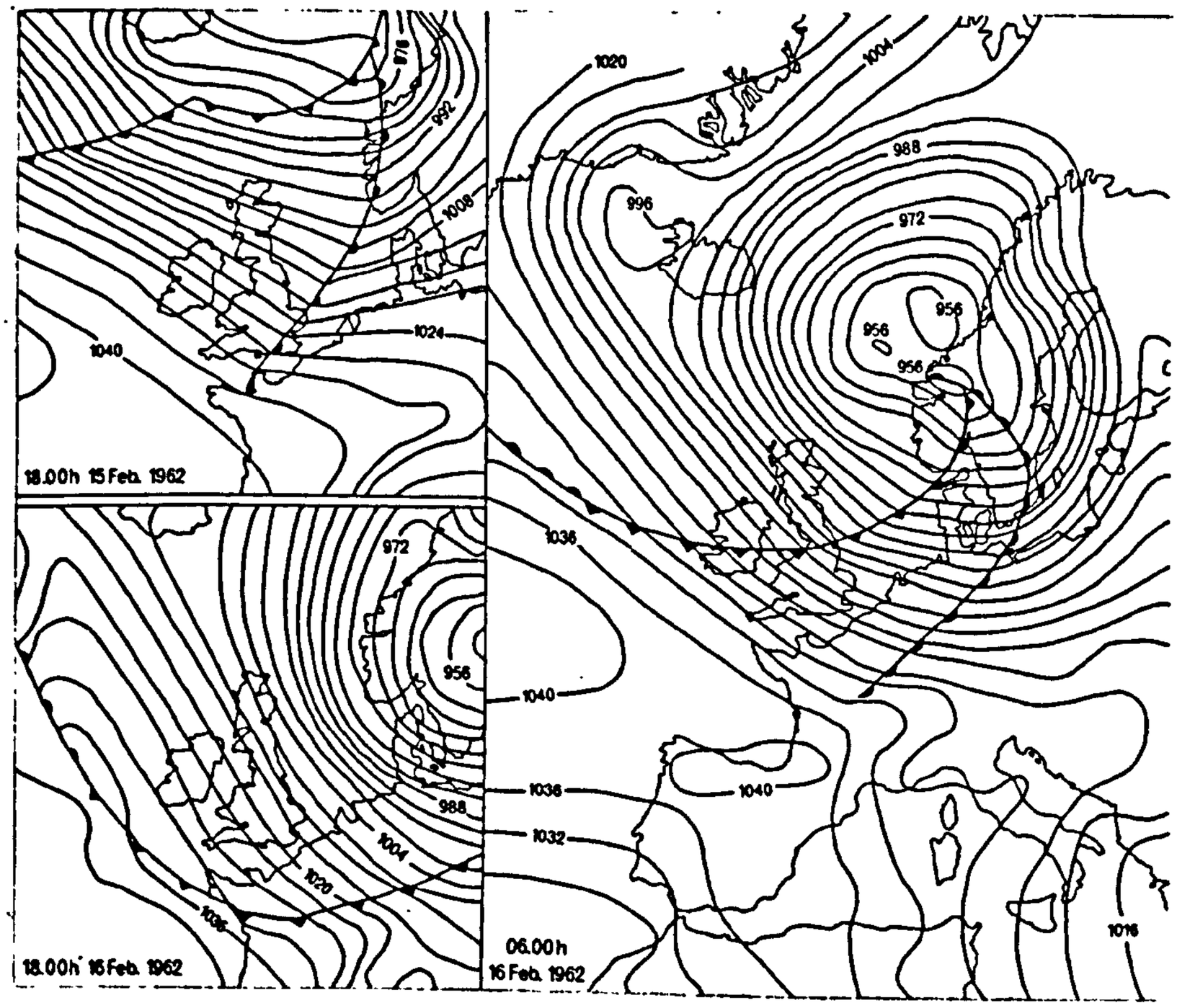

FIGURE 8·30
WEATHER CHARTS FOR THE STORM SURGE
OF 15th TO 17th FEBRUARY 1962

For boundary data the numerical model uses the measured surge at Immingham, presented by Heaps (1968), superimposed on the predicted tidal range from the Admiralty Tide Tables 1968, giving a total water level variation of around 6m. The wind stress and barometric pressure variations were considered to have a negligible effect in an estuary of this type and were dropped from the calculation.

The numerical scheme remained stable throughout the calculation, sample results are shown in Figures 8.31 and 8.33. Figures 8.31a to 8.31d show the computed tide plus surge levels compared with the predicted tide levels at locations within the Estuary. Comparisons between the computed tide plus surge are given in Figures 8.32a to 8.32d. From Figures 8.33a to 8.33d the amplification of the surge as it propagates up the Estuary can be seen.

8.15 THE INFLUENCE OF SPURN HEAD ON TIDE PROPAGATION IN THE HUMBER ESTUARY

8.15.1 PHYSICAL DESCRIPTION OF SPURN HEAD

Spurn Head, the sand and shingle spit that curves a good third of the way across the mouth of the Humber, is at the present time about 5km long. From its wedge-shaped root at Kilnsea it tapers to a neck which though the narrowest, is also the highest, part of Spurn; it rises to about 9m O.D. This narrow neck sweeps round to a wider, distal portion about two miles long, the seaward

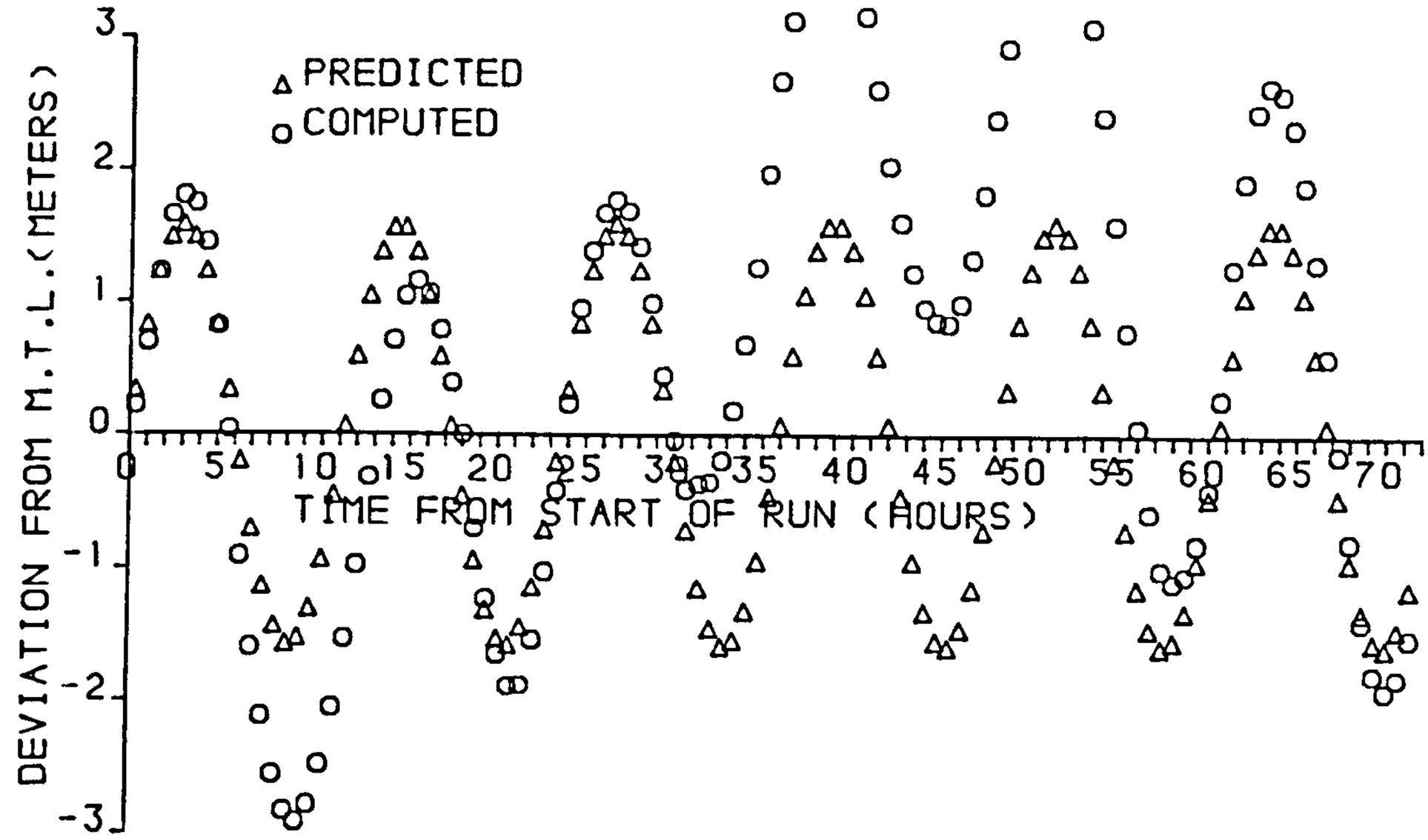

FIGURE 8·31a

HAMBURG SURGE LEVELS AT BULL SAND

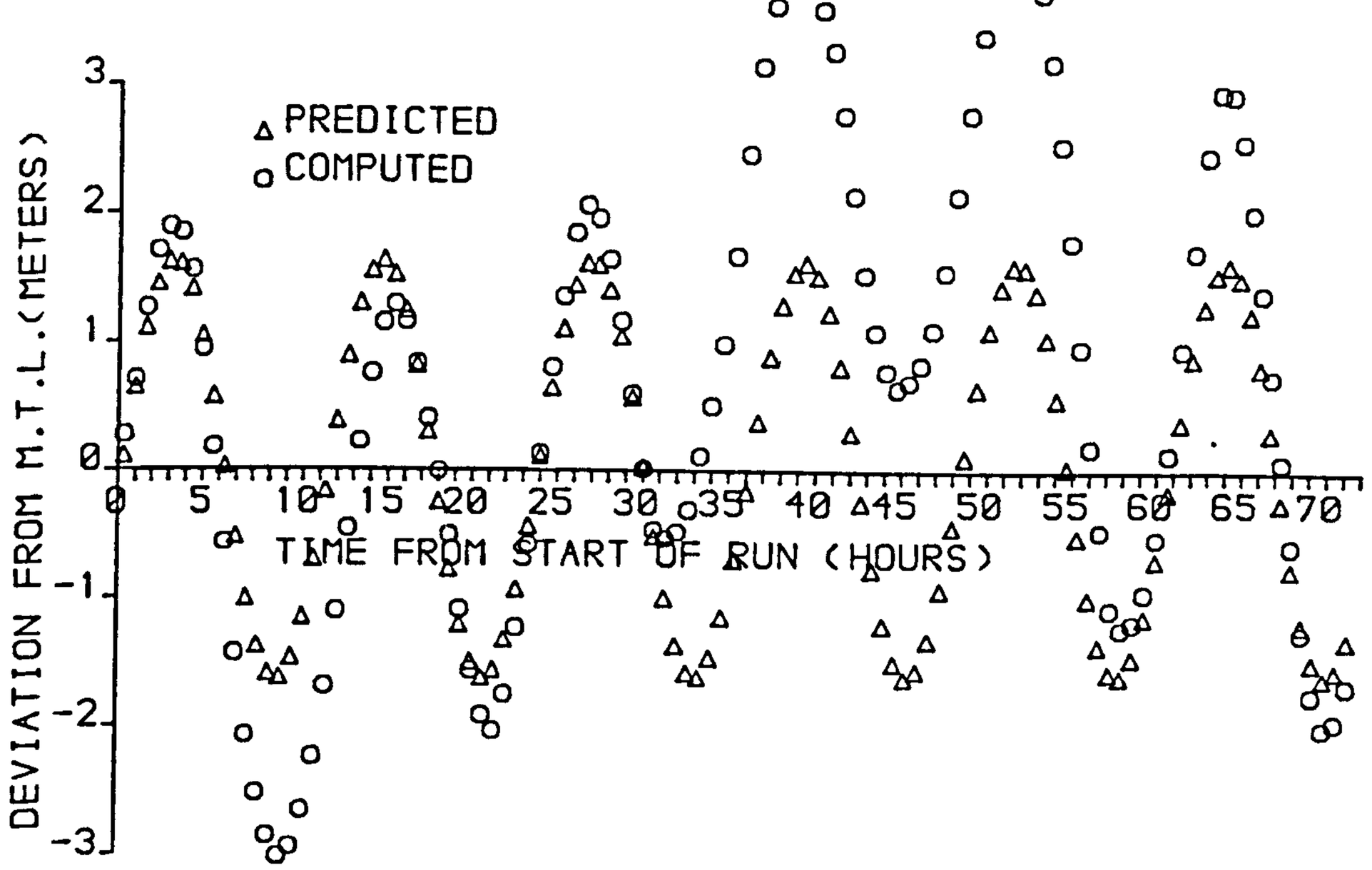

FIGURE 8·31b

HAMBURG SURGE LEVELS AT GRIMSBY

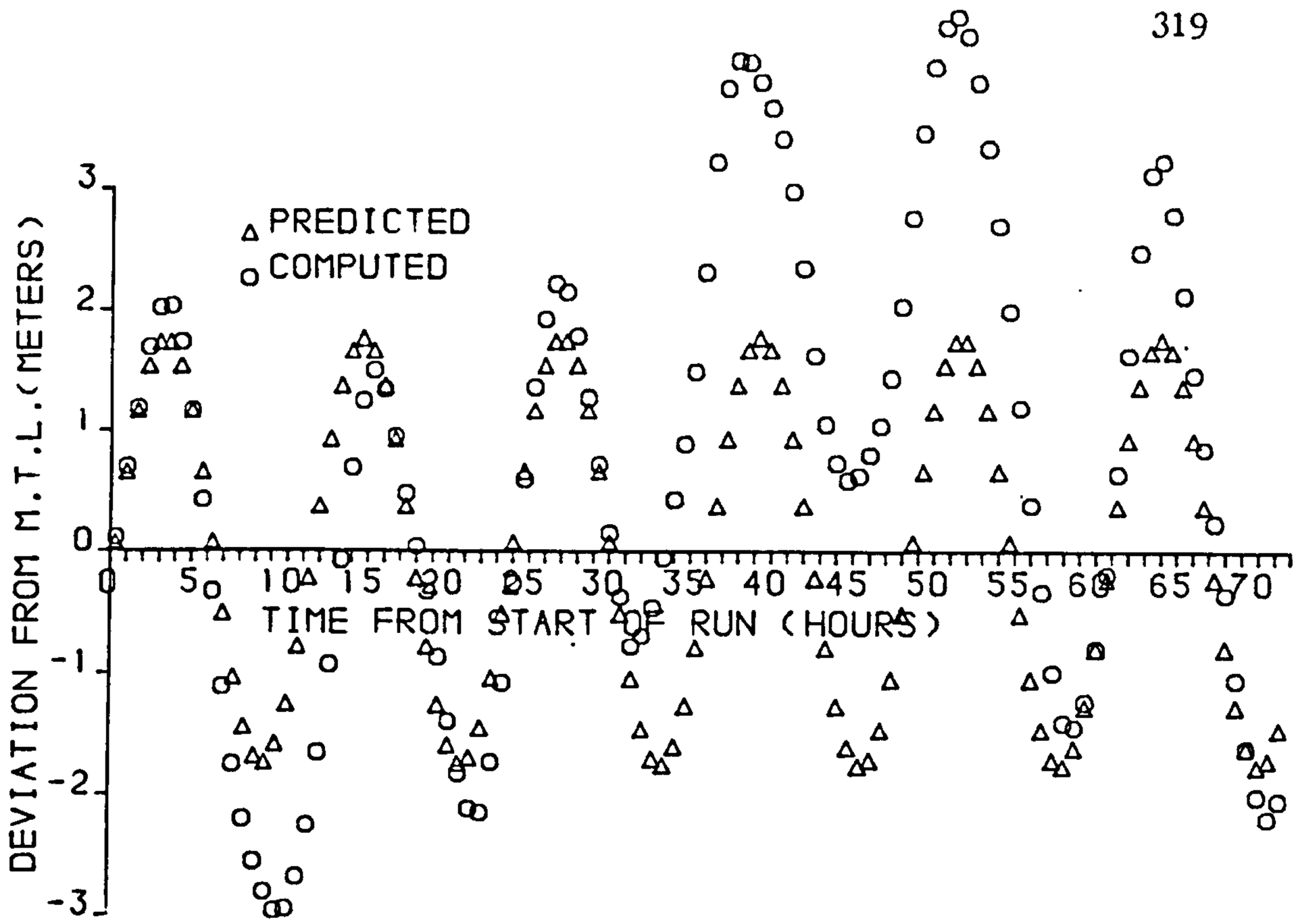

FIGURE 8·31 c

HAMBURG SURGE LEVELS AT IMMINGHAM

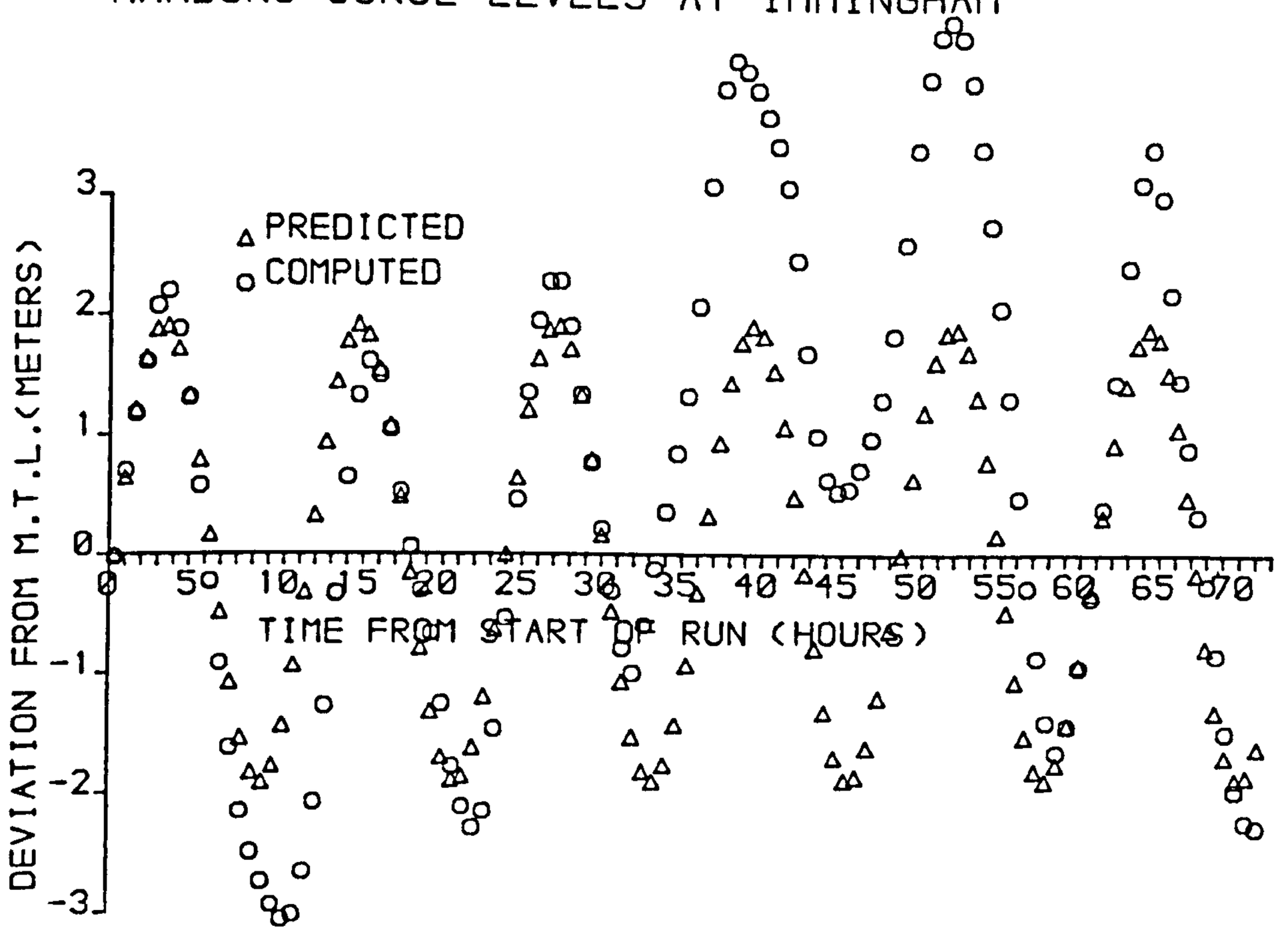

FIGURE 8·31 d

HAMBURG SURGE LEVELS AT HULL

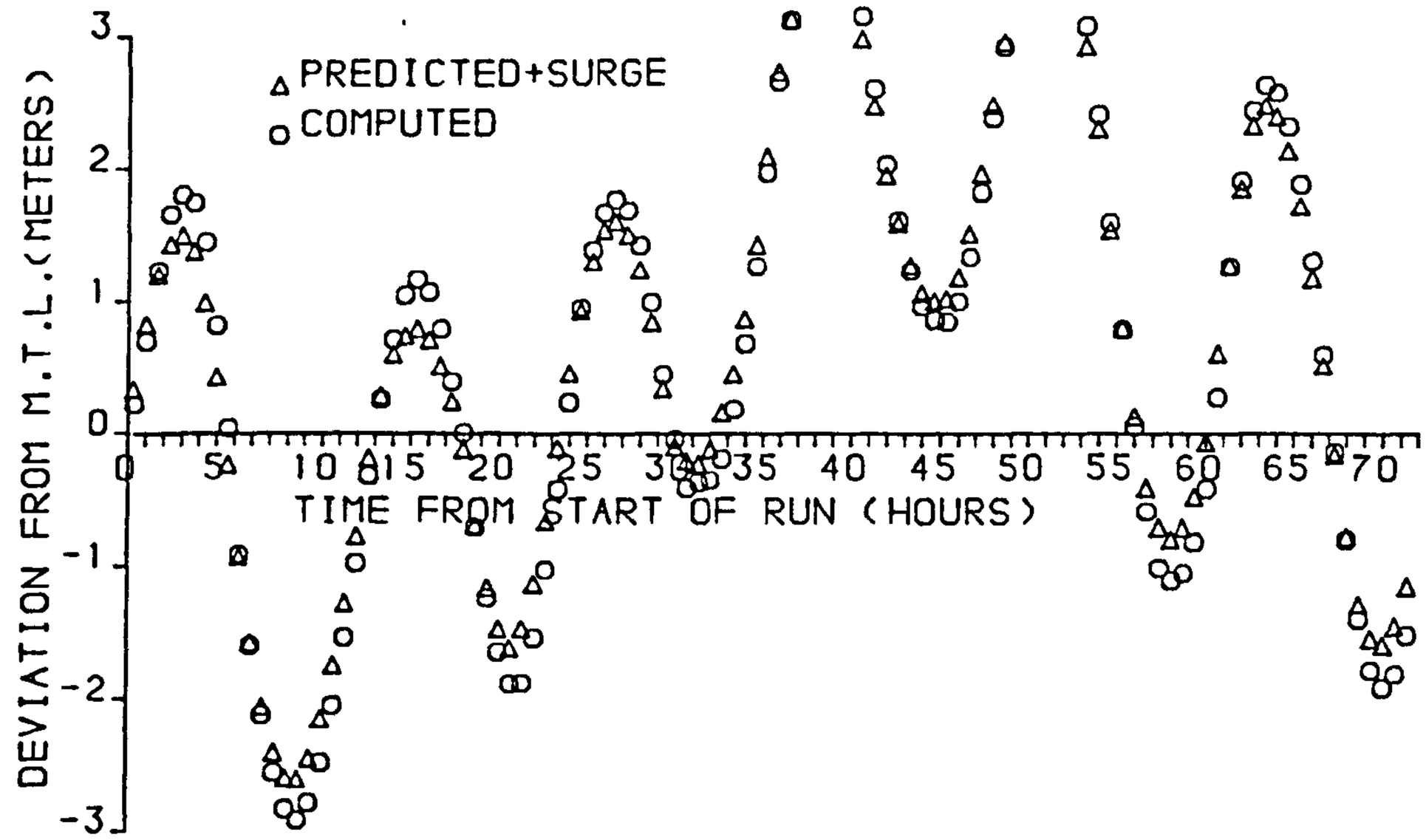

FIGURE 8·32a

HAMBURG SURGE LEVELS AT BULL SAND

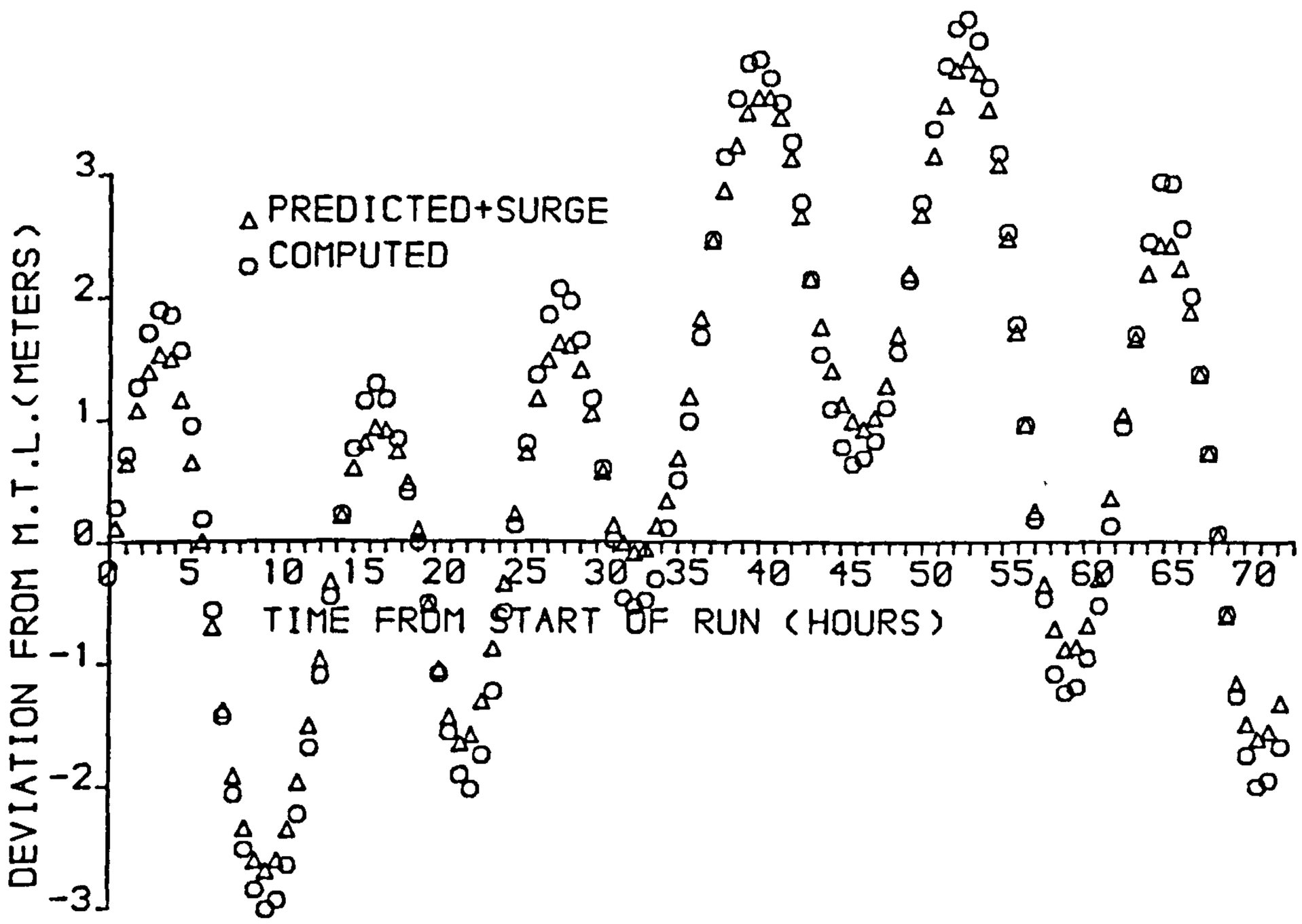

FIGURE 8·32b

HAMBURG SURGE LEVELS AT GRIMSBY

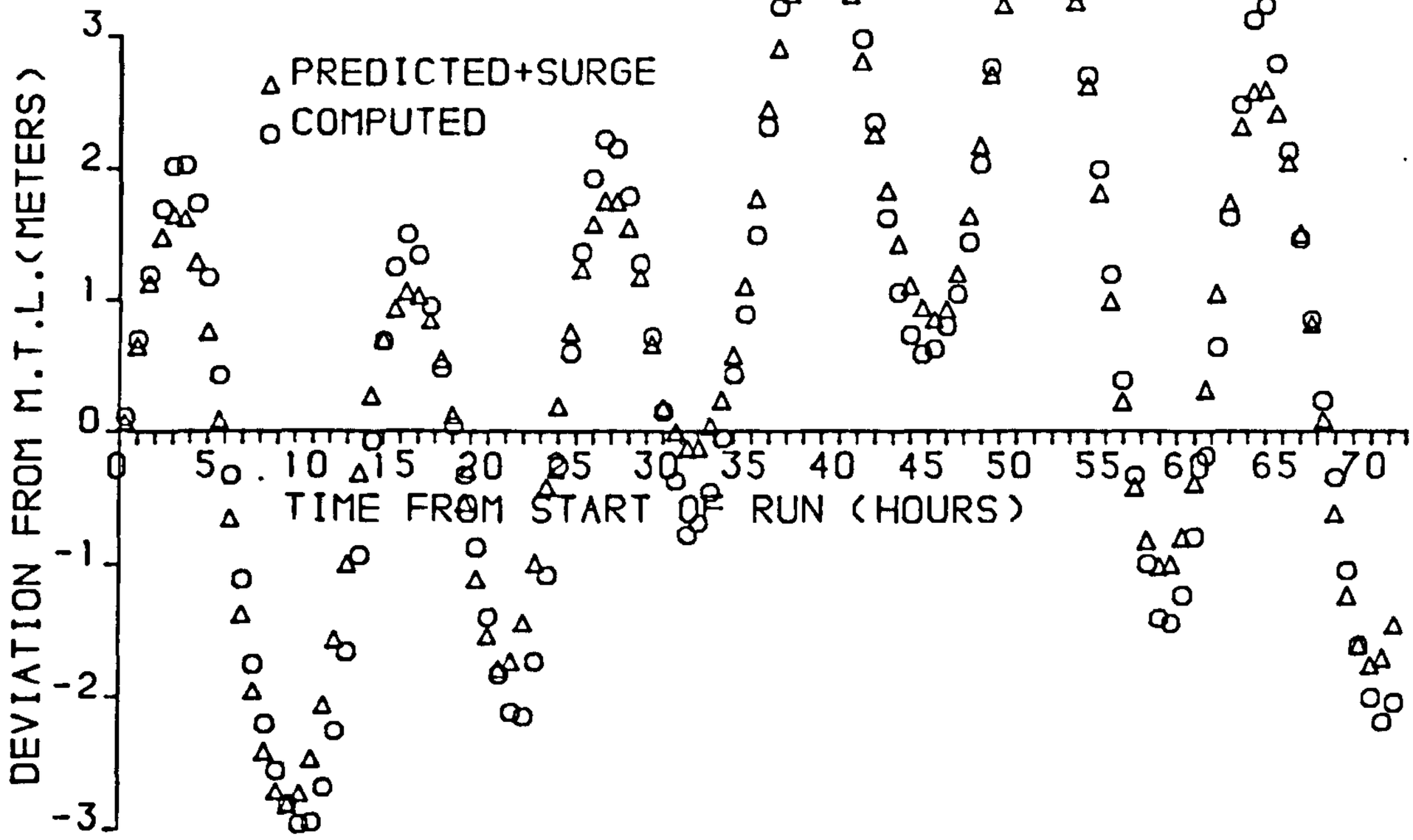

FIGURE 8·32c

HAMBURG SURGE LEVELS AT IMMINGHAM

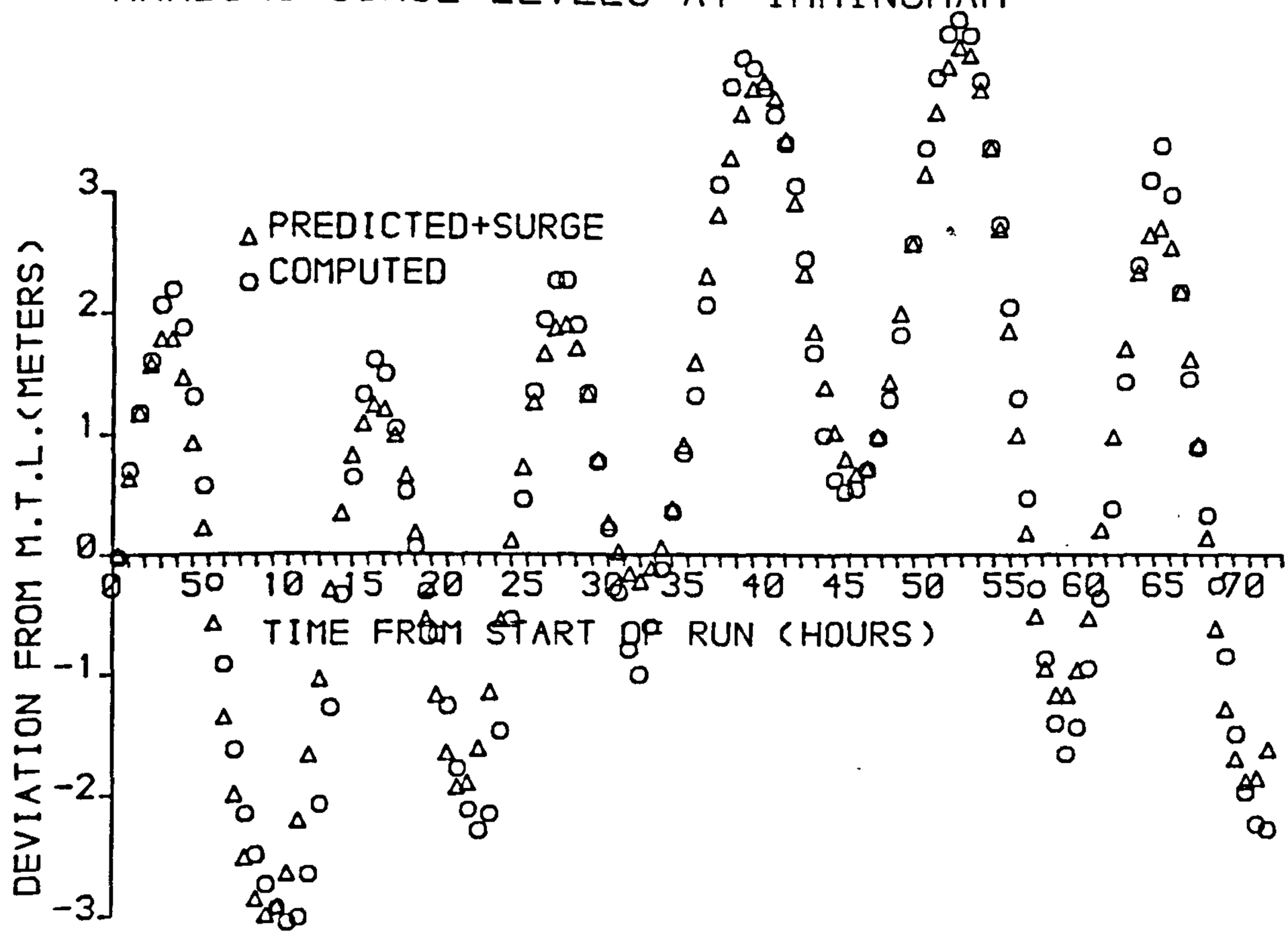

FIGURE 8·32d

HAMBURG SURGE LEVELS AT HULL

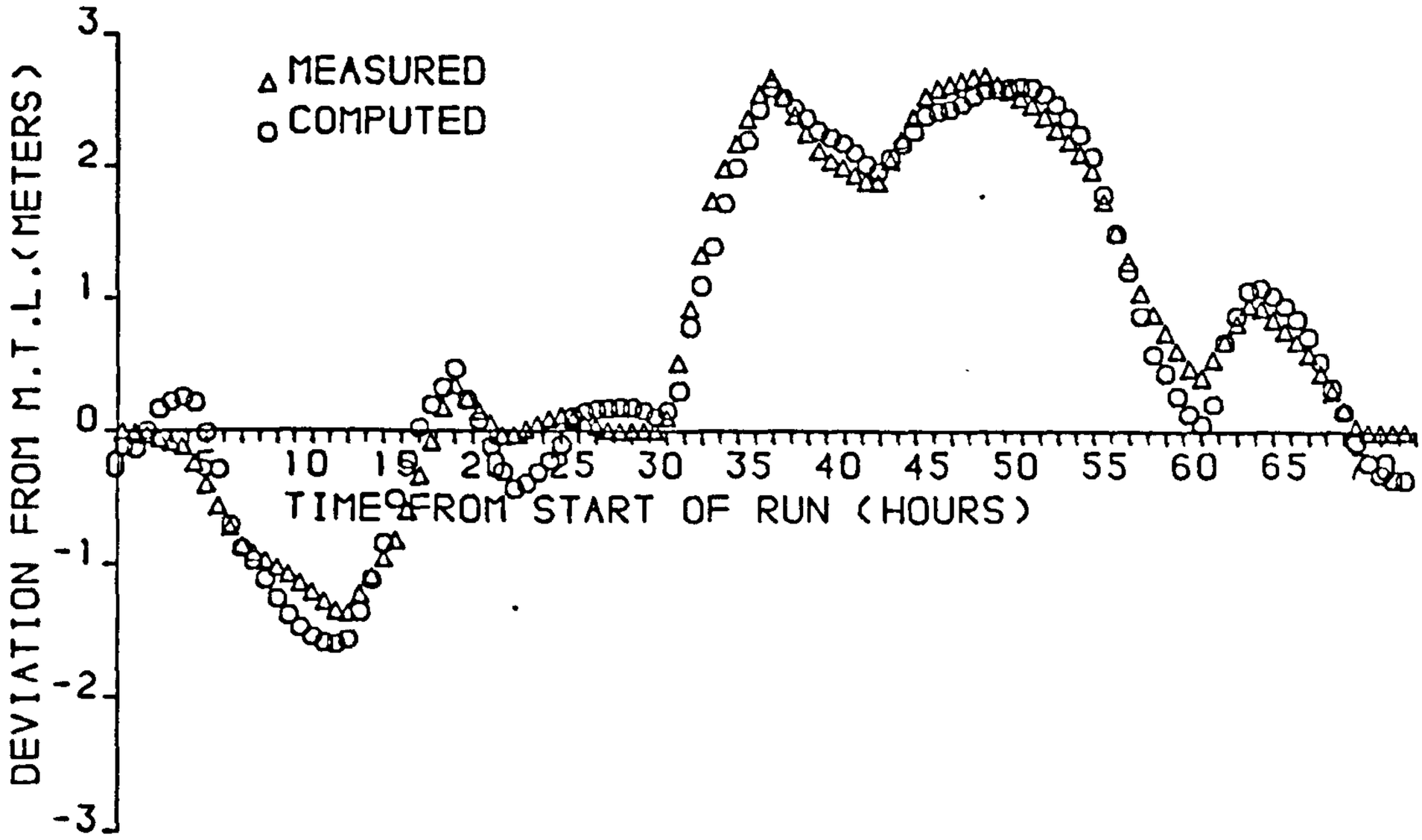

FIGURE 8·33 a

HAMBURG SURGE LEVELS AT BULL SAND

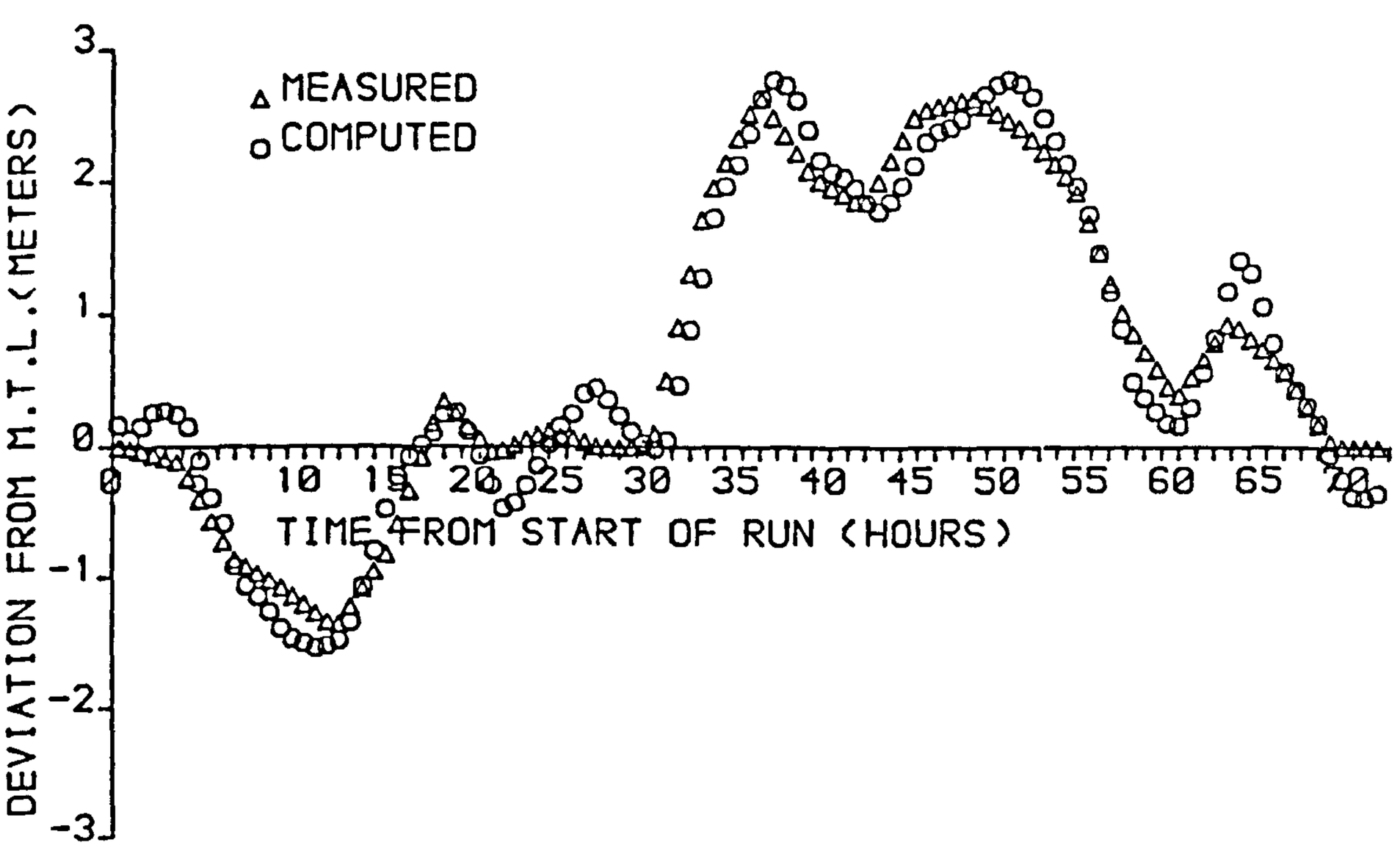

FIGURE 8·33 b

HAMBURG SURGE LEVELS AT GRIMSBY

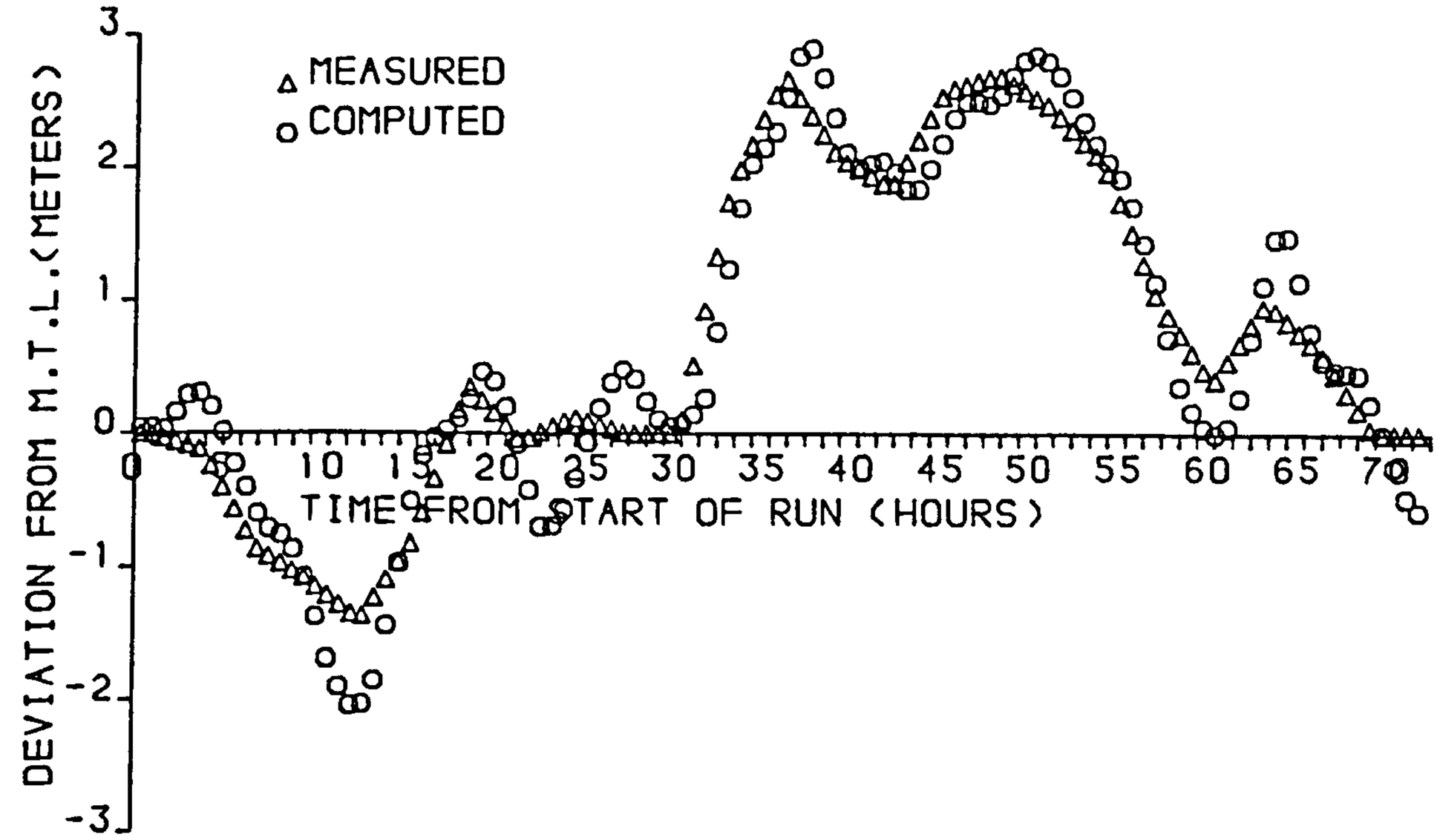

FIGURE 8·33c

HAMBURG SURGE LEVELS AT IMMINGHAM

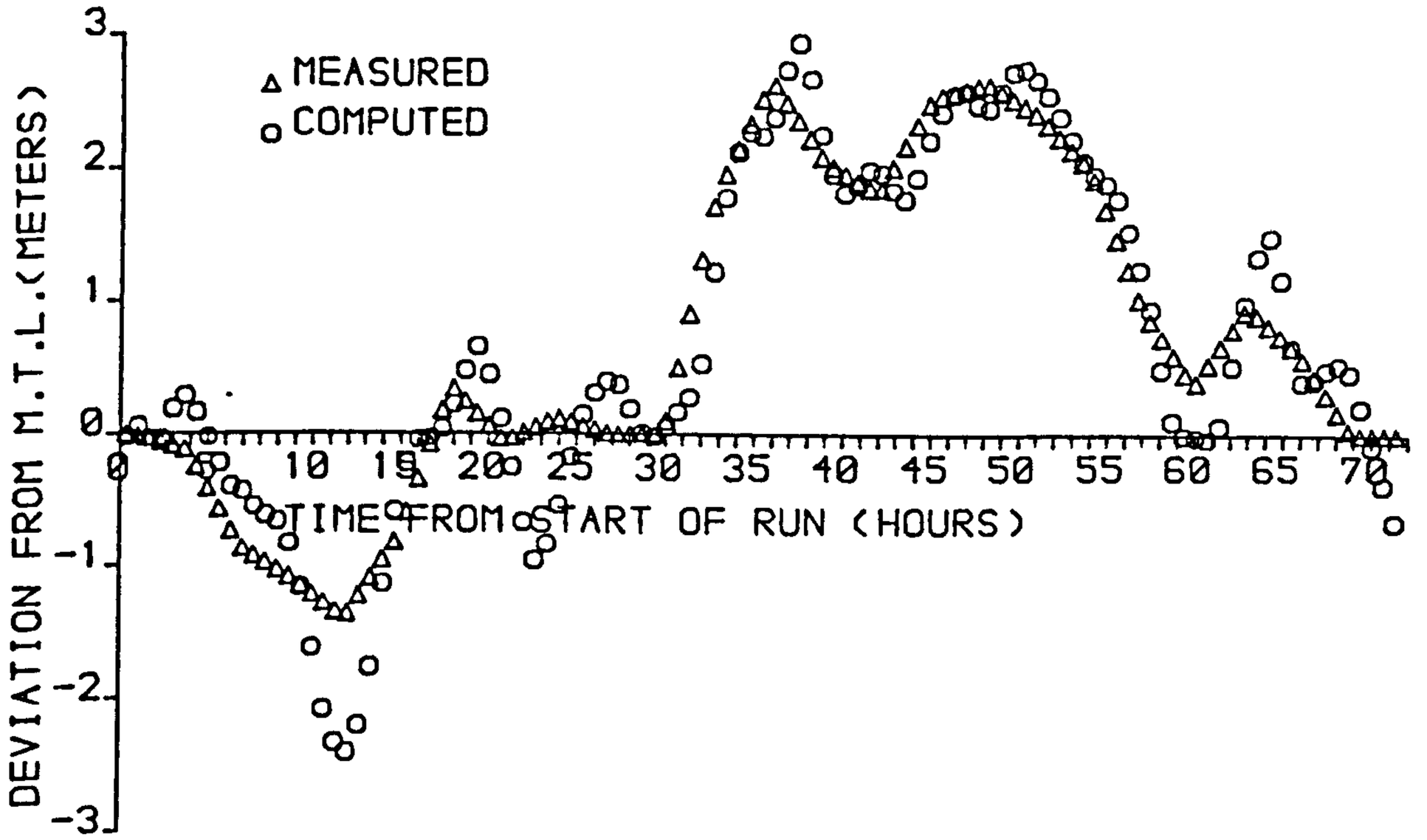

FIGURE 8·33d

HAMBURG SURGE LEVELS AT HULL

side of which is straight, the river side is irregular. A section near the northern end which bulges out into the river marks the place where the great breach of 1849 was sealed. Another bulge into the river right at the end gives the spit a broad tip with wide sand flats on the inside. The sea side maintains its straightness to the tip which slopes steeply down to depths of 25 to 27 metres.

Left to natural phenomena Spurn Head is not a permanent feature but undergoes cyclic phases of construction and destruction. The physical processes of sediment transport responsible for this are discussed by De Boer (1964). The net result is that approximately every 250 years Spurn Head reaches its maximum length. Then destructive forces take over, and it is gradually destroyed. Following this a new Spurn Head is built further west than its predecessor. In 1849 a destructive phase began with a major breach about 320 yards wide and 12 feet deep at ordinary high water. Other considerable breaches occurred in 1851 and 1856. De Boer suggests that breaching on this scale if left to develop would have resulted in the destruction of the spit and the beginning of a fresh cycle. However, fears for the effect on navigation in the estuary led to the breaches being sealed in 1852-56.

8.15.2 CASES CONSIDERED

To illustrate the use of the "weir" flow boundary condition and the predictive capacity of the numerical

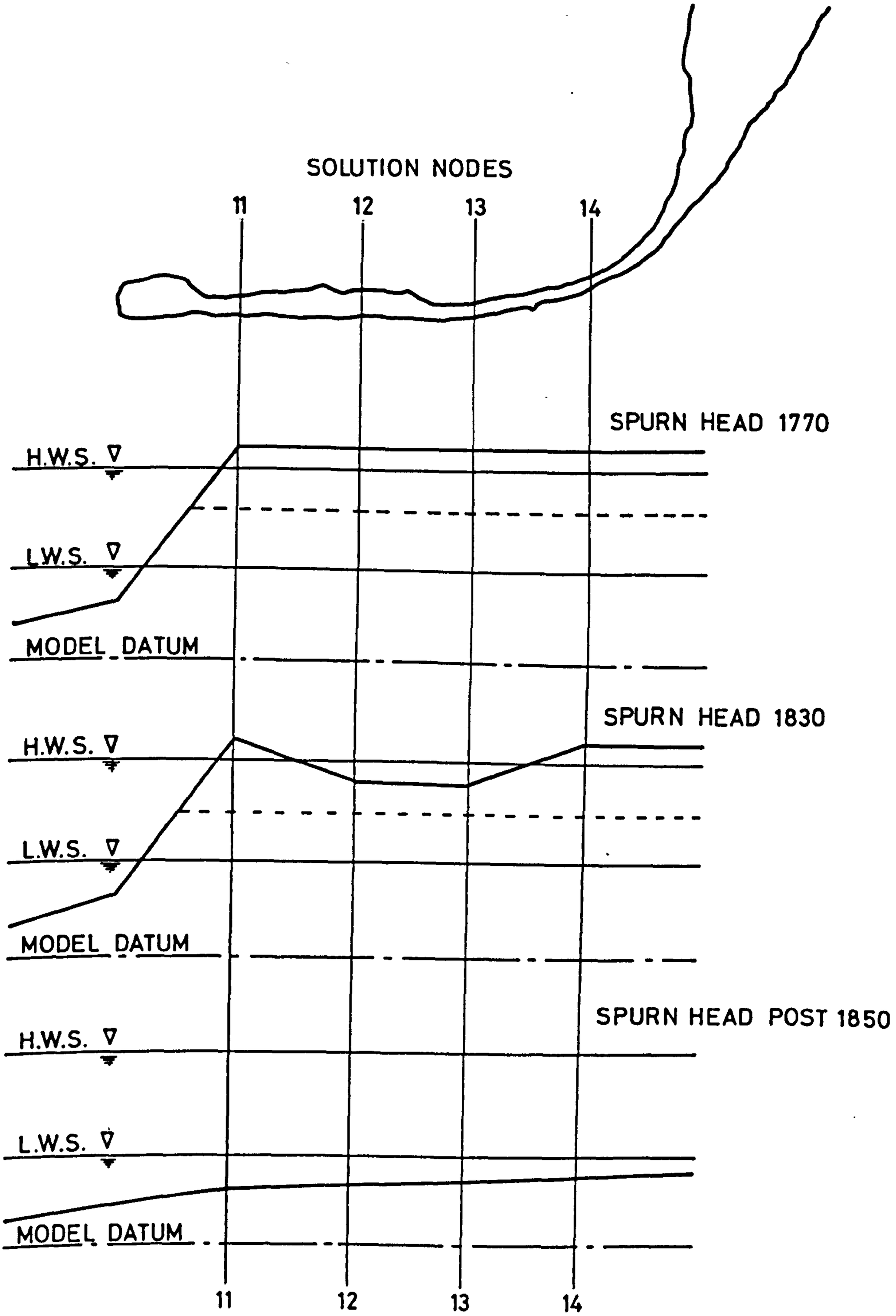
SOLUTION NODES
11
12
13
14
SPURN HEAD 1770
H.W.S.
L.W.S.
MODEL DATUM
SPURN HEAD 1830
H.W.S.
L.W.S.
MODEL DATUM
SPURN HEAD POST 1850
H.W.S.
L.W.S.
MODEL DATUM
11
12
13
14

FIGURE 8·34

model the effect of the decay of Spurn Head on spring tide propagation in the Humber has been assessed.

Three stages of decay of Spurn Head shown in Figure 8.34 have been considered. These correspond to dates around 1770, 1830 and post 1850 respectively. For the 1770 condition, no overtopping of Spurn Head with spring tides occurs, the top of the sand spit being 1.5m above spring tide level. De Boer (1964) reports that in 1830 the neck of Spurn Head was overtopped at high water springs and during rough weather with easterly winds. For this case the numerical model levels at two points on the neck are 1.5m and 2.0m below high water springs. The "weir" flow boundary condition is used in this case to model flows over the spit. Calibration of the "weir" flow coefficients Co and C_s was carried out by a back water curve integration assuming a steady flow condition over a 200m wide sand bank, the values used are 0.20 and 0.37 respectively. For the post 1850 case Spurn Head has been completely eroded with only the sand flats of Spurn Bight remaining.

Open boundary conditions are assumed to be unaffected by the changes at Spurn Head.

8.15.3 RESULTS

Variations in spring tide ranges resulting from changes in Spurn Head are given in Table 8.4. It can be seen that small reductions in the ranges have resulted both with the 1830 and post 1850 configurations. A hydrograph of flow over Spurn Head for the 1830 case is shown in Figure 8.35. During the calibration of the "weir" flow

POSITION	RANGES		
	1770	1830	Post 1850
BULL SAND	5.87	5.85	5.73
GRIMSBY	6.13	6.12	6.01
IMMINGHAM	6.34	6.33	6.23
HULL	6.65	6.64	6.55

Table 8.4

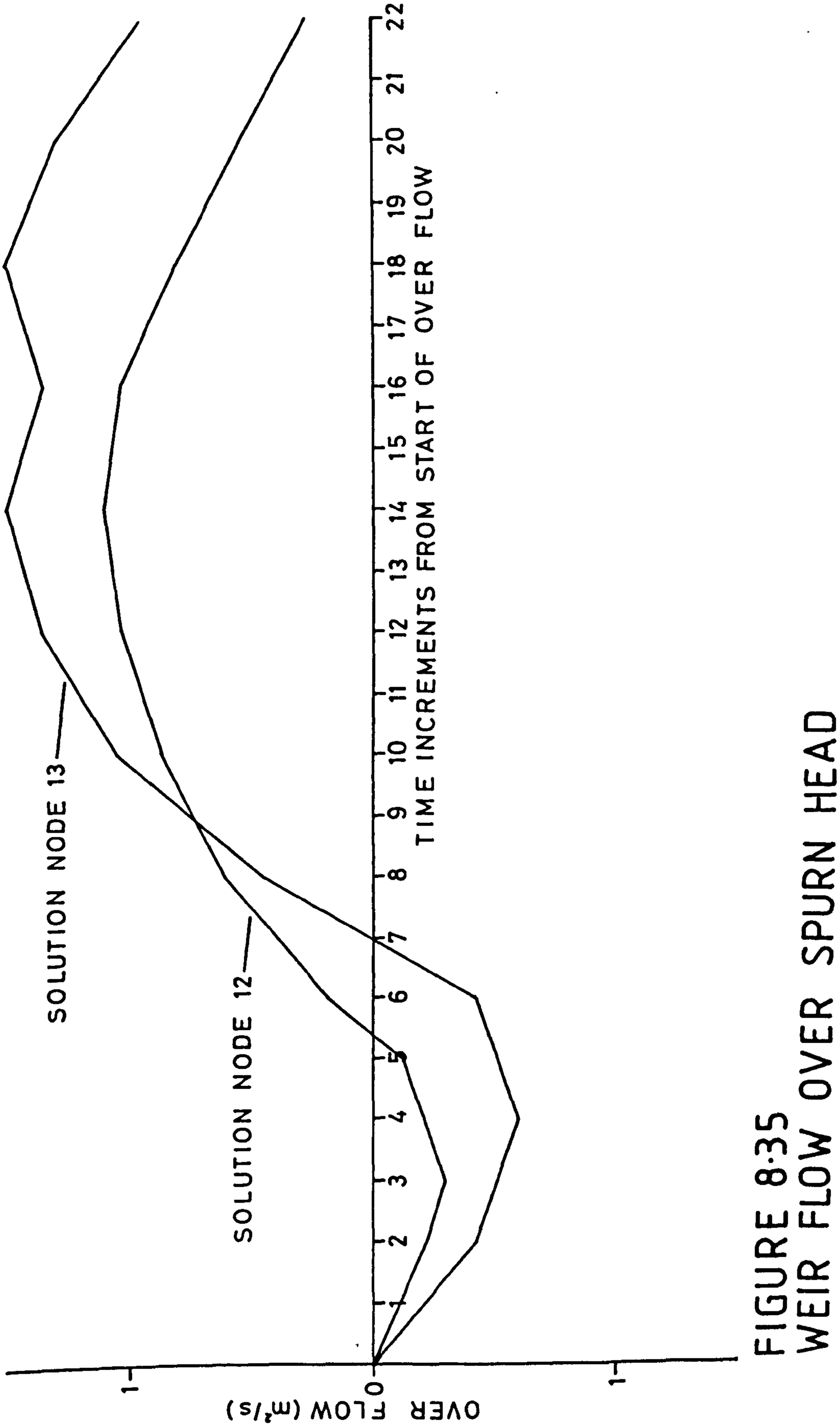

FIGURE 8.35
WEIR FLOW OVER SPURN HEAD

equation it was noted that use of high discharge coefficients resulted in oscillations appearing in the computed "weir" flows. The effect is probably due to insufficient account being taken of changes in downstream water level during a time increment. In the present example the discharge coefficient used was small enough to damp out these oscillations.

8.15.4 MODELLING THE EROSION OF SPURN HEAD

Historical evidence, de Boer (1964), indicates that once Spurn Head is overtopped erosion will occur rapidly. It may be possible to obtain an estimate of the rate of this erosion by incorporating a sediment transport equation in the numerical model. For example, the Engelund-Hansen formula developed for an uniform flow case:

$$q_b = 0.05\gamma_s \, u^2 \sqrt{\frac{Dso}{g(\gamma_s/\gamma - 1)}} \left[\tau_o / (\gamma_s - \gamma) \, Dso \right]^{3/2} \quad \text{Equation 8.1}$$

could be used. Where q_b is the sediment flow rate per unit breadth, γ_s is the mass per unit weight of sand, Dso the sediment diameter below which 50% of the sand grains lie and τ_o is the bed shear stress equal to $\gamma \, dS_o$, and S_o is the surface slope. All parameters in equation 8.1 can either be measured or obtained from the numerical solution, q_b could therefore be calculated and used to estimate the rate of erosion of the sand spit.

CHAPTER NINE

CONCLUSIONS

9.1

Today's civil engineers are looking more to computer simulation techniques to solve practical engineering problems than ever before. This move to computational methods has created a high demand for efficient and reliable engineering software. The aim of this research project was to go some way to meeting this demand in the field of free surface hydraulics.

This was achieved by the development of computational algorithms suitable as the basis of design systems to solve problems concerning long wave propagation both in river channels and coastal seas. These design systems are intended for use by practicing engineers with access to standard office computing facilities. Such users require that the algorithms be robust, efficient and have a low computer storage requirement. By robust it is meant that the models should be free from strict stability restraints permitting sensible results to be obtained irrespective of Courant number. This necessitates that care be taken by the operator to ensure that operating Courant numbers are not so high as to impair the accuracy of the results.

Efficiency is also greatly enhanced by freedom of choice of Courant number as physically realistic time increments can be used to model variations in flow parameters.

9.2 FLOOD ROUTING MODEL

With the aid of existing library programme facilities a design system for flood routing in a natural river channel and its associated washland areas has been developed. Algorithms for the simulation of conditions in the main river channel and the washland areas were presented in previous chapters.

The main channel algorithm solves the continuity and full dynamic equation in one plan dimension using a variation of the Preissmann implicit finite difference scheme. This scheme was chosen as it provided for easy inclusion of natural channel geometry, variable distance increments, control sections and a rating curve as the downstream boundary condition. The introduction of control sections into the scheme presented problems in accurately modelling the variation of energy gradient in the vicinity of the control section. This problem was overcome by modifying energy gradients by a variable weighting coefficient to provide a better simulation of the distance over which steep energy gradients act upstream of a control section.

The washland algorithm solves the continuity equation to estimate the volumes of water entering or leaving the main channel and the water levels in the washlands. An explicit solution of the continuity equation was chosen as it was originally thought that rates of change of water level in the washlands would be modest compared to those in the main channel. This proved to be false due to the large volumes of flood water which can flow over

the river banks for a relatively small head above bank level. This poor numerical representation made the model prone to instabilities manifest by large oscillations in the numerical solution for washland water levels. However, it was decided to persevere with the explicit representation rather than revert to an implicit one, as ultimately this would provide greater model flexibility. Eventually the problem was cured by what is essentially a single iteration of the explicit washland solution, initial estimates of lateral flows being improved by using first estimates of the washland water level. A similar problem was encountered by Price (1983) during the development of Hydraulic Research's EMBER model; in this case, the problem was solved by introducing smoothing techniques into the algorithm to damp out the oscillations. The author considers the iterative approach to be more physically realistic than the smoothing technique.

After development trials the model was used for a flood study in a natural river. A description of the problem and model results are given in Chapter Five. Here it is concluded that the model operated well, faithfully reproducing observed flood events before being used as a predictive tool to assess the effect of the proposed changes to the drainage system.

Although in its present condition the model can be used for real situations further developments are thought to be necessary. Firstly, a facility for introducing a singular head loss proportional to $u^2/2g$ at main channel solution nodes should be included. Such a feature would

be of advantage at constrictions in the main channel, such as bridges. At present such features are modelled by a local increase in the Manning's roughness coefficient. Secondly, further development of the washland algorithm to include flows along a flood plain between washlands is desirable. This could be achieved by including washland to washland flow terms in the washland continuity equation. Such an alteration will pose considerable computational difficulties and require a major research effort.

9.3 TIDAL MODEL

The first steps have been taken towards the development of a solution algorithm suitable for use in a design system for the solution of two plan dimension tide and storm surge propagation problems. The algorithm is shown to be stable over a range of Courant numbers although care should be taken to ensure that result accuracy is not affected by operating at excessively high values. The scheme's ability to handle flow round islands and in basins with highly variable bathymetry is demonstrated through the application to the Firth of Clyde. Storm surge phenomena have been successfully reproduced albeit in a manner highly dependent on prior knowledge of surge elevations at the model boundary. Further tests in larger sea areas where wind stress and barometric pressure gradients have a significant effect are required to assess the numerical representation of these terms.

A comparison between the efficiency of the present alternating direction implicit model and an x-y-t characteristic

model was undertaken. This showed the present model to require considerably less computer time than the characteristic model for a given simulation.

The present algorithm was also used to model conditions in the Humber Estuary. In this application it was possible to compare computed water levels and velocities with observed values. These comparisons indicated that the model accurately represented flow conditions within the Humber Estuary even at considerable distances upstream where shallow water effects are pronounced. The model's flexibility in handling boundary conditions was also demonstrated by the Humber Estuary application. In addition to the normal boundary conditions of flow or water level given as a function of time are included a moving shore line condition permitting the simulation of flooding and drying of sand flat areas, and a "weir" flow boundary condition providing a means of modelling the overtopping of sand spits and bars during storm surge events.

Although the scheme has been shown. to accurately reproduce the hydrodynamic features of tide and storm surge propagation a considerable amount of work remains to be carried out before it could be used successfully as a commercial model. The first step would be to reprogramme the algorithm paying particular attention to programme efficiency. On completion the computational speed of the model could be compared with a scheme based on the Leendertse method which solves the governing equations

using an extremely efficient tridiagonal elimination method for flows and water levels at alternating grid points. It would be expected that the present model would require greater computation time. Its economic viability, however, would depend on to what extent increased computer costs were offset by greater flexibility of boundary conditions. Further work is also required on the finite difference representation of convective terms. In the Firth of Clyde model these terms were considered to have negligable effect and were omitted from the calculation, while in the Humber Estuary model the terms were included in an explicit manner. Abbott (1979) and Weare (1976) both show how these terms may cause long term stability problems in the Leendertse scheme. Careful examination of these terms with regard to the present scheme is required before any conclusions regarding stability can be drawn. Examination of the influence of the Θ parameter is also required. In the applications undertaken so far the waves modelled have had wavelengths long enough to prevent significant numerical dissipation by use of $\Theta = 1.0$. If it were intended to use the model to study long wave phenomena with shorter periods, say for example harbour seiching, the effect on numerical results of using values less than 1.0 would need to be determined.

If the further developments indicated above were completed and the scheme were to prove itself as an economic concern subsidiary programmes for data and result manipulation

could then be developed. A start on this was made in the present work where it proved advantageous to develop plotting routines to aid in presenting results from the Firth of Clyde and the Humber Estuary in graphical form.

APPENDIX A

SOLUTION OF LINEAR EQUATIONS

A.1 INTRODUCTION

Modelling a physical system by an implicit finite difference scheme such as equations 3.6 and 3.22 requires the solution of a set of simultaneous equations, for each time increment. The computational procedure for this solution is simplified if the simultaneous equations are written in matrix notation. That is,

$$[R]\ [S] = [T] \qquad \text{Equation A.1}$$

where, R is the coefficient matrix, S is the vector of unknowns and T is a vector containing constants calculated from conditions at the start of the time increment.

Applying any pair of finite difference equations presented in the previous chapters to a solution region containing jj solution nodes gives:

$$[R]=\begin{bmatrix} r1 & r2 & r3 & r4 & . & . & & \\ r5 & r6 & r7 & r8 & . & . & & \\ & & . & . & . & . & & \\ & & & & r1_j & r2_j & r3_j & r4_j & . & . \\ & & & & r5_j & r6_j & r7_j & r8_j & . & . \\ & & & & & . & . & . & . & \\ & & & & & & r1_{jj-1} & r2_{jj-1} & r3_{jj-1} & r4_{jj-1} \\ & & & & & & r5_{jj-1} & r6_{jj-1} & r7_{jj-1} & r8_{jj-1} \end{bmatrix}$$

and,

$$S = \begin{bmatrix} W1_1^{n+1} \\ Q_1^{n+1} \\ \vdots \\ W1_j^{n+1} \\ Q_j^{n+1} \\ \vdots \\ W1_{jj}^{n+1} \\ Q_{jj}^{n+1} \end{bmatrix}$$

with,

$$T = \begin{bmatrix} G_1 \\ H_1 \\ G_j \\ H_j \\ \vdots \\ G_{jj} \\ H_{jj} \end{bmatrix}$$

Equations for evaluation of coefficients r and constant G and H are given in Chapter 3 for the one dimensional flood routing model and Chapter 6 for the two dimensional tidal model.

This set of 2(jj-1) simultaneous equations can be solved for the 2jj unknowns provided that appropriate boundary conditions are available.

A.2 BOUNDARY CONDITIONS

For solution of the simultaneous equation system

A.1, boundary data at the j = 1 and j = jj solution points are required. This data can be either a given value of an unknown or a relationship connecting two unknowns. A discussion of appropriate boundary conditions for real situations is given in sections 3.8 and 6.8.

For the present purpose it is sufficient to note that by transfer ing the product of the known boundary conditions and their coefficients to the right hand side vector T , equation A.1 becomes as shown overleaf.

A.3 CHOICE OF NUMERICAL METHOD

As already stated in Chapter 1, it is important that all programming be as efficient as possible. This is particularly true of the numerical method algorithm, as its execution can account for a large proportion of the total computation time. It was, therefore, necessary to chose, from the large number available, the numerical method particularly suited to the solution of equation A.2.

Adoption of a direct method as opposed to an iterative method was decided; the latter being more efficient when the simultaneous equations result in the formation of a sparse coefficient matrix, Johnson and Dean Reiss (1977). The most efficient direct methods are Gaussian elimination and LU decomposition. LU decomposition has special advantages when the coefficient matrix is tridiagonal in form, Johnson and Dean Reiss (1977) and Abbott (1979). In the present case, however, the finite difference formulation, see Chapters 3 and 6, results in a diagonal coefficient matrix

$$
\begin{bmatrix} W1_1 \end{bmatrix} \times \begin{bmatrix} Q_1 \text{ or } \underline{Q_1} \\ W1_2 \\ Q_2 \\ W1_3 \\ Q_3 \\ W1_4 \\ Q_4 \\ \vdots \\ W1_{jj-1} \\ Q_{jj-1} \\ \underline{Q_{jj} \text{ or } W1_{jj}} \end{bmatrix} = \begin{bmatrix} G_1 \\ H_1 \\ G_2 \\ H_2 \\ G_3 \\ H_3 \\ \vdots \\ G_{jj-2} \\ H_{jj-2} \\ O_{jj-1} \\ \underline{P_{jj-1}} \end{bmatrix}
$$

$$
\begin{bmatrix} \overline{r3}_{jj-2} & \overline{r4}_{jj-2} \\ r7_{jj-2} & r8_{jj-2} \\ r1_{jj-1} & r2_{jj-1} \\ \underline{r5_{jj-1}} & \underline{r6_{jj-1}} \end{bmatrix} \begin{bmatrix} r3_{jj-1} \\ \underline{r7_{jj-1}} \end{bmatrix}
$$

$$
\begin{bmatrix} \overline{r3}_2 & \overline{r4}_2 \\ r7_2 & r8_2 \\ r1_3 & r2_3 \\ \underline{r5_3} & \underline{r6_3} \end{bmatrix} \begin{bmatrix} r4_3 \\ r8_3 \\ \vdots \\ \underline{r2_{jj-2}} \\ r6_{jj-2} \\ \underline{\quad} \\ \underline{\quad} \end{bmatrix} \begin{bmatrix} r3_3 \\ r7_3 \\ \vdots \\ r1_{jj-2} \\ \underline{r5_{jj-2}} \end{bmatrix}
$$

$$
\begin{bmatrix} \overline{r1}_1 & \overline{r3}_1 \\ r2_1 & r7_1 \\ r5_1 & r6_1 \\ \underline{\quad} & \underline{\quad} \\ \underline{\quad} & \underline{\quad} \end{bmatrix} \begin{bmatrix} \overline{r2}_2 \\ r6_2 \\ \underline{\quad} \\ \underline{\quad} \\ \underline{\quad} \end{bmatrix} \begin{bmatrix} r1_2 \\ \underline{r5_2} \end{bmatrix}
$$

EQUATION A.2

with a band width of four. Hence a Gaussian elimination procedure, modified to take advantage of the diagonal nature of the matrix, was adopted.

A.4 MODIFIED GUASSIAN ELIMINATION ROUTINE

Guassian elimination is a variable elimination technique whereby the variables are eliminated one at a time to reduce the original system to an equivalent triangular system, from which a solution can be obtained by back substitution. In the present case it is possible to take advantage of the diagonal nature of the coefficient matrix, in equation A.2 to increase the method's efficiency.

From examination of the coefficient matrix in equation A.2 it can be seen that the forward reduction may be split into units with identical arithmetic for each unit. A typical unit is shown below:

$$\begin{bmatrix} r1_j & r2_j & r3_j \\ r4_j & r5_j & r6_j \\ 0 & r1_{j+1} & r2_{j+1} \\ 0 & r5_{j+1} & r6_{j+1} \end{bmatrix}$$

The arithmetic operations for each unit can now be defined. Noting that the two zero elements will always exist and need not be included in the forward reduction. The arithmetic operations are as follows:

$$C1 = -r4_j / r1_j$$

$$r5^*_j = r5j + C1 \times r2_j$$

$$r6^*_j = r6_j + C1 \times r3_j$$

$$H^*_j = H_j + C1 \times G_j$$

$$C2 = -r1_{j+1}/r5_j$$

$$r2^*_{j+1} = r2_{j+1} + C2 \times r6_j$$

$$G^*_{j+1} = G_{j+1} + C2 \times H_j$$

$$C3 = -r5_{j+1}/r5_j$$

$$r6^*_{j+1} = r6_{j+1} + C3 \times r6_j$$

$$H^*_{j+1} = H_{j+1} + C3 \times H_j$$

Equation A.3

To achieve the forward reduction for a total of 2(jj-1) simultaneous equations it is required that the operations defined in equation A.3 be repeated for j = 1 to j = jj-1. Leaving the elimination of the $r5_{jj-1}$ element to be carried out independently. This completed, the original system is now modified to the triangular system, equation A.4. (see overleaf).

With reference to equation A.4 it is evident that the back substitution also consists of repeatable units. A typical unit is shown below:

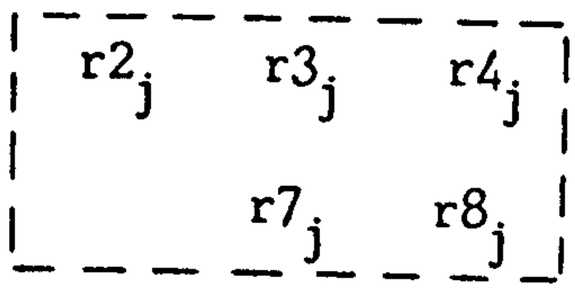

The arithmetic operations for back substitution of this unit are:

$$W1_j = (H^*_{j-1} + r8^*_{j-1} \times Q_j) / r7^*_{j-1}$$

$$Q_{j-1} = (G^*_{j-1} + r4^*_{j-1} \times Q_j + r3^*_{j-1} \times W1_j) / r2^*_{j-1}$$

Equation A.5

Hence, for the back substitution of 2(jj-1) equations it is necessary to start the procedure by calculating

$$
\begin{bmatrix}
r1^*_1 & r2^*_1 & r3^*_1 & & & & & & & \\
 & r4^*_1 & r5^*_1 & & & & & & & \\
 & & & r2^*_2 & r3^*_2 & r4^*_2 & & & & \\
 & & & & r7^*_2 & r8^*_2 & & & & \\
 & & & & & & r2^*_3 & r3^*_3 & r4^*_3 & \\
 & & & & & & & r7^*_3 & r8^*_3 & \\
 & & & & & & & & & \ddots \\
 & & & & & & & & & r2^*_{jj-2} \quad r3^*_{jj-2} \quad r4^*_{jj-2} \\
 & & & & & & & & & r7^*_{jj-2} \quad r8^*_{jj-2} \\
 & & & & & & & & & r2^*_{jj-1} \quad r3^*_{jj-1} \\
 & & & & & & & & & r6^*_{jj-1}
\end{bmatrix}
\times
\begin{bmatrix} Wl_1 \text{ or } G_1 \\ Wl_2 \\ Q_2 \\ Wl_3 \\ Q_3 \\ \vdots \\ Wl_{jj-2} \\ Q_{jj-2} \\ Wl_{jj-1} \\ Q_{jj-1} \\ Wl_{jj} \text{ or } Q_{jj} \end{bmatrix}
=
\begin{bmatrix} G_1 \\ H_1 \\ G_2 \\ H_2 \\ G_3 \\ H_3 \\ \vdots \\ G_{jj-2} \\ H_{jj-2} \\ G_{jj-1} \\ H_{jj-1} \end{bmatrix}
$$

EQUATION A.4

Wl_j or Q_j and Q_{jj-1} independently then repeating the operations defined by equation A.5 from j = jj-2 to j = 1.

After these operations the vector [S] will contain estimates for water level and flow at time (n+1)Δt.

A.5 EFFICIENCY OF MODIFIED GUASSIAN ELIMINATION ROUTINE

There are a number of aspects which must be considered for the practical and efficient implementation of any numerical procedure on a computer. Three such aspects that can influence the choice of algorithm are storage requirements, round-off errors and execution time.

A.5.1 EXECUTION TIME

The execution time required by a method is dependent upon the number of arithmetic operations required to solve the simultaneous equations. Hence a count of the number of arithmetic operations used by various methods, or indeed alternative formulations of the same method gives an estimate of their relative efficiency. The subsequent paragraph is a count of the number of arithmetic operations required by the modified Gaussian elimination routine of section A.3

A.5.1.1 OPERATIONS COUNT

To simplify the count consider division as a multiplication and substraction as an addition.

In the forward reduction phase it can be seen from equation A.3 that each repeatable unit requires

ten multiplications and seven additions. For 2(jj-1) simultaneous equations there will be jj-2 such units, with a further three multiplications and two additions required for the odd elimination. This gives totals of (jj-2) x 10 + 3 multiplications, and (jj-2) x 7 + 2 additions to triangularize the system.

From equation A.5 it is seen that each unit, for back substitution, requires five multiplications and three additions. The (jj-2) repetitions together with the three multiplications and one addition to start the process gives totals of (jj-2) x 5 + 3 multiplications and (jj-2) x 3 + 1 additions.

Hence for one complete solution, (jj-2) x 15 + 6 multiplications and (jj-2) x 10 + 3 additions are required. This shows a great improvement in efficiency over a standard Gaussian elimination, where approximately $(jj-1)^3/3$ multiplications are required for the forward reduction phase alone.

A.5.2 STORAGE REQUIREMENT

Another aspect affecting method efficiency is storage requirements. This was minimised in the present case by storing only non-zero elements of the coefficient matrix. In an array of dimensions (2jj x 4), see Table A.1.

For a system consisting of one hundred solution points, this approach results in 97% reduction in the capacity required to store the coefficient matrix.

A.5.3 ROUND-OFF ERRORS

The subsequent discussion deals with round-off errors

$r1_1$	$r2_1$	$r3_1$	0
$r5_1$	$r6_1$	$r7_1$	0
$r1_2$	$r2_2$	$r3_2$	$r4_2$
$r5_2$	$r6_2$	$r7_2$	$r8_2$
.	.	.	.
.	.	.	.
$r1_{jj-2}$	$r2_{jj-2}$	$r3_{jj-2}$	$r4_{jj-2}$
$r5_{jj-2}$	$r6_{jj-2}$	$r7_{jj-2}$	$r8_{jj-2}$
0	$r1_{jj-1}$	$r2_{jj-1}$	$r3_{jj-1}$
0	$r5_{jj-1}$	$r6_{jj-1}$	$r7_{jj-1}$

TABLE A.1

which arise as a result of the machine truncating numbers for storage purposes. They are present with all computational methods and can under certain circumstances grow to destroy the solution.

For Gaussian elimination the magnitude of round-off errors is a function of both the total number of arithmetic operations and the relative absolute values of the elements forming the coefficients C1, C2 and C3 in equation A.3. Their effect can be minimised by the use of double precision arithmetic and full or partial pivioting techniques, see Broyden (1975) and Johnson and Dean Reiss (1977).

In the present application it was anticipated that no detectable round-off errors would arise. As, in the case of open channel flow problems, the elements in the coefficient matrix are all approximately the same order of magnitude , the total number of arithmetic operations is relatively small.

APPENDIX B

LISTING OF FLOOD ROUTING MODEL

```
      PROGRAM(FLOOD)
      INPUT 5=CRO
      OUTPUT 6=LPO
      END
      MASTER MAIN
      DIMENSION QXA(42),WLA(42),
     1BNDC(8,100),ENDD(100),A(42),B(42),WLW(42),WQ(42),RES(100)
     1,BT(42),EA(42),EB(42),DX(42),AMAT(100,4)
     2,NJ(42),IPTS(42),X(42),TJ(42),AJ(42),XKJ(42),
     3WLD(10,42),T(10,42),XA(10,42),XK(10,42),XF(10,42),
     4WLI(10),TI(10),XAI(10),XKI(10),XFI(10),SF(5),QTJ(5)
     5,QLT(42),QL(10,42),QR(10,42),WLL(10,42),WLR(10,42)
     6,QDS(10),QLJ(42),QRJ(42),DQ(42),DQM(42)
     7,XWL(10,42),RWL(10,42),AWL(10,42),AWR(10,42),VILLE(11),
     8TF(5),SD(11),WWL(42),WWR(42),AL(42),AR(42),KAL(42),KAR(42)
     9,CL(5,42),KL(5,42),CR(5,42),KR(5,42),KABL(2,42),KABR(2,42)
     1,SGRAD(42),GCR(20),CCR(20),ICTRL(20)
      COMMON/BLOCKCT/CT1,CT2,CT3
      COMMON/BLOCKC/C1,C2,C3,C4,C5
      COMMON G
C
C     READ PARAMETER DATA.
C
      READ(5,1)DT
1     FORMAT(1F0.0)
      READ(5,2)JJ,NN
2     FORMAT(2I0)
      READ(5,6)G ,THETA
 6    FORMAT(2F0.0)
      READ(5,2)INDX,JNDX
C
C     READ SECTION PROPERTIES.
C
      DO 13 J=1,JJ
      READ(5,8)I,NJ(I),X(I),IPTS(I)
 8    FORMAT(2I0,F0.0,I0)
      IPTS(I)=10
      READ(5,9)(WLD(K,I),T(K,I),XA(K,I),XK(K,I),XF(K,I),K=1,IPTS(I))
 9    FORMAT(5F0.0)
13    CONTINUE
C
C     READ DOWNSTREAM RATEING CURVE.
C
      READ(5,15)(QDS(K),K=1,IPTS(JJ))
C
C     READ OVERBANK FLOW DATA.
C
      DO 23 J=1,JJ
      READ(5,24)I,K
24    FORMAT(2I0)
      IF(K.GT.0) GO TO 23
      READ(5,25)(WLL(K,I),QL(K,I),K=1,10)
      READ(5,25)(WLR(K,I),QR(K,I),K=1,10)
25    FORMAT(2F0.0)
23    CONTINUE
C
C     READ SUBMERGENCE RATIO CURVE.
C
      READ(5,55)(SD(K),K=1,10)
      READ(5,55)(VILLE(K),K=1,10)
 55   FORMAT(10F0.0)
```

```
C
C       READ IN STORAGE POND DATA.
C
        DO 14 J=1,JJ
        READ(5,12)KAL(J)
12      FORMAT(I0)
        IF(KAL(J).EQ.0) GOTO 31
        IF(J.EQ.1) GOTO 34
        IF(KAL(J).LE.KAL(J-1)) GOTO 3
34      KABL(1,KAL(J))=J
        KALJJ=KAL(J)
        READ(5,25)(XWL(K,KAL(J)),AWL(K,KAL(J)),K=1,10)
3       KABL(2,KAL(J))=J
31      READ(5,12)KAR(J)
        IF(KAR(J).EQ.0) GOTO 14
        IF(J.EQ.1)GOTO 36
        IF(KAR(J).LE.KAR(J-1)) GOTO 32
36      KABR(1,KAR(J))=J
        KARJJ=KAR(J)
        READ(5,25)(RWL(K,KAR(J)),AWR(K,KAR(J)),K=1,10)
32      KABR(2,KAR(J))=J
14      CONTINUE
C
C       READ IN INITIAL CONDITIONS.
C
        READ(5,15)(WLA(I),I=1,JJ)
        READ(5,15)(QXA(I),I=1,JJ)
        READ(5,15)(WWL(I),I=1,KALJJ)
        READ(5,15)(WWR(I),I=1,KARJJ)
   15 FORMAT(10F0.0)
C
C       CALCULATE VALUES OF DX BETWEEN SECTIONS.
C
        DO 16 J=1,JJ-1
        DX(J)=X(J+1)-X(J)
   16 CONTINUE
        DO 18 J=1,JJ
        IF(NJ(J).EQ.0) GOTO 18
C
C       READ INFLOW HYDROGRAPHS.
C
        READ(5,4)(BNDC(NJ(J),K),K=1,NN+1)
   18 CONTINUE
        IF(JNDX.GT.2) GOTO 7
C
C       READ DOWNSTREAM BOUNDARY CONDITIONS IF REQUIRED.
C
        READ(5,4)(BNDD(N),N=1,NN)
4       FORMAT(10F0.0)
7       CT1=1.0/DT
        CT2=0.5*CT1
        CT3=CT2/G
        C1=THETA
        C2=1.0-THETA
        C4=0.5/G
        C3=C1*C4
        C5=2.0*THETA
        I=0
C
C       ARRANGE BANK SECTIONS IN ORDER ELEVATION.
C
```

```
      DO 305 K=1,KALJJ
      I=1
      DO 305 J=KABL(1,K),KABL(2,K)
      L=I-1
307   IF(L.EQ.0) GOTO 306
      IF(WLL(1,J).GT.CL(L,K)) GOTO 306
      CL(L+1,K)=CL(L,K)
      KL(L+1,K)=KL(L,K)
      L=L-1
      GOTO 307
306   I=I+1
      CL(L+1,K)=WLL(1,J)
      KL(L+1,K)=J
305   CONTINUE
      I=0
      DO 312 K=1,KARJJ
      I=1
      DO 312 J=KABR(1,K),KABP(2,K)
      L=I-1
313   IF(L.EQ.0) GOTO 314
      IF(WLR(1,J).GT.CR(L,K)) GOTO 314
      CR(L+1,K)=CR(L,K)
      KR(L+1,K)=KR(L,K)
      L=L-1
      GOTO 313
314   I=I+1
      CR(L+1,K)=WLR(1,J)
      KR(L+1,K)=J
312   CONTINUE
C
C     SET CONTROL INDICATORS FOR SOLUTION AS ONE REACH.
C
      ICTRL(1)=1
      ICTRL(2)=JJ
      INDCR=0
      NCTRL=0
C
C     START OF TIME LOOP.
C
      DO 170 IT=1,NN
      N=0
C
C     INTERPOLATE SECTION PROPERTIES FOR USE IN THIS INCREMENT
C
      DO 17 J=1,JJ
      CALL COPY(WLD,WLI,J,IPTS(J))
      CALL INTERP(WLA(J),WLI,IPTS(J),K,P)
      AJ(J)=XA(K,J)+P*(XA(K+1,J)-XA(K,J))
      BT(J)=T(K,J)+P*(T(K+1,J)-T(K,J))
      XKJ(J)=XK(K,J)+P*(XK(K+1,J)-XK(K,J))
      EA(J)=ENRG(WLA(J),QXA(J),AJ(J))
      SGRAD(J)=(XK(K+1,J)-XK(K,J))/(WLD(K+1,J)-WLD(K,J))
   17 CONTINUE
      IF(JNDX.NE.3) GOTO 20
      BNDD(IT)=QDS(K)+P*(QDS(K+1)-QDS(K))
20    IF(JNDX.NE.4) GOTO 26
      ENDG=(QDS(K+1)-QDS(K))/(WLD(K+1,JJ)-WLD(K,JJ))
      BNDR=QXA(JJ)-BNDG*WLA(JJ)
26    TIME=(IT-1)*DT/3600
C
C     WRITE CONDITIONS AT START OF TIME INCREMENT.
```

```
C
      WRITE(6,66) TIME
   66 FORMAT(1H ,9HTIME HRS=,F10.3)
      WRITE(6,5)
 5    FORMAT(1H ,22HWATER LEVEL METRES ADD)
      WRITE(6,11)(WLA(J),J=1,JJ)
      WRITE(6,19)
 19   FORMAT(1H ,15HFLOWRATE CUMECS)
      WRITE(6,11)(QXA(J),J=1,JJ)
  11  FORMAT(1H ,10F8.3)
      WRITE(6,67)
67    FORMAT(1H ,25HWASHLAND LEVEL METERS ADD)
      WRITE(6,68)(WWL(J),J=1,KALJJ)
68    FORMAT(1H ,10HLEFT BANK ,10F10.3)
      WRITE(6,69)(WWR(J),J=1,KARJJ)
69    FORMAT(1H ,10HRIGHT BANK,10F10.3)
C
C     DETERMINE LATERAL FLOWS AND POND LEVELS ON LEFT BANK.
C
      DO 315 K=1,KALJJ
330   CALL COPY(XWL,WLI,K,10)
      CALL INTERP(WWL(K),WLI,10,N,P)
      AL(K)=AWL(N,K)+P*(AWL(N+1,K)-AWL(N,K))
      L=0
      DO 316 J=KABL(1,K),KABL(2,K)
      IF(KAL(J).NE.K) GOTO 316
      L=L+1
      CALL COPY(WLL,WLI,J,10)
   49 IF(WLA(J).GT.WWL(KAL(J)))GOTO 40
      S=1.0
      WU=WWL(KAL(J))
      WD=WLA(J)
      GOTO 41
   40 S=-1.0
      WU=WLA(J)
      WD=WWL(KAL(J))
   41 IF(WU.GT.WLI(1))GOTO 43
      QTJ(L)=0.0
      QLJ(J)=0.0
      DQ(J)=0.0
      GOTO 316
43    CALL INTERP(WU,WLI,10,N,P)
      DQ(J)=S*(QL(N+1,J)-QL(N,J))/(WLI(N+1)-WLI(N))
      QTJ(L)=S*(QL(N,J)+P*(QL(N+1,J)-QL(N,J)))
      SR=(WD-WLI(1))/(WU-WLI(1))
      CALL INTERP(SR,SD,10,N,P)
      SF(L)=VILLE(N)+P*(VILLE(N+1)-VILLE(N))
      QLJ(J)=QTJ(L)*SF(L)
      DQ(J)=DQ(J)*SF(L)
316   CONTINUE
      SUMQL=0.0
      GQ=0.
      DO 318 J=KABL(1,K),KABL(2,K)
      IF(KAL(J).NE.K) GOTO 318
      IF(QLJ(J).GT.0.0) GQ=GQ+DQ(J)*0.5
      SUMQL=SUMQL+QLJ(J)
318   CONTINUE
      WLF=-SUMQL/(AL(K)/DT+GQ)+WWL(K)
344   L=0
      GQ=0.0
      DO 340 J=KABL(1,K),KABL(2,K)
```

```
      IF(KAL(J).NE.K) GOTO 340
      L=L+1
      IF(QLJ(J))353,340,349
353   SR=(WLF-WLL(1,J))/(WLA(J)-WLL(1,J))
      GOTO 350
349   SR=(WLA(J)-WLL(1,J))/(WLF-WLL(1,J))
350   CALL INTERP(SR,SD,10,N,P)
      SF2=VILLE(N)+P*(VILLE(N+1)-VILLE(N))
      DQ(J)=DQ(J)/SF(L)
      QLJ(J)=QTJ(L)*0.5*SF(L)+QTJ(L)*SF2*0.5
      DQ(J)=0.5*(DQ(J)*SF(L)+DQ(J)*SF2)
      SUMQL=SUMQL+QTJ(L)*0.5*(SF2-SF(L))
      IF(QLJ(J).GT.0.0)GQ=GQ+0.5*DQ(J)
340   CONTINUE
      WLF=-SUMQL/(AL(K)/DT+GQ)+WWL(K)
345   L=0
      M=KABL(2,K)-KABL(1,K)+1
      IF(WWL(K).GE.WLF) GOTO 341
      DO 319 I=1,M
      J=KL(I,K)
      IF(KAL(J).NE.K) GOTO 319
      IF(CL(I,K).GE.WLF) GOTO 341
      IF(WLA(J).GT.CL(I,K)) GOTO 320
      IF(QLJ(J).GT.0.0) GOTO 319
      WRITE(6,710)
710   FORMAT(1H ,41H*****LEFT POND WATERLEVEL ABOVE BANK.****)
      TF(I)=(WLF-CL(I,K))/(WLF-WWL(K))
      X3=CL(I,K)
321   CALL COPY(WLL,WLI,J,10)
      DQ(J)=(QL(2,J)-QL(1,J))/(WLI(2)-WLI(1))
      DQ(J)=DQ(J)*TF(I)
      X1=AL(K)/DT
      X2=0.5*DQ(J)
      WLF=(WLF*X1+X2*X3)/(X1+X2)
      QLJ(J)=0.5*DQ(J)*(WLF-X3)
      GOTO 319
320   IF(WLF.LE.WLA(J).OR.QLJ(J).GT.0.0) GOTO 319
      TF(I)=(WLA(J)-WWL(K))/(WLF-WWL(K))
      WLF=WLF+QLJ(J)*DT/AL(K)
      QLJ(J)=QLJ(J)*TF(I)
      DQ(J)=DQ(J)*TF(I)
      WLF=WLF-QLJ(J)*DT/AL(K)
319   CONTINUE
341   WWL(K)=WLF
315   CONTINUE
C
C     WRITE LEFT LATERAL FLOWS.
C
      WRITE(6,52)
52    FORMAT(1H ,27HFLOWS OVER LEFT BANK CUMECS)
      WRITE(6,11)(QLJ(J),J=1,JJ)
C
C     DETERMINE LATERAL FLOWS AND POND WATER LEVELS ON RIGHT BANK.
C
      DO 323 K=1,KARJJ
335   CALL COPY(RWL,WLI,K,10)
      CALL INTERP(WWR(K),WLI,10,N,P)
      AR(K)=AWR(N,K)+P*(AWR(N+1,K)-AWR(N,K))
      L=0
      DO 324 J=KAER(1,K),KAER(2,K)
      IF(KAR(J).NE.K) GOTO 324
```

```
      L=L+1
   44 CALL COPY(WLR,WLI,J,10)
   51 IF(WLA(J).GT.WWR(KAR(J)))GOTO 45
      S=1.0
      WU=WWR(KAR(J))
      WD=WLA(J)
      GOTO 46
   45 S=-1.0
      WU=WLA(J)
      WD=WWR(KAR(J))
   46 IF(WU.GT.WLI(1))GOTO47
      QTJ(L)=0.0
      QRJ(J)=0.0
      DQM(J)=0.0
      GOTO 324
47    CALL INTERP(WU,WLI,10,N,P)
      DQM(J)=S*(QR(N+1,J)-QR(N,J))/(WLI(N+1)-WLI(N))
      QTJ(L)=S*(QR(N,J)+P*(QR(N+1,J)-QR(N,J)))
      SR=(WD-WLI(1))/(WU-WLI(1))
      CALL INTERP(SR,SD,10,N,P)
      SF(L)=VILLE(N)+P*(VILLE(N+1)-VILLE(N))
      DQM(J)=DQM(J)*SF(L)
      QRJ(J)=QTJ(L)*SF(L)
324   CONTINUE
      SUMQR=0.0
      GQ=0.
      DO 326 J=KAER(1,K),KABR(2,K)
      IF(KAR(J).NE.K) GOTO 326
      IF(QRJ(J).GT.0.0) GQ=GQ+DQM(J)*0.5
      SUMQR=SUMQR+QRJ(J)
326   CONTINUE
      WRF=-SUMQR/(AR(K)/DT+GQ)+WWF(K)
346   L=0
      GQ=0.0
      DO 347 J=KABR(1,K),KAER(2,K)
      IF(KAR(J).NE.K) GOTO 347
      L=L+1
      IF(QRJ(J))354,347,351
354   SR=(WRF-WLR(1,J))/(WLA(J)-WLR(1,J))
      GOTO 352
351   SR=(WLA(J)-WLR(1,J))/(WRF-WLR(1,J))
352   CALL INTERP(SR,SD,10,N,P)
      SF2=VILLE(N)+P*(VILLE(N+1)-VILLE(N))
      DQM(J)=DQM(J)/SF(L)
      QRJ(J)=QTJ(L)*0.5*SF(L)+QTJ(L)*SF2*0.5
      DQM(J)=0.5*(DQM(J)*SF(L)+DQM(J)*SF2)
      SUMQR=SUMQR+QTJ(L)*0.5*(SF2-SF(L))
      IF(QRJ(J).GT.0.0)GQ=GQ+0.5*DQM(J)
347   CONTINUE
      WRF=-SUMQR/(AR(K)/DT+GQ)+WWF(K)
348   L=0
      M=KABR(2,K)-KAER(1,K)+1
      IF(WWR(K).GE.WRF) GOTO 342
      DO 327 I=1,M
      J=KR(I,K)
      IF(KAR(J).NE.K) GOTO 327
      IF(CR(I,K).GE.WRF) GOTO 342
      IF(WLA(J).GT.CR(I,K)) GOTO 328
      IF(QRJ(J).GT.0.0) GOTO 327
      WRITE(6,711)
711   FORMAT(1H ,47H*****RIGHT POND WATERLEVEL ABOVE BANKLEVEL*****)
```

```
TF(I)=(WRF-CR(I,K))/(WRF-WWR(K))
X3=CR(I,K)
CALL COPY(WLR,WLI,J,10)
DQM(J)=(QR(2,J)-QR(1,J))/(WLI(2)-WLI(1))
DQM(J)=DQM(J)*TF(I)
X1=AR(K)/DT
X2=0.5*DQM(J)
WRF=(WRF*X1+X2*X3)/(X1+X2)
QRJ(J)=0.5*DQM(J)*(WRF-X3)
GOTO 327
IF(WRF.LE.WLA(J).OR.QRJ(J).GT.0.0) GOTO 327
TF(I)=(WLA(J)-WWR(K))/(WRF-WWR(K))
WRF=WRF+QRJ(J)*DT/AR(K)
QRJ(J)=QRJ(J)*TF(I)
DQM(J)=DQM(J)*TF(I)
WRF=WRF-QRJ(J)*DT/AR(K)
CONTINUE
WWR(K)=WRF
CONTINUE

WRITE RIGHT LATERAL FLOWS.

WRITE(6,53)
FORMAT(1H ,28HFLOWS OVER RIGHT BANK CUMECS)
WRITE(6,11)(QRJ(J),J=1,JJ)

CALCULATE TOTAL LATERAL FLOW INCLUDING TRIBUTARY IF NECESSARY.

DO 332 J=1,JJ
QLT(J)=QLJ(J)+QRJ(J)
IF(DQ(J).GT.0.0)DQ(J)=0.0
IF(DQM(J).LT.0.0)DQ(J)=DQ(J)+DQM(J)
IF(NJ(J).LT.2) GOTO 332
QLT(J-1)=QLT(J-1)+0.5*(BNDC(NJ(J),IT)+BNDC(NJ(J),IT+1))
CONTINUE

DETERMINE IF ANY EXISTING CONTROLS DROWNED OR IF ANY NEW CONTROLS FORMED

N=1
JA=ICTRL(N)
JAJ=ICTRL(N+1)
IF(JAJ.EQ.JJ) GOTO 290
S1=QXA(JAJ)/XKJ(JAJ)
S1=S1*S1
S2=QXA(JAJ+1)/XKJ(JAJ+1)
S2=S2*S2
F1=S2/(S1+S2)
F2=S1/(S1+S2)
EDS=EA(JAJ+1)+DX(JAJ)*(F1*S1+F2*S2)
ECR=EA(JAJ)
IF(EDS.LT.ECR) GOTO 310
WRITE(6,26)JAJ
FORMAT(1H ,21HCONTROL DROWNED AT J=,I3)
L=N
L=L+1
ICTRL(L)=ICTRL(L+1)
GCR(L)=GCR(L+1)
CCR(L)=CCR(L+1)
IF(ICTRL(L).EQ.JJ) GOTO 230
GOTO 220
NCRTL=NCTRL-1
```

```
      JA=JAJ
      GOTO 211
310   CALL COPY(WLD,WLI,JAJ,IPTS(JAJ))
      CALL INTERP(WLA(JAJ),WLI,IPTS(JAJ),K,P)
      QCR=XF(K,JAJ)+P*(XF(K+1,JAJ)-XF(K,JAJ))
      QCR=QCR*0.9
      GCR(N+1)=0.9*(XF(K+1,JAJ)-XF(K,JAJ))/(WLD(K+1,JAJ)-WLD(K,JAJ))
      CCR(N+1)=QCR-GCR(N+1)*WLA(JAJ)
280   IAI=JAJ-1
      IF(JA+1.EQ.JAJ) GOTO 180
      DO 180 J=JA+1,IAI
      CALL COPY(WLD,WLI,J,IPTS(J))
      CALL INTERP(WLA(J),WLI,IPTS(J),K,P)
      QCR=XF(K,J)+P*(XF(K+1,J)-XF(K,J))
      QCR=0.9*QCR
      IF(QCR-QXA(J).GE.0.01) GOTO 180
      WRITE(6,7)J
7     FORMAT(1H ,19HCRITICAL FLOW AT J=,I3)
      GCRT=0.9*(XF(K+1,J)-XF(K,J))/(WLD(K+1,J)-WLD(K,J))
      CCRT=QCR-GCRT*WLA(J)
      INDCR=1
      NCTRL=NCTRL+1
      L=NCTRL+1
260   ICTRL(L+1)=ICTRL(L)
      GCR(L+1)=GCR(L)
      CCR(L+1)=CCR(L)
      L=L-1
      IF(J.LT.ICTRL(L)) GOTO 260
270   ICTRL(L+1)=J
      GCR(L+1)=GCRT
      CCR(L+1)=CCRT
180   CONTINUE
      IF(JAJ.EQ.JJ) GOTO 290
      N=N+1
      GOTO 210
290   N=0
190   N=N+1
      JA=ICTRL(N)+1
      IF(JA.EQ.2)JA=1
      JAJ=ICTRL(N+1)
      IAJ=JAJ-JA
      IF(IAJ.NE.0) GOTO 200
      N=N+1
      JAJ=ICTRL(N+1)
      IAJ=JAJ-JA
200   JAJJ=IAJ*2
      JAJJJ=(IAJ+1)*2
C
C     CALCULATE R.H.S. VECTOR.
C
140    CALL AANDB(DT,DX,WLA,QXA,QLT,DQ,EA,A,E,AJ,ET,XKJ,AJ,
     1IAJ,JA,SGRAD)
       CALL VECT(A,E,RES,JAJ,JAJJ,JAJJJ)
C
C      FORM COEFFICIENT MATRIX.
C
       CALL FORM(QXA,AJ,AMAT,JAJJ,JA,DX,ET,XKJ,AJ,DQ,SGRAD)
       IF(ICTRL(N).EQ.1) GOTO 21
       BND1=QXA(JA-1)+QLT(JA-1)
       IND=2
       GOTO 22
```

```
21      BND1=BNDC(1,IT)
        IND=INDX
22      IF(ICTRL(N+1).EQ.JJ) GOTO 400
        JND=4
        GOTO 42
400     BND2=BNDD(IT)
        JND=JNDX
        GCR(N+1)=BNDG
        CCR(N+1)=BNDR
42      CALL BOUND(AMAT,RES,IND,JND,BND1,BND2,JAJJ,GCR(N+1),CCR(N+1))
C
C       SOLVE BY GAUSSIAN ELIMINATION.
C
        CALL GAUSS(AMAT,RES,JAJJ,JND,GCR(N+1),CCR(N+1))
        CALL SWITCH(RES,IND,JND,BND1,BND2,WLW,WQ,JAJ,JA
       1,JAJJ,JAJJJ)
        DO 130 J=JA,JAJ
        WLA(J)=WLW(J)
        QXA(J)=WQ(J)
  130   CONTINUE
        IF(JA.NE.1) GOTO 300
        WLA(1)=WLW(1)
        QXA(1)=WQ(1)
300     IF(JAJ.EQ.JJ) GOTO 170
        GOTO 190
170     CONTINUE
        STOP
        END
        SUBROUTINE AANDB(DT,DX,WL,QU,QL,DQL,E,A,B,AB,BT,XKJ,AJ
       1,IAN,IA,SGRAD)
        DIMENSION WL(42),QU(42),E(42),XKJ(42),AJ(42),
       1BT(42),DX(42),A(42),B(42),AB(42),AC(42),CL(42)
       2,SGRAD(42),DQL(42)
        COMMON/BLOCKCT/CT1,CT2,CT3
        COMMON/BLOCKC/C1,C2,C3,C4,C5
        COMMON G
        J=IA-1
        DO 45 K=1,IAN
        J=J+1
        DXI=1.0/DX(J)
6       A(K)=(WL(J)*BT(J)+WL(J+1)*BT(J+1))*CT2
       1-0.5*DXI*(QU(J+1)-QU(J))+(QL(J)-DQL(J)*WL(J)
       1/2.0)*DXI
        QD=QU(J)
        QE=QU(J+1)
        S1=QD*QD/(XKJ(J)*XKJ(J))
        S2=QE*QE/(XKJ(J+1)*XKJ(J+1))
        F1=S2/(S1+S2)
        F2=S1/(S1+S2)
        B(K)=(QU(J)/AJ(J)+QU(J+1)/AJ(J+1))*CT3+C2*DXI*(E(J)-E(J+1))
       1-F1*(1.0-C5*(1.0-SGRAD(J)*WL(J)/XKJ(J)))*S1
       2-F2*(1.0-C5*(1.0-SGRAD(J+1)*WL(J+1)/XKJ(J+1)))*S2
45      CONTINUE
30      RETURN
        END
        SUBROUTINE VECT(A,B,C,NAN,NANN,NANNN)
        DIMENSION A(42),B(42),C(100)
        J=0
        DO 20 N=1,NANN,2
        J=J+1
        C(N)=A(J)
```

```
      C(N+1)=B(J)
20    CONTINUE
30    RETURN
      END
      SUBROUTINE FORM(Q2,A2,XMAT,NANN,NA,DX,BT,XKJ,AJ,DQL,SGRAD)
      DIMENSION Q2(42),A2(42),XMAT(100,4),DX(42),BT(42)
     1,SGRAD(42),DQL(42),XKJ(42),AJ(42)
      COMMON/BLOCKCT/CT1,CT2,CT3
      COMMON/BLOCKC/C1,C2,C3,C4,C5
      J=NA
      NN=NANN-1
      K=NA-1
20    DO 30 N=1,NN,2
      K=K+1
      S1=Q2(J)*Q2(J)/(XKJ(J)*XKJ(J))
      S2=Q2(J+1)*Q2(J+1)/(XKJ(J+1)*XKJ(J+1))
      F1=S2/(S1+S2)
      F2=S1/(S1+S2)
      DXI=1.0/DX(K)
      A1=AJ(J)
      CA=Q2(J)*(C3*DXI/(A1*A1))
      CC=F1*C5*Q2(J)/(XKJ(J)*XKJ(J))
      CD=-F1*C5*SGRAD(J)*Q2(J)*Q2(J)/(XKJ(J)*XKJ(J)*XKJ(J))
      XMAT(N,1)=CT2*BT(K)-DQL(K)*0.5*DXI
      XMAT(N,2)=-0.5*DXI
      XMAT(N,3)=CT2*BT(K+1)
      J=J+1
      XMAT(N,4)=0.5*DXI
      I=N+1
      A3=AJ(J)
      CB=Q2(J)*(C3*DXI/(A3*A3))
      CE=F2*C5*Q2(J)/(XKJ(J)*XKJ(J))
      CF=-F2*C5*SGRAD(J)*Q2(J)*Q2(J)/(XKJ(J)*XKJ(J)*XKJ(J))
      XMAT(I,1)=-C1*DXI+CD
      XMAT(I,2)=CT3/A1-CA+CC
      XMAT(I,3)=C1*DXI+CF
      XMAT(I,4)=CT3/A3+CE+CE
30    CONTINUE
40    RETURN
      END
      SUBROUTINE BOUND(A,C,IND,JND,BND1,BND2,NANN,GCR,CCR)
      DIMENSION A(100,4),C(100)
      IF(IND.EQ.2) GOTO 10
      C(1)=C(1)-A(1,1)*BND1
      C(2)=C(2)-A(2,1)*BND1
      A(1,1)=A(1,2)
      A(1,2)=A(1,3)
      A(1,3)=A(1,4)
      A(2,1)=A(2,2)
      A(2,2)=A(2,3)
      A(2,3)=A(2,4)
      GOTO 30
10    C(1)=C(1)-A(1,2)*BND1
      C(2)=C(2)-A(2,2)*BND1
      A(1,2)=A(1,3)
      A(1,3)=A(1,4)
      A(2,2)=A(2,3)
      A(2,3)=A(2,4)
30    J=NANN-1
      IF(JND.GT.1) GOTO 50
      C(J)=C(J)-A(J,3)*BND2
```

```
      C(NANN)=C(NANN)-A(NANN,3)*BND2
      A(J,3)=A(J,4)
      A(NANN,3)=A(NANN,4)
      GOTO 60
50    IF(JND.GT.3) GOTO 20
      C(J)=C(J)-A(J,4)*BND2
      C(NANN)=C(NANN)-A(NANN,4)*BND2
      GOTO 60
20    A(NANN+1,3)=-GCR
      A(NANN+1,4)=1.0
      C(NANN+1)=CCR
60    RETURN
      END
      SUBROUTINE GAUSS(A,C,NANN,JND,GCR,CCR)
      DIMENSION A(100,4),C(100)
      IF(NANN.EQ.2) GOTO 40
      COEF=-A(2,1)/A(1,1)
      A(2,1)=0.0
      A(2,2)=A(2,2)+A(1,2)*COEF
      A(2,3)=A(2,3)+A(1,3)*COEF
      C(2)=C(2)+C(1)*COEF
      COEF=-A(3,1)/A(2,2)
      A(3,1)=0.0
      A(3,2)=A(3,2)+A(2,3)*COEF
      C(3)=C(3)+C(2)*COEF
      COEF=-A(4,1)/A(2,2)
      A(4,1)=0.0
      A(4,2)=A(4,2)+A(2,3)*COEF
      C(4)=C(4)+C(2)*COEF
      NN=NANN-3
      IF(NN.LT.3) GOTO 10
      DO 10 K=3,NN,2
      I=K+1
      J=K+2
      L=K+3
      COEF=-A(I,2)/A(K,2)
      A(I,2)=0.0
      A(I,3)=A(I,3)+A(K,3)*COEF
      A(I,4)=A(I,4)+A(K,4)*COEF
      C(I)=C(I)+C(K)*COEF
      COEF=-A(J,1)/A(I,3)
      A(J,1)=0.0
      A(J,2)=A(J,2)+A(I,4)*COEF
      C(J)=C(J)+C(I)*COEF
      COEF=-A(L,1)/A(I,3)
      A(L,1)=0.0
      A(L,2)=A(L,2)+A(I,4)*COEF
      C(L)=C(L)+C(I)*COEF
10    CONTINUE
      L=NANN
      J=NANN-1
      COEF=-A(L,2)/A(J,2)
      A(L,2)=0.0
      A(L,3)=A(L,3)+A(J,3)*COEF
      A(L,4)=A(L,4)+A(J,4)*COEF
      C(L)=C(L)+C(J)*COEF
      IF(JND.LT.4) GOTO 60
      COEF=-A(L,3)/A(L+1,3)
      A(L,4)=A(L,4)+COEF*A(L+1,4)
      CTEMP=(C(L)+COEF*C(L+1))/A(L,4)
      C(L+1)=(C(L+1)-CTEMP*A(L+1,4))/A(L+1,3)
```

```
      C(L)=C(L+1)
      C(L+1)=CTEMP
      C(L-1)=(C(L-1)-C(L)*A(L-1,3)-C(L+1)*A(L-1,4))/A(L-1,2)
      GOTO 70
60    C(NANN)=C(NANN)/A(NANN,3)
      C(NANN-1)=(C(NANN-1)-C(NANN)*A(NANN-1,3))/A(NANN-1,2)
70    K=NANN-2
      IF(K.EQ.2) GOTO 30
20    C(K)=(C(K)-C(K+1)*A(K,4))/A(K,3)
      K=K-1
      C(K)=(C(K)-C(K+1)*A(K,3)-C(K+2)*A(K,4))/A(K,2)
      K=K-1
      IF(K.EQ.2) GOTO 30
      GOTO 20
30    C(2)=(C(2)-C(3)*A(2,3))/A(2,2)
      C(1)=(C(1)-C(2)*A(1,2)-C(3)*A(1,3))/A(1,1)
      GOTO 50
40    A(3,2)=A(3,3)
      A(3,3)=A(3,4)
      COEF=-A(2,1)/A(1,1)
      A(2,2)=A(2,2)+COEF*A(1,2)
      A(2,3)=A(2,3)+COEF*A(1,3)
      C(2)=C(2)+COEF*C(1)
      COEF=-A(2,2)/A(3,2)
      A(2,3)=A(2,3)+COEF*A(3,3)
      CTEMP=(C(2)+COEF*C(3))/A(2,3)
      C(3)=(C(3)-A(3,3)*CTEMP)/A(3,2)
      C(2)=C(3)
      C(3)=CTEMP
      C(1)=(C(1)-A(1,3)*C(3)-A(1,2)*C(2))/A(1,1)
50    RETURN
      END
      SUBROUTINE SWITCH(RES,IND,JND,BND1,BND2,WL,Q,NN,II,NNN,N)
      DIMENSION RES(100),WL(42),Q(42)
      IS=NN-1
      JJ=2
      DO 10 I=II+1,IS
      WL(I)=RES(JJ)
      JJ=JJ+2
10    CONTINUE
      JJ=3
      DO 20 I=II+1,IS
      Q(I)=RES(JJ)
      JJ=JJ+2
20    CONTINUE
      IF(IND.EQ.2) GOTO 30
      WL(II)=BND1
      Q(II)=RES(1)
      GOTO 40
30    WL(II)=RES(1)
      Q(II)=END1
40    IF(JND.GT.1) GOTO 50
      WL(NN)=BND2
      Q(NN)=RES(NNN)
      GOTO 60
50    IF(JND.GT.3) GOTO 70
      WL(NN)=RES(NNN)
      Q(NN)=BND2
      GOTO 60
70    Q(NN)=RES(NNN+1)
      WL(NN)=RES(NNN)
```

```
60      RETURN
        END
        FUNCTION ENRG(WL,Q1,A1)
        COMMON/BLOCKC/C1,C2,C3,C4,C5
        ENRG=WL+(Q1*Q1)/(A1*A1)*C4
        RETURN
        END
        SUBROUTINE COPY(F,FI,I,IPTS)
        DIMENSION F(10,42),FI(10)
        DO 10 K=1,IPTS
        FI(K)=F(K,I)
    10  CONTINUE
        RETURN
        END
        SUBROUTINE INTERP(X,XF,IPTS,J,P)
        DIMENSION XF(10)
        IF(X.LE.XF(1) ) GO TO 10
        IF(X.GE.XF(IPTS)) GO TO 11
        DO 12 I=2,IPTS
        IF(X.LT.XF(I)) GO TO 13
   12   CONTINUE
   10   J=1
        P=0.0
        GO TO 14
   11   J=IPTS-1
        P=1.0
        GO TO 14
   13   J=I-1
        P=(X-XF(I-1))/(XF(I)-XF(I-1))
   14   RETURN
        END
        FINISH
```

APPENDIX C

LISTING OF TIDAL MODEL

```
      DIMENSION BNDA(17,1),BNDB(1,1),BNDC(1,1),BNDD(47,1),
     &Z(47,19),S(47),SF(47,19),WLVSTIM(4,360),XUS(47),
     &ZZC(4,80),IDIR(17),SPITX(2,17),XFLOW(47,19)
      DIMENSION XNAMES(12,10),ICOORDS(12,2),ABRV(12,2)
     &,ICE(12,2),VSX(8,200),VSY(8,200),VSC(8,200)
      COMMON/BLOCKA/US(47),DS(47),UF(47),DF(47),VS(47)
      COMMON/BLOCKB/ES(47),EF(47)
      COMMON/BLOCKC/C1,C2,C3,C4,C5
      COMMON/CT/CT1,CT2,CT3
      COMMON/CX/CX1,CX2,CX3,CX4,CX5,CX6,CX7,CX8,CX9
      COMMON/CY/CY1,CY2,CY3,CY4,CY5,CY6,CY7,CY8,CY9
      COMMON/BLOCKD/JJ,KK,NN,NAN
      COMMON/BLOCKE/DX,DY,DT
      COMMON/BLOCKF/A(47),B(47)
      COMMON/BLOCKG/AMAT(94,4),RES(94)
      COMMON/BOUNDX/INDX(47,4),JNDX(47,4),JSTART(47,4),JFINISH(47,4)
     &,NSTART(47,4),NFINISH(47,4),IXTYPE(47,4),NXREACH(47)
      COMMON/BOUNDY/INDY(19,4),JNDY(19,4),KSTART(19,4),KFINISH(19,4)
     &,IYTYPE(19,4),NYREACH(19),LSTART(19,4),LFINISH(19,4)
      COMMON/CONDA/WLA(47,19),DA(47,19),CXA(47,19),CYA(47,19)
      COMMON/CONDB/WLB(47,19),DB(47,19),CXB(47,19),CYB(47,19)
      COMMON/GRID/IGRIDX(47,19),IGRIDY(47,19)
      COMMON/ENERGY/EA(47,19),EB(47,19)
      COMMON G
      READ(1,*)DX,DY,DT
      READ(1,*)JJ,KK,NN,NXMAX,NYMAX,NPTS
      READ(1,*)G,THETA,EXWL
      READ(1,*)INCRS,CH,XLAT,OMEGA,DENWAT,DENAIR,WCOEFF
      READ(1,*)((SPITX(I,J),J=1,JJ),I=1,2)
      XLAT=XLAT*0.017453
      COF=2.0*OMEGA*SIN(XLAT)/G
      CH=CH*CH
      READ(9,707)((DA(K,J),J=1,JJ),K=1,KK)
      READ(9,707)((CYA(K,J),J=1,JJ),K=1,KK)
      READ(9,707)((CXA(K,J),J=1,JJ),K=1,KK)
      READ(9,707)((Z(K,J),J=1,JJ),K=1,KK)
      READ(9,705)((XFLOW(K,J),J=1,JJ),K=1,KK)
      READ(9,708)((SF(K,J),J=1,JJ),K=1,KK)
      READ(8,602)((IGRIDX(K,J),J=1,JJ),K=1,KK)
      READ(8,602)((IGRIDY(K,J),J=1,JJ),K=1,KK)
602   FORMAT(17I3)
      READ(5,608)((XNAMES(N,L),L=1,10),N=1,NPTS)
608   FORMAT(10A8)
      READ(5,703)((ABRV(N,L),L=1,2),N=1,NPTS)
703   FORMAT(2A3)
      READ(5,609)((ICOORDS(N,L),L=1,2),N=1,NPTS)
609   FORMAT(2I4)
      READ(12,*)NVS
      READ(12,*)((ICE(N,L),L=1,2),N=1,NVS)
      CALL BOUNDS(NXMAX,NYMAX,1)
      CT1=1.0/DT
      CT2=0.5*CT1
      CT3=CT2/3
      CX1=1.0/DX
      CX2=0.5*CX1
      CX3=THETA*CX1
      CX4=(1.0-THETA)*CX1
      CX5=0.25*CX1
      CY1=1.0/DY
      CY2=0.5*CY1
      CY3=THETA*CY1
```

```
      CY4=(1.0-THETA)*CY1
      CY5=0.25*CY1
      CC=G*DT
      CX6=CC*CX3
      CX7=CC*CX4
      CX8=0.5*CX6
      CX9=0.5*CX7
      CY6=CC*CY3
      CY7=CC*CY4
      CY8=0.5*CY6
      CY9=0.5*CY7
      C1=1.0/G
      C2=0.5*C1
      C3=0.125*C2
      C4=CX3*C2
      C5=CY3*C2
      MRS=FLOAT(NN)*DT/3600.0
      NISC=NN/INCRS+1
      TIME=0.0
      WRITE(3,706)JJ,KK,NISC
705   FORMAT(3I4,2F8.1)
706   FORMAT(3I4)
      WRITE(3,23)TIME
      WRITE(3,12)((DA(K,J),J=1,JJ),K=1,KK)
      WRITE(3,12)((CYA(K,J),J=1,JJ),K=1,KK)
      WRITE(3,12)((CXA(K,J),J=1,JJ),K=1,KK)
      DO 13 K=1,KK
      DO 13 J=1,JJ
      WLA(K,J)=DA(K,J)+Z(K,J)
   13 CONTINUE
      WRITE(6,*)WLA(47,10)
      DO 10 K=1,KK
      DO 10 I=1,NXREACH(K)
      MSTART(K,I)=JSTART(K,I)
      MFINISH(K,I)=JFINISH(K,I)
      DO 10 J=JSTART(K,I),JFINISH(K,I)
      EA(K,J)=ENFG(WLA(K,J),CXA(K,J),CYA(K,J),DA(K,J))
      DB(K,J)=DA(K,J)
10    CONTINUE
      DO 66 J=1,JJ
      DO 66 I=1,NYREACH(J)
      LSTART(J,I)=KSTART(J,I)
      LFINISH(J,I)=KFINISH(J,I)
   66 CONTINUE
      DO 170 ITIM=1,NN,2
      DO 305 J=1,JJ
      IDIR(J)=1
      IF(IFIX(SPITX(1,J)).EQ.0) GOTO 305
      IF(WLA(SPITX(1,J),J).GT.SPITX(2,J).AND.
     &WLA(SPITX(1,J),J).GT.WLA(SPITY(1,J)-1,J)) IDIR(J)=-1
  305 CONTINUE
      CALL ENBAND(Z,ITIM)
      CALL ENFANC(Z,SPITX,ITIM)
1011  CALL FCLNDS(NXMAX,NYMAX,ITIM)
1012  WRITE(6,1000)ITIM
1000  FORMAT(I4)
      READ(10,*)SURGE2
      WINDDIR=WINDDIR*0.0174532
      I=0
      AMP=2.75
      ENEX2=28.0+AMP*SIN(3.141527*2.0*(DT*FLOAT(ITIM)+33600.0)
```

```
     &/45000.0)
      WRITE(6,*)ENDX2
      DO 605 J=1,17
      ENDA(J,1)=ENDX2
605   CONTINUE
      DO 2001 J=1,47
      ENDB(J,1)=ENDX2
2001  CONTINUE
190   DO 301 K=1,KK
      IF(NXREACH(K).EQ.0)GOTO 301
      ND=NXREACH(K)+1
      DO 300 I=1,NXREACH(K)
      ND=ND-1
      END1=0.0
      IF(INDX(K,I).LT.2) END1=ENDB(K,1)
      END2=0.0
      IF(JNDX(K,I).LT.3) END2=ENDB(K,1)
      IF(IXTYPE(K,I).LT.3) GOTO 320
      JDIST=JFINISH(K,I)-JSTART(K,I)+1
      IAJ=JDIST-1
      JAJJ=IAJ*2
      DO 310 J=JSTART(K,I),JFINISH(K,I)
      IF(DA(K,J).LT.0.8) WRITE(6,6001)K,J
6001  FORMAT(2I4,12H DEPTHS ZERO)
      IF(DA(K,J).LT.0.8)WRITE(6,*)DA(K,J)
      XUS(J)=XFLOW(K,J)
      US(J)=QXA(K,J)
      DS(J)=DA(K,J)
      EF(J)=WLA(K,J)
      ES(J)=EA(K,J)
      QF(J)=QA(K,J)
      UF(J)=QYA(K,J)
      VS(J)=QYA(K,J)/QA(K,J)
      S(J)=SF(K,J)*QXA(K,J)/QA(K,J)-CDR*VS(J)
     &-WCOEFF*DENAIR*WINDS**2*SIN(WINDDIR)/(G*DENWAT*DA(K,J))
     &+DFDY/(G*DENWAT)
      VS(J)=VS(J)**2/(2.0*G)
310   CONTINUE
      CALL AANDB(IAJ,1,K,JSTART(K,I),JFINISH(K,I),XUS,S)
      CALL VECT(JAJJ,JAJJJ)
      CALL FORM(1,JAJJ,JSTART(K,I))
      CALL BCOND(INDX(K,I),JNDX(K,I),END1,END2,JAJJ)
      CALL GAUSS(JAJJ)
      CALL SWITCH(INDX(K,I),JNDX(K,I),END1,END2,
     &JSTART(K,I),JFINISH(K,I),JAJJ)
      GOTO 360
320   DO 330 J=JSTART(K,I),JFINISH(K,I)
      IF(IXTYPE(K,I).EQ.2) GOTO 350
      DF(J)=ENDA(J,1)
      GOTO 330
350   DF(J)=ENDB(J,1)
330   CONTINUE
      DO 340 J=JSTART(K,I),JFINISH(K,I)
      WLE(K,J)=DF(J)
      DE(K,J)=WLE(K,J)-Z(K,J)
      QXE(K,J)=0.0
      EE(K,J)=ENERG(WLE(K,J),QXE(K,J),QYA(K,J),DE(K,J))
340   CONTINUE
      GOTO 300
360   DO 820 J=JSTART(K,I),JFINISH(K,I)
      WLE(K,J)=DF(J)
```

```
      CXE(K,J)=UE(J)
      DB(K,J)=WLE(K,J)-Z(K,J)
      EE(K,J)=ENRG(WLE(K,J),CXE(K,J),CYA(K,J),DE(K,J))
820   CONTINUE
      DO 821 J=JSTART(K,I),JFINISH(K,I)
      F=2.0
      L2=J+1
      L1=J-1
      IF(J.EQ.JSTART(K,I)) GOTO 900
      IF(J.EQ.JFINISH(K,I)) GOTO 910
      GOTO 920
900   L1=J
      F=1.0
      GOTO 920
910   L2=J
      F=1.0
920   XFLOW(K,J)=(QXA(K,L2)-QXA(K,L1)+QXB(K,L2)-QXB(K,L1))/(F*DX*2.0)
821   CONTINUE
300   CONTINUE
301   CONTINUE
  250 DO 31 J=1,JJ
      IF(NYREACH(J).EQ.0) GOTO 31
      IF(IDIR(J).LT.0) I=NYREACH(J)+1
      IF(IDIR(J).GT.0) I=0
   30 IF(IDIR(J).LT.0) I=I-1
      IF(IDIR(J).GT.0) I=I+1
      IF(I.EQ.0.OR.I.GT.NYREACH(J)) GOTO 31
      IF(IDIR(J).LT.0) WRITE(6,8000)K,J
 8000 FORMAT(2I4,17HREVERSED SOLUTION)
      END1=0.0
      IF(J.EQ.4)END1=0.0
      IF(J.EQ.5)END1=0.0
      IF(J.EQ.6)END1=0.0
      IF(J.EQ.7)END1=0.0
      IF(JNOY(J,I).LT.3) END1=ENDA(J,1)
      END2=0.0
      IF(JNOY(J,I).LT.3) END2=ENDB(J,1)
      IF(IYTYPE(J,I).LT.3) GOTO 370
      IF(SPITX(1,J).EQ.0) GOTO 1020
      IF(WLA(SPITX(1,J),J).GT.SPITX(2,J).OR.
     &WLA(SPITX(1,J)-1,J).GT.SPITX(2,J)) GOTO 1010
      GOTO 1020
 1010 IF(JNOY(J,I).EQ.5.AND.IDIR(J).EQ.-1) END2=CYB(SPITX(1,J),J)
      IF(JNOY(J,I).EQ.5.AND.IDIR(J).EQ.1.AND.WLA(SPITX(1,J),J).
     &LT.SPITX(2,J)) END2=0.3*(WLA(SPITX(1,J)-1,J)-SPITX(2,J))*
     &SQRT(G*(WLA(SPITX(1,J)-1,J)-SPITX(2,J)))
      IF(JNOY(J,I).EQ.5.AND.IDIR(J).EQ.1.AND.WLA(SPITX(1,J),J).
     &GE.SPITX(2,J)) END2=0.42*(WLA(SPITX(1,J)-1,J)-SPITX(2,J))*
     &SQRT(G*(WLA(SPITX(1,J)-1,J)-WLA(SPITX(1,J),J)))
      IF(JNOY(J,I).EQ.5.AND.IDIR(J).EQ.-1.AND.WLA(SPITX(1,J)-1,J).
     &LT.SPITX(2,J)) END1=-0.3*(WLA(SPITX(1,J),J)-SPITX(2,J))*
     &SQRT(G*(WLA(SPITX(1,J),J)-SPITX(2,J)))
      IF(JNOY(J,I).EQ.5.AND.IDIR(J).EQ.-1.AND.WLA(SPITX(1,J)-1,J).
     &GE.SPITX(2,J)) END1=-0.42*(WLA(SPITX(1,J),J)-SPITX(2,J))*
     &SQRT(G*(WLA(SPITX(1,J),J)-WLA(SPITX(1,J)-1,J)))
      IF(JNOY(J,I).EQ.5.AND.IDIR(J).EQ.1) END1=CYB(SPITX(1,J)-1,J)
 1020 KDIST=KFINISH(J,I)-KSTART(J,I)+1
      IAK=KDIST-1
      KAKK=IAK*2
      DO 800 K=KSTART(J,I),KFINISH(J,I)
      XUS(K)=XFLOW(K,J)
```

```
      US(K)=CYA(K,J)
      DS(K)=DA(K,J)
      EF(K)=WLA(K,J)
      ES(K)=EA(K,J)
      DF(K)=DA(K,J)
      UF(K)=CYA(K,J)
      VS(K)=CXE(K,J)/DE(K,J)
      S(K)=SF(K,J)*CYA(K,J)/DA(K,J)+CDR*VS(K)
     &-WCDEFF*DENAIR*WINDS**2*COS(WINDDIF)/(G*DENWAT*DA(K,J))
     &+DFEYDY/(G*DENWAT)
      VS(K)=VS(K)**2/(2.0*G)
  300 CONTINUE
      CALL AANDE(IAK,2,J,KSTART(J,I),KFINISH(J,I),XUS,S)
   80 CALL VECT(KAKK,KAKKK)
      CALL FORM(2,KAKK,KSTART(J,I))
      CALL SOUND(INDY(J,I),JNDY(J,I),END1,END2,
     &KAKK)
      IF(J.NE.13)GOTO 805
  805 CALL GALSS(KAKK)
      CALL SWITCH(INDY(J,I),JNDY(J,I),END1,END2,
     &KSTART(J,I),KFINISH(J,I),KAKK)
      GOTO 65
  370 DO 360 K=KSTART(J,I),KFINISH(J,I)
      IF(IYTYPE(J,I).EQ.2) GOTO 350
      DF(K)=ENDC(K,1)
      GOTO 360
  350 DF(K)=ENDD(K,1)
  360 CONTINUE
      DO 730 K=KSTART(J,I),KFINISH(J,I)
      WLB(K,J)=DF(K)
      DB(K,J)=DF(K)-Z(K,J)
      CYB(K,J)=0.0
      EB(K,J)=ENRG(WLB(K,J),CXB(K,J),CYB(K,J),DB(K,J))
      U=CXB(K,J)/DB(K,J)
      V=CYB(K,J)/DB(K,J)
      SF(K,J)=SQRT(U*U+V*V)/(CH*DB(K,J))
  730 CONTINUE
      GOTO 30
   65 DO 60 K=KSTART(J,I),KFINISH(J,I)
      WLB(K,J)=DF(K)
      CYB(K,J)=UF(K)
      DB(K,J)=WLB(K,J)-Z(K,J)
      EB(K,J)=ENRG(WLB(K,J),CXB(K,J),CYB(K,J),DB(K,J))
      U=CXB(K,J)/DB(K,J)
      V=CYB(K,J)/DB(K,J)
      SF(K,J)=SQRT(U*U+V*V)/(CH*DB(K,J))
   60 CONTINUE
      GOTO 30
   31 CONTINUE
      TIME=FLOAT(ITIM)*DT
      IT=ITIM+1
      READ(10,*)SURGE2
      WINDIR=WINDDIR*0.017453
      I=0
      AMP=2.75
      END2=28.0+AMP*SIN(3.1415927*2.0*(DT*FLOAT(IT)+33600.0)
     &/43000.0)
      WRITE(6,*)END2
      DO 806 J=1,17
      ENDA(J,1)=END2
  806 CONTINUE
```

```
      DO 2000 J=1,47
      ENDB(J,1)=ENDX2
 2000 CONTINUE
      DO 401 J=1,JJ
      IF(NYREACH(J).EQ.0) GOTO 401
      IF(IDIR(J).LT.0) I=NYREACH(J)+1
      IF(IDIR(J).GT.0) I=0
  400 IF(IDIR(J).LT.0) I=I-1
      IF(IDIR(J).GT.0) I=I+1
      IF(I.EQ.0.OR.I.GT.NYREACH(J)) GOTO 401
      IF(IDIR(J).LT.0) WRITE(6,8000)K,J
      END1=0.0
      IF(J.EQ.4)END1=0.0
      IF(J.EQ.5)END1=0.0
      IF(J.EQ.6)END1=0.0
      IF(J.EQ.7)END1=0.0
      IF(INDY(J,I).LT.3) END1=ENDA(J,1)
      END2=0.0
      IF(JNDY(J,I).LT.3) END2=ENDB(J,1)
      IF(IYTYPE(J,I).LT.3) GOTO 420
      IF(SPITX(1,J).EQ.0) GOTO 1040
      IF(WLA(SPITX(1,J),J).GT.SPITX(2,J).OR.
     &WLA(SPITX(1,J)-1,J).GT.SPITX(2,J)) GOTO 1030
      GOTO 1040
 1030 IF(JNDY(J,I).EQ.5.AND.IDIR(J).EQ.-1) END2=QYA(SPITX(1,J),J)
      IF(JNDY(J,I).EQ.5.AND.IDIR(J).EQ.1.AND.WLA(SPITX(1,J),J).LT.
     &SPITX(2,J))END2=0.3*(WLA(SPITX(1,J)-1,J)-SPITX(2,J))*
     &SQRT(G*(WLA(SPITX(1,J)-1,J)-SPITX(2,J)))
      IF(JNDY(J,I).EQ.5.AND.IDIR(J).EQ.1.AND.WLA(SPITX(1,J),J).
     &GE.SPITX(2,J)) END2=0.42*(WLA(SPITX(1,J)-1,J)-SPITX(2,J))*
     &SQRT(G*(WLA(SPITX(1,J)-1,J)-WLA(SPITX(1,J),J)))
      IF(INDY(J,I).EQ.5.AND.IDIR(J).EQ.-1.AND.WLA(SPITX(1,J),J).LT.
     &SPITX(2,J)) END1=-0.3*(WLA(SPITX(1,J),J)-SPITX(2,J))*
     &SQRT(G*(WLA(SPITX(1,J),J)-SPITX(2,J)))
      IF(INDY(J,I).EQ.5.AND.IDIR(J).EQ.-1.AND.WLA(SPITX(1,J)-1,J).
     &GE.SPITX(2,J)) END1=-0.42*(WLA(SPITX(1,J),J)-SPITX(2,J))*
     &SQRT(G*(WLA(SPITX(1,J),J)-WLA(SPITX(1,J)-1,J)))
      IF(INDY(J,I).EQ.5.AND.IDIR(J).EQ.1) END1=QYA(SPITX(1,J)-1,J)
 1040 KDIST=KFINISH(J,I)-KSTART(J,I)+1
      IAK=KDIST-1
      KAKK=IAK*2
      DO 410 K=KSTART(J,I),KFINISH(J,I)
      XUS(K)=XFLOW(K,J)
      US(K)=QYE(K,J)
      DS(K)=DE(K,J)
      EF(K)=WLE(K,J)
      ES(K)=EE(K,J)
      DF(K)=DE(K,J)
      Q=(K)=QYE(K,J)
      VS(K)=QXE(K,J)/DE(K,J)
      S(K)=SF(K,J)*QYE(K,J)/DE(K,J)+CER*VS(K)
     &-WCOEFF*DENAIR*WINDS**2*COS(WINDDIR)/(G*DENWAT*DA(K,J))
     &+CFEYDY/(G*DENWAT)
      VS(K)=VS(K)**2/(2.0*G)
  410 CONTINUE
      CALL ADNCE(IAK,Z,J,KSTART(J,I),KFINISH(J,I),XUS,S)
      CALL VECT(KAKK,KAKKK)
      CALL FORM(Z,KAKK,KSTART(J,I))
      CALL BOUND(INDY(J,I),JNDY(J,I),END1,END2,
     &KAKK)
      CALL GAUSS(KAKK)
```

```
      CALL SWITCH(IKEY(J,I),JKEY(J,I),END1,END2,
     &KSTART(J,I),KFINISH(J,I),KAKK)
      GOTO 460
420   DO 430 K=KSTART(J,I),KFINISH(J,I)
      IF(IYTYPE(J,I).EQ.2) GOTO 450
      DF(K)=ENDC(K,1)
      GOTO 430
450   DF(K)=ENDC(K,1)
430   CONTINUE
      DO 440 K=KSTART(J,I),KFINISH(J,I)
      WLA(K,J)=DF(K)
      DA(K,J)=DF(K)-Z(K,J)
      CYA(K,J)=0.0
      EA(K,J)=ENRG(WLA(K,J),CXE(K,J),CYA(K,J),DA(K,J))
440   CONTINUE
      GOTO 400
460   DO 830 K=KSTART(J,I),KFINISH(J,I)
      WLA(K,J)=DF(K)
      CYA(K,J)=UF(K)
      DA(K,J)=WLA(K,J)-Z(K,J)
      EA(K,J)=ENRG(WLA(K,J),CXE(K,J),CYA(K,J),DA(K,J))
830   CONTINUE
      DO 831 K=KSTART(J,I),KFINISH(J,I)
      L2=K+1
      L1=K-1
      F=2.0
      IF(K.EQ.KSTART(J,I)) GOTO 930
      IF(K.EQ.KFINISH(J,I)) GOTO 940
      GOTO 950
930   L1=K
      F=1.0
      GOTO 950
940   L2=K
      F=1.0
950   XFLOW(K,J)=(CYF(L2,J)-CYF(L1,J)+CYA(L2,J)-CYA(L1,J))/(F*DY*2.0)
831   CONTINUE
      GOTO 400
401   CONTINUE
250   DO 101 K=1,KK
      IF(NXREACH(K).EQ.0) GOTO 101
      NC=NXREACH(K)+1
      DO 100 I=1,NXREACH(K)
      NC=NC-1
      END1=0.0
      IF(INDX(K,I).LT.3) END1=ENDC(K,1)
      END2=0.0
      IF(JNDX(K,I).LT.3) END2=ENDC(K,1)
      IF(IXTYPE(K,I).LT.2) GOTO 470
      JDIST=JFINISH(K,I)-JSTART(K,I)+1
      IAJ=JDIST-1
      JAJJ=IAJ*2
      DO 540 J=JSTART(K,I),JFINISH(K,I)
      XUS(J)=XFLOW(K,J)
      US(J)=CXE(K,J)
      DS(J)=DE(K,J)
      EF(J)=WLE(K,J)
      ES(J)=EE(K,J)
      DF(J)=DE(K,J)
      UF(J)=CXE(K,J)
      VS(J)=CYA(K,J)/DA(K,J)
      S(J)=SF(K,J)*CXE(K,J)/DE(K,J)-CDR*VS(J)
```

```
     &-WCOEFF*DENAIR*WINDS**2*SIN(WINDDIR)/(G*DENWAT*DA(K,J))
     &+DFBYDX/(G*DENWAT)
      VS(J)=VS(J)**2/(2.0*G)
540   CONTINUE
      CALL BANDS(IAJ,1,K,JSTART(K,I),JFINISH(K,I),XUS,S)
140   CALL VECT(JAJJ,JAJJJ)
      CALL FORM(1,JAJJ,JSTART(K,I))
      CALL BOUND(INDX(K,I),JNDX(K,I),END1,END2,JAJJ)
      CALL GAUSS(JAJJ)
      CALL SWITCH(INDX(K,I),JNDX(K,I),END1,END2,
     &JSTART(K,I),JFINISH(K,I),JAJJ)
      GOTO 135
470   DO 480 J=JSTART(K,I),JFINISH(K,I)
      IF(IXTYPE(K,I).EQ.2) GOTO 490
      DF(J)=ENDA(J,1)
      GOTO 480
490   DF(J)=ENDB(J,1)
480   CONTINUE
      DO 740 J=JSTART(K,I),JFINISH(K,I)
      WLA(K,J)=DF(J)
      DA(K,J)=WLA(K,J)-Z(K,J)
      QXA(K,J)=0.0
      EA(K,J)=ENRG(WLA(K,J),QXA(K,J),QYA(K,J),DA(K,J))
      U=QXA(K,J)/DA(K,J)
      V=QYA(K,J)/DA(K,J)
      SF(K,J)=SQRT(U*U+V*V)/(CH*DA(K,J))
740   CONTINUE
      GOTO 100
135   DO 130 J=JSTART(K,I),JFINISH(K,I)
      WLA(K,J)=DF(J)
      QXA(K,J)=UF(J)
      DA(K,J)=WLA(K,J)-Z(K,J)
      EA(K,J)=ENRG(WLA(K,J),QXA(K,J),QYA(K,J),DA(K,J))
      U=QXA(K,J)/DA(K,J)
      V=QYA(K,J)/DA(K,J)
      SF(K,J)=SQRT(U*U+V*V)/(CH*DA(K,J))
130   CONTINUE
100   CONTINUE
  101 CONTINUE
      QSPURN=0.0
      DO 8002 I=2,10
      QTEMP=SQRT(QXA(36,I)**2+QYA(36,I)**2)
      IF(QYA(36,I).LT.0.0)QTEMP=QTEMP*-1.0
      QSPURN=QSPURN+QTEMP
      IF(QYA(36,6).LT.0.0)QSTON=QSTON+QTEMP
      IF(QYA(36,6).GT.0.0).STOP=QSTOP+QTEMP
 8002 CONTINUE
      QGRIM=0.0
      DO 8001 I=3,6
      QTEMP=SQRT(QXA(24,I)**2+QYA(24,I)**2)
      IF(QYA(24,I).LT.0.0)QTEMP=QTEMP*-1.0
      QGRIM=QGRIM+QTEMP
      IF(QYA(24,6).LT.0.0)QGTON=QGTON+QTEMP
      IF(QYA(24,6).GT.0.0)QGTOP=QGTOP+QTEMP
 8001 CONTINUE
      QINN=0.0
      DO 8003 I=2,6
      QTEMP=SQRT(QXA(17,I)**2+QYA(17,I)**2)
      IF(QYA(17,I).LT.0.0) QTEMP=QTEMP*-1.0
      QINN=QINN+QTEMP
      IF(QYA(17,6).LT.0.0)QITON=QITON+QTEMP
```

```
      IF(CYA(17,4).GT.0.0)QITOP=QITOP+QTEMP
 8002 CONTINUE
      WRITE(11,*)QSPLRN,QGRIM,QIMM
      DO 650 NUM=1,NPTS
      WLVSTIM(NUM,IT/2)=WLA(ICCORDS(NUM,1),ICCORDS(NUM,2))
      CC(NUM,IT/2)=CYA(32,10+NUM)
  650 CONTINUE
      DO 695 NUM=1,NVS
      VSY(NUM,IT/2)=CYA(ICC(NUM,1),ICC(NLM,2))/DA(ICC(NUM,1),ICC(NUM,2))
      VSX(NUM,IT/2)=CXA(ICC(NUM,1),ICC(NLM,2))/DA(ICC(NUM,1),ICC(NUM,2))
      VSC(NUM,IT/2)=SQRT(VSY(NUM,IT/2)**2+VSX(NUM,IT/2)**2)
  695 CONTINUE
      TIME=FLOAT(IT)*DT
      FR1=FLOAT(ITIM)/FLOAT(INCRS)
      FR2=FLOAT(IT)/FLOAT(INCRS)
      IR1=ITIM/INCRS
      IR2=IT/INCRS
      XR1=FLOAT(IR1)
      XR2=FLOAT(IR2)
      IF(XR1.LT.FR1.AND.XR2.LT.FR2) GOTO 170
   23 FORMAT(F10.3)
   11 FORMAT(10F8.3/7F8.3)
   12 FORMAT(10F7.2/7F7.2)
      WRITE(3,23)TIME
      WRITE(3,12)((DA(K,J),J=1,JJ),K=1,KK)
      WRITE(3,12)((CYA(K,J),J=1,JJ),K=1,KK)
      WRITE(3,12)((CXA(K,J),J=1,JJ),K=1,KK)
  170 CONTINUE
      WRITE(11,*)QSTON,QSTOP
      WRITE(11,*)QGTON,QGTOP
      WRITE(11,*)QITON,QITOP
      WRITE(4,24)NPTS,NN/2,DT*2
   24 FORMAT(2I4,F8.1)
      DO 700 N=1,NPTS
      WRITE(4,701)(XNAMES(N,L),L=1,10)
  701 FORMAT(10A8)
  700 CONTINUE
      DO 720 N=1,NPTS
      WRITE(4,704)(AEQV(N,L),L=1,2)
  704 FORMAT(2A8)
  720 CONTINUE
      DO 710 N=1,NPTS
      WRITE(4,702)(ICCORDS(N,L),L=1,2)
  702 FORMAT(2I5)
  710 CONTINUE
      NTT=NN/2
      DO 690 L=1,NPTS
      WRITE(4,22)(WLVSTIM(L,N),N=1,NTT)
   22 FORMAT(10F8.3)
  690 CONTINUE
      DO 691 L=1,4
      WRITE(4,22)(QC(L,N),N=1,NTT)
  691 CONTINUE
      DO 695 L=1,NVS
      WRITE(2,22)(VSY(L,N),N=1,NN/2)
      WRITE(2,22)(VSX(L,N),N=1,NN/2)
      WRITE(2,22)(VSC(L,N),N=1,NN/2)
  695 CONTINUE
      WRITE(7,707)((DA(K,J),J=1,JJ),K=1,KK)
      WRITE(7,707)((CYA(K,J),J=1,JJ),K=1,KK)
      WRITE(7,707)((CXA(K,J),J=1,JJ),K=1,KK)
```

```
      WRITE(7,707)((Z(K,J),J=1,JJ),K=1,KK)
707   FORMAT(10F8.3/7F8.3)
      WRITE(7,705)((XFLOW(K,J),J=1,JJ),K=1,KK)
      WRITE(7,708)((SF(K,J),J=1,JJ),K=1,KK)
708   FORMAT(5E16.6,/,5E16.6,/,2E16.6)
      STOP
      END
      SUBROUTINE AANCE(IAN,IZ,N,ISTART,IFINISH,XLS,S)
      DIMENSION XLS(47),S(47)
      COMMON/CT/CT1,CT2,CT3
      COMMON/CX/CX1,CX2,CX3,CX4,CX5,CX6,CX7,CX8,CX9
      COMMON/CY/CY1,CY2,CY3,CY4,CY5,CY6,CY7,CY8,CY9
      COMMON/BLOCKA/LS(47),DS(47),UF(47),DF(47),VS(47)
      COMMON/BLOCKB/ES(47),EF(47)
      COMMON/BLOCKF/A(47),B(47)
      COMMON G
      N=0
      IF(IZ.EQ.1) GOTO 10
      DO 20 K=ISTART,IFINISH-1
      N=N+1
      A(N)=(EF(K)+EF(K+1))*CT2-CY2*(US(K+1)-US(K))
     &-(XUS(K)+XUS(K+1))*0.5
      B(N)=(US(K)/DS(K)+US(K+1)/DS(K+1))*CT3+CY4*(ES(K)-ES(K+1))
     &+(VS(K)-VS(K+1))*CY3-(S(K)+S(K+1))*0.5
20    CONTINUE
      GOTO 30
10    DO 40 K=ISTART,IFINISH-1
      N=N+1
      A(N)=(EF(K)+EF(K+1))*CT2-CX2*(US(K+1)-US(K))
     &-(XUS(K)+XUS(K+1))*0.5
      B(N)=(US(K)/DS(K)+US(K+1)/DS(K+1))*CT3+CX4*(ES(K)-ES(K+1))
     &+(VS(K)-VS(K+1))*CX3-(S(K)+S(K+1))*0.5
40    CONTINUE
30    RETURN
      END
      SUBROUTINE VECT(NANA,NANN)
      COMMON/BLOCKF/A(47),B(47)
      COMMON/BLOCKG/AMAT(94,4),RES(94)
      J=0
      DO 20 N=1,NANA,2
      J=J+1
      RES(N)=A(J)
      RES(N+1)=B(J)
20    CONTINUE
30    RETURN
      END
      SUBROUTINE FORM(IZ,NANA,ISTART)
      COMMON/CX/CX1,CX2,CX3,CX4,CX5,CX6,CX7,CX8,CX9
      COMMON/CY/CY1,CY2,CY3,CY4,CY5,CY6,CY7,CY8,CY9
      COMMON/CT/CT1,CT2,CT3
      COMMON/BLOCKC/C1,C2,C3,C4,C5
      COMMON/BLOCKA/LS(47),DS(47),UF(47),DF(47),VS(47)
      COMMON/BLOCKG/AMAT(94,4),RES(94)
      J=ISTART
      NN=NANA-1
      IF(IZ.EQ.1) GOTO 20
      DO 10 N=1,NN,2
      CA=UF(J)/(EF(J)*DF(J))*C5
      AMAT(N,1)=CT2
      AMAT(N,2)=-CY2
      AMAT(N,3)=CT2
```

```
      J=J+1
      AMAT(N,4)=CY2
      I=N+1
      CE=UF(J)/(DF(J)*DF(J))*C5
      AMAT(I,1)=-CY3
      AMAT(I,2)=CT3/DF(J-1)-CA
      AMAT(I,3)=CY3
      AMAT(I,4)=CT3/DF(J)+CE
10    CONTINUE
      GOTO 40
20    DO 30 N=1,NN,2
      CA=UF(J)/(DF(J)*DF(J))*C4
      AMAT(N,1)=CT2
      AMAT(N,2)=-CX2
      AMAT(N,3)=CT2
      J=J+1
      AMAT(N,4)=CX2
      I=N+1
      CE=UF(J)/(DF(J)*DF(J))*C5
      AMAT(I,1)=-CX3
      AMAT(I,2)=CT3/DF(J-1)-CA
      AMAT(I,3)=CX3
      AMAT(I,4)=CT3/DF(J)+CE
30    CONTINUE
40    RETURN
      END
      SUBROUTINE BOUND(IND,JND,END1,END2,NANN)
      COMMON/BLOCKG/AMAT(94,4),RES(94)
      IF(IND.GE.2) GOTO 10
      RES(1)=RES(1)-AMAT(1,1)*END1
      RES(2)=RES(2)-AMAT(2,1)*END1
      AMAT(1,1)=AMAT(1,2)
      AMAT(1,2)=AMAT(1,3)
      AMAT(1,3)=AMAT(1,4)
      AMAT(2,1)=AMAT(2,2)
      AMAT(2,2)=AMAT(2,3)
      AMAT(2,3)=AMAT(2,4)
      GOTO 30
10    RES(1)=RES(1)-AMAT(1,2)*BND1
      RES(2)=RES(2)-AMAT(2,2)*END1
      AMAT(1,2)=AMAT(1,3)
      AMAT(1,2)=AMAT(1,4)
      AMAT(2,2)=AMAT(2,3)
      AMAT(2,3)=AMAT(2,4)
30    J=NANN-1
      IF(J.EQ.1) GOTO 70
      L=3
      M=4
      GOTO 80
70    L=2
      M=3
80    IF(JND.GE.3) GOTO 50
      RES(J)=RES(J)-AMAT(J,L)*END2
      RES(NANN)=RES(NANN)-AMAT(NANN,L)*END2
      AMAT(J,L)=AMAT(J,M)
      AMAT(NANN,L)=AMAT(NANN,M)
      GOTO 60
50    RES(J)=RES(J)-AMAT(J,M)*BND2
      RES(NANN)=RES(NANN)-AMAT(NANN,M)*BND2
60    RETURN
      END
```

```
      SUBROUTINE GAUSS(NANN)
      COMMON/BLOCKG/AMAT(94,4),RES(94)
      IF(NANN.EQ.2) GOTO 60
      COEF=-AMAT(2,1)/AMAT(1,1)
      AMAT(2,1)=0.0
      AMAT(2,2)=AMAT(2,2)+AMAT(1,2)*COEF
      AMAT(2,3)=AMAT(2,3)+AMAT(1,3)*COEF
      RES(2)=RES(2)+RES(1)*COEF
      COEF=-AMAT(3,1)/AMAT(2,2)
      AMAT(3,1)=0.0
      AMAT(3,2)=AMAT(3,2)+AMAT(2,3)*COEF
      RES(3)=RES(3)+RES(2)*COEF
      COEF=-AMAT(4,1)/AMAT(2,2)
      AMAT(4,1)=0.0
      AMAT(4,2)=AMAT(4,2)+AMAT(2,3)*COEF
      RES(4)=RES(4)+RES(2)*COEF
      NN=NANN-3
      IF(NN.GT.1) GOTO 40
      COEF=-AMAT(4,2)/AMAT(3,2)
      AMAT(4,3)=AMAT(4,3)+AMAT(3,3)*COEF
      RES(4)=RES(4)+RES(3)*COEF
      GOTO 50
   40 DO 10 K=3,NN,2
      I=K+1
      J=K+2
      L=K+3
      COEF=-AMAT(I,2)/AMAT(K,2)
      AMAT(I,2)=0.0
      AMAT(I,3)=AMAT(I,3)+AMAT(K,3)*COEF
      AMAT(I,4)=AMAT(I,4)+AMAT(K,4)*COEF
      RES(I)=RES(I)+RES(K)*COEF
      COEF=-AMAT(J,1)/AMAT(I,3)
      AMAT(J,1)=0.0
      AMAT(J,2)=AMAT(J,2)+AMAT(I,4)*COEF
      RES(J)=RES(J)+RES(I)*COEF
      COEF=-AMAT(L,1)/AMAT(I,3)
      AMAT(L,1)=0.0
      AMAT(L,2)=AMAT(L,2)+AMAT(I,4)*COEF
      RES(L)=RES(L)+RES(I)*COEF
   10 CONTINUE
      COEF=-AMAT(L,2)/AMAT(J,2)
      AMAT(L,2)=0.0
      AMAT(L,3)=AMAT(L,3)+AMAT(J,3)*COEF
      RES(L)=RES(L)+RES(J)*COEF
   50 RES(NANN)=RES(NANN)/AMAT(NANN,3)
      RES(NANN-1)=(RES(NANN-1)-RES(NANN)*AMAT(NANN-1,3))/AMAT(NANN-1,2)
      K=NANN-2
      IF(K.EQ.2) GOTO 30
   20 RES(K)=(RES(K)-RES(K+1)*AMAT(K,4))/AMAT(K,2)
      K=K-1
      RES(K)=(RES(K)-RES(K+1)*AMAT(K,3)-RES(K+2)*AMAT(K,4))/AMAT(K,2)
      K=K-1
      IF(K.EQ.2) GOTO 30
      GOTO 20
   30 RES(2)=(RES(2)-RES(3)*AMAT(2,3))/AMAT(2,2)
      RES(1)=(RES(1)-RES(2)*AMAT(1,2)-RES(3)*AMAT(1,3))/AMAT(1,1)
      GOTO 70
   60 COEF=-AMAT(2,1)/AMAT(1,1)
      AMAT(2,2)=AMAT(2,2)+AMAT(1,2)*COEF
      RES(2)=RES(2)+RES(1)*COEF
      RES(2)=RES(2)/AMAT(2,2)
```

```
      RES(1)=(RES(1)-RES(2)*AMAT(1,2))/AMAT(1,1)
70    RETURN
      END
      SUBROUTINE SWITCH(IND,JND,END1,END2,ISTART,IFINISH,NNN)
      COMMON/BLOCKA/US(47),DS(47),UF(47),DF(47),VS(47)
      COMMON/BLOCKG/AMAT(94,4),RES(94)
      JJ=2
      DO 10 I=ISTART+1,IFINISH-1
      DF(I)=RES(JJ)
      JJ=JJ+2
10    CONTINUE
      JJ=3
      DO 20 I=ISTART+1,IFINISH-1
      UF(I)=RES(JJ)
      JJ=JJ+2
20    CONTINUE
      IF(IND.GE.3) GOTO 30
      DF(ISTART)=END1
      UF(ISTART)=RES(1)
      GOTO 40
30    DF(ISTART)=RES(1)
      UF(ISTART)=END1
40    IF(JND.GE.3) GOTO 50
      DF(IFINISH)=END2
      UF(IFINISH)=RES(NNN)
      GOTO 60
50    DF(IFINISH)=RES(NNN)
      UF(IFINISH)=END2
60    RETURN
      END
      FUNCTION ENRG(WL,Q1,Q2,D)
      COMMON/BLOCKC/C1,C2,C3,C4,C5
      CA=Q1/D
      CE=Q2/D
      ENRG=WL+(CA*Q2+CE*CE)*C2
      RETURN
      END
      SUBROUTINE BOUNDS(NXMAX,NYMAX,ITIM)
      COMMON/BLOCKD/JJ,KK,NN,NNN
      COMMON/BOUNDX/INDX(47,4),JNDX(47,4),JSTART(47,4),JFINISH(47,4)
     &,NSTART(47,4),NFINISH(47,4),IXTYPE(47,4),NXREACH(47)
      COMMON/BOUNDY/INDY(19,4),JNDY(19,4),KSTART(19,4),KFINISH(19,4)
     &,IYTYPE(19,4),NYREACH(19),LSTART(19,4),LFINISH(19,4)
      COMMON/GRID/IGRIDX(47,19),IGRIDY(47,19)
      IF(ITIM.EQ.47)WRITE(6,*)1,IGRIDY(31,13)
      DO 210 J=1,JJ
      IF(NYREACH(J).EQ.0) GOTO 210
      DO 201 I=1,NYREACH(J)
      K=KSTART(J,I)-1
220   IF(K.EQ.0) GOTO 230
      IF(IGRIDY(K,J).NE.-1) GOTO 230
      IF(IGRIDY(K+1,J).NE.4) GOTO 230
      IGRIDY(K+1,J)=0
      IGRIDY(K,J)=4
      K=K-1
      GOTO 220
230   K=KFINISH(J,I)+1
      IF(ITIM.EQ.47.AND.J.EQ.13)WRITE(6,*)2,IGRIDY(31,13)
240   IF(K.GT.KK) GOTO 310
      IF(IGRIDY(K,J).NE.-1) GOTO 201
      IF(IGRIDY(K-1,J).NE.4) GOTO 201
```

```
      IGRIDY(K-1,J)=0
      IGRIDY(K,J)=4
      IF(IGRIDY(K+1,J).EQ.4) GOTO 250
      K=K+1
      GOTO 240
  250 IGRIDY(K,J)=0
      IGRIDY(K+1,J)=0
  201 CONTINUE
      IF(ITIM.EQ.47.AND.J.EQ.13)WRITE(6,*)3,IGRIDY(31,13)
  310 K=1
  260 IF(IGRIDY(K,J).EQ.-1) GOTO 270
      K=K+1
      IF(K.GE.KK) GOTO 210
      GOTO 260
  270 IF(IGRIDY(K+1,J).EQ.0) GOTO 300
      IGRIDY(K,J)=4
  280 K=K+1
      IF(IGRIDY(K+1,J).NE.-1) GOTO 290
      IGRIDY(K,J)=0
      GOTO 280
  290 IGRIDY(K,J)=4
  300 K=K+1
      GOTO 260
  210 CONTINUE
      IF(ITIM.EQ.47.AND.J.EQ.13)WRITE(6,*)4,IGRIDY(31,13)
      ITEST=0
      DO 100 J=1,JJ
      IF(NYREACH(J).EQ.0) GOTO 100
      DO 101 I=1,NYREACH(J)
      K=KSTART(J,I)
      IF(IGRIDY(K,J).NE.-2) GOTO 110
      ITEST=1
  120 IGRIDY(K,J)=0
      IF(K.EQ.KFINISH(J,I)) GOTO 101
      K=K+1
      IF(IGRIDY(K,J).NE.-2) GOTO 180
      GOTO 120
  180 IGRIDY(K,J)=4
  110 N=KFINISH(J,I)
      IF(IGRIDY(N,J).NE.-2) GOTO 140
  130 IGRIDY(N,J)=0
      N=N-1
      IF(IGRIDY(N,J).NE.-2) GOTO 170
      GOTO 130
  170 IGRIDY(N,J)=4
  140 K=K+1
      IF(IGRIDY(K,J).EQ.-2) GOTO 150
      IF(K.GE.KFINISH(J,I)) GOTO 101
      GOTO 140
  150 IGRIDY(K-1,J)=4
  190 IGRIDY(K,J)=0
      K=K+1
      IF(IGRIDY(K,J).NE.-2) GOTO 200
      GOTO 190
  200 IGRIDY(K,J)=4
      GOTO 140
  101 CONTINUE
  100 CONTINUE
      DO 600 K=1,KK
      DO 600 L=1,NYMAX
      INDX(K,L)=0
```

```
      JNDX(K,L)=0
      JSTART(K,L)=0
      JFINISH(K,L)=0
      IXTYPE(K,L)=0
600   CONTINUE
      DO 603 J=1,JJ
      DO 603 L=1,NYMAX
      INDY(J,L)=0
      JNDY(J,L)=0
      KSTART(J,L)=0
      KFINISH(J,L)=0
      IYTYPE(J,L)=0
603   CONTINUE
      DO 510 J=1,JJ
      NYREACH(J)=1
      DO 520 K=1,KK
      IF(IGRIDY(K,J).LE.0) GOTO 520
      IF(KSTART(J,NYREACH(J)).EQ.0) GOTO 530
   10 KFINISH(J,NYREACH(J))=K
      JNDY(J,NYREACH(J))=IGRIDY(K,J)
      IYTYPE(J,NYREACH(J))=IGRIDX(K,J)
      IF(IYTYPE(J,NYREACH(J)).EQ.0)IYTYPE(J,NYREACH(J))=3
      NYREACH(J)=NYREACH(J)+1
      GOTO 520
  530 KSTART(J,NYREACH(J))=K
      INDY(J,NYREACH(J))=IGRIDY(K,J)
520   CONTINUE
      NYREACH(J)=NYREACH(J)-1
510   CONTINUE
      DO 550 K=1,KK
      NXREACH(K)=1
      DO 560 J=1,JJ
      IF(IGRIDX(K,J).LE.0) GOTC 560
      IF(JSTART(K,NXREACH(K)).EQ.0) GOTO 570
   30 JFINISH(K,NXREACH(K))=J
      JNDX(K,NXREACH(K))=IGRIDX(K,J)
      IXTYPE(K,NXREACH(K))=IGRIDY(K,J)
      IF(IXTYPE(K,NXREACH(K)).EQ.0)IXTYPE(K,NXREACH(K))=3
      NXREACH(K)=NXREACH(K)+1
      GOTC 560
570   JSTART(K,NXREACH(K))=J
      INDX(K,NXREACH(K))=IGRIDX(K,J)
560   CONTINUE
      NXREACH(K)=NXREACH(K)-1
550   CONTINUE
      RETURN
      END
      SUBROUTINE EXPAND(I,ITIM)
      DIMENSION I(47,19)
      COMMON/BLOCKD/JJ,KK,NN,NANA
      COMMON/BOUNDX/INDX(47,4),JNDX(47,4),JSTART(47,4),JFINISH(47,4)
     &,NSTART(47,4),NFINISH(47,4),IXTYPE(47,4),NXREACH(47)
      COMMON/BOUNDY/INDY(19,4),JNDY(19,4),KSTART(19,4),KFINISH(19,4)
     &,IYTYPE(19,4),NYREACH(19),LSTART(19,4),LFINISH(19,4)
      COMMON/GRID/IGRIDX(47,19),IGRIDY(47,19)
      COMMON/CONEA/WLA(47,19),DA(47,19),CXA(47,19),CYA(47,19)
      COMMON/CONEB/WLB(47,19),DB(47,19),CXB(47,19),CYB(47,19)
      COMMON/ENERGY/EA(47,19),EB(47,19)
      DO 10 K=1,KK
      DO 10 I=1,NXREACH(K)
      J=JFINISH(K,I)
```

```
      IF(JNDX(K,I).NE.4) GOTO 20
      IF(ITIM.GT.100) GOTO 30
      IF(WLA(K,J).LE.Z(K,J+1)+1.000) GOTO 30
      IF(IGRIDY(K,J+1).EQ.3) GOTO 30
      WRITE(6,1)J,K
    1 FORMAT(7HEXPAND ,2I4)
      DA(K,J+1)=WLA(K,J)-Z(K,J+1)
      EA(K,J+1)=WLA(K,J+1)
      UXA(K,J+1)=0.0
      UYA(K,J+1)=0.0
      WLA(K,J+1)=WLA(K,J)
      WLB(K,J+1)=WLA(K,J+1)
      DB(K,J+1)=DA(K,J+1)
      UXB(K,J+1)=UXA(K,J+1)
      UYB(K,J+1)=0.0
      IGRIDX(K,J)=0
      IGRIDX(K,J+1)=4
      IF(IGRIDY(K,J+1).EQ.0) IGRIDY(K,J+1)=-1
   30 IF(MFINISH(K,I).EQ.JFINISH(K,I)) GOTO 20
      J=MFINISH(K,I)
      IF(ITIM.LT.111) GOTO 20
      WRITE(6,3)K,J
    3 FORMAT(2I4,9H CONTRACT)
      IGRIDX(K,J)=4
   50 J=J+1
      IGRIDX(K,J)=0
      IGRIDY(K,J)=-2
      UXA(K,J)=0.0
      UYA(K,J)=0.0
      UXB(K,J)=0.0
      UYB(K,J)=0.0
      WLB(K,J)=Z(K,J)
      IF(J.EQ.JFINISH(K,I)) GOTO 20
      GOTO 50
   10 J=JSTART(K,I)
      IF(INDX(K,I).NE.4)GOTO 10
      IF(ITIM.GT.100) GOTO 40
      IF(WLA(K,J).LE.Z(K,J-1)+1.000)GOTO 40
      IF(IGRIDX(K,J-1).EQ.3) GOTO 10
      WRITE(6,1)J,K
      DA(K,J-1)=WLA(K,J)-Z(K,J-1)
      EA(K,J-1)=WLA(K,J)
      UXA(K,J-1)=0.0
      UYA(K,J-1)=0.0
      WLA(K,J-1)=WLA(K,J)
      WLB(K,J-1)=WLB(K,J-1)
      DB(K,J-1)=DA(K,J-1)
      UXB(K,J-1)=UXA(K,J-1)
      UYB(K,J-1)=0.0
      IGRIDX(K,J)=0
      IGRIDX(K,J-1)=4
      IF(IGRIDY(K,J-1).EQ.0) IGRIDY(K,J-1)=-1
   40 IF(MSTART(K,I).EQ.JSTART(K,I)) GOTO 10
      J=MSTART(K,I)
      IF(ITIM.LT.111) GOTO 10
      IGRIDX(K,J)=4
      WRITE(6,3)K,J
   60 J=J-1
      IGRIDX(K,J)=0
      IGRIDY(K,J)=-2
      UXA(K,J)=0.0
```

```
      DYA(K,J)=0.0
      DXB(K,J)=0.0
      DYB(K,J)=0.0
      WLA(K,J)=Z(K,J)
      IF(J.EQ.JSTART(K,I)) GOTO 10
      GOTO 60
10    CONTINUE
      RETURN
      END
      SUBROUTINE EXPAND(Z,SPITY,ITIM)
      DIMENSION Z(47,19),SPITX(2,17)
      COMMON/BLOCKC/JJ,KK,NN,KANN
      COMMON/BOUNDX/INDX(47,4),JNDX(47,4),JSTART(47,4),JFINISH(47,4)
     &,MSTART(47,4),MFINISH(47,4),IXTYPE(47,4),NXREACH(47)
      COMMON/BOUNDY/INDY(19,4),JNDY(19,4),KSTART(19,4),KFINISH(19,4)
     &,IYTYPE(19,4),NYREACH(19),LSTART(19,4),LFINISH(19,4)
      COMMON/GRID/IGRIDX(47,19),IGRIDY(47,19)
      COMMON/CONCA/WLA(47,19),DA(47,19),CXA(47,19),CYA(47,19)
      COMMON/CONCB/WLB(47,19),DB(47,19),CXB(47,19),CYB(47,19)
      DO 10 J=1,JJ
      IF(SPITX(1,J).EQ.0) GOTO 10
      K=IFIX(SPITX(1,J))
      IF(WLA(K,J).LE.SPITX(2,J)) GOTO 10
      IGRIDY(K-1,J)=5
10    CONTINUE
      RETURN
      END
```

REFERENCES

Abbott, M.B., and Isonescu, F. (1967)
"On the Numerical Computation of Nearly-Horizontal Flows", Journal of Hydraulic Research, Vol 5, No 2, pp 97-117.

Abbott, M.B. (1973)
"System 21, 'Jupiter' (A Design System for Two-Dimensional Nearly-Horizontal Flows)", Journal of Hydraulic Research, I.A.H.R., Vol 11, No 1.

Abbott, M.B. (1974)
"Continuous Flows, Discontinuous Flows and Numerical Analysis", Journal of Hydraulic Research, I.A.H.R., Vol 12, No 4, pp 417-468.

Abbott, M.B. (1976a)
"A Pathology of Mathematical Modelling", Journal of Hydraulic Research, I.A.H.R., Vol 14, No 4.

Abbott, M.B. (1976b)
"The Application of Design Systems to Problems of Unsteady Flow in Open Channels", International Symposium on Unsteady Flow in Open Channels, B.H.R.A. Fluid Eng., Cranfield, U.K.

Abbott, M.B. (1979a)
"Commercial and Scientific Aspects of Applied Mathematical Modelling", Advances in Engineering Software, Vol 1, pp 147-152.

Abbott, M.B. (1979b)
"Computational Hydraulics : Elements of the Theory of Free Surface Flows", Pitman Publishing Limited, London.

Al-Khairulla, L.M. (1977)
"A Mathematical Model of Stratified, Unsteady Open Channel Flow", Ph.D. Thesis, University of Strathclyde, Glasgow.

Ambrose, R.B. Jnr and Roesch, S. (1982)
"Dynamic Estuary Model Performance", Journal of the Environmental Engineering Division, A.S.C.E., Vol 108, No EE1, Feb, pp 51-71.

Amein, M. and Fang, C.S. (1970)
"Implicit Flood Routing in Natural Channels", Journal of the Hydraulics Division, A.S.C.E., Vol 96, No Hy12, Proc. Paper 7711, Dec, pp 2481-2501.

Amein, M. (1976)
"Field of Application of an Implicit Numerical Method", B.H.R.A. Fluid Eng., Cranfield, U.K.

Balafoutas, G.J. and Abbott, M.B. (1977)
"Two-Dimensional Model for Two-Layer Flow", Journal of the Engineering Mechanics Division, A.S.C.E, Vol 103, No EM5, Proc. Paper 13263, Oct, pp 789-806.

Barnett, A.G. (1970)
"Hydrodynamic Analysis of Surface Water . Flow", Ph.D. Thesis, University of Canterbury, Christchurch, New Zealand.

Bauer, S.W. and Schmidt, K.D. (1983)
"Irregular-Grid Finite Difference Simulation of Lake Geneva Surge", Journal of Hydraulic Engineering, Vol 109, No 10, Oct, Paper No 18307.

de Boer, G. (1964)
"Spurn Head : Its History and Evolution", Transactions of the Institute of British Geography, No 34, pp 71-89.

Broyden, C.G. (1975)
"Basic Matrices and Introduction to Matrix Theory and Practice", Macmillan.

Brutsaret, W. (1971)
"De Saint-Venant Equations Experimentally Verified", Journal of Hyraulics Division, A.S.C.E., Vol 97, No HY9, Proc. Paper 8378, Sept, pp 1387-1401.

Chowdhury, A.K.M. (1982)
"Numerical Models for Shallow Water Tides in x-y-t River Networks and x-y-t Space", Ph.D. Thesis, University of Strathclyde, Glasgow.

Chu, W. and Yeh, W. (1980)
"Two-Dimensional Tidally Averaged Estuarine Model", Journal of the Hydraulics Division, A.S.C.E., Vol 106, No HY4, Proc. Paper 15345, April, pp 501-518.

Cunge, J.A., Holly, F.M. and Verwey, A. (1980)
"Practical Aspects of Computational River Hydraulics", Pitman Publishing Limited, London.

Denman, N.E. (1973)
"The Humber Estuary Symposium", Humber Advisory Group, Dec.

Donald, A.S. (1981)
"The Numerical Simulation of Tide and Storm Surge Propagation in Two-Dimensional Space Using the Method of Characteristics" Ph.D. Thesis, University of Strathclyde, Glasgow.

Doodson, A.T. and Corkan, R. (1932)
"The Principle Constituent of the Tides in the English and Irish Channels", Philosophical Transactions of the Royal Society, A.234.

Doodson, A.T. and Warburg, H.D. (1941)
"Admiralty Manual of Tides", Her Majesty's Stationery Office.

Douglas, J. Jnr (1955)
"On the Numerical Integration of $\partial^2 u/\partial x^2 + \partial^2 u/\partial y^2 = \partial u/\partial t$ by Implicit Methods", Journal of the Society of Industrial Applied Mathematics, Vol 3, No 1, March, pp 42-65.

Dronkers, J.J. (1964)
"Tidal Computations in Rivers and Coastal Waters", North-Holland Publishing Company.

Dronkers, J.J. (1969)
"Tidal Computations for Rivers, Coastal Areas and Seas", Journal of the Hydraulics Division, A.S.C.E., Vol 95, No HY1, Proc. Paper 6341, Jan, pp 29-77.

Ellis, J. (1970)
"Unsteady Flow in a Channel of Variable Cross Section", Journal of the Hydraulics Division, A.S.C.E., Vol 96, No HY10, Proc. Paper 7583, Oct, pp 1927-1945.

Ellis, J. (1972)
"The Changing Tides of the River Clyde 1750 to 1980", The Institution of Engineers and Shipbuilders in Scotland.

Ellis, J. (1979)
"Unsteady Open Channel Flow Calculations", Annual Meeting of Hydraulic Specialists, Portsmouth Polytechnic, Sept.

Evans, E.P. (1977)
"The Behaviour of a Mathematical Model of Open Channel Flow", Proceedings 17th Congress I.A.H.R., Baden-Baden, Vol 2, pp 173-180.

Flather, R.A. and Heaps, N.S. (1975)
"Tidal Computations for Morecombe Bay", The Geophysical Journal, Vol 42, pp 489-517.

Fletcher, A.G. and Hamilton, W.S. (1967)
"Flood Routing in an Irregular Channel", Journal of the Engineering Mechanics Division, Proceedings of the American Society of Civil Engineers, Vol 93, No EM3, June.

Goldberg, D.E. and Wylie, E.B. (1983)
"Characteristics Method Using Time-Line Interpolations", Journal of Hydraulic Engineering, Vol 109, No 5, May, Paper No 17937.

Harleman, D. (1973)
Lectures Given at NATO Advanced Study Institute on Estuary Dynamics, Lisbon, June-July.

Harris, D.L. (1966)
"Hurricane Storm Surges", Hurricane Symposium American Society of Oceanography, pp 200-224.

Hartree, D.R. (1952)
"Numerical Analysis", Oxford University Press, London, England, pp 260-261.

Heaps, N.S. (1969)
"A Two-Dimensional Numerical Sea Model", Philosophical Transactions of the Royal Society, A 265, pp 93-137.

Henderson, F.M. (1966)
"Open Channel Flow", Macmillan.

Humber Advisory Group (1973)
"The Humber Estuary", Symposium, Dec.

Humber Estuary Research Committee (1974)
"Collection of Field Data for the Design and Operation of the Humber Tidal Model", Report No H1, Nov.

Hydraulics Research Station (1968)
"The Formation and Maintenance of a Navigation Channel in the Humber Estuary Through the Middle Shoal", Parts 1 and 2, Ex 386, Feb.

Hydraulics Research Station (1970)
"Killingholme Power Station : Estimation of Recirculation Performance of Cooling-Water Works", Part 1, Vol 1, Ex 495, June.

Hydraulics Research Station (1974)
"Killingholme Power Station : Prediction of Surface Flow Patterns", Ex 670, Jan.

Johnson, L.W. and Dean Reiss, R. (1977)
"Numerical Analysis", Addison-Wesley.

Katopodes, N. and Strelkoff, T. (1979)
"Two-Dimensional Shallow Water Wave Models", Journal of the Engineering Mechanics Division, A.S.C.E. Vol 105, EM2, Proc. Paper 14532, April, pp 317-806.

Lax, P.D. and Richtmyer, R.D. (1956)
"Survey of the Stability of Linear Finite Difference Equations", Communications on Pure and Applied Mathematics, Vol 9, pp 267-293.

Leendertse, J.J. (1967)
"Aspects of a Computational Model for Long-Period Water Wave Propagation", Memo RM 5294 - PR, Rand Corporation, May.

Lennon, G.W. (1963)
"The Identification of Weather Conditions Associated with the Generation of Major Storm Surges Along the West Coast of the British Isles", Quarterly Journal of the Royal Meteorological Society, Vol 89, pp 381-395.

Liu, S.K. and Leendertse, J.J. (1978)
"Multidimensional Numerical Modelling of Estuaries and Coastal Seas", Advances in Hydroscience, Vol 11, pp 95-164.

McDowell, D.M. and O'Connor, B.A. (1977)
"Hydraulic Behaviour of Estuaries", Macmillan.

Meyer, C. (1975)
"Special Problems Related to Linear Equation Solvers", Journal of the Structural Division, A.S.C.E., Vol 101, No 514, April, pp 869-890.

Muir Wood, A.M. and Fleming, C.A. (1981)
"Coastal Hydraulics (Second Edition)", Macmillan.

Peaceman, D.W. and Rachford, H.H. Jnr (1955)
"The Numerical Solution of Parabolic and Elliptic Differential Equations", Journal of the Society of Industrial Applied Mathematics, Vol 3, No 1, March, pp 28-41.

Price, R.K. (1974)
"Comparison of Four Numerical Methods for Flood Routing", Journal of the Hydraulic Division, A.S.C.E. Vol 100, HY7, July, pp 879-899.

Price, R.K. and Samuels, P.G. (1980)
"A Computational Hydraulic Model for Rivers", Proceedings of the Institution of Civil Engineers, Part 2, March, pp 87-96.

Raudkivi, A.S. and Callander, R.A. (1975)
"Advanced Fluid Mechanics : An Introduction", Edward Arnold (Publishers) Limited.

Reid, R.O. and Bodine, B.R. (1968)
"Numerical Model for Storm Surges in Galveston Bay", Journal of Waterways and Harbours Division, A.S.C.E., Vol 94, No WW1, Proc. Paper 5805, Feb, pp 33-57.

Roach, P.J. (1972)
"Computational Fluid Dynamics", Hermosa Publishers, Albuquerque, New Mexico.

Rossiter, J.R. (1968)
"Computer Methods in Tidal Hydraulics", Proceedings of the Institution of Civil Engineers, Vol 39, pp 175-179.

Samuels, P.G. (1983a)
"Two-Dimensional Modelling of Flood Flows Using the Finite Element Method", International Conference on the Hydraulic Aspects of Floods and Flood Control, London, Sept. 13-15.

Samuels, P.G. (1983b)
"Computational Modelling of Flood Flows in Embanked Rivers", International Conference on the Hydraulic Aspects of Floods and Flood Control, London, England. Sept 13-15.

Smith, A.A. (1968)
"A Numerical Analysis of the Effects of Proposed Flood Prevention Methods on the White Cart River", Report to the City Engineer, Corporation of Glasgow, University of Strathclyde.

Smith, G.D. (1978)
"Numerical Solution of Partial Differential Equations : Finite Difference Methods", Oxford Applied Mathematics and Computing Science Series, Claredon Press.

Sobey, R.J. (1970)
"Finite Difference Schemes Compared for Wave-Deformation Characteristics etc", Technical Memoir No 32, US Army Corps of Engineers, Coastal Engineering Research Center, Washington, D.C.

Stelling, S.G. (1980)
"Improved Stability of Dronkers Tidal Schemes", Journal of the Hydraulics Division, A.S.C.E. Vol 106, No HY8, Aug, pp 1365-1379.

Townson, J.M. (1974)
"An Application of the Method of Characteristics to Tidal Calculations in x-y-t Space", Journal of Hydraulic Research, I.A.H.R. Vol 12, No 4.

Townson, J.M., Davis, M.E. and Matsookis, P. (1980)
"Numerical Simulations of the Bristol Channel Tide", Proceedings of the Institution of Civil Engineers, Part 2, Vol 69, Sept, pp 671-685.

Vardy, A.E. (1976)
"On the Use of the Method of Characteristics for the Solution of Unsteady Flows in Networks", Second International Conference on Pressure Surges, Sept 22-24, BHRA, Fluid Engineering, Cranfield, England.

Vreugdenhil, C.B. (1978)
"Application of Finite-Difference Methods to Estuary Problems", Symposium on Mathematical Modelling of Esturine Physics, Aug 24-26, Hamburg.

Vreugdenhil, C.B. and Wijbenga, J.H. (1982)
"Computation of Flow Patterns in Rivers", Journal of the Hydraulics Division, A.S.C.E., Vol 108, No HY11, Nov.

Walden, R.F. (1973)
"Programming the Equations of Unsteady Flow", Master of Engineering Thesis, McMaster University, Nov 1973.

Weare, J.T. (1976)
"Instability in Tidal Flow Computational Schemes", Journal of the Hydraulics Division, A.S.C.E., Vol 102, No HY5, May, pp 569-580.

Weare, J.T. (1979)
"Errors Arising from Irregular Boundaries in ADI Solutions of the Shallow-Water Equations", International Journal for Numerical Methods in Engineering, Vol 14, 1979, pp 921-931.

Wen-Li Chaing and Jiin-Jen Lee (1982)
"Simulation of Large-Scale Circulation in Harbours", Journal of the Waterways, Port, Coastal and Ocean Division, A.S.C.E. Vol 108, No WW1, Feb.

Wylie, E.B. (1980)
"Inaccuracies in the Characteristics Method", A.S.C.E. Proceedings, Computer and Physical Modelling, Aug, pp 165-176.